CENTRAL NERVOUS SYSTEM EXTRACELLULAR VESICLES

EDITED BY: Dominic Martin Walsh, Francesc Xavier Guix and Grant Thomas Corbett

PUBLISHED IN: Frontiers in Neuroscience

frontiers Research Topics

frontiers

ISSN 1664-8714
ISBN 978-2-88963-953-3
DOI 10.3389/978-2-88963-953-3

About Frontiers

Frontiers is more than just an open-access publisher of scholarly articles: it is a pioneering approach to the world of academia, radically improving the way scholarly research is managed. The grand vision of Frontiers is a world where all people have an equal opportunity to seek, share and generate knowledge. Frontiers provides immediate and permanent online open access to all its publications, but this alone is not enough to realize our grand goals.

Frontiers Journal Series

The Frontiers Journal Series is a multi-tier and interdisciplinary set of open-access, online journals, promising a paradigm shift from the current review, selection and dissemination processes in academic publishing. All Frontiers journals are driven by researchers for researchers; therefore, they constitute a service to the scholarly community. At the same time, the Frontiers Journal Series operates on a revolutionary invention, the tiered publishing system, initially addressing specific communities of scholars, and gradually climbing up to broader public understanding, thus serving the interests of the lay society, too.

Dedication to Quality

Each Frontiers article is a landmark of the highest quality, thanks to genuinely collaborative interactions between authors and review editors, who include some of the world's best academicians. Research must be certified by peers before entering a stream of knowledge that may eventually reach the public - and shape society; therefore, Frontiers only applies the most rigorous and unbiased reviews.
Frontiers revolutionizes research publishing by freely delivering the most outstanding research, evaluated with no bias from both the academic and social point of view. By applying the most advanced information technologies, Frontiers is catapulting scholarly publishing into a new generation.

What are Frontiers Research Topics?

Frontiers Research Topics are very popular trademarks of the Frontiers Journals Series: they are collections of at least ten articles, all centered on a particular subject. With their unique mix of varied contributions from Original Research to Review Articles, Frontiers Research Topics unify the most influential researchers, the latest key findings and historical advances in a hot research area! Find out more on how to host your own Frontiers Research Topic or contribute to one as an author by contacting the Frontiers Editorial Office: researchtopics@frontiersin.org

CENTRAL NERVOUS SYSTEM EXTRACELLULAR VESICLES

Topic Editors:
Dominic Martin Walsh, Harvard Medical School, United States
Francesc Xavier Guix, Severo Ochoa Molecular Biology Center (CSIC-UAM), Spain
Grant Thomas Corbett, Harvard Medical School, United States

Citation: Walsh, D. M., Guix, F. X., Corbett, G. T., eds. (2020). Central Nervous System Extracellular Vesicles. Lausanne: Frontiers Media SA. doi: 10.3389/978-2-88963-953-3

Table of Contents

frontiers in Neuroscience

MINI REVIEW
published: 05 March 2019
doi: 10.3389/fnins.2019.00163

Therapeutic Potential of Extracellular Vesicles for the Treatment of Nerve Disorders

Luisa R. Galieva[1], *Victoria James*[2], *Yana O. Mukhamedshina*[1,3]* *and Albert A. Rizvanov*[1]

[1] *Institute of Fundamental Medicine and Biology, Kazan Federal University, Kazan, Russia,* [2] *School of Veterinary Medicine and Science, University of Nottingham, Nottingham, United Kingdom,* [3] *Department of Histology, Cytology, and Embryology, Kazan State Medical University, Kazan, Russia*

The use of extracellular vesicles (EVs) as cell free therapy is a promising approach to stimulate tissue regeneration including that of the nervous system. EVs transfer bioactive proteins and lipids, RNA and microRNAs, which play a relevant role in EV-mediated intercellular communication. The immunomodulatory, anti-inflammatory, and neuroprotective effects of mesenchymal stem cells-derived EVs have been well studied, knowledge of this paracrine mechanism and the availability of these cells, positions mesenchymal stem cells as a potential source of EVs for cell free therapy for a variety of regenerative and nervous system disorders. In this review, we focus on the immunomodulatory and neuroprotective effects of stem cells-derived EVs within *in vitro* and *in vivo* models of nerve disorders.

Keywords: extracellular vesicles, immunomodulatory effects, neuroprotective effects, mesenchymal stem cells, nerve disorders

OPEN ACCESS

Edited by:
Grant Thomas Corbett, Harvard Medical School, United States

Reviewed by:
Susanna Amadio, Fondazione Santa Lucia (IRCCS), Italy
Veronica Perez de la Cruz, Instituto Nacional de Neurología y Neurocirugía (INNN), Mexico

***Correspondence:**
Yana O. Mukhamedshina
yana.k-z-n@mail.ru

Specialty section:
This article was submitted to Neurodegeneration, a section of the journal Frontiers in Neuroscience

Received: *20 November 2018*
Accepted: *12 February 2019*
Published: *05 March 2019*

Citation:
Galieva LR, James V, Mukhamedshina YO and Rizvanov AA (2019) Therapeutic Potential of Extracellular Vesicles for the Treatment of Nerve Disorders. Front. Neurosci. 13:163. doi: 10.3389/fnins.2019.00163

INTRODUCTION

The need to improve the effectiveness of available therapeutic protocols used within the regenerative medicine field, has led to a number of different approaches. However, the nerve disorders still present a treatment challenge due to the low regenerative potential of the central nervous system (CNS). Stem cell therapy has been at the forefront of regenerative medicine for the last decade, but poor clinical trial reports have shifted the focus of researchers to develop improved protocols and complementary approaches. For example, it became apparent, that the therapeutic effect of stem cells can be enhanced through the expression of genes of neurotrophic factors using gene therapy approaches. Unfortunately, a hazard associated with inducing such genetic changes is the potential for stem cell transformation. Therefore, a critical need still exists for the development of new therapeutic approaches that do not carry the same potential risks.

Confirmation of the paracrine effects of stem cells and the relevance to tissue regeneration was a breakthrough in this area, paving the way for a series of subsequent studies to characterize and leverage this mechanism for therapeutic development. Gnecchi et al. were the first to show that conditioned medium from mesenchymal stem cells (MSCs) overexpressing the gene *Akt1* exerted cytoprotective effects on cardiomyocytes exposed to hypoxia *in vitro,* reduced acute myocardial infarction sizes and improved ventricular functions *in vivo* (Gnecchi et al., 2005, 2006). Takahashi et al. (2006) similarly found that injection of bone marrow mononuclear cells supernatants increased microvessel density and decreased the fibrotic area within an infarcted heart model, contributing to significant functional improvement. Subsequently, MSCs-derived conditional medium was reported to stimulate functional and morphological improvement in pathological conditions such as renal injury, myocardial infarction, and fulminant hepatic failure (Bi et al., 2007; Parekkadan et al., 2007; Timmers et al., 2007).

The results obtained supported a paracrine hypothesis of stem cell action in tissue protection and repair. It was subsequently established that these beneficial were attributable to soluble factors including extracellular vesicles (EVs) released from stem cells (Bruno et al., 2009; Lai et al., 2010; Xin et al., 2013a). The biogenesis and methodology of isolation of EVs has been described in several published reviews (Biancone et al., 2012; Akers et al., 2013; Koniusz et al., 2016). Therefore, in this mini review, we focus on the newly emerging field investigating the therapeutic potential of stem cell-derived EVs, produced *in vitro* and transplanted within the animals and patient for the treatment of nerve disorders.

IMMUNOMODULATORY AND NEUROPROTECTIVE EFFECTS OF STEM CELL-DERIVED EVS

By transferring bioactive proteins and lipids, RNA and microRNAs (miRNAs), EVs may play a crucial role in intercellular communication between stem cells and other cells within the tissue micro-environment (Camussi et al., 2013; Braccioli et al., 2014; Gomzikova and Rizvanov, 2017). The anti-inflammatory and neuroprotective effects of MSC-derived EVs and their paracrine mechanism of action have been well studied (Kalani et al., 2014; Börger et al., 2017).

EVs have been shown to be actively involved in processes of immune regulation such as stimulation of T-cell proliferation, apoptosis induction in activated cytotoxic T-cells, differentiation of monocytes into dendritic cells and B lymphocyte-mediated tumor suppression (Bobrie et al., 2011; Chaput and Théry, 2011; Taylor and Gercel-Taylor, 2011). It is not surprising that MSCs-derived EVs were also found to be immunologically active (Blazquez et al., 2014; Zhang et al., 2014; Bruno et al., 2015). The immunomodulatory properties of MSCs-derived EVs are reported to be the result of the suppression of TNF-a and IL-1b secretion, increasing the concentrations of TGF-b, regulatory T cells (Treg) and cytotoxic T lymphocyte-associated protein 4, inducing Th1 to Th2 cell conversion, reducing IFN-γ production and the potential of T cells to differentiate into Th17 cells (Mokarizadeh et al., 2012; Blazquez et al., 2014; Del Fattore et al., 2015; Chen et al., 2016b). However, some data indicate a lower *in vitro* immunomodulatory effect of MSC-derived EVs on T-cell proliferation and antibody formation, as compared with their cellular counterpart (Conforti et al., 2014). In a recent study, immunomodulatory effect inflammation-stimulated (TNF-α and IFN-γ) MSCs-derived EVs was evaluated (Harting et al., 2018). It was found, that thus obtained EVs have enhanced anti-inflammatory properties partially due to COX2/PGE2 pathway alteration.

Although EVs can exhibit a variety of different protein and nucleic acid cargos, their regenerative effects are mainly ascribed to the transfer of specific proteins and miRNAs (Collino et al., 2017). For example, EV cargos of miR-1000, miR-133b, miR-21, miR-34a, and miR-219 have been reported to exert a neuroprotective effect by regulating glutamate release at the synapse (Verma et al., 2015), promoting neural plasticity (Xin et al., 2013b), suppressing apoptosis (Ma et al., 2013; Vallabhaneni et al., 2015), and enhancing myelination (Pusic and Kraig, 2014b).

Despite knowledge of the function of some aspects of the EV cargo, further studies are required to fully understand the mechanisms that underpin the immunomodulatory and neuroprotective effects of EVs.

CURRENT PERSPECTIVES OF EVS IN THE TREATMENT OF NERVE DISORDERS

Although the therapeutic potential of EVs has not been fully elucidated, their use can be said to be most promising for the treatment of different disorders of the CNS, when drugs are of limited use due to their inability to penetrate the blood-brain barrier (BBB). EVs have been proposed to be transported across the interior of a cell via transcytosis, which may enable these EVs to cross the BBB. This has been experimentally confirmed, as EVs given intravenously (Alvarez-Erviti et al., 2011) or intranasally (Zhuang et al., 2011; Haney et al., 2015) were able to penetrate the BBB.

It should be noted that the therapeutic potential of EVs depends on the composition of their cargo. The cargo of EVs from different cell types can include a common set of biological molecules (nucleic acids, proteins, and lipids) and also molecules that reflect the cell source of the EVs and the physiological or pathological state of the cell source (Zhang et al., 2016; Reiner et al., 2017). In this regard, it is important to define the cargo of stem cell-derived EVs to further understand the mechanisms involved in regenerative processes during therapy. Currently, most studies evaluating the regenerative potential of stem cell-derived EVs focus on a general assessment of therapeutic efficacy without detailing the multiple physiological or biochemical changes occurring due to EVs specific cargo. Defining the EV cargo would allow subsequent manipulation, combining a specific set of proteins and RNAs which could efficiently modulate the course of nerve disorders (Selmaj et al., 2017).

The introduction of EV use into clinical practice has been limited by the ability to isolate sufficient EVs from culture systems and the heterogeneity of the cargo of naturally occurring EVs. Therefore, methods of obtaining "modified" EV have become a major focus for the field. In such a cases, EVs are most often derived from MSCs owing to the availability of these cells and the presence of positive properties mediated by their EVs, or induced pluripotent stem cells (iPS cells) whose EVs also demonstrate consistent regenerative abilities. EVs from both cell types have been proposed as a potential starting point for cell free therapy in nerve disorders (**Figure 1**).

Table 1 provides a summary of preclinical studies of EV use in both *in vitro* and *in vivo* models of nerve disorders.

Multiple Sclerosis (MS)

The success of remyelinating therapy in MS is mostly attributed to dendritic cell (DCs)-derived EVs (Pusic et al., 2014a), whereby EVs produced by IFN-γ-stimulated DCs increased

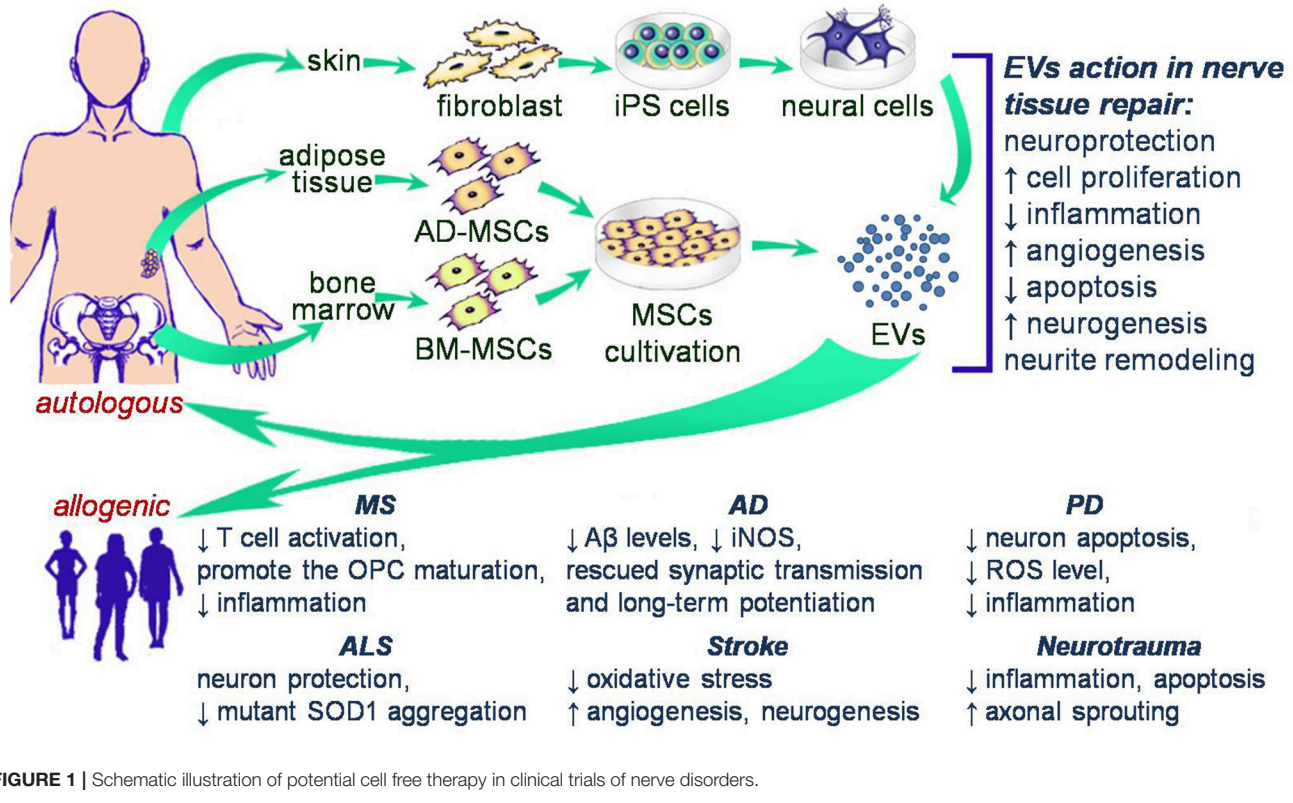

FIGURE 1 | Schematic illustration of potential cell free therapy in clinical trials of nerve disorders.

myelination and oxidative tolerance *in vitro* and *in vivo* (Pusic et al., 2014c). These changes are likely attributable to the high levels of miR-219 within the EVs, which is necessary and sufficient for oligodendrocyte precursor cell (OPC) differentiation, the formation and maintenance of compact myelin, and is deficient in human multiple sclerosis lesions (Junker et al., 2009; Dugas et al., 2010; Zhao et al., 2010). Pusic et al. (2014a) proposed that stimulated DCs-derived EVs contain high levels of specific anti-inflammatory miRNAs that may have an immunomodulatory role in suppressing the development of multiple sclerosis. Yu et al. (2013) demonstrated that EVs with membrane-associated TGF-β1 from gene-modified DCs prevented the de novo differentiation of Th17 cells by inhibiting DC IL-6 production, and were effective in inhibiting the development and progression of experimental autoimmune encephalomyelitis (EAE).

Zhuang et al. (2011) used EVs loaded with anti-inflammatory agents like curcumin or JSI124 for intranasal delivery to the brain. Effects of this route of delivery were evaluated in 3 different inflammation-mediated murine disease models: brain tumor-bearing, lipopolysaccharide (LPS)-induced brain inflammation, and EAE. Having given EVs with curcumin, mice were protected from LPS-induced brain inflammation and progression of EAE, brain tumor-bearing mice also showed a significant delay in brain tumor growth following curcumin loaded EV treatment. Intranasal administration of EVs has been shown to provide rapid transport to the brain, and subsequent absorption by the microglia.

A marked reduction in MS and EAE relapses have been observed during pregnancy (Confavreux et al., 1998). It was demonstrated in a mouse model of EAE that serum EVs suppressed T cell activation, promoted the maturation of OPC, and pregnancy-associated exosomes facilitated OPC migration into active CNS lesions (Williams et al., 2013). At the same time, serum EVs derived from non-pregnant mice were also able to reduce the severity of EAE. Thus, it was established that serum EVs are a prominent mediator both of immune modulation and neuroprotection which is especially pronounced during pregnancy.

Alzheimer's Disease (AD)

Wang et al. (2017) demonstrated the positive effect of using bone marrow MSC-derived EVs (BM-MSC-derived EVs) both *in vitro* and *in vivo*. Inducible nitric oxide synthase (iNOS) mRNA and protein levels were significantly reduced in cultured primary neurons prepared from APP/PS1 pups treated with BM-MSC-derived EVs. *In vivo* studies demonstrated improved cognitive behavior, rescued CA1 synaptic transmission, and long-term potentiation in APP/PS1 mice administrated with BM-MSC-derived EVs through an intracerebroventricular (i.c.v.) injection.

It has already been reported, that neutral endopeptidase (NEP) levels and activity are reduced in patients with AD (Yasojima et al., 2001). NEP was initially identified as a regulator of the Aβ level (Iwata et al., 2000). Katsuda et al. (2013) demonstrated NEP-specific enzyme activity could be exhibited by adipose tissue-derived MSC EVs (AD-MSC-derived EVs). Furthermore,

TABLE 1 | Preclinical trials using EVs.

Disease model	Source of EVs	Protocol details	Reported effects	Reference
MULTIPLE SCLEROSIS				
EAE in mice	EVs from bone marrow-derived DCs infected Ad/mTGF- 1 or Ad/sTGF-β1, ∼100 nm	10 μg EVs/mouse, intravenously	Prevented the *de novo* differentiation of Th17 cells via inhibiting IL-6 production, inhibited the development and progression of EAE	Yu et al., 2013
Primary OPC cultures	serum-derived EVs of pregnant and non-pregnant mice	Co-culture of primary OPC with EVs, for 72 h	Enhanced the function of OPCs	Williams et al., 2013
EAE in mice	∼100 nm	40 μg total protein of EVs/mouse, intravenously	Suppressed T cell activation, promoted the maturation of OPC, facilitated OPC migration into active CNS lesions	
Brain tumor-bearing mice model	Tumor cells-derived EVs with circumin or JSI124, ∼100 nm	12.5 pmol EVs, intranasally for 12 consecutive days	Significantly delayed brain tumor growth in the brain tumor model; protected against LPS-induced brain inflammation and the progression of EAE	Zhuang et al., 2011
LPS-induced brain inflammation		1.5 nmol EVs in 10 μl PBS/mouse, single intranasal administration		
EAE in mice		1.5 nmol EVs, intranasally for 26 consecutive days		
ALZHEIMER'S DISEASE				
N2a cells	AD-MSC-derived EVs, ∼100–200 nm	Co-culture of N2a cells with EVs, 500 μg protein/mL, up to 24 h	Decreased extracellular and intracellular Aβ levels in N2a cells	Katsuda et al., 2013
APP transgenic mice	Primary neuron culture-derived EVs	2 mg total protein of EVs/ml PBS by Alzet minipump at 0.25 ll/h for 14 days.	decreased Aβ and amyloid depositions	Yuyama et al., 2015
Primary cortical neuron culture from newborn APP/PS1 mice	BM-MSC-derived EVs, ∼100–140 nm	Co-culture of cortical neurons with EVs, 100 μg/ml EVs for 12 h	Reduced Aβ induced iNOS expression in primary neurons	Wang et al., 2017
APP/PS1 mice		100 μg EVs in 5 μl PBS/mouse, i.c.v. injection once per 2 days for 2 weeks	Improved cognitive behavior, rescued impairment of CA1 synaptic transmission, and long-term potentiation	
PARKINSON'S DISEASE				
6-OHDA induced apoptosis in DA neurons	SHEDs-derived EVs, ∼50–1000 nm	Co-culture of DA neurons with EVs, for 20 h	Suppressed 6-OHDA induced apoptosis	Jarmalavičiute et al., 2015
Cortical neurons and DA neurons from mouse pups	Macrophages—derived EVs incorporating therapeutic protein catalase, ∼100–200 nm	Co-culture of cortical neurons and DA neurons with EVs, 100 μg/mL total protein, for 24 h	Reduced ROS level	Haney et al., 2015
6-OHDA lesion of C57BL/6 mice		2.4×10^{10} EVs in 20 μl PBS/mouse, intranasally or intravenously	Anti-inflammatory effect, reduced microgliosis	
AMYOTROPHIC LATERAL SCLEROSIS				
NSC-34 cells expressing ALS mutations	ADSC-derived EVs, 30–120 nm	Co-culture of NSC-34 cells with 200 μg/ml EVs for up to 18 h	Protected cells from oxidative damage	Bonafede et al., 2016
G93A primary neuronal cell culture	AD-MSC-derived EVs, ∼100 nm	Co-culture of G93A cells with 200 μg/ml EVs, twice on day 2 and day 6	Reduced mutant SOD1 aggregation	Lee et al., 2016
STROKE				
MCAO in rats	BM-MSC-derived EVs, ∼100 nm	100 μg total protein of EVs in 500 μl PBS/rats, intravenously	Improved functional recovery and enhanced neurite remodeling, neurogenesis, and angiogenesis	Xin et al., 2013a
MCAO in mice	BM-MSC-derived EVs, ∼100 nm	EVs released by 2×10^6 MSCs diluted in 250 μl of saline, intravenously	Reduced post-ischemic motor coordination impairment, induced long-term neuroprotection, increased cell proliferation, stimulated neurogenesis, and angiogenesis	Doeppner et al., 2015

(Continued)

TABLE 1 | Continued

Disease model	Source of EVs	Protocol details	Reported effects	Reference
MCAO in rats	AD-MSC-derived EVs, ~100 nm	100 μg EVs/rat, intravenously	Reduced infiltration of $CD11^+$ and $CD68^+$ cells, decreased oxidative stress, increased angiogenesis	Chen et al., 2016a
Subcortical Stroke	AD-MSC-derived EVs, ~100 nm	100 μg total protein of EVs, intravenously	Rescued cognitive impairments, improved functional recovery and increased axonal sprouting	Otero-Ortega et al., 2017
NEUROTRAUMA				
TBI (controlled cortical impact, CCI) in rat	BM-MSC-derived EVs, ~100–150 nm	100 μg total protein of EVs in 500 μl PBS/rat, intravenously	Significantly improved spatial learning, sensorimotor functional recovery, reduced neuroinflammation, increased the number of newly formed mature neurons in the DG, increased the number of newly formed endothelial cells in the lesion boundary zone and DG	Zhang et al., 2015, 2017
TBI (controlled cortical impact, CCI) in mice	BM-MSC-derived EVs, ~200 nm	30 μg total protein of EVs (15×10^9)/mice, single intravenous injection	Rescued cognitive impairments	Kim et al., 2016
Contused SCI in rat	BM-MSC—derived EVs, ~20–130 nm	100 μg total protein of EVs (1×10^{10}) in 500 μl PBS/rat, intravenously	Decreased expression of proapoptotic protein (Bax) and pro-inflammatory cytokines (TNF-α and IL-1β), increased expression levels of anti-apoptotic (Bcl-2) and anti-inflammatory (IL-10) proteins	Huang et al., 2017
Contused SCI in rat	BM-MSC—derived EVs, ~30–150 nm	40 μg total protein of EVs (1×10^6) in 200 μL PBS/rat, 30 min and 1 day post-SCI, intravenously	Reduced the proportion of A1 astrocytes, decreased lesion area and expression of pro-inflammatory cytokines (TNFα, IL-1α, IL-1β), improved functional recovery	Wang et al., 2018
Contused SCI in rat	BM-MSC—derived EVs	1×10^9 of EVs in 1 ml PBS/rat, 3 h post-SCI, intravenously	Reduced neuroinflammation, decreased reactive microglia and astrocytes, improved functional recovery	Ruppert et al., 2018
Contused SCI in rat	BM-MSC- derived EVs, ~30–100 nm	2.5×10^9 in 200 μl PBS/rat, intravenously	Targeted the SCI site and might contribute to the therapeutic effects, target specifically to M2 macrophages	Lankford et al., 2018

it was indicated that AD-MSC-derived EVs when transferred to N2a cells (a fast-growing mouse neuroblastoma cell line overproducing human Aβ) contributed, at least in part, to a decrease in both extracellular and intracellular Aβ levels. That AD-MSCs expressed NEP at a higher level than BM-MSCs is an important observation highlighting the importance of MSC origin on function (Yasojima et al., 2001).

An alternative cellular source of EVs for therapeutic intervention in AD were used by Yuyama et al. (2015). These authors showed that intracerebral infusion of neuronal EVs into brains of APP transgenic mice decreased amyloid depositions, suggesting an important role for neuronal exosomes in clearing Aβ in brain, but not explaining mechanisms of EVs actions.

Parkinson's Disease (PD)

Haney et al. (2015) proposed a new EV-based technology for catalase delivery to the CNS to treat PD. Bovine liver derived catalase was loaded into EVs isolated from the mouse macrophage cell line (Raw 264.7). The *in vitro* study data demonstrated that reactive oxygen species (ROS) levels decreased when catalase-loaded EVs as well as empty ones were co-cultured with cortical neurons and dopaminergic (DA) neurons, although the effect of empty EVs was less significant. Administration of the same catalase loaded EVs to a model of 6-OHDA lesions in C57BL/6 female mice had an anti-inflammatory effect manifested as decreased microgliosis. It is important to note that there was no effect on microglia activation, or the number of DA neurons. It was hypothesized that EVs-mediated delivery of catalase to activated microglia, astrocytes, and neurons in the inflamed brain might result in ROS degradation and neuroprotection in PD patients.

Jarmalavičiute et al. (2015) demonstrated *in vitro* that EVs isolated from the supernatants of stem cells derived from the dental pulp of human exfoliated deciduous teeth (SHEDs), and grown on laminin-coated 3D alginate micro-carriers, suppressed 6-OHDA (6-hydroxy-dopamine) induced apoptosis in DA neurons. Interestingly, EVs from the same stem cells cultured under standard conditions possessed no such properties. These results confirm that EVs serve as a novel therapeutic approach in the treatment of Parkinson's disease, although the mechanism of action remains unclear.

Amyotrophic Lateral Sclerosis (ALS)

Bonafede et al. (2016) showed *in vitro*, that AD-stromal cell-derived EVs (AD-SC-derived EVs) were able to protect NSC-34 cells from oxidative damage, which is one of the main mechanisms of damage in ALS, increasing cell viability. They suggest the positive effect might be caused by secretion of miRNAs, which play a protective role via inhibition of apoptosis pathways, and promoting cell cycle progression and proliferation. AD-SC-derived EVs were shown *in vitro* to ameliorate SOD1 protein levels and aggregates in neuronal cells derived from G93A ALS mice. It was concluded that the abnormal expression of mitochondrial proteins in ALS cells could be rescued by application of AD-SC-derived EVs (Lee et al., 2016).

Stroke

When using BM-MSC-derived EVs in a model of middle cerebral artery occlusion (MCAO) ischemic lesion volumes reduced, however there was no significant difference compared to PBS-treated controls (Xin et al., 2013a). This study demonstrated that neurite remodeling improved, alongside increases in synaptic plasticity, neurogenesis and angiogenesis within the ischemic boundary zone. These improvements in function were proposed to be the result of miR133b activity on neurite remodeling, delivered to neural cells as part of the BM-MSC-derived EVs cargo (Xin et al., 2013b). In complementary study, intravenous injection of BM-MSC-derived EVs into an *in vivo* model of MCAO reduced post-ischemic motor coordination impairment, induced long-term neuroprotection, increased cell proliferation, and stimulated neurogenesis and angiogenesis (Doeppner et al., 2015).

Chen et al. (2016a) studied the effects of intravenous administration of AD-MSC-derived EVs and AD-MSCs in a model of MCAO. Results demonstrated that neurological impairment was reversed after treatment with AD-MSC-derived EVs an effect that was more significant when treatment used AD-MSCs. Reduced infiltration of CD11+ and CD68+ cells (two indicators of inflammation), decreased oxidative stress and increased angiogenesis were reported in both experimental groups.

Otero-Ortega et al. (2017) demonstrated in a model of subcortical stroke that after intravenous infusion, EVs were found in the brain and peripheral organs (the liver, lungs and the spleen). There was improved functional outcome, increased axonal sprouting, increased oligodendrocyte-associated marker expression and myelin formation, changes in white matter thickness and the restoration of tract connectivity at 28 days after EV administration. Proteomics analysis of the EVs identified 2,416 proteins that are implicated in repairing brain functions.

Neurotrauma

Zhang et al. (2015) demonstrated that BM-MSC-derived EVs effectively improved functional outcome by promoting endogenous angiogenesis, neurogenesis and reducing inflammation in rats after traumatic brain injury (TBI). In 2 years the same team of scientists reported the results of systemic administration of BM-MSC-derived EVs cultured under 2D and 3D conditions. This treatment did not alter cortical lesion volume but significantly improved cognitive and sensorimotor functional recovery, increased the number of newly formed mature neurons in the dentate gyrus (DG). It also increased the number of newly formed endothelial cells in the lesion boundary zone and DG, as well as reduced neuroinflammation. BM-MSC-derived EVs cultured under 3D conditions provided better outcome in spatial learning compared to EVs from a 2D culture (Zhang et al., 2017).

Kim et al. (2016) demonstrated that BM-MSC-derived EVs suppressed neuroinflammation after TBI in mice. It was also shown that an intravenous infusion of the isolated EVs shortly after induction of TBI rescued pattern separation and spatial learning impairments 1 month later.

Studies of the therapeutic potential of EVs in spinal cord injury (SCI) report that systemic administration of BM-MSC-derived EVs in contused SCI in rats attenuated cell apoptosis and inflammatory processes, stimulated angiogenesis, and promoted functional recovery. In particular, there was a downregulated expression of a pro-apoptotic protein (Bax) and pro-inflammatory cytokines (TNF-α and IL−1β), increased expression levels of anti-apoptotic (Bcl-2) and anti-inflammatory (IL-10) proteins (Huang et al., 2017). Furthermore, Lankford et al. (2018) demonstrated that intravenously delivered BM-MSC-derived EVs targeted the SCI site, might contribute to the therapeutic effects by specifically targeting M2 macrophages. EVs were detected in the area of SCI and the spleen, but not in the intact region of the spinal cord.

Recently, Wang et al. (2018) confirmed a comparable therapeutic effect of intravenously administered BM-MSC-derived EVs and BM-MSCs in SCI. The authors observed that BM-MSC-derived EVs reduced the proportion of neurotoxic astrocytes, probably via inhibiting nuclear translocation of NFκB p65, and exerted anti-inflammatory and neuroprotective effects following SCI. Similar results were obtained by Ruppert et al. (2018), who confirmed the anti-inflammatory and functional effects of intravenously delivered BM-MSC-derived EVs by means of a decreased in microglia activation markers rather than skewing microglial polarization.

Clinical Trials Using EVS in the Treatment of Nerve Disorders

The conceptual advance in our understanding of the therapeutic application of EVs as a regenerative strategy for neural tissue is relatively new. Therefore, a considerable number of studies are non-clinical, relying on *in vitro* and *in vivo* models. To date the Food and Drug Administration (FDA) have approved clinical trials using EVs as a treatment of ulcers (ClinicalTrials.gov Identifier: NCT02565264), sepsis (NCT02957279), macular hole (NCT03437759), and type 1 diabetes mellitus (NCT02138331). Based on pre-clinical studies of EV-mediated delivery of miR-124 promoting neurogenesis after ischemia (Yang et al., 2017), a further clinical trial using MSC-derived EVs in the treatment of acute ischemic stroke (NCT03384433) is planned for 2018–19, in which the effect of MSC-generated EVs will be examined in post-stroke phases 1 and 2.

CONCLUSION

Studies of the therapeutic potential of EVs in regenerative strategies strongly support the use of MSC-derived EVs in the treatment of nerve tissue disorders. MSC-derived EVs are reported to exert the majority of the positive effects seen with the direct use of MSCs as a therapy, but without the risks associated with stem cell transplantation (Gatti et al., 2011; Li et al., 2012; Konala et al., 2016). The rapid progression from non-clinical to clinical studies of MSC-derived EVs will uncover the exciting potential that EV-mediated cell free therapy may offer for the treatment of nerve disorders.

AUTHOR CONTRIBUTIONS

LG: collection of data on the characteristics of immunomodulatory and neuroprotective effects of EVs, compilation these data. VJ: collection of data on the transplantation EVs in neurodegeneration deseases, professional English editing. YM: collection of data on the transplantation EVs in stroke and traumatic injury, compilation these data, drawing **Figure 1**. AR: compilation of article content, writing some chapters.

FUNDING

This work was supported by a grant from the Russian Science Foundation No. 18-75-00043 YM. This work was performed in accordance with the Program of Competitive Growth of the Kazan Federal University and a subsidy allocated to the Kazan Federal University for the state assignment in the sphere of scientific activities. AR was supported by a state assignment 20.5175.2017/6.7 (Leading Researcher) of the Ministry of Education and Science of the Russian Federation.

REFERENCES

Akers, J. C., Gonda, D., Kim, R., Carter, B. S., and Chen, C. C. (2013). Biogenesis of extracellular vesicles (EV): exosomes, microvesicles, retrovirus-like vesicles, and apoptotic bodies. *J. Neuro Oncol.* 113, 1–11. doi: 10.1007/s11060-013-1084-8

Alvarez-Erviti, L., Seow, Y., Yin, H., Betts, C., Lakhal, S., and Wood, M. J. (2011). Delivery of siRNA to the mouse brain by systemic injection of targeted exosomes. *Nat. Biotechnol.* 29:341. doi: 10.1038/nbt.1807

Bi, B., Schmitt, R., Israilova, M., Nishio, H., and Cantley, L. G. (2007). Stromal cells protect against acute tubular injury via an endocrine effect. *J. Am. Soc. Nephrol.* 18, 2486–2496. doi: 10.1681/ASN.2007020140

Biancone, L., Bruno, S., Deregibus, M. C., Tetta, C., and Camussi, G. (2012). Therapeutic potential of mesenchymal stem cell-derived microvesicles. *Nephrol. Dialysis Transplant.* 27, 3037–3042. doi: 10.1093/ndt/gfs168

Blazquez, R., Sanchez-Margallo, F. M., de la Rosa, O., Dalemans, W., Alvarez, V., Tarazona, R., et al. (2014). Immunomodulatory potential of human adipose mesenchymal stem cells derived exosomes on *in vitro* stimulated T cells. *Front. Immunol.* 5:556. doi: 10.3389/fimmu.2014.00556

Bobrie, A., Colombo, M., Raposo, G., and Théry, C. (2011). Exosome secretion: molecular mechanisms and roles in immune responses. *Traffic* 12, 1659–1668. doi: 10.1111/j.1600-0854.2011.01225.x

Bonafede, R., Scambi, I., Peroni, D., Potrich, V., Boschi, F., Benati, D., et al. (2016). Exosome derived from murine adipose-derived stromal cells: neuroprotective effect on *in vitro* model of amyotrophic lateral sclerosis. *Exp. Cell Res.* 340, 150–158. doi: 10.1016/j.yexcr.2015.12.009

Börger, V., Bremer, M., Ferrer-Tur, R., Gockeln, L., Stambouli, O., Becic, A., et al. (2017). Mesenchymal stem/stromal cell-derived extracellular vesicles and their potential as novel immunomodulatory therapeutic agents. *Int. J. Mol. Sci.* 18:1450. doi: 10.3390/ijms18071450

Braccioli, L., van Velthoven, C., and Heijnen, C. J. (2014). Exosomes: a new weapon to treat the central nervous system. *Mol. Neurobiol.* 49, 113–119. doi: 10.1007/s12035-013-8504-9

Bruno, S., Deregibus, M. C., and Camussi, G. (2015). The secretome of mesenchymal stromal cells: role of extracellular vesicles in immunomodulation. *Immunol. Lett.* 168, 154–158. doi: 10.1016/j.imlet.2015.06.007

Bruno, S., Grange, C., Deregibus, M. C., Calogero, R. A., Saviozzi, S., Collino, F., et al. (2009). Mesenchymal stem cell-derived microvesicles protect against acute tubular injury. *J. Am. Soc. Nephrol.* 20, 1053–1067. doi: 10.1681/ASN.2008070798

Camussi, G., Deregibus, M. C., and Cantaluppi, V. (2013). Role of stem-cell-derived microvesicles in the paracrine action of stem cells. *Biochem. Soc. Trans.* 41, 283–287. doi: 10.1042/BST20120192

Chaput, N., and Théry, C. (2011). Exosomes: immune properties and potential clinical implementations. *Semin. Immunopathol.* 33, 419–440. doi: 10.1007/s00281-010-0233-9

Chen, K. H., Chen, C. H., Wallace, C. G., Yuen, C. M., Kao, G. S., Chen, Y. L., et al. (2016a). Intravenous administration of xenogenic adipose-derived mesenchymal stem cells (ADMSC) and ADMSC-derived exosomes markedly reduced brain infarct volume and preserved neurological function in rat after acute ischemic stroke. *Oncotarget* 7, 74537–74556. doi: 10.18632/oncotarget.12902

Chen, W., Huang, Y., Han, J., Yu, L., Li, Y., Lu, Z., et al. (2016b). Immunomodulatory effects of mesenchymal stromal cells-derived exosome. *Immunol. Res.* 64, 831–840. doi: 10.1007/s12026-016-8798-6

Collino, F., Pomatto, M., Bruno, S., Lindoso, R. S., Tapparo, M., Sicheng, W., et al. (2017). Exosome and microvesicle-enriched fractions isolated from mesenchymal stem cells by gradient separation showed different molecular signatures and functions on renal tubular epithelial cells. *Stem Cell Rev. Rep.* 13, 226–243. doi: 10.1007/s12015-016-9713-1

Confavreux, C., Hutchinson, M., Hours, M. M., Cortinovi,-Tourniaire, P., and Moreau, T. (1998). Rate of pregnancy-related relapse in multiple sclerosis. Pregnancy in multiple sclerosis group. *N. Engl. J. Med.* 339, 285–291. doi: 10.1056/NEJM199807303390501

Conforti, A., Scarsella, M., Starc, N., Giorda, E., Biagini, S., Proia, A., et al. (2014). Microvescicles derived from mesenchymal stromal cells are not as effective as their cellular counterpart in the ability to modulate immune responses *in vitro*. *Stem Cells Dev.* 23, 2591–2599. doi: 10.1089/scd.2014.0091

Del Fattore, A., Luciano, R., Pascucci, L., Goffredo, B. M., Giorda, E., Scapaticci, M., et al. (2015). Immunoregulatory effects of mesenchymal stem cell-derived extracellular vesicles on T lymphocytes. *Cell Transplant.* 24, 2615–2627. doi: 10.3727/096368915X687543

Doeppner, T. R., Herz, J., Görgens, A., Schlechter, J., Ludwig, A. K., Radtke, S., et al. (2015). Extracellular vesicles improve post-stroke neuroregeneration and prevent postischemic immunosuppression. *Stem Cells Transl. Med.* 4, 1131–1143. doi: 10.5966/sctm.2015-0078

Dugas, J. C., Cuellar, T. L., Scholze, A., Ason, B., Ibrahim, A., Emery, B., et al. (2010). Dicer1 and miR-219 Are required for normal oligodendrocyte differentiation and myelination. *Neuron* 65, 597–611. doi: 10.1016/j.neuron.2010.01.027

Gatti, S., Bruno, S., Deregibus, M. C., Sordi, A., Cantaluppi, V., Tetta, C., et al. (2011). Microvesicles derived from human adult mesenchymal stem cells protect against ischaemia–reperfusion-induced acute and chronic kidney injury. *Nephrology Dialysis Transplant.* 26, 1474–1483. doi: 10.1093/ndt/gfr015

Gnecchi, M., He, H., Liang, O. D., Melo, L. G., Morello, F., Mu, H., et al. (2005). Paracrine action accounts for marked protection of ischemic heart by Akt-modified mesenchymal stem cells. *Nat. Med.* 11:367. doi: 10.1038/nm0405-367

Gnecchi, M., He, H., Noiseux, N., Liang, O. D., Zhang, L., Morello, F., et al. (2006). Evidence supporting paracrine hypothesis for Akt-modified mesenchymal stem cell-mediated cardiac protection and functional improvement. *FASEB J.* 20, 661–669. doi: 10.1096/fj.05-5211com

Gomzikova, M. O., and Rizvanov, A. A. (2017). Current trends in regenerative medicine: from cell to cell-free therapy. *BioNanoScience* 7, 240–245. doi: 10.1007/s12668-016-0348-0

Haney, M. J., Klyachko, N. L., Zhao, Y., Gupta, R., Plotnikova, E. G., He, Z., et al. (2015). Exosomes as drug delivery vehicles for Parkinson's disease therapy. *J. Controlled Release* 207, 18–30. doi: 10.1016/j.jconrel.2015.03.033

Harting, M. T., Srivastava, A. K., Zhaorigetu, S., Bair, H., Prabhakara, K. S., Toledano Furman, N. E., et al. (2018). Inflammation-stimulated mesenchymal stromal cell-derived extracellular vesicles attenuate inflammation. *Stem Cells* 36, 79–90. doi: 10.1002/stem.2730

Huang, J. H., Yin, X. M., Xu, Y., Xu, C. C., Lin, X., Ye, F. B., et al. (2017). Systemic administration of exosomes released from mesenchymal stromal cells attenuates apoptosis, inflammation, and promotes angiogenesis after spinal cord injury in rats. *J. Neurotrauma* 34, 3388–3396. doi: 10.1089/neu.2017.5063

Iwata, N., Tsubuki, S., Takaki, Y., Watanabe, K., Sekiguchi, M., Hosoki, E., et al. (2000). Identification of the major Aβ 1–42-degrading catabolic pathway in brain parenchyma: suppression leads to biochemical and pathological deposition. *Nat. Med.* 6, 143–150. doi: 10.1038/72237

Jarmalavičiute, A., Tunaitis, V., Pivorait,e, U., Venalis, A., and Pivoriunas, A. (2015). Exosomes from dental pulp stem cells rescue human dopaminergic neurons from 6-hydroxy-dopamine–induced apoptosis. *Cytotherapy* 17, 932–939. doi: 10.1016/j.jcyt.2014.07.013

Junker, A., Krumbholz, M., Eisele, S., Mohan, H., Augstein, F., Bittner, R., et al. (2009). MicroRNA profiling of multiple sclerosis lesions identifies modulators of the regulatory protein CD47. *Brain 132(Pt* 12):3342–3352. doi: 10.1093/brain/awp300

Kalani, A., Tyagi, A., and Tyagi, N. (2014). Exosomes: mediators of neurodegeneration, neuroprotection and therapeutics. *Mol. Neurobiol.* 49, 590–600. doi: 10.1007/s12035-013-8544-1

Katsuda, T., Tsuchiya, R., Kosaka, N., Yoshioka, Y., Takagaki, K., Oki, K., et al. (2013). Human adipose tissue-derived mesenchymal stem cells secrete functional neprilysin-bound exosomes. *Sci. Rep.* 3:1197. doi: 10.1038/srep01197

Kim, D. K., Nishida, H., An, S. Y., Shetty, A. K., Bartosh, T. J., and Prockop, D. J. (2016). Chromatographically isolated CD63+ CD81+ extracellular vesicles from mesenchymal stromal cells rescue cognitive impairments after TBI. *Proc. Natl. Acad. Sci. U.S.A.* 113, 170–175. doi: 10.1073/pnas.1522297113

Konala, V. B., Mamidi, M. K., Bhonde, R., Das, A. K., Pochampally, R., Pal, R., et al. The current landscape of the mesenchymal stromal cell secretome: a new paradigm for cell-free regeneration., *Cytotherapy* (2016). 18, 13–24. doi: 10.1016/j.jcyt.2015.10.008

Koniusz, S., Andrzejewska, A., Muraca, M., Srivastava, A. K., Janowski, M., and Lukomska, B. (2016). Extracellular vesicles in physiology, pathology, and therapy of the immune and central nervous system, with focus on extracellular vesicles derived from mesenchymal stem cells as therapeutic tools. *Front. Cell. Neurosci.* 10:109. doi: 10.3389/fncel.2016.00109

Lai, R. C., Arslan, F., Lee, M. M., Sze, N. S., Choo, A., Chen, T. S., et al. (2010). Exosome secreted by MSC reduces myocardial ischemia/reperfusion injury. *Stem Cell Res.* 4, 214–222. doi: 10.1016/j.scr.2009.12.003

Lankford, K. L., Arroyo, E. J., Nazimek, K., Bryniarski, K., Askenase, P. W., and Kocsis, J. D. (2018). Intravenously delivered mesenchymal stem cell-derived exosomes target M2-type macrophages in the injured spinal cord. *PLoS ONE* 13:e0190358. doi: 10.1371/journal.pone.0190358

Lee, M., Ban, J. J., Kim, K. Y., Jeon, G. S., Im, W., Sung, J. J., et al. (2016). Adipose-derived stem cell exosomes alleviate pathology of amyotrophic lateral sclerosis *in vitro*. *Biochem. Biophys. Res. Commun.* 479, 434–439. doi: 10.1016/j.bbrc.2016.09.069

Li, T., Yan, Y., Wang, B., Qian, H., Zhang, X., Shen, L., et al. (2012). Exosomes derived from human umbilical cord mesenchymal stem cells alleviate liver fibrosis. *Stem Cells Dev.* 22, 845–854. doi: 10.1089/scd.2012.0395

Ma, Y., Bao-Han, W., Lv, X., Su, Y., Zhao, X., Yin, Y., et al. (2013). MicroRNA-34a mediates the autocrine signaling of PAR2-activating proteinase and its role in colonic cancer cell proliferation. *PLoS ONE* 8:e72383. doi: 10.1371/journal.pone.0072383

Mokarizadeh, A., Delirezh, N., Morshedi, A., Mosayebi, G., Farshid, A. A., and Mardani, K. (2012). Microvesicles derived from mesenchymal stem cells: potent organelles for induction of tolerogenic signaling. *Immunol. Lett.* 147, 47–54. doi: 10.1016/j.imlet.2012.06.001

Otero-Ortega, L., Laso-García, F., Gómez-de Frutos, M. D., Rodríguez-Frutos, B., Pascual-Guerra, J., Fuentes, B., et al. (2017). White matter repair after extracellular vesicles administration in an experimental animal model of subcortical stroke. *Sci. Rep.* 7:44433. doi: 10.1038/srep44433

Parekkadan, B., van Poll, D., Suganuma, K., Carter, E. A., Berthiaume, F., Tilles, A. W., et al. (2007). Mesenchymal stem cell-derived molecules reverse fulminant hepatic failure. *PLoS ONE* 2:e941. doi: 10.1371/journal.pone.0000941

Pusic, A. D., and Kraig, R. P. (2014b). Youth and environmental enrichment generate serum exosomes containing miR-219 that promote CNS myelination. *Glia* 62, 284–299. doi: 10.1002/glia.22606

Pusic, A. D., Pusic, K. M., Clayton, B. L., and Kraig, R. P. (2014c). IFNγ-stimulated dendritic cell exosomes as a potential therapeutic for remyelination. *J. Neuroimmunol.* 266, 12–23. doi: 10.1016/j.jneuroim.2013.10.014

Pusic, A. D., Pusic, K. M., and Kraig, R. P. (2014a). What are exosomes and how can they be used in multiple sclerosis therapy? *Expert Rev. Neurother. (2014)* 14, 353–355. doi: 10.1586/14737175.2014.890893

Reiner, A. T., Witwer, K. W., van Balkom, B. W. M., de Beer, J., Brodie, C., Corteling, R. L., et al. (2017). Concise review: developing best-practice models for the therapeutic use of extracellular vesicles. *Stem Cells Transl. Med.* 6, 1730–1739. doi: 10.1002/sctm.17-0055

Ruppert, K. A., Nguyen, T. T., Prabhakara, K. S., Toledano Furman, N. E., Srivastava, A. K., Harting, M. T., et al. (2018). Human mesenchymal stromal cell-derived extracellular vesicles modify microglial response and improve clinical outcomes in experimental spinal cord injury. *Sci. Rep.* 8:480. doi: 10.1038/s41598-017-18867-w

Selmaj, I., Mycko, M. P., Raine, C. S., and Selmaj, K. W. (2017). The role of exosomes in CNS inflammation and their involvement in multiple sclerosis. *J. Neuroimmunol.* 306, 1–10. doi: 10.1016/j.jneuroim.2017.02.002

Takahashi, M., Li, T. S., Suzuki, R., Kobayashi, T., Ito, H., Ikeda, Y., et al. (2006). Cytokines produced by bone marrow cells can contribute to functional improvement of the infarcted heart by protecting cardiomyocytes from ischemic injury. *Am. J. Physiol. Heart Circul. Physiol.* 291, H886–H893. doi: 10.1152/ajpheart.00142.2006

Taylor, D. D., and Gercel-Taylor, C. (2011). Exosomes/microvesicles: mediators of cancer-associated immunosuppressive microenvironments. *Semin. Immunopathol.* 33, 441–454. doi: 10.1007/s00281-010-0234-8

Timmers, L., Lim, S. K., Arslan, F., Armstrong, J. S., Hoefer, I. E., Doevendans, P. A., et al. (2007). Reduction of myocardial infarct size by human mesenchymal stem cell conditioned medium. *Stem Cell Res.* 1, 129–137. doi: 10.1016/j.scr.2008.02.002

Vallabhaneni, K. C., Penfornis, P., Dhule, S., Guillonneau, F., Adams, K. V., Mo, Y. Y., et al. (2015). Extracellular vesicles from bone marrow mesenchymal stem/stromal cells transport tumor regulatory microRNA, proteins, and metabolites. *Oncotarget* 6:4953. doi: 10.18632/oncotarget.3211

Verma, P., Augustine, G. J., Ammar, M. R., Tashiro, A., and Cohen, S. M. (2015). A neuroprotective role for microRNA miR-1000 mediated by limiting glutamate excitotoxicity. *Nat. Neurosci.* 18:379. doi: 10.1038/nn.3935

Wang, L., Pei, S., Han, L., Guo, B., Li, Y., Duan, R., et al. (2018). Mesenchymal stem cell-derived exosomes reduce A1 astrocytes via downregulation of phosphorylated NFκB P65 subunit in spinal cord injury. *Cell Physiol. Biochem.* 50, 1535–1559. doi: 10.1159/000494652

Wang, S. S., Jia, J., and Wang, Z. (2017). Mesenchymal stem cell-derived extracellular vesicles suppresses iNOS expression and ameliorates neural impairment in Alzheimer's disease mice. *J. Alzheimer's Dis.* 61, 1005–1013. doi: 10.3233/JAD-170848

Williams, J. L., Gatson, N. N., Smith, K. M., Almad, A., McTigue, D. M., Whitacre, C. C., et al. (2013). Serum exosomes in pregnancy-associated immune modulation and neuroprotection during CNS autoimmunity. *Clin. Immunol.* 149, 236–243. doi: 10.1016/j.clim.2013.04.005

Xin, H., Li, Y., Cui, Y., Yang, J. J., Zhang, Z. G., and Chopp, M. (2013a). Systemic administration of exosomes released from mesenchymal stromal cells promote functional recovery and neurovascular plasticity after stroke in rats. *J. Cereb. Blood Flow Metab.* 33, 1711–1715. doi: 10.1038/jcbfm.2013.152

Xin, H., Li, Y., Liu, Z., Wang, X., Shang, X., Cui, Y., et al. (2013b). MiR-133b promotes neural plasticity and functional recovery after treatment of stroke with multipotent mesenchymal stromal cells in rats via transfer of exosome-enriched extracellular particles. *Stem Cells* 31, 2737–2746. doi: 10.1002/stem.1409

Yang, J., Zhang, X., Chen, X., Wang, L., and Yang, G. (2017). Exosome mediated delivery of miR-124 promotes neurogenesis after ischemia. *Mol. Ther. Nucleic Acids*. 7, 278–287. doi: 10.1016/j.omtn.2017.04.010

Yasojima, K., Akiyama, H., McGeer, E. G., and McGeer, P. L. (2001). Reduced neprilysin in high plaque areas of Alzheimer brain: a possible relationship to deficient degradation of β-amyloid peptide. *Neurosci. Lett.* 297, 97–100. doi: 10.1016/S0304-3940(00)01675-X

Yu, L., Yang, F., Jiang, L., Chen, Y., Wang, K., Xu, F., et al. (2013). Exosomes with membrane-associated TGF-β1 from gene-modified dendritic cells inhibit murine EAE independently of MHC restriction. *Eur. J. Immunol.* 43, 2461–2472. doi: 10.1002/eji.201243295

Yuyama, K., Sun, H., Usuki, S., Sakai, S., Hanamatsu, H., Mioka, T., et al. (2015). A potential function for neuronal exosomes: sequestering intracerebral amyloid-β peptide. *FEBS Lett.* 589, 84–88. doi: 10.1016/j.febslet.2014.11.027

Zhang, B., Yeo, R. W., Tan, K. H., Lim, S. K., et al. (2016). Focus on extracellular vesicles: therapeutic potential of stem cell-derived extracellular vesicles. *Int. J. Mol. Sci.* 17:174. doi: 10.3390/ijms17020174

Zhang, B., Yin, Y., Lai, R. C., Tan, S. S., Choo, A. B., and Lim, S. K. (2014). Mesenchymal stem cells secrete immunologically active exosomes. *Stem Cells Dev.* 23, 1233–1244. doi: 10.1089/scd.2013.0479

Zhang, Y., Chopp, M., Meng, Y., Katakowski, M., Xin, H., Mahmood, A., et al. (2015). Effect of exosomes derived from multipluripotent mesenchymal stromal cells on functional recovery and neurovascular plasticity in rats after traumatic brain injury. *J. Neurosurg.* 122, 856–867. doi: 10.3171/2014.11.JNS14770

Zhang, Y., Chopp, M., Zhang, Z. G., Katakowski, M., Xin, H., Qu, C., et al. (2017). Systemic administration of cell-free exosomes generated by human bone marrow derived mesenchymal stem cells cultured under 2D and 3D conditions improves functional recovery in rats after traumatic brain injury. *Neurochem. Int.* 111, 69–81. doi: 10.1016/j.neuint.2016.08.003

Zhao, X., He, X., Han, X., Yu, Y., Ye, F., Chen, Y., et al. (2010). MicroRNA-mediated control of oligodendrocyte differentiation. *Neuron* 65, 612–626. doi: 10.1016/j.neuron.2010.02.018

Zhuang, X., Xiang, X., Grizzle, W., Sun, D., Zhang, S., Axtell, R. C., et al. (2011). Treatment of brain inflammatory diseases by delivering exosome encapsulated anti-inflammatory drugs from the nasal region to the brain. *Mol. Ther.* 19, 1769–1779. doi: 10.1038/mt.2011.164

Conflict of Interest Statement: The authors declare that the research was conducted in the absence of any commercial or financial relationships that could be construed as a potential conflict of interest.

frontiers in Neuroscience

ORIGINAL RESEARCH
published: 15 April 2019
doi: 10.3389/fnins.2019.00344

Leukocyte Derived Microvesicles as Disease Progression Biomarkers in Slow Progressing Amyotrophic Lateral Sclerosis Patients

Daisy Sproviero[1†], Sabrina La Salvia[1†], Federico Colombo[2], Susanna Zucca[1], Orietta Pansarasa[1], Luca Diamanti[3,4], Alfredo Costa[3,4], Luca Lova[3,5], Marta Giannini[1,3], Stella Gagliardi[1], Eliana Lauranzano[6], Michela Matteoli[6,7], Mauro Ceroni[3,4], Andrea Malaspina[8†] and Cristina Cereda[1†]*

[1] Genomic and Post-Genomic Center, IRCCS Mondino Foundation, Pavia, Italy, [2] Flow Cytometry and Cell Sorting Unit, Humanitas Clinical and Research Center – IRCCS, Rozzano, Italy, [3] Department of Brain and Behavioral Sciences, University of Pavia, Pavia, Italy, [4] Division of General Neurology, IRCCS Mondino Foundation, Pavia, Italy, [5] Becton Dickinson Italia S.p.A., Milan, Italy, [6] Laboratory of Pharmacology and Brain Pathology, Humanitas Clinical and Research Center – IRCCS, Rozzano, Italy, [7] IN-CNR, Milan, Italy, [8] Neurodegeneration Group, Centre for Neuroscience and Trauma, Blizard Institute, Queen Mary University of London, London, United Kingdom

OPEN ACCESS

Edited by:
Grant Thomas Corbett,
Harvard Medical School,
United States

Reviewed by:
Bradley Turner,
The Florey Institute of Neuroscience and Mental Health, Australia
Gérard Lizard,
Université de Bourgogne, France

***Correspondence:**
Cristina Cereda
cristina.cereda@mondino.it

[†] These authors have contributed equally to this work

Specialty section:
This article was submitted to Neurodegeneration, a section of the journal Frontiers in Neuroscience

Received: 20 December 2018
Accepted: 25 March 2019
Published: 15 April 2019

Citation:
Sproviero D, La Salvia S, Colombo F, Zucca S, Pansarasa O, Diamanti L, Costa A, Lova L, Giannini M, Gagliardi S, Lauranzano E, Matteoli M, Ceroni M, Malaspina A and Cereda C (2019) Leukocyte Derived Microvesicles as Disease Progression Biomarkers in Slow Progressing Amyotrophic Lateral Sclerosis Patients. Front. Neurosci. 13:344. doi: 10.3389/fnins.2019.00344

The lack of biomarkers in Amyotrophic Lateral Sclerosis (ALS) makes it difficult to determine the stage of the disease in patients and, therefore, it delays therapeutic trials. Microvesicles (MVs) are possible biomarkers implicated in physiological and pathological functions, however, their role in ALS remains unclear. We investigated whether plasma derived microvesicles could be overrepresented in a group of 40 patients affected by ALS compared to 28 Alzheimer's Disease (AD) patients and 36 healthy volunteers. Leukocyte derived MVs (LMVs) compared to endothelial, platelet, erythrocyte derived MVs, were mostly present in ALS patients compared to AD patients and healthy donors. Correlation analysis corrected for the presence of confounding variables (riluzole, age at onset, site of onset, gender) was tested between PRL (Progression Rate at the Last visit) and LMVs, and a statistically significant value was found (Pearson partial correlation $r = 0.407$, $p = 0.006$). We also investigated SOD1, TDP-43 intravesicular protein level in LMVs. Misfolded SOD1 was selectively transported by LMVs and its protein level was associated with the percentage of LMVs in slow progressing patients ($r = 0.545$, $p = 0.033$). Our preliminary findings suggest that LMVs are upregulated in ALS patients and they can be considered possible markers of disease progression.

Keywords: amyotrophic lateral sclerosis, biomarkers, disease progression, microvesicles, SOD1, TDP-43

INTRODUCTION

The discovery of disease biomarkers for prognostic purposes, clinical monitoring, and evaluation of treatment response is a major research endeavor in Amyotrophic Lateral Sclerosis (ALS), a fatal neurodegenerative disease caused by selective motor neuron death (Al-Chalabi and Hardiman, 2013; Al-Chalabi et al., 2016). Microvesicles (MVs), a subclass of

Abbreviations: ALS, amyotrophic lateral sclerosis; EVs, extracellular vesicles; LMVs leukocyte derived microvesicles; MVs, microvesicles.

extracellular vesicles, are biologically relevant, considering their cargo of RNAs, proteins, and surface receptors and they have potential to be used as biomarkers in both physiological and pathological states (Cocucci and Meldolesi, 2015). MVs (size: 100–1000 nm) are vesicles shed by budding of the plasma membrane of cells (Raposo and Stoorvogel, 2013; Lötvall et al., 2014; Cocucci and Meldolesi, 2015). They are present under physiological conditions, but they can be significantly elevated under various stimuli [increased (Ca^{2+}), cellular stress, cytokine exposure, etc.] and in pathological conditions, such as cancer and neurodegenerative diseases (Yáñez-Mó et al., 2015). Upon release from their cell of origin, MVs interact only with cells that they recognize for their receptors and, once recognized, they can fuse with the plasma membrane and discharge their cargo into the cytoplasm (Prada and Meldolesi, 2016). MVs have a central role in inflammatory processes (Carandini et al., 2015) and they could be plausible targets in any research into ALS, which is characterized by an activation of astrocytes and microglia (Henkel et al., 2004; Cereda et al., 2008) as an immunological reaction to motor neuron death. Immune responses can be triggered by pathological proteins, like SOD1 and TDP-43, which have relevance to neurodegeneration (Cereda et al., 2013; Amor et al., 2014). Misfolded SOD1 is able to activate microglia by binding to the CD14/TLR4 receptor (Beers et al., 2008) and expression of TDP-43 increases pro-inflammatory markers, like IL-6, and TNFa which in glial and neuronal cells from ALS patients can act as co-activators of NF-κB (Swarup et al., 2011). SOD1 and TDP-43 can be transported by extracellular vesicles (Feneberg et al., 2014; Hanspal et al., 2017; Sproviero et al., 2018), however, it is not known whether MVs protein cargo contributes to the progression of ALS pathology. We have previously demonstrated that plasma derived MVs of ALS patients were enriched with SOD1, TDP-43, and FUS compared to controls, but we didn't investigate if these proteins were transported by MVs of a specific origin. Zachau's group has previously demonstrated the presence of high level of LMVs (Leukocytes derived microvesicles-CD45+MVs) in the cerebrospinal fluid (CSF) of an ALS patient (Zachau et al., 2012). Here, we investigated the role of CD45 MVs sub-typing in blood for clinical stratification of ALS patients and MVs function, as potential carrier of misfolded proteins, alternative route for disease propagation.

MATERIALS AND METHODS

Standard Protocol Approvals, Registrations, and Patient Consents

The study protocol was approved by the Ethical Committee of the IRCCS Mondino Foundation (Pavia, Italy). Subjects participating in the study signed an informed consent (Protocol n°375/04 – version 07/01/2004). The study conformed the standards of the Declaration of Helsinki. Plasma was isolated from 40 sporadic ALS patients (SALS) (mean age at sampling: 67 ± 9.91). ALS diagnosis was made according to the revised El Escorial Criteria (Brooks et al., 2000). ALS individuals harboring mutations in the *SOD1, FUS/TLS, TARDBP, C9ORF72* were excluded from this study. Patients with concomitant infections (pneumonia and infection at the site of gastrostomy) were excluded and biological signs of inflammation present (CRP-ESR) were normal. Patients' demographic and clinical characteristics are reported in **Table 1**. Progression rate at the last visit (PRL) was calculated as 48 minus the ALS Functional Rating Scale–Revised score (ALSFRS) at the last visit divided by the disease duration (in months) from onset of symptoms to the last visit (48-ALSFRS/Δt) (Lu et al., 2015). Progression rate lower than 0.5, and higher than 0.5 were defined as slow (ALS-slow) and fast progressing ALS (ALS-fast), respectively. Thirty-six sex and age-matched healthy volunteers, not on any pharmacological treatment (mean age: 51.04 ± 9.9) were used as controls (CTRL). Plasma was also collected from 28 patients affected by Alzheimer's Disease (AD; mean age at sampling: 75.8 ± 7.3). Diagnosis of AD was based on Aging-Alzheimer's Association work group criteria (McKhann et al., 2011). AD patients were used as neurological controls to assay if the evaluated parameters are specific of the disease. All methods were performed in accordance with the relevant guidelines and regulations.

Blood Sample Collection and Isolation of MVs

Blood samples were obtained from patients with ALS and AD and healthy controls by peripheral venepuncture into BD Vacutainer™ blood collection tubes with Sodium Citrate (BD Biosciences, United States). Within 1 h, blood sample was centrifuged at low speed (1,000 × *g* for 20 min, 1600 × *g* for 15 min) to separate plasma and remove platelets. Platelet-free plasma was then transferred to a new tube and snap frozen at −80°C. Prior to the analysis, platelet-free plasma was thawed on ice and it was centrifuged at 20,000 × *g* for 1 h with Centrifuge 5427R (Eppendorf, Italy). The pellet was washed with 0.22 μm filtered PBS and centrifuged at 20,000 × *g* for 1 h. The pellet was then processed for MVs analysis. Western Blot analysis for MVs marker (Annexin V, Santa Cruz Biotechnology, United States) and EXOs marker (Alix, Abcam, United States) and Nanoparticle-tracking analysis (NTA) were run to confirm MVs purity (**Supplementary Figure S1**) as previously described (Sproviero et al., 2018).

Flow Cytometry Analysis of MVs

Microvesicles pellet was re-suspended in 1 ml of 0.22 μm filtered Annexin V binding buffer 1× (BD Biosciences, United States). MVs were incubated with conjugated primary antibody as listed

TABLE 1 | Demographic and clinical features of ALS patients.

Variables	Data
Age (years)	67.0 (SD 9.9; range:47–86)
Spinal/bulbar	32/8 (80/20)
ALS-FRSr†	35.8 (SD 8.5; range:6–48)
PRL†	Range 0.01–3.12
Fast/Slow	17/23

†*ALSFRS, ALS Functional Rating Scale; PRL, Progression Rate at last visit.*

in the antibody section. Samples were analyzed immediately after labeling, using a BD FACS Canto II with BD FACS Diva software (BD Biosciences, United States). A standardized calibrated-bead strategy using polystyrene beads (Megamix-Plus, BioCytex, France) was used, as previously described (Nielsen et al., 2014), to discriminate MVs from background noise. The polystyrene/latex beads used were a mix of fluorescent beads of varied diameters, selected to cover a theoretical MVs size range (0.16–0.20 and 0.2–0.5 μm), using SSC as a size-related parameter. Polystyrene/latex beads acquisition setting allows the cytometer to study MVs within a constant size region and getting reproducible MV counts. The range 0.16–0.20 μm was used to define the threshold background and MVs range was between 0.2 and 0.5 μm as shown in **Supplementary Figure S1**. MVs with positive staining for Annexin V and cell specific markers CD45 (leukocyte antigen), CD31 (endothelial cell antigen), CD61 (platelet antigen), and CD235a (erythrocyte antigen) were selected. Logarithmic amplification was used for all channels and results were referred to the percentage of Annexin V^+ MVs, co-expressing another specific cell lineage marker, as previously described in the literature (Robert et al., 2009).

Immunoprecipitation of Leukocyte Derived Microvesicles (LMVs)

Microvesicles were separated as described above and resuspended in PBS+BSA 1%. Anti-CD45 antibody (Santa Cruz Biotechnology, United States) was coupled to Dynabeads (Invitrogen, United States) and then incubated with MVs overnight at 4°C. Proteins retained (immunoprecipitated, IP) on the beads were recovered by adding cold Radio-Immunoprecipitation Assay (RIPA) buffer containing phosphatase and protease inhibitors (Sigma-Aldrich, Italy) and Laemmli buffer 2× and boiled at 95°C for 5 min to obtain $CD45^+$ MVs. Immunodepleted fraction (I-) and input (starting material of MVs) were lysed in cold RIPA buffer, mixed with Laemmli buffer 2× and denatured at 95°C for 10 min.

Western Blot Analysis

Proteins were fractionated by size on SDS Precast 8–16% polyacrylamide gels (BioRad, Italy), transferred to a nitrocellulose membrane using a *Trans*-blot Turbo (BioRad, Italy) and blocked with blocking solution (5% non-fat dry milk in Tween-20 Tris-Buffered Saline solution, TBS-T) for 1 h. Membranes were incubated overnight with primary antibody in blocking solution at 4°C. Membranes were then incubated for 1 h at room temperature with secondary antibodies. Antibodies used are listed in the antibodies section. Bands were visualized using an enhanced chemiluminescence detection kit (ECL Advance, GE Healthcare, United Kingdom). For subsequent immunoreactions, primary and secondary antibodies were removed from the membrane with stripping solution incubated for 20 min (100 mM Glycine, 0.1% NP-40, 1% SDS pH 2.2). Densitometric analysis of the bands was performed using ImageJ software (National Institutes of Health, United States).

Machine Learning Analysis

Orange software (Demsar et al., 2013) was used to perform an exploratory analysis of MVs distribution in CTRL and ALS groups, with a focus on the percentages of Annexin V^+ MVs expressing specific cell lineage markers. Logistic regression was performed and receiver operator characteristic (ROC) curves were computed (Cook, 2008). The percentages of Annexin V^+ MVs expressing the cell lineage markers ($CD45^+$/Annexin V^+, $CD235a^+$/Annexin V^+, $CD31^+$/Annexin V^+, $CD61^+$/Annexin V^+), were used as regressors for the multivariate analysis and referred to disease phenotypes as described in flow cytometry analysis. Briefly, multivariate logistic regression was performed to predict the class of each sample (healthy donors or patients) and to rank features based on mutual information criteria (Peng et al., 2002).

Antibodies

Antibodies, used for flow cytometry were mouse monoclonal anti-human CD45 (2D1) (ab 641417APC-H7); mouse monoclonal anti-human CD31 (MEC13.3) (ab 560983 PE); mouse monoclonal anti-human CD61 (RUU-PL7F12) (ab 347408 Per-cy); mouse monoclonal anti-human CD235a (GA-R2 (HIR2) (ab 563666 Pe-cy7) derivation and the apoptotic marker Annexin V (ab 550407 APC-BD) (BD Biosciences, United States). Immunoglobulin isotype-matched control antibodies were purchased from BD Biosciences, United States. Antibodies used for western blot were rabbit polyclonal primary antibody anti-CD45 (Santa Cruz Biotechnology, United States), mouse monoclonal anti-misfolded SOD1-DSE2-3H1 (kindly given by Prof. Neil R. Cashman) and mouse monoclonal anti-TDP-43 (Proteintech, United States). For phospho-TDP-43 we used the same antibody we utilized for the detection of TDP-43, which recognizes the intact 45 kDa protein as well as all post-translationally modified (phosphorylated and glycosylated forms) and truncated forms in multiple applications. Secondary antibodies used were donkey anti-rabbit or anti-mouse secondary peroxidase-conjugated antibody (GE Healthcare, United Kingdom).

Statistical Analysis

The statistical analysis was carried out using Graph Pad Prism 5.0 (GraphPad Inc., United States) and SPSS statistical package version 22 (IBM, United States). One-way ANOVA with Bonferroni's multiple comparison test was used and a value of $p < 0.05$ was considered significant. The Shapiro–Wilk test was used to test variables for normality distribution and Levene test was used to test the assumption of homogeneity. In order to determine the correlation between continuous variables, a Pearson's correlation test was applied when the variables were normally distributed and a Spearman's correlation test when the variables were not normally distributed. Categorical variables were tested using the non-parametric Mann–Whitney *U*-test. A partial correlation analysis (Pearson, one-tailed test) was applied to test the correlation between PRL and CD45, while correcting for the presence of confounding variables such as riluzole (Calvo et al., 2017) or other significant factors (age at

onset, site of onset, gender). A Log-transformation was used for some data if they were not normally distributed.

RESULTS

LMVs Are Elevated in Plasma of ALS Patients

Correct purification of MVs was confirmed by transmission electron microscopy (TEM), NTA and the detection of classical MVs enriched markers (**Supplementary Figures S1A–C**) as we previously described (Sproviero et al., 2018). In Sproviero et al. (2018), we demonstrated that 90% of MVs were smaller than 500 nm by NTA. For this reason we used specific polystyrene/latex beads in the range of 0.2–0.5 μm. The percentages of Annexin V+ MVs derived from platelets (CD61), erythrocytes (CD235a), leukocytes (CD45), and endothelium (CD31) were analyzed by flow cytometry. AD patients were used as neurological controls to assay if the evaluated parameters are specific of the disease. Annexin V, that binds phosphatidylserine, is used as common marker for MVs (Lötvall et al., 2014). Flow cytometry dot plots show higher levels of LMVs in ALS patients (**Figures 1A,B,D**). Specifically, we observed that 75% of ALS patients had higher levels of leukocyte derived MVs (LMVs, % CD45+/Annexin V+ MVs) as percentage of all MVs subsets than the mean of the non-neurological control individuals and AD patients considered in this study as neurological controls (**Figure 1C**, ANOVA followed by Bonferroni's test, $p < 0.0001$; $p < 0.001$, respectively). Conversely, percentages of Annexin V+ MVs derived from endothelium (CD31), erythrocytes (CD235a), and platelets (CD61) percentage (**Figures 1E–G**) of ALS patients were not different from those of healthy control subjects and AD patients. A Spearman correlation test was run among the four markers and the age (**Table 2**). Even if there was a significant correlation between age and CD45 MVs %, the data of the three groups didn't meet the assumption of homogeneity of regression slopes since the Levene test was significant ($F = 16.47$, p-value < 0.001), so we didn't correct for the age.

Multivariate logistic regression analysis (MLRA) was applied as a classification method for ALS and control data for the four markers (**Figures 2A–D**). $CD45^{+}$/Annexin V^{+} MVs were identified as the most informative feature to discriminate ALS subgroup from AD patients and healthy controls (**Figure 2A**). The ROC curve (**Figure 2E**) showed an area under the curve of 0.717 and accuracy of 0.653 in separating patients from healthy controls. In ALS patients, no difference was found in LMV% between male and female patients (Mann–Whitney U-test $p = 0.967$) (**Table 3**). There was no statistically significant

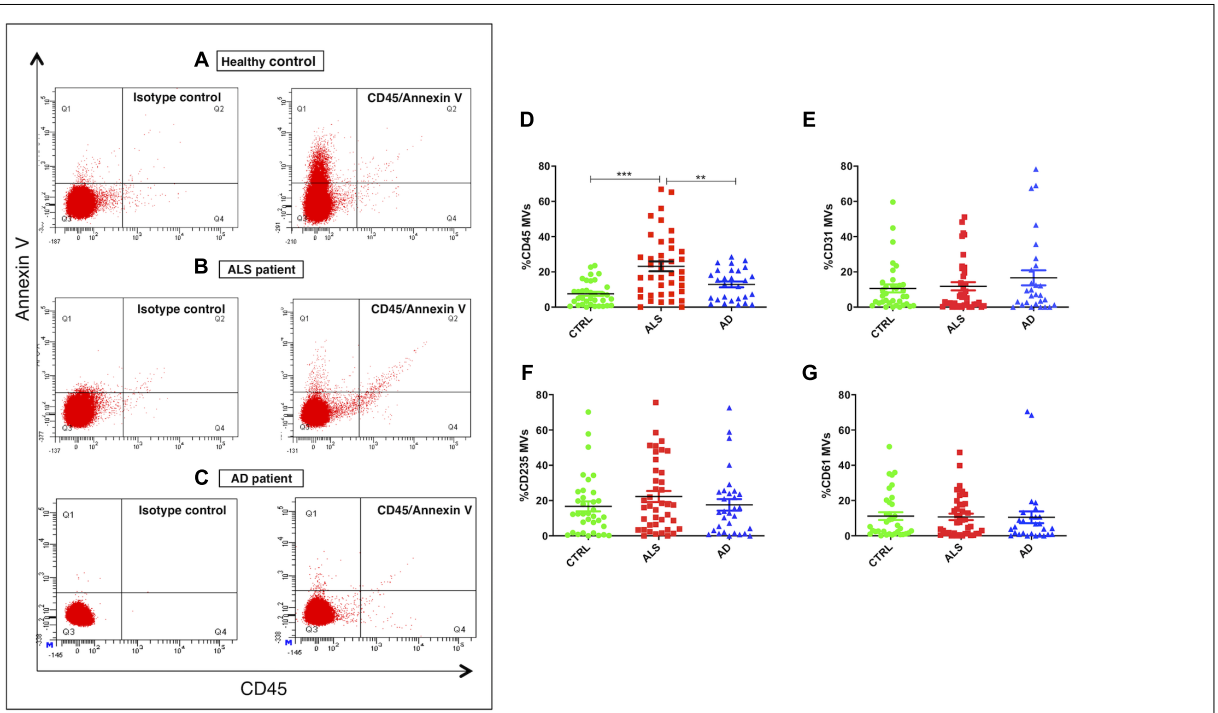

FIGURE 1 | LMVs overrepresentation in plasma from ALS patients. Flow cytometry dot plots of MVs isolated from plasma of a representative healthy control, an ALS patient and AD patient labeled with Annexin V and CD45 **(A–C)**. While healthy control **(A)** and AD patient **(C)** presented few events similar to isotype control, ALS patient **(B)** had higher % CD45+/Annexin V+ MVs. Dot plots of MVs isolated from plasma of ALS patients (red), healthy controls (green), and AD patients (blue) labeled with Annexin V and CD45 **(D)**, CD31 **(E)**, CD235A **(F)**, CD61 **(G)** markers. Results were referred as the percentage of Annexin V^{+} MVs expressing the cell lineage marker. While Annexin V+ MVs derived from endothelium (%CD31 MVs) **(E)**, erythrocytes (%CD235a MVs) **(F)**, platelets (%CD61 MVs) **(G)** were not different from the healthy control subjects and AD patients (ANOVA test, $p > 0.05$), the percentage of Annexin V+ MVs derived from leukocytes (%CD45 MVs) **(D)** was significantly enhanced in the plasma of ALS patients compared to the control group (ANOVA test, $^{***}p < 0.001$) and the AD patients (ANOVA test, $^{**}p < 0.01$). n CTRL = 36; n ALS = 40; n AD = 28.

TABLE 2 | Spearman correlation between CD45, CD235a, CD31, CD61% MVs, and age.

	Spearman's rho (*p*-value) §				
Variables	**CD45**	**CD235a**	**CD31**	**CD61**	**Age**
CD45	1	0.384 (0.000)***	0.093 (0.346)	0.117 (0.236)	0.290 (0.003)**
CD235a	0.384 (0.000)***	1	0.185 (0.060)	0.259 (0.008)**	0.186 (0.061)
CD31	0.093 (0.346)	0.185 (0.06)	1	0.651 (0.000)***	−0.023 (0.816)
CD61	0.117 (0.236)	0.259 (0.008)**	0.651 (0.000)***	1	−0.063 (0.527)

§,**Significant level, p-value < 0.05; **Significant level, p-value < 0.01, ***Significant level, p-value < 0.001.*

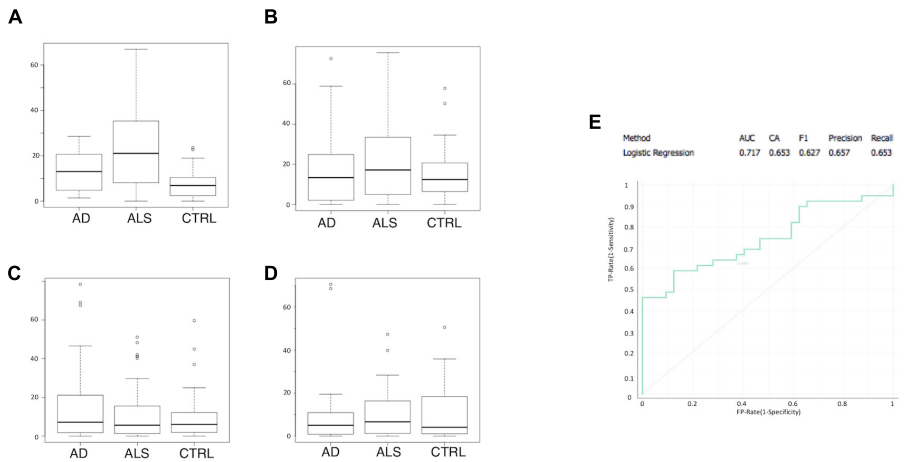

FIGURE 2 | CD45+/Annexin V+ MVs is the most informative feature to discriminate ALS group from AD patients and healthy matched control groups. Boxplot of percentage of marker positive MVs are shown for ALS, AD, and control samples: **(A)** CD45+/Annexin V+; **(B)** CD235a+/Annexin V+; **(C)** CD31+/Annexin V+; **(D)** CD61+/Annexin V+; **(E)** ROC curve for logistic regression with an AUC of 0.717 and an accuracy of 0.653.

correlation between age at onset and CD45 MVs (Spearman test, $r = 0.370$, $p = 0.072$) (**Table 3**).

LMVs Selective Enrichment of Misfolded SOD1

We have looked at whether LMVs (the most represented MVs in blood from ALS patients), carry different levels of misfolded SOD1 and TDP-43 proteins. LMVs (CD45+MVs) were isolated from plasma of 19 ALS patients (13 = Slow; 6 = Fast) and 10 healthy controls. LMVs of all patients analyzed were enriched with misfolded SOD1 and densitometric analysis of this protein, normalized against CD45, revealed a slight increase of this protein in ALS patients compared to controls (0.8431 ± 0.1236 for CTRL and 1.008 ± 0.1274 for ALS) (**Figure 3B**). The immunodepleted fraction (I-), which includes all CD45 negative MVs derived from other cells, did not show any or very little level of misfolded SOD1 (**Figure 3A**), found mainly in LMVs.

Leukocyte derived MVs of only 12 out of 19 patients carried a TDP-43 band at 45 kDa, which resembles the phosphorylated form of TDP-43 (p-TDP-43) (Steinacker et al., 2008). TDP-43 was found in IP fraction ($CD45^{+}$MVs) and in the immunodepleted (I-) fraction ($CD45^{-}$MVs) (**Figure 3A**). These results indicate that misfolded SOD1, but not TDP-43, may be compartmentalized in LMVs.

LMVs Correlation With Rate of Disease Progression and Misfolded SOD1 Enrichment

A Pearson partial correlation between LMVs and PRL was evaluated, since the variables were normally distributed. The

TABLE 3 | Clinical and phenotypic variables effect on PRL/LMVs/SOD1.

Variables	**Cases (N)**	**Age at onset rho (*p*-value)[§]**	**Bulbar_No bulbar (*p*-value)[†]**	**Gender_Code (*p*-value)[†]**	**Riluzole (*p*-value)[†]**
PRL	39	0.083 (0.375)	0.878	1.000	0.043 *
CD45	39	0.370 (0.072)	0.044*	0.967	0.294
SOD1	18	0.006 (0.491)	0.506	0.591	0.353

[†]*Mann–Whitney U-test;* [§]*Spearman's correlation test; *Significant level; p-value < 0.05.*

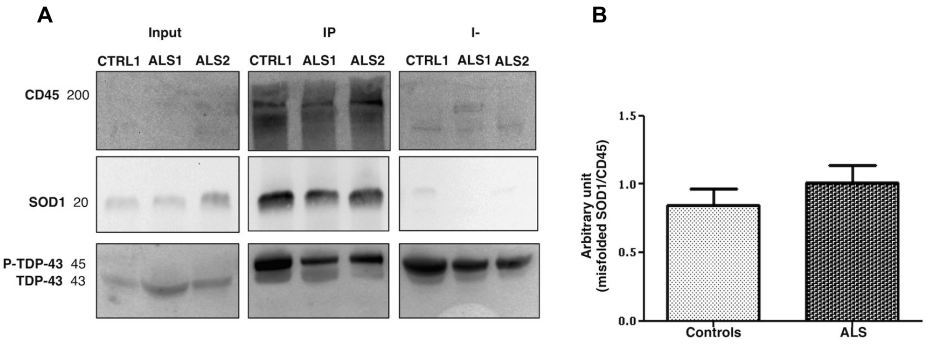

FIGURE 3 | Misfolded SOD1 enrichment in LMVs (CD45+ MVs) from ALS patients and controls. CD45+ MVs of patients (ALS 1 and ALS 2) and of CTRLs (CTRL1) were enriched with misfolded SOD1. Misfolded SOD1 was only found in LMVs. The cropped blots are used in the figure and full length blots are presented in **Supplementary Figure S2**. The immunodepleted (I-) fraction, which include all CD45 negative MVs from other cell origin, showed no or very little level of misfolded SOD1. TDP-43 was transported in its phosphorylated form by MVs of the IP and immunodepleted (I-) **(A)**. ALS 1 and ALS 2 are referred to two slow progressing patients. Input = MVs whole lysate-20% of the IP; IP = CD45 immunoprecipitated MVs (LMVs); I- = immunodepleted. **(B)** Densitometric analysis of misfolded SOD1, normalized to CD45 band, revealed slight increase of misfolded SOD1 in all ALS patients compared to controls (0.8431 ± 0.1236, CTRL n = 10; 1.008 ± 0.1274, ALS n = 18).

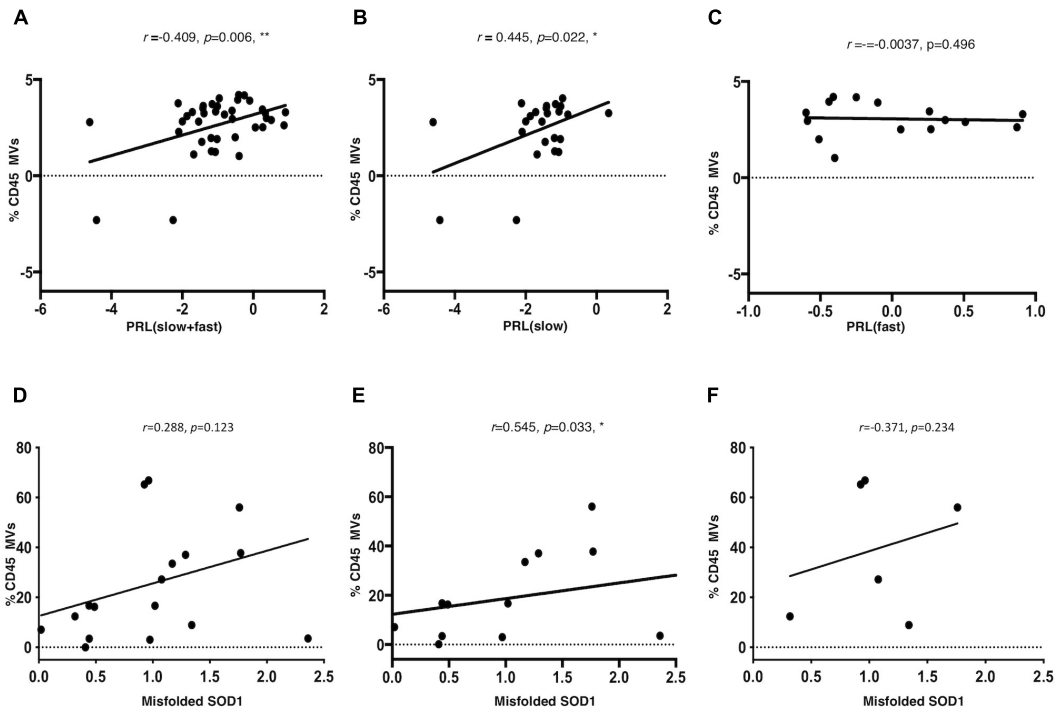

FIGURE 4 | LMVs percentage in ALS patients is correlated to progression rate at last visit and is correlated to misfolded SOD1 protein level in slow progressing ALS patients. The log of PRL and of LMVs was plotted and the line was drawn from the least squares regression. A significant correlation was found between LMVs and PRL (Pearson partial correlation r = 0.409, p = 0.006) **(A)**. The PRL of slow progressing patients was positively correlated to LMVs levels (% CD45 MVs) (Pearson partial correlation r = 0.432, p = 0.022) **(B)**. On the other hand, there was no correlation between LMVs levels and disease progression in fast progressing patients (Pearson partial correlation, r = –0.0037, p = 0.496) **(C)**. CD45+ MVs percentage (%) was directly correlated with misfolded SOD1. Densitometric analysis of misfolded SOD1 was correlated to the percentage of CD45 Annexin V (%CD45 MVs) by Spearman rank analysis. LMVs level was not associated to the densitometric level of misfolded SOD1 in ALS patients (Spearman test, r = 0.288, p = 0.123) **(D)**. We instead found a strong correlation between misfolded SOD1 protein level and LMVs in slow progressing patients (r = 0.545, p = 0.033) (n = 12) **(E)**. No statistically significant difference was found in fast progressing patients (r = –0.371, p = 0.234) (n = 6) **(F)**.

presence of a patient with a very fast progression was observed and excluded from the analysis (ALS 20, PRL = 3.12, >3sd from the mean of the PRL distribution). The cohort of patients included a number of six cases that were treated with riluzole medication, eight cases with bulbar onset and 32 with spinal onset. The effect of riluzole and site of onset on PRL were

considered and corrected. Other variables were tested, but resulted not statistically significant (**Table 3**). A significant correlation was found between LMVs and PRL (Pearson partial correlation, $r = 0.409$, $p = 0.006$) (**Figure 4A**). The inclusion of the outlier in the correlation analysis did not change the results (Pearson partial correlation, $r = 0.379$, $p = 0.009$).

Amyotrophic Lateral Sclerosis patients were separated according to PRL, into slow progressing (PRL < 0.5; $n = 23$) versus fast progressing (PRL > 0.5; $n = 17$). The PRL of slow progressing patients was positively correlated to LMVs levels (% CD45 MVs) ($r = 0.445$, $p = 0.022$) (**Figure 4B**). On the other hand, there was no correlation between LMVs levels and disease progression in fast progressing patients ($r = -0.0037$, $p = 0.496$) (**Figure 4C**). The correlation between the percentage of LMVs and misfolded SOD1 was tested for 19 patients. After removing an outlier for SOD1 (>3sd from distribution mean), LMVs level was not associated to the densitometric level of misfolded SOD1 in ALS patients (Spearman test, $r = 0.288$, $p = 0.123$) (**Figure 4D**). We instead found a strong correlation between misfolded SOD1 protein level and LMVs in slow progressing patients ($r = 0.545$, $p = 0.033$) ($n = 12$) (**Figure 4E**). No statistically significant difference was found in fast progressing patients ($r = -0.371$, $p = 0.234$) ($n = 6$). We also found no correlation between LMVs and p-TDP-43 ($r = -0.371$, $p = 0.146$) (**Figure 4F**).

DISCUSSION

Microvesicles are important mediators of cross-talk among cells and are emerging as new biomarkers of neurological diseases. In this study, for the first time, we have identified an over-representation of the blood CD45+ MVs (LMVs) component in ALS patients compared to healthy controls and to AD patients. Adding to previous observations of an enrichment of CD45+ MVs in CSF from ALS patients (Zachau et al., 2012), we are hinting at LMVs as readout of innate immune response activation at a systemic level in ALS patients. This observation is relevant considering the central role that MVs occupy in any endeavor to develop biomarkers of neurodegeneration.

The LMVs may originate from neutrophils, monocytes or macrophages, lymphocytes, and can also derive from T-cells activation (Zachau et al., 2012). T-regulatory lymphocytes (Tregs) are important immunomodulatory cells that regulate the balance between activation and suppression of the immune response and control microglia activation in the central nervous system. The involvement of T-cells in ALS is supported by a host of experimental data. Treg levels in peripheral blood of ALS patients are inversely correlated with disease severity (Henkel et al., 2013) and it has been shown that rapid disease progression in ALS is associated with a higher number of differentially expressed genes in monocytes (Zhao et al., 2017).

We have found that LMVs blood expression variably correlate to PRL in ALS individuals. LMVs peripheral expression is positively linked to a slower disease progression, but not with fast disease progression. This might depend on the reported Tregs (suppressor T cells) regulation, which modulate the immune system in slowly progressing patients (Henkel et al., 2013; Murdock et al., 2016).

In ALS, extracellular vesicles have been implicated in the release and uptake of misfolded proteins mainly *in vitro* cell culture (Gomes et al., 2007; Nonaka et al., 2013; Grad et al., 2014; Iguchi et al., 2016; Pinto et al., 2017). SOD1 misfolding has been reported in all ALS sub-types, including the non-SOD1-linked familial and sporadic cases (Shibata et al., 1994) and several studies propose that misfolded protein can be both secreted and taken up by the extracellular environment through exosomes (Gomes et al., 2007; Nonaka et al., 2013; Grad et al., 2014; Iguchi et al., 2016; Pinto et al., 2017).

CD45 can bind to heparan sulfate proteoglycans (Altin and Sloan, 1997), which have been shown to be involved in aggregate uptake of prion proteins (Coombe et al., 1994; Holmes et al., 2013), and therefore, this family of receptors can be involved in the propagation of misfolded SOD1 (Gomes et al., 2007; Grad et al., 2014). In this study, we show that LMVs (CD45+ MVs) selectively transport misfolded SOD1 (but not TDP-43) and that there is a strong correlation between misfolded SOD1 protein levels in LMVs mainly in slow progressing ALS patients. This finding may suggest that slow progression may be linked to the removal of potentially toxic proteins in MVs from the blood stream. Hence LMVs may have a neuroprotective role acting as physiological scavengers of misfolded SOD1 in slow progressing ALS patients as much as in healthy controls.

We have also found p-TDP-43 in LMVs from patients, but not specifically in LMVs. Pathological TDP-43 is hyper-phosphorylated and abnormally cleaved to generate aggregation-prone C-terminal fragments (CTFs) and it can propagate from cell to cell as p-TDP-43 aggregates (Lagier-Tourenne et al., 2010). However, in our study levels of LMVs were not correlated to TDP-43, in line with previous reports. TDP-43 has been previously reported in secreted exosomes from Neuro2a cells and primary neurons, but not in exosomes produced by CD45 positive astrocytes or microglia (Iguchi et al., 2016). Our data suggest that the regulation of LMVs formation may be key to the immune response to neurodegeneration, exerting a neuroprotective effect by SOD1 misfolded protein removal, impacting on speed of disease progression. These findings might open new avenues for biomarkers discovery and strategies for therapeutics, which enhance aggregated protein clearance.

ETHICS STATEMENT

The study protocol was approved by the Ethical Committee of the IRCCS Mondino Foundation (Pavia, Italy). Subjects participating in the study signed an informed consent (Protocol n°375/04 – version 07/01/2004). The study conformed the standards of the Declaration of Helsinki.

AUTHOR CONTRIBUTIONS

DS executed the experiments, designed the study, acquired and analyzed the data, drafted the manuscript, and created the figures. SLS executed the experiments, and acquired and analyzed the data. FC and LL executed the flow cytometry experiments, and acquired and analyzed the data. SZ performed the machine learning analysis and statistical analysis. OP acquired and analyzed the data. LD and MC recruited the ALS patients and analyzed the data. AC recruited the AD patients and analyzed the data. LL, SG, and EL analyzed the data. MG acquired the data. MM and AM analyzed the data and drafted the manuscript. CC conceived and designed the study, analyzed the data, and drafted the manuscript.

FUNDING

This work was supported by Italian Ministry of Health (Grant No. RC2017-2019). AriSLA Foundation for funding (Granulopathy-VCP and autophagolysosomal pathway: guardians of proteostasis and stress granule dynamics. Unraveling their implication in ALS); Fondazione Regionale per la Ricerca Biomedica for TRANS–ALS (Translating Molecular Mechanisms into ALS risk and patient's well-being: FRRB 2015-0023); European Union's Horizon 2020 Research and Innovation Program under grant agreement N° 643417 (Grant ID: 01ED1601A, CureALS).

ACKNOWLEDGMENTS

We thank Prof. Neil R. Cashman for the gift of the antibody DSE2-3H1. We also thank patients and families for contributing to this study.

SUPPLEMENTARY MATERIAL

The Supplementary Material for this article can be found online at: https://www.frontiersin.org/articles/10.3389/fnins.2019.00344/full#supplementary-material

FIGURE S1 | Microvesicles isolation. **(A)** Representative image of MVs (2 MVs of about 150 nm) from plasma obtained by transmission electron microscopy (TEM) (Scale bar: 100 nm); **(B)** Nanoparticle distribution by NTA confirmed the purity of MVs (mode = 137.8 +/− 6.0 nm) **(C)** Western Blot of MVs and EXOs markers in MVs and EXOs samples showed the presence of Annexin V in MVs lysate and Alix in EXOs lysate.

FIGURE S2 | Western blot analysis of co-immunoprecipitation of $CD45^+$ MVs with misfolded SOD1 and TDP-43 of **Figure 3A**. Immunoblots of MVs (input), immunoprecipitated CD45+ MVs (Bound) and of CD45- MVs (Unbound) from plasma of an healthy donor (CTRL1-lane 1, 4, 7) and two ALS patients (ALS 1-lane 2, 5, 8) and ALS 2-lane 3, 6, 9) with rabbit anti CD45 antibody **(A)**, misfolded SOD1 -3H1 **(B)**, TDP-43 **(C)**. Black squares show the cropping locations.

FIGURE S3 | Leukocyte derived MVs are enriched in ALS patients with a different trend from endothelial, platelet and erythrocyte derived MVs. The histogram represents the enrichment of CD45, CD31, CD61, and CD235a MVs in four representative ALS patients and CTRLs **(A)**. Flow cytometry dot plots of MVs isolated from plasma of a representative ALS patient labelled with CD45 and CD235a **(B)** and CD61 and CD31**(C)**.

REFERENCES

Al-Chalabi, A., and Hardiman, O. (2013). The epidemiology of ALS: a conspiracy of genes, environmental and time. *Nat. Rev. Neurol.* 9, 617–628. doi: 10.1038/nrneurol.2013.203

Al-Chalabi, A., Hardiman, O., Kiernan, M. C., Chiò, A., Rix-Brooks, B., and van den Berg, L. H. (2016). Amyotrophic lateral sclerosis: moving towards a new classification system. *Lancet Neurol.* 15, 1182–1194. doi: 10.1016/S1474-4422(16)30199-5

Altin, J. G., and Sloan, E. K. (1997). The role of CD45 and CD45-associated molecules in T cell activation. *Immunol. Cell Biol.* 75, 430–445. doi: 10.1038/icb.1997.68

Amor, S., Peferoen, L. A., Vogel, D. Y., Breur, M., van der Valk, P, Baker, D., et al. (2014). Inflammation in neurodegenerative diseases-an update. *Immunology* 142, 151–166. doi: 10.1111/imm.12233

Beers, D. R., Henkel, J. S., Zhao, W., Wang, J., and Appel, S. H. (2008). CD4+ T cells support glial neuroprotection, slow disease progression, and modify glial morphology in an animal model of inherited ALS. *Proc. Natl. Acad. Sci. U.S.A.* 105, 15558–15563. doi: 10.1073/pnas.0807419105

Brooks, B. R., Miller, R. G., Swash, M., and Munsat, T. L. (2000). World federation of neurology research group on motor neuron diseases. el escorial revisited: revised criteria for the diagnosis of amyotrophic lateral sclerosis. *Amyotroph. Lateral Scler. Other Motor Neuron Disord.* 1, 293–299. doi: 10.1080/146608200300079536

Calvo, A., Moglia, C., Lunetta, C., Marinou, K., Ticozzi, N., Ferrante, G. D., et al. (2017). Factors predicting survival in ALS: a multicenterItalian study. *J. Neurol.* 264, 54–63. doi: 10.1007/s00415-016-8313-y

Carandini, T., Colombo, F., Finardi, A., Casella, G., Garzetti, L., Verderio, C., et al. (2015). Microvesicles: what is the role in multiple sclerosis? *Front. Neurol.* 6:111. doi: 10.3389/fneur.2015.00111

Cereda, C., Baiocchi, C., Bongioanni, P., Cova, E., Guareschi, S., Metelli, M. R., et al. (2008). TNF and sTNFR1/2 plasma levels in ALS patients. *J. Neuroimmunol.* 194, 123–131. doi: 10.1016/j.jneuroim.2007.10.028

Cereda, C., Leoni, E., Milani, P., Pansarasa, O., Mazzini, G., Guareschi, S., et al. (2013). Altered intracellular localization of sod1 in leukocytes from patients with sporadic amyotrophic lateral sclerosis. *PLoS One* 8:e75916. doi: 10.1371/journal.pone.0075916

Cocucci, E., and Meldolesi, J. (2015). Ectosomes and exosomes: shedding the confusion between extracellular vesicles. *Trends Cell Biol.* 25, 364–372. doi: 10.1016/j.tcb.2015.01.004

Cook, N. R. (2008). Statistical evaluation of prognostic versus diagnosticmodels: beyond the ROC curve. *Clin. Chem.* 54, 17–23. doi: 10.1373/clinchem.2007.096529

Coombe, D. R., Watt, S. M., and Parish, C. R. (1994). Mac-1 CD11b/CD18 and CD45 mediate the adhesion of hematopoietic progenitor cells to stromal cell elements via recognition of stromal heparin sulfate. *Blood* 84, 739–752.

Demsar, J., Curk, T., Erjavec, A., Gorup, C., Hocevar, T., Milutinovic, M., et al. (2013). Orange: data mining toolbox in python. *J. Mach. Learn. Res.* 14, 2349–2353.

Feneberg, E., Steinacker, P., Lehnert, S., Schneider, A., Walther, P., Thal, D. R., et al. (2014). Limited role of free TDP-43 as a diagnostic tool in neurodegenerative diseases. *Amyotroph. Lateral Scler. Frontotemporal. Degener.* 15, 351–356. doi: 10.3109/21678421.2014.905606

Gomes, C., Keller, S., Altevogt, P., and Costa, J. (2007). Evidence for secretion of Cu, Zn superoxide dismutase via exosomes from a cell model of amyotrophic lateral sclerosis. *Neurosci. Lett.* 428, 43–46. doi: 10.1016/j.neulet.2007.09.024

Grad, L. I., Yerbury, J. J., Turner, B. J., Guest, W. C., Pokrishevsky, E., O'Neill, M. A., et al. (2014). Intercellular propagated misfolding of wild-type Cu/Zn superoxide dismutase occurs via exosome-dependent and independent

mechanisms. *Proc. Natl. Acad. Sci. U.S.A.* 111, 3620–3625. doi: 10.1073/pnas.1312245111

Hanspal, M. A., Dobson, C. M., Yerbury, J. J., and Kumita, J. R. (2017). The relevance of contact-independent cell-to-cell transfer of TDP-43 and SOD1 in amyotrophic lateral sclerosis. *Biochim. Biophys. Acta Mol. Basis Dis.* 1863, 2762–2771. doi: 10.1016/j.bbadis.2017.07.007

Henkel, J. S., Beers, D. R., Wen, S., Rivera, A. L., Toennis, K. M., Appel, J. E., et al. (2013). Regulatory T-lymphocytes mediate amyotrophic lateral sclerosis progression and survival. *EMBO Mol. Med.* 5, 64–79. doi: 10.1002/emmm.201201544

Henkel, J. S., Engelhardt, J. I., Siklós, L., Simpson, E. P., Kim, S. H., Pan, T., et al. (2004). Presence of dendritic cells, MCP-1, and activated microglia/macrophages in amyotrophic lateral sclerosis spinal cord tissue. *Ann. Neurol.* 55, 221–235. doi: 10.1002/ana.10805

Holmes, B. B., DeVos, S. L., Kfoury, N., Li, M., Jacks, R., Yanamandra, K., et al. (2013). Heparan sulfate proteoglycans mediate internalization and propagation of specific proteopathic seeds. *Proc. Natl. Acad. Sci. U.S.A.* 110, E3138–E3147. doi: 10.1073/pnas.1301440110

Iguchi, Y., Eid, L., Parent, M., Soucy, G., Bareil, C., and Riku, Y. (2016). Exosome secretion is a keypathway for clearance of pathological TDP-43. *Brain* 139, 3187–3201. doi: 10.1093/brain/aww237

Lagier-Tourenne, C., Polymenidou, M., and Cleveland, D. W. (2010). TDP-43 and FUS/TLS: emerging roles in RNA processing and neurodegeneration. *Hum. Mol. Genet.* 19, R46–R64. doi: 10.1093/hmg/ddq137

Lötvall, J., Hill, A. F., Hochberg, F., Buzás, E. I., Di Vizio, D., and Gardiner, C. (2014). Minimal experimental requirements for definition of extracellular vesicles and their functions: a position statement from the international society for extracellular vesicles. *J. Extracell. Vesicles* 3:26913. doi: 10.3402/jev.v3.26913

Lu, C. H., Macdonald-Wallis, C., Gray, E., Pearce, N., Petzold, A., Norgren, N., et al. (2015). Neurofilament light chain: a prognostic biomarker in amyotrophic lateral sclerosis. *Neurology* 84, 2247–2257. doi: 10.1212/WNL.0000000000001642

McKhann, G. M., Knopman, D. S., Chertkow, H., Hyman, B. T., Jack, C. R. Jr., Kawas, C. H., et al. (2011). The diagnosis of dementia due to Alzheimer's disease: recommendations from the national institute on aging-alzheimer's association work groups on diagnostic guidelines for alzheimer's disease. *Alzheimers Dement.* 7, 263–269. doi: 10.1016/j.jalz.2011.03.005

Murdock, B. J., Bender, D. E., Kashlan, S. R., Figueroa-Romero, C., Backus, C., Callaghan, B. C., et al. (2016). Increased ratio of circulating neutrophils to monocytes in amyotrophic lateral sclerosis. *Neurol. Neuroimmunol. Neuroinflamm.* 3:e242. doi: 10.1212/NXI.0000000000000242

Nielsen, M. H., Beck-Nielsen, H., Andersen, M. N., and Handberg, A. (2014). A flow cytometric method for characterization of circulating cell-derived microparticles in plasma. *J. Extracell. Vesicles* 3:3402. doi: 10.3402/jev.v3.20795

Nonaka, T., Masuda-Suzukake, M., Arai, T., Hasegawa, Y., Akatsu, H., Obi, T., et al. (2013). Prion-like properties of pathological TDP-43 aggregates from diseased brains. *Cell Rep.* 4, 124–134. doi: 10.1016/j.celrep.2013.06.007

Peng, C. Y. J., Kuk, L. L., and Ingersoll, G. M. (2002). An introduction to logistic regression analysis and reporting. *J. Educ. Res.* 96, 3–14. doi: 10.1080/00220670209598786

Pinto, S., Cunha, C., Barbosa, M., Vaz, A. R., and Brites, D. (2017). Exosomes from NSC-34 cells transfected with hSOD1-G93A are enriched in miR-124 and drive alterations in microglia phenotype. *Front. Neurosci.* 11:273. doi: 10.3389/fnins.2017.00273

Prada, I., and Meldolesi, J. (2016). Binding and fusion of extracellular vesicles to the plasma membrane of their cell targets. *Int. J. Mol. Sci.* 17:1296. doi: 10.3390/ijms17081296

Raposo, G., and Stoorvogel, W. (2013). Extracellular vesicles: exosomes, microvesicles.and friends. *J. Cell Biol.* 200, 373–383. doi: 10.1083/jcb.201211138

Robert, S., Poncelet, P., Lacroix, R., Arnaud, L., Giraudo, L., Hauchard, A., et al. (2009). Standardization of platelet-derived microparticle counting using calibrated beads and a cytomics FC500 routine flow cytometer: a first step towards multicenter studies? *J. Thromb. Haemost.* 7, 190–197. doi: 10.1111/j.1538-7836.2008.03200.x

Shibata, N., Hirano, A., Kobayashi, M., Sasaki, S., Kato, T., Matsumoto, S., et al. (1994). Cu/Zn superoxide dismutase-like immunoreactivity in Lewy body-like inclusions of sporadic amyotrophic lateral sclerosis. *Neurosci. Lett.* 179, 149–152. doi: 10.1016/0304-3940(94)90956-3

Sproviero, D., La Salvia, S., Giannini, M., Crippa, V., Gagliardi, S., Bernuzzi, S., et al. (2018). Pathological proteins are transported by extracellular vesicles of sporadic amyotrophic lateral sclerosis patients. *Front. Neurosci.* 12:487. doi: 10.3389/fnins.2018.00487

Steinacker, P., Hendrich, C., Sperfeld, A. D., Jesse, S., von Arnim, C. A., Lehnert, S., et al. (2008). TDP-43 incerebro-spinal fluid of patients with frontotemporal lobar degeneration and amyotrophic lateral sclerosis. *Arch. Neurol.* 65, 1481–1487. doi: 10.1001/archneur.65.11.1481

Swarup, V., Phaneuf, D., Dupré, N., Petri, S., Strong, M., Kriz, J., et al. (2011). Deregulation of TDP-43 in amyotrophic lateral sclerosis triggers nuclear factor κB–mediated pathogenic pathways. *J. Exp. Med.* 208, 2429–2447. doi: 10.1084/jem.20111313

Yáñez-Mó, M., Siljander, P. R., Andreu, Z., Zavec, A. B., Borràs, F. E., Buzas, E. I., et al. (2015). Biological properties of extracellular vesicles and their physiological functions. *J. Extracell. Vesicles* 4:27066. doi: 10.3402/jev.v4.27066

Zachau, A. C., Wallén, H., and Wetterberg, L. (2012). Leukocyte-derivedmicroparticles and scanning electron microscopicstructures in twofractions of freshcerebrospinalfluid in amyotrophic lateral sclerosis: a case report. *J. Med. Case Rep.* 6:274. doi: 10.1186/1752-1947-6-274

Zhao, W., Beers, D. R., Hooten, K. G., Sieglaff, D. H., Zhang, A., Kalyana-Sundaram, S., et al. (2017). Characterization of gene expression phenotype in amyotrophic lateral sclerosis monocytes. *JAMA Neurol.* 74, 677–685. doi: 10.1001/jamaneurol.2017.0357

Conflict of Interest Statement: LL is an employee of Becton Dickinson Italia S.p.A, which provided the antibodies used in this study.

The remaining authors declare that the research was conducted in the absence of any commercial or financial relationships that could be construed as a potential conflict of interest.

frontiers in Neuroscience

ORIGINAL RESEARCH
published: 18 April 2019
doi: 10.3389/fnins.2019.00361

Co-cultures of Glioma Stem Cells and Primary Neurons, Astrocytes, Microglia, and Endothelial Cells for Investigation of Intercellular Communication in the Brain

*Zhiyun Wei, Shubham Kale, Rachid El Fatimy, Rosalia Rabinovsky and Anna M. Krichevsky**

Department of Neurology, Brigham and Women's Hospital, Harvard Medical School, Boston, MA, United States

Intercellular communication within complex biological and pathological systems via extracellular vesicles (EVs) and secreted factors is a highly attractive area of research. However, cell models enabling investigation of such communication *in vitro* are limited. Commonly utilized is the supplementation of hyper-concentrated EVs or other extracellular factors to the recipient cell cultures. This approach requires purification of the secreted complexes and is confounded by the contamination of media components. Two-chamber co-cultures of donor and recipient cells separated by a pore membrane may represent a more physiological and better-controlled system for the investigation of intercellular communication. Yet, distinct culture conditions for different neural cell types often make them incompatible for co-culturing. Here we optimized short-term co-cultures of patient-derived low-passage glioma-initiating stem cells with normal cells of the brain microenvironment, such as primary neurons, astrocytes, microglia, and brain endothelial cells. We demonstrate the culture compatibility of these cell types and internalization of glioma-derived extracellular RNA by the normal recipient cells. The presented protocols are valuable for the investigation of intercellular communication between glioma brain tumor and cells of its microenvironment, including but not limited to the EVs-mediated communication.

RESEARCH IN CONTEXT

Cell-to-cell communication is essential in normal physiology and implicated in disease; however, experimental systems for its modeling *in vitro* are limited. Particularly, the investigation of communication between brain tumors and normal cells of the brain microenvironment has been challenged by the lack of adequate culture models. Here we developed co-cultures of glioma stem cells with various types of normal brain cells, including primary neurons, astrocytes, microglia, and brain endothelial cells, and demonstrated their utility for the study of intercellular communication. Detection of proposed markers in the recipient cells confirmed RNA transfer in these co-cultures.

Keywords: intercellular communication, extracellular vesicles, glioma stem cells, neurons, microglia, astrocytes

OPEN ACCESS

Edited by:
Francesc Xavier Guix, Severo Ochoa Molecular Biology Center (CSIC-UAM), Spain

Reviewed by:
Yu Fujita, The Jikei University School of Medicine, Japan
Rong Xu, La Trobe University, Australia

***Correspondence:**
Anna M. Krichevsky
akrichevsky@bwh.harvard.edu

Specialty section:
This article was submitted to Neurodegeneration, a section of the journal Frontiers in Neuroscience

Received: *17 December 2018*
Accepted: *29 March 2019*
Published: *18 April 2019*

Citation:
Wei Z, Kale S, El Fatimy R, Rabinovsky R and Krichevsky AM (2019) Co-cultures of Glioma Stem Cells and Primary Neurons, Astrocytes, Microglia, and Endothelial Cells for Investigation of Intercellular Communication in the Brain. Front. Neurosci. 13:361. doi: 10.3389/fnins.2019.00361

HIGHLIGHTS

- Culture conditions were optimized for co-culturing glioma stem cells with various types of primary normal brain cells.
- RNA transfer between donor and recipient cells was confirmed in the co-cultures.

INTRODUCTION

Intercellular communication is critical for all biological and pathological processes. Established secreted mediators of such communication include hormones, neurotransmitters, growth factors, cytokines, chemokines, and neurotrophins. More recently, additional routes of transmission, such as those mediated by extracellular vesicles (EVs) (Valadi et al., 2007; Skog et al., 2008) and extravesicular ribonucleoproteins (RNPs) (Vickers et al., 2011) carrying RNA, proteins, lipids and other cargo molecules, have also been extensively explored.

Investigation of these modes of communication is an especially active area of research in the field of cancer biology, as they are thought to contribute to the invasion, metastasis, angiogenesis, chemo-resistance, and immune tolerance of many malignancies (Hanahan and Weinberg, 2011). Among these malignancies is glioblastoma (GBM), the most common and invasive primary brain tumor that affects both adult and pediatric patients. The median survival of GBM patients is only about 14–15 months, despite aggressive treatments that include tumor resection followed by radiotherapy and chemotherapy. Investigation of the tumor cross-talk with other cells of the brain microenvironment may provide new avenues for the development of targeted therapeutic applications (reviewed by Broekman et al., 2018).

The most common approaches for the investigation of the intercellular communication rely on either a single-pulse or repeated supplementation of the purified and concentrated "agent" (e.g., EVs) to the recipient cells. However, such a strategy does not consider the local physiological concentration and the dynamics of release and uptake of the investigated factors. Another way of studying intercellular communication employs co-cultures of donor and recipient cells in common culture conditions, with a membrane separating the two cell types. Comparing to the previous strategy, co-culture experiments may better model the complex and persistent communication between the cells, physiological release-uptake dynamics, and enable assessment of multiple mediators of communication between the donor and recipient cultures. Such experimental design has been utilized in many studies, including those reporting miRNA transfer from cardiac fibroblast to cardiomyocytes (Bang et al., 2014) and between dendritic cells (Alexander et al., 2105), ncRNA transfer from cardiosphere-derived cells to macrophages (Cambier et al., 2107), mRNA transfer from acute myelogenous leukemia to stromal niche (Huan et al., 2103), DNA transfer between parasites (Regev-Rudzki et al., 2013), protein transfer from mesenchymal stromal cells to haematopoietic cells (Bauer et al., 2011), and virus transfer from infected hepatoma cells to plasmacytoid dendritic cells (Feng et al., 2014). In these cases, both donor and recipient cells share the same, or similar, routine culturing condition and require no additional optimization for co-culturing. However, the studies of intercellular communication in the brain and brain tumors are largely hampered by the difficulty in co-culturing glioma with primary neuroglial cells, as they have distinct culture conditions.

Here we screened multiple conditions and developed novel protocols for co-culturing patient-derived glioma-initiating stem cells (GSC), a key population of GBM cells that is considered most resistant to chemo- and radiotherapies and largely responsible for tumor recurrence, with primary neuronal, glial, and endothelial cells of the brain. We provide two new species-specific ncRNA markers to demonstrate extracellular RNA (exRNA) transfer from GSC to the normal cells. The established cell systems may provide a simple and physiologically relevant model for studying the bidirectional communication in malignant gliomas.

MATERIALS AND METHODS

Human GSC Cultures

Low passage GBM8 cells have been cultured as neurospheres in Neurobasal medium (Gibco) supplemented with 3 mM GlutaMAX (Gibco), 1× B-27 supplement (an optimized serum-free proprietary supplement commercially available from Gibco), 0.5× N-2 supplement (a chemically defined, serum-free supplement from Gibco; components include transferrin, insulin, progesterone, putrescine and selenite), 0.5% Antibiotic-Antimycotic Solution (Corning), 20 ng/mL EGF (R&D Systems, MN, United States), and 20 ng/mL FGF (PeproTech, NJ, United States). Mature neurospheres were dissociated using NeuroCult Chemical Dissociation Kit (Mouse) (Stemcell Technologies, Canada). Approximately 0.5×10^6 cells were seeded in 10 mL fresh media in a 10 cm dish (Corning), and 1/3 volume of fresh medium was added every 3 days. Mature neurospheres were usually formed within 7∼10 days.

Primary Neuron Cultures

Brain cortical tissues of E18 C57BL/6 mice were dissected, dissociated with papain (12 U/ml; Worthington) for 20 min at 37°C, and triturated to single cells using Pasteur pipettes. After dissociation, the cells were washed with DMEM-F12 (Corning) three times and pelleted at 300 *g* centrifugation. The cells were seeded on a poly-D-lysine (Sigma-Aldrich, MO, United States) coated 24-well plates, at 80,000 cells per cm^2. The seeding medium consisted of Neurobasal, 1× B-27, 1% Antibiotic-Antimycotic Solution (Corning), 0.5 mM GlutaMAX, and 2% FBS (Gibco). Next day, the seeding medium was replaced to the fresh culture medium with no FBS. After 5 days, the culture medium was supplemented with Ara-C (5 μM; Sigma-Aldrich) to deplete glial cells. Half

of the medium was replaced with the fresh culture medium twice a week.

Primary Glia Cultures

Brain cortical tissues of P1 C57BL/6 mice were cut to small pieces and dissociated with 0.25% Trypsin (Gibco) and 0.1 mg/mL DNase I (Roche) for 15 min at 37°C, with swirling every 3 min. After dissociation, the cells were washed with DMEM-F12 three times and pelleted at 300 *g* centrifugation. The cells collected from three pups were seeded in one T75 flask with culture medium consisted of DMEM-F12, 10% FBS, and 1% Antibiotic-Antimycotic Solution. The medium was changed to the fresh culture medium 3 days after seeding, and further replaced every 5–7 days. For astrocyte cultures, the flasks were shaken at 200 rpm at 37°C overnight three times to remove microglia, and then trypsinized and transferred to 24-well plates. For microglia cultures, the media was supplemented with a recombinant M-CSF mouse protein (10 ng/mL; Gibco). One week later, floating microglia were collected by pelleting the conditioned media at 300 g for 10 min, and then seeded on the poly-D-lysine coated 24-well plates, at 100,000 cells per cm^2 with fresh culture media.

Cultures of Brain Endothelial Cells

Mouse primary brain microvascular endothelial cells (MBEC) were purchased from Cell Biologics, IL, United States (Catalog# C57-6023; Lot# 070613T2MP) and cultured according to the manual, but with no heparin (as it interferes with EV uptake Atai et al., 2013; Christianson et al., 2013). Briefly, T25 flasks were pre-coated with Gelatin-based coating solution (Cell Biologics), 10^6 cells seeded in the Endothelial Cell Medium (Cell Biologics) and passaged 1:2 upon confluence. Low passages (1–4) have been used in this study.

Co-culture Conditions

The recipient normal cells of the brain were seeded in 24-well plates, as described above. One day later, small GBM8 neurospheres grown in GSC conditions were transferred to the upper chamber of the Millicell hanging insert with 1.0 μm pore size (Millipore). For co-cultures of GSCs with neurons, the optimized media consisted of Neurobasal, 1× B-27, 0.5× N-2 supplement, 0.5 mM GlutaMAX, and 1% Antibiotic-Antimycotic Solution. For co-cultures of GSCs with glia, the optimized media consisted of DMEM-F12, 1× B-27, 0.5× N-2 supplement, and 1% Antibiotic-Antimycotic Solution. For co-cultures of GSCs with endothelial cells, the optimized media consisted of Mouse Endothelial Cell Basal Medium (Cell Biologics), 1× B-27, 0.5× N-2, 0.1% VEGF, 0.1% ECGS, 0.1% EGF, 0.1% Hydrocortisone, 2 mM L-Glutamine and 1% Antibiotic-Antimycotic Solution.

Cell Imaging

Using the IN Cell Analyzer 2200 (GE Healthcare Life Sciences, PA, United States) the 24-well plates were automatically scanned with 81 photographs per well taken at days 3 and 6 of cell culturing in the experimental media. The representative images of neurospheres were adjusted by auto-contrast, and for adherent monolayer cultures, additionally, by Scott 5 HDR preset of the Photoshop (Adobe, CA, United States). All images have been processed in parallel, using identical settings.

RNA Isolation and qRT-PCR

Total RNA was isolated by miRCURY RNA Isolation Kit – Cell & Plant (Exiqon, Denmark), with on-column DNase treatment (Qiagen, Germany), after 3 days of co-culture. RNA quality was examined using Agilent 2100 Bioanalyzer (Agilent, CA, United States). qRT-PCR reactions were performed using miRCURY system (Exiqon) as previously reported (Wei et al., 2017) for small RNAs, and iScript system (Bio-Rad, CA, United States) for mRNAs, with the following DNA primers. Human RNY5 RNA (Christov et al., 2006): 5′-AGTTGGTCCGAGTGTTGTGG-3′ and 5′-AACAGCAAGCTAGTCAAGCG-3′; human RNU2-1 RNA: 5′-TTTGGAGCAGGGAGATG-3′ and 5′-CACCGTTCCTGGAGGTA-3′; mouse Actb: 5′-GGCACCACACCTTCTACAATG-3′ and 5′-GGTACGACCAGAGGCATACA-3′; mouse Gapdh: 5′-GAAGGTCGGTGTGAACGGATT-3′ and 5′-CGTGAGTGGAGTCATACTGGAAC-3′; mouse NeuN: 5′-GCACGGCATGACCCTCTACA-3′ and 5′-GTGGAGTTGCTGGTTGTCTGTC-3′; mouse Tuj1: 5′-CAGCGATGAGCACGGCATAGA-3′ and 5′-CCAGGTTCCAAGTCCACCAGAAT-3′; mouse Gfap: 5′-AACGACTATCGCCGCCAACTG-3′ and 5′-CGAGCAAGTGCCTCCTGGTAAC-3′; mouse Eaat1: 5′-TGCCTCTCCTCTACTTCCTG-3′ and 5′-CCACACCATTGTTCTCTTCCA-3′; mouse CD11b: 5′-AGCACCTCGGTATCAGCATATTG-3′ and 5′-GGTATTGCCATCAGCGTCCAT-3′; mouse Iba1: 5′-CAGACTGCCAGCCTAAGACA-3′ and 5′-GGATCATCGAGGAATTGCTTGT-3′; mouse CD31: 5′-TCCAACAGAGCCAGCAGTATGA-3′ and 5′-GCGATGACCACTCCAATGACAA-3′; mouse Cdh5: 5′-CCAGCGACACTTCTACCACTTC-3′ and 5′-CTGTCACTGGTCTTGCGGATG-3′. The U6 snRNA was quantified with LNA-containing primers (Exiqon) and used as the endogenous control for small RNAs.

Western Blot

Cell lysates containing equal amount of total proteins were separated by SDS-PAGE with 4–12% Blot Bis-Tris Plus Gels (Thermo Fisher Scientific), and transferred to 0.45 μm PVDF membrane (Thermo Fisher Scientific). After blocking with 5% (wt/vol) fat-free milk in Tris-buffered saline with 0.075% Tween-20 (TBST), the membranes were incubated overnight with diluted primary antibodies (Tuj-1: Abcam ab14545, 1:10000 dilution; GFAP: Sigma-Aldrich G9269, 1:7500 dilution; CD11b: Abcam ab133357, 1:2000 dilution; CD31: Cell Signaling Technology 3528S, 1:500 dilution; β-Actin: Abcam ab3280, 1:10000 dilution) at 4°C. The membranes were washed and incubated with horseradish peroxidase-conjugated secondary antibodies (Cell Signaling Technology 7074S and 7076S, 1:5000 dilution) for 1 h at room temperature. The blots were developed by the Amersham ECL Reagent (GE Healthcare).

RESULTS

GSCs Cultured in Alternative Conditions Change Their Morphology

For maintenance of the stem-cell-like properties, GSCs are typically cultured in a defined serum-free Neurobasal media, whereas primary astrocytes, microglia, and endothelial cells are cultured in distinct growth conditions, supplemented with FBS. Optimal growth conditions for GSCs and primary neurons are more similar, with the supplementation of N-2 and additional growth factors in GSC media, which suggest their better compatibility in the co-cultures.

To investigate whether GSCs can maintain their morphology in conditions used for culturing normal cells of the brain, we established small spheroids of GBM8 GSCs, and at day 3 after passaging, replaced the GSC growth medium with the media corresponding to either neuronal, glial, or endothelial cells, followed by the observation of GSC morphology over 6 days. As shown in **Figure 1A**, when cultured in the regular GSC medium, in 9 days GSCs grow into spheroids of variable sizes. Similar,

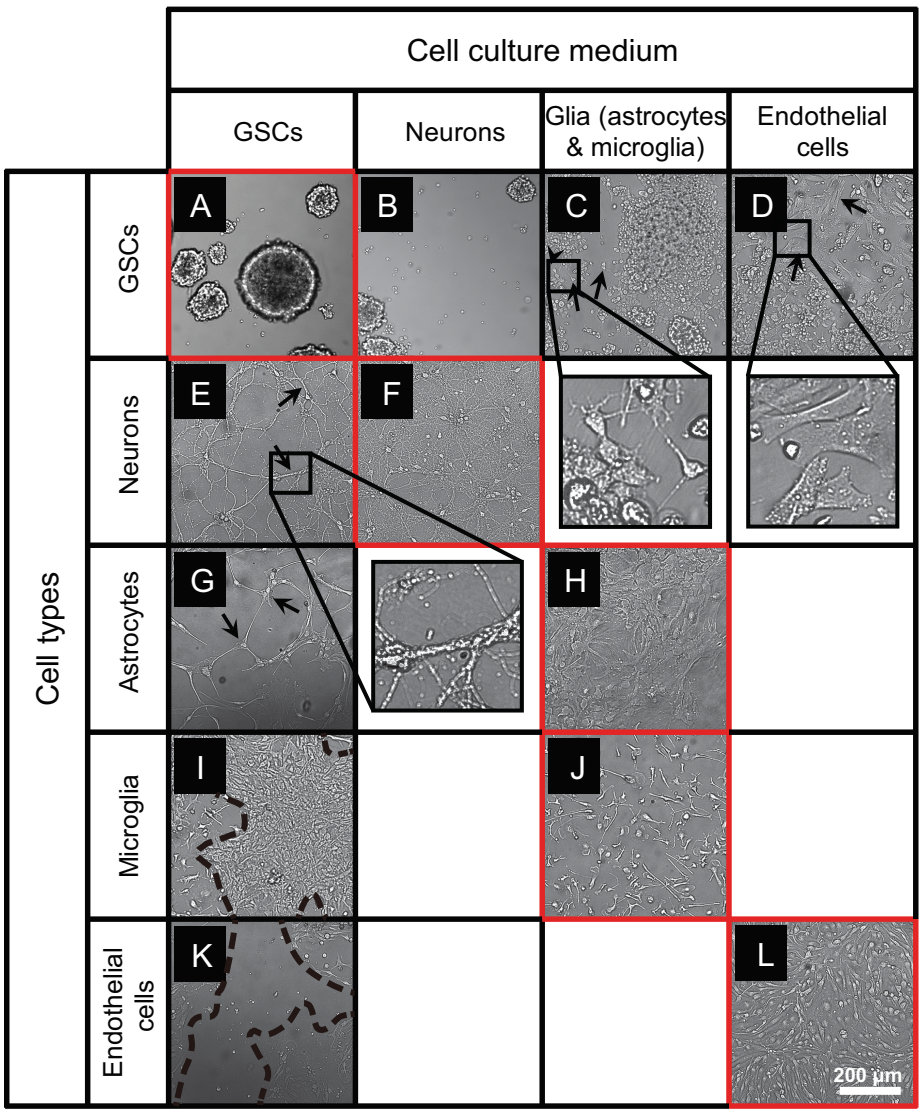

FIGURE 1 | Microscopy images of GSCs, primary neurons, astrocytes, microglia, and endothelial cells in various culture conditions. **(A–D)** Typical GBM8 spheroids cultured in GSC medium **(A)**, and their altered growth in neuron medium **(B)**, glia medium (**C**; alterations observed in 81 out of 81 images analyzed), and endothelial cell medium (**D**; observed in 81 out of 81 images analyzed). **(E,F)** Representative images of primary neurons cultured in regular medium **(F)** and their morphological changes in GSC medium (**E**; observed in 17 out of 81 images analyzed). **(G,H)** Representative images of primary astrocytes cultured in regular medium **(H)** and their morphological changes in GSC medium (**G**; observed in 5 out of 81 images). **(I,J)** Representative images of primary microglia cultured in regular medium **(J)** and their morphological changes in GSC medium (**I**; observed in 30 out of 81 images). **(K,L)** Representative images of primary brain endothelial cells cultured in regular medium **(L)** and their morphological changes in GSC medium (**K**; observed in 78 out of 81 images). Typical morphological alterations are depicted by arrows, arrowhead, and dashed lines. Images were taken 6 days after medium change. *N* = at least two independent experiments/condition.

albeit smaller GSC spheroids are formed in the neuronal media lacking N-2 supplements (**Figure 1B**). However, as expected, when cultured in the FBS-containing media used for glial or endothelial cells, small gliomaspheres became adherent to the plate surface and exhibit altered morphology, indicative of their differentiation (**Figures 1C,D**). Most of the cells spread out of the initial spheres to form monolayer or multilayer colonies. In the glial medium that is essentially similar to the media used for GSC differentiation, GSCs developed multiple extended processes (arrows in **Figure 1C**) with frequent branching (arrowhead in **Figure 1C**), resembling the premature primary astrocytes (observed in 81 out of 81 images analyzed). In the endothelial medium, GSCs exhibit fibroblastic morphology with bipolar or multipolar elongated shapes (arrows in **Figure 1D**; observed in 81 out of 81 images analyzed).

Primary Brain Cells Change Their Morphology When Cultured in GSC Media

To examine the compatibility of primary neurons, astrocytes, microglia, and endothelial cells with GSC medium, we established individual cultures of these cells using their optimal growth conditions, then replaced the media with the GSC medium, and observed their growth over 6 days. Primary neuronal cultures grown in the GSC media at DIV10 to 16 exhibited altered cell morphology and reduced complexity, with fewer and less branched processes (arrows in **Figure 1E**, compared to **Figure 1F**).

Primary astrocytes usually maintain their morphology and remain adherent and healthy for several months, as shown in **Figure 1H**. However, when the pre-established monolayer of astrocytes was exposed to the GSC medium, the cells dramatically changed their shape, become slender and more elongated, and the cultures lost their typical dense monolayer appearance (arrows in **Figure 1G**).

Microglia cultured in the established optimal conditions is firmly attached to the polylysine matrix, displays a typical ramified morphology, and remains quiescent (**Figure 1J**). However, when cultured in the GSC media, microglia became activated and proliferative, giving rise to large colonies (area surrounded by dashed lines in **Figure 1I**).

Finally, the cultures of primary brain endothelial cells (**Figure 1L**) exhibited significant cell death and quickly degenerated when grown in the GSC medium (**Figure 1K**). Taken together, these results indicate that the culture conditions utilized for GSCs and normal primary cells of the brain are incompatible and cannot be for co-culture experiments.

Optimization of Co-culture Conditions for GSC and Primary Normal Cells of the Brain

To optimize the GSC co-cultures with normal cells of the brain, for each pair of cell types we tested several media compositions based on their original recipes (**Supplementary Table S1**) and observed the cell growth and morphology over time. The co-culture conditions were optimized to enable the maintenance of the undifferentiated neurosphere state by GSCs (**Figures 2A–C**) and preserve the original morphologies of the counterpart normal cells (**Figures 2D–G**) for at least 6 days. Loss of neuronal processes has been rarely observed in the optimized conditions (in only 4/81 images in the co-culture conditions, which is similar to 3/81 rate observed in normal neuronal cultures). Abnormal morphologies were not observed for astrocytes, microglia or endothelial cells in the optimized co-culture conditions. As expected, the B27 supplement was necessary to maintain the undifferentiated status of GSCs while FBS triggered their differentiation. Growth factors (EGF and FGF) appear to significantly alter the morphology of neurons and astrocytes and induce proliferation of microglia. They have been, therefore, omitted from the corresponding co-culture media. On the other hand, replacing FBS with B27 did not trigger significant morphological changes of primary glial and endothelial cells. Glutamine supplementation had significant effects on GSC and neurons (with low concentrations being toxic to the former and high concentrations to the latter) and, thus, had to be balanced for their co-cultures. N2 supplementation did not have major effects on the co-cultures. Furthermore, mRNA and protein levels of the representative markers for each recipient cell type have not changed under the corresponding co-culture conditions (**Figure 3**). Final compositions of the media supporting the co-cultures of GSCs with normal neurons, astrocytes, microglia, and brain endothelial cells are described in the Section "Materials and Methods."

Validation of Intercellular RNA Transfer in Co-cultures

To validate a cross-talk between GSC and normal cells in the optimized co-culture conditions, human GSCs were co-cultured with various types of primary mouse brain cells, including neurons, astrocytes, microglia and endothelial cells, and the transfer of GSC-derived exRNA to the normal cells was assessed. The RNA was isolated from the recipient normal mouse cells after 3 days of co-culturing, and the levels of specific RNA markers in these cells were examined. We tested the transfer of snRNA and Y RNA, two classes of ncRNA abundantly released by GSCs (Wei et al., 2017). While human-specific RNAs such as RNU2-1 snRNA and RNY5 were undetectable in the monocultures of mouse primary microglia, they were strongly elevated in the microglia co-cultured with human GBM8 neurospheres (**Figure 4**). Similar results were observed for the recipient primary cultures of neurons, astrocytes, and endothelial cells (**Figure 4**). These experiments confirmed RNA transfer from human GSCs to the mouse recipient cells in co-cultures and thus demonstrated the application of this protocols for investigation of the intercellular communication between GSCs and normal cells of glioma microenvironment *in vitro*.

DISCUSSION

Although it is gaining increased attention in recent years, intercellular communication in the brain tumor microenvironment remains among the least investigated

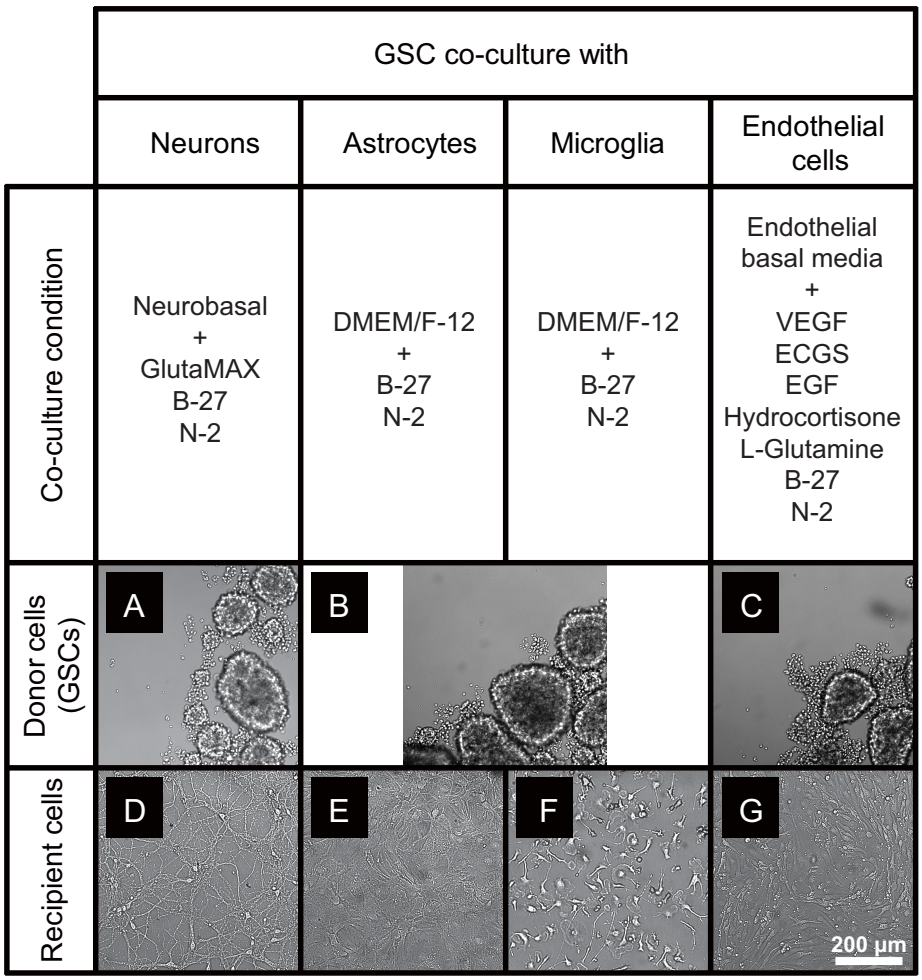

FIGURE 2 | GSC and normal cell types of the brain maintained in the optimized co-culture conditions for 6 days. **(A–C)** GBM8 spheroids in co-culture media optimized for neurons **(A)**, glia **(B)**, and endothelial cells **(C)**. **(D–G)** Representative images of primary neurons **(D)**, astrocytes **(E)**, microglia **(F)**, and brain endothelial cells **(G)** in the corresponding co-culture media. *N* = at least two independent experiments/condition.

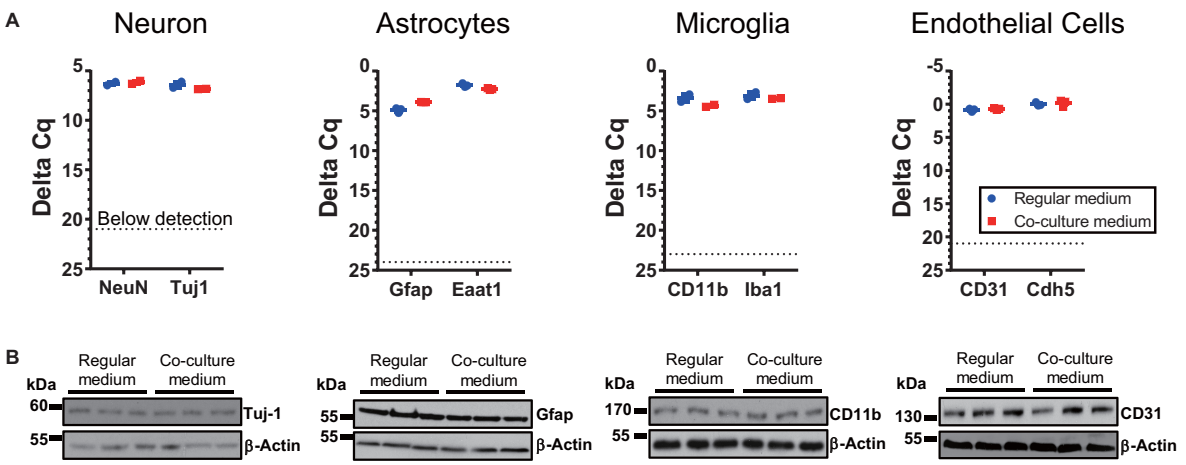

FIGURE 3 | Expression of cell-type specific markers for cells cultured under regular conditions and the optimized co-culture conditions. No significant difference was observed, based on RNA **(A)** and protein levels **(B)**. *N* = 3 wells per culture condition.

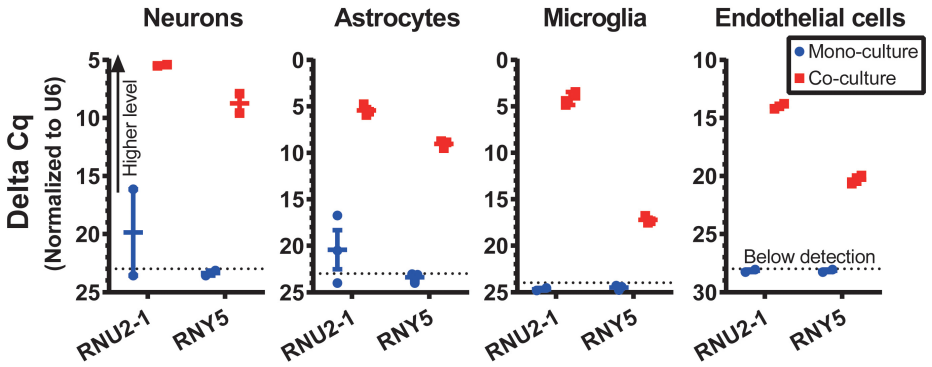

FIGURE 4 | RNA transfer from human GSCs to mouse primary neurons, astrocytes, microglia, and endothelial cells was assessed for human-specific transcripts by qRT-PCR. *N* = 3 wells per culture condition, after 3 days in co-culture.

topics in the pathology of malignant gliomas. The impact of the intercellular interactions occurring in the brain on the glioma initiation, growth, and therapy resistance has not been thoroughly elucidated. Previous studies mostly focused on the secreted molecules that mediate communication, such as hormones, growth factors, cytokines, and chemokines. EVs and extravesicular RNP complexes carrying heterogeneous cargo (e.g., proteins, nucleic acids, and lipids) have been proposed as additional potent and more complex communication vehicles. Notably, the *in vitro* modeling of such complex interactions underlying the growth of intracranial tumors remains one of the major impediments in the field.

Most studies of the intercellular communication *in vitro* rely on the pulse supplementation of an experimental factor derived from the donor cells to the recipient cells. While such traditional strategy is merited for specific molecular agents/mediators (e.g., cytokines), it can be suboptimal for more complex mediators, such as EVs. It is currently unclear how to dose and time this type of experiments so that they mimic the physiology and dynamics of EV/RNP release and uptake; therefore, it is common to simply apply a pulse of hyper-concentrated preparations of EVs to the recipient cells. In addition, since any fresh media contain active ingredients that may cause false-positive results, designing suitable controls for such experiments is challenging (Wei et al., 2016; Tosar et al., 2017). Co-culturing diverse cell types may provide the better, more physiological approach for studying the intercellular communication among them. However, the caveat, especially concerning the difficult-to-culture primary and low passage cells of the brain and brain tumors, is their poor compatibility in culture. The cells of the CNS such as neurons, astrocytes, microglia, and brain derived endothelial cells are highly sensitive and require specific, distinct conditions for their growth *in vitro*. Optimized protocols for co-culturing these cells with glioma will advance the investigation of intercellular communication between brain tumors and brain microenvironment, mediated by EVs and other means (Broekman et al., 2018).

Here we optimized conditions for co-culturing four major types of normal brain cells with glioma-initiating cells so that they could be maintained together and retain their normal phenotypes for at least 6 days. This time frame is generally sufficient for a diverse set of molecular and phenotypic assays. In addition to revealing the impact of a broad EV population or the entire secretome, specific EV subclasses varying by their sizes (e.g., oncosomes, microvesicles, and exosomes) can be studied in such two-chamber systems separated by the membranes with different pore sizes. For example, modification of the assay to employ the inserts with either 0.2 μm and 20 nm pores will assess the relative contributions of EVs and RNPs.

In this study, we also propose several human-specific RNA markers that provide positive controls for RNA transfer studies and can be utilized for the studies of exRNA secretion and uptake mechanism. While the focus of exRNA field remains largely on miRNAs due to their enrichment in EVs and important regulatory potential, other classes of regulatory transcripts are abundantly released by various types of cells (Wei et al., 2017; Chiou et al., 2018; Driedonks and Nolte-'t Hoen, 2018; Hinger et al., 2018; Rimer et al., 2108; Elsemuller et al., 2019). The copy numbers of some non-miRNA transcripts in the extracellular space are significantly higher than those of even the most abundant miRNAs (Wei et al., 2017). While the biological impact of their intercellular transfer is largely unknown, the presented protocols may aid the corresponding investigation. Here we demonstrated the transfer of two classes of highly abundant ncRNA, snRNA, and Y RNA, from glioma cells to the normal cells of the brain. Overall, the established protocols are valuable for the investigation of intercellular communication between glioma brain tumor and its microenvironment, including but not limited to the EVs-mediated communication.

ETHICS STATEMENT

All animal experiments have been approved by the Brigham and Women's Hospital Institutional Animal Care and Use Committee.

AUTHOR CONTRIBUTIONS

AK conceived the study. ZW and AK designed the experiments and wrote the manuscript. ZW, SK, and REF performed the experiments. RR assisted with experiments. All authors revised and approved the manuscript.

FUNDING

This work was supported by the U19 CA179563 grant and U19 administrative supplement through the NIH Common Fund and the Office of Strategic Coordination/Office of the NIH Director, R01 CA215072, and R21 NS098051 grants.

ACKNOWLEDGMENTS

We thank Ramil Arora for assisting with experiments and members of Krichevsky laboratory for helpful discussions.

SUPPLEMENTARY MATERIAL

The Supplementary Material for this article can be found online at: https://www.frontiersin.org/articles/10.3389/fnins.2019.00361/full#supplementary-material

TABLE S1 | Tested medium compositions and their effects on cell growth and morphology. Optimal medium compositions for co-cultures are highlighted in red. *N* = at least two independent experiments/condition.

REFERENCES

Alexander, M., Hu, R., Runtsch, M. C., Kagele, D. A., Mosbruger, T. L., Tolmachova, T., et al. (2105). Exosome-delivered microRNAs modulate the inflammatory response to endotoxin. *Nat. Commun.* 6:7321. doi: 10.1038/ncomms8321

Atai, N. A., Balaj, L., van Veen, H., Breakefield, X. O., Jarzyna, P. A., Van Noorden, C. J., et al. (2013). Heparin blocks transfer of extracellular vesicles between donor and recipient cells. *J. Neurooncol.* 115, 343–351. doi: 10.1007/s11060-013-1235-y

Bang, C., Batkai, S., Dangwal, S., Gupta, S. K., Foinquinos, A., Holzmann, A., et al. (2014). Cardiac fibroblast-derived microRNA passenger strand-enriched exosomes mediate cardiomyocyte hypertrophy. *J. Clin. Invest.* 124, 2136–2146. doi: 10.1172/JCI70577

Bauer, N., Wilsch-Brauninger, M., Karbanova, J., Fonseca, A. V., Strauss, D., Freund, D., et al. (2011). Haematopoietic stem cell differentiation promotes the release of prominin-1/CD133-containing membrane vesicles–a role of the endocytic-exocytic pathway. *EMBO Mol. Med.* 3, 398–409. doi: 10.1002/emmm.201100147

Broekman, M. L., Maas, S. L. N., Abels, E. R., Mempel, T. R., Krichevsky, A. M., and Breakefield, X. O. (2018). Multidimensional communication in the microenvirons of glioblastoma. *Nat. Rev. Neurol.* 14, 482–495. doi: 10.1038/s41582-018-0025-8

Cambier, L., de Couto, G., Ibrahim, A., Echavez, A. K., Valle, J., Liu, W., et al. (2107). Y RNA fragment in extracellular vesicles confers cardioprotection via modulation of IL-10 expression and secretion. *EMBO Mol. Med.* 9, 337–352. doi: 10.15252/emmm.201606924

Chiou, N. T., Kageyama, R., and Ansel, K. M. (2018). Selective export into extracellular vesicles and function of tRNA fragments during T cell activation. *Cell Rep.* 25, 3356–3370.e4. doi: 10.1016/j.celrep.2018.11.073

Christianson, H. C., Svensson, K. J., van Kuppevelt, T. H., Li, J. P., and Belting, M. (2013). Cancer cell exosomes depend on cell-surface heparan sulfate proteoglycans for their internalization and functional activity. *Proc. Natl. Acad. Sci. U.S.A.* 110, 17380–17385. doi: 10.1073/pnas.1304266110

Christov, C. P., Gardiner, T. J., Szuts, D., and Krude, T. (2006). Functional requirement of noncoding Y RNAs for human chromosomal DNA replication. *Mol. Cell. Biol.* 26, 6993–7004. doi: 10.1128/MCB.01060-06

Driedonks, T. A. P., and Nolte-'t Hoen, E. N. M. (2018). Circulating Y-RNAs in extracellular vesicles and ribonucleoprotein complexes; implications for the immune system. *Front. Immunol.* 9:3164. doi: 10.3389/fimmu.2018.03164

Elsemuller, A. K., Tomalla, V., Gartner, U., Troidl, K., Jeratsch, S., Graumann, J., et al. (2019). Characterization of mast cell-derived rRNA-containing microvesicles and their inflammatory impact on endothelial cells. *FASEB J.* 33, 5457–5467. doi: 10.1096/fj.201801853RR

Feng, Z., Li, Y., McKnight, K. L., Hensley, L., Lanford, R. E., Walker, C. M., et al. (2014). Human pDCs preferentially sense enveloped hepatitis A virions. *J. Clin. Invest.* 125, 169–176. doi: 10.1172/JCI77527

Hanahan, D., and Weinberg, R. A. (2011). Hallmarks of cancer: the next generation. *Cell* 144, 646–674. doi: 10.1016/j.cell.2011.02.013

Hinger, S. A., Cha, D. J., Franklin, J. L., Higginbotham, J. N., Dou, Y., Ping, J., et al. (2018). Diverse long RNAs are differentially sorted into extracellular vesicles secreted by colorectal cancer cells. *Cell Rep.* 25, 715–725.e4. doi: 10.1016/j.celrep.2018.09.054

Huan, J., Hornick, N. I., Shurtleff, M. J., Skinner, A. M., Goloviznina, N. A., Roberts, C. T. Jr., et al. (2103). RNA trafficking by acute myelogenous leukemia exosomes. *Cancer Res.* 73, 918–929. doi: 10.1158/0008-5472.CAN-12-2184

Regev-Rudzki, N., Wilson, D. W., Carvalho, T. G., Sisquella, X., Coleman, B. M., Rug, M., et al. (2013). Cell-cell communication between malaria-infected red blood cells via exosome-like vesicles. *Cell* 153, 1120–1133. doi: 10.1016/j.cell.2013.04.029

Rimer, J. M., Lee, J., Holley, C. L., Crowder, R. J., Chen, D. L., Hanson, P. I., et al. (2108). Long-range function of secreted small nucleolar RNAs that direct 2'-O-methylation. *J. Biol. Chem.* 293, 13284–13296. doi: 10.1074/jbc.RA118.003410

Skog, J., Würdinger, T., van Rijn, S., Meijer, D. H., Gainche, L., Sena-Esteves, M., (2008). Glioblastoma microvesicles transport RNA and proteins that promote tumour growth and provide diagnostic biomarkers. *Nat. Cell Biol.* 10, 1470–1476. doi: 10.1038/ncb1800

Tosar, J. P., Cayota, A., Eitan, E., Halushka, M. K., and Witwer, K. W. (2017). Ribonucleic artefacts: are some extracellular RNA discoveries driven by cell culture medium components? *J. Extracell. Vesicles* 6:1272832. doi: 10.1080/20013078.2016.1272832

Valadi, H., Ekstrom, K., Bossios, A., Sjostrand, M., Lee, J. J., and Lotvall, J. O. (2007). Exosome-mediated transfer of mRNAs and microRNAs is a novel mechanism of genetic exchange between cells. *Nat. Cell Biol.* 9, 654–659. doi: 10.1038/ncb1596

Vickers, K. C., Palmisano, B. T., Shoucri, B. M., Shamburek, R. D., and Remaley, A. T. (2011). MicroRNAs are transported in plasma and delivered to recipient cells by high-density lipoproteins. *Nat. Cell Biol.* 13, 423–433. doi: 10.1038/ncb2210

Wei, Z., Batagov, A. O., Carter, D. R., and Krichevsky, A. M. (2016). Fetal bovine serum RNA interferes with the cell culture derived extracellular RNA. *Sci. Rep.* 6:31175. doi: 10.1038/srep31175

Wei, Z., Batagov, A. O., Schinelli, S., Wang, J., Wang, Y., El Fatimy, R., et al. (2017). Coding and noncoding landscape of extracellular RNA released by human glioma stem cells. *Nat. Commun.* 8:1145. doi: 10.1038/s41467-017-01196-x

Conflict of Interest Statement: The authors declare that the research was conducted in the absence of any commercial or financial relationships that could be construed as a potential conflict of interest.

frontiers in Neuroscience

PERSPECTIVE
published: 08 May 2019
doi: 10.3389/fnins.2019.00452

Neuron-Derived Exosome Proteins May Contribute to Progression From Repetitive Mild Traumatic Brain Injuries to Chronic Traumatic Encephalopathy

Edward J. Goetzl[1], Aurélie Ledreux[2]*, Ann-Charlotte Granholm[2], Fanny M. Elahi[3], Laura Goetzl[4], Jade Hiramoto[5] and Dimitrios Kapogiannis[6]**

[1] Department of Medicine, University of California, San Francisco, San Francisco, CA, United States, [2] Knoebel Institute for Healthy Aging, University of Denver, Denver, CO, United States, [3] Department of Neurology, Memory and Aging Center, University of California, San Francisco, San Francisco, CA, United States, [4] Department of Obstetrics, Gynecology and Reproductive Sciences, Health Sciences Center at Houston, University of Texas, Houston, TX, United States, [5] Division of Vascular Surgery, Department of Surgery, University of California, San Francisco, San Francisco, CA, United States, [6] Laboratory of Neurosciences, Intramural Research Program, National Institute on Aging, Baltimore, MD, United States

OPEN ACCESS

Edited by:
Francesc Xavier Guix,
Severo Ochoa Molecular Biology Center (CSIC-UAM), Spain

Reviewed by:
Ye Xiong,
Henry Ford Health System, United States
Bogdan A. Stoica,
University of Maryland, Baltimore, United States

***Correspondence:**
Edward J. Goetzl
edward.goetzl@ucsf.edu
Aurélie Ledreux
aurelie.ledreux@du.edu
Dimitrios Kapogiannis
kapogiannisd@nih.gov

Specialty section:
This article was submitted to Neurodegeneration, a section of the journal Frontiers in Neuroscience

Received: 22 February 2019
Accepted: 23 April 2019
Published: 08 May 2019

Citation:
Goetzl EJ, Ledreux A, Granholm A-C, Elahi FM, Goetzl L, Hiramoto J and Kapogiannis D (2019) Neuron-Derived Exosome Proteins May Contribute to Progression From Repetitive Mild Traumatic Brain Injuries to Chronic Traumatic Encephalopathy. Front. Neurosci. 13:452. doi: 10.3389/fnins.2019.00452

The recent recognition that Alzheimer disease-like pathology may be found in chronic traumatic encephalopathy (CTE) even after acute mild traumatic brain injury (mTBI) has increased the urgency of elucidating mechanisms, identifying biomarkers predictive of high risk of development of CTE, and establishing biomarker profiles indicative of impactful effects of treatments. Of the many proteins that are loaded into neuron-derived exosomes (NDEs) from damaged neurons after acute TBI, the levels of prion cellular protein (PRPc), coagulation factor XIII (XIIIa), synaptogyrin-3, IL-6, and aquaporins remain elevated for months. Prolonged heightened expression of aquaporins and IL-6 may account for the persistent central nervous system edema and inflammation of CTE. PRPc, XIIIa and synaptogyrin-3 bind and concentrate neurotoxic forms of oligomeric amyloid β peptides or P-tau for delivery into neurons at or distant from the site of trauma. Our progression factor hypothesis of CTE asserts that physiological neuronal proteins, such as PRPc, XIIIa, synaptogyrin-3, IL-6 and aquaporins, that increase in concentration in neurons and NDEs for months after acute TBI, are etiological contributors to CTE by either direct actions or by recruiting neurotoxic forms of Aβ peptides or P-tau. Such progression factors also may be useful new targets for development of drugs to prevent CTE.

Keywords: amyloid, cellular prion protein, phospho-tau, synaptogyrin-3, Alzheimer disease

Abbreviations: Aβ42, β amyloid peptide 1-42; APP, amyloid precursor protein; BACE-1, beta-secretase-1 or beta-site amyloid precursor protein cleaving enzyme 1; BBB, blood-brain barrier; CTE, chronic traumatic encephalopathy; DU, University of Denver; MCP, monocyte chemoattractant protein; mTBI, mild TBI; NDE, neuron-derived exosome; NKCC-1, sodium-potassium-chloride co-transporter-1; PRPc, cellular prion protein; Rab 7, Rab 10, Rab 35, ras-related small GTPase 7, 10, 35; TBI, traumatic brain injury; UC, University of California; UCH-L1, ubiquitin C-terminal hydrolase L1; XIIIa, coagulation factor XIII.

INTRODUCTION

Traumatic brain injury (TBI) is the term used to describe mechanical injury to the parenchymal tissues and meninges of the brain, and the subsequent series of further damaging proteolytic, oxidative, inflammatory, and proteinopathic responses (Langlois et al., 2006; Roozenbeek et al., 2013; Quillinan et al., 2016). Several million TBIs occur annually in the United States, of which approximately 80% are defined as mild traumatic brain injury (mTBI) (Faul and Coronado, 2015; Taylor et al., 2017). A high frequency of repetitive mTBIs is observed in young adults from participation in sports and from the shock waves created by military explosives (Broglio et al., 2009; Champion et al., 2009; Wilk et al., 2012; Papa et al., 2015; McKee et al., 2016). It is clear that moderate and severe TBI predispose to both more prevalent and earlier onset Alzheimer disease, and to CTE (Barnes et al., 2014; Gardner et al., 2014; McKee et al., 2016; Perry et al., 2016). Despite the far higher prevalence of mTBI than moderate and severe TBI, it has only recently been recognized that repetitive mTBIs also increase the risk of subsequent development of CTE and dementia (Crane et al., 2016; Barnes et al., 2018). Our understanding of the mechanisms of acute mTBI resulting from a single concussive blow and CTE following repeated episodes of acute mTBI is incomplete, in part due to the past lack of sensitive and accurate biomarkers for the many constituent abnormalities.

The complex matrix of pathways interacting in the course of an mTBI begin with disruption of the blood-brain barrier (BBB) and axonal injury. BBB damage is manifested maximally within hours by morphological changes in endothelial cells, pericytes and astrocytes, increases in the number of perivascular monocytes, and elevated blood levels of tight-junction and astrocyte-specific proteins (Blyth et al., 2009; Higashida et al., 2011; Obermeier et al., 2013; Kuriakose et al., 2018). Subsequent edema of neurons and interstitial tissues follows with increased brain tissue levels of proteins from damaged neuronal framework structures, channels, transporters, and vesicle transport systems (Hue et al., 2016; Kuriakose et al., 2018). Inflammation develops in the same time period of initial responses to acute mTBI, as shown by increased brain tissue levels of cytokines, such as IFN-α, IL-1β, IL-6, and MCP, oxygen radicals and matrix metalloproteinases (Helmy et al., 2011; Woodcock and Morganti-Kossmann, 2013; Yan et al., 2014; Gyoneva and Ransohoff, 2015; Lozano et al., 2015; Simon et al., 2017; Roselli et al., 2018). This period also is characterized by increased expression of stress response and pro-apoptotic factor genes (Mettang et al., 2018).

Onset of more persistent features of CTE months or years after a TBI may be foreshadowed by sustained neuronal elevations of elements of proteinopathic neurodegeneration and chronic inflammation (DeKosky et al., 2013). Although neuropathogenic bridges linking acute mTBI to CTE are poorly understood, some mechanisms have been recognized. Within 24 h of acute TBI in rats, hippocampal and cortical brain tissues showed transient increases in beta-secretase-1 (BACE-1) (Blasko et al., 2004). In humans suffering single-incident severe TBI, increases in brain tissue levels of APP and Aβ peptides as well as diffuse Aβ plaques may be found within hours and persist variably (DeKosky et al., 2013). In contrast, the predominant early neuropathology in CTE following repetitive mTBIs is patchy distribution of neuropil threads and neurofibrillary tangles of P-tau throughout the neocortex (DeKosky et al., 2013). Plasma levels of tau-positive exosomes were abnormally elevated in former professional football players, exposed to repetitive mTBIs, and these increases correlated with decreases in memory and psychomotor speed (Stern et al., 2016). Although many abnormalities of cognition and affect or mood are similar in subjects suffering from CTE after acute severe TBI or repetitive mTBI, relationships between these neurocognitive abnormalities and differing proteinopathic etiologic mechanisms have not been delineated (Prince and Bruhns, 2017; Roy et al., 2017; Dailey et al., 2018).

Investigations of a wide range of neurally derived proteins and of systemic predominantly lipid metabolites in CSF and plasma have not yielded biomarkers that reliably assess the severity of mTBI, predict progression of mTBI to CTE, or offer useful targets for therapy (DeKosky et al., 2013; Agoston et al., 2017; Werhane et al., 2017; Kim et al., 2018). Changes in blood levels of some individual proteins, such as tau, s100B, neurofilament light chain, ubiquitin protein hydrolase-1 and neuron-specific enolase, showed moderate diagnostic and/or prognostic value in some circumstances, but had limited neural specificity, late expression and lack of cross-correlation (Di Battista et al., 2013). A comprehensive gas chromatographic analysis of sera obtained within 2 weeks of mTBI or more severe TBI showed elevations of two medium-chain fatty acids and 2,3-bisphosphoglyceric acid, that were significantly associated with the severity of TBI and added value to clinical and radiological imaging results (Oresic et al., 2016). Six plasma metabolites, including two fatty acids, three phospholipids and tauroursodeoxycholic acid, that were quantified at <6 h to 7 days after mTBI, significantly distinguished mTBI athletes from matched uninjured teammate controls throughout the week after mTBI (Fiandaca et al., 2018). However, as for the prior investigation of metabolomic lipids, these analytes have no known specific CNS functions and statistical characteristics of data for two independent cohorts showed major differences. It thus seems appropriate now to investigate subjects with acute or chronic repetitive mTBI by quantifying alterations in levels of their endosomal and other membrane CNS proteins, that are accessible in the protected cargo of plasma NDEs. The multiphasic and multicomponent set of events characteristic of all TBIs has suggested the importance of selecting biomarkers that probe both intracellular processes and diverse relevant mechanisms.

PLASMA NEURON-DERIVED EXOSOME PROTEIN ABNORMALITIES IN mTBI

Application of established technology to enrich the NDE subset of extracellular vesicles in plasma has permitted initial elucidation of the changes in exosome trafficking and levels of cargo proteins characteristic of mTBIs. A study of military personnel suffering mTBI and subsequent chronic unspecific CNS symptoms revealed significant increases in CD81 exosome marker-normalized NDE levels of total tau, Aβ42, and IL-10 relative to deployed controls without a history of mTBI

(Gill et al., 2018). Although the precise timing of episodes of mTBI was not determinable, most had been in combat at least once during the year preceding testing. Significant associations were identified between post-concussive symptoms and increases in NDE tau and between symptoms of post-traumatic stress disorder and increases in NDE IL-10 (Gill et al., 2018).

A recent investigation of plasma levels of NDEs and a broader profile of NDE cargo proteins has been conducted in college athletes aged 18–26 years, who provided plasma within 1 week after a sports-related mTBI (acute mTBI, $n = 18$) or 3 months or longer after two to four mTBIs (chronic mTBI, $n = 14$) (Goetzl et al., 2019). Plasma levels of NDEs, assessed by closely correlated counts and levels of extracted CD81 exosome marker, were significantly depressed by a mean of 45% in acute mTBI ($P < 0.0001$), as compared to teammates without TBI ($n = 21$), but not in chronic mTBI. Mean CD81-normalized NDE concentrations of a range of functional brain proteins were significantly abnormal relative to those of uninjured teammate controls in acute but not chronic mTBI groups, including ras-related small GTPase 10 (Rab 10), 73% decrease; annexin VII, 8.8-fold increase; UCH-L1, 2.5-fold increase; αII spectrin fragments, 1.9-fold increase; claudin-5, 2.7-fold increase; and sodium-potassium-chloride cotransporter-1 (NKCC-1), 2.8-fold increase (all acute increases were significantly different from controls, $P < 0.0001$). Three physiological neural proteins whose NDE levels changed significantly in acute mTBI also maintained lesser alterations in chronic TBI. Aquaporin 4 showed 8.9-fold ($P < 0.0001$) and 3.6-fold ($P = 0.0004$) increases, and synaptogyrin-3 showed 3.1-fold ($P < 0.0001$) and 1.3-fold ($P = 0.041$) increases, whereas ras-related small GTPase 35 (Rab 35) exhibited 56% ($P < 0.0001$) and 33% ($P = 0.0045$) decreases, respectively, in acute and chronic mTBI. In chronic mTBI, there were elevated CD81-normalized NDE levels of usually neuropathologic β-amyloid peptide 1–42 (Aβ42), 1.6-fold ($P < 0.0001$ relative to controls); XIIIa, 1.3-fold ($P = 0.042$); P-T181-tau, 2.2-fold ($P < 0.0001$); P-S396-tau, 1.6-fold ($P < 0.01$); IL-6, 16-fold ($P < 0.0001$); and prion cellular protein (PRPc), 5.1-fold ($P < 0.0001$), with lesser or greater (XIIIa, IL-6, PRPc) increases in acute mTBI.

The acute decreases in Rab 10 and Rab 35 levels in NDEs, that are presumed to reflect neuronal levels of these small GTPases involved in vesicular formation, trafficking and secretion, may account for the observed acute decreases in plasma levels of NDEs, as discussed in the next section (**Figure 1**). The sustained decrease in NDE level of Rab35 distinguishes this response from the transient acute decrease in NDE level of Rab10. Levels of other NDE cargo proteins, that represent disposal of damaged neuronal proteins, instead significantly increased after acute mTBI but these increases were not all sustained in chronic mTBI. Of the acute mTBI NDE cargo responders, annexin VII has roles in neuronal survival and membrane transport functions, UCH-L1 targets damaged proteins by ubiquitination for elimination, αII spectrin with actin constitutes the neuronal periodic skeleton, claudin-5 is a component of the tight junction of the BBB, and NKCC-1 and aquaporins, respectively control ion and water movements required for normal neuronal functions (Creutz, 1992; Ohara et al., 1998; Brophy et al., 2011; Scharfman and Binder, 2013; Morita et al., 2014). In contrast, the NDE proteins that increased in concentration after chronic repetitive mTBIs without (only P-S396-tau) or with significant increases in acute mTBI are regarded predominantly as mediators of proteinopathic neurodegeneration, including total tau, P-T181-tau, P-S396-tau, Aβ42, IL-6, PRPc, and XIIIa. Of this group, PRPc and XIIIa, as well as the acute responder synaptogyrin-3 remain elevated through repetitive mTBIs and bind, concentrate and deliver the mediators of proteinopathic neurodegeneration P-tau or Aβ42 to other neurons.

Hypoxic or ischemic CNS damage in two disease states evoked some of the same changes in plasma levels of NDEs and/or cargo proteins as were observed in mTBI. In the first example, ten patients undergoing multi-branched endovascular repair of aortic aneurysms were studied pre-operatively, immediately postoperatively and the day after surgery. This form of surgery is often associated with ischemic hyperglycemic spinal damage and prolonged lower extremity weakness despite application of intra-operative counter-measures (Hiramoto et al., 2017). The mean level of NDEs fell significantly after surgery and returned the following day to that observed pre-operatively. The NDE mean level of Rab 10 also decreased post-operatively and rose to near normal the next day. NDE mean levels of PRPc, neurofilament light chain, NKCC-1, aquaporins and several synaptic proteins increased significantly after surgery and decreased to near normal the next day. This contrasts with the sustained elevations of PRPc, aquaporins and synaptogyrin-3 after mTBI. NDE levels of differently phosphorylated forms of insulin receptor signaling protein, changed post-operatively in accordance with development of insulin resistance. The mean NDE level of several other proteins, such as IL-6, rose post-operatively, and fell the next day, but remained significantly higher than that seen pre-operatively, which again raised the possibility of a subset of neural protein progression factors that might mediate subacute or chronic injury after hypoxia or ischemia.

The second example is neonatal hypoxemic-ischemic encephalopathy and early identification of affected infants that are not responding to standard therapeutic hypothermia. Neonatal NDEs in plasma obtained at 8, 10 and 14 h after initiation of hypothermia were enriched by absorption with anti-Contactin-2 antibody (Goetzl et al., 2018). CD81-normalized levels of neonatal NDE synaptopodin, synaptophysin, neuron-specific enolase and mitochondrial cytochrome C oxidase were quantified immunochemically. The most promising marker for all clinical outcomes was NDE synaptopodin, as the slope of change in its NDE level between 8 and 14 h of hypothermia was associated with clinically significant outcomes including persistent seizure activity requiring treatment ($p = 0.02$) and length of hospital stay ($P < 0.001$).

Rab SMALL GTPases AND NDE TRAFFICKING in mTBIs

Rab small GTPases, the largest branch of the Ras superfamily, are highly abundant, and diverse organizers of intracellular membrane trafficking in the CNS (Kiral et al., 2018). The state

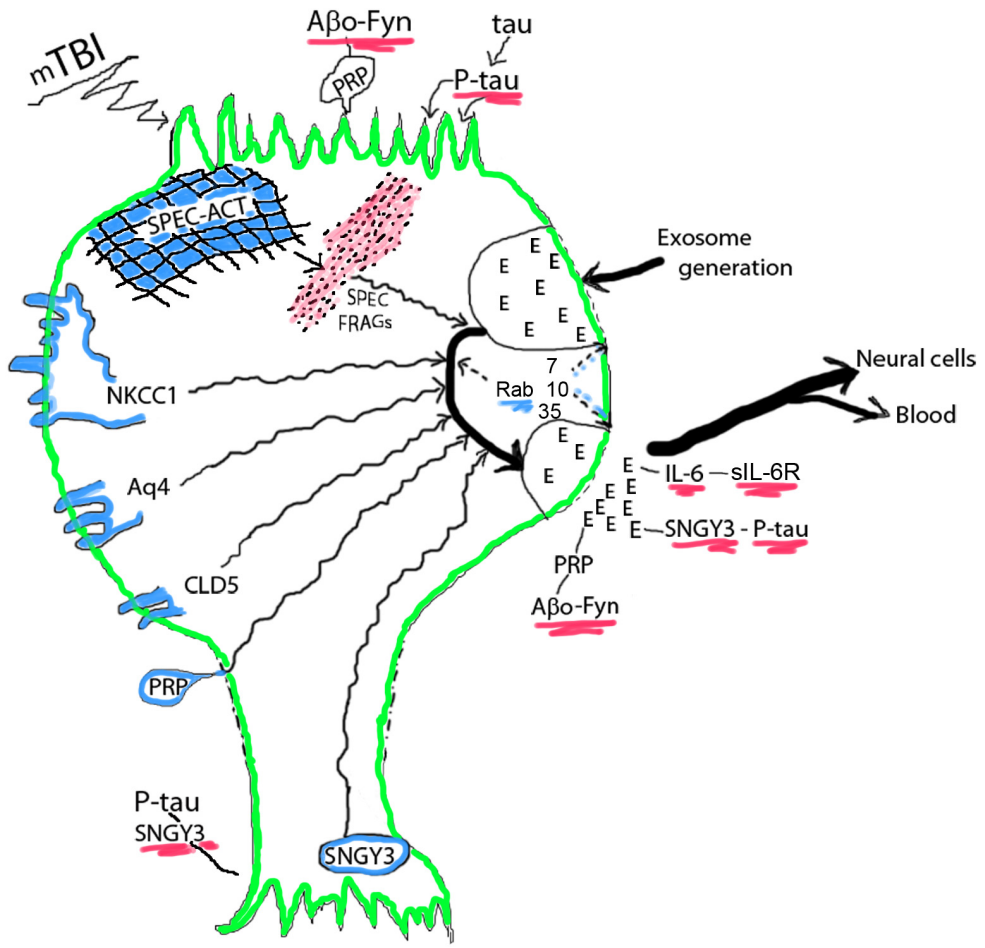

FIGURE 1 | Acute mTBI-evoked alterations in NDEs. NDEs are generated at the plasma membrane surface of the cell body, loaded with diverse neuronal proteins in their endosomal course in multivesicular bodies, and secreted through secretory type multivesicular bodies. Cargo proteins are from membrane structures or the spectrin (SPEC)-actin (ACT) matrix and their levels in NDEs increase after mTBI. The small GTPases Rab 7, 10, 35, and others regulate the processes of NDE generation, trafficking and secretion, that all diminish after mTBI reduces Rab levels. Progression factors bind, concentrate and deliver neurotoxic proteins: oligomeric Aβ peptides (Aβo) by PRPc in a trimolecular complex with Fyn kinase at dendritic surfaces and in NDEs, P-tau by synaptogyrin-3 (SNGY3) at axonal and synaptic surfaces and in NDEs, and IL-6 by soluble(s)IL-6Rs. E, exosome. Color depictions are green for neuronal boundary, blue for normal cellular proteins that are found in NDE cargo and red for disrupted neuronal matrix proteins and neurotoxic progression factor complexes.

of membrane association and activity of Rab GTPases are highly dependent on controlling interactions with numerous classes of accessory proteins. In the CNS, most Rab GTPases have multiple functions. For example, Rab 7 in neurons is a critical regulator of multivesicular body maturation from early endosomes, fusion of multivesicular bodies with lysosomes to form autolysosomes, and retrograde axonal transport of vesicles with the motor protein dynein into neuron cell bodies. Similarly, Rab 35 is important for the rejuvenation of synaptic vesicles from sorting/recycling endosomes and influences neuronal actin dynamics, largely by activating Rho GTPases (Chua et al., 2010). In contrast to the increases in some neuronal Rab GTPases observed in many neurodegenerative diseases (Kiral et al., 2018), NDE levels of Rab 7, Rab 10, and Rab 35 decrease in acute mTBI. Any NDE-related functional significance of decreased levels of some Rab GTPases in acute mTBI remains to be established.

POTENTIAL NDE PROTEIN PROGRESSION FACTORS IN THE CONTINUUM FROM REPETITIVE mTBIs TO CHRONIC TRAUMATIC ENCEPHALOPATHY (CTE)

It is too early in the course of elucidating acute mTBI-initiated pathways of pathogenesis of CTE for meaningful speculation about critical mechanisms. Further, we have no data for contributions of NDE miRNAs or lipids, or of astrocyte- or microglia-derived exosomes. However, a tentative analytical

integration of existing data has identified several proteins in NDEs that may serve as factors mediating progression from repetitive mTBIs to CTE. Neuronal proteins that are elevated in NDEs acutely after mTBIs and remain significantly increased for 3 months or longer at levels higher than seen acutely include the directly neurotoxic Aβ42 and P-T181-tau (Goetzl et al., 2019). Neuronal proteins that are elevated in NDEs acutely after mTBIs and remain significantly increased for 3 months or longer at levels lower than seen acutely are aquaporins, synaptogyrin-3 and XIIIa, which lack direct neurotoxicity, as well as IL-6 and PRPc, that may diminish neuronal viability (Goetzl et al., 2019). Each of these latter mTBI-generated proteins is a candidate progression factor that promotes sustained neurotoxicity indirectly through enhancement of Aβ42 or P-tau effects or by other mechanisms.

In the model proposed, mTBI damages and releases from neuronal membranes and other structures a wide range of functional proteins that are loaded into NDEs in endosomal pathways (**Figure 1**). No relationships have yet been established between the severity of a single mTBI and the magnitude or duration of increases in NDE levels of the proteins being removed by the exosomal pathway, but indirect evidence suggests that most such increases last for less than 3 months after a single mTBI. Transient decreases in NDE levels and presumptively neuronal levels of Rab 7, 10, and 35 reduce formation and secretion of NDEs for days after an acute mTBI with potential back-up of released proteins in the neurons. mTBI increases NDE and neuronal levels of the binding partners PRPc with Aβ peptides, especially oligomeric forms of Aβ (Aβo), synaptogyrin-3 with P-tau species, and IL-6 with soluble IL-6 receptors (sIL-6Rs). Neurotoxic concentrations of PRPc-Aβ peptide complexes at dendrites, synaptogyrin-3- P-tau complexes at synapses, and IL-6-sIL-6R complexes accumulate both in and on neurons of origin at the site of mTBI and in NDEs that transport them into neighboring neurons not damaged directly by the inciting mTBI (**Figure 1**). Sustained increases in aquaporins promote edema and in IL-6 maintain chronic inflammation after mTBIs. Thus acute changes of mTBI may progress to pathogenesis of early CTE with increasing probability after subsequent repetitive mTBIs (**Figure 2**).

The postulated stages of mTBI induction of CTE are illustrated schematically from normal to mild deterioration after one mTBI to advanced CTE pathology after repeated mTBIs (mTBIn) (**Figure 2**). After a single mTBI, APP and BACE1 in exosomes from reactive astrocytes (AG) and to a lesser extent from damaged neurons are transferred to lesional and distant neurons. This initiates increased neuronal production of Aβ peptides, their

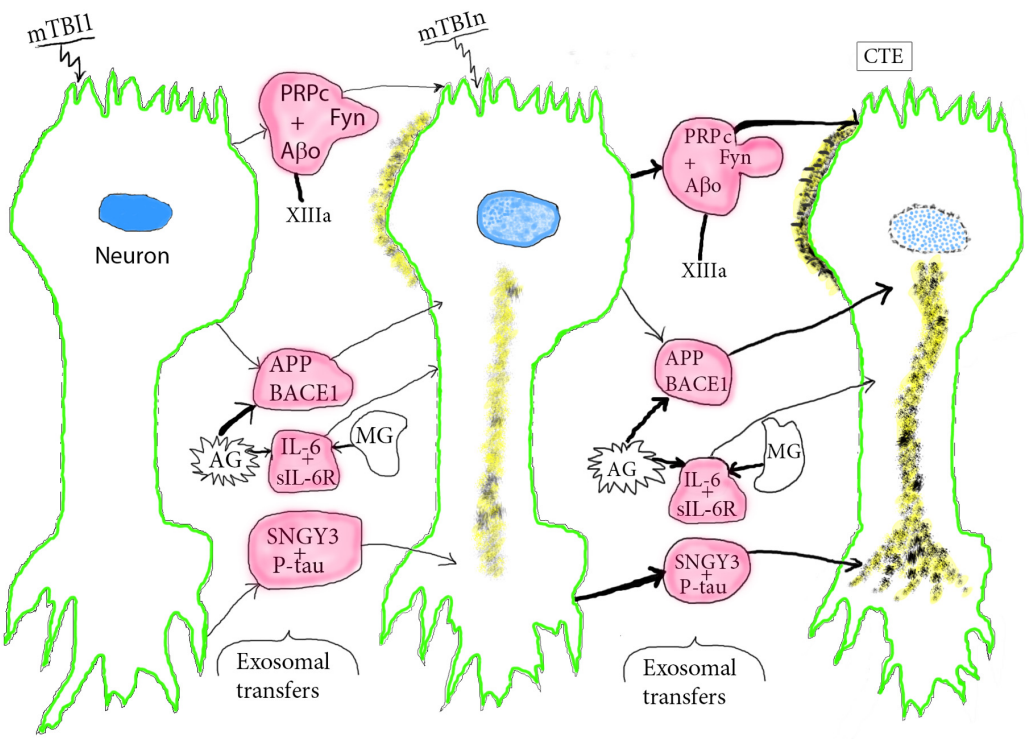

FIGURE 2 | Course of pathogenesis of CTE by repetitive mTBIs. An initial mTBI leads to neuronal production of NDEs containing pathogenic complexes composed of PRPc+Aβo+Fyn, SNGY3+P-tau, and IL-6-sIL-6R that begin to damage the donor neurons at sites of mTBI and other neurons that receive the neurotoxic NDEs. Microglia (MG) and astrocytes (AG) produce MDEs and ADEs, respectively, that carry increased levels of APP, BACE-1, and IL-6 capable of further neurotoxic damage of neurons that receive these other sets of exosomes. This series of processes increases with subsequent episodes of mTBI and is enhanced by other progression factors, such as XIIIa that promotes oligomerization of Aβ to Aβo. P-tau neuropil fibers and Aβo deposits increase in size and density with repetitive mTBIs and lead to neuronal apoptosis. Color depictions are green for neuronal boundary, blue for the degenerating nucleus, yellow for Aβ, P-tau deposits, and red for NDEs with progression factor complexes and AG/MG products.

oligomerization to Aβo that is catalyzed in part by increased levels of XIIIa (Hur et al., 2019), and beginning aggregation into loose deposits on neurons (**Figure 2**, second stage). IL-6-sIL-6R complexes in exosomes from reactive AG and microglia (MG) are secreted in part in their respective ADEs and MDEs for transfer to neurons, which mediates a sustained neuronal inflammatory response. PRPc-Fyn kinase-Aβ peptide complexes with XIIIa-oligomerized Aβ (Aβo) are transferred by NDEs to dendrites of other neurons and synaptogyrin-3 (SNGY-3)-P-tau complexes are transferred by NDEs and concentrated in axonal and presynaptic areas of other neurons to begin formation of loose P-tau strands and tangles. Repetitive mTBIs result in enhancement of all of these exosomal transfer processes with greater neuronal proteinopathic deposition of Aβo and forms of P-tau followed by early neuronal apoptosis in stage 3 (**Figure 2**). In summary, mTBI-derived CTE progression factors such as PRPc, XIIIa and SNGY-3, may act by binding to, concentrating and delivering to neurons neurotoxic Aβ peptides and various forms of P-tau. Others act independently of neurotoxic mediators, as exemplified by IL-6, which is bound by sIL-6Rs that dominate in neural tissues, link as the IL-6-sIL-6R complex to glycoprotein 130 on neurons and transmit neurodegenerative signals to the affected neurons (Erta et al., 2012; Rothaug et al., 2016). Accessory ligands for aquaporins have not been identified.

The many means for validation of the progression factor hypothesis of mediation of CTE by repetitive mTBIs include simple definitions of the time-courses of changes in NDE levels of three classes of relevant biomarkers. First, NDE levels of acute biomarkers, such as annexin VII, claudin-5, UCH-L1, spectrin fragments and NKCC-1, should only be elevated in the several weeks after each mTBI. Second, acute NDE increases in levels of Aβ peptide and P-tau mediators of proteinopathic toxicity should increase progressively and persist longer after each episode of mTBI. Third, NDE levels of the progression factors XIIIa, PRPc, SNGY-3, and possibly IL-6 and aquaporins should remain on elevated plateaus for months to years between episodes of mTBI. It also remains to be established if there are any relationships between the severity of a single mTBI or the stage of advancement to CTE and the NDE level of any of the biomarkers. Changes in the NDE level and duration of elevation of some biomarkers of mTBI also hopefully may provide information about the effectiveness of a therapeutic agent or program. Finally, this model may encourage extending drug discovery for mTBI and possibly Alzheimer disease to agents that alter neuronal expression of progression factors and their binding of Aβ peptides and P-tau species.

DATA AVAILABILITY

The datasets for this manuscript are not publicly available because data are available in Goetzl et al. (2019) cited reference. Requests to access the datasets should be directed to edward.goetzl@ucsf.edu.

ETHICS STATEMENT

This study was carried out in accordance with the recommendations of the University of California, San Francisco, San Francisco, CA, United States and University of Denver Human Research Institutional Review Committees with written informed consent from all subjects. All subjects gave written informed consent in accordance with the Declaration of Helsinki. The protocol was approved by the University of California, San Francisco and University of Denver Human Research Institutional Review Committees.

AUTHOR CONTRIBUTIONS

EG and DK formulated the conceptual framework of this perspective and prepared the draft manuscript. All authors analyzed the findings reported, edited the manuscript, and approved the final version submitted.

FUNDING

The research described was supported by a pilot grant to Drs. Ledreux and Granholm-Bentley from the Knoebel Institute for Healthy Aging and by support of Drs. Mustapic and Kapogiannis from the Intramural Program of the National Institute on Aging of the NIH.

ACKNOWLEDGMENTS

The authors are grateful to Judith H. Goetzl for preparation of the graphic illustrations.

REFERENCES

Agoston, D. V., Shutes-David, A., and Peskind, E. R. (2017). Biofluid biomarkers of traumatic brain injury. *Brain Inj.* 31, 1195–1203. doi: 10.1080/02699052.2017.1357836

Barnes, D. E., Byers, A. L., Gardner, R. C., Seal, K. H., Boscardin, W. J., and Yaffe, K. (2018). Association of mild traumatic brain injury with and without loss of consciousness with dementia in US military veterans. *JAMA Neurol.* 75, 1055–1061. doi: 10.1001/jamaneurol.2018.0815

Barnes, D. E., Kaup, A., Kirby, K. A., Byers, A. L., Diaz-Arrastia, R., and Yaffe, K. (2014). Traumatic brain injury and risk of dementia in older veterans. *Neurology* 83, 312–319. doi: 10.1212/WNL.0000000000000616

Blasko, I., Beer, R., Bigl, M., Apelt, J., Franz, G., Rudzki, D., et al. (2004). Experimental traumatic brain injury in rats stimulates the expression, production and activity of Alzheimer's disease beta-secretase (BACE-1). *J. Neural Transm.* 111, 523–536. doi: 10.1007/s00702-003-0095-6

Blyth, B. J., Farhavar, A., Gee, C., Hawthorn, B., He, H., Nayak, A., et al. (2009). Validation of serum markers for blood-brain barrier disruption in traumatic brain injury. *J. Neurotrauma* 26, 1497–1507. doi: 10.1089/neu.2008-0738

Broglio, S. P., Sosnoff, J. J., Shin, S., He, X., Alcaraz, C., and Zimmerman, J. (2009). Head impacts during high school football: a biomechanical assessment. *J. Athl. Train* 44, 342–349. doi: 10.4085/1062-6050-44.4.342

Brophy, G. M., Mondello, S., Papa, L., Robicsek, S. A., Gabrielli, A., Tepas, J., et al. (2011). Biokinetic analysis of ubiquitin C-terminal

hydrolase-L1 (UCH-L1) in severe traumatic brain injury patient biofluids. *J. Neurotrauma* 28, 861–870. doi: 10.1089/neu.2010.1564

Champion, H. R., Holcomb, J. B., and Young, L. A. (2009). Injuries from explosions: physics, biophysics, pathology, and required research focus. *J. Trauma* 66, 1468–1477; discussion 1477. doi: 10.1097/TA.0b013e3181a27e7f

Chua, C. E., Lim, Y. S., and Tang, B. L. (2010). Rab35–a vesicular traffic-regulating small GTPase with actin modulating roles. *FEBS Lett.* 584, 1–6. doi: 10.1016/j.febslet.2009.11.051

Crane, P. K., Gibbons, L. E., Dams-O'Connor, K., Trittschuh, E., Leverenz, J. B., Keene, C. D., et al. (2016). Association of traumatic brain injury with late-life neurodegenerative conditions and neuropathologic findings. *JAMA Neurol.* 73, 1062–1069. doi: 10.1001/jamaneurol.2016.1948

Creutz, C. E. (1992). The annexins and exocytosis. *Science* 258, 924–931. doi: 10.1126/science.1439804

Dailey, N. S., Smith, R., Bajaj, S., Alkozei, A., Gottschlich, M. K., Raikes, A. C., et al. (2018). Elevated aggression and reduced white matter integrity in mild traumatic brain injury: a DTI study. *Front. Behav. Neurosci.* 12:118. doi: 10.3389/fnbeh.2018.00118

DeKosky, S. T., Blennow, K., Ikonomovic, M. D., and Gandy, S. (2013). Acute and chronic traumatic encephalopathies: pathogenesis and biomarkers. *Nat. Rev. Neurol.* 9, 192–200. doi: 10.1038/nrneurol.2013.36

Di Battista, A. P., Rhind, S. G., and Baker, A. J. (2013). Application of blood-based biomarkers in human mild traumatic brain injury. *Front. Neurol.* 4:44. doi: 10.3389/fneur.2013.00044

Erta, M., Quintana, A., and Hidalgo, J. (2012). Interleukin-6, a major cytokine in the central nervous system. *Int. J. Biol. Sci.* 8, 1254–1266. doi: 10.7150/ijbs.4679

Faul, M., and Coronado, V. (2015). Epidemiology of traumatic brain injury. *Handb. Clin. Neurol.* 127, 3–13.

Fiandaca, M. S., Mapstone, M., Mahmoodi, A., Gross, T., Macciardi, F., Cheema, A. K., et al. (2018). Plasma metabolomic biomarkers accurately classify acute mild traumatic brain injury from controls. *PLoS One* 13:e0195318. doi: 10.1371/journal.pone.0195318

Gardner, R. C., Burke, J. F., Nettiksimmons, J., Kaup, A., Barnes, D. E., and Yaffe, K. (2014). Dementia risk after traumatic brain injury vs nonbrain trauma: the role of age and severity. *JAMA Neurol.* 71, 1490–1497. doi: 10.1001/jamaneurol.2014.2668

Gill, J., Mustapic, M., Diaz-Arrastia, R., Lange, R., Gulyani, S., Diehl, T., et al. (2018). Higher exosomal tau, amyloid-beta 42 and IL-10 are associated with mild TBIs and chronic symptoms in military personnel. *Brain Inj.* 32, 1277–1284. doi: 10.1080/02699052.2018.1471738

Goetzl, E. J., Elahi, F. M., Mustapic, M., Kapogiannis, D., Pryhoda, M., Gilmore, A., et al. (2019). Altered levels of plasma neuron-derived exosomes and their cargo proteins characterize acute and chronic mild traumatic brain injury. *FASEB J.* 33, 5082–5088. doi: 10.1096/fj.201802319R

Goetzl, L., Merabova, N., Darbinian, N., Martirosyan, D., Poletto, E., Fugarolas, K., et al. (2018). Diagnostic potential of neural exosome cargo as biomarkers for acute brain injury. *Ann. Clin. Transl. Neurol.* 5, 4–10. doi: 10.1002/acn3.499

Gyoneva, S., and Ransohoff, R. M. (2015). Inflammatory reaction after traumatic brain injury: therapeutic potential of targeting cell-cell communication by chemokines. *Trends Pharmacol. Sci.* 36, 471–480. doi: 10.1016/j.tips.2015.04.003

Helmy, A., De Simoni, M. G., Guilfoyle, M. R., Carpenter, K. L., and Hutchinson, P. J. (2011). Cytokines and innate inflammation in the pathogenesis of human traumatic brain injury. *Prog. Neurobiol.* 95, 352–372. doi: 10.1016/j.pneurobio.2011.09.003

Higashida, T., Kreipke, C. W., Rafols, J. A., Peng, C., Schafer, S., Schafer, P., et al. (2011). The role of hypoxia-inducible factor-1alpha, aquaporin-4, and matrix metalloproteinase-9 in blood-brain barrier disruption and brain edema after traumatic brain injury. *J. Neurosurg.* 114, 92–101. doi: 10.3171/2010.6.JNS10207

Hiramoto, J. S., Fernandez, C., Gasper, W., Vartanian, S., Reilly, L., and Chuter, T. (2017). Lower extremity weakness is associated with elevated blood and cerebrospinal fluid glucose levels following multibranched endovascular aortic aneurysm repair. *J. Vasc. Surg.* 65, 311–317. doi: 10.1016/j.jvs.2016.08.111

Hue, C. D., Cho, F. S., Cao, S., Nicholls, R. E., Vogel Iii, E. W., and Sibindi, C. (2016). Time course and size of blood-brain barrier opening in a mouse model of blast-induced traumatic brain injury. *J. Neurotrauma* 33, 1202–1211. doi: 10.1089/neu.2015.4067

Hur, W. S., Mazinani, N., Lu, X. J. D., Yefet, L. S., Byrnes, J. R., Ho, L., et al. (2019). Coagulation factor XIIIa cross-links amyloid beta into dimers and oligomers and to blood proteins. *J. Biol. Chem.* 294, 390–396. doi: 10.1074/jbc.RA118.005352

Kim, H. J., Tsao, J. W., and Stanfill, A. G. (2018). The current state of biomarkers of mild traumatic brain injury. *JCI Insight* 3:97105. doi: 10.1172/jci.insight.97105

Kiral, F. R., Kohrs, F. E., Jin, E. J., and Hiesinger, P. R. (2018). Rab GTPases and membrane trafficking in neurodegeneration. *Curr. Biol.* 28, R471–R486. doi: 10.1016/j.cub.2018.02.010

Kuriakose, M., Rama Rao, K. V., Younger, D., and Chandra, N. (2018). Temporal and spatial effects of blast overpressure on blood-brain barrier permeability in traumatic brain injury. *Sci. Rep.* 8:8681. doi: 10.1038/s41598-018-26813-7

Langlois, J. A., Rutland-Brown, W., and Wald, M. M. (2006). The epidemiology and impact of traumatic brain injury: a brief overview. *J. Head. Trauma Rehabil.* 21, 375–378. doi: 10.1097/00001199-200609000-00001

Lozano, D., Gonzales-Portillo, G. S., Acosta, S., de la Pena, I., Tajiri, N., Kaneko, Y., et al. (2015). Neuroinflammatory responses to traumatic brain injury: etiology, clinical consequences, and therapeutic opportunities. *Neuropsychiatr. Dis. Treat.* 11, 97–106. doi: 10.2147/NDT.S65815

McKee, A. C., Alosco, M. L., and Huber, B. R. (2016). Repetitive head impacts and chronic traumatic encephalopathy. *Neurosurg. Clin. N. Am.* 27, 529–535. doi: 10.1016/j.nec.2016.05.009

Mettang, M., Reichel, S. N., Lattke, M., Palmer, A., Abaei, A., Rasche, V., et al. (2018). IKK2/NF-kappaB signaling protects neurons after traumatic brain injury. *FASEB J.* 32, 1916–1932. doi: 10.1096/fj.201700826R

Morita, Y., Callicott, J. H., Testa, L. R., Mighdoll, M. I., Dickinson, D., and Chen, Q. (2014). Characteristics of the cation cotransporter NKCC1 in human brain: alternate transcripts, expression in development, and potential relationships to brain function and schizophrenia. *J. Neurosci.* 34, 4929–4940. doi: 10.1523/JNEUROSCI.1423-13.2014

Obermeier, B., Daneman, R., and Ransohoff, R. M. (2013). Development, maintenance and disruption of the blood-brain barrier. *Nat. Med.* 19, 1584–1596. doi: 10.1038/nm.3407

Ohara, O., Ohara, R., Yamakawa, H., Nakajima, D., and Nakayama, M. (1998). Characterization of a new beta-spectrin gene which is predominantly expressed in brain. *Brain Res. Mol. Brain Res.* 57, 181–192. doi: 10.1016/s0169-328x(98)00068-0

Oresic, M., Posti, J. P., Kamstrup-Nielsen, M. H., Takala, R. S. K., Lingsma, H. F., and Mattila, I. (2016). Human serum metabolites associate with severity and patient outcomes in traumatic brain injury. *EBioMedicine* 12, 118–126. doi: 10.1016/j.ebiom.2016.07.015

Papa, L., Ramia, M. M., Edwards, D., Johnson, B. D., and Slobounov, S. M. (2015). Systematic review of clinical studies examining biomarkers of brain injury in athletes after sports-related concussion. *J. Neurotrauma* 32, 661–673. doi: 10.1089/neu.2014.3655

Perry, D. C., Sturm, V. E., Peterson, M. J., Pieper, C. F., Bullock, T., and Boeve, B. F. (2016). Association of traumatic brain injury with subsequent neurological and psychiatric disease: a meta-analysis. *J. Neurosurg.* 124, 511–526. doi: 10.3171/2015.2.JNS14503

Prince, C., and Bruhns, M. E. (2017). Evaluation and treatment of mild traumatic brain injury: the role of neuropsychology. *Brain Sci.* 7:E105.

Quillinan, N., Herson, P. S., and Traystman, R. J. (2016). Neuropathophysiology of brain injury. *Anesthesiol. Clin.* 34, 453–464. doi: 10.1016/j.anclin.2016.04.011

Roozenbeek, B., Maas, A. I., and Menon, D. K. (2013). Changing patterns in the epidemiology of traumatic brain injury. *Nat. Rev. Neurol.* 9, 231–236. doi: 10.1038/nrneurol.2013.22

Roselli, F., Chandrasekar, A., and Morganti-Kossmann, M. C. (2018). Interferons in traumatic brain and spinal cord injury: current evidence for translational application. *Front. Neurol.* 9:458. doi: 10.3389/fneur.2018.00458

Rothaug, M., Becker-Pauly, C., and Rose-John, S. (2016). The role of interleukin-6 signaling in nervous tissue. *Biochim. Biophys. Acta* 1863(6 Pt A), 1218–1227. doi: 10.1016/j.bbamcr.2016.03.018

Roy, D., Vaishnavi, S., Han, D., and Rao, V. (2017). Correlates and prevalence of aggression at six months and one year after first-time traumatic brain injury.

J. Neuropsychiatry Clin. Neurosci. 29, 334–342. doi: 10.1176/appi.neuropsych.16050088

Scharfman, H. E., and Binder, D. K. (2013). Aquaporin-4 water channels and synaptic plasticity in the hippocampus. *Neurochem. Int.* 63, 702–711. doi: 10.1016/j.neuint.2013.05.003

Simon, D. W., McGeachy, M. J., Bayir, H., Clark, R. S. B., Loane, D. J., and Kochanek, P. M. (2017). The far-reaching scope of neuroinflammation after traumatic brain injury. *Nat. Rev. Neurol.* 13:572. doi: 10.1038/nrneurol.2017.116

Stern, R. A., Tripodis, Y., Baugh, C. M., Fritts, N. G., Martin, B. M., Chaisson, C., et al. (2016). Preliminary study of plasma exosomal Tau as a potential biomarker for chronic traumatic encephalopathy. *J. Alzheimers Dis.* 51, 1099–1109. doi: 10.3233/JAD-151028

Taylor, C. A., Bell, J. M., Breiding, M. J., and Xu, L. (2017). Traumatic brain injury-related emergency department visits, hospitalizations, and deaths - United States, 2007 and 2013. *MMWR Surveill. Summ.* 66, 1–16. doi: 10.15585/mmwr.ss6609a1

Werhane, M. L., Evangelista, N. D., Clark, A. L., Sorg, S. F., Bangen, K. J., Tran, M., et al. (2017). Pathological vascular and inflammatory biomarkers of acute- and chronic-phase traumatic brain injury. *Concussion* 2:CNC30. doi: 10.2217/cnc-2016-0022

Wilk, J. E., Herrell, R. K., Wynn, G. H., Riviere, L. A., and Hoge, C. W. (2012). Mild traumatic brain injury (concussion), posttraumatic stress disorder, and depression in U.S. soldiers involved in combat deployments: association with postdeployment symptoms. *Psychosom. Med.* 74, 249–257. doi: 10.1097/PSY.0b013e318244c604

Woodcock, T., and Morganti-Kossmann, M. C. (2013). The role of markers of inflammation in traumatic brain injury. *Front. Neurol.* 4:18. doi: 10.3389/fneur.2013.00018

Yan, E. B., Satgunaseelan, L., Paul, E., Bye, N., Nguyen, P., Agyapomaa, D., et al. (2014). Post-traumatic hypoxia is associated with prolonged cerebral cytokine production, higher serum biomarker levels, and poor outcome in patients with severe traumatic brain injury. *J. Neurotrauma* 31, 618–629. doi: 10.1089/neu.2013.3087

Conflict of Interest Statement: The authors declare that the research was conducted in the absence of any commercial or financial relationships that could be construed as a potential conflict of interest.

The handling Editor declared a past co-authorship with one of the authors DK.

frontiers in Neuroscience

MINI REVIEW
published: 02 July 2019
doi: 10.3389/fnins.2019.00698

Propagation of Tau via Extracellular Vesicles

*Mar Pérez[1], Jesús Avila[2,3] and Félix Hernández[2,3]**

[1] Departamento de Anatomía Histología y Neurociencia, Facultad de Medicina UAM, Madrid, Spain, [2] Network Center for Biomedical Research in Neurodegenerative Diseases (CIBERNED), Madrid, Spain, [3] Centro de Biología Molecular Severo Ochoa (CSIC-UAM), Madrid, Spain

Extracellular vesicles (EVs), like exosomes, play a critical role in physiological processes, including synaptic transmission and nerve regeneration. However, exosomes in particular can also contribute to the development of neurodegenerative conditions such as Alzheimer's disease (AD), Parkinson's disease, and prion diseases. All of these disorders are characterized by protein aggregation and deposition in specific regions of the brain. Several lines of evidence indicate that protein in exosomes is released from affected neurons and propagated along neuroanatomically connected regions of the brain, thus spreading the neurodegenerative disease. Also, different cell types contribute to the progression of tauopathy, such as microglia. Several groups have reported tau release via exosomes by cultured neurons or cells overexpressing human tau. Although the exact mechanisms underlying the propagation of protein aggregates are not fully understood, recent findings have implicated EVs in this process. The AD brain has two hallmarks, namely the presence of amyloid-β-containing plaques and neurofibrillary tangles, the latter formed by hyperphosphorylated tau protein. Both amyloid peptide and tau protein are present in specific exosomes. This review summarizes recent advances in our understanding of exosomes in the pathology of AD, with a special focus on tau protein.

Keywords: tau propagation, extracellular vesicle, neurodegenerative disease, tau protein, Alzheimer's disease

OPEN ACCESS

Edited by:
Grant Thomas Corbett, Harvard Medical School, United States

Reviewed by:
Ioannis Sotiropoulos, University of Minho, Portugal
Rostislav Skrabana, Institute of Neuroimmunology (SAS), Slovakia

***Correspondence:**
Félix Hernández
fhernandez@cbm.csic.es

Specialty section:
This article was submitted to Neurodegeneration, a section of the journal Frontiers in Neuroscience

Received: *05 April 2019*
Accepted: *19 June 2019*
Published: *02 July 2019*

Citation:
Pérez M, Avila J and Hernández F (2019) Propagation of Tau via Extracellular Vesicles. Front. Neurosci. 13:698. doi: 10.3389/fnins.2019.00698

INTRODUCTION

Brain microtubules were first isolated and characterized in the 1970s (Weisenberg, 1972). This study revealed the presence of a main protein, tubulin, and several others described as microtubule-associated proteins (MAPs) in these structures. One of these MAPs, tau, was first characterized by Kirschner's group (Weingarten et al., 1975). Similar to other MAPs, the function of tau was found to be related to an increase in microtubule stabilization (Drubin and Kirschner, 1986), which prevents cell proliferation and facilitates neuronal differentiation. Recent discoveries about partners (End binding proteins 1 and 3, tRNA), different subcellular localizations (nucleus, nucleolus, plasma membrane, dendrites and dendritic spines) or association with cellular organelles (ribosomes, endoplasmic reticulum and the Golgi apparatus) for tau suggest additional roles. According to these studies, tau should be implicated on mechanisms of synaptic plasticity, structural architecture of heterochromatin, chromosome stability or regulating the cellular transcriptome (for more detail see review Sotiropoulos et al., 2017).

Although tau is mainly an intracellular protein, there are reports indicating that extracellular tau is present in brain interstitial fluid (Yamada et al., 2011), its amount decreasing in this medium during sleep (Lucey et al., 2019). Secreted tau may be implicated in some features of sleep (Cantero et al., 2010; Lucey et al., 2019). However, independently of this notion, secreted tau protein is present *in vivo*, and its secretion appears to be regulated.

TAU SECRETION AND ITS REGULATION

The presence of extracellular tau suggests that it is secreted under physiological conditions. In this regard, it has been proposed that intracellular tau is released upon an increase in neuronal activity (Pooler et al., 2013; Yamada et al., 2014). In addition to neuron activity-dependent tau secretion, the extracellular form of the protein may arise by other mechanisms, such as neuron death (Gomez-Ramos et al., 2006), intracellular tau accumulation (Simon et al., 2012), a tauopathy (Clavaguera et al., 2009), or modulation by tau mutations (Karch et al., 2012). In the case of neuron death, intracellular proteins like tau are released into the extracellular space.

Intracellular tau accumulation can arise due to aging. In this regard, tau accumulation in older adults is associated with hippocampal hyperactivity (Huijbers et al., 2019). Also, an increase in intracellular levels of tau can result from pathological disorders related to a decrease in the turnover of this protein. This reduction can be caused by impaired tau degradation through two main systems, the ubiquitin-proteasome pathway and the autophagy-lysosomal pathway (Wang et al., 2009; Chesser et al., 2013; Lee et al., 2013; Guo et al., 2017). Recently, a third degradative pathway, the endolysosomal system, has been proposed for neurodegenerative disorders such as AD or Parkinson's disease (Vaz-Silva et al., 2018). Rab35 and the endosomal sorting complex required for transport (ESCRT) machinery should be involved in the delivery of tau to lysosomes via early endosomes and multivesicular bodies. Intracellular tau accumulation may facilitate post-translational modifications, like phosphorylation or truncation, in the protein (Avila et al., 2004), and the modified tau isoform can also be secreted.

Hyperphosphorylation is one of the most important post-translational modifications in AD and related tauopathies (Medina et al., 2016). An increase in phosphorylation at T181 (Vanmechelen et al., 2000) or T231 (Hampel et al., 2005) has been described in the cerebrospinal fluid of AD patients, although a decrease with the progression of AD has also been reported (Hampel et al., 2001). Thus, a tau mutant mimicking phosphorylation is more efficiently secreted than one mimicking dephosphorylation in Hela cells (Plouffe et al., 2012). However, it is still unclear whether phosphorylation regulates tau secretion, since both phosphorylated and unphosphorylated tau species have been detected in the extracellular space. Studies carried out in primary cortical neurons showed the release of unphosphorylated tau in control conditions (Pooler et al., 2013), while other groups have reported that cortical neurons secrete phosphorylated and unphosphorylated Tau species in response to various insults (Plouffe et al., 2012). Further research is needed to elucidate how tau phosphorylation contributes to the secretion of this protein. However, one point to keep in mind is the observation that extracellular tau is dephosphorylated in the AD brain by tissue Non-specific alkaline phosphatases (Diaz-Hernandez et al., 2010).

TAU SECRETION IN CELL CULTURE MODELS

The transfer of tau in Non-neuronal cell cultures may take place upon tau secretion (Frost et al., 2009), and in a direct way it has been demonstrated that the accumulation of tau in Non-neuronal cells promotes its secretion to the extracellular space in nacked (free) form or via membrane vesicles (Simon et al., 2012). This secretion could occur by accumulation of the whole tau molecule or by accumulation of tau fragments (Perez et al., 2016). Post-translational modifications like phosphorylation or truncation may regulate tau secretion in Non-neuronal cell models (Diaz-Hernandez et al., 2010; Plouffe et al., 2012). Also, secretion of truncated tau forms has been reported in neuronal cells (Kim et al., 2010; Kanmert et al., 2015). In this regard, a number of mechanisms explaining the secretion of truncated (and/or aggregated) tau and tau in free form (Kfoury et al., 2012) have been put forward.

Regarding the factors involved in the secretion of tau in cell culture models, End-binding proteins bind to the N-terminal end of human tau protein (Sayas et al., 2019). This observation suggests that the interaction of EB proteins with tau facilitates the localization of tau close to cellular membrane and its further secretion. However, more analysis is needed to confirm this notion.

POSSIBLE MECHANISMS OF TAU SECRETION

The molecular mechanisms responsible for the secretion of tau in its different forms: unmodified, phosphorylated, truncated, etc, are unclear. It has been postulated that secretion takes place through a Non-vesicular (free protein) secretory pathway, because tau lacks a signal sequence to regulate its transport to the endoplasmic reticulum, a step needed in the conventional secretary pathway (Yamada, 2017). On the other hand, the Golgi dynamics in neurons has been linked to the regulation of tau secretion (Mohamed et al., 2017). Also, mitochondria damage in neurons and Non-neuronal cells may also be involved in the modulation of tau secretion (Shafiei et al., 2017). Although it is not clear how tau can be localized at the cell membrane, several reports demonstrate its presence at the membrane (Brandt et al., 1995; Arrasate et al., 2000), a localization that could favor its further secretion. Also, tau is found present at various cell protrusions like dendritic spines (Ittner et al., 2010), growth cones (Dotti et al., 1987), axonal grains (Dennissen et al.,

2016) and presynaptic compartments (Zhou et al., 2017). In the postsynaptic compartment, tau binds to presynaptic vesicles through the transmembrane vesicle protein synaptogyrin-3, as found in the brain of AD patients (McInnes et al., 2018). A reduction of synaptogyrin-3 prevents the association of presynaptic tau with vesicles and may facilitate neurotransmitter release (McInnes et al., 2018).

In contrast, an unconventional secretory pathway is the one involving protein secretion through extracellular vesicles such as exosomes and microvesicles. This mechanism has been proposed to decrease the levels of some intracellular proteins (Simons and Raposo, 2009). Wang et al. (2017) have demonstrated that tau may be released via exosomes by neurons or cultured cells and the release of exosomes is enhanced by neuronal activity. Furthermore, Asai et al. (2015) have suggested that microglia may phagocytize tau-containing neurons and would secrete tau in exosomes, in order to facilitate its propagation to neurons. Recently, Katsinelos et al. (2018) have characterized a mechanism in which hyperphosphorylated tau is secreted through direct translocation across the plasma membrane. $PI(4,5)P_2$ and proteoglycans are involved in this secretion process.

Additionally, the involvement of larger extracellular vesicles, ectosomes, has been proposed (Dujardin et al., 2014).

Multivesicular bodies (MVBs; late endocytic compartments) can fuse with the plasma membrane to release intraluminal vesicles into the extracellular medium, and once secreted, these vesicles are called the exosomes (Fuster-Matanzo et al., 2015) (**Figure 1**). In contrast, microvesicles arise by outward budding of the plasma membrane (Simons and Raposo, 2009; Gangalum et al., 2011).

EXOSOMES AND INTERACTIONS WITH THE CELL SURFACE OF TARGET CELLS

Exosomes are defined as signaling organelles involved in health or in disease signaling pathways (Corrado et al., 2013). Measuring between 30 and 150 nm, these extracellular vesicles were first described almost 40 years ago (Trams et al., 1981). They are composed by a membrane that contains proteins like tetraspanins, flotillin and cell-specific receptors, and lipid rafts containing cholesterol, sphingomyelin and ceramide (DeLeo and Ikezu, 2018). The vesicle itself holds different types of proteins,

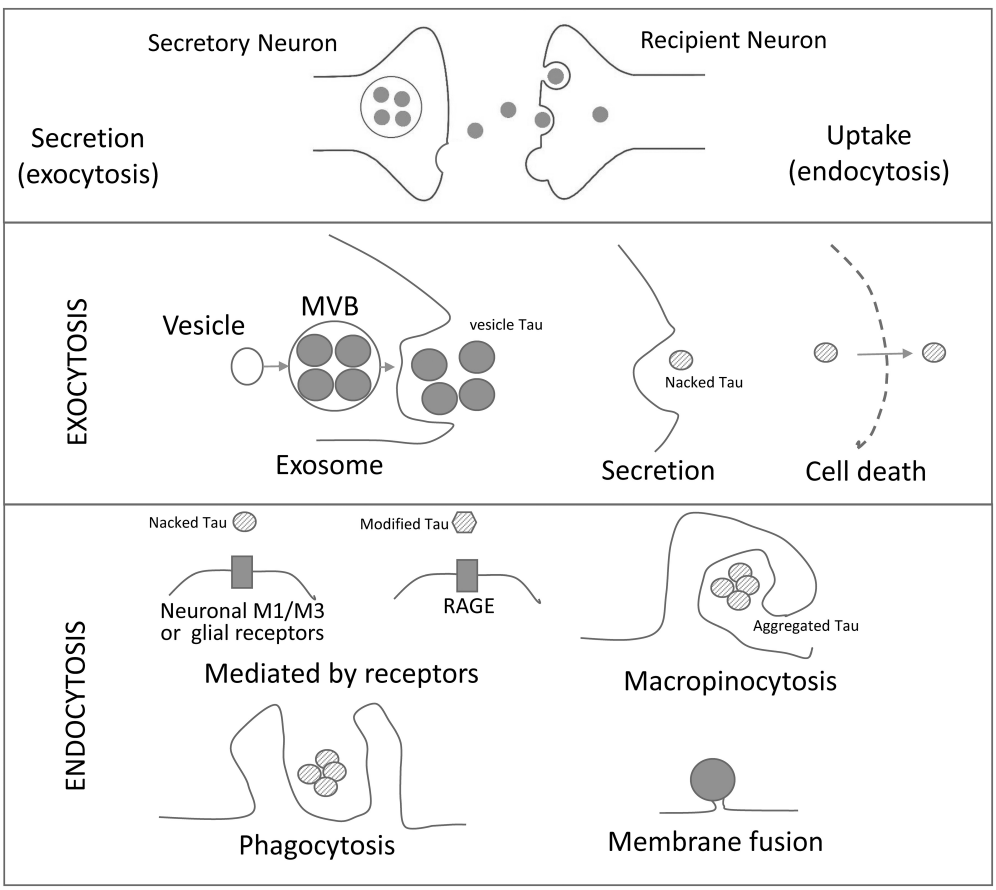

FIGURE 1 | Schematic Representation of Cell-to-Cell Transmission of Tau Pathology. Tau seeds are released from neurons by different exocytosic mechanisms (exosome, secretion and neuronal death). The released tau is taken up by neurons or glial cells by a variety of mechanisms (mediated by receptors, micropinocytosis, phagocytosis and/or membrane fusion of exosomes. RAGE: receptor for advanced glycation endproducts. M1/M3: muscarinic receptors.

nucleic acids (like miRNAs) or protein nucleic acid complexes depending of the cell types from which they are released (Corrado et al., 2013). Also, exosomes can also be found in several body fluids like plasma, saliva, urine, cerebrospinal fluid, amniotic fluid, colostrum, breast milk, synovial fluid, semen and pleural ascites (Corrado et al., 2013; McKelvey et al., 2015). For this reason, exosomes have been used as biomarkers of different diseases. Recently, a precipitation/immunoaffinity system has been developed to isolate neuron-derived as well as astrocyte-derived exosomes in the blood of Alzheimer's disease patients. Results from these studies suggest that neuronal exosomes from blood plasma and that measurement of certain forms of tau in neuronal exosomes can be used as a diagnostic and prognostic biomarker to the disease (Goetzl et al., 2018; Guix et al., 2018).

The membranes of some types of exosomes contain proteins with the capacity to interact with the plasma membrane proteins of their target cells. For instance, B-lymphocytes exosomes bear integrin that are capable to interact with fibroblasts (Clayton et al., 2004). However, less specific links, mainly through the extracellular matrix (Corrado et al., 2013), may contribute to the interaction with target cells. In general, several mechanisms have been put forward to explain the interaction of exosomes with target cells that results in cell membrane fusion, phagocytosis, macropinocytosis, and receptor-mediated endocytosis (McKelvey et al., 2015) (**Figure 1**).

NEURON-DERIVED EXOSOMES AND NEURODEGENERATION

Neuron-derived exosomes containing specific proteins related to neurological disorders can be released from the neurons affected. In the case of AD, the presence of exosomes containing tau or amyloid-β peptide has been reported. Exosomes can transport the amyloid-β peptide or fragments of its precursor protein (APP; Rajendran et al., 2006; Sharples et al., 2008; Perez-Gonzalez et al., 2012; Sardar Sinha et al., 2018). Furthermore, aggregated tau has been reported in brain exosomes of mouse models of tauopathy (Baker et al., 2016; Polanco et al., 2016). In these animal models, neuronal exosomes containing human mutated tau are toxic to the recipient neurons *in vivo* (Winston et al., 2018). Also, tau exosomes could be used as biomarkers not only for AD but also Down syndrome and Parkinson's disease (Shi et al., 2016; Hamlett et al., 2018). With respect to phosphorylation, tau secreted by exosomes is phosphorylated at some AD epitopes (Hampel et al., 2004; Saman et al., 2012).

Indeed, it has been suggested that the tau efflux from the Central Nervous System via exosomes is increased in Parkinson's disease but not in AD (Shi et al., 2016). However, exosomes containing tau protein have been found in human biofluids in AD patients (Fiandaca et al., 2015; Guix et al., 2018) and the release and *trans*-synaptic transmission of tau via exosomes has been also described (Wang et al., 2017).

TAU TRANSMISSION FROM CELL TO CELL

The exact mechanism of tau release is unclear, and some studies have demonstrated that both vesicle-bound and soluble free extracellular populations of tau exist (Saman et al., 2012; Kanmert et al., 2015; Wang et al., 2017). Furthermore, neuron death results in the release of tau into the extracellular space. Soluble-free tau protein can interact with M1/M3 muscarinic receptors which may be present, not only in neurons but also in some glia (Santello et al., 2019). The reception of tau by these receptors may lead to an increase in intracellular calcium (Gomez-Ramos et al., 2008; Diaz-Hernandez et al., 2010). On the other hand, extracellular tau reacts with fractalkine receptors in microglia (Bolos et al., 2017; Perea et al., 2018) and this interaction may contribute to tau propagation (Asai et al., 2015).

Tau propagation implicates its cellular uptake by surroundings cells. Clathrin-mediated endocytosis, micropinocytosis, or direct membrane fusion have been proposed as possible mechanisms of tau uptake (Christianson and Belting, 2014; Calafate et al., 2016; McInnes et al., 2018).

The discovery of tau spreading has prompted several researchers to focus on the development of tau antibodies as immunotherapies to block the cell-to-cell transmission of pathological tau (Boutajangout et al., 2011; Chai et al., 2011; Yanamandra et al., 2013; Dai et al., 2018).

FUTURE

Further research should address exosomes containing tau. These vesicles contain proteins and nucleic acids and sometimes complexes of both. Tau is a nucleic acid-binding protein (Villasante et al., 1981; Sultan et al., 2011) and, inside the exosome, it can be bound to a specific nucleic acid. This binding could result in conformational changes in the tau molecule, which would lead to diverse tau-prion strains (Holmes et al., 2013; Sharma et al., 2018). In summary, a better characterization of tau isoforms present in exosomes would help us to understand the mechanism of tau propagation.

AUTHOR CONTRIBUTIONS

All authors listed have made a substantial, direct and intellectual contribution to the work, and approved it for publication.

FUNDING

This study was funded by grants from Spanish Ministry of Science, Innovation and Universities (BFU2016-77885-P), the Comunidad de Madrid, through EU structural funds (S2017/BMD-3700 NEUROMETAD-CM), CIBERNED (ISCIII), and the Fundacion Ramon Areces.

REFERENCES

Arrasate, M., Perez, M., and Avila, J. (2000). Tau dephosphorylation at tau-1 site correlates with its association to cell membrane. *Neurochem. Res.* 25, 43–50.

Asai, H., Ikezu, S., Tsunoda, S., Medalla, M., Luebke, J., Haydar, T., et al. (2015). Depletion of microglia and inhibition of exosome synthesis halt tau propagation. *Nat. Neurosci.* 18, 1584–1593. doi: 10.1038/nn.4132

Avila, J., Lucas, J. J., Perez, M., and Hernandez, F. (2004). Role of tau protein in both physiological and pathological conditions. *Physiol. Rev.* 84, 361–384. doi: 10.1152/physrev.00024.2003

Baker, S., Polanco, J. C., and Gotz, J. (2016). Extracellular vesicles containing P301L mutant tau accelerate pathological tau phosphorylation and oligomer formation but do not seed mature neurofibrillary tangles in ALZ17 mice. *J. Alzheimers Dis.* 54, 1207–1217. doi: 10.3233/jad-160371

Bolos, M., Llorens-Martin, M., Perea, J. R., Jurado-Arjona, J., Rabano, A., Hernandez, F., et al. (2017). Absence of CX3CR1 impairs the internalization of Tau by microglia. *Mol. Neurodegener.* 12:59. doi: 10.1186/s13024-017-0200-1

Boutajangout, A., Ingadottir, J., Davies, P., and Sigurdsson, E. M. (2011). Passive immunization targeting pathological phospho-tau protein in a mouse model reduces functional decline and clears tau aggregates from the brain. *J. Neurochem.* 118, 658–667. doi: 10.1111/j.1471-4159.2011.07337.x

Brandt, R., Leger, J., and Lee, G. (1995). Interaction of tau with the neural plasma membrane mediated by tau's amino-terminal projection domain. *J. Cell Biol.* 131, 1327–1340. doi: 10.1083/jcb.131.5.1327

Calafate, S., Flavin, W., Verstreken, P., and Moechars, D. (2016). Loss of Bin1 promotes the propagation of Tau pathology. *Cell Rep.* 17, 931–940. doi: 10.1016/j.celrep.2016.09.063

Cantero, J. L., Hita-Yanez, E., Moreno-Lopez, B., Portillo, F., Rubio, A., and Avila, J. (2010). Tau protein role in sleep-wake cycle. *J. Alzheimers Dis.* 21, 411–421. doi: 10.3233/JAD-2010-100285

Chai, X., Wu, S., Murray, T. K., Kinley, R., Cella, C. V., Sims, H., et al. (2011). Passive immunization with anti-Tau antibodies in two transgenic models: reduction of Tau pathology and delay of disease progression. *J. Biol. Chem.* 286, 34457–34467. doi: 10.1074/jbc.M111.229633

Chesser, A. S., Pritchard, S. M., and Johnson, G. V. (2013). Tau clearance mechanisms and their possible role in the pathogenesis of Alzheimer disease. *Front. Neurol.* 4:122. doi: 10.3389/fneur.2013.00122

Christianson, H. C., and Belting, M. (2014). Heparan sulfate proteoglycan as a cell-surface endocytosis receptor. *Matrix Biol.* 35, 51–55. doi: 10.1016/j.matbio.2013.10.004

Clavaguera, F., Bolmont, T., Crowther, R. A., Abramowski, D., Frank, S., Probst, A., et al. (2009). Transmission and spreading of tauopathy in transgenic mouse brain. *Nat. Cell Biol.* 11, 909–913. doi: 10.1038/ncb1901

Clayton, A., Turkes, A., Dewitt, S., Steadman, R., Mason, M. D., and Hallett, M. B. (2004). Adhesion and signaling by B cell-derived exosomes: the role of integrins. *FASEB J.* 18, 977–979. doi: 10.1096/fj.03-1094fje

Corrado, C., Raimondo, S., Chiesi, A., Ciccia, F., De Leo, G., and Alessandro, R. (2013). Exosomes as intercellular signaling organelles involved in health and disease: basic science and clinical applications. *Int. J. Mol. Sci.* 14, 5338–5366. doi: 10.3390/ijms14035338

Dai, C. L., Hu, W., Tung, Y. C., Liu, F., Gong, C. X., and Iqbal, K. (2018). Tau passive immunization blocks seeding and spread of Alzheimer hyperphosphorylated Tau-induced pathology in 3 x Tg-AD mice. *Alzheimers Res. Ther.* 10:13. doi: 10.1186/s13195-018-0341-7

DeLeo, A. M., and Ikezu, T. (2018). Extracellular vesicle biology in alzheimer's disease and related tauopathy. *J. Neuroimmune Pharmacol.* 13, 292–308. doi: 10.1007/s11481-017-9768-z

Dennissen, F. J., Anglada-Huguet, M., Sydow, A., Mandelkow, E., and Mandelkow, E. M. (2016). Adenosine A1 receptor antagonist rolofylline alleviates axonopathy caused by human Tau DeltaK280. *Proc. Natl. Acad. Sci. U.S.A.* 113, 11597–11602. doi: 10.1073/pnas.1603119113

Diaz-Hernandez, M., Gomez-Ramos, A., Rubio, A., Gomez-Villafuertes, R., Naranjo, J. R., Miras-Portugal, M. T., et al. (2010). Tissue-nonspecific alkaline phosphatase promotes the neurotoxicity effect of extracellular tau. *J. Biol. Chem.* 285, 32539–32548. doi: 10.1074/jbc.M110.145003

Dotti, C. G., Banker, G. A., and Binder, L. I. (1987). The expression and distribution of the microtubule-associated proteins tau and microtubule-associated protein 2 in hippocampal neurons in the rat in situ and in cell culture. *Neuroscience* 23, 121–130. doi: 10.1016/0306-4522(87)90276-4

Drubin, D. G., and Kirschner, M. W. (1986). Tau protein function in living cells. *J. Cell Biol.* 103, 2739–2746. doi: 10.1083/jcb.103.6.2739

Dujardin, S., Begard, S., Caillierez, R., Lachaud, C., Delattre, L., Carrier, S., et al. (2014). Ectosomes: a new mechanism for non-exosomal secretion of tau protein. *PLoS One* 9:e100760. doi: 10.1371/journal.pone.0100760

Fiandaca, M. S., Kapogiannis, D., Mapstone, M., Boxer, A., Eitan, E., Schwartz, J. B., et al. (2015). Identification of preclinical Alzheimer's disease by a profile of pathogenic proteins in neurally derived blood exosomes: a case-control study. *Alzheimers Dement.* 11, 600.e1–607.e1. doi: 10.1016/j.jalz.2014.06.008

Frost, B., Jacks, R. L., and Diamond, M. I. (2009). Propagation of tau misfolding from the outside to the inside of a cell. *J. Biol. Chem.* 284, 12845–12852. doi: 10.1074/jbc.M808759200

Fuster-Matanzo, A., Gessler, F., Leonardi, T., Iraci, N., and Pluchino, S. (2015). Acellular approaches for regenerative medicine: on the verge of clinical trials with extracellular membrane vesicles? *Stem Cell Res. Ther.* 6:227. doi: 10.1186/s13287-015-0232-9

Gangalum, R. K., Atanasov, I. C., Zhou, Z. H., and Bhat, S. P. (2011). AlphaB-crystallin is found in detergent-resistant membrane microdomains and is secreted via exosomes from human retinal pigment epithelial cells. *J. Biol. Chem.* 286, 3261–3269. doi: 10.1074/jbc.M110.160135

Goetzl, E. J., Abner, E. L., Jicha, G. A., Kapogiannis, D., and Schwartz, J. B. (2018). Declining levels of functionally specialized synaptic proteins in plasma neuronal exosomes with progression of Alzheimer's disease. *FASEB J.* 32, 888–893. doi: 10.1096/fj.201700731R

Gomez-Ramos, A., Diaz-Hernandez, M., Cuadros, R., Hernandez, F., and Avila, J. (2006). Extracellular tau is toxic to neuronal cells. *FEBS Lett.* 580, 4842–4850. doi: 10.1016/j.febslet.2006.07.078

Gomez-Ramos, A., Diaz-Hernandez, M., Rubio, A., Miras-Portugal, M. T., and Avila, J. (2008). Extracellular tau promotes intracellular calcium increase through M1 and M3 muscarinic receptors in neuronal cells. *Mol. Cell Neurosci.* 37, 673–681. doi: 10.1016/j.mcn.2007.12.010

Guix, F. X., Corbett, G. T., Cha, D. J., Mustapic, M., Liu, W., Mengel, D., et al. (2018). Detection of aggregation-competent tau in neuron-derived extracellular vesicles. *Int. J. Mol. Sci.* 19:E663. doi: 10.3390/ijms19030663

Guo, T., Noble, W., and Hanger, D. P. (2017). Roles of tau protein in health and disease. *Acta Neuropathol.* 133, 665–704. doi: 10.1007/s00401-017-1707-9

Hamlett, E. D., Ledreux, A., Potter, H., Chial, H. J., Patterson, D., Espinosa, J. M., et al. (2018). Exosomal biomarkers in Down syndrome and Alzheimer's disease. *Free Radic. Biol. Med.* 114, 110–121. doi: 10.1016/j.freeradbiomed.2017.08.028

Hampel, H., Buerger, K., Kohnken, R., Teipel, S. J., Zinkowski, R., Moeller, H. J., et al. (2001). Tracking of Alzheimer's disease progression with cerebrospinal fluid tau protein phosphorylated at threonine 231. *Ann. Neurol.* 49, 545–546. doi: 10.1002/ana.111.abs

Hampel, H., Burger, K., Pruessner, J. C., Zinkowski, R., Debernardis, J., Kerkman, D., et al. (2005). Correlation of cerebrospinal fluid levels of tau protein phosphorylated at threonine 231 with rates of hippocampal atrophy in Alzheimer disease. *Arch. Neurol.* 62, 770–773.

Hampel, H., Teipel, S. J., Fuchsberger, T., Andreasen, N., Wiltfang, J., Otto, M., et al. (2004). Value of CSF beta-amyloid1-42 and tau as predictors of Alzheimer's disease in patients with mild cognitive impairment. *Mol. Psychiatry* 9, 705–710. doi: 10.1038/sj.mp.4001473

Holmes, B. B., Devos, S. L., Kfoury, N., Li, M., Jacks, R., Yanamandra, K., et al. (2013). Heparan sulfate proteoglycans mediate internalization and propagation of specific proteopathic seeds. *Proc. Natl. Acad. Sci. U.S.A.* 110, E3138–E3147. doi: 10.1073/pnas.1301440110

Huijbers, W., Schultz, A. P., Papp, K. V., Lapoint, M. R., Hanseeuw, B., Chhatwal, J. P., et al. (2019). Tau accumulation in clinically normal older adults is associated with hippocampal hyperactivity. *J. Neurosci.* 39, 548–556. doi: 10.1523/JNEUROSCI.1397-18.2018

Ittner, L. M., Ke, Y. D., Delerue, F., Bi, M., Gladbach, A., Van Eersel, J., et al. (2010). Dendritic function of tau mediates amyloid-beta toxicity in Alzheimer's disease mouse models. *Cell* 142, 387–397. doi: 10.1016/j.cell.2010.06.036

Kanmert, D., Cantlon, A., Muratore, C. R., Jin, M., O'malley, T. T., Lee, G., et al. (2015). C-Terminally truncated forms of Tau, but not full-length Tau or its C-terminal fragments, are released from neurons independently of cell death. *J. Neurosci.* 35, 10851–10865. doi: 10.1523/JNEUROSCI.0387-15.2015

Karch, C. M., Jeng, A. T., and Goate, A. M. (2012). Extracellular Tau levels are influenced by variability in Tau that is associated with tauopathies. *J. Biol. Chem.* 287, 42751–42762. doi: 10.1074/jbc.M112.380642

Katsinelos, T., Zeitler, M., Dimou, E., Karakatsani, A., Muller, H. M., Nachman, E., et al. (2018). Unconventional secretion mediates the trans-cellular spreading of Tau. *Cell Rep.* 23, 2039–2055. doi: 10.1016/j.celrep.2018.04.056

Kfoury, N., Holmes, B. B., Jiang, H., Holtzman, D. M., and Diamond, M. I. (2012). Trans-cellular propagation of Tau aggregation by fibrillar species. *J. Biol. Chem.* 287, 19440–19451. doi: 10.1074/jbc.M112.346072

Kim, W., Lee, S., Jung, C., Ahmed, A., Lee, G., and Hall, G. F. (2010). Interneuronal transfer of human tau between Lamprey central neurons in situ. *J. Alzheimers Dis.* 19, 647–664. doi: 10.3233/JAD-2010-1273

Lee, M. J., Lee, J. H., and Rubinsztein, D. C. (2013). Tau degradation: the ubiquitin-proteasome system versus the autophagy-lysosome system. *Prog. Neurobiol.* 105, 49–59. doi: 10.1016/j.pneurobio.2013.03.001

Lucey, B. P., Mccullough, A., Landsness, E. C., Toedebusch, C. D., Mcleland, J. S., Zaza, A. M., et al. (2019). Reduced non-rapid eye movement sleep is associated with tau pathology in early Alzheimer's disease. *Sci. Transl. Med.* 11:eaau6550. doi: 10.1126/scitranslmed.aau6550

McInnes, J., Wierda, K., Snellinx, A., Bounti, L., Wang, Y. C., Stancu, I. C., et al. (2018). Synaptogyrin-3 mediates presynaptic dysfunction induced by Tau. *Neuron* 97, 823.e8–835.e8. doi: 10.1016/j.neuron.2018.01.022

McKelvey, K. J., Powell, K. L., Ashton, A. W., Morris, J. M., and Mccracken, S. A. (2015). Exosomes: mechanisms of uptake. *J. Circ. Biomark.* 4:7. doi: 10.5772/61186

Medina, M., Hernandez, F., and Avila, J. (2016). New features about Tau function and dysfunction. *Biomolecules* 6:E21. doi: 10.3390/biom6020021

Mohamed, N. V., Desjardins, A., and Leclerc, N. (2017). Tau secretion is correlated to an increase of Golgi dynamics. *PLoS One* 12:e0178288. doi: 10.1371/journal.pone.0178288

Perea, J. R., Avila, J., and Bolos, M. (2018). Dephosphorylated rather than hyperphosphorylated Tau triggers a pro-inflammatory profile in microglia through the p38 MAPK pathway. *Exp. Neurol.* 310, 14–21. doi: 10.1016/j.expneurol.2018.08.007

Perez, M., Cuadros, R., Hernandez, F., and Avila, J. (2016). Secretion of full-length tau or tau fragments in a cell culture model. *Neurosci. Lett.* 634, 63–69. doi: 10.1016/j.neulet.2016.09.026

Perez-Gonzalez, R., Gauthier, S. A., Kumar, A., and Levy, E. (2012). The exosome secretory pathway transports amyloid precursor protein carboxyl-terminal fragments from the cell into the brain extracellular space. *J. Biol. Chem.* 287, 43108–43115. doi: 10.1074/jbc.M112.404467

Plouffe, V., Mohamed, N. V., Rivest-Mcgraw, J., Bertrand, J., Lauzon, M., and Leclerc, N. (2012). Hyperphosphorylation and cleavage at D421 enhance tau secretion. *PLoS One* 7:e36873. doi: 10.1371/journal.pone.0036873

Polanco, J. C., Scicluna, B. J., Hill, A. F., and Gotz, J. (2016). Extracellular vesicles isolated from the brains of rTg4510 mice seed Tau protein aggregation in a threshold-dependent manner. *J. Biol. Chem.* 291, 12445–12466. doi: 10.1074/jbc.M115.709485

Pooler, A. M., Phillips, E. C., Lau, D. H., Noble, W., and Hanger, D. P. (2013). Physiological release of endogenous tau is stimulated by neuronal activity. *EMBO Rep.* 14, 389–394. doi: 10.1038/embor.2013.15

Rajendran, L., Honsho, M., Zahn, T. R., Keller, P., Geiger, K. D., Verkade, P., et al. (2006). Alzheimer's disease beta-amyloid peptides are released in association with exosomes. *Proc. Natl. Acad. Sci. U.S.A.* 103, 11172–11177. doi: 10.1073/pnas.0603838103

Saman, S., Kim, W., Raya, M., Visnick, Y., Miro, S., Saman, S., et al. (2012). Exosome-associated tau is secreted in tauopathy models and is selectively phosphorylated in cerebrospinal fluid in early Alzheimer disease. *J. Biol. Chem.* 287, 3842–3849. doi: 10.1074/jbc.M111.277061

Santello, M., Toni, N., and Volterra, A. (2019). Astrocyte function from information processing to cognition and cognitive impairment. *Nat. Neurosci.* 22, 154–166. doi: 10.1038/s41593-018-0325-8

Sardar Sinha, M., Ansell-Schultz, A., Civitelli, L., Hildesjo, C., Larsson, M., Lannfelt, L., et al. (2018). Alzheimer's disease pathology propagation by exosomes containing toxic amyloid-beta oligomers. *Acta Neuropathol.* 136, 41–56. doi: 10.1007/s00401-018-1868-1

Sayas, C. L., Medina, M., Cuadros, R., Olla, I., Garcia, E., Perez, M., et al. (2019). Role of tau N-terminal motif in the secretion of human tau by end binding proteins. *PLoS One* 14:e0210864. doi: 10.1371/journal.pone.0210864

Shafiei, S. S., Guerrero-Munoz, M. J., and Castillo-Carranza, D. L. (2017). Tau oligomers: cytotoxicity, propagation, and mitochondrial damage. *Front. Aging Neurosci.* 9:83. doi: 10.3389/fnagi.2017.00083

Sharma, A., Bhattarai, P., and Sharma, A. (2018). eFAST for the diagnosis of a perioperative complication during percutaneous nephrolithotomy. *Crit. Ultrasound J.* 10, 7. doi: 10.1186/s13089-018-0088-1

Sharples, R. A., Vella, L. J., Nisbet, R. M., Naylor, R., Perez, K., Barnham, K. J., et al. (2008). Inhibition of gamma-secretase causes increased secretion of amyloid precursor protein C-terminal fragments in association with exosomes. *FASEB J.* 22, 1469–1478. doi: 10.1096/fj.07-9357com

Shi, M., Kovac, A., Korff, A., Cook, T. J., Ginghina, C., Bullock, K. M., et al. (2016). CNS tau efflux via exosomes is likely increased in Parkinson's disease but not in Alzheimer's disease. *Alzheimers Dement.* 12, 1125–1131. doi: 10.1016/j.jalz.2016.04.003

Simon, D., Garcia-Garcia, E., Royo, F., Falcon-Perez, J. M., and Avila, J. (2012). Proteostasis of tau. Tau overexpression results in its secretion via membrane vesicles. *FEBS Lett.* 586, 47–54. doi: 10.1016/j.febslet.2011.11.022

Simons, M., and Raposo, G. (2009). Exosomes–vesicular carriers for intercellular communication. *Curr. Opin. Cell Biol.* 21, 575–581. doi: 10.1016/j.ceb.2009.03.007

Sotiropoulos, I., Galas, M. C., Silva, J. M., Skoulakis, E., Wegmann, S., Maina, M. B., et al. (2017). Atypical, non-standard functions of the microtubule associated Tau protein. *Acta Neuropathol. Commun.* 5:91. doi: 10.1186/s40478-017-0489-6

Sultan, A., Nesslany, F., Violet, M., Begard, S., Loyens, A., Talahari, S., et al. (2011). Nuclear tau, a key player in neuronal DNA protection. *J. Biol. Chem.* 286, 4566–4575. doi: 10.1074/jbc.M110.199976

Trams, E. G., Lauter, C. J., Salem, N. Jr., and Heine, U. (1981). Exfoliation of membrane ecto-enzymes in the form of micro-vesicles. *Biochim. Biophys. Acta* 645, 63–70. doi: 10.1016/0005-2736(81)90512-5

Vanmechelen, E., Vanderstichele, H., Davidsson, P., Van Kerschaver, E., Van Der Perre, B., Sjogren, M., et al. (2000). Quantification of tau phosphorylated at threonine 181 in human cerebrospinal fluid: a sandwich ELISA with a synthetic phosphopeptide for standardization. *Neurosci. Lett.* 285, 49–52. doi: 10.1016/s0304-3940(00)01036-3

Vaz-Silva, J., Gomes, P., Jin, Q., Zhu, M., Zhuravleva, V., Quintremil, S., et al. (2018). Endolysosomal degradation of Tau and its role in glucocorticoid-driven hippocampal malfunction. *EMBO J.* 37:e99084. doi: 10.15252/embj.201899084

Villasante, A., Corces, V. G., Manso-Martinez, R., and Avila, J. (1981). Binding of microtubule protein to DNA and chromatin: possibility of simultaneous linkage of microtubule to nucleic and assembly of the microtubule structure. *Nucleic Acids Res.* 9, 895–908. doi: 10.1093/nar/9.4.895

Wang, Y., Balaji, V., Kaniyappan, S., Kruger, L., Irsen, S., Tepper, K., et al. (2017). The release and trans-synaptic transmission of Tau via exosomes. *Mol. Neurodegener.* 12:5. doi: 10.1186/s13024-016-0143-y

Wang, Y., Martinez-Vicente, M., Kruger, U., Kaushik, S., Wong, E., Mandelkow, E. M., et al. (2009). Tau fragmentation, aggregation and clearance: the dual role of lysosomal processing. *Hum. Mol. Genet.* 18, 4153–4170. doi: 10.1093/hmg/ddp367

Weingarten, M. D., Lockwood, A. H., Hwo, S. Y., and Kirschner, M. W. (1975). A protein factor essential for microtubule assembly. *Proc. Natl. Acad. Sci. U.S.A.* 72, 1858–1862. doi: 10.1073/pnas.72.5.1858

Weisenberg, R. C. (1972). Microtubule formation in vitro in solutions containing low calcium concentrations. *Science* 177, 1104–1105. doi: 10.1126/science.177.4054.1104

Winston, C. N., Goetzl, E. J., Baker, L. D., Vitiello, M. V., and Rissman, R. A. (2018). Growth hormone-releasing hormone modulation of neuronal exosome biomarkers in mild cognitive impairment. *J. Alzheimers Dis.* 66, 971–981. doi: 10.3233/JAD-180302

Yamada, K. (2017). Extracellular Tau and its potential role in the propagation of Tau pathology. *Front. Neurosci.* 11:667. doi: 10.3389/fnins.2017.00667

Yamada, K., Cirrito, J. R., Stewart, F. R., Jiang, H., Finn, M. B., Holmes, B. B., et al. (2011). In vivo microdialysis reveals age-dependent decrease of brain interstitial fluid tau levels in P301S human tau transgenic mice. *J. Neurosci.* 31, 13110–13117. doi: 10.1523/JNEUROSCI.2569-11.2011

Yamada, K., Holth, J. K., Liao, F., Stewart, F. R., Mahan, T. E., Jiang, H., et al. (2014). Neuronal activity regulates extracellular tau in vivo. *J. Exp. Med.* 211, 387–393. doi: 10.1084/jem.20131685

Yanamandra, K., Kfoury, N., Jiang, H., Mahan, T. E., Ma, S., Maloney, S. E., et al. (2013). Anti-tau antibodies that block tau aggregate seeding in vitro markedly decrease pathology and improve cognition in vivo. *Neuron* 80, 402–414. doi: 10.1016/j.neuron.2013.07.046

Zhou, L., Mcinnes, J., Wierda, K., Holt, M., Herrmann, A. G., Jackson, R. J., et al. (2017). Tau association with synaptic vesicles causes presynaptic dysfunction. *Nat. Commun.* 8:15295. doi: 10.1038/ncomms15295

Conflict of Interest Statement: The authors declare that the research was conducted in the absence of any commercial or financial relationships that could be construed as a potential conflict of interest.

frontiers in Neuroscience

BRIEF RESEARCH REPORT
published: 03 September 2019
doi: 10.3389/fnins.2019.00942

IFNγ-Stimulated Dendritic Cell Exosomes for Treatment of Migraine Modeled Using Spreading Depression

*Kae M. Pusic, Lisa Won, Richard P. Kraig and Aya D. Pusic**

Department of Neurology, The University of Chicago, Chicago, IL, United States

Migraine is a common headache disorder characterized by unilateral, intense headaches. In migraine with aura, the painful headache is preceded by focal neurological symptoms that can be visual, sensory, or motor in nature. Spreading depression (the most likely cause of migraine with aura and perhaps related headache pain) results in increased neuronal excitability and related increases in inflammation and production of reactive oxygen species. This in turn can promote the transformation of low-frequency, episodic migraine into higher-frequency and eventually chronic migraine. Though migraine affects 11% of adults worldwide, with 3% experiencing chronic headache, existing therapies offer only modest benefits. Here, we focus on the mechanisms by which environmental enrichment (i.e., volitionally increased intellectual, social, and physical activity) mitigates spreading depression. In prior work, we have shown that exposure to environmental enrichment reduces susceptibility to spreading depression in rats. This protective effect is at least in part due to environmental enrichment-mediated changes in the character of serum exosomes produced by circulating immune cells. We went on to show that environmental enrichment-mimetic exosomes can be produced by stimulating dendritic cells with low levels of interferon gamma (a cytokine that is phasically increased during environmental enrichment). Interferon gamma-stimulated dendritic cell exosomes (IFNγ-DC-Exos) significantly improve myelination and reduce oxidative stress when applied to hippocampal slice cultures. Here, we propose that they may also be effective against spreading depression. We found that administration of IFNγ-DC-Exos reduced susceptibility to spreading depression *in vivo* and *in vitro*, suggesting that IFNγ-DC-Exos may be a potential therapeutic for migraine.

Keywords: exosomes, dendritic cells, interferon gamma, environmental enrichment, oxidative stress, migraine, spreading depression

OPEN ACCESS

Edited by:
Grant Thomas Corbett, Brigham and Women's Hospital, Harvard Medical School, United States

Reviewed by:
Wensheng Lin, University of Minnesota Twin Cities, United States
Robert H. Miller, George Washington University, United States

***Correspondence:**
Aya D. Pusic
apusic@bsd.uchicago.edu

Specialty section:
This article was submitted to Neurodegeneration, a section of the journal Frontiers in Neuroscience

Received: *03 June 2019*
Accepted: *21 August 2019*
Published: *03 September 2019*

Citation:
Pusic KM, Won L, Kraig RP and Pusic AD (2019) IFNγ -Stimulated Dendritic Cell Exosomes for Treatment of Migraine Modeled Using Spreading Depression. Front. Neurosci. 13:942. doi: 10.3389/fnins.2019.00942

INTRODUCTION

Migraine is a neurological disorder characterized by episodic severe and painful headaches lasting between 4 and 72 h. In one-third of migraine patients, headaches are preceded by focal neurological symptoms. Spreading depression (SD) is the most likely cause of migraine aura and perhaps related headache pain (Leao, 1944; Milner, 1958; Moskowitz et al., 1993; Noseda and Burstein, 2013; Pietrobon and Moskowitz, 2013). Production of the pro-inflammatory cytokine

tumor necrosis factor alpha (TNFα) is increased following SD (Kunkler et al., 2004). TNFα enhances synaptic efficacy by increasing membrane expression of excitatory α-amino-3-hydroxy-5-methyl-4-isoxazolepropionic acid receptors and decreasing membrane expression of inhibitory γ-aminobutyric acid-A receptors (Stellwagen et al., 2005). Increased neuronal excitability in turn leads to increased production of reactive oxygen species, both of which promote subsequent occurrence of SD (Grinberg et al., 2012, 2013). This feedback cycle may be involved in the transformation of low-frequency migraine to higher-frequency and chronic migraine.

Our lab studies the mechanisms underlying environmental enrichment-based neuroprotection. Environmental enrichment (EE) consists of exposure to increased physical, intellectual and social activity, and has wide-ranging physiological and behavioral effects, including enhancing cognition, memory, learning, behavior and motor coordination (van Praag et al., 2000). Although the majority of EE studies have been conducted in rodents, it has been determined that EE is effective in a wide variety of animals, including non-human primates (Singhal et al., 2014). To date, these animal studies have shown that EE has beneficial effects in neurological diseases such as Huntington's disease (van Dellen et al., 2000), Alzheimer's disease (Jankowsky et al., 2005), and traumatic brain injury (Passineau et al., 2001). While it is more difficult to determine the effect of a robust EE paradigm in human patients, there is significant evidence that EE (which in humans includes "creative thought") is likewise beneficial in humans.

Exposure to increased physical exercise is an important component of EE, and has been linked to improved outcomes in several neurological disorders, including depression (Strohle et al., 2010), schizophrenia (Beebe et al., 2005), epilepsy (Arida et al., 2010) and migraine (Darabaneanu et al., 2011; Varkey et al., 2011; Irby et al., 2016; Lemmens et al., 2019). Engaging in increased intellectual activity, another component of EE, is thought to play a role in creating a "cognitive reserve" that lessens the impact of brain diseases on cognitive impairment (Stern, 2012; Crescentini et al., 2014). Likewise, numerous studies report that social engagement and an active lifestyle can protect against dementia (Fratiglioni et al., 2004). In addition, EE has well-documented effects on the immune system. Much of this work has been conducted in the context of immune (dys)function with age or in response to infection. This is important, as age is a critical factor in the progression of many neurological diseases (Mattson et al., 2002; Sim et al., 2002). Despite the many benefits of EE, clinical implementation may be difficult. As a result, we have studied the signaling involved in EE-based neuroprotection with the goal of developing effective mimetics as an alternative.

We first focused on exosomes derived from the serum of EE-exposed rats. When applied to hippocampal slice cultures or nasally administered to naïve rats, these exosomes significantly increase myelin content, oligodendrocyte precursor cell and neural stem cell levels, and reduce oxidative stress (Pusic and Kraig, 2014). We next used rat bone marrow-derived dendritic cells (DCs) as a scalable, exogenous source of similarly pro-myelinating exosomes. Primary rat DC cultures were stimulated with low-level interferon gamma (IFNγ), a pro-inflammatory cytokine that phasically increases during EE. Exosomes released by IFNγ-stimulated DCs (IFNγ-DC-Exos) also increase myelination and oxidative tolerance *in vitro* and *in vivo* (Pusic A. D. et al., 2014).

Since EE has been clinically shown to reduce migraine frequency (Darabaneanu et al., 2011; Varkey et al., 2011), we also explored the mechanism of EE-mediated mitigation of SD. We found that exposure to an EE paradigm significantly reduces SD susceptibility in rats (Pusic K. M. et al., 2014). Mimicking the cytokine signaling of EE through administration of interleukin-11, insulin-like growth factor-1 or phasic administration of IFNγ likewise reduced susceptibility to SD (Pusic K. M. et al., 2014; Pusic and Kraig, 2015; Grinberg et al., 2017).

Based on the body of work outlined above, work presented here takes the next logical step to determine whether EE mimetic IFNγ-DC-Exos are also protective against SD. Treatment with IFNγ-DC-Exos reduced susceptibility to SD in hippocampal slice cultures. When nasally administered to rats, IFNγ-DC-Exos reduced susceptibility to SD, promoted a reduction in microglial M1 product iNOS, and reduced oxidative-stress mediated damage. These results provide the first evidence that IFNγ-DC-Exos, a naturally occurring biologic, is effective against SD. Accordingly, further study of this biologic as a potential therapeutic for migraine is warranted.

METHODS

Animal Care

Wistar rats were obtained from Charles River Laboratories (Wilmington, MA, United States) and were used in accordance with the University of Chicago Animal Care and Use Committee. Untimed pregnant Wistar female rats were single-housed with Enviro-dri paper bedding (Shepherd, Watertown, TN, United States) and Nestlets (Ancare Corporation, Bellmore, NY, United States) and pups (culled to ten at birth) were used for hippocampal slice cultures. Male Wistar rats (10–12 weeks old) were double-housed and used for bone marrow isolations.

Slice Culture Preparation and Use

P9–P10 rat pups were used to make hippocampal slice cultures (350 μm) as previously described (Kunkler and Kraig, 1997). After 18 days *in vitro* (DIV) cultures were transferred to a serum-free medium, which does not activate microglia and does not contain horse serum-derived exosomes, thus allowing for accurate assessment of the impact of exosome treatments (Pusic and Kraig, 2014). Cultures were used when mature, at 21–35 DIV. All cultures were screened for viability by staining with Sytox (Invitrogen, Carlsbad, CA, United States), a fluorescent cell death marker. Cultures with any evidence of pyramidal cell layer death were excluded.

Exosome treatments were applied to the media of slice cultures and incubated for 3 days. Treatments consisted of 100 μg of exosomes in 50 μL. All experimental measurements were compared to age-matched control slice cultures.

Slice culture electrophysiology was performed as previously described (for details see Pusic et al., 2011). Briefly, a

hippocampal slice culture insert was placed in a 35 mm culture dish filled with 1.5 mL of serum-free culture medium and secured in place. A sterile cotton strip saturated in medium was placed along the inner wall of the insert to provide necessary humidity. Next, the insert-dish assembly sealed with polyvinyl chloride wrap (Thermo Fisher Scientific, Waltham, MA, United States) and placed into a recording chamber (PDMI-2; Harvard Apparatus, Holliston, MA, United States) that maintains temperature at 36°C and 5% carbon dioxide, 95% air. Recording microelectrodes and a specially fabricated bipolar stimulating electrode were positioned into slice cultures using WR 60 manipulators (Narishige International, Amytiville, NY, United States) on an inverted microscope stage (DMIRBE; Leica, Wetzlar, Germany).

Interstitial DC recordings were made using an Axoprobe A1 amplifier system coupled to a Digidata 1422A analog-digital conversion board (Axon Instruments, Burlington, CA, United States). Bipolar electrical stimuli were provided via a digital Master-8 stimulator (A.M.P. Instruments, Jerusalem, Israel) coupled to a model BSI-2 isolator (Bak Electronics, Inc., Umatilla, FL, United States). To determine SD threshold, stimulation [10 pulses, 10 Hz (100 μs/pulse)] was applied at half the current required for eliciting maximal field potential, and increased (every 3 min) until SD was induced.

Isolation of Dendritic Cells

Immature bone marrow cells were isolated from Wistar rats, as previously described (Powell et al., 2003; Pusic A. D. et al., 2014). Briefly, animals were anesthetized with progressive exposure to 100% carbon dioxide and then immediately decapitated. Using aseptic techniques, bone marrow was aspirated out of the femurs and tibias and stromal cells were purified through the passage of bone and debris through a strainer. Red blood cell lysis buffer (0.15 M NH_4Cl, 10 mM $KHCO_3$, and 0.1 mM EDTA) was used to remove the red blood cells. Cells were then washed and plated in 6-well plates at a density of 10^6 cells/mL in RPMI 1640 (Invitrogen) containing 10% FBS (Invitrogen) and 20 ng/mL of GM-CSF (PeproTech Inc., Rocky Hill, NJ, United States) for differentiation into bone marrow derived DCs. Media was changed on day two and five. DCs in suspension were harvested on day seven and transferred to new plates.

Generation and Isolation of Dendritic Cell-Derived Exosomes

For generation of DC exosomes, media was prepared using 10% exosome-depleted FBS (System Biosciences, Palo Alto, CA). Day seven bone marrow dendritic cells were plated at 10^6 cells/mL and placed in media alone or stimulated with media containing 500U of IFNγ (R&D Systems, Minneapolis, MN, United States). Three days later, culture media was collected and spun down to remove any cells and debris. Exosomes were then isolated using ExoQuick (System Biosciences). ExoQuick was added to culture media at a ratio of 1:5, incubated at 4°C overnight, and exosomes were precipitated by centrifugation at 2000×*g* for 30 min. The exosome pellet was resuspended in 100 μL of sterile phosphate buffered saline at a pH of 7.3. Isolation of exosomes was confirmed via immunoblot for two exosomal protein markers, CD63 and Alix (AbD Serotec, Kidlington, United Kingdom) (Schorey and Bhatnagar, 2008) and electron microscopy (Thery et al., 2006) (data not shown). Quantification of exosomes was performed by BCA assay (Thermo Fisher Scientific) of protein content.

Intranasal Administration of IFNγ-DC-Exos

Wistar rats were nasally administered exosome preparations as previously described (Pusic A. D. et al., 2014). Briefly, rats were placed in a fume hood with a heat lamp and thermo-regulator to maintain temperatures at 37°C. Isoflurane (Butler Schein Animal Health, Dublin, OH, United States) anesthesia was delivered via a nose cone (five percent induction and two-three percent maintenance, delivered in oxygen). Animals were placed in a supine position, and 100 μg of exosomes in 50 μL were administered over a 20 min period at a rate of 5 μL every 2 min to alternating nostrils (Liu et al., 2001). Sham animals were administered 50 μL of sodium succinate vehicle alone, following the protocol above.

One or three days later, animals were anesthetized with progressive exposure to 100% carbon dioxide and decapitated. Brains were rapidly removed, flash frozen in isopentane, and stored at −80°C until further use.

Whole Animal Electrophysiology

Whole animal SD recordings were completed using aseptic techniques (Kraig et al., 1991; Pusic K. M. et al., 2014). Male Wistar (300–400 gm) rats were anesthetized with isoflurane in oxygen (five percent induction, three percent during surgical procedures, two-three percent during recordings) via inhalational mask with outflow gas exhausted via vacuum to prevent room contamination. Arterial oxygen was monitored throughout with an oximeter (Nonin Medical, Plymouth, MN, United States) and ranged from 95 to 100%. Animals were continuously monitored for uniform respiratory rate and depth of respiration as well as animal color and periodic absence of withdrawal to hind paw pinch (National Research Council, 2011; Tremoleda et al., 2012).

Once anesthetized, animals were mounted in a standard table-top nose clamp and ear bars and kept warm with an overhead infrared lamp to keep core temperature at 37°C in preparation for cranial surgery. Eyes were coated with Artificial Tears (Akorn, Lake Forest, IL, United States) and the head was shaved and cleansed with Betadine (Purdue Products L.P., Stamford, CT, United States). Next, 0.05 mL of 0.25% Bupivacaine (Hospira Inc., Lake Forest, IL, United States) was injected subcutaneously to either side of what would become a midline scalp incision minutes later. A midline scalp incision was made from just behind the eyes to the lambdoid suture area. The skin was spread laterally and skull scraped free of connective tissue. Skull hemostasis was achieved using Bone Wax (CP Medical Inc., Portland, OR, United States). Two 1–2 mm craniotomies were made in the left skull under saline cooling and without damaging the underlying dura. The KCl stimulation craniotomy was placed

−2.0 mm from bregma and 1.5 mm to the left of the sagittal suture. The recording craniotomy was placed −6.0 mm from bregma and 4.5 mm lateral to the sagittal suture.

After craniotomy surgery, anesthetized animals were quickly transferred to a stereotaxic recording setup where gaseous anesthesia, oxygen monitoring, and warming was continued. The skull was warmed (37°C) directly with sterile saline superfusion. For interstitial DC recordings, a 2–4 μm tip microelectrode was positioned 750 μm below the pial surface at the posterior craniotomy with a Canberra micromanipulator (Narishige) and recordings begun using an Axoprobe A1 amplifier system and Digidata 1422A analog-digital conversion board run on a PC-based computer system. For KCl-induced SD threshold measurements, a microelectrode with tip broken to 8–12 μm (1.0 mm outside diameter, 0.58 mm inside diameter; Sutter Lambda SC, Novato, CA, United States) and filled with 0.5 M KCl was positioned 750 μm below the pial surface at the anterior craniotomy. Micro-injections of KCl were administered via pressure from a Picospritzer-II electronic valve system (Parker Hannifin, Hollis, NH, United States), whose injection periods were registered directly to the permanent digital recording of interstitial DC potential changes (Grinberg et al., 2017). Injections of KCl were doubled in duration every four-to-five minutes if the previous injection failed to elicit an SD. Upon successful SD induction (i.e., SD threshold), the injection electrode was pulled up and an injection of the same pressure and duration was reproduced into 3-In-ONE^{TM} light machine oil (WD-40 Company, San Diego, CA, United States) contained in a depression well microscope slide (VWR Scientific Products, Buffalo Grove, IL, United States). The injection volume was calculated by measuring the injection sphere diameter in oil with a calibrated eye-piece micrometer on a compound microscope. As previously noted (Grinberg et al., 2017), injection volumes measured from injection into machine oil likely do not fully reflect injections made *in vivo* (Nicholson, 2001). However, any discrepancies would not be consequential as they would be a systemic error that would be equally applied to all experimental conditions.

Protein Carbonyl Measurement

Protein carbonyl levels were measured utilizing the Protein Carbonyl Content Assay Kit (Abcam, Cambridge, MA, United States) according to manufacturer's protocol. Briefly, protein was extracted from the neocortex of animals nasally administered IFNγ-DC-Exos or sodium succinate vehicle (sham) using RIPA buffer. Protein homogenate was treated with streptozocin to remove any nucleic acid contaminates. Samples were reacted with 2, 4-Dinitrophenylhydrazine followed by quantification of the acid hydrazones at 405 nm. BCA assays (Thermo Fisher Scientific) were simultaneously run and a standard curve constructed for the calculation of protein carbonyl content based on optical density.

RT-qPCR

RNA was isolated by TRIzol extraction followed by miRNeasy mini kit (Qiagen, Hilden, Germany) spin column-based purification. Total RNA concentrations were determined using a Take3 Micro-Volume plate, read in a Synergy HTX multi-mode reader (BioTek Instruments, Winooski, VT, United States). Equal amounts of RNA for each sample were reverse transcribed in a T100 thermocycler (Bio-Rad, Hercules, CA, United States) using the iScript cDNA synthesis kit (Bio-Rad) following manufacturer's protocol. Real-time PCR reactions were performed using iQ SYBR Green Supermix (Bio-Rad) on the CFX96 Real Time PCR Detection System (Bio-Rad). All primers (see **Table 1**) were used at 10 nM (Integrated DNA Technologies, Inc., Coralville, IA, United States). Each sample was normalized to an endogenous control, Rpl13a, and the fold changes for each gene assayed was determined via the delta Ct method (Pfaffl, 2001).

Data Handling and Statistics

All data were analyzed using SigmaStat software (Systat Software Inc., San Jose, CA, United States). All data were subject to normality testing (p-value to reject: 0.05). Controls in each treatment group were scaled to 1.0 with experimental data scaled proportionally and expressed as mean ± standard error of the mean. Statistical tests are noted in the figure legends.

RESULTS

IFNγ-DC-Exos Increased SD Threshold in Slice Cultures

Preliminary work to determine the efficacy of IFNγ-DC-Exos at increasing SD threshold was done in hippocampal slice cultures. Slice cultures were treated with 100 μg of IFNγ-DC-Exos (as before, see Pusic A. D. et al., 2014) or left untreated (Control) and SD threshold measured three days later. Treatment with IFNγ-DC-Exos evoked a significant, greater than 12-fold increase

TABLE 1 | RT-qPCR Primer Sequences.

Gene	GenBank Accession #	Primer	Sequence (5′–3′)
TNFα	NM_012675.3	F R	ACCACGCTCTTCTGTCTACTGA CTGATGAGAGGGAGCCCATTTG
IL-11	NM_133519.4	F R	GCTGACAAGGCTTCGAGTAG TCTTTAGGGAAGGACCAGCT
CD32	NM_175756.1	F R	CCAAACTCGGAGAGAAGCCT CTTCGGAAGACCTGCATGAGA
CD86	NM_020081.1	F R	GAGCTCTCAGTGATCGCCAA CAAACTGGGGCTGCGAAAAA
Arg-1	NM_017134.3	F R	TGGACCCTGGGGAACACTAT GTAGCCGGGGTGAATACTGG
CD206	NM_001106123.2	F R	AGTCTGCCTTAACCTGGCAC AGGCACATCACTTTCCGAGG
iNOS	NM_012611.3	F R	AGAGACGCTTCTGAGGTTCC GTTGTTGGGCTGGGAATAGC
TGFβ	NM_031131.1	F R	ACCGCAACAACGCAATCTATG TTCCGTCTCCTTGGTTCAGC
IL-10	NM_012854.2	F R	GCTCAGCACTGCTATGTTGC AATCGATGACAGCGTCGCA
Rpl13α	NM_173340.2	F R	TTGCTTACCTGGGGCGTCT CCTTTTCCTTCCGTTTCTCCTC

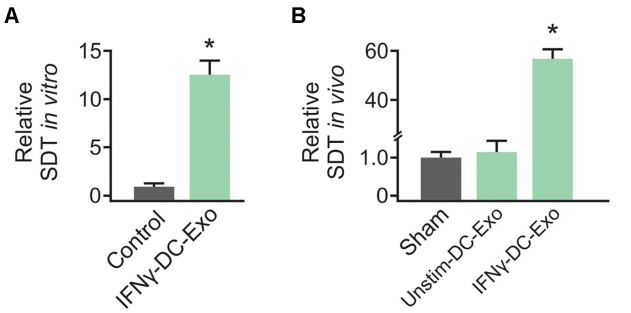

FIGURE 1 | IFNγ-DC-Exosomes increase spreading depression threshold *in vitro* and *in vivo*. **(A)** When applied to naïve hippocampal slice cultures, IFNγ-stimulated dendritic cell exosomes (IFNγ-DC-Exos) significantly (*$p \leq 0.001$) increased spreading depression threshold three days later, compared to untreated control slices. **(B)** Nasally administering IFNγ-DC-Exos to rats likewise significantly (*$p \leq 0.001$) increased the threshold to neocortical spreading depression one day later when compared to untreated sham animals, or animals nasally administered unstimulated dendritic cell exosomes (Unstim-DC-Exos). Significance determined by ANOVA plus *post hoc* Holm-Sidak testing.

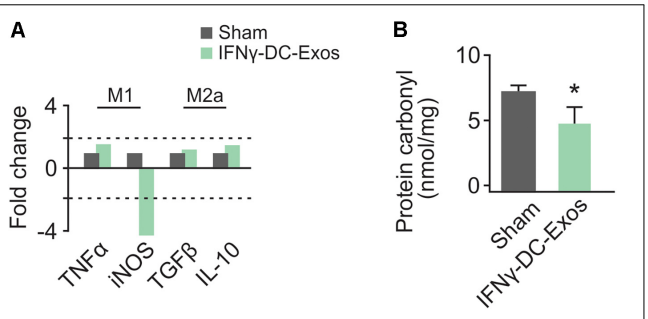

FIGURE 2 | Nasal administration of IFNγ-DC-Exosomes reduces oxidative stress. **(A)** Nasal administration of IFNγ-DC-Exos significantly reduced expression of the M1 polarization product iNOS by 4.37-fold compared to expression levels in Sham animals. Significance was determined by greater than 2-fold change. Though there was no significant change in other M1 and M2a markers measured, this reduction in iNOS was reflected by a similarly significant (*$p = 0.035$) reduction in **(B)** protein carbonyl content in Sham versus IFNγ-DC-Exo-treated animals. Significance determined by ANOVA plus *post hoc* Holm-Sidak testing.

in SD threshold compared to untreated control slices. Specific values were: Control: 1.00 ± 0.45; IFNγ-DC-Exos: 12.5 ± 1.52 (n = 8/group) (**Figure 1A**). This allowed us to proceed to *in vivo* experiments.

Nasal Administration of IFNγ-DC-Exos Increased SD Threshold

Male Wistar rats were nasally administered IFNγ-DC-Exos (100 μg in 50 μL), unstimulated dendritic cell exosomes (unstim-DC-Exos) or vehicle alone (control/sham) and SD threshold determined one day later. IFNγ-DC-Exo treatment significantly increased threshold to SD when compared to age and treatment-matched sham and age-matched untreated control animals. Specific values were: Sham: 1.00 ± 0.14; unstim-DC-Exo: 1.10 ± 0.28; IFNγ-DC-Exos: 57.0 ± 4.27 (n = 3–5/group) (**Figure 1B**).

Nasal Administration of IFNγ-DC-Exos Altered Microglial Polarization

As no significant differences have been observed in unstim-DC-Exo treated versus sodium succinate-treated animals thus far, we proceeded with IFNγ-DC-Exos versus sodium succinate (Sham) for subsequent experiments. Male Wistar rats were once again nasally administered IFNγ-DC-Exos or sodium succinate. One day later, brains were harvested and RT-qPCR was performed for M1 and M2a gene expression. M1 polarization was determined by measuring expression levels of M1 products TNFα and iNOS. Similarly, M2a polarization was determined by measuring expression levels of M2a products TGFβ and IL-10. A significant decrease (4.37-fold) was found in iNOS mRNA expression in IFNγ-DC-Exo- treated brains versus untreated brains, though no significant change (<2-fold) was seen in M1-specific TNFα or M2a-specific TGFβ and IL-10 mRNA levels (**Figure 2A**). This may indicate that IFNγ-DC-Exo treatment reduces M1 microglial polarization, as microglia are a primary source of iNOS in the CNS (Dringen, 2005).

Nasal Administration of IFNγ-DC-Exos Reduced Protein Carbonyl Content

Neocortical tissue was collected for determination of protein carbonyl content three days after nasal administration. Although protein carbonylation is reactive oxygen species-mediated and does not encompass reactive nitrogen species-mediated damage, its measurement is accepted as a reliable indicator for the extent of oxidative damage (Ghezzi and Bonetto, 2003). Relative to sham animals administered vehicle alone, IFNγ-DC-Exo-treated rat brains contained significantly reduced baseline levels of carbonylated protein [Sham: 7.25 ± 0.83 (n = 7); IFNγ-DC-Exos: 4.58 ± 0.55 (n = 5)] (**Figure 2B**).

DISCUSSION

This study is based on the premise that EE has great potential as a therapeutic for a wide range of neurological disorders, including migraine. A large body of literature provides evidence suggesting that EE has a beneficial impact on human brain health. Unfortunately, it can be prohibitively difficult to implement a robust EE paradigm in patients. As a result, there is increased interest in development of effective EE-mimetics (McOmish and Hannan, 2007). To this end, our lab studies the role of exosomes in EE and the use of dendritic cells as a scalable *ex vivo* source of EE-mimetic exosomes.

In prior work, we have shown that IFNγ-stimulated dendritic cell-derived exosomes reduce oxidative stress and improve recovery from a demyelinating injury in slice cultures (Pusic A. D. et al., 2014). We have also illustrated a link between myelin integrity and susceptibility to SD (Pusic et al., 2015). This led us to explore the ability of IFNγ-DC-Exos to mitigate SD as a model of migraine with aura.

Here, we demonstrate that IFNγ-DC-Exos indeed protect against SD. The ∼12-fold increase in SD threshold in slice cultures was modest, but encouraging. In the *in vivo* condition, IFNγ-DC-Exos produced a much more robust, 57-fold increase in SD threshold. While this is roughly equivalent to the protection seen with nasally administered IFNγ (∼63-fold; Pusic and Kraig, 2015), administration of IFNγ-DC-Exos does not have the same potential for negative side effects as use of a pro-inflammatory cytokine does.

Crosstalk between inflammation and oxidative stress is likely involved in SD. In prior work, we have shown that microglial polarization state is a key factor in determining SD susceptibility. Microglia, like macrophages, can be polarized by cytokines and other factors in the microenvironment to adopt anti- or pro-inflammatory phenotypes with distinct functions. These phenotypic types range from a classically activated (M1) state to an alternatively activated (M2a) state (Ransohoff and Perry, 2009). It is important to note that these polarization states are plastic, and the classifications designated here represent extremes along a spectrum of phenotypes.

Spreading depression creates an M1-skewed microglial phenotype that may increase susceptibility to subsequent SD (Pusic K. M. et al., 2014). M1 microglia produce reactive oxygen species and pro-inflammatory cytokines, including TNFα which can increase neuronal excitability and promote initiation of SD (Durafourt et al., 2012; Grinberg et al., 2012, 2013; Ajmone-Cat et al., 2013). This pro-inflammatory environment may also be responsible for transient gray matter myelin disruption following SD (Pusic et al., 2015). Conditions of increased inflammation and oxidative stress deplete intracellular glutathione levels and activate neutral sphingomyelinase-2 (Liu et al., 1998; Jana and Pahan, 2007). Myelin contains neutral sphingomyelinases (Chakraborty et al., 1997) whose activity leads to sphingomyelin hydrolysis, ceramide formation and other downstream reactions with deleterious effects on myelin integrity. Given that demyelination in the cuprizone model of MS increases susceptibility to SD (Hoffmann et al., 2008), we suggest that SD-induced demyelination may also contribute to increased SD susceptibility by enhancing aberrant excitability, via ephaptic transmission between demyelinated fibers.

Nasal administration of IFNγ-DC-Exos reduced levels of iNOS mRNA (a product of M1 polarization) and decreased protein carbonyl content, suggesting that IFNγ-DC-Exos create an environment of decreased oxidative stress. This conclusion is supported by prior work demonstrating that IFNγ-DC-Exo treatment reduces menadione-induced oxidative stress and increases microglial glutathione in hippocampal slice cultures (Pusic A. D. et al., 2014). While we acknowledge that other neuronal cell types produce iNOS, microglia are a major cellular source in the CNS (Dringen, 2005). Furthermore, we have previously shown that rats exposed to EE have significantly lower M1 and higher M2a levels than non-enriched animals, and found evidence that EE protection against SD is in part mediated by decreased generation of oxidants and pro-inflammatory cytokines from M1 microglia (Pusic K. M. et al., 2014).

Finally, we have demonstrated in several instances (Pusic and Kraig, 2014; Pusic A. D. et al., 2014) that exosomes can be nasally administered to impact brain function. Here, we have extended those studies to show that nasal administration of exosomes can effectively decrease susceptibility to SD in an *in vivo* model of migraine. While we can infer that exosomes enter the CNS through measurement of these functional effects, we have not yet directly tracked exosomes through imaging studies. Future studies should also involve tracking exosomes post-nasal administration to whole animals to determine the efficiency of this delivery route to the brain, the rate of entry and clearance, and cellular uptake.

In conclusion, work here discusses several mechanisms by which exosome-based neuroimmune signaling contributes to neuroprotection resulting from EE, and advocates use of EE-mimetic exosomes as neurotherapeutics.

DATA AVAILABILITY

The datasets generated for this study are available on request to the corresponding author.

ETHICS STATEMENT

Animal Subjects: The animal study was reviewed and approved by The University of Chicago Animal Care and Use Committee.

AUTHOR CONTRIBUTIONS

AP and KP conceived the study and wrote the manuscript. All authors performed the experiments and analyzed the data, read and commented on the final version of the manuscript and approved the submission.

FUNDING

This work was supported by the National Institutes of Health Common Fund, through the Office of Strategic Coordination/Office of the Director (UH2 TR000918 and UH3TR000918), core facilities funds from the National Center for Advancing Translational Sciences of the National Institutes of Health (UL1 TR000430) a CTSA award to AP from the National Center for Advanced Translational Sciences and the National Institute of Neurological Disorders and Stroke (NS-019108).

ACKNOWLEDGMENTS

We acknowledge the continued support from the Polsky Center for Entrepreneurship and Innovation at The University of Chicago for their assistance in our exosome-based research and patent portfolio that is directed to development of IFNγ-DC-Exos as a novel therapeutic for neurological disorders.

REFERENCES

Ajmone-Cat, M. A., Mancini, M., De Simone, R., Cilli, P., and Minghetti, L. (2013). Microglial polarization and plasticity: evidence from organotypic hippocampal slice cultures. *Glia* 61, 1698–1711. doi: 10.1002/glia.22550

Arida, R. M., Scorza, F. A., and Cavalheiro, E. A. (2010). Favorable effects of physical activity for recovery in temporal lobe epilepsy. *Epilepsia* 51(Suppl. 3), 76–79. doi: 10.1111/j.1528-1167.2010.02615.x

Beebe, L. H., Tian, L., Morris, N., Goodwin, A., Allen, S. S., and Kuldau, J. (2005). Effects of exercise on mental and physical health parameters of persons with schizophrenia. *Issues Ment. Health Nurs.* 26, 661–676. doi: 10.1080/01612840590959551

Chakraborty, G., Ziemba, S., Drivas, A., and Ledeen, R. W. (1997). Myelin contains neutral sphingomyelinase activity that is stimulated by tumor necrosis factor-alpha. *J. Neurosci. Res.* 50, 466–476.

Crescentini, C., Urgesi, C., Fabbro, F., and Eleopra, R. (2014). Cognitive and brain reserve for mind-body therapeutic approaches in multiple sclerosis: a review. *Restor. Neurol. Neurosci.* 32, 575–595. doi: 10.3233/rnn-130364

Darabaneanu, S., Overath, C. H., Rubin, D., Luthje, S., Sye, W., Niederberger, U., et al. (2011). Aerobic exercise as a therapy option for migraine: a pilot study. *Int. J. Sports Med.* 32, 455–460. doi: 10.1055/s-0030-1269928

Dringen, R. (2005). Oxidative and antioxidative potential of brain microglial cells. *Antioxid. Redox Signal.* 7, 1223–1233. doi: 10.1089/ars.2005.7.1223

Durafourt, B. A., Moore, C. S., Zammit, D. A., Johnson, T. A., Zaguia, F., Guiot, M. C., et al. (2012). Comparison of polarization properties of human adult microglia and blood-derived macrophages. *Glia* 60, 717–727. doi: 10.1002/glia.22298

Fratiglioni, L., Paillard-Borg, S., and Winblad, B. (2004). An active and socially integrated lifestyle in late life might protect against dementia. *Lancet Neurol.* 3, 343–353. doi: 10.1016/s1474-4422(04)00767-7

Ghezzi, P., and Bonetto, V. (2003). Redox proteomics: identification of oxidatively modified proteins. *Proteomics* 3, 1145–1153. doi: 10.1002/pmic.200300435

Grinberg, Y. Y., Dibbern, M. E., Levasseur, V. A., and Kraig, R. P. (2013). Insulin-like growth factor-1 abrogates microglial oxidative stress and TNF-alpha responses to spreading depression. *J. Neurochem.* 126, 662–672. doi: 10.1111/jnc.12267

Grinberg, Y. Y., van Drongelen, W., and Kraig, R. P. (2012). Insulin-like growth factor-1 lowers spreading depression susceptibility and reduces oxidative stress. *J. Neurochem.* 122, 221–229. doi: 10.1111/j.1471-4159.2012.07763.x

Grinberg, Y. Y., Zitzow, L. A., and Kraig, R. P. (2017). Intranasally administered IGF-1 inhibits spreading depression in vivo. *Brain Res.* 1677, 47–57. doi: 10.1016/j.brainres.2017.09.022

Hoffmann, K., Lindner, M., Groticke, I., Stangel, M., and Loscher, W. (2008). Epileptic seizures and hippocampal damage after cuprizone-induced demyelination in C57BL/6 mice. *Exp. Neurol.* 210, 308–321. doi: 10.1016/j.expneurol.2007.11.005

Irby, M. B., Bond, D. S., Lipton, R. B., Nicklas, B., Houle, T. T., and Penzien, D. B. (2016). aerobic exercise for reducing migraine burden: mechanisms, markers, and models of change processes. *Headache* 56, 357–369. doi: 10.1111/head.12738

Jana, A., and Pahan, K. (2007). Oxidative stress kills human primary oligodendrocytes via neutral sphingomyelinase: implications for multiple sclerosis. *J. Neuroimmune Pharmacol.* 2, 184–193. doi: 10.1007/s11481-007-9066-2

Jankowsky, J. L., Melnikova, T., Fadale, D. J., Xu, G. M., Slunt, H. H., Gonzales, V., et al. (2005). Environmental enrichment mitigates cognitive deficits in a mouse model of Alzheimer's disease. *J. Neurosci.* 25, 5217–5224. doi: 10.1523/jneurosci.5080-04.2005

Kraig, R. P., Dong, L. M., Thisted, R., and Jaeger, C. B. (1991). Spreading depression increases immunohistochemical staining of glial fibrillary acidic protein. *J. Neurosci.* 11, 2187–2198.

Kunkler, P. E., Hulse, R. E., and Kraig, R. P. (2004). Multiplexed cytokine protein expression profiles from spreading depression in hippocampal organotypic cultures. *J. Cereb. Blood Flow Metab* 24, 829–839. doi: 10.1097/01.Wcb.0000126566.34753.30

Kunkler, P. E., and Kraig, R. P. (1997). Reactive astrocytosis from excitotoxic injury in hippocampal organ culture parallels that seen in vivo. *J. Cereb. Blood Flow Metab.* 17, 26–43. doi: 10.1097/00004647-199701000-199701005

Leao, A. A. P. (1944). Spreading depression of activity in the cerebral cortex. *J. Neurophysiol.* 7, 359–390.

Lemmens, J., De Pauw, J., Van Soom, T., Michiels, S., Versijpt, J., van Breda, E., et al. (2019). The effect of aerobic exercise on the number of migraine days, duration and pain intensity in migraine: a systematic literature review and meta-analysis. *J. Headache Pain* 20:16. doi: 10.1186/s10194-019-0961-8

Liu, B., Andrieu-Abadie, N., Levade, T., Zhang, P., Obeid, L. M., and Hannun, Y. A. (1998). Glutathione regulation of neutral sphingomyelinase in tumor necrosis factor-alpha-induced cell death. *J. Biol. Chem.* 273, 11313–11320. doi: 10.1074/jbc.273.18.11313

Liu, X. F., Fawcett, J. R., Thorne, R. G., DeFor, T. A., and Frey, W. H. (2001). Intranasal administration of insulin-like growth factor-I bypasses the blood-brain barrier and protects against focal cerebral ischemic damage. *J. Neurol. Sci.* 187, 91–97.

Mattson, M. P., Chan, S. L., and Duan, W. (2002). Modification of brain aging and neurodegenerative disorders by genes, diet, and behavior. *Physiol. Rev.* 82, 637–672. doi: 10.1152/physrev.00004.2002

McOmish, C. E., and Hannan, A. J. (2007). Enviromimetics: exploring gene environment interactions to identify therapeutic targets for brain disorders. *Expert Opin. Ther. Targets* 11, 899–913. doi: 10.1517/14728222.11.7.899

Milner, P. M. (1958). Note on a possible correspondence between the scotomas of migraine and spreading depression of Leao. *Electroencephalogr. Clin. Neurophysiol.* 10:705.

Moskowitz, M. A., Nozaki, K., and Kraig, R. P. (1993). Neocortical spreading depression provokes the expression of c-fos protein-like immunoreactivity within trigeminal nucleus caudalis via trigeminovascular mechanisms. *J. Neurosci.* 13, 1167–1177.

National Research Council (2011). *Guide for the Care and Use of Laboratory Animals*, 8th Edn. Washington, DC: The National Academies Press.

Nicholson, C. (2001). Diffusion and related transport mechanisms in brain tissue. *Rep. Prog. Phys.* 64:815.

Noseda, R., and Burstein, R. (2013). Migraine pathophysiology: anatomy of the trigeminovascular pathway and associated neurological symptoms, CSD, sensitization and modulation of pain. *Pain* 154(Suppl. 1), S44–S53. doi: 10.1016/j.pain.2013.07.021

Passineau, M. J., Green, E. J., and Dietrich, W. D. (2001). Therapeutic effects of environmental enrichment on cognitive function and tissue integrity following severe traumatic brain injury in rats. *Exp. Neurol.* 168, 373–384. doi: 10.1006/exnr.2000.7623

Pfaffl, M. W. (2001). A new mathematical model for relative quantification in real-time RT-PCR. *Nucleic Acids Res.* 29, e45. doi: 10.1093/nar/29.9.e45

Pietrobon, D., and Moskowitz, M. A. (2013). Pathophysiology of migraine. *Annu. Rev. Physiol.* 75, 365–391. doi: 10.1146/annurev-physiol-030212-183717

Powell, T. J., Jenkins, C. D., Hattori, R., and MacPherson, G. G. (2003). Rat bone marrow-derived dendritic cells, but not ex vivo dendritic cells, secrete nitric oxide and can inhibit T-cell proliferation. *Immunology* 109, 197–208. doi: 10.1046/j.1365-2567.2003.01639.x

Pusic, A. D., Grinberg, Y. Y., Mitchell, H. M., and Kraig, R. P. (2011). Modeling neural immune signaling of episodic and chronic migraine using spreading depression in vitro. *J. Vis. Exp.* 52:e2910. doi: 10.3791/2910

Pusic, A. D., and Kraig, R. P. (2014). Youth and environmental enrichment generate serum exosomes containing miR-219 that promote CNS myelination. *Glia* 62, 284–299. doi: 10.1002/glia.22606

Pusic, A. D., and Kraig, R. P. (2015). Phasic treatment with interferon gamma stimulates release of exosomes that protect against spreading depression. *J. Interferon Cytokine Res.* 35, 795–807. doi: 10.1089/jir.2015.0010

Pusic, A. D., Mitchell, H. M., Kunkler, P. E., Klauer, N., and Kraig, R. P. (2015). Spreading depression transiently disrupts myelin via interferon-gamma signaling. *Exp. Neurol.* 264, 43–54. doi: 10.1016/j.expneurol.2014.12.001

Pusic, A. D., Pusic, K. M., Clayton, B. L., and Kraig, R. P. (2014). IFNgamma-stimulated dendritic cell exosomes as a potential therapeutic for remyelination. *J. Neuroimmunol.* 266, 12–23. doi: 10.1016/j.jneuroim.2013.10.014

Pusic, K. M., Pusic, A. D., Kemme, J., and Kraig, R. P. (2014). Spreading depression requires microglia and is decreased by their M2a polarization from environmental enrichment. *Glia* 62, 1176–1194. doi: 10.1002/glia.22672

Ransohoff, R. M., and Perry, V. H. (2009). Microglial physiology: unique stimuli, specialized responses. *Annu. Rev. Immunol.* 27, 119–145. doi: 10.1146/annurev.immunol.021908.132528

Schorey, J. S., and Bhatnagar, S. (2008). Exosome function: from tumor immunology to pathogen biology. *Traffic* 9, 871–881. doi: 10.1111/j.1600-0854.2008.00734.x

Sim, F. J., Zhao, C., Penderis, J., and Franklin, R. J. (2002). The age-related decrease in CNS remyelination efficiency is attributable to an impairment of both oligodendrocyte progenitor recruitment and differentiation. *J. Neurosci.* 22, 2451–2459.

Singhal, G., Jaehne, E. J., Corrigan, F., and Baune, B. T. (2014). Cellular and molecular mechanisms of immunomodulation in the brain through environmental enrichment. *Front. Cell Neurosci.* 8:97. doi: 10.3389/fncel.2014.00097

Stellwagen, D., Beattie, E. C., Seo, J. Y., and Malenka, R. C. (2005). Differential regulation of AMPA receptor and GABA receptor trafficking by tumor necrosis factor-alpha. *J. Neurosci.* 25, 3219–3228. doi: 10.1523/jneurosci.4486-04.2005

Stern, Y. (2012). Cognitive reserve in ageing and Alzheimer's disease. *Lancet Neurol.* 11, 1006–1012. doi: 10.1016/s1474-4422(12)70191-6

Strohle, A., Stoy, M., Graetz, B., Scheel, M., Wittmann, A., Gallinat, J., et al. (2010). Acute exercise ameliorates reduced brain-derived neurotrophic factor in patients with panic disorder. *Psychoneuroendocrinology* 35, 364–368. doi: 10.1016/j.psyneuen.2009.07.013

Thery, C., Amigorena, S., Raposo, G., and Clayton, A. (2006). Isolation and characterization of exosomes from cell culture supernatants and biological fluids. *Curr. Protoc. Cell Biol.* 30, 3.22.1–3.22.29. doi: 10.1002/0471143030.cb0322s30

Tremoleda, J. L., Kerton, A., and Gsell, W. (2012). Anaesthesia and physiological monitoring during in vivo imaging of laboratory rodents: considerations on experimental outcomes and animal welfare. *EJNMMI Res.* 2:44. doi: 10.1186/2191-219x-2-44

van Dellen, A., Blakemore, C., Deacon, R., York, D., and Hannan, A. J. (2000). Delaying the onset of huntington's in mice. *Nature* 404, 721–722. doi: 10.1038/35008142

van Praag, H., Kempermann, G., and Gage, F. H. (2000). Neural consequences of environmental enrichment. *Nat. Rev. Neurosci.* 1, 191–198. doi: 10.1038/35044558

Varkey, E., Cider, A., Carlsson, J., and Linde, M. (2011). Exercise as migraine prophylaxis: a randomized study using relaxation and topiramate as controls. *Cephalalgia* 31, 1428–1438. doi: 10.1177/0333102411419681

Conflict of Interest Statement: AP, KP, and RK are co-inventors listed on the following issued and pending patent applications: United States Patent No. 10,231,997 issued March 19, 2019; United States Patent Application No. 16/259,563 filed January 28, 2019; Canadian Patent Application No. CA2882248 filed August 15, 2013, European Patent Application No. 13829748.6 filed August 15, 2013; and Australian Patent No. AU2013302526 issued July 5, 2018; all dealing with the use of exosomes to reduce oxidative stress in the central nervous system and promote remyelination of damaged neurons.

The remaining author declares that the research was conducted in the absence of any commercial or financial relationships that could be construed as a potential conflict of interest.

frontiers in Neuroscience

ORIGINAL RESEARCH
published: 02 October 2019
doi: 10.3389/fnins.2019.01005

Assessing Neuronal and Astrocyte Derived Exosomes From Individuals With Mild Traumatic Brain Injury for Markers of Neurodegeneration and Cytotoxic Activity

Charisse N. Winston[1], Haylie K. Romero[2], Maya Ellisman[1], Sophie Nauss[1], David A. Julovich[3], Tori Conger[3], James R. Hall[3], Wendy Campana[2,4], Sid E. O'Bryant[3], Caroline M. Nievergelt[5,6], Dewleen G. Baker[5,6], Victoria B. Risbrough[5,6†] and Robert A. Rissman[1,4*†]*

[1] Department of Neurosciences, University of California, San Diego, La Jolla, CA, United States, [2] Department of Anesthesiology, University of California, San Diego, La Jolla, CA, United States, [3] Department of Pharmacology and Neuroscience, Institute for Translational Research, University of North Texas Health Science Center, Fort Worth, TX, United States, [4] VA San Diego Healthcare System, La Jolla, CA, United States, [5] Center of Excellence for Stress and Mental Health, La Jolla, CA, United States, [6] Department of Psychiatry, University of California, San Diego, La Jolla, CA, United States

OPEN ACCESS

Edited by:
Francesc Xavier Guix,
Severo Ochoa Molecular Biology Center (CSIC-UAM), Spain

Reviewed by:
Edward J. Goetzl,
University of California, San Francisco, United States
Rodolfo Gabriel Gatto,
University of Illinois at Chicago, United States

***Correspondence:**
Victoria B. Risbrough
vrisbrough@ucsd.edu
Robert A. Rissman
rrissman@ucsd.edu

† These authors have contributed equally to this work as senior authors

Specialty section:
This article was submitted to Neurodegeneration, a section of the journal Frontiers in Neuroscience

Received: 29 May 2019
Accepted: 04 September 2019
Published: 02 October 2019

Citation:
Winston CN, Romero HK, Ellisman M, Nauss S, Julovich DA, Conger T, Hall JR, Campana W, O'Bryant SE, Nievergelt CM, Baker DG, Risbrough VB and Rissman RA (2019) Assessing Neuronal and Astrocyte Derived Exosomes From Individuals With Mild Traumatic Brain Injury for Markers of Neurodegeneration and Cytotoxic Activity. Front. Neurosci. 13:1005. doi: 10.3389/fnins.2019.01005

Mild traumatic brain injury (mTBI) disproportionately affects military service members and is very difficult to diagnose. To-date, there is currently no blood-based, diagnostic biomarker for mTBI cases with persistent post concussive symptoms. To examine the potential of neuronally-derived (NDE) and astrocytic-derived (ADE) exosome cargo proteins as biomarkers of chronic mTBI in younger adults, we examined plasma exosomes from a prospective longitudinal study of combat-related risk and resilience, marine resiliency study II (MRSII). After return from a combat-deployment participants were interviewed to assess TBI exposure while on deployment. Plasma exosomes from military service members with mTBI (mean age, 21.7 years, n = 19, avg. days since injury 151), and age-matched, controls (deployed service members who did not endorse a deployment-related TBI or a pre-deployment history of TBI; mean age, 21.95 years, n = 20) were precipitated and enriched against a neuronal adhesion protein, L1-CAM, and an astrocyte marker, glutamine aspartate transporter (GLAST) using magnetic beads to immunocapture the proteins and subsequently selected by fluorescent activated cell sorting (FACS). Extracted protein cargo from NDE and ADE preparations were quantified for protein levels implicated in TBI neuropathology by standard ELISAs and on the ultra-sensitive single molecule assay (Simoa) platform. Plasma NDE and ADE levels of Aβ42 were significantly higher while plasma NDE and ADE levels of the postsynaptic protein, neurogranin (NRGN) were significantly lower in participants endorsing mTBI exposure compared to controls with no TBI history. Plasma NDE and ADE levels of Aβ40, total tau, and neurofilament light (NFL), P-T181-tau, P-S396-tau were either undetectable or not significantly different between the two groups. In an effort to understand the pathogenetic potential of NDE and ADE cargo

proteins, neuron-like cultures were treated with NDE and ADE preparations from TBI and non-TBI groups. Lastly, we determined that plasma NDE but not ADE cargo proteins from mTBI samples were found to be toxic to neuron-like recipient cells *in vitro*. These data support the presence of markers of neurodegeneration in NDEs of mTBI and suggest that these NDEs can be used as tools to identify pathogenic mechanisms of TBI.

Keywords: traumatic brain injury, neuronal exosomes, astrocytes, amyloid, tau

INTRODUCTION

Traumatic brain injury (TBI) is a global public health concern. Epidemiological data suggests approximately 10 million people worldwide will sustain a TBI each year (Hyder et al., 2007). This is likely a gross underestimation as many mTBI cases go unreported, especially amongst sports athletes and military service members (Langlois et al., 2006). Approximately 75% of all TBI cases are mild TBI (mTBI) or concussions (Holm et al., 2005; Langlois et al., 2006). mTBI typically results in short-lived, neurological impairment that resolves spontaneously within 12 months (Binder, 1986; Karr et al., 2014). However, 5–20% of mTBI cases experience chronic, post concussive symptoms long after the injury (Ponsford et al., 2011; Karr et al., 2014; Eme, 2017). The underestimation of reported head injury cases and the chronic sequelae of TBI signifies the need for better diagnostic tools and therapeutic interventions for head injury patients.

Mild TBI diagnosis is complicated by the lack of interdisciplinary consensus regarding what constitutes a mTBI (Kulbe and Geddes, 2016; Prince and Bruhns, 2017). Because of this, the current criteria for mTBI can be difficult to assess in patients with pre-existing neurological conditions, intoxicated patients, and children (Kulbe and Geddes, 2016). In military populations, the recognition of mTBI is further complicated by the delay in diagnosis due to lengthy deployments (Marion et al., 2011). Many mTBI diagnoses are primarily based on the subjective nature of patients self-reporting mTBI symptoms and are likely to not be assessed until months or years after the initial impact (Kulbe and Geddes, 2016; Prince and Bruhns, 2017).

The current state of mTBI diagnostics includes expensive neuroimaging modalities (Lee and Huang, 2014; Shin et al., 2017) and cerebral spinal fluid (CSF) sampling (Agoston et al., 2017). Post concussive symptomology is insensitive to current neuroimaging techniques while CSF sampling is invasive and imposes an additional health risk to the patient. The urgent need to identify pre-symptomatic, neuropathological changes in the brain at earlier and more treatable timepoints has fueled research into biofluid biomarkers, specifically those obtained from plasma and serum. Extensive research has identified number of promising blood-based and CSF biomarkers of head injury including tau, neurofilament (NF), glial fibrillary acidic protein (GFAP), ubiquitin carboxyl-terminal hydrolase isoenzyme L1 (UCHL1), neuron-specific enolase (NSE), myelin basic protein (MBP), and calcium-binding protein (s100β). Many of these markers demonstrate high diagnostic accuracy for the acute stages of severe TBI (Agoston et al., 2017; Kim et al., 2018) while GFAP has recently emerged as demonstrating high diagnostic accuracy in differentiating mTBI patients from controls (Bogoslovsky et al., 2017). Work from our lab and others demonstrated the utility of neuronally derived, plasma exosomes (NDEs) as biomarkers for elucidating the neurodegenerative stages of AD and other diseases (Fiandaca et al., 2015; Goetzl et al., 2016a, 2018a; Hamlett et al., 2016; Stern et al., 2016; Winston et al., 2016; Ngolab et al., 2017). However, limited research has been conducted to assess the diagnostic potential of blood-based exosomes as a measurement of acute and chronic sequelae of mTBI (Gill et al., 2018; Goetzl et al., 2018c, 2019).

The acute and chronic sequelae of mTBI involves the activation of a diverse cascade of pathophysiological processes and events (DeKosky et al., 1998; Povlishock and Katz, 2005). Axonal damage, disruption of cytoskeletal networks along with the redistribution of neurofilament proteins are all thought to be the primary determinant of outcome following mTBI (Shahim et al., 2018) and severe TBI (Hamberger et al., 2003; Johnson et al., 2013). Because of this, many biofluid biomarker studies target cytoskeletal proteins including the microtubule stabilizing protein, tau and Neurofilament light (NFL). NFL is neuron specific, cytoskeletal protein found in myelinated axons. Axonal damage liberates tau and NFL from axons and releases it into the CSF and blood (Lin et al., 2018). Several longitudinal and prospective cohort studies support serum NFL as an ultrasensitive biomarker for mTBI, sports-related, repeat concussion (Shahim et al., 2017, 2018) and AD (Lin et al., 2018). Moreover, tau and phosphorylated epitopes of tau (p-tau) has been detected immediately after severe TBI (Tsitsopoulos and Marklund, 2013); plasma tau has been reported to be increased in military populations approximately 12 months after TBI (McKee et al., 2009; Rubenstein et al., 2015); and abnormal p-tau accumulation can be detected in post mortem brain many years after head injury (McKee et al., 2013; Tsitsopoulos and Marklund, 2013).

Neuroinflammation is also a well characterized pathological hallmark of head injury (Karve et al., 2016). Astrocytes, one of the major resident glial cells in the brain, were once thought to only provide structural support in the central nervous system (CNS) (Montgomery, 1994). Today, there is a greater appreciation for the diverse role that astrocytes play in the healthy CNS and following CNS insult and disease (Karve et al., 2016; Xiong et al., 2018). Previously, exosomes derived from astrocytes (ADEs) contained proteins associated with the generation of the toxic Aβ42 peptide (Goetzl et al., 2016b) and complement proteins that were associated with neurotoxic reactive astrocytes

(Goetzl et al., 2018b; Winston et al., 2019). Similarly, cargo proteins of plasma ADEs accurately differentiated AD patients from age-matched controls (Goetzl et al., 2016b) and were found to be predictive biomarker of MCI conversion to AD (Goetzl et al., 2018b; Winston et al., 2019).

To examine NDE and ADE cargo proteins as biomarkers of chronic mTBI, we leveraged plasma samples from the Marine Resiliency Study II (MRSII), a prospective study of combat-related neurocognitive outcomes in 1,040 Marine and Navy service members (Glenn et al., 2017). Participants were assessed at pre-deployment and again at 4–6 months after returning from a combat deployment to Afghanistan for mental and physical health and cognitive performance. In the current study, we used plasma samples from 39 participants of this cohort (controls, $n = 20$; mTBI, $n = 19$), to isolate exosomes.

Exosomes were enriched by magnetic-bead immunocapture against the neural adhesion marker, L1CAM and the astrocytic marker, glutamine aspartate transporter (GLAST). Subsequently, all BAE (bead-antibody-exosome) preparations were FACS sorted. Protein cargo from NDE and ADE preparations were extracted, followed by quantitative determination of TBI-related markers via human specific ELISAs. The markers chosen were Aβ42, Aβ40, NFL, total tau, phosphorylated tau epitopes, T181 and S396, and calmodulin-binding, postsynaptic protein neurogranin (NRGN).

Absorption of NDE cargo from other neurodegenerative disorders are toxic to receipt cells *in vivo* (Winston et al., 2018), however, the pathogenic potential of plasma NDE and ADE cargo proteins from TBI samples has yet to be investigated. Lastly, we determined if cargo proteins from NDEs and ADEs were toxic to recipient cells *in vitro*.

MATERIALS AND METHODS

Baseline Characteristics of Study Participants

Participants in this study, a subset of MRS-II participants, were all male, with a mean age at pre-deployment of 21.87 (SD = 2.76). On average assessments were given at 4 weeks (SD = 4.9) prior to deployment and again at 22 weeks (SD = 22.4) following deployment (Marine Resiliency Study II; Moore et al., 2017). MRS-II TBI assessment methodology mirrored that of MRS, which assessed life-time head injury (up to a maximum 5) at pre-deployment, and combat-related head injuries, defined as any head injury sustained between the pre- and post-deployment assessments (Yurgil et al., 2014). Detailed MRS methodology has been reported elsewhere (Baker et al., 2012); only descriptions of measures relevant to the present study are presented here. Demographic information (age, ethnicity, race) was collected via self-report surveys before deployment and was included in analysis as potential covariates. Head injury events were assessed via interview before deployment and after deployment. Interviewers gathered details of each reported injury, including injury cause or mechanism and symptom severity. TBI was defined as any head injury that resulted in loss of consciousness (LOC) or altered mental status (i.e., dazed, confused, or seeing stars, and/or posttraumatic amnesia (National Center for Injury Prevention and Control, 2003; von Holst and Cassidy, 2004; Helmick et al., 2006). Any head injury resulting in LOC and/or altered mental state (AMS; i.e., dazed, confused, "seeing stars," and/or posttraumatic amnesia [PTA]) was defined as TBI (National Center for Injury Prevention and Control, 2003; O'Neil et al., 2014; Yurgil et al., 2014). For this study we selected post-deployment plasma samples from participants who self-reported multiple (2+) head injuries during the index deployment ($n = 17$ mean age, 21.74 ± 0.9; average number of TBI, 2.526 ± 0.1772, average number of days between most recent deployment TBI and sample collection 151 ± 112 days). In the TBI exposed group, 94% reported at least one injury that involved LOC, with the majority (82%) experiencing LOC < 15 min. Although the utility of neuroimaging has improved for mTBI diagnoses (Salat et al., 2017) imaging was not conducted on these participants. Moreover, no participant endorsed an injury with fracture or head wound. At the time of sample collection participants were asked if they were experiencing any current problems from the TBI, including memory problems, balance problems, headaches, sensitivity to light, irritability, and/or sleep problems. 94% endorsed experiencing at least one current symptom (average number of symptoms endorsed 3 ± 1.5). 76% of participants endorsed a blast/explosion-related TBI. Trauma- and deployment-exposed controls who did not endorse a history of TBI were selected for similarities in age, ethnicity/race, # of months in the military and range of trauma-symptoms as assessed by the Clinician Administered PTSD Symptom Scale (CAPS, version for DSM-IV) (Blake et al., 1995). The CAPS is a structured interview that is considered the gold standard for assessment of PTSD symptom severity. At the time of assessment, blood was drawn into EDTA-treated tubes, after which plasma was isolated for storage in −80°C freezers. See Demographics **Table 1** for details.

This study was approved by the institutional review boards of the University of California, San Diego; the Veterans Affairs San Diego Research Service; and the Naval Health Research

TABLE 1 | Demographics, military, and TBI history.

	No history of TBI	TBI
Age (years)	22.0 ± 1.2	21.7 ± 0.7
Race/Ethnicity	70% Caucasian, 5% African American, 15% Hispanic, 10% Asian/Other	71% Caucasian, 6% African American, 12% Hispanic, 11% Asian/Other
# Months in military	36.5 ± 12.1	32.9 ± 9.8
PTSD symptoms	23.25 ± 25	35.11 ± 25
Deployment stress	0.27 ± 0.61	0.79 ± 0.63*
Average # of TBI	0	2.59 ± 0.8

*Measures are means ± SD. PTSD Symptoms assessed by Clinician Administered PTSD Symptom Scale for DSM-IV (Blake et al., 1995). Deployment Stress assessed using the Deployment Risk and Resiliency Inventory (variable is based on a composite score across four scales: post-battle experiences, combat experience, deployment concern, difficult living, and working environment (Vogt et al., 2013). *$p < 0.05$ vs. No history of TBI group, $t_{34} = -2.55$.*

Center and written informed consent was obtained from all participants.

Enrichment of Neuronal-Derived (NDEs) and Astrocyte-Derived Exosomes (ADEs) From Human Plasma via Bead Antibody Exosome (BAE) – FITC Complex and FACS Sort

Exosome isolation was conducted per manufacturer's instructions (System Biosciences, Inc., Mountain view, CA, United States; Catalog # EXOQ5TM-1). Briefly, 250 μL of human plasma were incubated with 2.5 μL purified thrombin (System Biosciences, Inc.; Catalog # TMEXO-1) at room temperature for 5 min. After centrifugation at 10,000 rmp for 5 min, supernatants were incubated with 63 μL ExoQuick Exosome Precipitation solution (System Biosciences, Inc.; Catalog # EXOQ5TM-1) for 30 min at 4°C. Resultant suspensions were centrifuged at 1,500 × *g* for 1 h at 4°C. Supernatant was collected and the resultant pellet was suspended in 300 μL of 1× phosphate buffer saline (PBS) (diluted from 10× PBS; Thermo Fisher Scientific; Catalog# AM9625) with Halt protease and phosphatase inhibitor cocktail EDTA-free (Thermo Fisher Scientific; Catalog # 78443) and stored at −80°C until immunochemical enrichment of exosomes from both neural and astrocytic sources.

Neural and astrocyte enrichment was conducted per manufacturer's instructions (System Biosciences, Inc.; Catalog # CSFLOWBASICA-1). Briefly, 40 μL of 9.1 μm, streptavidin magnetic Exo-Flow beads (System Biosciences, Inc.; Catalog # CSFLOWBASICA-1) were incubated with 100 ng/μL of mouse anti-human CD171 (L1CAM, neural adhesion protein) biotinylated antibody (clone 5G3, eBioscience/Thermo Fisher Scientific; Catalog # 13-1719-82) or mouse anti-human GLAST (ACSA-1) biotinylated antibody (Miltenyi Biotec, Inc., Auburn, CA, United States; Catalog # 130-118-984) for 2 h on ice, with gently flicking every 30 min to mix. Bead-antibody (Ab) complex was washed three times in Bead Wash Buffer (Systems Biosciences, Inc.; CSFLOWBASICA-1) using a magnetic stand. Bead-Ab complex was suspended with 400 μL of Bead Wash Buffer and 100 μL of total exosome suspensions rotating overnight at 4°C. Bead-Ab-exosome (BAE) complex was washed three times with Bead Wash Buffer then suspended in 240 μL of Exosome Stain Buffer and 10 μL of Exo-FITC Exosome FACS stain (Systems Biosciences, Inc.; Catalog # CSFLOWBASICA-1) for 2 h on ice, with gently flicking to mix. BAE-FITC complex was washed Three times in Bead Wash Buffer then suspended in 300 μL of Bead Wash Buffer prior to loading into BD FACS Aria II for sorting.

Flow-sorted, BAE-FITC complexes were incubated with 300 μL of Exosome elution buffer (System Biosciences, Inc.; Catalog # CSFLOWBASICA-1) at 25°C for 30 min. Finally, supernatant containing eluted exosomes were incubated with 1 μL of Exo-FlowIP clearing reagent (System Biosciences, Inc.; Catalog # EXOFLOW32A) at 37°C for 30 min then stored at −80°C.

Quantification of NDE and ADE Protein Cargo by Human-Specific Enzyme Linked Immunosorbent Assays (ELISAs) and Using the Single Molecule Array (Simoa) Technology

Protein concentrations for eluted NDE and ADE suspensions were determined using the Pierce bicinchoninic acid (BCA) Protein Assay kit (Thermo Fisher Scientific; Catalog # 23225). Mammalian protein extraction reagent (M-PER) (Thermo Fisher Scientific; Catalog # 78501) with protease and phosphatase inhibitors are mixed with eluted NDE and ADE suspensions prior to ELISA quantification.

L1CAM-positive (NDE) cargo proteins and GLAST-positive (ADE) cargo proteins were quantified by human-specific ELISAs for P-T181-tau (Fujirebio US, Inc., Alpharetta, GA, United States; Catalog # 81582), Aβ1–42 (Cusabio, American Research Products, Waltham, MA, United States; Catalog # CSB-E10684h), P-S396-tau (Life Technologies/Invitrogen, Camarillo, CA, United States; Catalog # KHB7031), neurogranin (Cloud Clone Corp., American Research Products-Katy, TX, United States; Catalog # CEA404Hu), and tetraspanning exosome marker CD81 (Cusabio, American Research Products, Waltham, MA, United States; Catalog # CSB-EL004960HU) with verification of the CD81 antigen standard curve using purified human recombinant CD81 antigen (Origene Technologies, Inc., Rockville, MD, United States; Catalog # TP317508), according to suppliers' directions. The mean value for all determinations of CD81 in each assay group was set at 1.00, and the relative values for each sample were used to normalize their recovery.

Neurofilament light, Aβ40 and total tau were measured using the Single Molecule Array (Simoa) technology (Simoa; Quanterix, Lexington, MA, United States) which enables detection of these biomarkers in human plasma, serum, CSF and enriched exosomes. The Simoa Human NF-Light Advantage kit (NFL) (Catalog # 103400) was used to determine the amount of NFL. The Simoa Human Neurology 3-Plex "A" (3-Plex) (Catalog # 101995) was used to quantitatively determine the amount of Ab42, Ab40, and Tau. Tests were performed to optimize dilution factors and centrifugation. 4× dilution factor was found to be suitable for the samples. After thawing, the samples were vortexed and spun at 10,000 g for 5 min; the supernatant was directly transferred to a 96 well plate (90 μL for singlet or 125 μL for duplicate). For NFL, a recombinant NFL calibration curve was constructed and transferred to the 96 well plate (334 μl). Calibration curve range was 0–500 pg/mL and with the dynamic range of 0–2000 pg/mL. Control samples (analog 200 pg/mL and digital 10 pg/mL) and inter-assay control (pooled normal plasma) were all transferred to the 96 well plate (90 μL for singlet or 125 μL for duplicate). The 96 well plate was loaded onboard and the desired dilution factor for the samples was created by the Simoa HD-1 analyzer. Utilizing a Two-step procedure in a reaction cuvette, samples were incubated with antibody coated paramagnetic beads and biotinylated antibody detector simultaneously. After a wash, streptavidin-conjugated β-galactosidase (SBG) reagent was added binding the biotinylated antibodies leading to SBG enzyme labeling of the captured

NFL. After a second wash, the beads were re-suspended in resorufin β-D-galactopyranoside (RGP) reagent, transferred to a Simoa disk array and sealed. The NFL proteins captured by the antibody coated paramagnetic beads and labeled with the SBG reagent hydrolyze the RGP substrate to produce a fluorescence signal (Abs/Em = 573/585 nm). The fluorescent signal values generated from the calibration curve of known concentrations were fit using a 4-parameter logistic curve and $1/y^2$ weighting. The unknown samples and control samples concentrations were calculated from 4PL curve fit. Lower Limit of Detection of NFL was reported at 0.038 pg/mL and the Lower Limit of Quantification at 0.174 pg/mL.

Multiplexed detection of Aβ40 and total tau was accomplished by labeling beads with dyes of various wavelengths and concentrations creating distinct subpopulations of beads. Antibodies for each specific protein were immobilized to these color-encoded beads. Mixture of these beads were incubated with each sample generating detection of multiple proteins. From the materials provided, a recombinant 3-Plex calibration curve was constructed and transferred to the 96 well plate (334 μl). Calibration ranges for Aβ42, Aβ40, and total tau was 0–60, 0–140, and 0–100 pg/mL and dynamic ranges of 0–240, 0–560, and 0–400 pg/mL, respectively. Aβ40 and total tau control samples (analog 87.0, 393, and 99.5 pg/mL and digital 3.20, 22.4, and 2.24 pg/mL, respectively) and inter-assay control (pooled normal plasma) were all transferred to the 96 well plate (90 μL for singlet or 125 μL for duplicate). The 96 well plate was loaded onboard and the desired dilution factor for the samples was created by the Simoa HD-1 analyzer. A two-step process in a reaction cuvette was used and samples were incubated with antibody coated paramagnetic beads and biotinylated antibody detector simultaneously. After a wash, streptavidin-conjugated β-galactosidase (SBG) reagent was added binding the biotinylated antibodies leading to SBG enzyme labeling of the captured Aβ40 and total tau. After a second wash, the beads were re-suspended in resorufin β-D-galactopyranoside (RGP) reagent, transferred to a Simoa disk array and sealed. Aβ40 and total tau captured by the antibody coated paramagnetic beads and labeled with the SBG reagent hydrolyze the RGP substrate to produce a fluorescence signal (Abs/Em = 573/585 nm). As with NFL the fluorescent signal values generated from the calibration curve of known concentrations were fit using a 4-parameter logistic curve and $1/y^2$ weighting. The sample and control concentrations were calculated from 4PL curve fit. Lower limit of detection for Aβ40 and total tau was reported at 0.196 and 0.019 pg/mL, respectively, and the lower limit of quantification for Aβ40 and total tau was reported at 0.675 and 0.063 pg/mL, respectively.

Differentiation and Exosome Treatment of PC12 Cells and Human Neuroblastoma SH-SY5Y Cells

PC12 cells were cultured in a 5% CO2 humidified atmosphere at 37°C. Cells were cultured in PDL-coated Sarstedt plastic T75 tissue culture flasks in DMEM supplemented with 10% horse serum and 5% fetal bovine serum. For exosome treatment, cells were transferred to poly-D-lysine (PDL)-coated, Olympus flat bottom, 12-well plates and plated at a density of 14,000 cells/well. Differentiation was induced by culturing cells in serum free media and 50 ng/ml NGF. After 48 h, PC12 cells showed signs of differentiation that included neurite sprouting. NDEs and ADEs preparations (100 ng/mL) from control and TBI samples were applied to NGF + PC12 cells and incubated for 48 h. Following the experiment, phase contrast images of PC12 cells were collected using a Nikon digital camera attached to a Zeiss Axiovert 35 microscope. Subsequently, cell culture media was collected and stored at −20°C.

Human neuroblastoma SH-SY5Y cells were maintained and differentiated as previously described (Kim et al., 2015). Briefly, cells were maintained in MEM:F12 + 10% FBS and incubated at 37°C in 5% CO2. For differentiation, cells were plated on rat tail collagen coated glass cover slips in MEM:F12 + 3% FBS supplemented with 15nM retinoic acid. Cells were refed every 2 days for 7 days for complete differentiation. NDEs preparations from control, TBI, and AD samples (100 ng/mL) were applied to SH-SY5Y cells and incubated for 48 h. Following the experiment, cell culture media was collected and stored at −20°C.

Homogeneous Membrane Integrity Assay

CtyoTox-ONE™ Homogeneous Membrane Integrity Assay was performed per manufactures instructions (Promega Corporation, Madison, WI, Catalog # G7890). Briefly, cell culture media from NDE and ADE-treated NGF + PC12 cells and SH-SY5Y cells were incubated with 2 μL of Lysis solution (per 100 μL original volume) for 25 min at 22°C and then aliquoted, in triplicate, into a 96 well assay plate. Equal volume of CytoTox-ONE™ Reagent (100 uL) was added to each well containing cell culture media and incubated at 22°C for 10 min. 50 μL of stop solution was added prior to measuring fluorescent intensity at 562 nm using the iMark™ Microplate Absorbance Reader (Bio-Rad Laboratories, Hercules, CA, United States).

Statistical Analyses

Statistical significance of differences between means for cross-sectional groups mTBI and control were determined with an unpaired, non-parametric Mann–Whitney *t*-test (Prism 6; GraphPad Software, La Jolla, CA, United States). Receiver operating characteristic (ROC) analyses were conducted to assess the sensitivity of exosome cargo proteins in distinguishing among the two patient groups (Prism 6; GraphPad Software). ROC analyses were conducted under the non-parametric distribution assumption for standard error of area to determine the performance of classifier models (SPSS v21.0, IBM).

RESULTS

Validating Neural and Astrocytic Enrichment of NDEs and ADEs From Human Plasma Using FACS Analysis

A bead-antibody-exosome (BAE) – FITC complex was generated to enrich for neuronally derived (NDEs) and astrocyte derived

(ADEs) exosomes from human plasma (**Figure 1A**). Mouse anti-human CD171 (L1CAM) or GLAST (ACSA-1) biotinylated antibody was coupled to magnetic streptavidin beads followed by the binding of plasma exosomes isolated from matched young, healthy military service members with no history of TBI and service members endorsing > 1 combat-related mTBI events within the past 4–6 months. The resultant BAE complex was coupled to a FITC fluorescent tag that only binds to exosomes (Exo-FITC, System Biosciences Inc.) and subsequently sorted based green fluorescent intensity. As a negative control, the resultant non-exosome, bead – antibody – FITC (BA – FITC) complex was sorted to confirm Exo-FITC secondary antibody only binds to exosomes (**Figure 1B**).

Fluorescent activated cell sorting analysis demonstrated that less than 0.5% of the particles are FITC-positive in the non-exosome, negative controls (BA-FITC) (**Figure 1B**) while the exosome preparations derived from control and TBI groups (**Figure 1B**) were between 76.4 and 99.8% Exo-FITC-positive (n = 19–20/group). The significant degree in flow separation from the non-exosome control demonstrates flow cytometry is an efficient method for validating neural and astrocytic enrichment of NDEs and ADEs from human plasma. The number of FITC positive (FITC+) events were quantified. We determined that the recovery of NDEs and ADEs following FACS were not significantly different between service members with mTBI and those with no TBI history (**Figure 1C**). Resultant exosome preparations were confirmed by ELISA against the exosome membrane protein marker, CD81 (**Figure 1D**). Similarly, plasma NDE levels for CD81 were not statistically different between the two patient populations (**Figure 1D**).

Plasma NDE and ADE Levels of Aβ42 Are Increased While Plasma NDE and ADE Levels of NRGN Are Decreased in Young Service Members With Multiple mTBI Compared to Service Members With No TBI History

Previously, we reported plasma NDE levels of Aβ42, P-tau-T181, P-tau-S396 increased while plasma NDE levels of NRGN

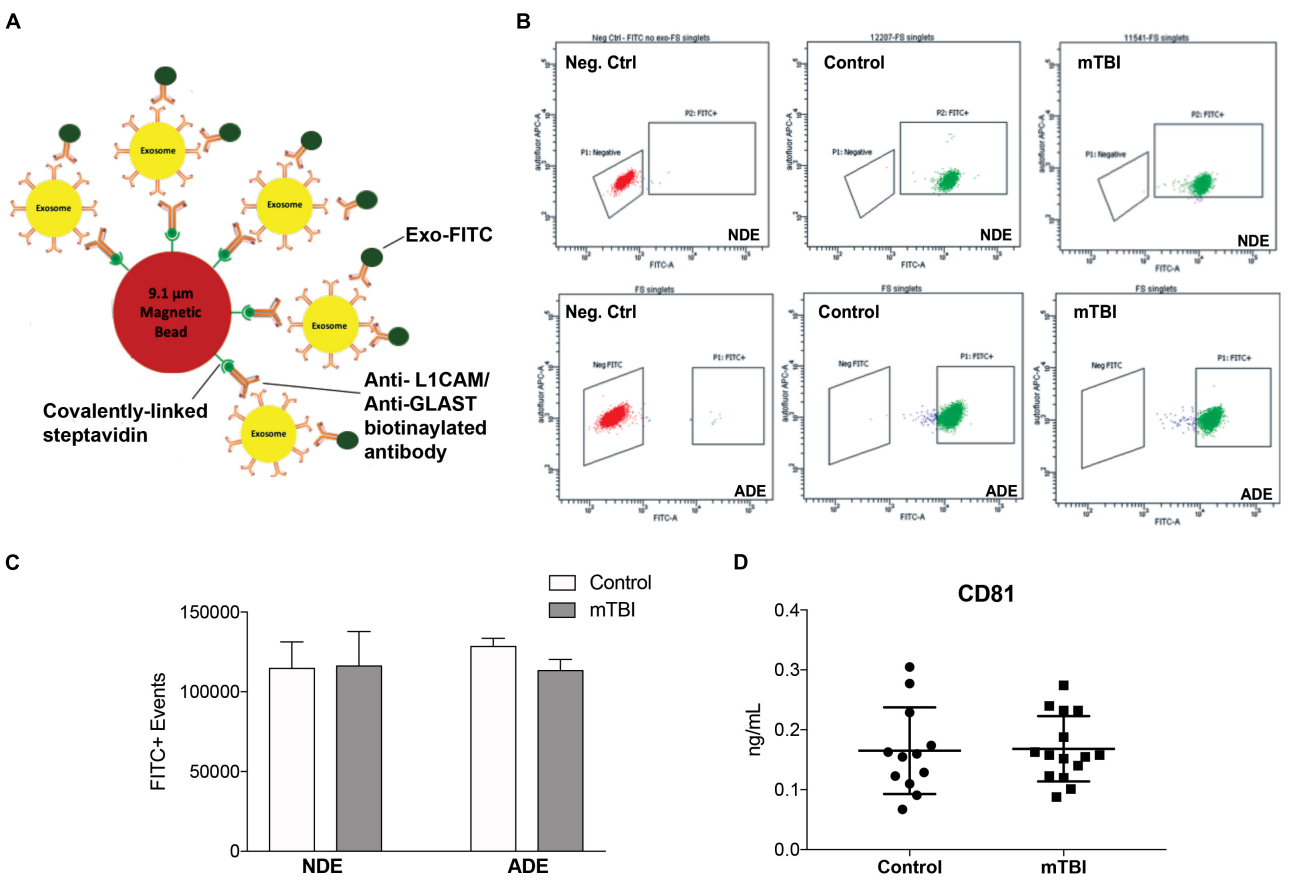

FIGURE 1 | Fluorescent activated cell sorting (FACS) enrichment of plasma NDEs from service members with and without mTBI during deployment. Schematic cartoon of FACS enrichment via the formation of a bead-antibody-exosome (BAE) – FITC complex **(A)**. Representative FACS plot for non-exosome, negative control (red) and BAE – FITC complexes exosomes (green) isolated from control subject, 12207 (age: 22) and mTBI subject, 11541 (age: 21) and enriched against anti-human CD171 biotin (L1CAM) or anti-GLAST antibody **(B)**. Total number of FITC+ events were not significantly different between the two populations (**C**; 114719 ± 3712 FITC+ events vs. 116121 ± 4969 FITC+ events). Plasma NDE and ADE concentrations of exosome marker, CD81 were not statistically different between the two populations as measured by standard ELISA **(D)**.

decreased in MCI (mean age, 68.7 years) and AD (71.1 years) patients as compared to age-matched controls (mean age, 70.8 years) (Winston et al., 2016, 2019). Here, we observed that plasma NDE and ADE levels of Aβ42 (**Figure 2A**, $P < 0.05$) were significantly increased and levels of NRGN (**Figure 2B**, $P < 0.05$) were significantly decreased in mTBI samples as compared to age matched controls with no TBI history. Plasma NDE and ADE levels of P-T181-tau were not significantly different between the two groups (**Figure 2C**). Plasma NDE levels of P-S396-tau were not significantly different between the two groups while plasma ADE levels of P-S396-tau were elevated in the mTBI group as compared to controls, however, these data failed to reach significance (**Figure 2D**). Across groups, ADE cargo showed higher levels of Aβ42 (**Table 2**, 1.18 pg/mL ADEs vs. 0.29 pg/mL NDEs) and P-396-tau (**Table 2**, 16.26 pg/mL ADEs vs. 5.47 pg/mL NDEs) compared to plasma NDE cargo. All NDE and ADE concentrations for biomarkers analyzed were normalized against CD81 (**Figure 1D**).

Quantitative determination of NDE cargo proteins on the Simoa platform revealed plasma NDE levels of Aβ40 (**Figure 3A**), NFL (**Figure 3B**), and total tau (**Figure 3C**) were not significantly different between the two patient populations while plasma ADE levels Aβ40, total tau, and NFL were negligible or undetectable on the Simoa platform.

Plasma NDE Cargo Protein From Service Members With mTBI Are Toxic to Recipient Cells *in vitro*

Lastly, we determined the pathogenic potential of plasma NDE and ADE cargo protein *in vitro*. The neuronal-like characteristics of differentiated PC12 cells are well documented (Greene and Tischler, 1976) and serve as an excellent *in vitro* model system for the study of neuronal function and survival. Differentiated PC12 cells (NGF + PC12 cells) were incubated with 100 ng/mL of NDE or ADE preparations for 48 h (averaged triplicates; $n = 4$ individual samples/group). Exosome-induced cytotoxicity was assessed by measuring the amount of lactate dehydrogenase (LDH) released into the cell culture media. LDH is a soluble protein that is found in all living cells. The release of LDH into the surrounding media is a result of compromised membrane integrity and a marker of cell death.

After 48 h, wells treated with plasma NDEs from mTBI individuals displayed overt signs of cytotoxicity. Representative

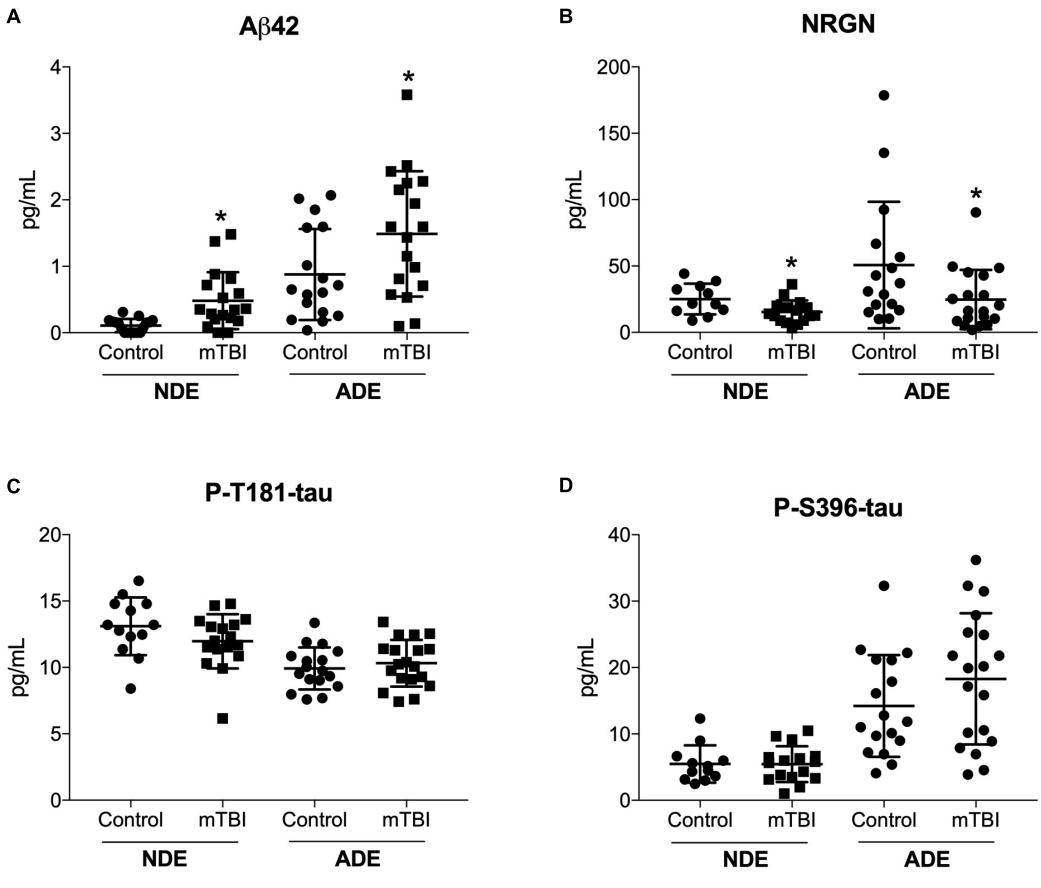

FIGURE 2 | Human plasma NDE and ADE levels Aβ1–42 and NRGN differentiate young mTBI individuals from individuals with no TBI history. Plasma NDE and ADE **(A)** concentrations of Aβ42 were significantly higher, whereas plasma NDE and ADE **(B)** concentrations of NRGN were significantly lower in young individuals with mTBI ($n = 17$) compared to age-matched controls ($n = 20$). Plasma NDE and ADE concentrations of P-T181-tau **(C)**, and P-S396-tau **(D)** were not significantly different between the two groups. Non-parametric *t*-test, $^*P < 0.05$ vs. control.

TABLE 2 | Plasma NDE and ADE protein quantification as measured by ELISA and the Sioma platform.

NDE – Hu ELISA			ADE – Hu ELISA		
Protein Cargo	**Control pg/ml ± S.E.M.**	**mTBI pg/ml ± S.E.M**	**Protein Cargo**	**Control pg/ml ± S.E.M.**	**mTBI pg/ml ± S.E.M**
Aβ42	0.11 ± 0.02	0.48 ± 0.10*	Aβ42	0.88 ± 0.17	1.49 ± 0.22*
NRGN	25.13 ± 3.49	15.45 ± 2.16*	NRGN	50.77 ± 11.92	24.74 ± 5.11*
P-T181-tau	13.10 ± 0.60	11.97 ± 0.49	P-T181-tau	9.93 ± 0.39	10.32 ± 0.40
P-S396-tau	5.48 ± 0.81	5.45 ± 0.68	P-S396-tau	14.22 ± 1.86	18.30 ± 2.27
NDE – Quanterix Simoa			**ADE – Quanterix Simoa**		
Protein Cargo	**Control pg/ml ± S.E.M.**	**mTBI pg/ml ± S.E.M**	**Protein Cargo**	**Control pg/ml ± S.E.M.**	**mTBI pg/ml ± S.E.M**
Aβ40	0.99 ± 0.19	0.75 ± 0.18	Aβ40	0	0
Total Tau	1.55 ± 0.17	1.69 ± 0.18	Total Tau	0.13 ± 0.01	0.12 ± 0.01
NFL	1.47 ± 0.17	1.57 ± 0.14	NFL	0.02 ± 0.01	0.02 ± 0.01

*Quantitative determination of NDE and ADE cargo proteins were conducted using an unpaired, non-parametric Mann–Whitney t-test. Plasma NDE and ADE concentrations of Aβ42 were significantly higher, whereas plasma NDE and ADE concentrations of NRGN were significantly lower in young individuals with mTBI (n = 17) compared to age-matched controls (n = 20). *P < 0.05. Cross sectional analysis revealed that plasma concentrations of ADE cargo (control + mTBI) were significantly higher for Aβ42 (1.18 pg/mL ADEs vs. 0.29 pg/mL NDEs, P < 0.05) and P-396-tau (16.26 pg/mL ADEs vs. 5.47 pg/mL NDEs; P < 0.01) as compared to plasma concentrations of NDE cargo (control + mTBI).*

photomicrographs depicted signs of dendritic blebbing, suppressed neurite outgrowth, and cell death (**Figure 4A**). Compared to controls (100% viability), there was approximately threefold (286.7%) increase in exosome-induced cytotoxicity in wells that were treated with NDEs derived from mTBI individuals (**Figure 4B**, $P < 0.05$).

Next, we aimed to replicate our findings in a different *in vitro* model system. Differentiated human neuroblastoma SH-SY5Y cells were treated with 100 ng/mL NDE or ADE preparations for 48 h (averaged triplicates; $n = 4$ samples/group). Treatment of SH-SY5Y cells with plasma NDE preparations from patients diagnosed with AD was included as a positive control. Again, we observed approximately threefold (265.8%) increase in exosome-induced cytotoxicity in wells that were treated with NDEs derived from samples of service members with mTBI. In wells that were treated with NDEs derived from AD patients, we observed approximately fourfold (450.3%) increase in exosome-induced cytotoxicity as compared to NDEs derived from controls (**Figure 4C**, $P < 0.05$). Interestingly, plasma ADE cargo proteins from service members with mTBI did not induce cytotoxicity or compromise the membrane integrity of NGF + PC12 cells or SH-SY5Y cells (**Figures 4B,C**).

Together, these data suggest that plasma NDE cargo proteins from individuals exposed to multiple recent (within 4–6 months) mTBI events are toxic to neuron-like cells *in vitro*. Furthermore, plasma exosomes from different cell types mediate divergent biological processes in the CNS.

DISCUSSION

In the current study, we report, for the first time, that plasma NDE and ADE levels of Aβ42 and NRGN can differentiate military service members with mTBI from those with no TBI with moderate sensitivity and accuracy (see ROC analysis, **Table 3**). Because of the matched control strategy these differences are unlikely to be due to age, race/ethnicity, # months in military or PTSD symptoms. Plasma NDE and ADE levels of Aβ42 were significantly increased (**Figure 2A**) while plasma NDE and ADE levels of NRGN (**Figure 2B**) were significantly decreased in the group with combat-related mTBI, as compared to those without mTBI. Plasma ADE levels of P-S396-tau were elevated in the mTBI group as compared to controls, however, these findings failed to reach significance (**Figure 2D**). Interestingly, plasma NDE and ADE levels of Aβ40, P-T181-tau, total tau, and NFL were either undetectable or not significantly different between the two groups.

Given that TBI can initiate the abnormal accumulation of Aβ and tau (Tsitsopoulos and Marklund, 2013), it was surprising to see that plasma NDE and ADE levels of total tau, P-T181-tau, P-S396-tau were not significantly different between the two groups. Surprisingly, cross sectional analysis revealed that total plasma concentrations of ADE cargo (control + mTBI) were significantly higher for Aβ42 (see **Table 2**; $P < 0.05$) and P-396-tau (see **Table 2**; $P < 0.01$) as compared to total plasma concentrations of NDE cargo (control + mTBI). It's not well understood why total levels of for Aβ42 and P-396-tau were higher in ADEs as compared to NDEs. Studies have demonstrated that astrocytes undergo phagocytosis in response to damaged neighboring cells (Liddelow and Barres, 2017; Wakida et al., 2018). Thus, its plausible that injury induced accumulation of Aβ42 and P-396-tau activated a phagocytic response in astrocytes. This response could result in higher levels of said proteins within astrocytes that are subsequently exocytosed and trafficked to the periphery via ADEs. Future studies include determining how exosome biogenesis and function differ between various cell populations.

Here, we detect changes in protein levels contained within exosomes. However, many of the previous studies reported elevated levels of Aβ42, total tau and p-tau in serum and/or CSF. One recent study reported elevated levels of exosomal p-tau and total tau in individuals who sustained > 3 mTBI injuries

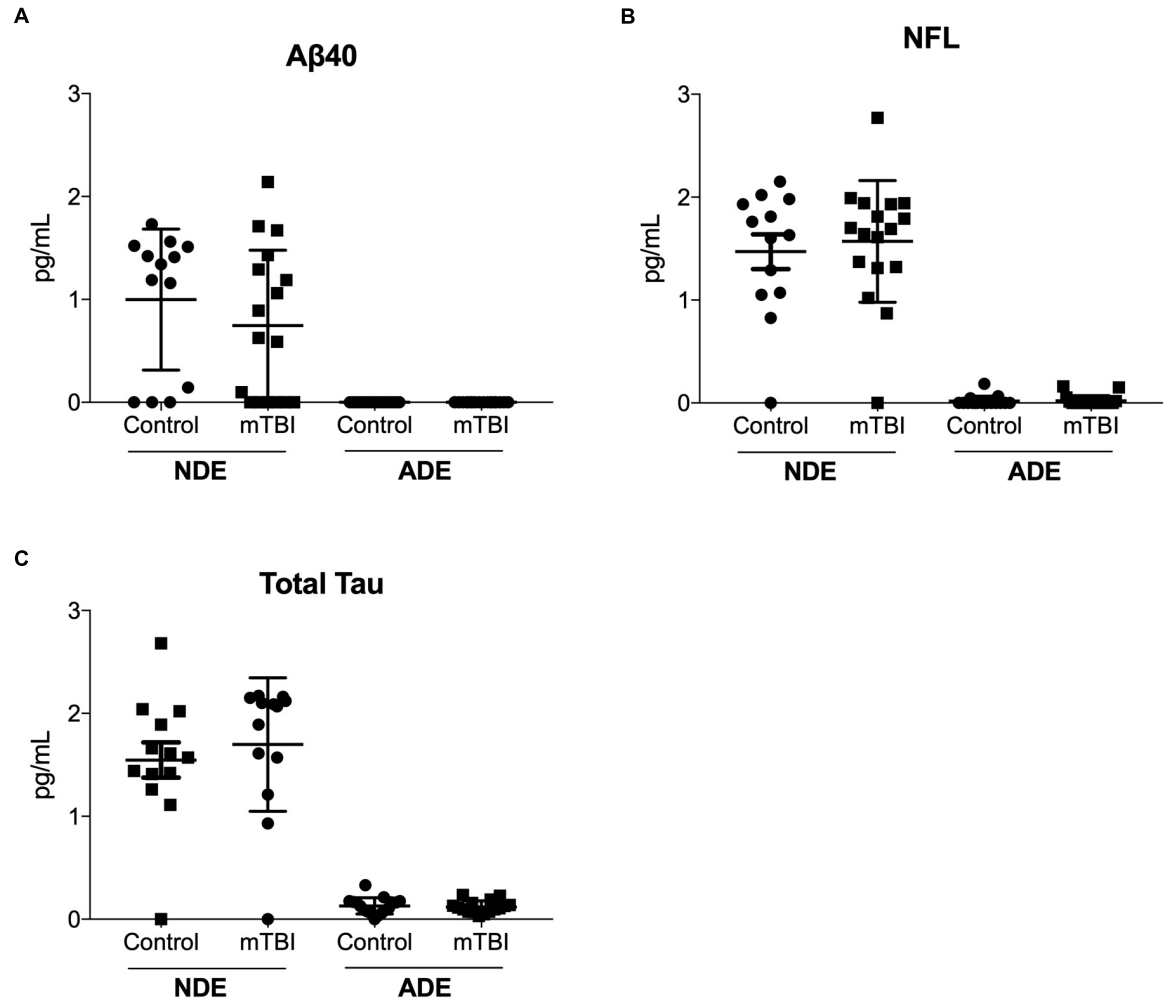

FIGURE 3 | Plasma NDE levels of Aβ40, total tau, and NFL are not significantly different between individuals with and without mTBI. Plasma NDE levels of Aβ40 **(A)**, NFL **(B)**, and total tau **(C)**, were not significantly different between the two populations while plasma ADE Aβ40 **(A)**, NFL **(B)**, and total tau **(C)** were not detectable by the Simoa Assay.

as compared to healthy controls and to those who sustained 2 or fewer mTBIs (Kenney et al., 2018). Interestingly, Kenney et al. (2018) reported Aβ42 and Aβ40 were undetectable in total exosomes derived from military veterans and controls. Gill et al. (2018) extracted NDEs from plasma and reported tau, Aβ42 and IL-10 were elevated in military servicemembers who had a mTBI and experienced a LOC of 20 min or less. In each of these studies, including the current study, biomarker quantification was assessed in patients with varying injury severity (mild to moderate); the number of self-reported mTBI varied amongst the study participants; some participants reported LOC while others did not; and the source of biomarker quantification also varied (total exosomal content vs. NDEs/ADEs). Understanding how all of these factors impact the expression of various TBI-related, exosome cargo proteins in the blood will aid in developing better mTBI diagnostics, prognostics, and would further elucidate mTBI pathophysiology.

Retrospective cohort studies confirm the relationship between age, injury severity, and outcome following TBI (LeBlanc et al., 2006). The age of onset is likely another factor that impacts the utility of blood-based, exosome biomarkers for mTBI. Our study participants were 10–20 years younger than the aforementioned studies (Gill et al., 2018; Kenney et al., 2018) and upward of 40–50 years younger than study participants of other exosome-related, biomarker studies (Fiandaca et al., 2015; Winston et al., 2016, 2019). It's not fully understood why certain proteins are packaged into exosomes and trafficked into the periphery, however, the temporal profile of blood-based biomarkers may vary across different age groups. Exosomes are known to shuttle cargo, including proteins and micro RNA (miRNA) between cells and aid in the removal of excess or damaged, intracellular proteins and their cellular contents (Rajendran et al., 2006; Kalani et al., 2014; Budnik et al., 2016). However, the basic mechanisms behind exosome transport and function in the

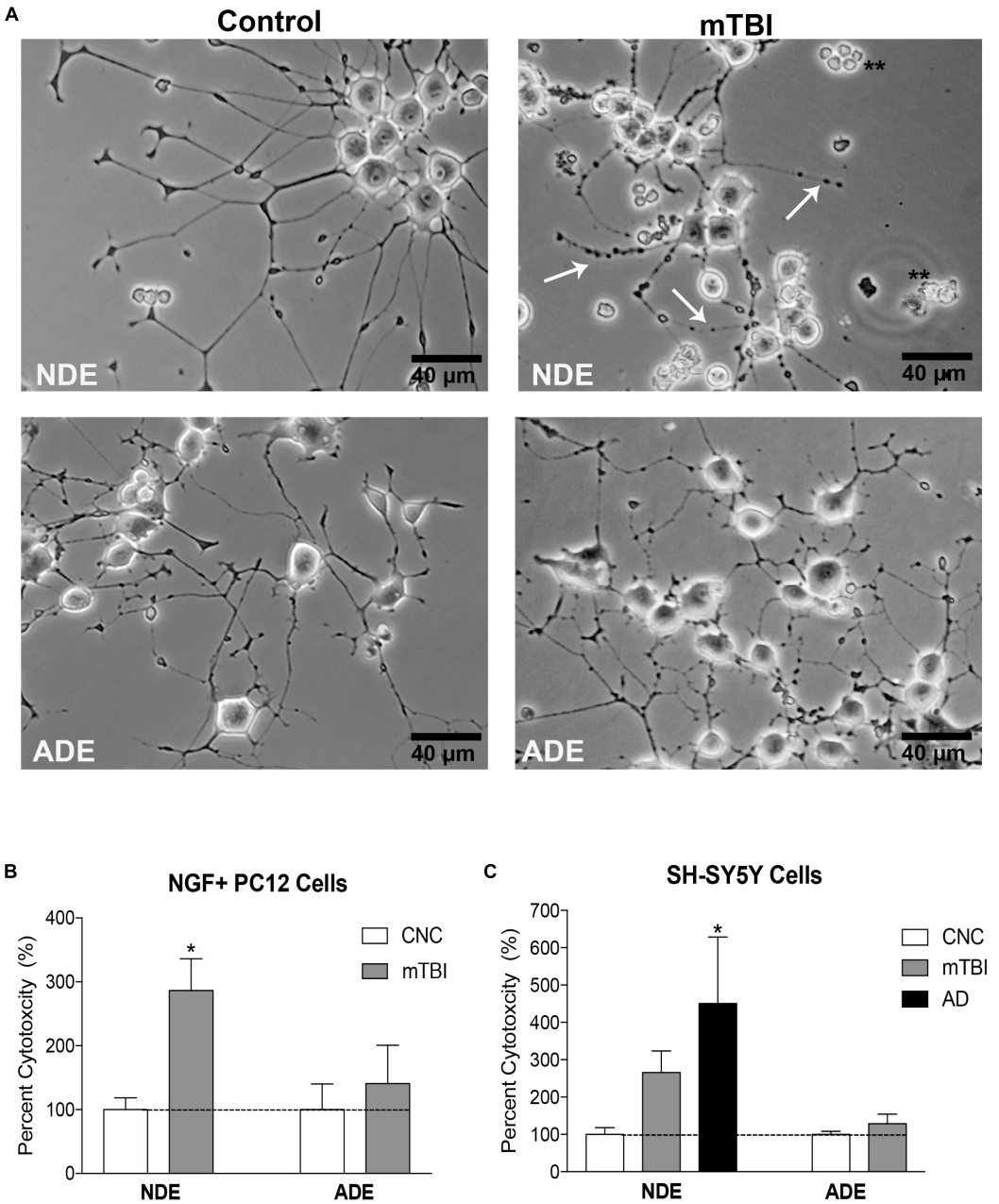

FIGURE 4 | Plasma NDE cargo from individuals with mTBI compromise membrane integrity and are toxic to neuron-like cells *in vitro*. Differentiated PC12 cells and SH-SY5Y cells were incubated with 100 ng/ml of NDE and ADE for 48 h. Representative photomicrographs indicate exosome-induced cytotoxicity. Signs of cytotoxicity include dendritic blebbing (indicated by arrows), suppressed neurite outgrowth and cell death in NGF + PC12 cells **(A)**. Compared to controls (100% viability), there was a threefold increase in exosome-induced cytotoxicity (LDH release) in wells that were treated with NDEs derived from service members with mTBI **(B)**, $*P < 0.05$ vs. control, dashed horizontal line represents 100% viability. SH-SY5Y cells were treated with NDE and ADE preparations from control and mTBI service members and AD patients. A similar level of cytotoxicity was observed in cultured SH-SY5Y. A threefold increase in exosome-induced cytotoxicity (LDH release) was observed in wells that were treated with NDEs derived from mTBI samples and a fourfold increase exosome-induced cytotoxicity in wells that were treated with NDEs derived from AD samples as compared to NDEs derived from control samples **(C)**. Non-parametric *t*-test; $*P < 0.05$ vs. control, dashed horizontal line represents 100% viability.

healthy and diseased CNS are still unknown (Hessvik and Llorente, 2018). In order to enhance the clinical utility of exosomes in therapy and diagnosis, it is essential that we gain a better understanding of these cellular processes (Hessvik and Llorente, 2018). Moreover, creating a profile with age-appropriate NDE and ADE biomarkers will also enhance the diagnostic and prognostic utility of blood-based exosome biomarkers for mTBI.

TABLE 3 | Receiver Operating Curve analysis for biomarker sensitivity for cargo proteins measured by standard ELISA.

NDE			ADE		
Protein cargo	**Sensitivity (% ±SEM)**	**Confidence interval (%)**	**Protein cargo**	**Sensitivity (% ±SEM)**	**Confidence interval (%)**
A042	84.6 ± 0.7	70.1–98.4	Aβ42	69.4 ± 0.08	51.8–87.1
NRGN	74.4 ± 0.9	55.1–93.7	NRGN	71.1 ± 0.09	53.9–88.1

The risk of developing of chronic traumatic encephalopathy (CTE) is a growing concern for military personnel and sports athletes (Randolph et al., 2013; Chauhan, 2014; Tartaglia et al., 2014). CTE is a slowly progressing neurodegenerative disease that typically affects those who suffer repeat mTBI over extended periods of time. CTE is a clinically and neuropathologically distinct tauopathy that can only be diagnosed post mortem (McKee et al., 2009). The ultimate concern, especially in younger patients, is continued exposure of repeat-mTBI during the latency period. Identifying blood-based, exosome biomarkers for mTBI would also serve is useful prognostic biomarkers for the progression of mTBI to CTE (Stern et al., 2016). Recently, Goetzl et al. (2019) quantified NDE cargo proteins in young sports athletes (mean age, 20.67 years) who sustained repeat-mTBI acutely (7 days) and chronically (3–12 months) prior to the time of blood donation. They determined plasma NDE levels of Aβ42 and P-T181-tau were elevated in acute and chronic mTBI patients while plasma NDE levels of P-S396-tau were elevated only in chronic mTBI patients as compared to controls (Goetzl et al., 2019). These data suggest that the diagnostic potential of the blood-based, exosome cargo proteins, Aβ42 and p-tau, are sensitive to varying inter-injury intervals (latency period between mTBI). In our study, blood collection occurred 4–6 months after the service members returned from deployment. These differences may also help explain why we didn't observe a significant difference in plasma NDE and ADE levels of p-tau and total tau between the two patient populations.

Interestingly, we observed no difference in plasma NDE levels of NFL between the two patient groups despite numerous studies suggesting serum and CSF NFL is a highly sensitive biomarker for concussion (Shahim et al., 2017, 2018). Shahim et al. (2017) reported levels of serum NFL levels were elevated between 7–10 days after a bout in young amateur boxers (mean age, 21.5 years), however, after 3 months of rest, serum NFL levels were significantly decreased in the amateur boxers (Shahim et al., 2017). Although, very few studies have quantified NFL in exosomes (Kawata et al., 2018), it's likely that NFL may only serve as an acute biomarker for mTBI. Plasma ADE levels of NFL (and Aβ40) derived from the two groups were undetectable. It's plausible that the release of NFL from the neuronal cytoskeleton may not be readily taken up by astrocytes, or these markers are immediately degraded following astrocyte absorption.

It's evident by these recent findings that there is not a single, "one-size fits all" biomarker suitable for mTBI diagnosis. The discrepancies across all of these studies call into question the approach that has been used to identify blood-based biomarkers for mTBI. The handful of previously identified biomarkers were derived from studies that screened biofluids for markers that were known to be associated with severe TBI pathophysiology (Agoston et al., 2017). This approach has limited the success for blood-based biomarker diagnostics for mTBI as the etiology for both conditions are not the same. Using an unbiased discovery approach, to identify and generate a panel with multiple blood-based biomarkers that are unique to mTBI and that accurately represent mTBI pathophysiology will likely be more efficacious than assessing the sensitivity of a single biomarker.

The ability to detect neurological biomarkers in biofluids, other than CSF, and at very low levels has also been challenging and has further limited the utility of blood-based biomarkers for mTBI. Moreover, the hesitancy to use exosome cargo as biomarkers for mTBI is derived from the lack of conclusive evidence that altered levels of exosome cargo proteins accurately reflect disease pathogenesis in the CNS. Exosomes have been shown to act as nano-surrogates of their cells of origin and possess unique signatures which reflect the status of the cell. Therefore, using CNS-derived exosomes to quantify levels of protein biomarkers may be more relevant than free circulating protein levels in whole blood.

Lastly, we investigated the pathogenetic potential of plasma NDE and ADE exosome cargo proteins in neuron-like cells. Work from our lab and others demonstrated that NDEs can propagate toxic proteins *in vivo* (Reilly et al., 2017) and induce toxicity to recipient cells *in vitro* (Winston et al., 2018). In the current study, we confirmed that plasma NDEs are toxic to recipient cells, and we report, for the first time that plasma ADEs were not toxic to neuron-like cells. Plasma NDEs and ADEs both contained detectable levels of Aβ42 and p-tau, however, only the cargo proteins from plasma NDEs of individuals with mTBI were toxic to neuron-like cells *in vitro*.

One explanation is ADEs are not easily taken up by neuronal-like cells. Alternatively, the reduced concentration of Aβ42 and p-tau in plasma ADEs as compared to plasma NDEs were insufficient to induce cytotoxicity. It's also plausible that plasma ADEs contained anti-inflammatory cytokines and other trophic molecules that attenuated cytotoxicity in recipient cells. We hypothesize that NDEs and ADEs have dual neuroprotective and neurotoxic roles in the CNS. One study reported that exosomes from astrocytes release inflammatory cytokines, including IL-1β, to induce an inflammatory response (Kalani et al., 2014) while another study determined that neuronal exosomes contain proteins, such as Ndfip1 and Nedd4, which are thought to play an important role in removing toxic proteins after injury (Putz et al., 2008). We acknowledge the limitations of our cytotoxicity assays which include the use

"neuron-like" cells vs. primary neuronal and astrocyte cultures. Despite these limitations, we report similar results in two distinct cell culture model systems. Future studies will include primary cultured cells from neurons and astrocytes and exosome treatment in pre-clinical animal models. Lastly, levels of complement proteins (Winston et al., 2019) and pro- and/or anti-inflammatory cytokines were not quantified in the current study, however, that is also future direction. Addressing this in future studies will provide better insight into the dual role that plasma exosomes derived from astrocytes may play in mTBI and other neurodegenerative diseases. Further investigation is needed to determine how exosomes from different cells mediate divergent biological processes in the healthy CNS and during CNS injury and disease.

Additional limitations to the study should also be considered. This was a male, military sample and thus may not be generalized to other forms of mTBI in civilians or in women. Imaging and helmet sensor verification for the injuries was not available thus case-control selection was based on self-report, a common problem for military mTBI studies. Indeed, retrospective self-report is most commonly all that is available for clinical TBI diagnoses in the Veteran population, and thus identification of potential biomarkers through exosome cargo may yield important future clinical applications. Studies are now ongoing to identify the timecourse of these proteins following injury and to disentangle if these proteins predict long-term chronicity and/or comorbidity with other disorders such as PTSD and neurodegenerative disorders in Veterans that endorse prior TBI.

DATA AVAILABILITY STATEMENT

All datasets generated for this study are included in the manuscript/supplementary files.

ETHICS STATEMENT

The studies involving human participants were reviewed and approved by UCSD and VA San Diego. The patients/participants provided their written informed consent to participate in this study.

AUTHOR CONTRIBUTIONS

CW and RR designed the study. CW evaluated the patients. CW, ME, SN, HR, DJ, TC, and JH performed the laboratory work. CW, RR, VR, and SO wrote the manuscript. WC helped design the present study, specifically the *in vitro* assays. VR initiated and helped to design the present study and supervised the original sample collection study (MRSII) and sample selection. DB administratively oversaw MRS data collection activities. CN and DB supervised the collection and storage of the samples and associated demographic, health, and TBI data, and edited the manuscript.

FUNDING

This study was supported by grants AG057459, AG057469, AG051848, AG018440, and ADRC P50 AG005131 from the National Institute on Aging, and VA Merit Awards BX003040 and BX004312 to RR and VA Merit Award BX004312, Department of Defense W81XWH1810761, P50 MH096889-06 to VR, VA Merit Award RX002484 to WC, and the VA Center of Excellence for Stress and Mental Health funding to VR, CN, and DB. This work was performed with the support of the Flow Cytometry Core at the San Diego Center for AIDS Research (P30 AI036214), the VA San Diego Health Care System, and the San Diego Veterans Medical Research Foundation.

REFERENCES

Agoston, D. V., Shutes-David, A., and Peskind, E. R. (2017). Biofluid biomarkers of traumatic brain injury. *Brain Inj.* 31, 1195–1203. doi: 10.1080/02699052.2017.1357836

Baker, D. G., Nash, W. P., Litz, B. T., Geyer, M. A., Risbrough, V. B., Nievergelt, C. M., et al. (2012). Predictors of risk and resilience for posttraumatic stress disorder among ground combat marines: methods of the Marine Resiliency Study. *Prev. Chronic Dis.* 9:E97.

Binder, L. M. (1986). Persisting symptoms after mild head injury: a review of the postconcussive syndrome. *J. Clin. Exp. Neuropsychol.* 8, 323–346. doi: 10.1080/01688638608401325

Blake, D. D., Weathers, F. W., Nagy, L. M., Kaloupek, D. G., Gusman, F. D., Charney, D. S., et al. (1995). The development of a clinician-administered PTSD Scale. *J. Trauma Stress* 8, 75–90.

Bogoslovsky, T., Wilson, D., Chen, Y., Hanlon, D., Gill, J., Jeromin, A., et al. (2017). Increases of plasma levels of glial fibrillary acidic protein, tau, and amyloid β up to 90 days after traumatic brain injury. *J. Neurotrauma* 34, 66–73. doi: 10.1089/neu.2015.4333

Budnik, V., Ruiz-Cañada, C., and Wendler, F. (2016). Extracellular vesicles round off communication in the nervous system. *Nat. Rev, Neurosci.* 17, 160–172. doi: 10.1038/nrn.2015.29

Chauhan, N. B. (2014). Chronic neurodegenerative consequences of traumatic brain injury. *Restor. Neurol. Neurosci.* 32, 337–365.

DeKosky, S. T., Kochanek, P. M., Clark, R. S., Ciallella, J. R., and Dixon, C. E. (1998). Secondary injury after head trauma: subacute and long-term mechanisms. *Semin. Clin, Neuropsychiatry* 3, 176–185.

Eme, R. (2017). Neurobehavioral outcomes of mild traumatic brain injury: a mini review. *Brain Sci.* 7:E46. doi: 10.3390/brainsci7050046

Fiandaca, M. S., Kapogiannis, D., Mapstone, M., Boxer, A., Eitan, E., Schwartz, J. B., et al. (2015). Identification of preclinical Alzheimer's disease by a profile of pathogenic proteins in neurally derived blood exosomes: a case-control study. *Alzheimers Dement* 11:600-7.e1. doi: 10.1016/j.jalz.2014.06.008

Gill, J., Mustapic, M., Diaz-Arrastia, R., Lange, R., Gulyani, S., Diehl, T., et al. (2018). Higher exosomal tau, amyloid-beta 42 and IL-10 are associated with mild TBIs and chronic symptoms in military personnel. *Brain Inj.* 32, 1277–1284. doi: 10.1080/02699052.2018.1471738

Glenn, D. E., Acheson, D. T., Geyer, M. A., Nievergelt, C. M., Baker, D. G., Risbrough, V. B., et al. (2017). Fear learning alterations after traumatic brain injury and their role in development of posttraumatic stress symptoms. *Depress. Anxiety* 34, 723–733. doi: 10.1002/da.22642

Goetzl, E. J., Abner, E. L., Jicha, G. A., Kapogiannis, D., and Schwartz, J. B. (2018a). Declining levels of functionally specialized synaptic proteins in plasma neuronal exosomes with progression of Alzheimer's disease. *FASEB J.* 32, 888–893. doi: 10.1096/fj.201700731R

Goetzl, E. J., Schwartz, J. B., Abner, E. L., Jicha, G. A., and Kapogiannis, D. (2018b). High complement levels in astrocyte-derived exosomes of Alzheimer disease. *Ann. Neurol.* 83, 544–552. doi: 10.1002/ana.25172

Goetzl, L., Merabova, N., Darbinian, N., Martirosyan, D., Poletto, E., Fugarolas, K., et al. (2018c). Diagnostic potential of neural exosome cargo as biomarkers. for acute brain injury. *Ann. Clin, Transl. Neurol.* 5, 4–10. doi: 10.1002/acn3.499

Goetzl, E. J., Elahi, F. M., Mustapic, M., Kapogiannis, D., Pryhoda, M., Gilmore, A., et al. (2019). Altered levels of plasma neuron-derived exosomes and their cargo proteins characterize acute and chronic mild traumatic brain injury. *FASEB J.* 33, 5082–5088. doi: 10.1096/fj.201802319R

Goetzl, E. J., Kapogiannis, D., Schwartz, J. B., Lobach, I. V., Goetzl, L., Abner, E. L., et al. (2016a). Decreased synaptic proteins in neuronal exosomes of frontotemporal dementia, and Alzheimer's disease. *FASEB J.* 30, 4141–4148. doi: 10.1096/fj.201600816r

Goetzl, E. J., Mustapic, M., Kapogiannis, D., Eitan, E., Lobach, I. V., Goetzl, L., et al. (2016b). Cargo proteins of plasma astrocyte-derived exosomes in Alzheimer's disease. *FASEB J.* 30, 3853–3859. doi: 10.1096/fj.201600756r

Greene, L. A., and Tischler, A. S. (1976). Establishment of a noradrenergic clonal line of rat adrenal pheochromocytoma cells which respond to nerve growth factor. *Proc. Natl. Acad. Sci. U.S.A.* 73, 2424–2428. doi: 10.1073/pnas.73.7.2424

Hamberger, A., Huang, Y. L., Zhu, H., Bao, F., Ding, M., Blennow, K., et al. (2003). Redistribution of neurofilaments and accumulation of beta-amyloid protein after brain injury by rotational acceleration of the head. *J. Neurotrauma* 20, 169–178. doi: 10.1089/08977150360547080

Hamlett, E. D., Goetzl, E. J., Ledreux, A., Vasilevko, V., Boger, H. A., LaRosa, A., et al. (2016). Neuronal exosomes reveal Alzheimer's disease biomarkers in down syndrome. *Alzheimers Dement* 13, 541–549. doi: 10.1016/j.jalz.2016.08.012

Helmick, K., Guskiewicz, K., Barth, J., Cantu, R., Kelly, J. P., McDonald, E., et al. (2006). *Defense and Veterans Brain Injury Center Working Group on the Acute Management of mild Traumatic Brain Injury in Military Operational Settings: Clinical Practice Guideline and Recommendations*. Washington, DC: Defense and Veterans Brain Injury Center.

Hessvik, N. P., and Llorente, A. (2018). Current knowledge on exosome biogenesis and release. *Cell Mol. Life Sci.* 75, 193–208. doi: 10.1007/s00018-017-2595-9

Holm, L., Cassidy, J. D., Carroll, L. J., Borg, J., and Neurotrauma Task Force on Mild Traumatic Brain Injury of the Who Collaborating Centre, (2005). Summary of the WHO collaborating centre for neurotrauma task force on mild traumatic brain injury. *J. Rehabil. Med.* 37, 137–141. doi: 10.1080/16501970510027321

Hyder, A. A., Wunderlich, C. A., Puvanachandra, P., Gururaj, G., and Kobusingye, O. C. (2007). The impact of traumatic brain injuries: a global perspective. *NeuroRehabilitation* 22, 341–353.

Johnson, V. E., Stewart, W., and Smith, D. H. (2013). Axonal pathology in traumatic brain injury. *Exp. Neurol.* 246, 35–43. doi: 10.1016/j.expneurol.2012.01.013

Kalani, A., Tyagi, A., and Tyagi, N. (2014). Exosomes: mediators of neurodegeneration, neuroprotection and therapeutics. *Mol. Neurobiol.* 49, 590–600. doi: 10.1007/s12035-013-8544-1

Karr, J. E., Areshenkoff, C. N., and Garcia-Barrera, M. A. (2014). The neuropsychological outcomes of concussion: a systematic review of meta-analyses on the cognitive sequelae of mild traumatic brain injury. *Neuropsychology* 28, 321–336. doi: 10.1037/neu0000037

Karve, I. P., Taylor, J. M., and Crack, P. J. (2016). The contribution of astrocytes and microglia to traumatic brain injury. *Br. J. Pharmacol.* 173, 692–702. doi: 10.1111/bph.13125

Kawata, K., Mitsuhashim, M., and Aldret, R. (2018). A preliminary report on brain-derived extracellular vesicle as novel blood biomarkers for sport-related concussions. *Front. Neurol.* 9:239. doi: 10.3389/fneur.2018.00239

Kenney, K., Qu, B. X., Lai, C., Devoto, C., Motamedi, V., Walker, W. C., et al. (2018). Higher exosomal phosphorylated tau and total tau among veterans with combat-related repetitive chronic mild traumatic brain injury. *Brain Inj.* 32, 1276–1284. doi: 10.1080/02699052.2018.1483530

Kim, C., Rockenstein, E., Spencer, B., Kim, H. K., Adame, A., Trejo, M., et al. (2015). Antagonizing neuronal toll-like receptor 2 prevents synucleinopathy by activating autophagy. *Cell Rep.* 13, 771–782. doi: 10.1016/j.celrep.2015.09.044

Kim, H. J., Tsao, J. W., and Stanfill, A. G. (2018). The current state of biomarkers of mild traumatic brain injury. *JCI Insight* 3:97105. doi: 10.1172/jci.insight.97105

Kulbe, J. R., and Geddes, J. W. (2016). Current status of fluid biomarkers in mild traumatic brain injury. *Exp. Neurol,* 275(Pt 3), 334–352. doi: 10.1016/j.expneurol.2015.05.004

Langlois, J. A., Rutland-Brown, W., and Wald, M. M. (2006). The epidemiology and impact of traumatic brain injury: a brief overview. *J. Head Trauma Rehabil.* 21, 375–378. doi: 10.1097/00001199-200609000-00001

LeBlanc, J., de Guise, E., Gosselin, N., and Feyz, M. (2006). Comparison of functional outcome following acute care in young, middle-aged and elderly patients with traumatic brain injury. *Brain Inj.* 20, 779–790. doi: 10.1080/02699050600831835

Lee, R. R., and Huang, M. (2014). Magnetoencephalography in the diagnosis of concussion. *Prog. Neurol. Surg.* 28, 94–111. doi: 10.1159/000358768

Liddelow, S. A., and Barres, B. A. (2017). Reactive astrocytes: production, function, and therapeutic potential. *Immunity* 46, 957–967. doi: 10.1016/j.immuni.2017.06.006

Lin, Y. S., Lee, W. J., Wang, S. J., and Fuh, J. L. (2018). Levels of plasma neurofilament light chain and cognitive function in patients with Alzheimer or Parkinson disease. *Sci. Rep.* 8:17368. doi: 10.1038/s41598-018-35766-w

Marion, D. W., Curley, K. C., Schwab, K., Hicks, R. R., and mTBI Diagnostics Workgroup, (2011). Proceedings of the military mTBI Diagnostics Workshop, St. Pete Beach. *J Neurotrauma* 28, 517–526. doi: 10.1089/neu.2010.1638

McKee, A. C., Cantu, R. C., Nowinski, C. J., Hedley-Whyte, E. T., Gavett, B. E., Budson, A. E., et al. (2009). Chronic traumatic encephalopathy in athletes: progressive tauopathy after repetitive head injury. *J. Neuropathol. Exp. Neurol.* 68, 709–735. doi: 10.1097/NEN.0b013e3181a9d503

McKee, A. C., Stern, R. A., Nowinski, C. J., Stein, T. D., Alvarez, V. E., Daneshvar, D. H., et al. (2013). The spectrum of disease in chronic traumatic encephalopathy. *Brain* 136(Pt 1), 43–64. doi: 10.1093/brain/aws307

Montgomery, D. L. (1994). Astrocytes: form, functions, and roles in disease. *Vet. Pathol.* 31, 145–167. doi: 10.1177/030098589403100201

Moore, T. M., Risbrough, V. B., Baker, D. G., Larson, G. E., Glenn, D. E., Nievergelt, C. M., et al. (2017). Effects of military service and deployment on clinical symptomatology: The role of trauma exposure and social support. *J. Psychiatr. Res.* 95, 121–128. doi: 10.1016/j.jpsychires.2017.08.013

National Center for Injury Prevention and Control (2003). *Report to Congress on Mild Traumatic Brain Injury in the United States: Steps to Prevent a Serious Public Health Problem*. Atlanta, GA: Centers for Disease Control and Prevention.

Ngolab, J., Trinh, I., Rockenstein, E., Mante, M., Florio, J., Trejo, M., et al. (2017). Brain-derived exosomes from dementia with Lewy bodies propagate α-synuclein pathology. *Acta Neuropathol. Commun.* 5:46. doi: 10.1186/s40478-017-0445-5

O'Neil, M. E., Carlson, K. F., Storzbach, D., Brenner, L. A., Freeman, M., Quiñones, A. R., et al. (2014). Factors associated with mild traumatic brain injury in veterans and military personnel: a systematic review. *J. Int. Neuropsychol. Soc.* 20, 249–261. doi: 10.1017/S1355617714000204

Ponsford, J., Cameron, P., Fitzgerald, M., Grant, M., and Mikocka-Walus, A. (2011). Long-term outcomes after uncomplicated mild traumatic brain injury: a comparison with trauma controls. *J. Neurotrauma* 28, 937–946. doi: 10.1089/neu.2010.1516

Povlishock, J. T., and Katz, D. I. (2005). Update of neuropathology and neurological recovery after traumatic brain injury. *J. Head Trauma Rehabil.* 20, 76–94. doi: 10.1097/00001199-200501000-00008

Prince, C., and Bruhns, M. E. (2017). Evaluation and treatment of mild traumatic brain injury: the role of neuropsychology. *Brain Sci.* 7:E105.

Putz, U., Howitt, J., Lackovic, J., Foot, N., Kumar, S., Silke, J., et al. (2008). Nedd4 family-interacting protein 1 (Ndfip1) is required for the exosomal secretion of Nedd4 family proteins. *J. Biol. Chem.* 283, 32621–32627. doi: 10.1074/jbc.M804120200

Rajendran, L., Honsho, M., Zahn, T. R., Keller, P., Geiger, K. D., Verkade, P., et al. (2006). Alzheimer's disease beta-amyloid peptides are released in association with exosomes. *Proc. Natl. Acad. Sci. U.S.A.* 103, 11172–11177. doi: 10.1073/pnas.0603838103

Randolph, C., Karantzoulis, S., and Guskiewicz, K. (2013). Prevalence and characterization of mild cognitive impairment in retired national football league players. *J. Int. Neuropsychol. Soc.* 19, 873–880. doi: 10.1017/S1355617713000805

Reilly, P., Winston, C. N., Baron, K., Trejo, M., Rockenstein, E. M., Akers, J. C., et al. (2017). Novel human neuronal tau model exhibiting neurofibrillary tangles

and transcellular propagation. *Neurobiol. Dis.* 106, 222–234. doi: 10.1016/j.nbd.2017.06.005

Rubenstein, R., Chang, B., Davies, P., Wagner, A. K., Robertson, C. S., and Wang, K. K. (2015). A novel, ultrasensitive assay for tau: potential for assessing traumatic brain injury in tissues and biofluids. *J. Neurotrauma* 32, 342–352. doi: 10.1089/neu.2014.3548

Salat, D. H., Robinson, M. E., Miller, D. R., Clark, D. C., and McGlinchey, R. E. (2017). Neuroimaging of deployment-associated traumatic brain injury (TBI) with a focus on mild TBI (mTBI) since 2009. *Brain Inj.* 31, 1204–1219. doi: 10.1080/02699052.2017.1327672

Shahim, P., Tegner, Y., Marklund, N., Blennow, K., and Zetterberg, H. (2018). Neurofilament light and tau as blood biomarkers for sports-related concussion. *Neurology* 90, e1780–e1788. doi: 10.1212/WNL.0000000000005518

Shahim, P., Zetterberg, H., Tegner, Y., and Blennow, K. (2017). Serum neurofilament light as a biomarker for mild traumatic brain injury in contact sports. *Neurology* 88, 1788–1794. doi: 10.1212/WNL.0000000000003912

Shin, S. S., Bales, J. W., Edward Dixon, C., and Hwang, M. (2017). Structural imaging of mild traumatic brain injury may not be enough: overview of functional and metabolic imaging of mild traumatic brain injury. *Brain Imaging Behav.* 11, 591–610. doi: 10.1007/s11682-017-9684-0

Stern, R. A., Tripodis, Y., Baugh, C. M., Fritts, N. G., Martin, B. M., Chaisson, C., et al. (2016). Preliminary study of plasma exosomal tau as a potential biomarker for chronic traumatic encephalopathy. *J. Alzheimers Dis.* 51, 1099–1109. doi: 10.3233/JAD-151028

Tartaglia, M. C., Hazrati, L. N., Davis, K. D., Green, R. E., Wennberg, R., Mikulis, D., et al. (2014). Chronic traumatic encephalopathy and other neurodegenerative proteinopathies. *Front. Hum. Neurosci.* 8:30. doi: 10.3389/fnhum.2014.00030

Tsitsopoulos, P. P., and Marklund, N. (2013). Amyloid-beta peptides and tau protein as biomarkers in cerebrospinal and interstitial fluid following traumatic brain injury: a review of experimental and clinical studies. *Front. Neurol.* 4:79. doi: 10.3389/fneur.2013.00079

Vogt, D., Smith, B. N., King, L. A., King, D. W., Knight, J., and Vasterling, J. J. (2013). Deployment risk and resilience inventory-2 (DRRI-2): an updated tool for assessing psychosocial risk and resilience factors among service members and veterans. *J. Trauma Stress* 26, 710–717. doi: 10.1002/jts.21868

von Holst, H., and Cassidy, J. D. (2004). Mandate of the WHO collaborating centre task force on mild traumatic brain injury. *J. Rehabil. Med.* 36(43 Suppl.), 8–10. doi: 10.1080/16501960410023633

Wakida, N. M., Cruz, G. M. S., Ro, C. C., Moncada, E. G., Khatibzadeh, N., Flanagan, L. A., et al. (2018). Phagocytic response of astrocytes to damaged neighboring cells. *PLoS One* 13:e0196153. doi: 10.1371/journal.pone.0196153

Winston, C. N., Aulston, B., Rockenstein, E. M., Adame, A., Prikhodko, O., Dave, K. N., et al. (2018). Neuronal exosome-derived human tau is toxic to recipient mouse neurons in vivo. *J. Alzheimers Dis.* 67, 541–553. doi: 10.3233/JAD-180776

Winston, C. N., Goetzl, E. J., Akers, J. C., Carter, B. S., Rockenstein, E. M., Galasko, D., et al. (2016). Prediction of conversion from mild cognitive impairment to dementia with neuronally derived blood exosome protein profile. *Alzheimers Dement* 3, 63–72. doi: 10.1016/j.dadm.2016.04.001

Winston, C. N., Goetzl, E. J., Schwartz, J. B., Elahi, F. M., and Rissman, R. A. (2019). Complement protein levels in plasma astrocyte-derived exosomes are abnormal in conversion from mild cognitive impairment to Alzheimer's disease dementia. *Alzheimers Dement* 11, 61–66. doi: 10.1016/j.dadm.2018.11.002

Xiong, Y., Mahmood, A., and Chopp, M. (2018). Current understanding of neuroinflammation after traumatic brain injury and cell-based therapeutic opportunities. *Chin. J, Traumatol.* 21, 137–151. doi: 10.1016/j.cjtee.2018.02.003

Yurgil, K. A., Barkauskas, D. A., Vasterling, J. J., Nievergelt, C. M., Larson, G. E., Schork, N. J., et al. (2014). Association between traumatic brain injury and risk of posttraumatic stress disorder in active-duty Marines. *JAMA Psychiatry* 71, 149–157. doi: 10.1001/jamapsychiatry.2013.3080

Conflict of Interest: The authors declare that the research was conducted in the absence of any commercial or financial relationships that could be construed as a potential conflict of interest.

frontiers in Neuroscience

ORIGINAL RESEARCH
published: 09 October 2019
doi: 10.3389/fnins.2019.01059

Proteomic Profiling of Extracellular Vesicles Isolated From Cerebrospinal Fluid of Former National Football League Players at Risk for Chronic Traumatic Encephalopathy

*Satoshi Muraoka[1], Mark P. Jedrychowski[2], Harutsugu Tatebe[3], Annina M. DeLeo[1], Seiko Ikezu[1], Takahiko Tokuda[4], Steven P. Gygi[2], Robert A. Stern[5,6] and Tsuneya Ikezu[1,5]**

[1] Department of Pharmacology and Experimental Therapeutics, Boston University School of Medicine, Boston, MA, United States, [2] Department of Cell Biology, Harvard Medical School, Boston, MA, United States, [3] Department of Medical Innovation and Translational Medical Science, Kyoto Prefectural University of Medicine, Kyoto, Japan, [4] Department of Molecular Pathobiology of Brain Diseases, Kyoto Prefectural University of Medicine, Kyoto, Japan, [5] Department of Neurology, Alzheimer's Disease Center, CTE Center, Boston University School of Medicine, Boston, MA, United States, [6] Department of Neurosurgery, and Anatomy & Neurobiology, Boston University School of Medicine, Boston, MA, United States

OPEN ACCESS

Edited by:
Francesc Xavier Guix,
Severo Ochoa Molecular Biology Center (CSIC-UAM), Spain

Reviewed by:
Fiona Crawford,
The Roskamp Institute, United States
Andrej Kovac,
Slovak Academy of Sciences (SAS), Slovakia

***Correspondence:**
Tsuneya Ikezu
tikezu@bu.edu

Specialty section:
This article was submitted to Neurodegeneration, a section of the journal Frontiers in Neuroscience

Received: 30 May 2019
Accepted: 20 September 2019
Published: 09 October 2019

Citation:
Muraoka S, Jedrychowski MP, Tatebe H, DeLeo AM, Ikezu S, Tokuda T, Gygi SP, Stern RA and Ikezu T (2019) Proteomic Profiling of Extracellular Vesicles Isolated From Cerebrospinal Fluid of Former National Football League Players at Risk for Chronic Traumatic Encephalopathy. Front. Neurosci. 13:1059. doi: 10.3389/fnins.2019.01059

Chronic Traumatic Encephalopathy (CTE) is a tauopathy that affects individuals with a history of repetitive mild traumatic brain injury, such as American football players. Initial neuropathologic changes in CTE include perivascular deposition of phosphorylated microtubule-associated protein tau (p-tau) neurofibrillary tangles and other aggregates in neurons, astrocytes and cell processes in an irregular pattern often at the depths of the cortical sulci. In later stages, the p-tau depositions become widespread and is associated with neurodegeneration. Extracellular vesicles (EVs) are known to carry neuropathogenic molecules, most notably p-tau. We therefore examined the protein composition of EVs isolated from the cerebrospinal fluid (CSF) of former National Football League (NFL) players with cognitive and neuropsychiatric dysfunction, and an age-matched control group (CTRL) with no history of contact sports or traumatic brain injury. EVs were isolated from the CSF samples using an affinity purification kit. Total tau (t-tau) and tau phosphorylated on threonine181 ($p\text{-}tau_{181}$) in CSF-derived EVs from former NFL players and CTRL participants were measured by ultrasensitive immunoassay. The t-tau and $p\text{-}tau_{181}$ levels of CSF-derived EV were positively correlated with the t-tau and $p\text{-}tau_{181}$ levels of total CSF in former NFL players, respectively, but not in the CTRL group. 429 unique proteins were identified from CSF-derived EVs and quantified by TMT-10 plex method. The identified protein molecules were significantly enriched for the extracellular exosome molecules, Alzheimer's disease pathway and Age/Telomere Length ontology as determined by DAVID Gene Ontology analysis. Ingenuity pathway analysis of the differentially expressed EV proteins revealed enrichment of canonical

liver/retinoid X receptor activation pathway. Upstream effect analysis predicted MAPT (tau) as an upstream regulator in former NFL players. These data will be useful for understanding the EV-mediated disease spread and development of novel EV biomarkers for CTE and related disorders.

Keywords: chronic traumatic encephalopathy, cerebrospinal fluid, extracellular vesicles, microtubule-associated protein tau, proteome, tauopathy, football

INTRODUCTION

Chronic Traumatic Encephalopathy (CTE) is a neurodegenerative tauopathy associated with repetitive mild traumatic brain injury, including concussion and subconcussion. CTE was first described in boxers in the 1920s and 1930s as "punch drunk," (Martland, 1928) or "dementia pugilistica," (Millspaugh, 1937) but has been more recently identified in other contact/collision sports athletes (including American football, soccer, ice hockey, and rugby players) (McKee et al., 2013, 2016; Bieniek et al., 2015; Ling et al., 2017; Mez et al., 2017; Tagge et al., 2018). Similar to other neurodegenerative diseases, CTE can only be diagnosed conclusively by neuropathologic examination. It is characterized by the perivascular deposition of phosphorylated microtubule-associated protein tau (p-tau) neurofibrillary tangles and other aggregates in neurons, astrocytes and cell processes in an irregular pattern often at the depths of the cortical sulci. In later stages, the p-tau depositions becomes widespread and is associated with neurodegeneration (McKee et al., 2015; Mez et al., 2017). CTE has a unique neuropathology from other tauopathies and the tau filaments of CTE are distinct from those in Alzheimer's disease (AD) (McKee et al., 2016; Falcon et al., 2019).

Currently, CTE cannot be diagnosed during life. A recent study provided preliminary support for the positron emission tomography (PET) imaging p-tau ligand flortaucipir to detect CTE in living former National Football League (NFL) players (Stern et al., 2019). However, PET imaging for routine diagnostic or screening purposes is limited due to its expense and lack of availability. Accessible fluid biomarkers could be more useful for assessing the presence of CTE Cerebrospinal fluid (CSF) measures of total tau (t-tau), p-tau, and amyloid-β peptide (Ab) are widely accepted as diagnostic and prognostic biomarkers for AD (Meredith et al., 2013; Galasko and Shaw, 2017). In an initial study of CSF in the detection of CTE, there were no significant differences between former NFL players and controls in CSF t-tau and p-tau levels. However CSF t-tau in the former NFL players was associated with exposure to repetitive head impacts (RHIs) (Alosco et al., 2018).

Extracellular vesicles (EVs), including exosomes (50–150 nm), ectosomes/microvesicles (150–1000 nm), and apoptotic bodies (1000–5000 nm) are released from neurons, glia, and various other cells into the extracellular space (Perez-Gonzalez et al., 2012; DeLeo and Ikezu, 2018). They contain microRNA, mRNA, and proteins that could be transferred to recipient cells for intracellular communication. EVs are found in all bodily fluids including blood, saliva, and CSF. In the central nervous system (CNS), it has been reported that tau, Aβ, alpha-synuclein, and prion protein are presented in EVs, and that the EVs in the brain play important roles in AD, Parkinson's disease, and prion diseases (Asai et al., 2015; Quek and Hill, 2017). In recent years, the proteins or microRNA present in EVs have emerged as an attractive target for neuronal disease detection and monitoring (Stern et al., 2016; DeLeo and Ikezu, 2018; Gill et al., 2018; Ko et al., 2018; Delpech et al., 2019). Other studies have reported proteomics analysis of EVs isolated from CSF, providing protein profiling on the composition of CSF-derived EVs as potential biomarkers for neurodegenerative diseases with high specificity (Chiasserini et al., 2014; Lee et al., 2016; Manek et al., 2018). Here, we aimed to identify a potential biomarker for diagnosing and monitoring of CTE, and we establish the proteomic profile of CSF-derived EVs in former NFL players using the ultrasensitive immunoassay and mass spectrometry.

MATERIALS AND METHODS

Sample Selection

The CSF samples were obtained from the National Institutes of Health–funded study, "Diagnosing and Evaluating Traumatic Encephalopathy using Clinical Tests" (DETECT) at Boston University School of Medicine (BUSM). Participants included in the current study were 15 former NFL players with cognitive and neuropsychiatric symptoms and a control group (CTRL) of 16 asymptomatic same-age men without a history of contact/collision sports or traumatic brain history. The DETECT study procedures, including lumbar puncture and neuropsychological assessment, have been described elsewhere (Alosco et al., 2017, 2018). An estimate of the cumulative number of repetitive head impacts from football was calculated for NFL participants (Montenigro et al., 2017). The Institutional Review Board at Boston University Medical Campus approved the protocol and all participants provided informed consent.

Purification of EVs From Human CSF Samples

The EV fraction was isolated from CSF samples using the MagCapture Exosome Isolation Kit PS (#293-77601 Fujifilm WAKO Pure Chemical Corporation, Japan). Briefly, the CSF samples were centrifuged at 1,200 g for 20 min at 4°C, then the supernatant was centrifuged at 10,000 g for 30 min at 4°C. The supernatant was filtered by 0.22 μm Spin-X centrifuge tube (#CLS8160 Corning, United States), then the EV fraction was isolated from the flow-through using the MagCapture Exosome Isolation Kit PS, according to the manufacturer's instructions.

Measurement of Total Tau (t-Tau) and Tau Phosphorylated on Threonine 181 (p-Tau$_{181}$)

M-PER® Mammalian Protein Extraction Reagent (#78503 PIERCE) was added to the isolated EV fraction using MagCapture Exosome Isolation Kit PS with Halt^{TM} Protease and Phosphatase Inhibitor Cocktail (#78442 Thermo Fisher Scientific, United States) and was mixed by vortexing for 15 min. The lysed EVs were filtered by 0.45 μm Spin-X centrifuge tube (#CLS8162 Corning, United States). The EV t-tau and p-tau$_{181}$ were measured using modified the Human Total Tau Simoa kit (Quanterix, Lexington, MA) on the Simoa HD-1 analyzer (Quanterix). Briefly, this kit is an updated version of the Simoa assay. It uses a monoclonal capture antibody that reacts with an epitope in the mid-region of all tau isoforms in combination with a detection antibody that reacts with an epitope at the N-terminus of t-tau for t-tau immunoassay or in PHF-tau (AT270, Thermo Fisher Scientific) for p-tau$_{181}$ immunoassay. We used t-tau or human tau (p-tau$_{181}$) as standards in the Human Tau ELISA^{TM} kit or Human Tau [pT181] phosphoELISA^{TM} ELISA kit (Invitrogen, Thermo Fisher Scientific) for each assay, respectively (Tatebe et al., 2017). All CSF-derived EV samples were diluted 4x with the Tau 2.0 Sample Diluent (Invitrogen, Thermo Fisher Scientific) prior to the assays, to minimize matrix effects, and were analyzed in duplicate on one occasion. The relative concentration estimates of t-tau and p-tau$_{181}$ were calculated according to the standard curve. For CSF t-tau and p-tau$_{181}$, the levels were measured using the multiplex xMAP Luminex platform (Luminex Corp., Austin, TX, United States) with Fujirebio (INNO-BIA AlzBio3, Ghent, Belgium) immunoassay kit-based reagents (Alosco et al., 2018).

Nanosight Tracking Analysis (NTA)

All samples were diluted in double-filtered PBS (dfPBS, with 0.22 μm pore-size) at least 1:10 to obtain particles within the target reading range for the Nanosight 300 machine (Malvern Panalytical Inc.), which was 10-100 particles per frame. Using a stage pump system four 30-s videos were taken for each sample at 21°C. Analysis of particle counts was carried out in the Nanosight NTA 3.2 software (Malvern Panalytical Inc.) with a detection threshold of 5.

SDS-PAGE and In-Gel Digestion

Ice-cold 100% (w/v) trichloroacetic acid (TCA) (#T6399 Sigma-Aldrich) was added to the isolated EV fraction to a final concentration of 20% of TCA, then the mixed sample was incubated for 30 min on ice and was centrifuged at 15,000 g for 20 min at 4°C. The pellet was then washed twice with ice-cold acetone (#179124 Sigma-Aldrich). After drying, the pellet was resuspended in Laemmli sample buffer (#1610747 Bio-Rad) with 5 mM dithiothreitol (# 43815 Sigma-Aldrich), reduced for 20 min at 65°C, and alkylated with 15 mM iodoacetamide (# I1149 Sigma-Aldrich) for 20 min at room temperature in the dark. Subsequently, the samples were run in a 4–20% gradient gel (#4561096 Bio-Rad) until the dye front was 10 mm from the top of the gel. The gels were washed twice with distilled water, fixed with 100% Methanol, and stained with GelCode Blue Stain Reagent (#24590 Thermo Fisher Scientific) for 16 hrs. Each lane was then individually removed from the gel. Gel pieces were then transferred to 1.5 mL tubes and destained twice using 50% acetonitrile (J. T. Baker, United States) in 25 mM HEPES (pH 8.8) at 22°C, for 15 min with shaking, and dehydrated with 100% acetonitrile for additional 10 min with shaking, for a total of three times. The destained gel piece was dried up using SpeedVac Concentrators (Thermo Fisher Scientific). The gel pieces were digested with proteomic grade trypsin (#03708985 Roche, United States) in 25 mM HEPES overnight at 37°C. The digested peptide was extracted with 70% acetonitrile/1% formic acid, and were removed the gel by Ultrafree-MC Centrifugal Filter (#UFC30L Millipore United States). The digested peptides were reconstituted in 25 μL of 200 mM EPPS (pH 8.0) and vortexed for 5 min.

Peptide Labeling With TMT 10-Plex Isobaric Labeling Kit

Tandem mass tag (TMT) labeling was performed according to the manufacturer's instructions (#90409 Thermo Fisher Scientific). In brief, 4 μL of TMT reagent (20 ng/μL) was added to the digested peptides. Following incubation at room temperature for 1 h, the reaction was quenched with 2 μL of 5% hydroxylamine for 15 min. The TMT-labeled peptide samples were pooled at a 1:1 ratio across 10 samples. The combined sample was added into 100 μL of 20% formic acid, 2 mL of 1% formic acid, desalted via StageTip, dried by vacuum centrifugation, and resuspended in 5% acetonitrile and 5% formic acid for nano-liquid chromatography and tandem mass-spectrometry (NanoLC-MS/MS).

Nano-Liquid Chromatography and Tandem Mass-Spectrometry

NanoLC–MS/MS analysis was conducted by an LTQ-Orbitrap Fusion Lumos mass spectrometer (Thermo Fisher Scientific) equipped with a Proxeon EASY-nanoLC 1200 liquid chromatography pump (Thermo Fisher Scientific, San Jose, CA, United States). Peptides were separated on a 100 μm inner diameter microcapillary column packed with ∼40 cm of Accucore 150 resin (2.6 μm, 150 Å, Thermo Fisher Scientific). We loaded 4 μL onto the column and separation was achieved using a 180 min gradient of 8 to 23% acetonitrile in 0.125% formic acid at a flow rate of ∼550 nL/min. The analysis used an MS3 based TMT method, which has been shown to reduce ion interference. The scan sequence began with an MS1 spectrum (Orbitrap; resolution 120,000; mass range 400–1400 m/z; automatic gain control (AGC) target 5×10^5; maximum injection time 100 ms). Precursors for MS^2/MS^3 analysis were selected using a Top10 method. MS2 analysis consisted of collision-induced dissociation (quadrupole ion trap; AGC 2×10^4; normalized collision energy (NCE) 35; maximum injection time 150 ms). Following acquisition of each MS^2 spectrum, we collected an MS^3 spectrum using our recently described method in which multiple MS^2 fragment ions were captured in the MS^3 precursor population using isolation waveforms with multiple frequency notches. MS^3 precursors were fragmented by high energy collision-induced

dissociation (HCD) and analyzed using the Orbitrap (NCE 65; AGC 1×10^5; maximum injection time 150 ms, resolution was 50,000 at 200 Th).

Mass-Spectrometry Data Analysis

A compendium of in-house developed software was used to convert mass spectrometric data (Raw file) to the mzXML format, as well as to correct monoisotopic m/z measurements (Elias and Gygi, 2007). Database searching included all entries from the *Homo sapiens* UniProt database (downloaded October, 2018). This database was concatenated with one composed of all protein sequences in the reversed order. Searches were performed using a 50 ppm precursor ion tolerance for total protein level profiling (McAlister et al., 2014). The product ion tolerance was set to 0.9 Da. These wide mass tolerance windows were chosen to maximize sensitivity in conjunction with SEQUEST searches and linear discriminant analysis. TMT tags on lysine residues and peptide N termini (+ 229.163 Da) and carbamidomethylation of cysteine residues (+ 57.021 Da) were set as static modifications, while oxidation of methionine residues (+ 15.995 Da) was set as a variable modification. Peptide-spectrum matches (PSMs) were adjusted to a 1% false discovery rate (FDR). Filtering was performed using an in-house linear discrimination analysis (LDA) method to create one combined filter parameter from the following peptide ion and MS2 spectra metrics: SEQUEST parameters XCorr and ΔCn, peptide ion mass accuracy and charge state, in-solution charge of peptide, peptide length and mis-cleavages. Linear discrimination scores were used to assign probabilities to each MS2 spectrum for being assigned correctly and these probabilities were further used to filter the dataset with an MS2 spectra assignment FDR of smaller than a 1% at the protein level (Huttlin et al., 2010). For TMT-based reporter ion quantitation, we extracted the summed signal-to-noise (S/N) ratio for each TMT channel and found the closest matching centroid to the expected mass of the TMT reporter ion. PSMs were identified, quantified, and collapsed to a 1% peptide false discovery rate (FDR) and then collapsed further to a final protein-level FDR of 1%. Moreover, protein assembly was guided by principles of parsimony to produce the smallest set of proteins necessary to account for all observed peptides. Proteins were quantified by summing reporter ion counts across all matching PSMs. PSMs with poor quality, MS^3 spectra with more than eight TMT reporter ion channels missing, MS^3 spectra with TMT reporter summed signal-to-noise ratio less than 100, or no MS^3 spectra were excluded from quantification. The mass spectrometry proteomics data have been deposited to the ProteomeXchange Consortium via the PRIDE partner repository with the dataset identifier PXD015358 (Perez-Riverol et al., 2019). Protein quantitation values were exported for further analysis in Microsoft Excel or Prism 6. Each reporter ion channel was summed across all quantified proteins.

Statistical Analysis

Statistical analysis was conducted using IBM SPSS software ver.25 and GraphPad Prism 6. Between group comparisons were analyzed by non-parametric Mann-Whitney U or one-way ANOVA followed by Bonferroni correction for multiple comparisons. Bivariate correlation analysis examined differences between former NFL players and controls in EV t-tau, EV p-tau$_{181}$, proteomics data, and demographics data using IBM SPSS software ver.25. The Gene Ontology of identified proteins were elucidated by DAVID Bioinformatics Resources 6.8. The Protein networks and pathway analysis were generated using Ingenuity Pathway Analysis (IPA)[1]. The Venn diagram and Heatmap analysis were generated using Venny_2.1[2] and MeV_4_8[3].

RESULTS

Workflow for Proteome Analysis of Former NFL Players CSF Derived EVs

The experimental workflow is summarized in **Figure 1**. The EVs were isolated from former NFL players CSF and an age-matched control group (CTRL) with no history of contact sports or traumatic brain injury using the MagCapture Exosome isolation kit. For EV t-tau and p-tau$_{181}$ immunoassays, the 10 former NFL players and 8 CTRLs isolated EVs were lysed with M-Per lysis buffer and then measured the levels of t-tau and p-tau$_{181}$ in EVs or total CSF were measured by ultrasensitive or conventional immunoassay (see Materials and Methods) (**Supplementary Table S1**). For the proteome profiling, the CSF samples were analyzed as (1) 4 pooled samples from either 2 or 4 former NFL players or CTRL individuals and as (2) individual samples from 4 former NFL players and 5 CTRLs (**Table 1** and **Supplementary Table S1**). The isolated EVs were run in the SDS-PAGE for in-gel digestion, the digested peptides were then labeled with TMT 10-plex isobaric labeling kit, and analyzed by high sensitivity mass spectrometry (see Materials and Methods).

Biochemical Characterization of Former NFL Players CSF-Derived EVs

To measure the concentration and size of EVs in CSF, we examined former NFL players and control CSF-derived EVs using nanoparticle tracking analysis (NTA, **Supplementary Figure S1**). The EV concentrations in former NFL players and CTRLs CSF had no significant difference (p = 0.9628). The mode size distribution peaked at 86 nm in former NFL players CSF and at 88 nm in CTRLs (p = 0.9628) (**Figure 2A**). To characterize the CSF-derived EVs, we isolated EVs from the CSF samples of former NFL players and CTRLs using the MagCapture Exosome Isolation kit. First, we measured the concentration of total tau (t-tau) and phosphorylated tau protein at threonine 181 (p-tau$_{181}$) in isolated EVs and total CSF from the 10 former NFL players and 8 CTRLs by ultrasensitive immunoassay or multiplex Luminex assay. Both t-tau and p-tau could be detected in both former NFL players and CTRLs CSF-derived EVs and total CSF samples. However, there was no significant difference between former NFL players and CTRLs (t-tau: p = 0.8688 and p-tau$_{181}$: p = 0.2682 in CSF-derived EVs; t-tau: p = 0.3031 and

[1]https://www.qiagenbioinformatics.com/products/ingenuity-pathway-analysis/
[2]http://bioinfogp.cnb.csic.es/tools/venny/
[3]http://mev.tm4.org

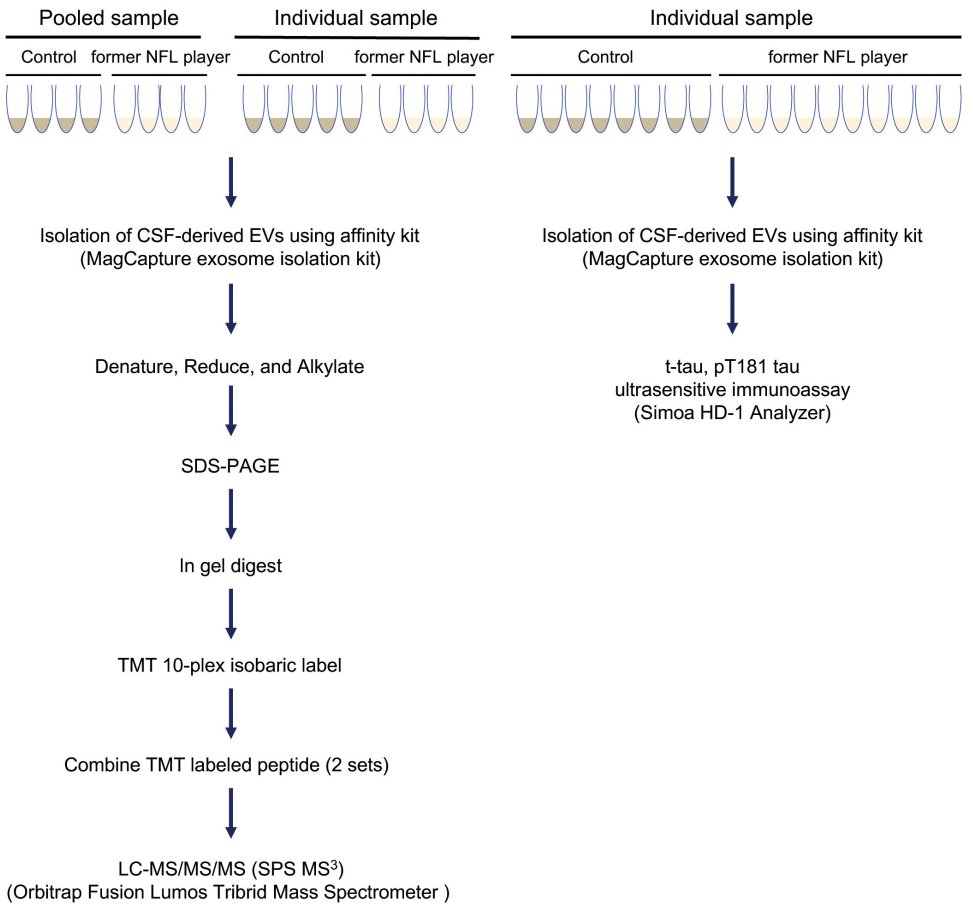

FIGURE 1 | Workflow used in proteomics analysis of former NFL players CSF-derived EVs: EVs were isolated from control and former NFL players CSF using MagCapture Isolation kit. For pooled proteomics analysis, 4 pooled samples from former NFL players or CTRLs were tested. For individual proteomics analysis, samples from 4 former NFL players and 5 CTRLs were tested. The isolated EVs were denatured, reduced, and alkylated and run on 4–20% gradient SDS-PAGE gel. The protein band was cut out of the gel followed by trypsin digestion and labeled with TMT 10-plex isobaric label kit. The combing TMT-labeled peptide was analyzed by MS^3 on Orbitrap Fusion Lumos Tribrid Mass Spectrometer. For immunoassays, EV samples from 10 former NFL players and 8 CTRLs were tested. Total tau (t-tau) and tau phosphorylated at threonine 181 (p-tau_{181}) in CSF-derived EV or total CSF samples were measured by ultrasensitive or conventional immunoassay (Simoa or multiplex Luminex systems), respectively.

p-tau_{181}: $p = 0.9477$ in total CSF) (**Figures 2B,C**). The level of EV p-tau_{181} was significantly correlated with EV t-tau ($r = 0.870$, $p < 0.0001$) (**Figure 2D**). Unexpectedly, the EV t-tau levels were lower than those of EV p-tau_{181}. One possible explanation is that the majority of tau in the CSF EVs is fragmented. Next, we assessed the correlation of CSF-derived EV t-tau, p-tau_{181} and total CSF t-tau, p-tau_{181} by Pearson's correlation analysis. There is a positive correlation between CSF t-tau, p-tau_{181} and EV t-tau, p-tau_{181} levels in former NFL players (t-tau: $r = 0.812$, $p = 0.0044$; p-tau_{181}: $r = 0.627$, $p = 0.0524$) (**Figure 2E**), but not in the CTRL group (t-tau: $r = -0.492$, $p = 0.2150$; p-tau_{181}: $r = -0.530$, $p = 0.1770$) (data not shown).

TMT-Based Proteomic Analysis of EV Proteins Isolated From the CSF of Former NFL Players and CTRL Group

To generate EV protein profiling of former NFL players' CSF, we analyzed EV proteins isolated from the former NFL players and CTRL cohorts by NanoLC-MS/MS using TMT-based labeling (Paulo et al., 2018). We identified a total of 429 unique proteins across both cohorts (**Supplementary Tables S2, S3**). The identified proteins were compared with the top 100 EV proteins

TABLE 1 | Patient information.

	Control (n = 16)	NFL player (n = '15)	p-value[a]
Age, mean	57.06 ± 6.95	56.33 ± 7.31	0.7178
BMI, mean	27.81 ± 3.43	33.07 ± 4.66	0.0008
Duration of football play, mean year	–	18.87 ± 3.96	–
Years in NFL, mean year	–	8.40 ± 3.48	–
Cumulative Head Impact Index[b]	–	20728.46 ± 6739.56	–

[a]*The statistical significance of the differences were calculated using Mann-Whitney test.* [b]*Estimated number of football-related repetitive head impacts (Montenigro et al., 2017).*

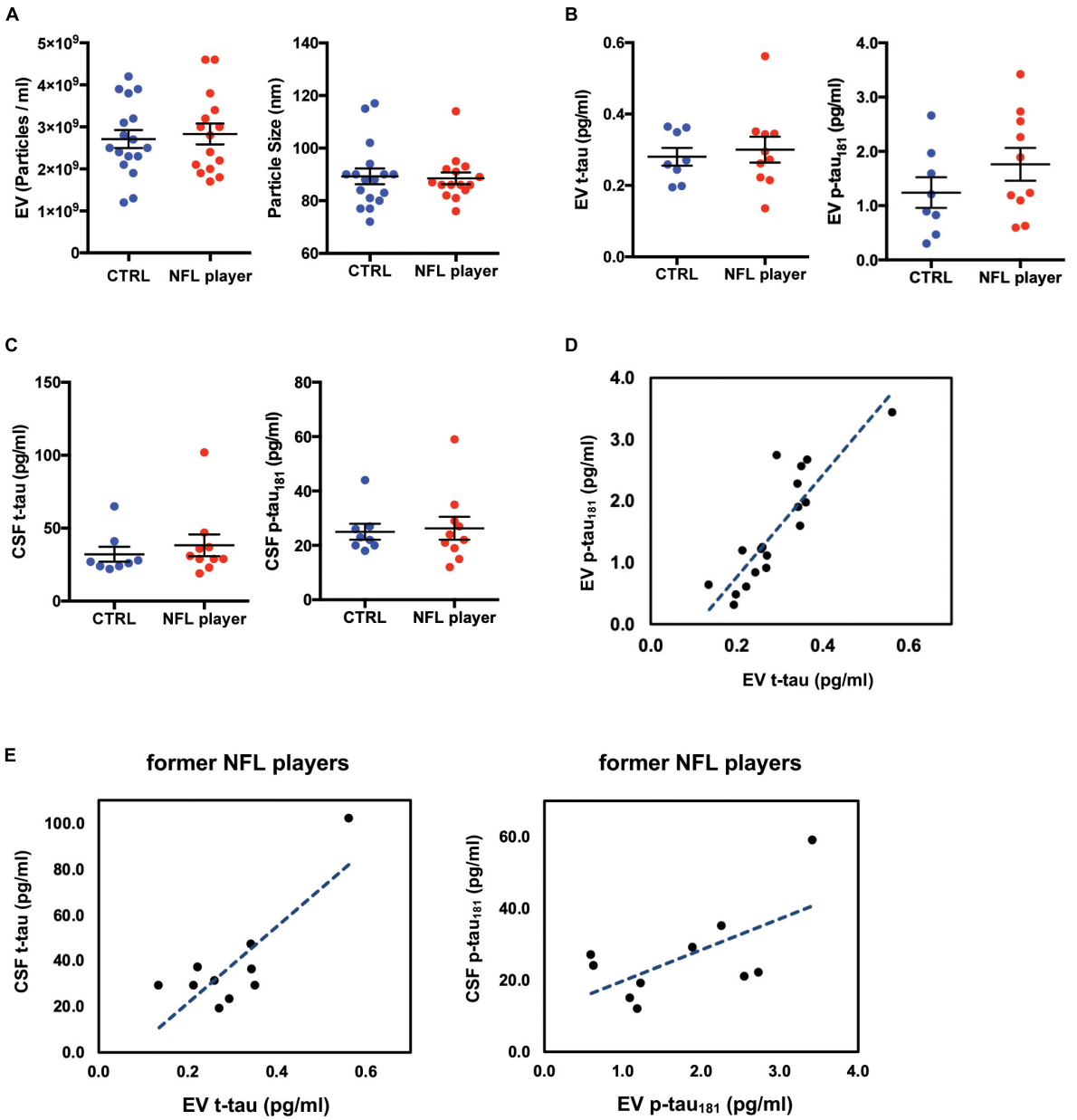

FIGURE 2 | Biochemical characteristic of CSF-derived EVs isolated from former NFL players. **(A)** Left: Particle numbers of CSF-derived EV fraction from CTRL or former NFL players by Nanoparticle tracking analysis ($p = 0.9628$ by Mann-Whitney test). Right: Particle size of CSF-derived EV fraction ($p = 0.9628$). **(B)** T-tau and p-tau$_{181}$ levels in CSF-derived EVs by ultrasensitive immunoassay. Left: EV t-tau levels ($p = 0.8688$). Right: EV p-tau$_{181}$ levels ($p = 0.2682$). **(C)** T-tau and p-tau$_{181}$ levels in total CSF by multiplex Luminex platform. Left: CSF t-tau ($p = 0.3031$). Right: CSF p-tau$_{181}$ ($p = 0.9477$). **(D)** Scattered plot of t-tau and p-tau$_{181}$ in CSF derived EV samples ($r = 0.870$, $p < 0.0001$). **(E)** Left: Scattered plot of t-tau levels in CSF-derived EV and in total CSF in the former NFL players ($r = 0.812$, $p = 0.0044$). Right: Scattered plot of p-tau$_{181}$ levels in CSF-derived EV and in total CSF in the former NFL players ($r = 0.627$, $p = 0.0524$).

from the EVpedia database (Kim et al., 2015). The comparison revealed that 62 of the top 100 EV proteins were expressed in the CSF-derived EVs (**Figure 3A**). The 381 proteins remaining after exclusion of keratins and immunoglobulins were examined with respect to Cellular component, Tissue expression, and Disease annotation by Gene Ontology analysis in the Database for Annotation, Visualization and Integrated Discovery (DAVID). Among these 381 proteins, 73.9% of them were annotated to be the Extracellular exosome ontology (**Figure 3B**), indicative of the purity of our CSF-derived EV samples. Furthermore, 11.8% of the identified molecules were enriched for the Alzheimer's disease or Aging/Telomere Length pathway, which was related to AD and senescence-associate genetic alteration (**Figure 3C**). The EV samples were enriched in exosomal markers, including Rab GTPases, immune receptors, flotillins, annexins, tetraspanins, apolipoproteins, heat shock proteins, and ESCRT associated

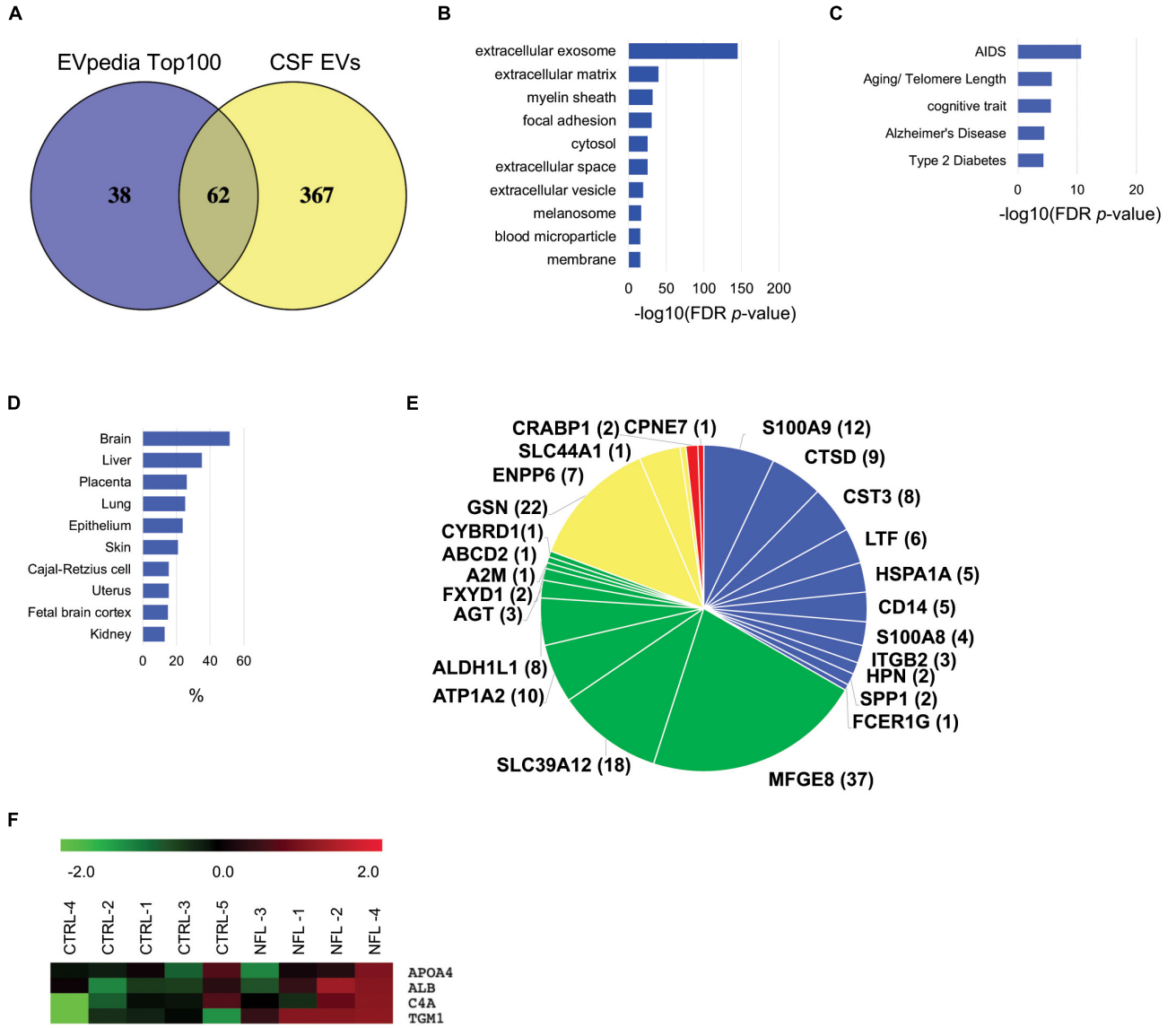

FIGURE 3 | Bioinformatic characterization of former NFL players CSF-derived EV proteome dataset: **(A)** Venn diagram of the 429 proteins identified in CSF-derived EV and EVpedia Top 100. **(B)** Gene Ontology (GO) analysis using DAVID Bioinformatics Resources 6.8. The GO term of Top10 Cellular Component with –log10 (FDR *p*-value). **(C)** The GO term of Top5 Disease Ontology with –log10 (FDR *p*-value). **(D)** The GO term of Top10 Tissue Expression Ontology with% enrichment. **(E)** Enrichment of brain cell-specific markers in CSF-derived EV proteins. The brain cell-specific markers were searched using Barres Brain RNA-Seq datasets. Blue: Microglia, Green: Astrocytes, Yellow: Oligodendrocytes, Red: neurons. The parentheses show the number of identified peptides by LC-MS/MS. **(F)** Heatmap of EV proteins in individual proteome dataset. Each row in the heat map show a protein, and each column represent CTRL and former NFL players. Red indicate up-regulate expression and Green show down-regulate.

proteins (**Table 2**). Using tissue expression analysis, we observed enrichment of 196 proteins (51.6%) derived from brain tissues (**Figure 3D**). We searched for brain cell-specific markers within the EV proteomics dataset using the Brain RNA-Seq database created by Barres Lab (Zhang Y. et al., 2014). Several proteins in our dataset were identified in the database as enriched markers for microglia (S100A9, CTSD, CST3, LTF, HSPA1A, CD14, S100A8, ITGB2, HPN, SPP1, FCER1G), astrocyte markers (MFGE8, SLC39A12, ATP1A2, ALDH1L1, AGT, FXYD1, A2M, ABCD2, CYBRD1), oligodendrocyte markers (GSN, ENPP6, SLC44A1) and neuron markers (CRABP1, CPNE7) (**Figure 3E**). These data indicated that the CSF-derived EVs were secreted from brain cells, and presumably mainly from glial cells. Using individual proteome dataset, we investigated differences in the expression of EV proteins between the 4 former NFL players and 5 CTRL groups. However, no molecules were significantly altered between former NFL players and control groups based on the criteria of at least >1.5 or <0.67-fold-change with an adjusted *p* value of <0.05. Next, we performed semi-supervised hierarchical clustering of differentially expressed proteins across

TABLE 2 | Identification of exosomal markers in CSF-derived EV.

		Pooled proteome	Individual proteome
Family[a]	Gene name	Identified peptide[b]	Identified peptide
RAB	RAB10	1	0
IR	HLA-A	4	1
	HLA-DRA	3	2
	HLA-DRB1	2	2
	HLA-DRB5	2	0
	CD14	3	2
	CD59	7	4
FLOT	FLOT1	1	0
ANXA	ANXA1	3	5
	ANXA2	26	14
	ANXA4	3	4
	ANXA5	12	12
	ANXA6	11	5
	ANXA7	3	0
	ANXA11	3	1
TSPAN	CD9	9	3
	CD81	8	3
	CD82	2	0
	TSPAN4	0	2
APO	APOA1	18	1
	APOA4	6	7
	APOD	11	1
	APOE	26	18
HSP	HSPA1A	4	1
	HSPA8	18	11
	HSPB1	3	3
	HSPD1	8	0
	HSPE1	2	0
	HSP90AA1	10	1
	HSP90AB1	7	0
ESCRT-AP	PDCD6IP	18	13
	SDCBP	16	9

[a]RAB, Rab GTPases; IR, immune receptor; FLOT, flotillin; ANXA, annexin; TSPAN HSP, tetraspanin; APO, apolipoprotein; HSP, heat shock prottein; ESCRT-AP, ESCRT associated proteine. [b]The identified peptid shows count by LC-MS/MS.

the individual proteomics dataset using Pearson Correlation metric and Average Linkage clustering as parameters for the Raw (proteins). Proteins cluster if they are differentially expressed between former NFL players and CTRLs (**Figure 3F**). The TGM1 protein, which was colocalized with aggregated Ab in senile plaques (SPs) and tau in Neurofibrillary tangles (NFTs) (Wilhelmus et al., 2009), in the cluster showed significant difference in expression level, but did not meet the pre-specified fold change cut-off (fold change = 1.18, $p = 0.0259$).

Networks Analysis for Former NFL Players CSF-Derived EV Individual Proteome Dataset

To assess enriched canonical pathways, upstream, and functional networks in the differentially expressed 61 EV proteins in the former NFL players (fold-change: >1.2 or <0.83), we analyzed the individual sample datasets using Ingenuity Pathway Analysis (IPA). Among top 10 differentially regulated canonical pathway, liver/retinoid X receptor (LXR/RXR) activation pathway, which was associated with ALB, C4A, FGA, S100A8, TF, TTR and SERPINA1, was upregulated in the former NFL players (**Figure 4A** and **Table 3**). Interestingly, MAPT (tau) was predicted as an upstream regulator protein for 10 differentially expressed EV proteins in the former NFL players (**Figure 4B**). Finally, we identified the signaling network for the connecting the tauopathy and MAPT regulating proteins (**Figure 4C**), suggesting the potential use of these molecules for the assessment of molecular changes induced by tau accumulation or tauopathy development in the CNS.

DISCUSSION

In this study, we performed digital ELISA analysis of t-tau and p-tau$_{181}$ and NanoLC–MS/MS analysis in CSF-derived EVs from former NFL players for the first time. We found that t-tau and p-tau$_{181}$ levels of CSF-derived EV were positively correlated with the t-tau and p-tau$_{181}$ levels of total CSF in former NFL players, but not in the CTRL group. We also identified 429 unique proteins from CSF-derived EVs, which were significantly enriched for the extracellular exosome molecules, Alzheimer's disease pathway and Age/Telomere Length ontology as determined by DAVID Gene Ontology analysis. Ingenuity pathway analysis of the differentially expressed EV proteins revealed enrichment of canonical liver/retinoid X receptor activation pathway. Finally, upstream effect analysis predicted MAPT (tau) as an upstream regulator in former NFL players.

As for tau levels in the CSF-derived EVs, the t-tau levels in the CSF-derived EV samples was lower than expected and accounted for less than 20% of p-tau$_{181}$ levels. One explanation for this finding is that EVs in CSF might contain an N-terminal-deleted fragment of tau, which might be undetected by the tau ELISA kit. We used a commercial Human Tau ELISA^{TM} kit and modified Human Tau [pT181] phosphoELISA^{TM} kit for this study. The total tau ELISA kit uses a capture antibody that reacts with mid-region of tau and a detection antibody that recognizes the N-terminal region. However, the modified phosphoELISA kit uses a capture antibody that recognizes the mid-region of tau and a detection antibody that reacts with p-tau$_{181}$. When t-tau and p-tau$_{181}$ in the CSF from the same former NFL players and CTRLs were measured by Fujirebio kit, which uses mid-region capture antibody for t-tau or p-tau$_{181}$ specific antibody in mid-region for p-tau and mid-region-specific detector antibody for both t-tau and p-tau detection, the CSF level of t-tau was higher than p-tau. Chen et al. (2019) reported that N-terminal and mid-region containing fragments of tau were elevated in CSF with AD and MCI, but did not detect full-length tau in the CSF. Other studies indicated that the N-terminal fragments of tau were secreted by activated neurons, which was increased in

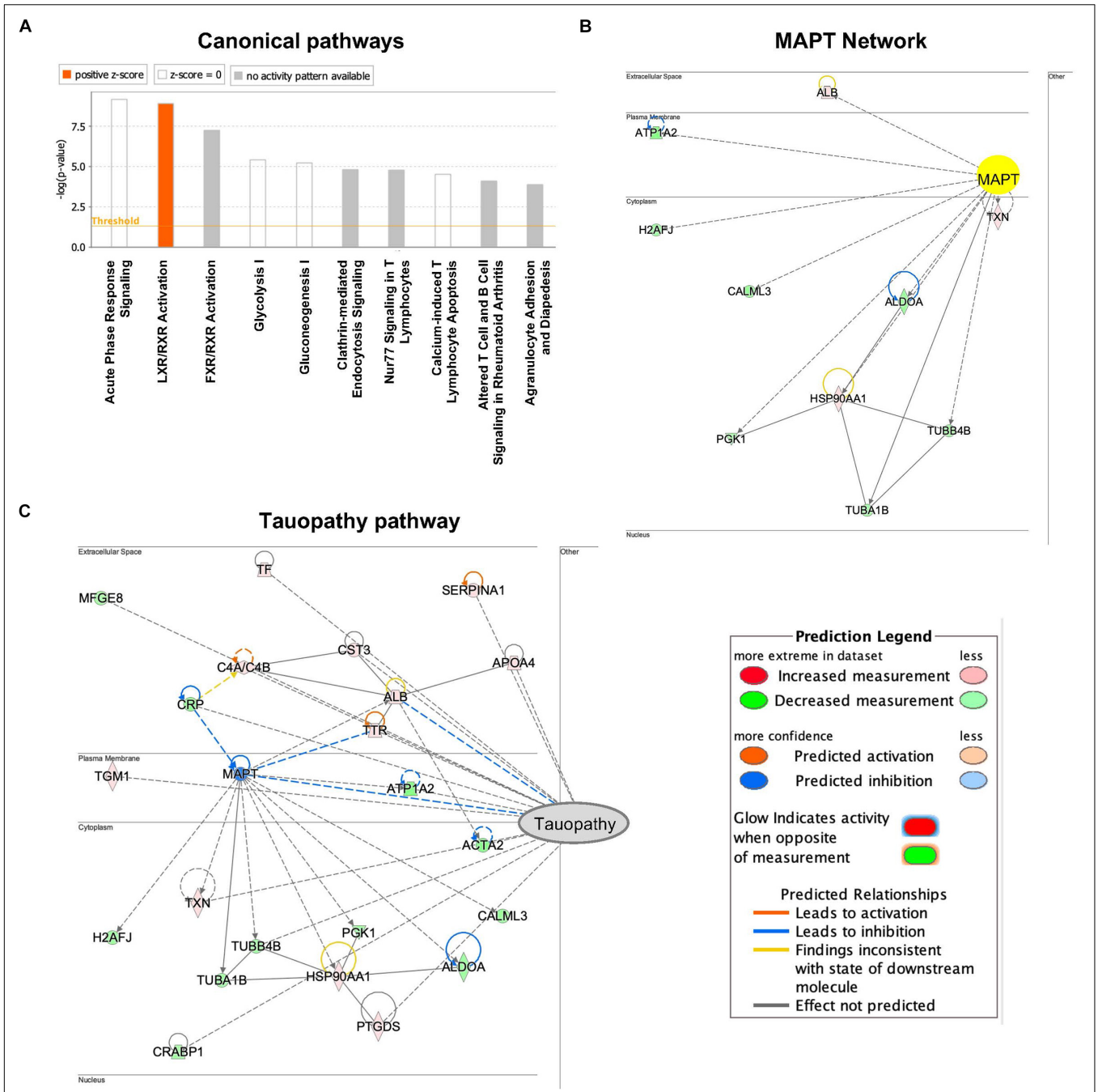

FIGURE 4 | Networks produced by Ingenuity pathway analysis based on CSF-derived EV proteome dataset from individual former NFL players: **(A)** The canonical pathways that were up- and down-regulated in former NFL players compared to controls. Upregulated pathways are denoted in red. **(B)** Upstream effect analysis of differentially expressed EV proteins in former NFL players. IPA predicted MAPT (tau) as activated and suppressed upstream regulator protein. Up-regulated protein is denoted in red and down-regulated protein is shown green. Solid and dashed lines are indicated direct and indirect interactions, respectively. **(C)** IPA-based protein network in neurological disease based on tauopathy. The intensity of the node color shows the degree of up–regulation (red) or down–regulation (green).

CSF from AD patients (Chen et al., 2019; Cicognola et al., 2019). Moreover, Zhao et al. (2016) reported that caspase-2-cleaved tau fragment were elevated in AD tissue, which was infiltrated into dendritic spines and ultimately induced memory dysfunction in their mouse models. On other hands, in the hippocampal tissue of AD patients, Calpain 1 and 2-cleaved tau fragments were found, but could not induce their phosphorylation or cytotoxicity (Ferreira and Bigio, 2011; Garg et al., 2011). In addition to caspase and calpain, thrombin, asparagine endopeptidase and cathepsins have been reported

TABLE 3 | Canonical pathways generated from protein lists comprised of significant proteins by Ingenuity Pathway Analysis.

Canonical pathway	Associated with the canonical pathway[a]	Ratio	−log (*p*-value)
Acute phase response signaling	ALB, C4A, CRABP1, CRP, FGA, FN1, SERPINA1.TF, TTR	9/178	9.178
LXR/RXR activation	ALB, APOA4, C4A, FGA, S100A8, SERPINA1, TF, TTR	8/128	8.928
FXR/RXR activation	ALB, APOA4, C4A, FGA, SERPINA1, TF, TTR	7/137	7.256
Glycolysis 1	ALDOA, C3, PGK1, C9	4/42	5.412
Gluconeogenesis 1	ALDOA, C3, PGK1, C9	4/47	5.213
Clathrin mediated endocytosis signaling	ACTA2, ALB, APOA4, S100A8, SERPINA1, TF	6/212	4.796
77 signaling in T lymphocytes	CALML5, FCER1G, HLA-A, HLA-DRB1	4/60	4.788
Calcium-induced T lymphocyte apoptosis	CALML5, FCER1G, HLA-A, HLA-DRB1	4/70	4.521
Altered T cell and B cell signaling in rheumatoid arthritis	FCER1G, HLA-A, HLA-DRB1, SPP1	4/90	4.093
Agranulocyte adhesion and diapedesis	ACTA2, FN1, GNAI2, MYH9, RDX	5/193	3.886

[a]*ALB, albumin; C4A, complement C4-A; CRABP1, cellular retinoic acid-binding protein 1; CRP, C-reactive protein; FGA, fibrinogen alpha chain; FN1, fibronectin; SERPINA1, alpha-1-antitrypsin; TF, Serotransferrin; TTR, transthyretin; APOA4, apolipoprotein A-IV; S100A8, Protein S100-A8; ALDOA, fructose-bisphosphate aldolase A; C3, complement C3; PGK1, phosphoglycerate kinase 1; C9, complement C9; ACTA2, actin aortic smooth muscle; FCER1G, high affinity immunoglobulin epsilon receptor subunit gamma; HLA-A, HLA class I histocompatibility antigen A-2 alpha chain; HLA-DRB1, HLA class II histocompatibility antigen DRB1-14 beta chain; SPP1, osteopontin; GNAI2, guanine nucleotide-binding protein G(i) subunit alpha-2; MYH9, myosin-9; RDX, radixin.*

to be tau-cleaving enzymes (Zhang Z. et al., 2014). Calpain-1 and Caspase-14 were identified in CSF-derived EVs in the present proteome analysis; therefore, this suggests that CSF-derived EVs might be contained N-terminal-deletion fragments of tau. Future studies are necessary to determine whether fragments of tau are present in specific brain cell type-specific derived EVs within CSF.

There is accumulating interest in proteomic analysis of CSF and CSF-derived EVs to identify biomarkers for neurodegenerative disorders. Here, we report the first proteomic analysis of CSF-derived EV samples isolated from former NFL players. Our proteomic analysis reports a slightly higher enrichment rate of EV-specific molecules in our CSF-derived EV preparation than previous reports, despite the lower number of identified molecules (Street et al., 2012; Chiasserini et al., 2014; Lee et al., 2016; Manek et al., 2018). The MagCapture exosome isolation kit employed here has been reported to have a higher purity of EV than other exosome isolation kits, resulting in the lower protein yields (Nakai et al., 2016). For these reasons, although we used 3 mL of CSF per sample in the present study, the number of identified proteins was lower than other have reported. In this individual proteomics study, we analyzed 4 former NFL players and 5 CTRL groups but found no significant differences between the groups. This could be due to the small sample size and some of the NFL players may not have CTE although they are high risk group. A further study is necessary with increased sample size and follow up with the former NFL players. When our proteomics dataset was compared with the CSF proteome dataset, only 114 proteins were commonly detected between total CSF and CSF-derived EVs, and they were mostly non-EV molecules (Dayon et al., 2019). On the other hand, our proteomic profiling data indicated that CSF-derived EVs are enriched in molecules from microglia, astrocytes, oligodendrocytes, and neurons to a lesser extent. Moreover, in CSF derived EVs, proteins specific to such brain cell as microglia (S100A9, CTSD, CST3, LTF, HSPA1A, CD14, S1008, ITGB2, SPP1), astrocytes (MFGE8, SLC39A12, ATP1A2, AGT, A2M), oligodendrocytes (GSN), and neurons (CRABP1) were identified commonly in the present study as well as by previously published proteomics studies on pooled human CSF samples (Chiasserini et al., 2014). Canonical pathway analysis revealed that enrichment of acute phase response and LXR/RXR activation, suggesting the elevation of inflammatory conditions and lipid biosynthesis pathway in the CSF-derived EVs from former NFL players. Researchers have reported the LXR/RXR pathway has important neuroprotective roles in neurodegenerative disease, including stroke, ALS, AD, and PD (Nam et al., 2016). In AD, LXR/RXR pathway has a role in microglial activity or in clearance of amyloid beta from the brain (Moutinho and Landreth, 2017). In former NFL players with risk of CTE, the LXR/RXR pathway might be able to affect neuronal survival and regulate microglia activity. Future exploration is needed to elucidate the activation of this pathway in CTE.

In summary, we have quantified tau levels and proteomic profiles in CSF-derived EVs from former NFL players in this study, identified unique enrichment of Alzheimer's disease pathway and Age/Telomere Length ontology, canonical liver/retinoid X receptor activation pathway, and predicted MAPT (tau) as an upstream regulator in former NFL players. Fluid and neuroimaging biomarkers have been mainly focused on tau: Tau PET imaging has been developed as an important tool for CTE diagnosis (Stern et al., 2019) and total tau and exosomal tau were identified as blood-based biomarker in CTE (Stern et al., 2016). The CSF is an attractive biofluid for biomarker discovery research with abundant proteins associated with neurodegenerative diseases in early stages in comparison to blood samples (Alosco et al., 2018). Our results suggested that p-tau$_{181}$ in CSF-derived EVs and a combination of several cell type-specific molecules are potential monitoring biomarkers in former NFL players at risk for CTE. Further investigations are necessary to confirm these biomarkers, including additional validation sets, and to clarify the implications of the correlation

of this marker with disease, and to elucidate the mechanisms of EV secretion from the brain cell types in former NFL players.

DATA AVAILABILITY STATEMENT

The datasets generated for this study can be found in the ProteomeXchange Consortium via the PRIDE partner repository with the dataset identifier PXD015358 (http://www.proteomexchange.org).

ETHICS STATEMENT

The studies involving human participants were reviewed and approved by the Boston University School of Medicine. The patients/participants provided their written informed consent to participate in this study.

AUTHOR CONTRIBUTIONS

SM, RS, and TI designed the research. SM, MJ, HT, and AD performed the research. SM, MJ, SG, TT, and TI analyzed the data. RS provided the CSF samples. SM and TI wrote the manuscript. SM, MJ, AD, SI, RS, and TI edited the manuscript.

FUNDING

This work was in part funded by the Aethlon Medical, Inc. (TI), Cure Alzheimer's Fund (TI), NIH RF1AG054199 (TI), NIH R56AG057469 (TI), R01NS078337 (RS), U01NS093334 (RS), P30AG13846 (RS), and AMED 17dk0207042s0101 (TT).

ACKNOWLEDGMENTS

We thank the Ikezu lab members (K. Yukawa-Takamatsu and M. B. Botros) for experimental supports.

SUPPLEMENTARY MATERIAL

The Supplementary Material for this article can be found online at: https://www.frontiersin.org/articles/10.3389/fnins.2019.01059/full#supplementary-material

FIGURE S1 | NTA plot of average size and concentration of EVs from former NFL player and CTRL CSF: The black line shows the fitting curve. Red line represents the error bar. The y axis is the concentration of particles. The x axis is the size of particle. **(A)** Former NFL player, **(B)** CTRL.

TABLE S1 | The sample size of each groups in this study.

TABLE S2 | Proteins identified and quantified in TMT-labeled experiment.

TABLE S3 | Peptides identified and quantified in TMT-labeled experiment.

REFERENCES

Alosco, M. L., Jarnagin, J., Tripodis, Y., Platt, M., Martin, B., Chaisson, C. E., et al. (2017). Olfactory function and associated clinical correlates in former national football league players. *J. Neurotrauma* 34, 772–780. doi: 10.1089/neu.2016.4536

Alosco, M. L., Tripodis, Y., Fritts, N. G., Heslegrave, A., Baugh, C. M., Conneely, S., et al. (2018). Cerebrospinal fluid tau, Aβ, and sTREM2 in former national football league players: modeling the relationship between repetitive head impacts, microglial activation, and neurodegeneration. *Alzheimers Dement* 14, 1159–1170. doi: 10.1016/j.jalz.2018.05.004

Asai, H., Ikezu, S., Tsunoda, S., Medalla, M., Luebke, J., Haydar, T., et al. (2015). Depletion of microglia and inhibition of exosome synthesis halt tau propagation. *Nat. Neurosci.* 18, 1584–1593. doi: 10.1038/nn.4132

Bieniek, K. F., Ross, O. A., Cormier, K. A., Walton, R. L., Soto-Ortolaza, A., Johnston, A. E., et al. (2015). Chronic traumatic encephalopathy pathology in a neurodegenerative disorders brain bank. *Acta Neuropathol.* 130, 877–889. doi: 10.1007/s00401-015-1502-4

Chen, Z., Mengel, D., Keshavan, A., Rissman, R. A., Billinton, A., Perkinton, M., et al. (2019). Learnings about the complexity of extracellular tau aid development of a blood-based screen for Alzheimer's disease. *Alzheimers Dement* 15, 487–496. doi: 10.1016/j.jalz.2018.09.010

Chiasserini, D., van Weering, J. R. T., Piersma, S. R., Pham, T. V., Malekzadeh, A., Teunissen, C. E., et al. (2014). Proteomic analysis of cerebrospinal fluid extracellular vesicles: a comprehensive dataset. *J. Proteom.* 106, 191–204. doi: 10.1016/j.jprot.2014.04.028

Cicognola, C., Brinkmalm, G., Wahlgren, J., Portelius, E., Gobom, J., Cullen, N. C., et al. (2019). Novel tau fragments in cerebrospinal fluid: relation to tangle pathology and cognitive decline in Alzheimer's disease. *Acta Neuropathol.* 137, 279–296. doi: 10.1007/s00401-018-1948-2

Dayon, L., Cominetti, O., Wojcik, J., Galindo, A. N., Oikonomidi, A., Henry, H., et al. (2019). Proteomes of paired human cerebrospinal fluid and plasma: relation to blood-brain barrier permeability in older adults. *J. Proteome Res.* 18, 1162–1174. doi: 10.1021/acs.jproteome.8b00809

DeLeo, A. M., and Ikezu, T. (2018). Extracellular vesicle biology in Alzheimer's disease and related tauopathy. *J. Neuroimmune Pharmacol.* 13, 292–308. doi: 10.1007/s11481-017-9768-z

Delpech, J.-C., Herron, S., Botros, M. B., and Ikezu, T. (2019). Neuroimmune crosstalk through extracellular vesicles in health and disease. *Trends Neurosci.* 42, 361–372. doi: 10.1016/j.tins.2019.02.007

Elias, J. E., and Gygi, S. P. (2007). Target-decoy search strategy for increased confidence in large-scale protein identifications by mass spectrometry. *Nat. Methods* 4, 207–214. doi: 10.1038/nmeth1019

Falcon, B., Zivanov, J., Zhang, W., Murzin, A. G., Garringer, H. J., Vidal, R., et al. (2019). Novel tau filament fold in chronic traumatic encephalopathy encloses hydrophobic molecules. *Nature* 568, 420–423. doi: 10.1038/s41586-019-1026-5

Ferreira, A., and Bigio, E. H. (2011). Calpain-mediated tau cleavage: a mechanism leading to neurodegeneration shared by multiple tauopathies. *Mol. Med.* 17, 676–685. doi: 10.2119/molmed.2010.00220

Galasko, D. R., and Shaw, L. M. (2017). Alzheimer disease: CSF biomarkers for Alzheimer disease - approaching consensus. *Nat. Rev. Neurol.* 13, 131–132. doi: 10.1038/nrneurol.2017.11

Garg, S., Timm, T., Mandelkow, E.-M., Mandelkow, E., and Wang, Y. (2011). Cleavage of Tau by calpain in Alzheimer's disease: the quest for the toxic 17 kD fragment. *Neurobiol. Aging* 32, 1–14. doi: 10.1016/j.neurobiolaging.2010.09.008

Gill, J., Mustapic, M., Diaz-Arrastia, R., Lange, R., Gulyani, S., Diehl, T., et al. (2018). Higher exosomal tau, amyloid-beta 42 and IL-10 are associated with mild TBIs and chronic symptoms in military personnel. *Brain Inj.* 32, 1277–1284. doi: 10.1080/02699052.2018.1471738

Huttlin, E. L., Jedrychowski, M. P., Elias, J. E., Goswami, T., Rad, R., Beausoleil, S. A., et al. (2010). A tissue-specific atlas of mouse protein phosphorylation and expression. *Cell* 143, 1174–1189. doi: 10.1016/j.cell.2010.12.001

Kim, D.-K., Lee, J., Kim, S. R., Choi, D.-S., Yoon, Y. J., Kim, J. H., et al. (2015). EVpedia: a community web portal for extracellular vesicles research. *Bioinformatics* 31, 933–939. doi: 10.1093/bioinformatics/btu741

Ko, J., Hemphill, M., Yang, Z., Sewell, E., Na, Y. J., Sandsmark, D. K., et al. (2018). Diagnosis of traumatic brain injury using miRNA signatures in nanomagnetically isolated brain-derived extracellular vesicles. *Lab Chip* 18, 3617–3630. doi: 10.1039/c8lc00672e

Lee, J., McKinney, K. Q., Pavlopoulos, A. J., Han, M. H., Kim, S.-H., Kim, H. J., et al. (2016). Exosomal proteome analysis of cerebrospinal fluid detects biosignatures of neuromyelitis optica and multiple sclerosis. *Clin. Chim. Acta* 462, 118–126. doi: 10.1016/j.cca.2016.09.001

Ling, H., Neal, J. W., and Revesz, T. (2017). Evolving concepts of chronic traumatic encephalopathy as a neuropathological entity. *Neuropathol. Appl. Neurobiol.* 43, 467–476. doi: 10.1111/nan.12425

Manek, R., Moghieb, A., Yang, Z., Kumar, D., Kobessiy, F., Sarkis, G. A., et al. (2018). Protein biomarkers and neuroproteomics characterization of microvesicles/exosomes from human cerebrospinal fluid following traumatic brain injury. *Mol. Neurobiol.* 55, 6112–6128. doi: 10.1007/s12035-017-0821-y

Martland, H. S. (1928). Punch drunk. *JAMA* 91, 1103–1107. doi: 10.1001/jama.1928.02700150029009

McAlister, G. C., Nusinow, D. P., Jedrychowski, M. P., Wühr, M., Huttlin, E. L., Erickson, B. K., et al. (2014). MultiNotch MS3 enables accurate, sensitive, and multiplexed detection of differential expression across cancer cell line proteomes. *Anal. Chem.* 86, 7150–7158. doi: 10.1021/ac502040v

McKee, A. C., Cairns, N. J., Dickson, D. W., Folkerth, R. D., Keene, C. D., Litvan, I., et al. (2016). The first NINDS/NIBIB consensus meeting to define neuropathological criteria for the diagnosis of chronic traumatic encephalopathy. *Acta Neuropathol.* 131, 75–86. doi: 10.1007/s00401-015-1515-z

McKee, A. C., Stein, T. D., Kiernan, P. T., and Alvarez, V. E. (2015). The neuropathology of chronic traumatic encephalopathy. *Brain Pathol.* 25, 350–364. doi: 10.1111/bpa.12248

McKee, A. C., Stern, R. A., Nowinski, C. J., Stein, T. D., Alvarez, V. E., Daneshvar, D. H., et al. (2013). The spectrum of disease in chronic traumatic encephalopathy. *Brain* 136, 43–64. doi: 10.1093/brain/aws307

Meredith, J. E., Sankaranarayanan, S., Guss, V., Lanzetti, A. J., Berisha, F., Neely, R. J., et al. (2013). Characterization of novel CSF Tau and ptau biomarkers for Alzheimer's disease. *PLoS One* 8:e76523. doi: 10.1371/journal.pone.0076523

Mez, J., Daneshvar, D. H., Kiernan, P. T., Abdolmohammadi, B., Alvarez, V. E., Huber, B. R., et al. (2017). Clinicopathological evaluation of chronic traumatic encephalopathy in players of American football. *JAMA* 318, 360–370. doi: 10.1001/jama.2017.8334

Millspaugh, J. A. (1937). Dementia pugilistica. *U.S. Nav. Med. Bull.* 35, 297–303.

Montenigro, P. H., Alosco, M. L., Martin, B. M., Daneshvar, D. H., Mez, J., Chaisson, C. E., et al. (2017). Cumulative head impact exposure predicts later-life depression, apathy, executive dysfunction, and cognitive impairment in former high school and college football players. *J. Neurotrauma* 34, 328–340. doi: 10.1089/neu.2016.4413

Moutinho, M., and Landreth, G. E. (2017). Therapeutic potential of nuclear receptor agonists in Alzheimer's disease. *J. Lipid Res.* 58, 1937–1949. doi: 10.1194/jlr.R075556

Nakai, W., Yoshida, T., Diez, D., Miyatake, Y., Nishibu, T., Imawaka, N., et al. (2016). A novel affinity-based method for the isolation of highly purified extracellular vesicles. *Sci. Rep.* 6:33935. doi: 10.1038/srep33935

Nam, K. N., Mounier, A., Fitz, N. F., Wolfe, C., Schug, J., Lefterov, I., et al. (2016). RXR controlled regulatory networks identified in mouse brain counteract deleterious effects of Aβ oligomers. *Sci. Rep.* 6:24048. doi: 10.1038/srep24048

Paulo, J. A., Jedrychowski, M. P., Chouchani, E. T., Kazak, L., and Gygi, S. P. (2018). Multiplexed isobaric tag-based profiling of seven murine tissues following in vivo nicotine treatment using a minimalistic proteomics strategy. *Proteomics* 18:e1700326. doi: 10.1002/pmic.201700326

Perez-Gonzalez, R., Gauthier, S. A., Kumar, A., and Levy, E. (2012). The exosome secretory pathway transports amyloid precursor protein carboxyl-terminal fragments from the cell into the brain extracellular space. *J. Biol. Chem.* 287, 43108–43115. doi: 10.1074/jbc.M112.404467

Perez-Riverol, Y., Csordas, A., Bai, J., Bernal-Llinares, M., Hewapathirana, S., Kundu, D. J., et al. (2019). The PRIDE database and related tools and resources in 2019: improving support for quantification data. *Nucleic Acids Res.* 47, D442–D450. doi: 10.1093/nar/gky1106

Quek, C., and Hill, A. F. (2017). The role of extracellular vesicles in neurodegenerative diseases. *Biochem. Biophys. Res. Commun.* 483, 1178–1186. doi: 10.1016/j.bbrc.2016.09.090

Stern, R. A., Adler, C. H., Chen, K., Navitsky, M., Luo, J., Dodick, D. W., et al. (2019). Tau Positron-Emission Tomography in Former National Football League Players. *N. Engl. J. Med.* 380, 1716–1725. doi: 10.1056/NEJMoa1900757

Stern, R. A., Tripodis, Y., Baugh, C. M., Fritts, N. G., Martin, B. M., Chaisson, C., et al. (2016). Preliminary study of plasma exosomal tau as a potential biomarker for chronic traumatic encephalopathy. *J. Alzheimers Dis.* 51, 1099–1109. doi: 10.3233/JAD-151028

Street, J. M., Barran, P. E., Mackay, C. L., Weidt, S., Balmforth, C., Walsh, T. S., et al. (2012). Identification and proteomic profiling of exosomes in human cerebrospinal fluid. *J. Transl. Med.* 10:5. doi: 10.1186/1479-5876-10-5

Tagge, C. A., Fisher, A. M., Minaeva, O. V., Gaudreau-Balderrama, A., Moncaster, J. A., Zhang, X.-L., et al. (2018). Concussion, microvascular injury, and early tauopathy in young athletes after impact head injury and an impact concussion mouse model. *Brain* 141, 422–458. doi: 10.1093/brain/awx350

Tatebe, H., Kasai, T., Ohmichi, T., Kishi, Y., Kakeya, T., Waragai, M., et al. (2017). Quantification of plasma phosphorylated tau to use as a biomarker for brain Alzheimer pathology: pilot case-control studies including patients with Alzheimer's disease and down syndrome. *Mol. Neurodegener.* 12:63. doi: 10.1186/s13024-017-0206-8

Wilhelmus, M. M. M., Grunberg, S. C. S., Bol, J. G. J. M., van Dam, A.-M., Hoozemans, J. J. M., Rozemuller, A. J. M., et al. (2009). Transglutaminases and transglutaminase-catalyzed cross-links colocalize with the pathological lesions in Alzheimer's disease brain. *Brain Pathol.* 19, 612–622. doi: 10.1111/j.1750-3639.2008.00197.x

Zhang, Y., Chen, K., Sloan, S. A., Bennett, M. L., Scholze, A. R., O'Keeffe, S., et al. (2014). An RNA-sequencing transcriptome and splicing database of glia, neurons, and vascular cells of the cerebral cortex. *J. Neurosci.* 34, 11929–11947. doi: 10.1523/JNEUROSCI.1860-14.2014

Zhang, Z., Song, M., Liu, X., Kang, S. S., Kwon, I.-S., Duong, D. M., et al. (2014). Cleavage of tau by asparagine endopeptidase mediates the neurofibrillary pathology in Alzheimer's disease. *Nat. Med.* 20, 1254–1262. doi: 10.1038/nm.3700

Zhao, X., Kotilinek, L. A., Smith, B., Hlynialuk, C., Zahs, K., Ramsden, M., et al. (2016). Caspase-2 cleavage of tau reversibly impairs memory. *Nat. Med.* 22, 1268–1276. doi: 10.1038/nm.4199

Conflict of Interest: TI has sponsored research agreement from Aethlon Medical, Inc., for this study.

The remaining authors declare that the research was conducted in the absence of any commercial or financial relationships that could be construed as a potential conflict of interest.

frontiers in Neuroscience

ORIGINAL RESEARCH
published: 18 October 2019
doi: 10.3389/fnins.2019.01067

Considerations and Implications in the Purification of Extracellular Vesicles – A Cautionary Tale

*Yi Xin Fiona Lee[1,2], Henrik Johansson[3], Matthew J. A. Wood[1] and Samir El Andaloussi[1,4]**

[1] Department of Physiology, Anatomy and Genetics, University of Oxford, Oxford, United Kingdom, [2] Genome Institute of Singapore, Agency for Science, Technology and Research, Singapore, Singapore, [3] Cancer Proteomics Mass Spectrometry, Science for Life Laboratory, Department of Oncology-Pathology, Karolinska Institutet, Stockholm, Sweden, [4] Department of Laboratory Medicine, Karolinska Institutet, Stockholm, Sweden

Extracellular vesicles (EVs) are nano-sized particles constitutively released from cells into all biological fluids. Interestingly, these vesicles contain genetic cargoes including proteins, RNA and bioactive lipids that can be functionally delivered and affect recipient cells. As a result, there is growing interest in studying EVs in pathological conditions, including central nervous system (CNS)-related diseases, as EVs may be used for diagnostic purposes or as therapeutic agents. However, one major bottleneck is the need for better EV purification strategies when considering complex biological sources such as serum/protein-rich media or plasma. In this study, we have performed a systematic comparison study between the current gold-standard method: ultracentrifugation, to an alternative: size-exclusion chromatography (LC), using induced pluripotent stem cell (iPSC) derived complex media as a model system. We demonstrate that LC allows for derivation of purer EVs from iPSCs, which was previously impossible with the original UC method. Importantly, our study further highlights the various drawbacks when using the conventional UC approach that lead to misinterpretation of EV data. Lastly, we describe novel data on our iPSC-EVs; how they could relate to stem cell biology and discuss their potential use as EV therapeutics for CNS diseases.

Keywords: extracellular vesicles, stem cells, proteomics, exosomes, isolation, purification

OPEN ACCESS

Edited by:
Grant Thomas Corbett, Brigham and Women's Hospital and Harvard Medical School, United States

Reviewed by:
In-Hyun Park, Yale University, United States
Valentina Bonetto, Istituto Di Ricerche Farmacologiche Mario Negri, Italy

***Correspondence:**
Samir El Andaloussi
Samir.El-Andaloussi@ki.se

Specialty section:
This article was submitted to Neurodegeneration, a section of the journal Frontiers in Neuroscience

Received: *08 July 2019*
Accepted: *24 September 2019*
Published: *18 October 2019*

Citation:
Lee YXF, Johansson H, Wood MJA and El Andaloussi S (2019) Considerations and Implications in the Purification of Extracellular Vesicles – A Cautionary Tale. Front. Neurosci. 13:1067. doi: 10.3389/fnins.2019.01067

INTRODUCTION

The very first report on secretory material from cells was by Wolf in 1967; here he observed the presence of minute phospholipid-rich, pro-coagulant substance from fresh platelet-free plasma which he then termed as "platelet-dusts" (Wolf, 1967). Subsequently, more studies revealed that these "dusts" were actually membranous nanosized particles that contained functional molecules, had downstream effects on recipient cells and could be collected from various bodily fluids (Raz et al., 1978; Trams et al., 1981). Based on the state of cells and mechanisms of release, these particles can be broadly classified into three main populations: "exosomes"- a pool of vesicles originating from the multivesicular endosome; "microvesicles"- a heterogeneous set of particles which directly shed off the plasma membrane, and "apoptotic bodies"- a much larger group of micelles which bleb off dying cells undergoing apoptosis (Harding et al., 1984; Pan et al., 1985; Raposo et al., 1996). Despite such known differences, there still appears to be significant overlaps in both molecular composition and size across all three populations. As it is challenging to purify each individual

group, there has been an active shift to use "extracellular vesicles (EVs)" as a collective term to instead describe these secretory vesicles (Bobrie et al., 2012; Gould and Raposo, 2013).

EVs as Communicators of Physiology and Disease

Historically, EVs were postulated to be the "garbage trucks" of cells; helping to remove unwanted molecular material out of cells. However, there are an increasing number of studies describing dedicated protein and RNA machineries that regulate the sorting of specific molecular contents (proteins and RNA) into and onto these vesicles (Szostak et al., 2014; Villarroya-Beltri et al., 2014; Janas et al., 2015; Hung and Leonard, 2016; Ragusa et al., 2017; Moreno-Gonzalo et al., 2018; Sork et al., 2018). Subsequently, these EVs serve as delivery men by following the unique "addresses" on their surface. Thus, EVs ferry their well-protected molecular cargoes within the bi-lipid boundaries and elicit phenotypic effects on recipient targets, some of which may locate at distal sites from their origin.

The presence and involvement of EVs in biology is best understood in the areas of immunology and cancer. Notably, EVs from dendritic cells can mimic their parental source to aid in antigen presentation and elicit a T cell response in normal physiological processes (Raposo et al., 1996; Zitvogel et al., 1998; Théry et al., 2001; Utsugi-Kobukai et al., 2003; Segura et al., 2005a,b). However, not all EV-mediated communications are beneficial, as in disease settings EVs can aid in the spread of pathogenesis. For example, EVs from primary cancer cells assist in the preparation of the pre-metastasis niche for colonization of migratory cancer cells (Janowska-Wieczorek et al., 2005; Peinado et al., 2012). Interestingly, one study found that subpopulations of EVs are secreted by a single pool of breast cancer cells and that each EV subtype can influence the formation of micro-metastases in the different organs, depending on the types of surface integrins (Hoshino et al., 2015).

EVs Contribute to Intercellular Brain Communication

The brain is a complex organ consisting of myriad neural networks between the multitudes of cell types. Hence, it is no surprise that there has been a steadily increasing body of evidence showing how EVs contribute to normal brain function and in central nervous system (CNS)-related diseases (Thompson et al., 2016). As in other body systems, all cell types of the brain, including neurons, oligodendrocytes, astrocytes and microglial cells, release EVs (Fauré et al., 2006; Krämer-Albers et al., 2007; Antonucci et al., 2012; Wang et al., 2012). Depending on the cell source and the physiological state, the characteristics of secreted EVs can vary accordingly and induce different functions in the brain. For example, EVs from neurons present the AMPA receptor subunit GluR2 and this contributes to synapse maturation and plasticity (Lachenal et al., 2011). Alternatively, EVs from neurons are enriched in syndecans and tetraspanins (e.g., CD81), which are important signaling cues (Bahi and Dreyer, 2005; Hienola et al., 2006). Hence, EVs can assist in neurite outgrowth and axon path finding. In other instances, EVs can act as important tools for the cross talk between different cell types in the brain, such as when oligodendrocytes release EVs in response to neuronal activity. These EVs carry metabolites such as catalase, which can be delivered back to the neurons for trophic support (Frühbeis et al., 2013). Similarly, Schwann cells have been shown to release EVs upon axonal damage (Krämer-Albers et al., 2007), where they could be active at the injury site and aid in axonal regeneration.

Technical Issues in EV Research-Purification Strategies

Despite growing knowledge of the importance of EVs to multicellular functions, there is still a lack of consensus on the methodologies for purifying EVs from cells. To date, the most common strategy remains differential ultracentrifugation (UC) due to its accessibility in most laboratories (Théry et al., 2006). However, with improved technologies for EV phenotyping, it is becoming increasingly evident that this "gold-standard" UC protocol suffers from several drawbacks; most of which are related to the yield, purity and physical integrity of EVs (Cvjetkovic et al., 2014; Nordin et al., 2015).

To address this issue, alternative methods for EV purification have been exploited. These include precipitation-based strategies; some of which can be coupled with antibody-capture methods on microfluidic devices or the use of magnetic nanowires (Ghosh et al., 2014; Kanwar et al., 2014; Lim et al., 2019; Sunkara et al., 2019). However, these methods may not be scalable, often compromise on EV purity (Yamada et al., 2012) and require more studies on if the purified EVs can be efficiently eluted and remain complementary to use for any downstream functional characterization. One other method which has gained popularity in recent years is size-exclusion liquid chromatography (LC). Unlike UC, the LC process does not require high speed spins and is scalable for large volume samples when combined with a pre-concentration step. All in all, many supporting reports have verified the feasibility of using LC for EV purification in several serum-free cell culture-based systems and in biological fluids (Chen et al., 2011; Arslan et al., 2013; Böing et al., 2014; Nordin et al., 2015; Welton et al., 2015; Mol et al., 2017; Oeyen et al., 2018; Lane et al., 2019; Takov et al., 2019).

Generally in EV research, it is required to use serum-free or exosome-cleared FBS for collection of conditioned media, as regular serum contains numerous microvesicles that can contaminate and confound the downstream analysis of the intended cellular EVs (Noerholm et al., 2012; Shelke et al., 2014; Wei et al., 2016; Kornilov et al., 2018; Lehrich et al., 2018). However, this becomes an issue when considering cell types which will change in serum-depleted media, such as stem cells. In all the previously studies on protocol comparison (Rood et al., 2010; Alvarez et al., 2012; Tauro et al., 2012; Rekker et al., 2014; Zhang et al., 2014; Livshits et al., 2015; Stranska et al., 2018; Takov et al., 2019), none have compared purification of EVs from protein-rich, complex media sources such as stem cell media. Here, we describe a systematic comparison study between UC and LC purified EVs from iPSCs. Interestingly, we find that their molecular contents vary based on protocol, which

will have implications on the interpretation of EV content and functionality. Lastly, we cross compared EVs to their parental sources and discuss the feasibility of using these iPSCs for CNS related research.

MATERIALS AND METHODS

Cell Culture of Pluripotent Stem Cell Lines and Embryonic Fibroblasts

Mouse embryonic fibroblasts (MEFs, derived from Dr. Paul Fairchild's lab) were grown in complete MEF growth media comprising of DMEM (Life Technologies) supplemented with 15% FBS and 50 μg/ml Penicillin/Streptomycin (P/S). To prepare feeders for stem cell culture, MEFs were treated with mitomycin-C (Sigma, United Kingdom) at 1 mg/ml of MEF media for 2 h. The treated MEFs were then washed three times with PBS and re-plated on fresh culture flasks. Mouse stem cell lines [embryonic stem cells (ESCs): ESF121, ESF116 and induced pluripotent stem cells (iPSCs): iMEF14, iMEF19]; all derived from Dr. Paul Fairchild's lab (Fairchild et al., 2000) were first cultured on mitomycin-C treated MEFs feeders. When the cells reached 80% confluence, one-tenth of the cells were plated on fresh feeders while the remainder were plated on 0.1% gelatin-coated plates. For both feeder and feeder-free conditions, cells were cultured in complete mouse stem cell media comprised of DMEM (Lonza, United Kingdom) supplemented with 15% knockout serum-replacement supplement (KOSR) (Life Technologies, United Kingdom), 2 mM L-glutamine (Life Technologies), 1 mM sodium pyruvate (Life Technologies), 0.1 mM non-essential amino acids (Life Technologies), 50 (μg/ml of P/S, 0.2 mM 2-mercaptoethanol (Sigma) and 106 units of mouse leukaemia inhibitory factor (mLIF, Miltenyi Biotec, United Kingdom). All cells were cultured at 37°C with 5% CO_2.

Collection of Conditioned Media (CM) for EV Purification

For the initial data shown in **Supplementary Figure S1**, pre-spun stem cell (PS) media described here was complete stem cell media that had been pre-spun at 120,000 *g* for 16 h prior to use. The OptiMEM (OM) media was OptiMEM (Life Technologies) supplemented with 50 μg/ml of P/S. For both ESC and iPSC cell lines, the stem cells were cultured twice on 0.1% gelatin-coated plates to get rid of any contaminating feeder cells prior to use for EV collection. For each cell line, 1M cells were initially seeded on a single 10 cm plate. When cells reached 70% confluence (48 or 72 h after plating), the growth media was removed; cells were washed with PBS and replaced with fresh stem cell media, PS or OM depending on the experimental set-up. Conditioned media (CM), ranging from 150–200 ml, was then collected 48 h after media change; cells were harvested by trypsin and counted with a hemocytometer. For each collection, the total CM was first centrifuged at 300 *g*, 5 min to get rid of cellular debris. The supernatant was decanted and further centrifuged at 2,000 *g*, 10 min to get rid of larger particles before subjecting to filtration through a 0.22 μm syringe filter. Subsequently, the CM was split equally into two volumes for UC and LC purification concurrently.

Purification of EVs

Purification of EVs by Differential Centrifugation Protocol (UC)

The UC protocol used for purification of EVs is based on an established protocol described by Théry et al. (2006). Briefly, the filtered CM was spun at 120,000 *g*, 70 min to pellet EVs. To eliminate any protein contaminations, the pellet was re-suspended in 25 ml of PBS and spun again at 120,000 *g* for 70 min. All centrifugation steps were performed at 4°C. The resultant pellet was then re-suspended in 100 μl of PBS and used fresh for analysis or kept at −80°C for further proteomics analysis.

Purification of EVs by Size-Exclusion Liquid Chromatography Protocol (LC)

The LC protocol used for purification of EVs was based on the method described by Taylor et al. (2011), with some slight modifications. Briefly, the filtered CM was concentrated using the Amicon 100k-Da molecular weight cut-off (MWCO) filters (Millipore, United Kingdom) at 3,500 *g* for 15 min. The concentrate retentate was then loaded onto a Sephacryl S-400 16/60 LC column (GE Healthcare, Sweden) and run with PBS at 0.5 ml/min. Fixed-volume 2 ml fractions of the eluted solutions were then collected with a fraction collector. Based on the 280 nm LC chromatograph, fractions covering the first 280 nm LC peak, designated as "F1," were pooled and concentrated with Amicon 10-kDa MWCO filters (Millipore) at 3,500 *g* for 15 min down to 100 μl of PBS and used fresh for analysis or kept at −80°C for further proteomics analysis. All centrifugation and LC processes were done at 4°C.

Sucrose Gradient Density Centrifugation of EVs

The sucrose gradient density centrifugation protocol used here was based from the protocol described by Théry et al. (2006). Briefly, hydroxyethylpiperazine-*N*′-2-ethanesulfonic acid (HEPES)/sucrose stock solution was prepared by mixing 428 g of protease-free sucrose (Sigma) in 500 ml of 20 mM of HEPES buffer. The pH was adjusted to 7.4 with 1M sodium hydroxide (NaOH) and stored at 4°C. Prior to construction of the sucrose gradient, the HEPES/sucrose stock solution was diluted with 20 mM HEPES buffer to generate 10 concentrations of sucrose solutions (0.25–2.5M with 0.25 increments). The EV sample collected after UC and LC was pre-mixed with either 0.25 or 2.5 M of HEPES/sucrose stock to 1 ml total volume and loaded at either at the top or bottom of the linear sucrose gradient respectively. The sucrose gradient was then centrifuged at 200,000 *g* for 16 h or 72 h at 4°C in a SW 40 swing rotor (Beckman Coulter). One ml fractions were carefully collected from the top and each fraction was weighed to obtain an estimated density of each fraction. Each 1ml sucrose fraction was subsequently diluted in 25 ml of PBS and centrifuged at 120,000 *g* for 70 min at 4°C to wash and pellet the particles. The resultant UC pellet of each fraction was re-suspended in 50 μl of PBS and subjected to molecular analysis.

Quantification and Characterization of EVs

Nanoparticle Tracking Analysis (NTA)

NTA allows for the quantification of total particle amounts and size distribution of particles based on Brownian motion of particles. All NTA was done with the NTA2.3 software on the NS500 Nanosight machine (Nanosight, Malvern, United Kingdom). Before each run, the NS500 measurements were calibrated with known concentrations of 100 nm silica microspheres to obtain optimum acquisition detector settings and post-acquisition settings. For all our recordings, we used a camera level of 14 (shutter speed 600, camera gain 250) and automatic function for all post-acquisition settings: detection threshold level 5, blur and minimum expected particle size. EV samples were diluted in PBS prior measurement, starting at an initial dilution of 1:100, and then further adjusted for each sample individually to achieve a particle count of between 2×10^8 per ml to 1×10^9 per ml. Once the dilution of the sample was determined, the sample was loaded in the sample chamber and the camera focus was adjusted to make the particles appear as sharp dots of light. Using the *script control* facility on the NTA2.3 software, we recorded five 30 s videos for each sample; incorporating a sample advance and 5 s delay between each recording. The measurements were then analyzed using the *batch process* facility and results were exported as Microsoft Excel spreadsheets for further analysis. If the profiles were not in agreement, measurements were then repeated.

Protein Quantification of EVs and Cell Lysates

Extracellular vesicles and cell lysates were quantified using the microBCA or the BCA assay kit (Thermo Scientific Fisher) respectively as indicated by the manufacturer's instructions.

Western Blotting (WB)

Depending on the experimental set-up, either a fixed volume or a set number of particles (as calculated by NTA) from the re-suspension of EV pellet was used. For cells, after trypsin treatment, cells were collected with PBS and spun at 1,500 *g*, 5 min to pellet cells. Cells were washed in PBS and pellet at 1,500 *g*, 5 min again. The supernatant was decanted and the cell pellet was lysed in radioimmunoprecipitation assay (RIPA) buffer for 1 h at 4°C. The mixture was then spun at 16,000 *g*, 20 min. The supernatants were then measured for protein concentration and fixed proteins amounts were used for WB. The EV/cell sample was mixed with 2x Laemilli sample buffer (Bio-Rad, United Kingdom) containing 5% β-mercaptanol and heated at 100°C for 10 min. Samples were then spun-down briefly before being loaded in 1.5 mm, 12% home-made Tris/Glycine SDS-polyacrylamide gels and ran at 170 V for 70 min in running buffer, until the dye front reaches the bottom of the tank. Proteins on the gel were transferred to a polyvinylidene fluoride (PVDF) membrane (Millipore) at 100 V for 70 min in transfer buffer containing 20% methanol. Membranes were then incubated in blocking buffer [5% fat free milk in Tris Buffer Saline with 0.1% Tween-20 (TBS-T, Sigma)] for 60 min at room temperature (RT) on a rocker with gentle shaking. After blocking, the membrane was incubated with freshly prepared primary antibody solution [from Abcam, United Kingdom: anti-Alix, ab117600; anti-Tsg101, ab30871; anti-CD9, ab92726; anti-Calnexin, ab22595; anti-Oct4, ab19857, anti-β-actin, ab8268, all used at 1:1000; from Santa Cruz: anti-CD81(H-121), sc-9158 used at 1:100] overnight at 4°C or 2 h at RT. Membranes were then washed three times 10 min each using washing buffer (TBS-T) with vigorous shaking before adding the secondary antibody solution [all from LiCOR, United Kingdom: Goat anti-mouse IgG IRDye® 800CW (925-32210) and 680RD (925-68070); Goat anti-rabbit IgG IRDye® 800CW (925-32211) abd 680RD (925-68071), all used at 1:10000] and incubated for 2 h at RT. After secondary incubation, membranes were washed three times 10 min each with TBS-T and visualized by scanning both 700- and 800 nm channels on the LI-COR Odyssey CLx infrared imaging system. For re-probing on the same membrane, the membrane was first washed three times 10 min each before re-incubation with the next primary antibody.

Transmission Electron Microscopy (TEM)

A 200 mesh nickel carbon/formvar grid (AgarScientific) was placed onto a 10 μl droplet of the EV suspension for 15 min. The grid was then blotted dry with filter paper, immediately transferred to a 15 μl droplet of 2% uranyl acetate for 1 min and protected from light. The grid was again blotted dry with filter paper before being transferred to a 15 μl droplet of filtered distilled and deionized water (ddH_20) for 1 min. The grid was then blotted dry and left to air dry on the bench top for 15 min. EVs negatively stained on this grid was then visualized with a JEOL 1010 transmission electron microscope (JEOL, Tokyo, Japan).

Trizol Extraction of RNA From EVs and Cells

Total RNA from EVs and cells were extracted based on the manufacturer's protocol. Briefly, 75 μl of the EV suspension or 2×10^5 cells were mixed in Trizol LS (Life Technologies) and incubated for 5 min at RT. Sixty μl of chloroform was then added and tubes were shaken for 15 s. The mixed samples were then incubated for 15 min at RT before being centrifuged at 12,000 *g* for 15 min at 4°C to derive the three distinct phases. The upper colorless phase was transferred to a new tube and 150 μl of isopropanol with 1 μl of glycogen was added. The sample was vortex briefly and incubated at RT for 10 min. The sample was then centrifuged at 12,000 *g* for 10 min at 4°C and the supernatant were discarded. The remaining white RNA pellet was washed with 300 μl of 75% ethanol and then spun down at 7,500 *g* for 5 min at 4°C. The ethanol was then discarded, and the pellet was air-dried for 5–10 min, till it turned transparent, and then re-dissolved in 20 μl of RNase-free water. The mixture was then incubated at 55–60°C for 15 min on a heat block. RNA concentrations of the samples were then measured using the Quant-iT™ RiboGreen® RNA Assay Kit (Life Technologies).

RNA Profiling With Agilent Bioanalyzer Software

Quality and size of the EV and cellular RNA were detected using capillary electrophoresis with the Agilent RNA 6000 Pico kit and Agilent RNA small RNA kit on an Agilent 2100 Bioanalyzer® (Agilent Technologies, Santa Clara, CA, United States) according to the manufacturer's protocol.

LC/MS/MS Proteomic Analysis

As both mouse iPSCs and ESCs were derived off the same strain background (CBA/Ca) and derived using the same methodology, we proceeded with proteomics analysis on one of the miPSC line- iMEF14 and one of the mESC line- ESF121. For each cell and EV sample, three biological replicates were prepared and analyzed (**Supplementary Table S1**). All cells and EVs were concentrated by speedvac and lysed with 1% SDS, 25 mM HEPES, 1 mM DTT. Lysates were heated to 95°C for 5 min followed by sonication for 1 min and centrifugation at 14,000 *g* for 15 min. The supernatant was mixed with 1 mM DTT, 8 M urea, 25 mM HEPES, pH 7.6 and transferred to a 10-kDa cut-off centrifugation filtering unit (Pall, Nanosep®), and centrifuged at 14,000 *g* for 15 min, followed by an addition of the 8 M urea buffer and centrifugation again. Proteins were alkylated by 50 mM iodoacetamide (IAA) in 8 M urea, 25 mM HEPES for 10 min, The proteins were then centrifuged at 14,000 *g* for 15 min followed by 2 more additions and centrifugations with 8 M urea, 25 mM HEPES. Trypsin (Promega) in 250 mM urea, 50 mM HEPES was added to the cell lysate at a ratio of 1:50 trypsin:protein and incubated overnight at 37°C. The filter units were centrifuged at 14,000 *g* for 15 min followed by another centrifugation with milli-Q water (MQ) and the flow-through was collected. Peptides were cleaned by a strata-X-C-cartridge (Phenomenex).

Before analysis on the Q Exactive (Thermo Fischer Scientific, San Jose, CA, United States), peptides were separated using an Agilent 1200 nano-LC system. Samples were trapped on a Zorbax 300SB-C18, and separated on a NTCC-360/100-5-153 (Nikkyo Technos., Ltd.) column using a gradient of A [3% acetonitrile (ACN), 0.1% formic acid (FA)] and B (95% ACN, 0.1% FA), ranging from 7 to 40% B in 240 min with a flow of 0.4 μl/min. The Q Exactive was operated in a data dependent manner, selecting top 5 precursors for fragmentation by HCD. The survey scan was performed at 70,000 resolution from 300–1700 *m/z,* using lock mass at *m/z* 445.120025, with a max injection time of 100 ms and target of 1×10^6 ions. For generation of HCD fragmentation spectra, a max ion injection time of 500 ms and AGC of 1×10^5 were used before fragmentation at 30% normalized collision energy, 17,500 resolution. Precursors were isolated with a width of 2 *m/z* and put on the exclusion list for 70 s. Single and unassigned charge states were rejected from precursor selection.

Proteome discoverer 1.3 with sequest-percolator was used for protein identification. Precursor mass tolerance was set to 10 ppm and for fragments to 0.02 Da. Oxidized methionine and was set as dynamic modification, and carbamidomethylation as static modification. Spectra were matched to a combined *Mus musculus* and *Bos taurus* ensembl 72 database, and results were filtered to 1% FDR. Identifications in *Bos taurus* was considered to originate from FBS and removed. For this set of LC-MS/MS, the reference list used was generated based on all proteins identified within this stem cell set. In this proteomics run, only a short gradient of the cellular and vesicular proteome was subjected to analysis. Hence, the overall proteome of the cell described here may only recapitulate a portion of the total proteome as expected. For classification of commonly identified proteins when comparing two sample types, we calculated the ratio of area of proteins of one sample over the other. Proteins that had a twofold change in ratio were designated to be "up-regulated." These groups were then analyzed in the online platform: Panther to evaluate enrichment of Gene ontology (GO) (Mi et al., 2013, 2019).

Statistics

The Student's *t*-test was used when comparing EVs derived by the UC versus LC purification.

RESULTS

Alternative Forms of Serum-Depleted Media Not Feasible for Stem Cells

In our study, mouse induced pluripotent stem cells (iPSCs) were used as a model for sensitive cells that require complex media types for their cultivation. Unlike differentiated cells, serum is crucial for the maintenance of stem cells in their undifferentiated state. However, in EV research, the use of serum is problematic as serum contains microvesicles, which could be co-purified and interfere with the downstream analysis of EVs. Hence, we used knockout serum replacement (KOSR), which is devoid of serum microvesicles. However, KOSR could still contain other undefined components, which could confound the EV purity.

To evaluate the background particulate counts in KOSR-supplemented (SR) media, we applied the UC purification protocol to unconditioned media and analyzed the pellet. In parallel, two other media types commonly used in EV research were compared; pre-spun SR-media (PS) and serum-free OptiMEM (OM). Interestingly, NTA measurements indicated the presence of nanoparticles in all pellets, most significantly in the SR-media pellet (**Supplementary Figures S1A,B**). Notably, the mode sizes of these nanoparticles appeared to be similar to that of EVs. Next, we assessed the growth and morphology of stem cells in these alternative media types. After a 48 h incubation period, we found that both iPSCs (**Supplementary Figures S1C,D**) and ESCs (**Supplementary Figures S1F,G**) grew differently in these three media types. In PS media, cells appeared less viable based on cell morphology and had much lower total cell counts as compared to regular SR media. In OM media, stem cells proliferated at a higher rate and some colonies displayed altered morphology. As for EVs, the greatest number of particles was recovered from SR CM, followed by OM and lastly PS media (**Supplementary Figures S1E,H**). As we were concerned with the cellular changes caused by the switch in media type, we decided to continue with SR media for subsequent comparisons between UC and LC protocol.

LC Enabled Purification of Stem Cell EVs in a Reproducible Fashion

Since SR media does not contain serum, the detection of vesicles by NTA in the UC pellet of SR media led us to question the nature of these particles. We hypothesized that these "particles" were macromolecular structures of protein aggregates that formed during the high-speed centrifugation.

In LC, there is a lack of high-speed spins. Hence, we fractionated CM from stem cells on the size-exclusion column. Generally, the total protein and particle number profiles overlapped well, such that the fractions with the highest amounts of protein corresponded to the fractions with the highest number of particles (**Figure 1A**). Overall, we grouped and pooled the fractions into four general fractions: F1–F4. NTA profiles of these four fractions showed that the greatest number of particles to be in F1 followed by F2, while F3 and F4 contained very few particles (**Figure 1B**). When we compared their particle size distribution graphs, the peak of particle concentration in F1 was significantly higher in cell-derived samples than that of media alone (**Figure 1C**). Moreover, the presence of EVs exclusively in F1 was confirmed through the detection of common EV markers (Alix and CD9) (**Figure 1D**). Importantly, this showed that stem cell media contains a fair amount of macromolecular proteins that may appear as particles on NTA. Unlike in LC, these contaminating proteins are inseparable from EVs in the UC process. Furthermore, the LC process was highly reproducible across replicate runs, as seen by the protein chromatographs, western blotting and small RNA profile analysis of replicate collections (**Figures 1E–H**).

UC Pelleting Led to Co-precipitation of Non-vesicular Proteins and RNAs With EVs

When comparing UC and LC side-by-side, we detected higher particle yield and total protein and RNA amounts after UC as compared to LC (**Figures 2A–D**). However, this contradicted our previous study on serum-free culture samples (Nordin et al., 2015). To understand the reasons underlying the differences, we analyzed the expression levels of common EV markers following both types of collection. Interestingly, when normalized by particle numbers, we detected stronger expression of both Alix and CD9 in LC purified than UC purified samples, whereas OCT-4, a marker of pluripotency, showed the reverse trend (**Figure 2E**). Next, we compared the expression of the same EV markers in parental cells and EVs based on a fixed protein amount. Unexpectedly, there was no enrichment of EV markers in the UC pellet as compared to cells. To complement our molecular profiling, we next assessed how the biophysical properties of EVs differed by purification protocol. Overall, TEM imaging showed a general cloudy background in the UC samples, which made it difficult to discriminate EVs. In contrast, LC samples had a cleaner background where particles were more easily detected (**Figure 2G**). Lastly, we calculated the particle per protein ratio (P/μg) and compared them to benchmark values suggested for EV purity (**Table 1**). Here, the P/μg ratio for UC sample was classified as impure, while the LC samples had slightly higher P/μg ratios and were considered of low vesicular purity (**Table 2**).

One of the methods proposed for deriving pure, clinical-grade EVs is by floating EVs on a discontinuous sucrose gradient overnight (Lamparski et al., 2002), where pure EVs should float at a specific density range of 1.15–1.19 g/ml (Théry et al., 2006). Here, we compared EV purity after loading the sucrose gradient either above (bottom-loading) or below the UC pellet (top-loading). Interestingly, we found a discrepancy in the fractions enriched for EV markers and peak particle counts between the two loading types. After bottom-loading, the purified sample unexpectedly peaked in fractions 7–8, which correspond to a density of 1.21–1.22 g/ml (**Figures 3A,B**). These fractions also contained the greatest amounts of protein (**Figure 3C**). Hence, we speculated that non-vesicular proteins attached to EVs during the UC process and that this prevented the migration of EVs to their real densities. When further increasing the fractionation time in the sucrose gradient to 72 h, we began to detect more expression of the EV marker CD81 in the expected fractions of pure EVs (**Figures 3D–I**). Overall, we here show that initial quantification of particle counts and molecular content (proteins and RNAs) in UC pellets were inaccurate. Despite additional prolonged periods of clean-up by either sucrose gradient centrifugation or LC (**Supplementary Figure S2**), we achieved only a marginal improvement in the purity of EVs isolated by UC.

EVs From iPSCs and ESCs Have Similar Size Distribution Profiles and Expression of EV Markers

Using the LC method, we next proceeded to purify EVs from two mouse ESCs lines and two iPSCs lines. From the LC chromatograph, it was observed that all four EV fractionation processes generally showed a similar 280 nm absorbance pattern across the eluted volume (**Figures 4A,C**). As we were only interested in the EVs, we pooled LC fractions across the region where EVs eluted (F1) and analyzed the particles with NTA. As shown in **Figures 4B,D,E**, the particle size distribution profiles overlapped within each cell type. Moreover, TEM on EVs from both mouse ESCs and iPSCs corroborated the NTA measurements and showed that the particles from both cell types appeared similar. Furthermore, similar levels of EV markers (Alix and CD9) were detected in both mouse iPSC and ESC-derived EVs (**Figures 4F,G**). Lastly, when analyzing the P/μg ratio of EVs from all four cell lines, we found that all samples were of similar purity (**Figure 4H**).

EVs From ESCs and iPSCs Contain Similar Proteins That Differ Greatly From Their Parental Cells

To characterize our EVs more deeply, unbiased LC-MS/MS proteomics analysis were performed on both cell lysates and EVs from our iPSC and ESC lines. As we suspected remnants of contaminating proteins within our EV samples, LC-MS/MS was first performed on unconditioned stem cell media. Overall, 35 cow and 29 mouse proteins were detected (**Table 3**),

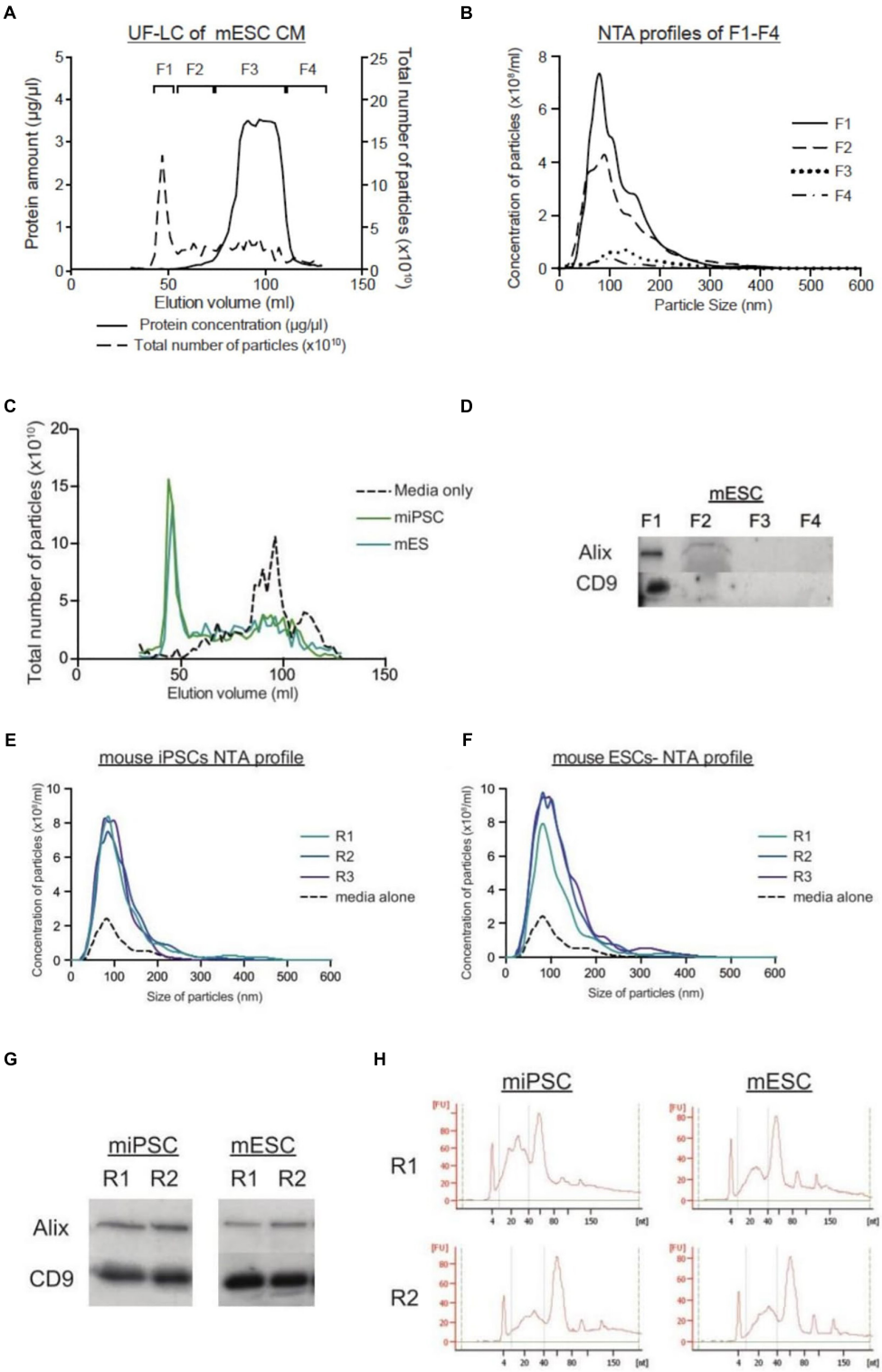

FIGURE 1 | LC protocol allows for purification of EVs in a reproducible manner. **(A)** Graph showing the protein concentration (µg/µl) and the total number of particles (x10^{10}) across the LC run. **(B)** NTA size distribution graphs of the four fractions from mESCs, where F1 is expected to contain the most EVs. **(C)** Graphs comparing the total number of particles (x10^{10}) collected through the elution courses of unconditioned media, and CM from miPSCs and mESCs. **(D)** Representative western blots for EV markers (Alix and CD9) in mESC CM. NTA size distribution profiles of the EVs collected from LC-F1 in three replicates (R1–R3) of CM from miPSC **(E)** and mESC **(F)**. **(G)** Representative western blotting pictures for EV markers (Alix and CD9) in duplicate EVs samples (R1–R2) from miPSCs and mESCs. **(H)** Small RNA Bioanalyzer profiles of duplicate EV samples (R1–R2) from miPSCs and mESCs.

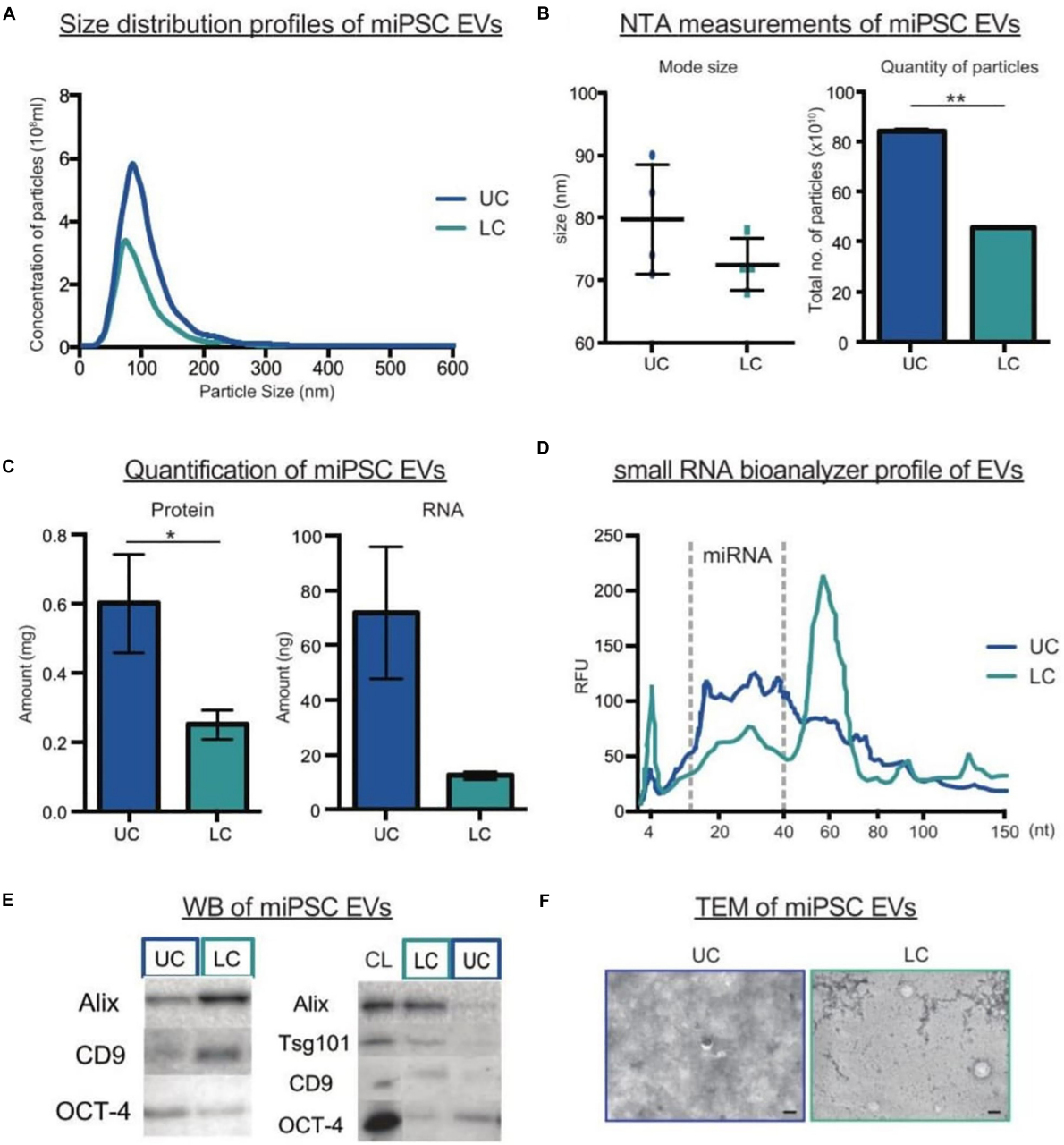

FIGURE 2 | Comparison of miPSCs EVs purified by UC or LC. **(A)** NTA size distribution profiles of EVs purified by UC or LC. **(B)** The mode size (nm) and total number of particles (x10^{10}) detected by NTA in UC or LC purified samples ($n = 4$, bars represent mean ± SD, $^{**}p < 0.01$). **(C)** Protein and RNA quantification of EVs in UC and LC purified samples ($n = 4$, bars represent mean ± SD, $^{*}p < 0.05$). **(D)** Small RNA Bioanalyzer profiles from UC and LC purified samples **(E)** Representative western blots of UC and LC purified samples. The left panel compares equal numbers of particles (4×10^{10}), while the right panel compares equal amount of protein from (10 μg) of cell lysate (CL) and EV samples. **(F)** Representative TEM images of EVs purified by UC or LC. The scale bar corresponds to 100 nm.

with the majority of proteins belonging to common protein groups such as albumin, fibronectin, heat shock protein and keratins (**Tables 4–6**). Importantly, many of these proteins were also detected in high abundance within our EV samples (**Supplementary Figure S3**). To avoid ambiguity, we removed the entire set of proteins present in media and our EV samples from downstream analysis.

After filtering, a total of 1387 proteins were detected in EVs from either iPSCs or ESCs, where 33.1% of them were present in both groups (**Figure 5A**). Although there were many more proteins found exclusively in iPSC-EVs than in ESC-EVs (593 vs. 35), GO annotations showed that many of these proteins had similar molecular functions, such as protein binding and cytosolic localization. Next, we considered the 459 proteins which

TABLE 1 | Table showing the suggested purity index by Webber and Clayton 2013.

Purity index	P/μg
High vesicular purity	$>3 \times 10^{10}$
Low vesicular purity	2×10^{9}–2×10^{10}
Unpure vesicles	1.5×10^{9}

TABLE 2 | Table showing the purity ratios of UC and LC samples from both stem cell types.

P/μg	miPSC	mESC
UC pellet	1.6×10^{9}	4.5×10^{8}
LC sample	3.6×10^{9}	6.2×10^{9}

were common to both types of EVs and divided them into three groups: proteins with similar expression, proteins over-represented in iPSC-EVs and proteins over-represented in ESC-EVs. In general, most of these common proteins were found at similar levels in both groups (**Figure 5B**). As expected, both EVs were enriched in proteins with GO terms such as EV, extracellular exosome, membrane-bound exosome and vesicle (**Figure 5C**). Moreover, known EV markers like CD9 and CD81 were abundant in both samples and were cross validated by western blotting (**Figure 5D**). On the other hand, a few GO terms were significantly different between the two groups. For example, GO terms for translation initiation factor activity, translation factor activity, RNA binding and protein hetero oligomerization were over-represented in EVs from iPSCs, while proteins associated with the plasma membrane were over-represented in EVs from ESCs (**Figure 5E**).

To analyze if the similarities in the EVs was related to their parental cells, we next compared the cellular proteomes of matched iPSCs and ESCs to their respective EVs. As expected, more proteins were detected in cells than in EVs (3565 versus 1387). Of the proteins identified, 71.6% overlapped in both cell types (**Figure 6A**). As for proteins exclusive to each cell type, most of them mapped to the same GO terms (e.g., nucleotide and RNA binding, organelle and membrane). Similar to before, common proteins were separated into three groups; those expressed similarly in both, those over-represented in iPSCs and those over-represented in ESCs. Although there were variations in GO term enrichments between the two cell types, none of these differences were found to be significant. Interestingly, the scatter plot of individual proteins showed the exception of two outliers: mitochondrial ribosomal protein S25 (MRPS25) and activating signal co-integrator 1 complex subunit 3 (ASCC3), both of which were more abundant in ESCs than in iPSCs (**Figure 6B**).

Next, we compared each EV sample back to their parent cells. Interestingly, the overlap of cellular proteins in their corresponding EVs was quite low; 28.5% for iPSCs and 15.5% for ESCs (**Figures 6C,E**). This was further supported by the scatter plots showing correlation expression of all identified proteins in EVs versus cells (**Figures 6D,F**). To understand the nature of these differences, we applied GO analysis to the different groups of proteins. In the iPSC set, GO terms for translation initiation factor activity, translation factor activity, RNA binding, extracellular matrix and extracellular space were all found to be over-represented in EVs. In contrast, proteins with GO terms for structural constituent of ribosome, mRNA binding, cytosolic part and intracellular non-membrane-bounded organelle were over-represented in cells (**Figure 6G**). As proteins detected in ESC-EVs, we observed an enrichment in GO terms for glycolipid binding, G-protein beta/gamma-subunit complex binding, external side of plasma membrane and extracellular matrix component in the EVs. In contrast, ESC proteins were over-represented in proteins with GO terms for the structural constituent of cytoskeleton, histone binding, protein-DNA complex assembly and chromatin assembly or disassembly, as compared to EVs (**Figure 6H**). Interestingly, there were some GO terms which were similarly enriched in EVs and cells across both stem cell types. For example, the GO term basal lamina was enriched in EVs from both iPSCs and ESCs when compared to their parent cells. On the other hand, GO terms for protein-DNA complex subunit organization, DNA replication-dependent nucleosome organization, nuclear chromosome and nuclear nucleosome were enriched in both cell samples as compared to their EVs (**Figure 6I**).

DISCUSSION

In this study, we cross compared the isolation of EVs from complex, protein rich media using two methods: the gold-standard of UC versus an LC method. Due to the presence of microvesicles in serum, many researchers have turned to alternative media types like pre-spun media or entirely serum-free solutions reconstituted with recombinant protein substitutes for serum component (Li et al., 2015). Unfortunately, there have been doubts about the clearance efficiency of microvesicles from pre-spun media (Kornilov et al., 2018), and it is not feasible to reconstitute serum components for certain sensitive cell types. Here, we have demonstrated the phenotypic changes that occur in stem cells after short term incubation in these different media types. Although serum-free alternatives for cell types such as neurons and astrocytes have been developed (Brewer, 1995; Pozzi et al., 2017), these remain poorly defined, protein rich alternatives that may induce unwanted molecular changes and lead to growth of selective populations (Balvers et al., 2013). Despite the growing number of studies comparing EV isolation methods, there is still only limited knowledge about the molecular profiles of EVs collected from protein rich media types and their implications on molecular contents of EVs.

In our findings, we highlight various problems associated with the UC protocol. First, we identify an issue with high particle counts in UC pellets from unconditioned media, despite the lack of serum in KOSR. However, when we fractionated the unconditioned media with LC, most particles were found in later fractions corresponding with high protein amounts. Hence, this led us to speculate that the high-speed spins in UC promote the precipitation of protein aggregates, which then appear as nano-sized particles on NTA.

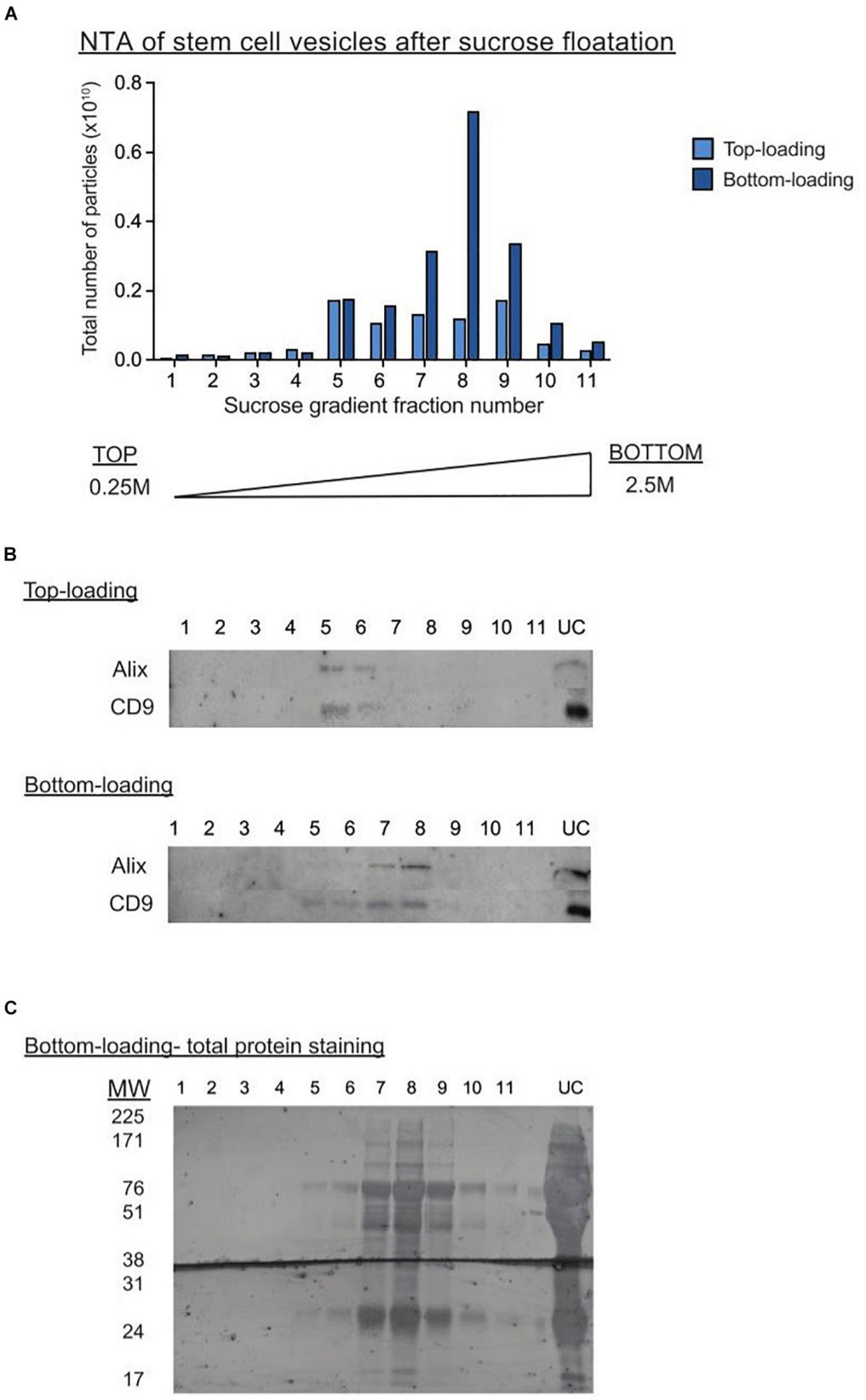

FIGURE 3 | Continued

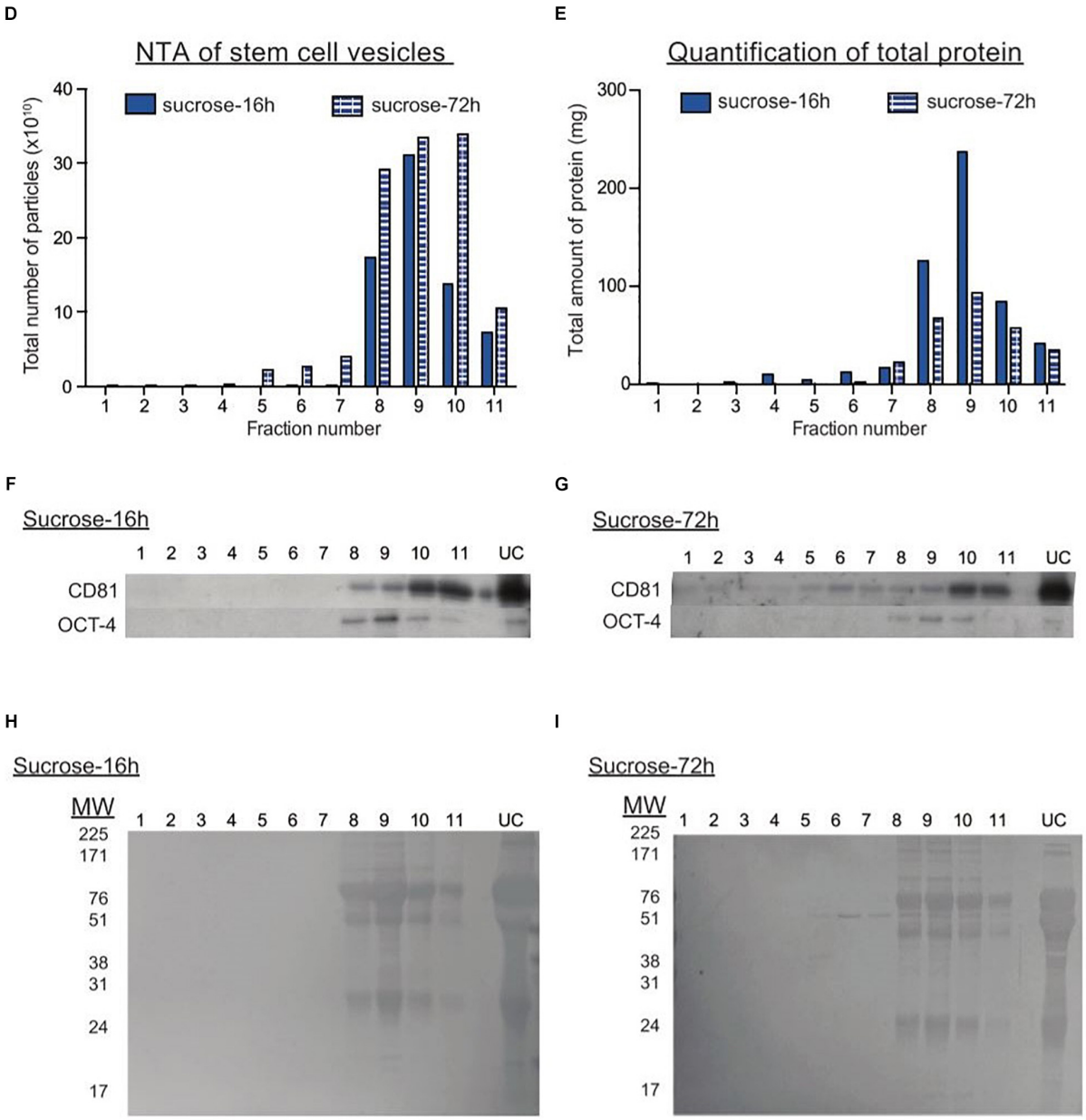

FIGURE 3 | Sucrose gradient fractionation of UC pellets indicates the co-precipitation of non-vesicular proteins with EVs. **(A)** Graph showing the total number of particles detected in each sucrose gradient fraction after top (light blue) or bottom loading (dark blue) the sample. The fractions are numbered from the top to the bottom of the gradient. **(B)** Representative western blots for EV markers in the top and bottom loaded gradient fractions. UC represents the original UC pellet input material. **(C)** Total protein staining of gradient fractions from the bottom loaded sample. **(D,E)** Graphs showing the total number of particles **(D)** or protein **(E)** detected in each gradient fraction after UC samples were bottom-loaded and centrifuged for 16 h (dark blue bar) or 72 h (striped blue bars). Representative western blots for EV (CD81) and pluripotency (OCT4) markers in UC samples centrifuged on the sucrose gradient for either 16 h **(F)** or 72 h **(G)**. Total protein staining of gradient fractions from UC samples centrifuged on the sucrose gradient for either 16 h **(H)** or 72 h **(I)**.

In our side-by-side comparison of UC and LC, the UC pellet contained more particles, protein and RNA than the LC sample. This result was rather unexpected, as the opposite trend was previously reported in serum-free CM (Nordin et al., 2015). As we are aware that protein aggregates in the UC pellet can appear as particles on the NTA, we remain unsure of the reliability of our NTA and protein quantifications. Thus, we used multitude of other technologies for our subsequent detailed comparison and characterization studies.

First, we checked the expression levels of well-established EV and stem cell markers when loading equal numbers of particles. Surprisingly, the expression level of OCT-4 was inversely correlated to that of the EV markers. Although OCT-4 is reported to be present in ESC-EVs (Ratajczak et al., 2006),

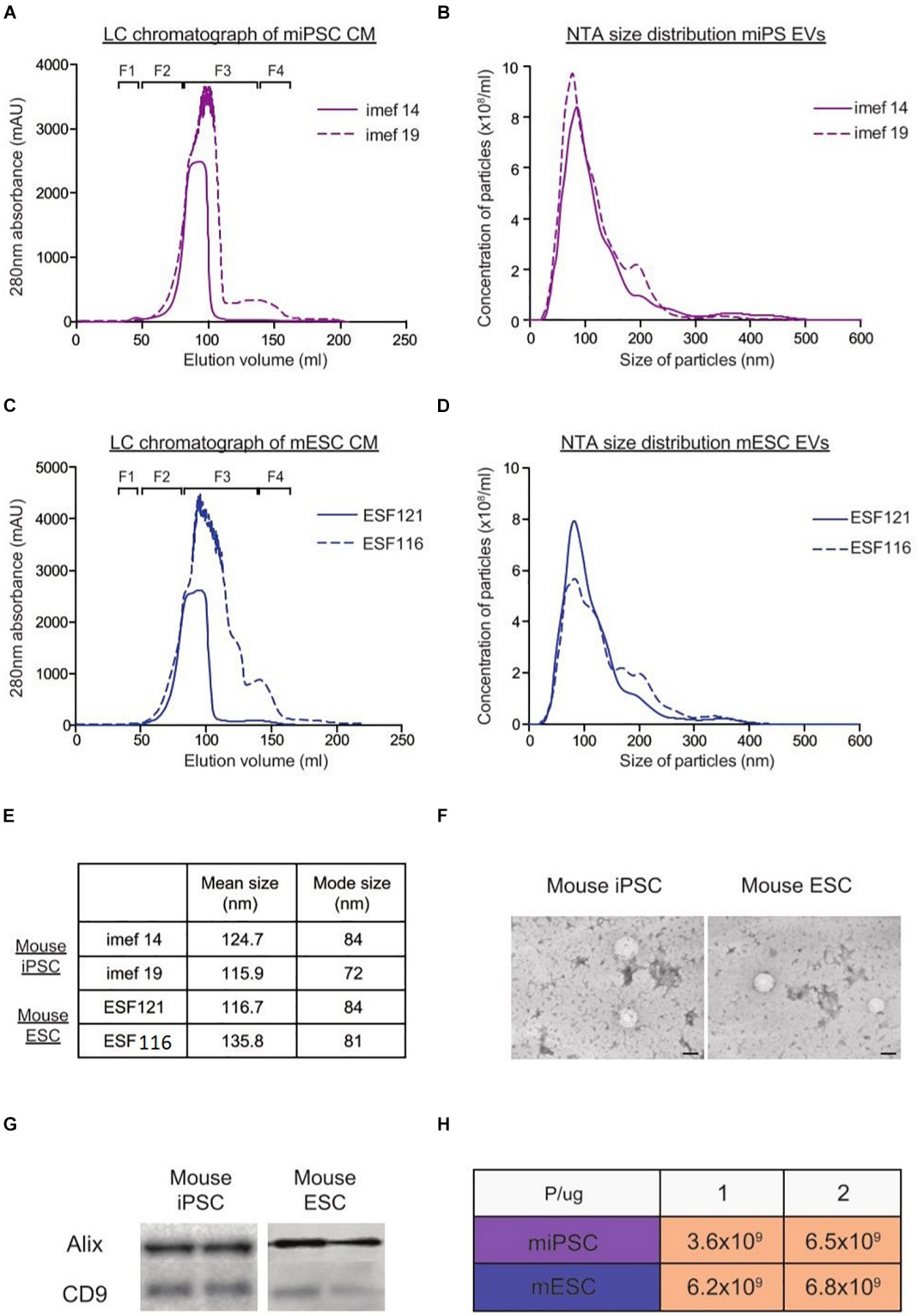

		Mean size (nm)	Mode size (nm)
Mouse iPSC	imef 14	124.7	84
	imef 19	115.9	72
Mouse ESC	ESF121	116.7	84
	ESF116	135.8	81

P/ug	1	2
miPSC	$3.6x10^9$	$6.5x10^9$
mESC	$6.2x10^9$	$6.8x10^9$

FIGURE 4 | Characterization of EVs from mouse iPSCs and ESCs with NTA, TEM and western blotting. Representative LC chromatographs of two different mouse iPSC cell lines (imef14 and imef19) **(A)** and mouse ESC cell line (ESF121 and ESF116) **(B)**. NTA size distribution profiles of EVs from mouse iPSCs **(C)** and mouse ESCs **(D)**. **(E)** Table showing the mean and mode sizes of EVs from mouse iPSCs and ESCs. **(F)** Representative TEM images of EVs from mouse iPSCs and mouse ESCs. **(G)** Representative western blots of EV markers (Alix and CD9) in replicate samples of EVs from mouse iPSCs and mouse ESCs. **(H)** Table showing the P/μg ratio of EVs purified from mouse iPSCs and ESCs.

TABLE 3 | Table showing the list of cow proteins exclusively identified in the media sample.

Species of protein	Name of protein	Accession number
Bos taurus	Alpha-1-acid glycoprotein	Q3SZR3
	Alpha-1 -antiproteinase	P34955
	Alpha-1 B-glycoprotein	Q2KJF1
	Alpha-2-antiplasmin	P28800
	Alpha-2-HS-glycoprotein	P12763
	Alpha-2-macroglobulin	Q7SIH1
	Antithrombin-III	F1MSZ6
	Apolipoprotein A-I	P15497
	Apolipoprotein A-IV	F1N3Q7
	C1QC protein (Fragment)	Q1RMH5
	Complement C3	G3×7A5
	Complement component C9	Q3MHN2
	FGG protein	Q3SZZ9
	Fibrinogen alpha chain	A5PJE3
	Fibrinogen beta chain	F1MAV0
	Gelsolin	F1MJH1
	Haptoglobin	G3 × 6K8
	Hemoglobin subunit beta	P02070
	Inter-alpha-trypsin inhibitor heavy chain H1	F1MMP5
	Inter-alpha-trypsin inhibitor heavy chain H4	F1MMD7
	Leucine-rich alpha-2-glycoprotein 1	Q2KIF2
	Protein AMBP	F1MMK9
	Prothrombin	P00735
	Serotransferrin	Q29443
	Serpin A3-5	A2I7N1
	Serpin A3-7	A2I7N3
	Uncharacterized protein (Fragment)	G3N0V0
	Uncharacterized protein (Fragment)	G5E513
	Uncharacterized protein	F1N514
	Uncharacterized protein	F1N076
	Uncharacterized protein	E1BH06
	Uncharacterized protein	F1MLW8
	Uncharacterized protein	F1MCF8
	Vitamin D-binding protein	F1N5M2

TABLE 4 | Table showing the list of mouse proteins exclusively identified in the media sample.

Species of protein	Class of protein	Name of protein	Accession number
Mus musculus	Fibronectin	Fibronectin	A0A087WS56
		Fibronectin	B7ZNJ1
	Heat shock protein	Heat shock protein 75 kDa, mitochondrial	Q9CQN1
		Heat shock protein HSP 90-alpha	P07901
		Heat shock protein HSP 90-beta	P11499
	Keratin	Keratin, type I cytoskeletal 16	Q9Z2K1
		Keratin, type I cytoskeletal 17	Q9QWL7
		Keratin, type I cytoskeletal 18	P05784
		Keratin, type I cytoskeletal 19	P19001
		Keratin, type II cytoskeletal 2 epidermal	Q3TTY5
		Keratin, type II cytoskeletal 8	P11679
	L-lactate dehydrogenase	L-lactate dehydrogenase A chain	P06151
		L-lactate dehydrogenase B chain	P16125
	Others	Actin, cytoplasmic 1	P60710
		Annexin (Fragment)	B0V2N7
		Apolipoprotein B-100 (Fragment)	E9Q1Y3
		Apoptosis facilitator Bcl-2-like protein 14	Q9CPT0
		Beta-actin-like protein 2	Q8BFZ3
		Complement component C8 beta chain	Q8BH35
		E3 ubiquitin-protein ligase TRIP12	A0A087WNZ7
		Filamin-C	D3YW87
		Fructose-bisphosphate aldolase A	P05064
		Gelsolin	P13020
		Hemoglobin subunit alpha	P01942
		Histone H4	P62806
		Junction plakoglobin	Q02257
		Rho guanine nucleotide exchange factor 9 (Fragment)	S4R1J2
		Ubiquitin-associated domain-containing protein 2	Q8R1K1

more recent work has shown that OCT-4 can also be secreted from cells directly into the extracellular environment (Wang and Jauch, 2014). Hence, we speculate that some portion of this secreted OCT-4 protein in the CM might pellet together with stem cell EVs during the UC process. This hypothesis would explain the high particle counts and levels of OCT-4 detected by western blotting in UC-purified EVs. Apart from proteins, we also observed significant differences in other EV properties after isolation with UC and LC, such as their small RNA profiles and TEM images of vesicles. In the latter, we hypothesized that the presence of free protein in the UC pellet would contribute to the cloudy background that interfered with our visualization of the EVs. Furthermore, the P/μg ratio was lower after UC than LC purification; which corroborated our data suggesting that the UC pellet displayed lower vesicle purity. However, here we realize that interpretation of the vesicle purity ratio (P/μg) may need to be re-considered for protein rich substances. Since some protein aggregates may be mistakenly counted as EVs when using NTA, purified samples with more protein aggregates would appear to have a higher purity ratio than they do.

Next, we subjected the UC pellet to additional clean-up strategies to test for the presence of contaminating proteins. The first clean up strategy we attempted was sucrose gradient centrifugation. Previously, it has been reported that EVs float at 1.15–1.19 g/ml, which is slightly different to vesicles originating from cellular organelles such as the endoplasmic reticulum

TABLE 5 | Table showing the list of mouse proteins exclusively identified in the gelatin sample.

Species of protein	Class of protein	Name of protein	Accession number
Mus musculus	Collagen	Collagen alpha -1 (I) chain	P11087
		Collagen alpha-1 (II) chain	P28481
		Collagen alpha-1 (III) chain	P08121
		Collagen alpha-1 (V) chain	088207
		Collagen alpha-2 (I) chain	Q01149
	Others	Ig gamma-2A chain C region secreted form	P01864
		Ig heavy chain V region MOPC 47A	P01786
		Protein Ahnak	E9Q616
		Protein BC067074 (Fragment)	F6Z6Y0

List excludes the detection of 8 uncharacterized sus scrofa proteins.

TABLE 6 | Table showing the list of proteins commonly identified in both the media and gelatin sample.

Species of protein	Class of protein	Name of protein	Accession number
Bos taurus	Albumin	Serum albumin	P02769
Mus musculus	Keratin	Keratin, type II cytoskeletal 79	Q8VED5
		Keratin, type II cytoskeletal 75	Q8BGZ7
		Keratin, type II cytoskeletal 5	Q922U2
		Keratin, type II cytoskeletal 1	P04104
		Keratin, type I cytoskeletal 10	A2A513

List excludes 2 uncharacterized sus scrofa proteins.

(1.18–1.25 g/ml) or the Golgi (1.05–1.12 g/ml) (Théry et al., 2006). These floatation intervals have been verified on EVs from different cellular sources and found to be reproducible regardless of the method of loading the EV sample on the top or bottom of the sucrose gradient. However, others have debated that overnight centrifugation was insufficient for vesicles to efficiently penetrate in the denser fractions and reach density equilibrium within 16 h centrifugation period (Yuana et al., 2014; Iwai et al., 2016). Hence, we here tested both loading strategies (top versus bottom) and at two different lengths of centrifugation timings (16 h versus 72 h). Unexpectedly, there was great inconsistency in the fractions showing the highest total particle counts and expression of EV markers between the two loading strategies. In the bottom-loaded sample, the gradient fractions positive for EV markers overlapped with those containing non-vesicular protein bands. Hence, we hypothesize that the EVs in the UC pellet may be associated with protein aggregates and thus float at these higher densities instead of their actual density.

Interestingly, with the longer overnight centrifugation, the expression of CD81 became more diverse. We hypothesized that after this longer incubation period, a portion of EVs were able to escape from the protein aggregates and float at their expected densities. In hindsight though, CD81 expression still appeared relatively higher in the higher density fractions. Despite this data, it is very difficult to conclude whether the particles appearing at higher densities and stained positively for CD81 are EVs bound to non-vesicular proteins or they could be true EVs that float at a higher density. However, there is the possibility that some of these EV-protein associations are transient, whilst others may be more permanent due the high gravitational forces inherent in the UC procedure. Another strategy we tried was to fractionate the UC pellet on an LC column. Interestingly, this revealed an additional protein peak immediately after the initial EV peak, though the particles in this second peak did not express any of the EV markers we tested. This result further supports our previous deduction that proteins can appear as particles on the NTA. From these results, we conclude that UC purification of EVs may require additional clean-up to increase the purity of EVs, despite that these steps would compromise the final EV yield as seen by another recent study (Onódi et al., 2018).

When applying LC to stem cell CM, the fractionation pattern was reproducible across replicates and consistent across the two stem cell types. However, we noticed that there was a lack of distinct cut-off points between the particle and protein peaks in the LC profile of stem cell CM. This led us to speculate that, due to the high protein content in the media, the resolution of fractionation may require more improvements; this can be in the form of sequential LC steps or with an alternative taller column. We briefly tested the sequential LC approach here and noticed that in the second LC run there was slightly lower expression of the transmembrane protein CD9, while the opposite was true for the intraluminal protein (Tsg101) (**Supplementary Figure S4**). Interestingly, this suggests that more caution is required when checking the expression of established EV markers identification. In this scenario, the lower expression of CD9 in the second LC may indicate that some CD9 initially detected might be contributed by non-EV proteins.

Despite our efforts to clean-up the EV product, there remains the presence of huge protein bands as seen by Ponceau S staining. From literature, KOSR contains high amounts of albumin and other proteins to replace the serum component. We postulated that the pre-concentration step with spin filters might have caused the capture of these protein aggregates in the filters. To bypass this, one could consider the use of tangential flow filtration (TFF) devices, which function through diafiltration-based processes. On the other hand, some contaminating proteins on EVs may be due to the presence of cell adhesion molecules like connexins, integrins and cadherins (Albelda and Buck, 1990; Sakisaka, 2005; Shimaoka et al., 2019) which would make EVs particularly adhesive to free proteins in the circulation.

Unlike previous studies on stem cell derived-EVs, which were collected from serum-free conditions (Ratajczak et al., 2006; Yuan et al., 2009; Katsman et al., 2012), we used serum-replacement media to avoid the differentiation of our stem cells in the absence of serum. To identify the background of proteins in the unconditioned media, we applied the use of a mass spectrometry method. We found a relatively high amount of cow albumin and keratin proteins. As the serum-replacement media contained AlbuMax^{TM} (Life Technologies, United Kingdom), we believed that this was the main source of cow albumin in our samples and pre-filtered these proteins out of downstream analysis.

Generally, the EVs from iPSCs and ESCs have relatively similar proteomes. Although there was a disparity in the total number of proteins detected in the iPSC-EVs and ESC-EVs, most of the specifically expressed proteins did not show a significant

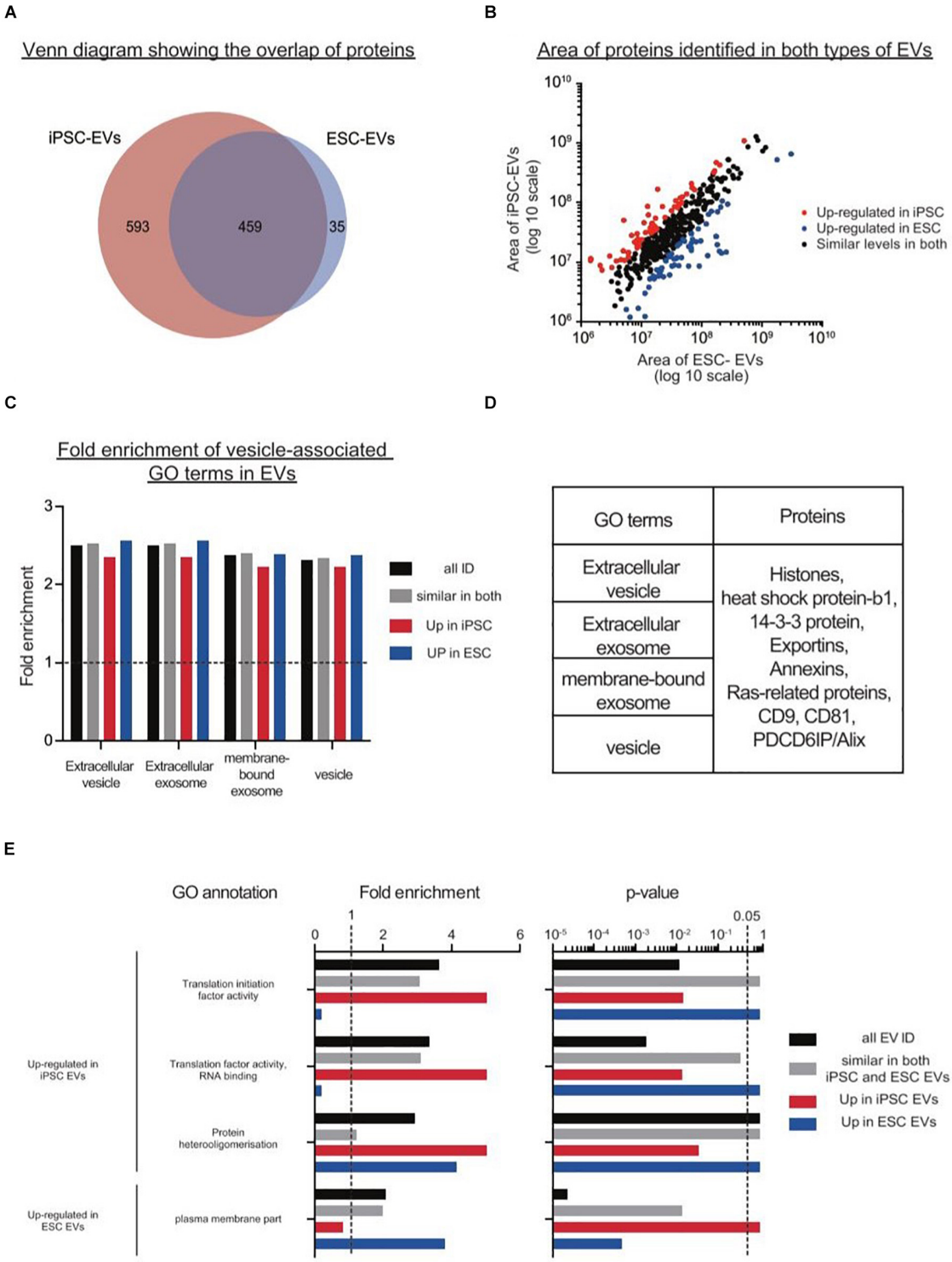

FIGURE 5 | Proteomics analysis on EVs from mouse iPSCs and ESCs. **(A)** Venn diagram showing the overlap of proteins identified in the two types of stem cell EVs. **(B)** Scatter plot showing the correlation between the areas of commonly identified proteins in both iPSC-EVs and ESC-EVs. All proteins were classified into three distinct groups: up-regulated in iPSC-EVs (red dots), up-regulated in ESC-EVs (blue dots) and of similar levels in both iPSC and ESC-derived EVs (black dots). **(C)** Graph showing the fold enrichments of iPSC-EVs and ESC-EVs over the reference list, in four vesicle-related GO terms: extracellular vesicle, extracellular exosome, membrane-bound exosome and vesicle. **(D)** List of individual proteins identified in these same four GO terms. **(E)** A subset of significantly enriched GO terms for proteins up regulated in iPSC or ESC-derived EVs. Proteins are grouped under four categories: all EV IDs (black bar), proteins at similar levels in both iPSC-EVs and ESC-EVs (gray bar), up-regulated in iPSC-EVs (red bar) and up-regulated in ESC-EVs (blue bar).

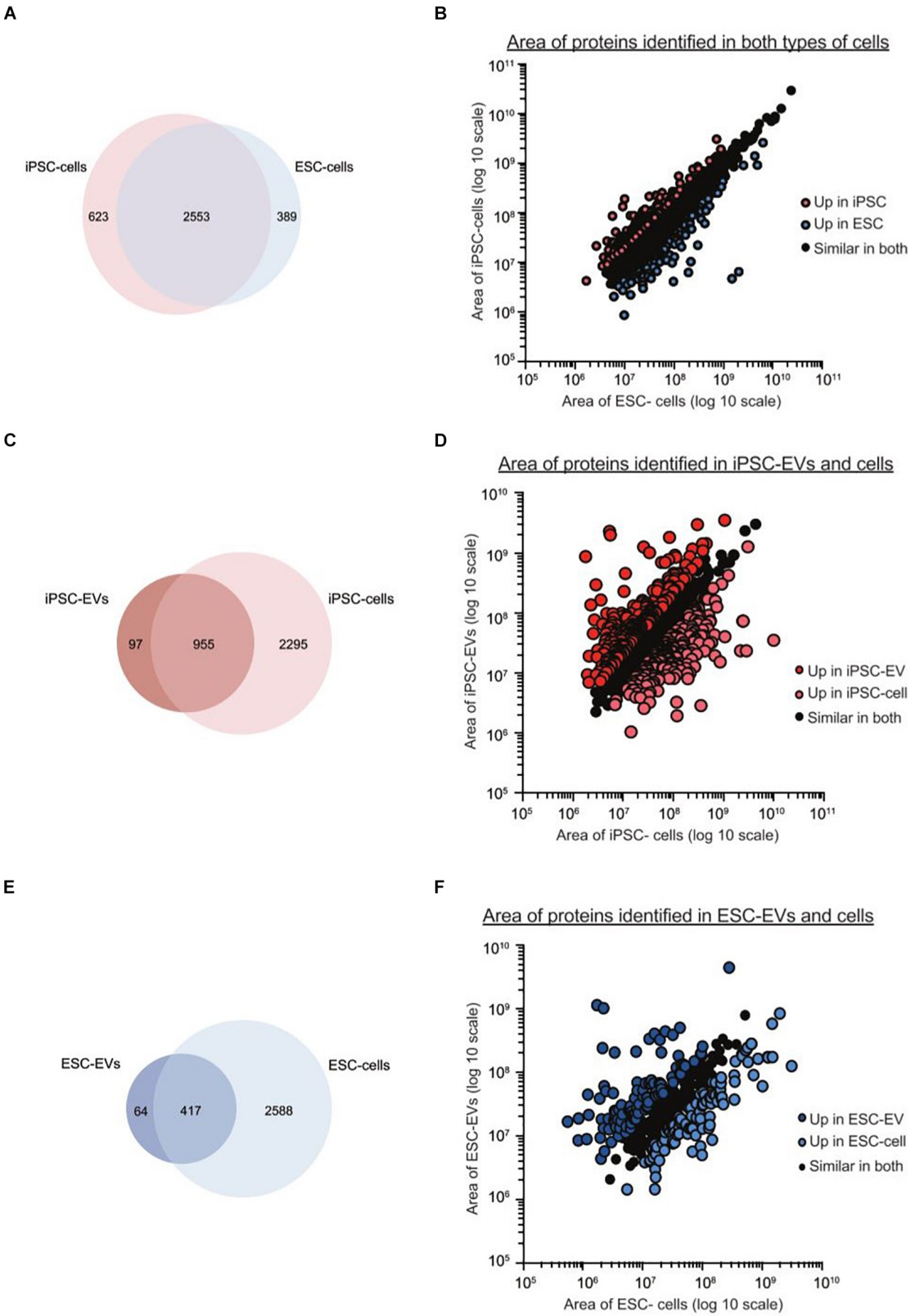

FIGURE 6 | Continued

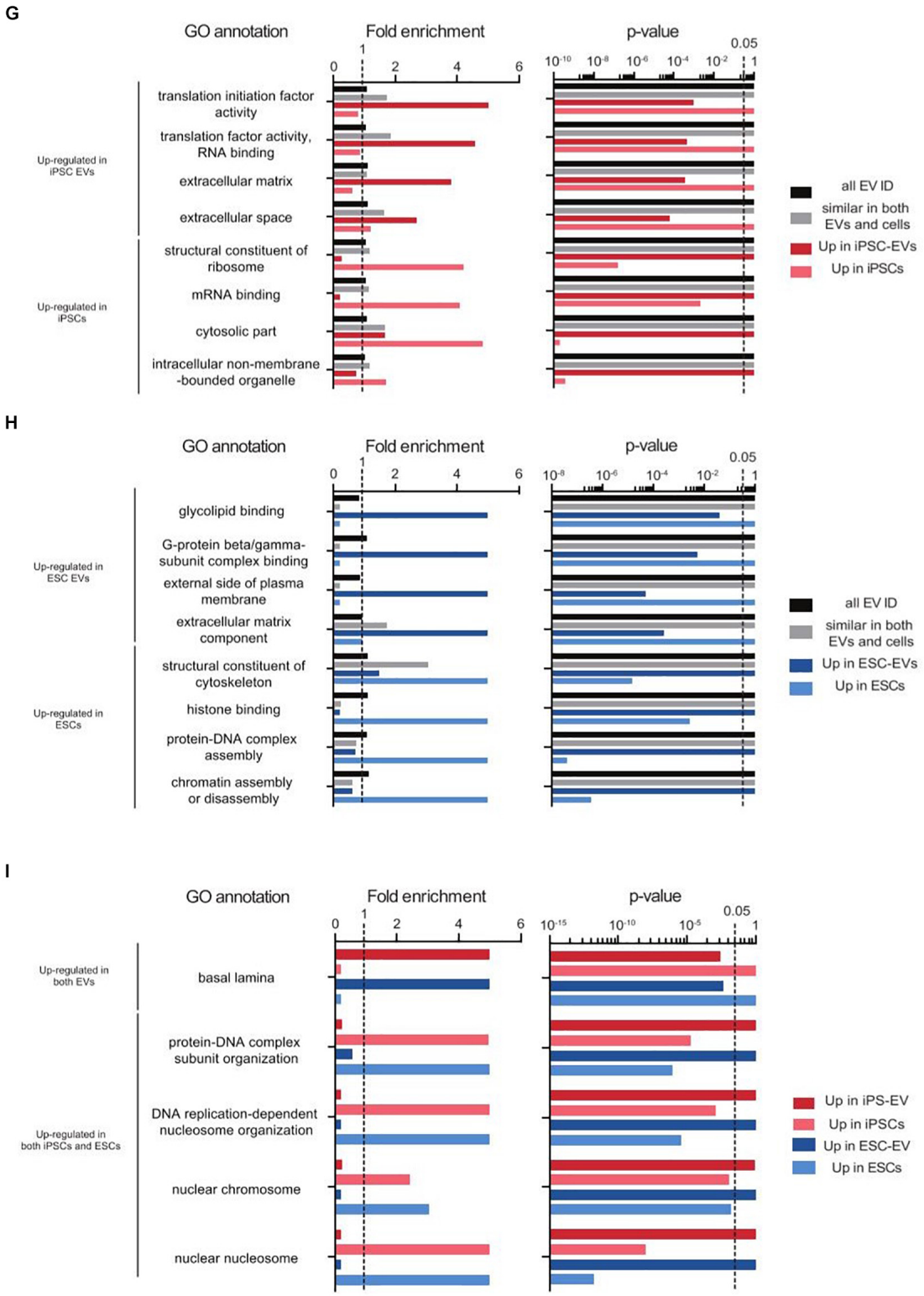

FIGURE 6 | Preliminary proteomics comparing GO terms of proteins from mouse iPSC and ESC EVs and cells. Venn diagram showing the overlap of proteins identified in the two types of stem cells **(A)**, in mouse iPSC-EVs and iPSCs **(B)** and in mouse ESC-EVs and ESCs **(C)**. Scatter plots showing the correlation between the areas of commonly identified proteins in each of these three pairing: iPSCs versus ESCs **(D)**, iPSC-EVs versus iPSCs **(E)** and ESC-EVs versus ESCs **(F)**. All proteins were classified into three distinct groups as indicated in the graphs. A subset of significantly enriched GO terms for proteins considered to be up regulated in either iPSCs or ESCs **(G)**, iPSC-EVs or iPSCs **(H)**, and ESC-EVs or ESCs **(I)**.

difference in GO terms enrichments and may not impact on cell functionality. Furthermore, our proteomics data highlighted the identities of other EV markers, which could serve as useful indicators for future studies on stem cell EVs.

Next, to trace if the similarities between EVs was related to their parental cells, we analyzed the proteomes of the cells from which the EVs were derived from. Although the proteomes of both stem cell types were highly similar, there was much less overlap between EVs and their corresponding parental source. This was largely due to the lower overall number of detected proteins in EVs than in cells. This is not at all unexpected, as it can be attributed to the size differences between a vesicle (100 nm) and a cell (>5 μm). However, the enrichment of specific GO terms in EVs over cells illustrates the differences between their biological contents and may be linked to their downstream functionality. In hindsight though, we cannot be certain how the background from the basal media may have also affected the LC-MS run and the downstream protein readout.

There is an overwhelming amount of research commenting on the similarities and differences between ESCs and iPSCs (Boulting et al., 2011; Narsinh et al., 2011; Phanstiel et al., 2011), and the variation between ESC and iPSC clones due to the type of donor cells (Ward et al., 2004; Osafune et al., 2008; Narsinh et al., 2011), their methylation status and transcriptomes (Kim et al., 2011; Lister et al., 2011; Ohi et al., 2011).

On the other hand, There have only been a handful of published proteomics studies on mouse (Graumann et al., 2007) and human iPSCs and ESCs (Phanstiel et al., 2011; Munoz et al., 2014), all of which have been performed on different ESC and iPSC lines. There have also been some recent studies on EVs from iPSCs and iPSC-derivatives (Zhou et al., 2016; Liu et al., 2017; Zhu et al., 2017; Ding et al., 2018; Dougherty et al., 2018; La Greca et al., 2018; Oh et al., 2018), though there is yet to be any proteomic data on EVs from pluripotent cell sources. Hence, due to the variation between lines, the biological data here might not be applicable to all other pluripotent stem cells.

In neurological diseases, standard methods of monitoring such as CT or MRI scans are costly, less sensitive and requires expertise interpretation. The use of traditional tissue biopsy or blood liquid biopsy in CNS-related disease has been elusive due to the presence of the blood brain barrier functions (Daneman and Prat, 2015). Recently though, some have capitalized on EVs in the cerebrospinal fluid (CSF) to monitor the brain and CNS (Welton et al., 2017; Thompson et al., 2018; Miller et al., 2019; Otake et al., 2019). However, the lumbar tap procedure for CSF extraction is painful and often only very small volumes of CSF can be extracted. Hence, we envision here that our study will assist other EV researchers on the methodology for EV purification from these precious sources.

Besides biology, EVs can also be exploited by loading therapeutic cargoes; both naturally and after engineering. In the former, there are many excellent reviews on how EVs from mesenchymal stem cells (MSCs) can alleviate disease through EV therapy in CNS-related diseases (Kawikova and Askenase, 2015; Koniusz et al., 2016; Luarte et al., 2016). On the other hand, others have cleverly designed targeting moieties on the surface of EVs and encapsulated genetic cargoes or drugs for therapeutic purposes (Alvarez-Erviti et al., 2011; El Andaloussi et al., 2013; Kalani et al., 2016; Usman et al., 2018). Here, we describe EVs from iPSCs that may serve as an alternative resource. Furthermore, we performed unbiased protein characterization of these EVs with the hope that this can assist in the future design and molecular engineering of EVs for specific personalized therapy.

CONCLUSION

Here, we describe a study investigating the isolation of EVs from protein-rich complex media types, using stem cells as a model. Initially, our step-by-step comparison between UC and LC contradicted our expectations. Using additional technologies, we illustrate the possible causes and sources of protein contamination in the UC pellet and how they can be reduced with additional clean-up steps. However, these processes are somewhat inefficient and compromise on the final output. On the other hand, although LC was a better alternative to UC, the resultant EV population still appears to be of low purity. The purity of EVs is of great importance in all forms of EV research, from deducing biological functions to use as therapeutic agents, as contaminations may confound interpretations. Furthermore, we highlight the need to be cautious when using current tools for the interpretation of EVs purified from complex media or biological fluids. Lastly, we analyzed the protein content of these EVs and briefly discuss their potential in future CNS-related research.

DATA AVAILABILITY STATEMENT

All datasets generated for this study are included in the manuscript/**Supplementary Files**.

AUTHOR CONTRIBUTIONS

YL performed all the experiments and wrote the manuscript. HJ performed the proteomics. MW and SE conceptualized the study and provided critical discussions on the overall study and manuscript.

FUNDING

YL is funded by the Agency for Science Technology and Research, Singapore. SE is funded by the Swedish Medical Research Council, the Swedish Foundation for Strategic Research (SSF-IRC), and Evox Therapeutics.

ACKNOWLEDGMENTS

We would like to thank Mr. Tim Davis and Dr. Paul Fairchild for kindly sharing their mouse ESCs and iPSCs lines. We would also like to thank Dr. Daniel Hagey for critical and useful discussions on the manuscript.

SUPPLEMENTARY MATERIAL

The Supplementary Material for this article can be found online at: https://www.frontiersin.org/articles/10.3389/fnins.2019.01067/full#supplementary-material

FIGURE S1 | Alternative types of serum-depleted media for EV collection from stem cells. **(A)** NTA size distribution profiles of UC pellets after centrifugation of the three types of media: KOSR-supplemented stem cell media (SR), Pre-spun stem cell media (PS) and serum-free media/OptiMEM (OM). **(B)** Table showing the mode size (nm) and concentration of particles (x10^9/ml) detected in the UC pellet of each media type. Representative bright-field images of mouse iPSCs **(C)** and mouse ESCs **(F)** after 48 h culture in SR, PS, or OM. Graphs comparing the total number of viable cells in the miPSCs **(D)** and mESCs **(E)** cultures at CM collection. Graphs comparing the total concentration of particles (x10^{10}/ml) detected by NTA in the UC pellet of miPSCs **(G)** and mESCs **(H)** in the three different media types.

FIGURE S2 | LC fractionation of UC pellets reveals co-precipitation of non-vesicular proteins with EVs in the UC pellet. **(A)** Schematic outline of the LC fractionation protocol of UC pellets. **(B)** LC chromatograph showing the 280 nm absorbance of the elution course from the LC column for three replicate samples (R1–R3). The first fraction (pink box) corresponds to the region where EVs elute. The second fraction (orange box) shows the appearance of another peak after the EVs. **(C)** NTA size distribution profiles of particles in the original UC sample (blue), and in the first (box 1; UC-LC1) and second (box 2; UC-LC2) LC fractions. **(D)** Graph on the left shows the mode size (nm) of particles in the original UC pellet, UC-LC1 and UC-LC2 (n = 3, bar represents mean ± SD). Graph on the right shows the percentage of particles detected in the UC pellet versus UC-LC1 (n = 3, bar represents mean ± SD). **(E)** Representative western blots for EV (Alix and CD9) and pluripotency (OCT4) markers when loading the same amount of particles from the UC pellet and UC-LC1 fraction. **(F)** Total protein staining of the UC pellet, UC-LC1 and UC-LC2. **(G)** Representative TEM images of the UC pellet and UC-LC1. Here the UC-LC1 sample appears to have a decreased background as compared to UC. The scale bar corresponds to 100 nm.

FIGURE S3 | Detection of non-mouse proteins in mouse derived EVs. Scatter plot showing the areas of proteins identified in the preliminary analysis of iPSC- and ESC-EV samples. Proteins from mouse (black dots), cow (red dots) and pig (blue dots) are indicated.

FIGURE S4 | Sequential LC fraction improves EV purity marginally. **(A)** Schematic outline of the sequential LC fractionation set-up. **(B)** LC chromatograph showing the 280 nm absorbance of the elution course from the LC column for three replicate samples (R1–R3). The first fraction (green box) corresponds to the region where EVs elute. **(C)** NTA size distribution profiles of particles in the first LC sample versus the second LC run (LC′1). **(D)** On the left, the mode size of particles in the original LC sample and the LC′1 sample appears to be similar (n = 3). On the right, graph showing overall percentage of particles recovered as compared to the input material. **(E)** Representative western blotting pictures when loading the same amount of particles for LC and LC'1. **(F)** Total protein staining of the membrane with LC and LC'1 samples.

TABLE S1 | Table showing the protein expression of replicate runs of cells and EVs purified from mouse ESC and mouse iPSC.

REFERENCES

Albelda, S. M., and Buck, C. A. (1990). Integrins and other cell adhesion molecules. *FASEB J.* 4, 2868–2880. doi: 10.1096/fasebj.4.11.2199285

Alvarez, M. L., Khosroheidari, M., Kanchi Ravi, R., and DiStefano, J. K. (2012). Comparison of protein, microRNA, and mRNA yields using different methods of urinary exosome isolation for the discovery of kidney disease biomarkers. *Kidney Int.* 82, 1024–1032. doi: 10.1038/ki.2012.256

Alvarez-Erviti, L., Seow, Y., Yin, H., Betts, C., Lakhal, S., and Wood, M. J. A. (2011). Delivery of siRNA to the mouse brain by systemic injection of targeted exosomes. *Nat. Biotechnol.* 29, 341–345. doi: 10.1038/nbt.1807

Antonucci, F., Turola, E., Riganti, L., Caleo, M., Gabrielli, M., Perrotta, C., et al. (2012). Microvesicles released from microglia stimulate synaptic activity via enhanced sphingolipid metabolism. *EMBO J.* 31, 1231–1240. doi: 10.1038/emboj.2011.489

Arslan, F., Lai, R. C., Smeets, M. B., Akeroyd, L., Choo, A., Aguor, E. N. E., et al. (2013). Mesenchymal stem cell-derived exosomes increase ATP levels, decrease oxidative stress and activate PI3K/Akt pathway to enhance myocardial viability and prevent adverse remodeling after myocardial ischemia/reperfusion injury. *Stem Cell Res.* 10, 301–312. doi: 10.1016/j.scr.2013.01.002

Bahi, A., and Dreyer, J.-L. (2005). Cocaine-induced expression changes of axon guidance molecules in the adult rat brain. *Mol. Cell. Neurosci.* 28, 275–291. doi: 10.1016/j.mcn.2004.09.011

Balvers, R. K., Kleijn, A., Kloezeman, J. J., French, P. J., Kremer, A., van den Bent, M. J., et al. (2013). Serum-free culture success of glial tumors is related to specific molecular profiles and expression of extracellular matrix-associated gene modules. *Neuro Oncol.* 15, 1684–1695. doi: 10.1093/neuonc/not116

Bobrie, A., Colombo, M., Krumeich, S., Raposo, G., and Théry, C. (2012). Diverse subpopulations of vesicles secreted by different intracellular mechanisms are present in exosome preparations obtained by differential ultracentrifugation. *J. Extracell. Vesicles* 1:18397. doi: 10.3402/jev.v1i0.18397

Böing, A. N., van der Pol, E., Grootemaat, A. E., Coumans, F. A. W., Sturk, A., and Nieuwland, R. (2014). Single-step isolation of extracellular vesicles by size-exclusion chromatography. *J. Extracell. Vesicles* 3:23430. doi: 10.3402/jev.v3.23430

Boulting, G. L., Kiskinis, E., Croft, G. F., Amoroso, M. W., Oakley, D. H., Wainger, B. J., et al. (2011). A functionally characterized test set of human induced pluripotent stem cells. *Nat. Biotechnol.* 29, 279–286. doi: 10.1038/nbt.1783

Brewer, G. J. (1995). Serum-free B27/neurobasal medium supports differentiated growth of neurons from the striatum, substantia nigra, septum, cerebral cortex, cerebellum, and dentate gyrus. *J. Neurosci. Res.* 42, 674–683. doi: 10.1002/jnr.490420510

Chen, T. S., Arslan, F., Yin, Y., Tan, S. S., Lai, R. C., Choo, A. B. H., et al. (2011). Enabling a robust scalable manufacturing process for therapeutic exosomes through oncogenic immortalization of human ESC-derived MSCs. *J. Transl. Med.* 9:47. doi: 10.1186/1479-5876-9-47

Cvjetkovic, A., Lötvall, J., and Lässer, C. (2014). The influence of rotor type and centrifugation time on the yield and purity of extracellular vesicles. *J. Extracell. Vesicles* 3:23111. doi: 10.3402/jev.v3.23111

Daneman, R., and Prat, A. (2015). The blood–brain barrier. *Cold Spring Harb. Perspect. Biol.* 7:a020412. doi: 10.1101/cshperspect.a020412

Ding, Q., Sun, R., Wang, P., Zhang, H., Xiang, M., Meng, D., et al. (2018). Protective effects of human induced pluripotent stem cell-derived exosomes on high glucose-induced injury in human endothelial cells. *Exp. Ther. Med.* 15, 4791–4797. doi: 10.3892/etm.2018.6059

Dougherty, J. A., Kumar, N., Noor, M., Angelos, M. G., Khan, M., Chen, C.-A., et al. (2018). Extracellular vesicles released by human induced-pluripotent stem cell-derived cardiomyocytes promote angiogenesis. *Front. Physiol.* 9:1794. doi: 10.3389/fphys.2018.01794

El Andaloussi, S., Mäger, I., Breakefield, X. O., and Wood, M. J. A. (2013). Extracellular vesicles: biology and emerging therapeutic opportunities. *Nat. Rev. Drug Discov.* 12, 347–357. doi: 10.1038/nrd3978

Fairchild, P. J., Brook, F. A., Gardner, R. L., Graça, L., Strong, V., Tone, Y., et al. (2000). Directed differentiation of dendritic cells from mouse embryonic stem cells. *Curr. Biol.*10, 1515–1518. doi: 10.1016/s0960-9822(00)00824-821

Fauré, J., Lachenal, G., Court, M., Hirrlinger, J., Chatellard-Causse, C., Blot, B., et al. (2006). Exosomes are released by cultured cortical neurones. *Mol. Cell. Neurosci.* 31, 642–648. doi: 10.1016/j.mcn.2005.12.003

Frühbeis, C., Fröhlich, D., Kuo, W. P., Amphornrat, J., Thilemann, S., Saab, A. S., et al. (2013). Neurotransmitter-triggered transfer of exosomes mediates oligodendrocyte-neuron communication. *PLoS Biol.* 11:e1001604. doi: 10.1371/journal.pbio.1001604

Ghosh, A., Davey, M., Chute, I. C., Griffiths, S. G., Lewis, S., Chacko, S., et al. (2014). Rapid isolation of extracellular vesicles from cell culture and biological fluids

using a synthetic peptide with specific affinity for heat shock proteins. *PLoS One* 9:e110443. doi: 10.1371/journal.pone.0110443

Gould, S. J., and Raposo, G. (2013). As we wait: coping with an imperfect nomenclature for extracellular vesicles. *J. Extracell. Vesicles* 2:20389. doi: 10.3402/jev.v2i0.20389

Graumann, J., Hubner, N. C., Kim, J. B., Ko, K., Moser, M., Kumar, C., et al. (2007). Stable isotope labeling by amino acids in cell culture (SILAC) and proteome quantitation of mouse embryonic stem cells to a depth of 5,111 proteins. *Mol. Cell. Proteomics* 7, 672–683. doi: 10.1074/mcp.M700460-MCP200

Harding, C., Heuser, J., and Stahl, P. (1984). Endocytosis and intracellular processing of transferrin and colloidal gold-transferrin in rat reticulocytes: demonstration of a pathway for receptor shedding. *Eur. J. Cell Biol.* 35, 256–263.

Hienola, A., Tumova, S., Kulesskiy, E., and Rauvala, H. (2006). N-syndecan deficiency impairs neural migration in brain. *J. Cell Biol.* 174, 569–580. doi: 10.1083/jcb.200602043

Hoshino, A., Costa-Silva, B., Shen, T.-L., Rodrigues, G., Hashimoto, A., Tesic Mark, M., et al. (2015). Tumour exosome integrins determine organotropic metastasis. *Nature* 527, 329–335. doi: 10.1038/nature15756

Hung, M. E., and Leonard, J. N. (2016). A platform for actively loading cargo RNA to elucidate limiting steps in EV-mediated delivery. *J. Extracell. Vesicles* 5:31027. doi: 10.3402/jev.v5.31027

Iwai, K., Minamisawa, T., Suga, K., Yajima, Y., and Shiba, K. (2016). Isolation of human salivary extracellular vesicles by iodixanol density gradient ultracentrifugation and their characterizations. *J. Extracell. Vesicles* 5:30829. doi: 10.3402/jev.v5.30829

Janas, T., Janas, M. M., Sapoń, K., and Janas, T. (2015). Mechanisms of RNA loading into exosomes. *FEBS Lett.* 589, 1391–1398. doi: 10.1016/j.febslet.2015.04.036

Janowska-Wieczorek, A., Wysoczynski, M., Kijowski, J., Marquez-Curtis, L., Machalinski, B., Ratajczak, J., et al. (2005). Microvesicles derived from activated platelets induce metastasis and angiogenesis in lung cancer. *Int. J. Cancer* 113, 752–760. doi: 10.1002/ijc.20657

Kalani, A., Chaturvedi, P., Kamat, P. K., Maldonado, C., Bauer, P., Joshua, I. G., et al. (2016). Curcumin-loaded embryonic stem cell exosomes restored neurovascular unit following ischemia-reperfusion injury. *Int. J. Biochem. Cell Biol.* 79, 360–369. doi: 10.1016/j.biocel.2016.09.002

Kanwar, S. S., Dunlay, C. J., Simeone, D. M., and Nagrath, S. (2014). Microfluidic device (ExoChip) for on-chip isolation, quantification and characterization of circulating exosomes. *Lab. Chip* 14, 1891–1900. doi: 10.1039/c4lc00136b

Katsman, D., Stackpole, E. J., Domin, D. R., and Farber, D. B. (2012). Embryonic stem cell-derived microvesicles induce gene expression changes in Müller cells of the retina. *PLoS One* 7:e50417. doi: 10.1371/journal.pone.0050417

Kawikova, I., and Askenase, P. W. (2015). Diagnostic and therapeutic potentials of exosomes in CNS diseases. *Brain Res.* 1617, 63–71. doi: 10.1016/j.brainres.2014.09.070

Kim, K., Zhao, R., Doi, A., Ng, K., Unternaehrer, J., Cahan, P., et al. (2011). Donor cell type can influence the epigenome and differentiation potential of human induced pluripotent stem cells. *Nat. Biotechnol.* 29, 1117–1119. doi: 10.1038/nbt.2052

Koniusz, S., Andrzejewska, A., Muraca, M., Srivastava, A. K., Janowski, M., and Lukomska, B. (2016). Extracellular vesicles in physiology, pathology, and therapy of the immune and central nervous system, with focus on extracellular vesicles derived from mesenchymal stem cells as therapeutic tools. *Front. Cell. Neurosci.* 10:109. doi: 10.3389/fncel.2016.00109

Kornilov, R., Puhka, M., Mannerström, B., Hiidenmaa, H., Peltoniemi, H., Siljander, P., et al. (2018). Efficient ultrafiltration-based protocol to deplete extracellular vesicles from fetal bovine serum. *J. Extracell. Vesicles* 7:1422674. doi: 10.1080/20013078.2017.1422674

Krämer-Albers, E.-M., Bretz, N., Tenzer, S., Winterstein, C., Möbius, W., Berger, H., et al. (2007). Oligodendrocytes secrete exosomes containing major myelin and stress-protective proteins: trophic support for axons? *Proteomics Clin. Appl.* 1, 1446–1461. doi: 10.1002/prca.200700522

La Greca, A., Solari, C., Furmento, V., Lombardi, A., Biani, M. C., Aban, C., et al. (2018). Extracellular vesicles from pluripotent stem cell-derived mesenchymal stem cells acquire a stromal modulatory proteomic pattern during differentiation. *Exp. Mol. Med.* 50:119. doi: 10.1038/s12276-018-0142-x

Lachenal, G., Pernet-Gallay, K., Chivet, M., Hemming, F. J., Belly, A., Bodon, G., et al. (2011). Release of exosomes from differentiated neurons and its regulation by synaptic glutamatergic activity. *Mol. Cell. Neurosci.* 46, 409–418. doi: 10.1016/j.mcn.2010.11.004

Lamparski, H. G., Metha-Damani, A., Yao, J.-Y., Patel, S., Hsu, D.-H., Ruegg, C., et al. (2002). Production and characterization of clinical grade exosomes derived from dendritic cells. *J. Immunol. Methods* 270, 211–226. doi: 10.1016/s0022-1759(02)00330-7

Lane, R. E., Korbie, D., Trau, M., and Hill, M. M. (2019). Optimizing size exclusion chromatography for extracellular vesicle enrichment and proteomic analysis from clinically relevant samples. *Proteomics* 19:e1800156. doi: 10.1002/pmic.201800156

Lehrich, B., Liang, Y., Khosravi, P., Federoff, H., and Fiandaca, M. (2018). Fetal bovine serum-derived extracellular vesicles persist within vesicle-depleted culture media. *Int. J. Mol. Sci.* 19:3538. doi: 10.3390/ijms19113538

Li, J., Lee, Y., Johansson, H. J., Mäger, I., Vader, P., Nordin, J. Z., et al. (2015). Serum-free culture alters the quantity and protein composition of neuroblastoma-derived extracellular vesicles. *J. Extracell. Vesicles* 4:26883. doi: 10.3402/jev.v4.26883

Lim, J., Choi, M., Lee, H., Kim, Y.-H., Han, J.-Y., Lee, E. S., et al. (2019). Direct isolation and characterization of circulating exosomes from biological samples using magnetic nanowires. *J. Nanobiotechnology* 17:1. doi: 10.1186/s12951-018-0433-433

Lister, R., Pelizzola, M., Kida, Y. S., Hawkins, R. D., Nery, J. R., Hon, G., et al. (2011). Hotspots of aberrant epigenomic reprogramming in human induced pluripotent stem cells. *Nature* 471, 68–73. doi: 10.1038/nature09798

Liu, X., Li, Q., Niu, X., Hu, B., Chen, S., Song, W., et al. (2017). Exosomes secreted from human-induced pluripotent stem cell-derived mesenchymal stem cells prevent osteonecrosis of the femoral head by promoting angiogenesis. *Int. J. Biol. Sci.* 13, 232–244. doi: 10.7150/ijbs.16951

Livshits, M. A., Khomyakova, E., Evtushenko, E. G., Lazarev, V. N., Kulemin, N. A., Semina, S. E., et al. (2015). Isolation of exosomes by differential centrifugation: theoretical analysis of a commonly used protocol. *Sci. Rep.* 5:17319. doi: 10.1038/srep17319

Luarte, A., Bátiz, L. F., Wyneken, U., and Lafourcade, C. (2016). Potential therapies by stem cell-derived exosomes in CNS diseases: focusing on the neurogenic niche. *Stem Cells Int.* 2016, 1–16. doi: 10.1155/2016/5736059

Mi, H., Muruganujan, A., and Thomas, P. D. (2013). PANTHER in 2013: modeling the evolution of gene function, and other gene attributes, in the context of phylogenetic trees. *Nucleic Acids Res.* 41, D377–D386. doi: 10.1093/nar/gks1118

Mi, H., Muruganujan, A., Huang, X., Ebert, D., Mills, C., Guo, X., et al. (2019). Protocol update for large-scale genome and gene function analysis with the PANTHER classification system (v.14.0). *Nat. Protoc.* 14, 703–721. doi: 10.1038/s41596-019-0128-8

Miller, A. M., Shah, R. H., Pentsova, E. I., Pourmaleki, M., Briggs, S., Distefano, N., et al. (2019). Tracking tumour evolution in glioma through liquid biopsies of cerebrospinal fluid. *Nature* 565, 654–658. doi: 10.1038/s41586-019-0882-883

Mol, E. A., Goumans, M.-J., Doevendans, P. A., Sluijter, J. P. G., and Vader, P. (2017). Higher functionality of extracellular vesicles isolated using size-exclusion chromatography compared to ultracentrifugation. *Nanomedicine* 13, 2061–2065. doi: 10.1016/j.nano.2017.03.011

Moreno-Gonzalo, O., Fernandez-Delgado, I., and Sanchez-Madrid, F. (2018). Post-translational add-ons mark the path in exosomal protein sorting. *Cell. Mol. Life Sci.* 75, 1–19. doi: 10.1007/s00018-017-2690-y

Munoz, J., Low, T. Y., Kok, Y. J., Chin, A., Frese, C. K., Ding, V., et al. (2014). The quantitative proteomes of human-induced pluripotent stem cells and embryonic stem cells. *Mol. Syst. Biol.* 7, 550–550. doi: 10.1038/msb.2011.84

Narsinh, K. H., Sun, N., Sanchez-Freire, V., Lee, A. S., Almeida, P., Hu, S., et al. (2011). Single cell transcriptional profiling reveals heterogeneity of human induced pluripotent stem cells. *J. Clin. Invest.* 121, 1217–1221. doi: 10.1172/JCI44635

Noerholm, M., Balaj, L., Limperg, T., Salehi, A., Zhu, L. D., Hochberg, F. H., et al. (2012). RNA expression patterns in serum microvesicles from patients with glioblastoma multiforme and controls. *BMC Cancer* 12:22. doi: 10.1186/1471-2407-12-22

Nordin, J. Z., Lee, Y., Vader, P., Mäger, I., Johansson, H. J., Heusermann, W., et al. (2015). Ultrafiltration with size-exclusion liquid chromatography for high yield isolation of extracellular vesicles preserving intact biophysical and functional properties. *Nanomedicine* 11, 879–883. doi: 10.1016/j.nano.2015.01.003

Oeyen, E., Van Mol, K., Baggerman, G., Willems, H., Boonen, K., Rolfo, C., et al. (2018). Ultrafiltration and size exclusion chromatography combined with asymmetrical-flow field-flow fractionation for the isolation and characterisation of extracellular vesicles from urine. *J. Extracell. Vesicles* 7:1490143. doi: 10.1080/20013078.2018.1490143

Oh, M., Lee, J., Kim, Y., Rhee, W., and Park, J. (2018). Exosomes derived from human induced pluripotent stem cells ameliorate the aging of skin fibroblasts. *Int. J. Mol. Sci.* 19:1715. doi: 10.3390/ijms19061715

Ohi, Y., Qin, H., Hong, C., Blouin, L., Polo, J. M., Guo, T., et al. (2011). Incomplete DNA methylation underlies a transcriptional memory of somatic cells in human iPS cells. *Nat. Cell Biol.* 13, 541–549. doi: 10.1038/ncb2239

Onódi, Z., Pelyhe, C., Terézia Nagy, C., Brenner, G. B., Almási, L., Kittel, Á., et al. (2018). Isolation of high-purity extracellular vesicles by the combination of iodixanol density gradient ultracentrifugation and bind-elute chromatography from blood plasma. *Front. Physiol.* 9:1479. doi: 10.3389/fphys.2018.01479

Osafune, K., Caron, L., Borowiak, M., Martinez, R. J., Fitz-Gerald, C. S., Sato, Y., et al. (2008). Marked differences in differentiation propensity among human embryonic stem cell lines. *Nat. Biotechnol.* 26, 313–315. doi: 10.1038/nbt1383

Otake, K., Kamiguchi, H., and Hirozane, Y. (2019). Identification of biomarkers for amyotrophic lateral sclerosis by comprehensive analysis of exosomal mRNAs in human cerebrospinal fluid. *BMC Med. Genomics* 12:7. doi: 10.1186/s12920-019-0473-z

Pan, B. T., Teng, K., Wu, C., Adam, M., and Johnstone, R. M. (1985). Electron microscopic evidence for externalization of the transferrin receptor in vesicular form in sheep reticulocytes. *J. Cell Biol.* 101, 942–948. doi: 10.1083/jcb.101.3.942

Peinado, H., Alečkovič, M., Lavotshkin, S., Matei, I., Costa-Silva, B., Moreno-Bueno, G., et al. (2012). Melanoma exosomes educate bone marrow progenitor cells toward a pro-metastatic phenotype through MET. *Nat. Med.* 18, 883–891. doi: 10.1038/nm.2753

Phanstiel, D. H., Brumbaugh, J., Wenger, C. D., Tian, S., Probasco, M. D., Bailey, D. J., et al. (2011). Proteomic and phosphoproteomic comparison of human ES and iPS cells. *Nat. Methods* 8, 821–827. doi: 10.1038/nmeth.1699

Pozzi, D., Ban, J., Iseppon, F., and Torre, V. (2017). An improved method for growing neurons: comparison with standard protocols. *J. Neurosci. Methods* 280, 1–10. doi: 10.1016/j.jneumeth.2017.01.013

Ragusa, M., Barbagallo, C., Cirnigliaro, M., Battaglia, R., Brex, D., Caponnetto, A., et al. (2017). Asymmetric RNA distribution among cells and their secreted exosomes: biomedical meaning and considerations on diagnostic applications. *Front. Mol. Biosci.* 4:66. doi: 10.3389/fmolb.2017.00066

Raposo, G., Nijman, H. W., Stoorvogel, W., Liejendekker, R., Harding, C. V., Melief, C. J., et al. (1996). B lymphocytes secrete antigen-presenting vesicles. *J. Exp. Med.* 183, 1161–1172. doi: 10.1084/jem.183.3.1161

Ratajczak, J., Miekus, K., Kucia, M., Zhang, J., Reca, R., Dvorak, P., et al. (2006). Embryonic stem cell-derived microvesicles reprogram hematopoietic progenitors: evidence for horizontal transfer of mRNA and protein delivery. *Leukemia* 20, 847–856. doi: 10.1038/sj.leu.2404132

Raz, A., Barzilai, R., Spira, G., and Inbar, M. (1978). Oncogenicity and immunogenicity associated with membranes isolated from cell-free ascites fluid of lymphoma-bearing mice. *Cancer Res.* 38, 2480–2485.

Rekker, K., Saare, M., Roost, A. M., Kubo, A.-L., Zarovni, N., Chiesi, A., et al. (2014). Comparison of serum exosome isolation methods for microRNA profiling. *Clin. Biochem.* 47, 135–138. doi: 10.1016/j.clinbiochem.2013.10.020

Rood, I. M., Deegens, J. K. J., Merchant, M. L., Tamboer, W. P. M., Wilkey, D. W., Wetzels, J. F. M., et al. (2010). Comparison of three methods for isolation of urinary microvesicles to identify biomarkers of nephrotic syndrome. *Kidney Int.* 78, 810–816. doi: 10.1038/ki.2010.262

Sakisaka, T. (2005). Cell adhesion molecules in the CNS. *J. Cell Sci.* 118, 5407–5410. doi: 10.1242/jcs.02672

Segura, E., Amigorena, S., and Théry, C. (2005a). Mature dendritic cells secrete exosomes with strong ability to induce antigen-specific effector immune responses. *Blood Cells. Mol. Dis.* 35, 89–93. doi: 10.1016/j.bcmd.2005.05.003

Segura, E., Nicco, C., Lombard, B., Véron, P., Raposo, G., Batteux, F., et al. (2005b). ICAM-1 on exosomes from mature dendritic cells is critical for efficient naive T-cell priming. *Blood* 106, 216–223. doi: 10.1182/blood-2005-01-0220

Shelke, G. V., Lässer, C., Gho, Y. S., and Lötvall, J. (2014). Importance of exosome depletion protocols to eliminate functional and RNA-containing extracellular vesicles from fetal bovine serum. *J. Extracell. Vesicles* 3:24783. doi: 10.3402/jev.v3.24783

Shimaoka, M., Kawamoto, E., Gaowa, A., Okamoto, T., and Park, E. (2019). Connexins and integrins in exosomes. *Cancers* 11:106. doi: 10.3390/cancers11010106

Sork, H., Corso, G., Krjutskov, K., Johansson, H. J., Nordin, J. Z., Wiklander, O. P. B., et al. (2018). Heterogeneity and interplay of the extracellular vesicle small RNA transcriptome and proteome. *Sci. Rep.* 8:10813. doi: 10.1038/s41598-018-28485-28489

Stranska, R., Gysbrechts, L., Wouters, J., Vermeersch, P., Bloch, K., Dierickx, D., et al. (2018). Comparison of membrane affinity-based method with size-exclusion chromatography for isolation of exosome-like vesicles from human plasma. *J. Transl. Med.* 16:1. doi: 10.1186/s12967-017-1374-6

Sunkara, V., Kim, C.-J., Park, J., Woo, H.-K., Kim, D., Ha, H. K., et al. (2019). Fully automated, label-free isolation of extracellular vesicles from whole blood for cancer diagnosis and monitoring. *Theranostics* 9, 1851–1863. doi: 10.7150/thno.32438

Szostak, N., Royo, F., Rybarczyk, A., Szachniuk, M., Blazewicz, J., del Sol, A., et al. (2014). Sorting signal targeting mRNA into hepatic extracellular vesicles. *RNA Biol.* 11, 836–844. doi: 10.4161/rna.29305

Takov, K., Yellon, D. M., and Davidson, S. M. (2019). Comparison of small extracellular vesicles isolated from plasma by ultracentrifugation or size-exclusion chromatography: yield, purity and functional potential. *J. Extracell. Vesicles* 8:1560809. doi: 10.1080/20013078.2018.1560809

Tauro, B. J., Greening, D. W., Mathias, R. A., Ji, H., Mathivanan, S., Scott, A. M., et al. (2012). Comparison of ultracentrifugation, density gradient separation, and immunoaffinity capture methods for isolating human colon cancer cell line LIM1863-derived exosomes. *Methods* 56, 293–304. doi: 10.1016/j.ymeth.2012.01.002

Taylor, D. D., Zacharias, W., and Gercel-Taylor, C. (2011). "Exosome Isolation for Proteomic Analyses and RNA Profiling," in *Serum/Plasma Proteomics*, eds R. J. Simpson, and D. W. Greening, (Totowa, NJ: Humana Press), 235–246. doi: 10.1007/978-1-61779-068-3_15

Théry, C., Amigorena, S., Raposo, G., and Clayton, A. (2006). Isolation and characterization of exosomes from cell culture supernatants and biological fluids. *Curr. Protoc. Cell Biol.* Chapter 3:Unit 3.22. doi: 10.1002/0471143030.cb0322s30

Théry, C., Boussac, M., Véron, P., Ricciardi-Castagnoli, P., Raposo, G., Garin, J., et al. (2001). Proteomic analysis of dendritic cell-derived exosomes: a secreted subcellular compartment distinct from apoptotic vesicles. *J. Immunol.* 166, 7309–7318. doi: 10.4049/jimmunol.166.12.7309

Thompson, A. G., Gray, E., Heman-Ackah, S. M., Mäger, I., Talbot, K., Andaloussi, S. E., et al. (2016). Extracellular vesicles in neurodegenerative disease - pathogenesis to biomarkers. *Nat. Rev. Neurol.* 12, 346–357. doi: 10.1038/nrneurol.2016.68

Thompson, A. G., Gray, E., Mager, I., Fischer, R., Thézénas, M.-L., Charles, P. D., et al. (2018). UFLC-Derived CSF extracellular vesicle origin and proteome. *Proteomics* 18:e1800257. doi: 10.1002/pmic.201800257

Trams, E. G., Lauter, C. J., Salem, N., and Heine, U. (1981). Exfoliation of membrane ecto-enzymes in the form of micro-vesicles. *Biochim. Biophys. Acta* 645, 63–70. doi: 10.1016/0005-2736(81)90512-5

Usman, W. M., Pham, T. C., Kwok, Y. Y., Vu, L. T., Ma, V., Peng, B., et al. (2018). Efficient RNA drug delivery using red blood cell extracellular vesicles. *Nat. Commun.* 9:2359. doi: 10.1038/s41467-018-04791-4798

Utsugi-Kobukai, S., Fujimaki, H., Hotta, C., Nakazawa, M., and Minami, M. (2003). MHC class I-mediated exogenous antigen presentation by exosomes secreted from immature and mature bone marrow derived dendritic cells. *Immunol. Lett.* 89, 125–131. doi: 10.1016/s0165-2478(03)00128-7

Villarroya-Beltri, C., Baixauli, F., Gutiérrez-Vázquez, C., Sánchez-Madrid, F., and Mittelbrunn, M. (2014). Sorting it out: regulation of exosome loading. *Semin. Cancer Biol.* 28, 3–13. doi: 10.1016/j.semcancer.2014.04.009

Wang, G., Dinkins, M., He, Q., Zhu, G., Poirier, C., Campbell, A., et al. (2012). Astrocytes secrete exosomes enriched with proapoptotic ceramide and prostate

apoptosis response 4 (PAR-4): potential mechanism of apoptosis induction in Alzheimer disease (AD). *J. Biol. Chem.* 287, 21384–21395. doi: 10.1074/jbc.M112.340513

Wang, X., and Jauch, R. (2014). OCT4: a penetrant pluripotency inducer. *Cell Regen.* 3:6. doi: 10.1186/2045-9769-3-6

Ward, C. M., Barrow, K. M., and Stern, P. L. (2004). Significant variations in differentiation properties between independent mouse ES cell lines cultured under defined conditions. *Exp. Cell Res.* 293, 229–238. doi: 10.1016/j.yexcr.2003.10.017

Wei, Z., Batagov, A. O., Carter, D. R. F., and Krichevsky, A. M. (2016). Fetal bovine serum RNA interferes with the cell culture derived extracellular RNA. *Sci. Rep.* 6:31175. doi: 10.1038/srep31175

Welton, J. L., Loveless, S., Stone, T., von Ruhland, C., Robertson, N. P., and Clayton, A. (2017). Cerebrospinal fluid extracellular vesicle enrichment for protein biomarker discovery in neurological disease; multiple sclerosis. *J. Extracell. Vesicles* 6:1369805. doi: 10.1080/20013078.2017.1369805

Welton, J. L., Webber, J. P., Botos, L.-A., Jones, M., and Clayton, A. (2015). Ready-made chromatography columns for extracellular vesicle isolation from plasma. *J. Extracell. Vesicles* 4:27269. doi: 10.3402/jev.v4.27269

Wolf, P. (1967). The nature and significance of platelet products in human plasma. *Br. J. Haematol.* 13, 269–288. doi: 10.1111/j.1365-2141.1967.tb08741.x

Yamada, T., Inoshima, Y., Matsuda, T., and Ishiguro, N. (2012). Comparison of methods for isolating exosomes from bovine milk. *J. Vet. Med. Sci.* 74, 1523–1525. doi: 10.1292/jvms.12-0032

Yuan, A., Farber, E. L., Rapoport, A. L., Tejada, D., Deniskin, R., Akhmedov, N. B., et al. (2009). Transfer of microRNAs by embryonic stem cell microvesicles. *PLoS One* 4:e4722. doi: 10.1371/journal.pone.0004722

Yuana, Y., Levels, J., Grootemaat, A., Sturk, A., and Nieuwland, R. (2014). Co-isolation of extracellular vesicles and high-density lipoproteins using density gradient ultracentrifugation. *J. Extracell. Vesicles* 3:23262. doi: 10.3402/jev.v3.23262

Zhang, Z., Wang, C., Li, T., Liu, Z., and Li, L. (2014). Comparison of ultracentrifugation and density gradient separation methods for isolating Tca8113 human tongue cancer cell line-derived exosomes. *Oncol. Lett.* 8, 1701–1706. doi: 10.3892/ol.2014.2373

Zhou, J., Ghoroghi, S., Benito-Martin, A., Wu, H., Unachukwu, U. J., Einbond, L. S., et al. (2016). Characterization of induced pluripotent stem cell microvesicle genesis, morphology and pluripotent content. *Sci. Rep.* 6:19743. doi: 10.1038/srep19743

Zhu, Y., Wang, Y., Zhao, B., Niu, X., Hu, B., Li, Q., et al. (2017). Comparison of exosomes secreted by induced pluripotent stem cell-derived mesenchymal stem cells and synovial membrane-derived mesenchymal stem cells for the treatment of osteoarthritis. *Stem Cell Res. Ther.* 8:64. doi: 10.1186/s13287-017-0510-9

Zitvogel, L., Regnault, A., Lozier, A., Wolfers, J., Flament, C., Tenza, D., et al. (1998). Eradication of established murine tumors using a novel cell-free vaccine: dendritic cell-derived exosomes. *Nat. Med.* 4, 594–600. doi: 10.1038/nm0598-594 doi: 10.1038/nm0598-594

Conflict of Interest: MW and SE are founders and shareholders of Evox Therapeutics.

The remaining authors declare that the research was conducted in the absence of any commercial or financial relationships that could be construed as a potential conflict of interest.

frontiers in Neuroscience

ORIGINAL RESEARCH
published: 26 November 2019
doi: 10.3389/fnins.2019.01208

miR-212 and miR-132 Are Downregulated in Neurally Derived Plasma Exosomes of Alzheimer's Patients

Diana J. Cha[1†], David Mengel[1,2,3†], Maja Mustapic[4], Wen Liu[1], Dennis J. Selkoe[1], Dimitrios Kapogiannis[4], Douglas Galasko[5], Robert A. Rissman[5,6], David A. Bennett[7] and Dominic M. Walsh[1,8]*

[1] Laboratory for Neurodegenerative Disease Research, Ann Romney Center for Neurologic Diseases, Brigham and Women's Hospital, Harvard Medical School, Boston, MA, United States, [2] Department of Neurodegenerative Diseases, Hertie-Institute for Clinical Brain Research and Center of Neurology, University of Tübingen, Tübingen, Germany, [3] German Center for Neurodegenerative Diseases, University of Tübingen, Tübingen, Germany, [4] Laboratory of Neurosciences, National Institute on Aging, National Institutes of Health, Baltimore, MD, United States, [5] Department of Neurosciences, University of California, San Diego, La Jolla, CA, United States, [6] VA San Diego Healthcare System, La Jolla, CA, United States, [7] Rush Alzheimer's Disease Center, Rush Medical College, Chicago, IL, United States, [8] Alzheimer's Disease and Dementia Research Unit, Biogen Inc., Cambridge, MA, United States

OPEN ACCESS

Edited by:
Efrat Levy,
New York University, United States

Reviewed by:
Scott Edward Counts,
Michigan State University, United States
Daniela Galimberti,
University of Milan, Italy
P. Hemachandra Reddy,
Texas Tech University Health Sciences Center, United States

***Correspondence:**
Dominic M. Walsh
dwalsh3@bwh.harvard.edu

[†]These authors have contributed equally to this work

Specialty section:
This article was submitted to Neurodegeneration, a section of the journal Frontiers in Neuroscience

Received: *21 August 2019*
Accepted: *25 October 2019*
Published: *26 November 2019*

Citation:
Cha DJ, Mengel D, Mustapic M, Liu W, Selkoe DJ, Kapogiannis D, Galasko D, Rissman RA, Bennett DA and Walsh DM (2019) miR-212 and miR-132 Are Downregulated in Neurally Derived Plasma Exosomes of Alzheimer's Patients. Front. Neurosci. 13:1208. doi: 10.3389/fnins.2019.01208

It was recently discovered that brain cells release extracellular vesicles (EV) which can pass from brain into blood. These findings raise the possibility that brain-derived EV's present in blood can be used to monitor disease processes occurring in the cerebrum. Since the levels of certain micro-RNAs (miRNAs) have been reported to be altered in Alzheimer's disease (AD) brain, we sought to assess miRNA dysregulation in AD brain tissue and to determine if these changes were reflected in neural EVs isolated from blood of subjects with AD. To this end, we employed high-content miRNA arrays to search for differences in miRNAs in RNA pools from brain tissue of AD (n = 5), high pathological control (HPC) (n = 5), or cognitively intact pathology-free controls (n = 5). Twelve miRNAs were altered by >1.5-fold in AD compared to controls, and six of these were also changed compared to HPCs. Analysis of hits in brain extracts from 11 AD, 7 HPCs and 9 controls revealed a similar fold difference in these six miRNAs, with three showing statistically significant group differences and one with a strong trend toward group differences. Thereafter, we focused on the four miRNAs that showed group differences and measured their content in neurally derived blood EVs isolated from 63 subjects: 16 patients with early stage dementia and a CSF Aβ42+ tau profile consistent with AD, 16 individuals with mild cognitive impairment (MCI) and an AD CSF profile, and 31 cognitively intact controls with normal CSF Aβ42+ tau levels. ROC analysis indicated that measurement of miR-132-3p in neurally-derived plasma EVs showed good sensitivity and specificity to diagnose AD, but did not effectively separate

individuals with AD-MCI from controls. Moreover, when we measured the levels of a related miRNA, miR-212, we found that this miRNA was also decreased in neural EVs from AD patients compared to controls. Our results suggest that measurement of miR-132 and miR-212 in neural EVs should be further investigated as a diagnostic aid for AD and as a potential theragnostic.

Keywords: blood biomarker, extracellular vesicles, L1CAM, micro-RNA, mild cognitive impairment, qRT-PCR

INTRODUCTION

Alzheimer's disease is a devastating disorder for which there is no cure or effective treatment. Symptom onset is insidious and even in sophisticated centers clinical diagnosis is imperfect (Salloway et al., 2014; Monsell et al., 2015). Advances in brain imaging and the development of robust immunoassays to measure tau and amyloid β-protein (Aβ) in cerebrospinal fluid (CSF) have greatly aided diagnosis (Blennow et al., 2012). Specifically, measurement of tau and Aβ in CSF, or quantitation of amyloid or tangle pathology by PET imaging, can be used to identify mild cognitive impairment (MCI), a frequent precursor of AD (Jack et al., 2013; Bao et al., 2017), and use of these markers is now common in clinical research (Blennow et al., 2012; Jack et al., 2013). But PET imaging is expensive and is restricted to use in certain geographies. Assessment of markers in CSF is more amendable for general use, but CSF sampling remains unpopular with patients. Thus, there is a pressing need for less costly and intrusive, and more widely available biomarkers that can replace or supplement current CSF and PET markers (Bateman et al., 2019). Measurement of a blood-based analyte would be ideal since blood collection is widely accepted by patients and can be done almost anywhere.

Unlike CSF, the contents of blood are influenced by many organs and therefore changes in blood analytes are often not sensitive to minor changes that occur in brain. For instance, while the levels of Aβ42 in CSF change early in AD, measurement of Aβ42 in plasma has not proved as useful (Janelidze et al., 2016). The discovery that brain cells release extracellular vesicles (EVs) and a portion of these enter the bloodstream offers the potential of monitoring changes occurring in the brain by isolating EVs from venous blood. EVs are small packages of cytosol encapsulated by a lipid bilayer and are released by all cells, including neurons and glia (Fruhbeis et al., 2012; Raposo and Stoorvogel, 2013; Paolicelli et al., 2019). *Exosome* is the term most frequently applied to EVs, but there are many classes of EVs, primarily defined by their cellular origin. Exosomes arise through the endolysosomal pathway and are specifically formed by inward budding of multivesicular bodies to produce intraluminal vesicles. After maturation, multivesicular bodies can fuse with the plasma membrane and exosomes are released (Pan et al., 1985; Johnstone et al., 1987).

A series of recent papers on neural exosomes isolated from blood plasma (Fiandaca et al., 2015; Goetzl et al., 2015a,b; Kapogiannis et al., 2015; Abner et al., 2016) has caused huge excitement among the neuroscience biomarker community (Galasko, 2015; Heinzelman et al., 2016; Vella et al., 2016). The method used employs a proprietary reagent, ExoQuick, to precipitate total "exosomes" from plasma, followed by enrichment of material of "neural" origin using an antibody to the neural cell adhesion molecules, L1CAM (Fiandaca et al., 2015). In two independent studies, analysis of samples prepared using this protocol revealed significant increases in pT181-tau, pS396-tau and Aβ1-42 in patients with AD vs. those from age-matched normal cognitively intact controls (Fiandaca et al., 2015; Winston et al., 2016). Other protein cargo in neural exosomes have also been found to change in AD (Goetzl et al., 2019). However, the ability to discriminate AD from AD-MCI and controls required a statistical approach that constrains comparison across cohorts analyzed on different occasions. Furthermore, a more recent publication employing a similar method failed to detect elevation of pT181-tau or Aβ1-42 in neural exosomes from AD subjects (Guix et al., 2018).

Micro-RNAs (miRNA) are small non-coding RNA molecules which base-pair with complementary sequences within mRNA to decrease post-transcriptional gene expression (O'Brien et al., 2018) and accumulating evidence indicates that the expression of certain miRNAs are altered in AD (Lau et al., 2013; Patrick et al., 2017; Pichler et al., 2017; El Fatimy et al., 2018; Swarbrick et al., 2019). However, it is unknown whether miRNA dysregulation in the brain is reflected in neural exosomes. To this end, we performed an unbiased analysis of miRNAs in human brain tissue to inform miRNA candidates for targeted analysis in neurally derived plasma exosomes. First, we measured miRNAs in pooled RNA isolated from five individuals with AD, five cognitively intact high pathology controls (HPCs), and five pathology-free controls. HPC refers to subjects with sufficient amyloid plaques and neurofibrillary tangles to be diagnosed as AD, but at the time of death these individuals had no evidence of cognitive impairment. Recently, it had been suggested to consider such individuals as AD stage 1 and 2 (Jack et al., 2018). Results were highly similar across the pooled and individual brain samples. In a total of 27 individual brain samples: 9 controls, 7 HPC and 11 AD, miR-182-5p, miR-591, miR-32-3p, and miR-132-3p were dysregulated in AD vs. both controls and HPC.

Armed with this information, we asked whether the miRNAs changed in AD brain were also altered in neural exosomes isolated from plasma. Since, diagnosis of AD based on clinical criteria alone is uncertain (Monsell et al., 2015) we were careful to use specimens from individuals whose clinical diagnosis was confirmed by the best current biomarkers – CSF Aβ42 and tau. Using plasma from patients that conformed to these criteria we prepared neural exosomes from 31 cognitively intact biomarker-negative controls, 16 CSF biomarker-positive MCI, and 16

CSF biomarker-positive AD. RNA was extracted from neural exosomes, reversed transcribed and analyzed by qRT-PCR for the four miRNAs most altered in AD brains. miR-132 was decreased by ∼9-fold in AD exosomes vs. controls, and ∼5.4 fold in AD vs. AD-MCI. Since miRNAs within the same cluster are often co-regulated, we also measured miR-212, a miRNA in tandem to miR-132. Strikingly, the levels of miR-212 were reduced fourfold in AD samples compared to controls. These results suggest that concerted dysregulation of miR-132 and miR-212 occurs in AD and that measuring the levels of these miRNAs in neurally derived exosomes may offer a window on changes occurring in AD brain. Our results in neural exosomes are consistent with prior studies that detected down-regulation of miR-132 and miR-212 in AD brain (Pichler et al., 2017) and down-regulation of miR-132 in blood (Denk et al., 2018).

MATERIALS AND METHODS

Brain Donors

Human specimens were obtained from Rush Alzheimer's Disease Center, Rush University Medical Center and used in accordance with the Partners Institutional Review Board (Protocol: Walsh BWH 2011). Samples of frozen frontal cortex were from the Religious Orders Study (ROS), a longitudinal clinical-pathological cohort study in aging and Alzheimer's Disease (Bennett et al., 2018). Participants from religious communities were enrolled at a time when they were free of known dementia. The study was approved by the Institutional Review Board of Rush University Center. All participants signed an informed consent, Anatomic Gift Act, and a repository consent to allow their data and biospecimens to be shared for research. They were followed over time until brain donation. Overall follow-up and autopsy rates were about 95%. Each participant underwent uniform structured annual cognitive and clinical evaluations. A diagnosis AD dementia required evidence of meaningful cognitive decline in two domains of cognition, one of which was episodic memory. Clinical summary diagnostic opinion was made *post-mortem* based on all available clinical information by a neurologist blinded to pathologic data. A neuropathologic diagnosis of high (1), intermediate (2), low (3), or no AD (4) was based on the modified NIA-Reagan Diagnosis of AD. This assessment relies on the severity and distribution of both neurofibrillary tangles and neuritic plaques (Bennett et al., 2006). Individuals were categorized as controls, high pathology controls (HPC), or AD based on combined clinical and pathological criteria (**Table 1**). Individuals with an NIA-Reagan score of 1 or 2 and a clinical diagnosis of AD dementia were defined AD (n = 11), whereas patients with an NIA-Reagan Score of 1 or 2 and no evidence of dementia were designated HPC (n = 8). Patients in the control group had an NIA-Reagan score of 3 and no evidence of dementia.

Study Participants, CSF and Blood Collection

Specimens were from research participants in the UCSD Shiley-Marcos Alzheimer's Disease Research Center, collected and used in accordance with IRB approval (**Table 2**). Each participant donated both ETDA plasma and CSF, which were obtained using standardized protocols. CSF was collected into polypropylene tubes, centrifuged at 1,500 × g for 10 min, and aliquoted into polypropylene storage tubes. Blood was drawn on the same day as lumbar puncture, and plasma was isolated and aliquoted. On the day of analysis, samples were thawed at room temperature, and used for subsequent exosome isolation.

Subjects were designated as AD, MCI, and controls based on cognitive testing (MMSE) and CSF biomarker criteria. Control subjects (n = 16) had an MMSE ≥ 28, a CSF Innotest tau/Aβ ratio < 0.5 and Aβ > 500 pg/mL (mean Innotest tau level: 248.6 ± 111.5 pg/mL; mean Innotest Aβ1-42 level: 911.2 ± 245.1 pg/mL). AD-MCI and AD subjects had a CSF Innotest tau/Aβ ratio ≥ 1 and Aβ < 650 pg/mL. AD subjects (n = 31) had a CSF AD biomarker profile (mean Innotest tau level: 699.6 ± 219.7 pg/mL; mean Innotest Aβ1-42 level: 500.0 ± 81.9 pg/mL) and an MMSE score of 15–24 points, whereas AD-MCI (n = 16) subjects had a CSF AD biomarker profile (mean Innotest tau level: 723.1 ± 218.8 pg/mL; mean Innotest Aβ1–42 level: 470.3 ± 90.5 pg/mL) and an MMSE score of 25–29 points. CSF levels of Aβ and tau yielded clear separation of diagnostic groups (**Supplementary Figure S1**).

Generation of Induced Neurons (iNs) From Human Induced Pluripotent Stem Cells (iPSCs) and Isolation of Exosomes From Conditioned Media

Neurogenin 2 (Ngn2)-induced human neurons were prepared as before (Guix et al., 2018). In brief, YZ1 iPSCs were maintained in medium containing DMEM/F12, Knockout Serum Replacement, penicillin/streptomycin, L-glutamine, MEM-NEAA, and β-mercaptoethanol (all from Invitrogen, Carlsbad, CA, United States) which was supplemented with 10 μg/mL basic fibroblast growth factor (bFGF; Millipore-Sigma, Burlington, MA, United States). For viral infection, iPSCs were plated at a density of 95,000 cells/cm^2. Ultrapure lentiviral titers (Alstem, Richmond, CA, United States) were used at the following concentrations: Tet-*O*-Ngn2-puro: 0.1 μL/50,000 cells; Tet-*O*-FUW-EGFP: 0.05 μL/50,000 cells; FUdeltaGW-rtTA: 0.11 μL/50,000 cells. Ngn-2 expression was induced by addition of doxycycline on iN day 1 at a concentration of 2 μg/mL. On iN day 2, puromycin was added at 20 μg/mL, and this concentration was maintained thereafter. On iN day 4, cells were plated on Matrigel (Corning, NY, United States)-coated 100 mm dishes (650,000 cells) and cultured in Neurobasal media (Gibco, Carlsbad, CA, United States) containing Glutamax, 20% dextrose, MEM-NEAA, B27 and 10 ng/mL BDNF, CNTF, GDNF (PeproTech, Rocky Hill, NY, United States). Conditioned media (CM) was collected on iN D21-33, pooled, and processed in batches of 30 mL. First, CM was centrifuged at 300 × g and 4°C for 10 min to pellet floating cells. Next, the upper 97% was recovered, and centrifuged at 2,000 × g and 4°C to pellet apoptotic bodies. Then, the upper 97% was recovered, diluted in neurobasal media, and centrifuged at 10,000 × g and 4°C for 30 min to pellet microvesicles and cell debris. Finally, the upper

TABLE 1 | Demographics and clinical characteristics of brain donors.

Disease Designation	ApoE genotype	Age at death (years)†	Last visit before death (months)	Cognitive Diagnosis	NIA Reagan	CERAD Score	Braak Stage
CTL*	3,3	85–90	10	2	3	4	3
CTL*	2,3	90—95	2	1	3	4	3
CTL*	3,3	90–95	7	2	3	4	3
CTL*	3,3	100–105	10	1	3	4	4
CTL*	3,3	80–85	10	2	3	4	1
CTL	2,3	85–90	3	2	3	3	3
CTL	3,3	90–95	53	2	3	3	2
CTL	3,3	80–85	12	1	3	2	0
CTL	3,3	80–85	1	1	3	3	1
HPC*‡	3,3	90–95	5	1	1	1	5
HPC*	3,3	90–95	7	1	2	1	4
HPC*	3,4	80–85	5	1	2	1	3
HPC*	3,4	80–85	2	1	2	1	4
HPC*	3,4	80–85	2	1	2	2	4
HPC	3,3	80–85	9	1	2	2	4
HPC	3,4	80–85	12	1	2	2	3
HPC	3,3	90–95	11	1	2	2	3
AD*	3,3	85–90	10	4	1	1	5
AD*	4,4	80–85	8	4	1	1	5
AD*	3,4	100–105	4	4	1	1	5
AD*	3,4	70–75	10	4	1	1	5
AD*	3,3	90–95	11	4	1	1	5
AD	4,4	90–95	11	4	2	1	4
AD	3,3	90–95	5	4	1	1	5
AD	3,3	85–90	12	4	1	1	5
AD	3,3	95–100	9	4	1	1	5
AD	2,4	85–90	4	4	2	2	3
AD	3,4	85–90	4	4	2	2	3

*CTL, control; HPC, high pathology control; AD, Alzheimer's Disease; Cognitive Diagnosis: 1 (no cognitive impairment), 2 (mild cognitive impairment), 4 (Alzheimer's Disease Dementia); NIA-Reagan: 1 (high likelihood of AD), 2 (intermediate likelihood of AD), 3 (low likelihood of AD); CERAD score: 1 (definite AD), 2 (probable AD), 3 (possible AD), 4 (no AD); Braak stage: 0 (no NFT pathology), I and II (NFT pathology confined to the enthorinal region), III and IV (involvement of limbic regions), V and VI (moderate to severe neocortical involvement). *Used for miRNA high content arrays †age-range is given to preserve anonymity of participants. ‡This brain was used only for the pooled analysis and not for assessment of individual brains. Gray represents brain samples from the control group, pink represents HPC, and orange represents AD.*

97% was recovered and subjected to centrifugation at 100,000 × *g* and 4°C for 70 min to pellet exosomes.

RNA Isolation and miRNA Analysis From Brain Tissue

Gray matter from frozen cortex was dissected on dry ice. Total RNA was extracted from ∼20 mg gray matter using a miRNeasy Advanced Kit (Qiagen, Louisville, KY, United States) according to the manufacturer's guidance. Briefly, samples were suspended in 200 μL ice cold RIPA buffer followed by addition of 120 μL kit-provided RPL buffer. Tissue was homogenized by gently pipetting samples up and down. Forty μL kit-provided RPP buffer was added to samples and vortexed for ∼30 s to facilitate precipitation of proteins. Samples were then centrifuged at 12,000 × *g* for 3 min to pellet the precipitate and debris, and approximately 230 (μL of supernatant was transferred to a new 1.5 mL tube. An equal volume of isopropanol was added and mixed by pipetting before transferring the entire sample to an RNeasy UCP MinElute column. Columns containing sample were centrifuged at 12,000 (x g for 1 minute. Flow-through was discarded and columns were washed according to the manufacturer"s protocol. RNA was eluted with two rounds of 20 (L RNase-free water. RNA yield and quality were quantified on a nanodrop. Fifty ng/μL aliquots of RNA were prepared and stored at −20°C.

One hundred and fifty ng of RNA was used for reverse transcription (RT) using a miSCRIPT RT II kit (Qiagen, Louisville, KY, United States), where samples were incubated at 37°C for 60 min followed by inactivation at 95°C for 5 min. RT efficiency was determined by measuring levels of miRTC, a RT control.

RNA Isolation and miRNA Analysis From iN Cells and iN-Derived Exosomes

iN cells were harvested and centrifuged at 300 × *g* for 10 min to pellet cells. Cell pellets were washed with PBS and lysed with RPL buffer. Exosomes from iN CM were isolated by differential centrifugation as described above,

TABLE 2 | Demographics and clinical characteristics of plasma donors.

Disease Designation	Age-range (years)†	CSF A(β 1-42 (pg/mL)	CSF Tau (pg/mL)
NCI	75—80	602	254
NCI	75—80	592	244
NCI	75–80	948	302
NCI	70–75	899	235
NCI	65–70	1095	229
NCI	75–80	1014	281
NCI	65–70	1425	456
NCI	75–80	586	74
NCI	70–75	976	257
NCI	65–70	1107	294
NCI	80–85	822	214
NCI	65–70	883	268
NCI	67–70	1114	333
NCI	70–75	1284	443
NCI	75–80	1513	551
NCI	65–70	689	126
NCI	75–80	734	231
NCI	65–70	585	72
NCI	75–80	878	173
NCI	65–70	992	145
NCI	65–70	1122	333
NCI	75–80	570	225
NCI	65–70	965	247
NCI	80–85	958	221
NCI	75–80	654	153
NCI	65–70	609	139
NCI	70–75	764	175
NCI	70–75	878	279
NCI	75–80	863	136
NCI	65–70	1006	174
NCI	75–80	1119	442
AD-MCI	75–80	589	1090
AD-MCI	55–60	325	712
AD-MCI	70–75	516	522
AD-MCI	70–75	549	590
AD-MCI	80–85	513	762
AD-MCI	70–75	359	778
AD-MCI	75–80	507	734
AD-MCI	70–75	458	610
AD-MCI	65–70	517	851
AD-MCI	55–60	442	529
AD-MCI	60–65	450	681
AD-MCI	80–85	568	670
AD-MCI	70–75	637	723
AD-MCI	65–70	510	516
AD-MCI	75–80	585	1315
AD-MCI	60–65	475	486
AD	65–70	532	938
AD	75–80	361	426
AD	75–80	406	690
AD	70–75	383	401
AD	65–70	528	582
AD	75–80	379	441
AD	60–65	546	782
AD	80–85	547	1123
AD	75–80	542	758
AD	60–65	462	831
AD	60–65	630	676
AD	75–80	430	496
AD	70–75	609	912
AD	60–65	364	793
AD	80–85	409	429
AD	65–70	397	916

NCI, no cognitive impairment; AD-MCI, mild cognitive impairment due to Alzheimer's Disease; AD, Alzheimer's Disease. †Age-range is given to preserve anonymity of participants.

washed with PBS, and lysed in RPL buffer. Subsequent steps were followed identically to the isolation of miRNA from brain tissue.

Isolation of Exosomes and Enrichment of Neuronal Exosomes

To verify that our methods could reliably detect miRNA expression in an exosomal fraction of human plasma, and to optimize preparative and analytical methods prior to processing precious clinical samples, we first tested experimental conditions using human plasma (each in technical duplicate) from two healthy volunteers.

The method to isolate neuron-derived exosomes from plasma has been validated and described in detail before (Guix et al., 2018), and is a slightly modified version of the procedure pioneered by the Goetzl/Kapogiannis group (Kapogiannis et al., 2015). Five μL thrombin (System Bioscience, Palo Alto, CA, United States) was added to 500 μL aliquots of plasma to induce clot formation and allow the removal of fibrin and related proteins. Reactions were mixed by inversion and incubated for 30 min at room temperature before dilution with 495 μL Ca^{2+}- and Mg^{2+}-free Dulbecco's Phosphate-Buffered Saline (DPBS) (Sigma-Aldrich, St. Louis, MO, United States) containing 3x phosphatase (Thermo Fisher, Carlsbad, CA, United States) and protease (Roche, Branchburg, NJ, United States) inhibitors. Thereafter, the samples were centrifuged at 6000 × *g* for 20 min at 4°C and the supernatant transferred to a new tube. Next, 252 μL ExoQuick (System Bioscience, Palo Alto, CA, United States) was added to the supernatants, samples mixed by inversion and left to stand at 4°C for 1 h. Vesicles present in the serum were recovered by centrifugation at 1500 × *g* for 20 min at 4°C and resuspended by vortexing in 500 μL MilliQ water containing 3 × phosphatase and protease inhibitors. ExoQuick pellets were then mixed overnight at 4°C on a vertical rotating mixer.

To isolate neuronal exosomes from the suspensions of total plasma exosomes, 4 μg biotinylated anti-L1CAM antibody (eBioscience, San Diego, CA, United States) in 42 μL 3% bovine serum albumin in DPBS (BSA/DPBS) was added to the

resuspended vesicles and incubated on a rotating mixer for 1 h at 4°C. Thereafter, 15 μL of pre-washed Streptavidin-Plus UltraLink Resin (Thermo Fisher, Danvers, MA, United States) in 25 μL 3% BSA/DPBS was added to each sample and incubated for 4 h at 4°C with rotation. Neuronal exosomes bound to the antibody/resin complex were recovered by centrifugation at 200 × *g* for 10 min at 4°C, and washed once with 3% BSA/DPBS before elution in 200 μL 0.1 M glycine (pH 3.0). Resin was removed by centrifugation at 4500 × *g* for 5 min at 4°C. Thereafter, 195 μL supernatant was neutralized with 15 μL of 1 M TrisHCl (pH 8.0) and exosomes were lysed by adding 360 μL M-PER (Thermo Fisher, Carlsbad, CA, United States), 25 μL 3% BSA/DPBS containing 1× phosphatase and protease inhibitors, and 2 freeze-thaw cycles before downstream analysis.

RNA isolation from neural exosomes was performed identically to brain samples, with the following modifications: total exosomes (Exoquick pellets), neural exosomes (L1CAM immunoisolates), or irrelevant/non-specific exosomes (46-4 immunoisolates) were mixed with 240 μL RPL buffer, followed by 80 μL RPP buffer. All subsequent steps were performed as for RNA isolation from brain tissue.

Bioanalyzer analysis showed that samples were enriched with small RNA species following elution from RNeasy UCP MinElute columns.

We cannot completely rule out that some plasma RNA outside of exosomes might be isolated along with exosomal RNA in our protocol. However, this seems unlikely, since free-floating RNA is rapidly degraded in plasma, and RNA protected in RNA-binding proteins or lipids would not allow isolation by L1CAM immunoprecipitation.

miRNA Quantitative PCR Array

The miRNA expression profile of RNA extracted from brain tissue was analyzed using a miScript miRNA PCR Array Human miRBase Profiler HC Plate 1, MIHS-3401Z (Qiagen, Hilden, Germany). Each array contains 372 unique miRNA assays, 3 snoRNA and 3 snRNA housekeeping genes, duplicate RT primer assays to evaluate RT efficiency, and duplicate PCR primer assays to evaluate the efficiency of the qPCR reaction (for a full list of miRNAs detectable using miScript arrays see: https://b2b.qiagen.com/~/media/genetable/mi/hs/34/mihs-3401z). Six μL RNA (initial concentration = 50 ng/μL) was prepared in 20 μL reverse-transcription reactions (final concentration = 15 ng/μL) using miScript HiSpec Buffer where mature miRNAs are polyadenylated by Poly(A)polymerase and reverse transcribed into cDNA using oligo-dT primers. The oligo-dT primers have a 3′ degenerate anchor and a universal tag sequence on the 5′ end, allowing amplification of mature miRNA in real-time PCR. Each reverse-transcription reaction was further diluted with 90 μL RNAse-free water (4.5 fold dilution) before being used as template for real-time PCR analysis on the miScript miRNA HC PCR Array. The array contained miRNA-specific miScript primers, the miScript SYBR Green kit with the miScript universal primer (reverse primer), and QuantiTect SYBR Green PCR Master Mix. miRNA cDNA was quantified using a ViiA 7 Real-Time PCR System (Applied Biosystems, Waltham, MA, United States). The thermal cycling protocol was as follows: 95°C for 10 min (PCR activation step), 45 amplification cycles at 94°C for 15 s (denaturation), at 55°C for 30 s (annealing), and at 70°C for 30 s (extension), followed by fluorescence data collection. A no-template control (NTC) of RNase-free water was co-purified and profiled like the samples to measure background.

We used the 3 snoRNAs and 3 snRNAs in addition to miR-16 as endogenous normalization controls in the arrays. MicroRNA expression was quantified as delta Ct values, where Ct = threshold cycle, delta Ct = (Ct target miRNA minus the average Ct of the 7 normalization controls). Relative miRNA expression was calculated as ddCt (AD vs. CTRL) = mean dCtAD – mean dCtCTRL or ddCt (AD vs. HPC) = mean dCtAD – mean dHPC. Higher values indicate higher expression. Signals with a ddCt $\geq |0.58|$, which corresponds to a fold change of $\geq |1.5|$, were considered as differentially regulated. The assay showed good technical reproducibility when repeated three times on three different days (**Supplementary Figure S2**).

Quantitative PCR of Individual miRNAs

QPCR of individual miRNAs was carried out as described for the miRNA array with the following modifications: cDNA was diluted 1:100 with RNAse free water in primer specific qPCR for each miR. For qPCR validation in brains, miR-16 and SNORD95 was used as endogenous normalization controls, whereas miR-16 alone was used as normalization control for qPCR of miRNAs in neural exosomes. miR-16 has been evaluated as an endogenous normalization control in plasma, and similar plasma levels were found in AD and controls (Bhatnagar et al., 2014). Moreover, several previous studies found miR-16 levels to be consistent across AD and control brains (Hebert et al., 2008; Banzhaf-Strathmann et al., 2014). A list of all primers used for qRT-PCR is presented in **Supplementary Table S1**.

Statistics

Statistical analyses were carried out using GraphPad Prism, version 8 (La Jolla, CA, United States). The Shapiro–Wilk test was used to determine normal distribution of data. Significance was determined by one-way ANOVA followed by Tukey's *post hoc* test for normally distributed data. Otherwise, Kruskal–Wallis test followed by Dunn's *post hoc* test was used. Mean age of brain and plasma donors was highly similar between diagnostic groups, and the age-distribution did not differ significantly. Thus, we did not control for age in our analyses. *P*-values are reported without correction for multiple testing because of the exploratory nature of this study. The significance threshold was set to a two-sided $p < 0.05$.

RESULTS

miRNAs Are Altered in AD Brains

To determine whether miRNAs are dysregulated in AD brain, we pooled RNA isolated from the brains of five individuals who died with AD, five individuals who had AD pathology but were without cognitive impairment at the time of death, and

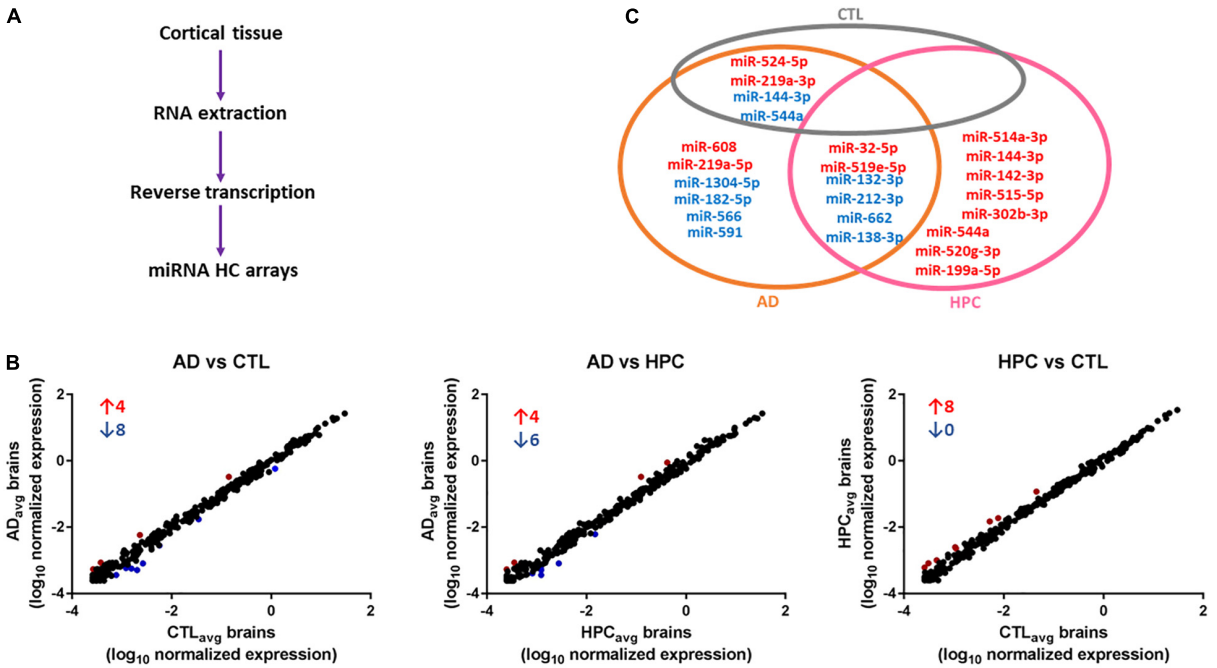

FIGURE 1 | miRNAs are differentially expressed in AD compared to control and HPC brains. **(A)** Workflow of miRNA candidate discovery. RNA was isolated from cortical brain tissue of individuals who were cognitively intact (n = 5), AD (n = 5) or HPC (n = 5) (see **Table 1** for demographic data). RNA from the 5 control, 5 AD or 5 HPC brains were pooled and used as template for cDNA synthesis. cDNA from pooled control, AD or HPC were used as templates for qRT-PCR. **(B)** Comparative analysis of profiled miRNAs between disease groups. miRNAs that are upregulated (red) and downregulated (blue) by >2-fold are indicated. Each point represents log10(2-ΔΔCt) average values from each cDNA pool run in triplicate (3 plates). **(C)** miRNAs that were significantly altered by >2-fold. A total of 16 miRNAs were dysregulated in AD brains compared to control or HPC brains. Six of those miRNAs were consistently altered specifically in AD brains (miR-608, -219a-5p, 1304-5p, -182-5p, -566, -591). Six additional miRNAs were upregulated >2-fold in AD brains compared to control, but <2-fold compared to HPC brains (miR-32-5p, -519e-5p, 132-3p, 212-3p, -662, -138-3p). Red text = upregulated miRNAs; blue text = downregulated miRNAs.

five individuals who were without cognitive impairment normal and free of AD pathology (**Table 1**). RNA was extracted from cortical gray matter, pooled, reverse transcribed into cDNA, and cDNA was used for miRNA assays (**Figure 1A**). Since it is often difficult to distinguish miRNAs that are altered due to disease from normal aging, comparative analysis of profiled miRNAs was performed between AD brains relative to control, and relative to HPC. Of the 372 miRNAs that were measured, 12 miRNAs were changed >2-fold in AD brains compared to controls (4 miRNAs were up- and 8 mIRNAs were downregulated, respectively) (**Table 3** and **Figure 1B**). Compared to HPC brains, 10 miRNAs were changed >2-fold (4 up- and 6 downregulated, respectively) (**Table 3** and **Figure 1B**). Six miRNAs were up (miR-608, miR-219a-5p) or downregulated (miR-566, -182-5p, -591, -1304-5p), specifically in AD brains vs. both HPCs and controls (**Figure 1C** and **Table 3**). Compared to controls, 8 miRNAs were increased in HPC brains no miRNAs were decreased (**Figure 1B**, right panel).

To assess the robustness of the findings obtained using miRNA array analysis, we used miR-specific qRT-PCR to measure levels of the 12 miRNAs that were found to be most changed in our array experiments. In our initial qRT-PCR we used exactly the same pools as employed for the array analysis. The changes detected by array analysis of pooled brain RNA (**Table 3**) were largely confirmed by qRT-PCR analysis of individual miRs (**Table 4**, columns 1 and 2). Nine of 12 miRs showed the same directional and comparable magnitude changes by both

TABLE 3 | miRNAs significantly changed by ≥2-fold in AD.

	ARRAY POOLED sample			
	AD (n = 5) vs. CTL (n = 5)		AD (n = 5) vs. HPC (n = 5)	
	Fold-change	p-value	Fold-change	p-value
miR-566	−3.96	0.04	−2.40	0.13
miR-182-5p	−3.27	0.02	−3.42	0.01
miR-1304-5p	−2.74	<0.01	−2.16	0.01
miR-591	−2.13	0.07	−3.41	0.03
miR-132-3p	−2.08	<0.01	−1.74	<0.01
miR-138-1-3p	−2.07	0.01	−1.55	0.11
miR-662	−2.02	<0.01	−1.68	<0.01
miR-212-3p	−2.00	<0.01	−1.74	<0.01
miR-519e-5p	2.05	<0.01	1.25	0.21
miR-608	2.28	0.39	2.43	0.39
miR-219a-5p	2.34	<0.01	2.66	<0.01
miR-32-5p	2.50	0.04	1.42	0.20

miRs with a >2 fold change in AD compared to CTL and HPC are displayed in bold font. miRs with decreased expression in AD brain are shown blue, whereas those with a increased expression are displayed in red.

TABLE 4 | qPCR validation of miRs.

	qPCR validation							
	Pooled samples		Individual brains contained in pools		All individual brains			
	AD (*n* = 5) vs. CTL (*n* = 5)	AD (*n* = 5) vs. HPC (*n* = 5)	AD (*n* (=5) vs. CTL (n (=5)	AD (n (=5) vs HPC (n (=5)	AD (n ((=11) vs. CTL (n ((=9)		AD (n ((=11) vs. HPC (n ((=7)	
	Fold-change	Fold-change	Fold-change	Fold-change	Fold-change	*p*-value	Fold-change	*p*-value
miR-566	−1.35	−1.05	−2.35	−1.41	−1.35	>0.99	−1.36	>0.99
miR-182-5p	−15.78	−5.79	−2.76	−1.66	−2.23	0.01	−1.76	0.11
miR-1304-5p	1.20	1.34	−1.99	−1.43	−1.41	0.03	−1.20	>0.99
miR-591	2.92	−1.14	−3.53	−1.15	−1.85	0.64	−3.01	0.99
miR-132-3p	−2.14	−1.24	−2.92	−1.57	−2.52	0.13	−2.34	0.09
miR-138-1-3p	1.07	−1.03	−1.66	−1.12	−1.52	0.21	−1.59	>0.99
miR-662	−1.39	−1.18	−2.26	−1.45	−1.47	0.18	−1.55	>0.99
miR-212-3p	1.33	1.14	−1.91	−1.05	−1.44	0.42	−1.59	0.16
miR-519e-5p	−1.02	1.53	1.13	1.38	1.33	0.67	1.23	>0.99
miR-608	1.35	1.17	1.31	1.08	1.57	>0.99	1.06	>0.99
miR-219a-5p	11.50	2.77	2.79	1.39	2.13	0.29	2.55	0.06
miR-32-5p	5.57	4.12	2.57	1.87	1.81	0.02	1.04	>0.99

miRs with decreased expression in AD brain are shown blue, whereas those with a increased expression are displayed in red.

arrays and qRT-PCR, but miR-1304, miR-138-1-3p, and miR-519e-5p changed in opposite directions (compare **Tables 3**, **4**). Thereafter, we undertook qRT-PCR analysis of RNA preparations from each of the 15 individual brains used for the initial pools. When values were averaged for each disease group (i.e., for the 5 AD, the 5 HPC and the 5 controls) the direction of change detected by qRT-PCR and array analysis were in complete agreement (compare **Tables 3**, **4**, columns 3 and 4). We then went on to use qRT-PCR to measure the levels of the same 12 miRs using RNA isolated from a total of 27 brains (11 AD, 7 HPC, and 9 cognitively intact controls). Here the results were similar to those obtained using array analysis of pooled samples (**Table 3**) and of the 15 individual samples (**Table 4**, compare columns 3 and 4 vs. columns 5 and 6). Two of these 12 miRNAs (miR-182-5p, miR-32-5p) were significantly changed from controls. miR-132-3p was significantly different between disease groups ($p < 0.05$), but did not reach statistical significance in pair-wise comparisons (control vs. AD, $p = 0.130$, HPC vs. AD, $p = 0.094$). miR-219a-5p showed a strong trend for change between disease groups ($p = 0.051$) (**Figure 2**). It is important to note that levels of miR-9, a neuron-specific miR, was unchanged between disease groups ($p = 0.769$). The latter finding indicates that dysregulation of miR-182-5p, miR-32-5p, and miR-132-3p are disease-specific.

miRNAs Can Be Detected in Neural Exosomes Derived From Blood

To determine whether miRNAs can be reliably detected in neural Exosomes, we initially measured reference miRNAs in exosomes isolated from human iPSC-derived cortical neurons (iNs) (Guix et al., 2018). Ubiquitously expressed miR-16 (Chevillet et al., 2014) was detected with cycle threshold (Ct) values of 27 and 31 in iN cell lysates and their exosomes, respectively. Neuron-specific miR-9 (Coolen et al., 2013) was readily detected in both iN cell lysates (Ct = 25) and exosome (Ct = 32), whereas miR-451a, a peripherally expressed miRNA was barely detectable with ct values near the upper limit of reliable quantitation. These data are consistent with the relative enrichment of neuronal miRs in neurons and neuron-derived exosomes, and support the use of miR-9 and miR-451a as markers to assess the neuronal origin of exosomes (**Figure 3A**).

Next, we examined whether we could discern a difference in the levels of miR-9 and miR451-a in total plasma exosomes vs. neural exosomes isolated from plasma using L1CAM (**Figure 4B**). Exosomes were isolated from the plasma of two healthy donors. RNA was extracted from total ExoQuick pellets or L1CAM-precipitated neural exosomes and used for qPCR (**Figure 3B**). MiR-9 was low in total exosomes (Ct = 34-37), while miR-451a was higher (Ct = 26-31). In contrast, L1CAM-isolated exosomes had high levels of miR-9 (Ct = 27-33), suggesting the L1CAM IP effectively enriched for neural exosomes (**Figure 3C**). The fact that we observed comparable levels of miR-451a in both total and L1CAM exosomes suggest our neural exosome preparation contained both neural and peripheral exosomes. Values for the house-keeping miR-16 were similar (Ct = 30–33) in both L1CAM and total exosomes. Notably, immunoprecipitation with the non-specific mAb, 46-4, did not lead to an enrichment of the neural miR-9. Together, these results confirm that measurement of miR-9 can be used to assess neural enrichment.

Levels of miR-132 and miR-212 Are Decreased in Neural Exosomes in Alzheimer's Disease

Diagnosis of AD based on clinical criteria alone is imperfect and typically 20–30% of individuals diagnosed as having AD have other neurological disorders, and considerable numbers

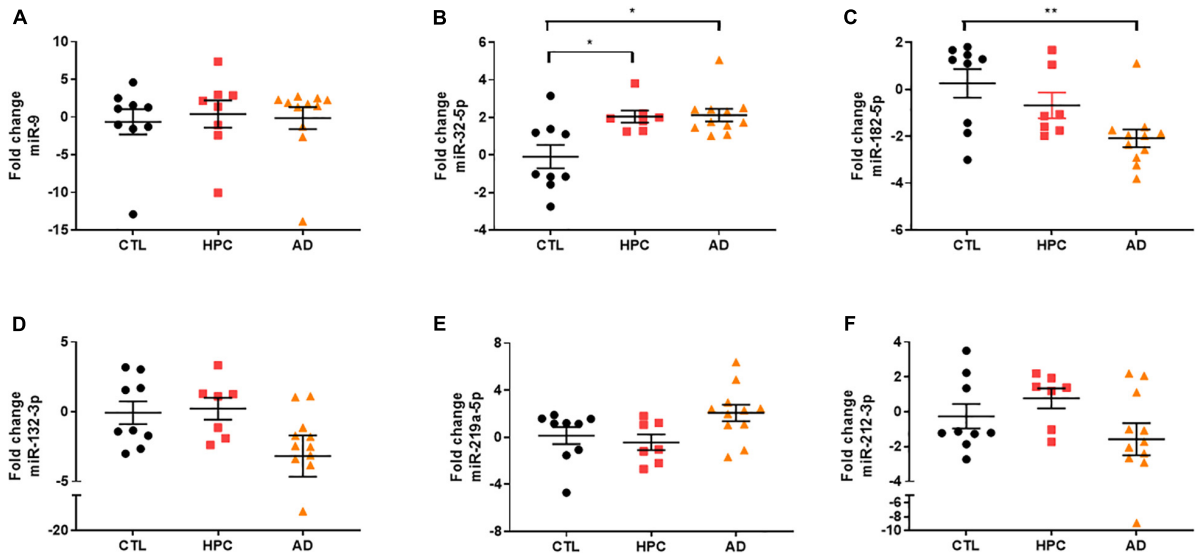

FIGURE 2 | miRNA validation in AD brain tissue by qRT-PCR. miRNA candidates were measured by miRNA-specific qRT PCR. **(A)** Neuron-specific miR-9 levels, which was similar between disease groups in array analysis, were also unchanged by qRT-PCR [$X^2(2) = 0.5263$, $p = 0.769$]. Two of the original hits **(B)** miR-182-5p (** = 0.009) and **(C)** miR-32-5p (control vs. HPC, * = 0.049; control vs. HPC, * = 0.025) identified by miRNA arrays were validated by qRT-PCR. **(D)** miR-132-3p was significantly changed between disease groups [$X^2(2) = 6.156$, $p = 0.046$], but did not reach statistical significance in pair-wise comparisons. **(E)** MiR-219a-5p showed a strong trend for change between the three disease groups [$X^2(2) = 5.906$, $p = 0.051$]. **(F)** miR-212-3p levels were not significantly changed between disease groups. Fold change was determined by $2^{-\Delta\Delta Ct}$ relative to miR-16. Significance was determined by Kruskal–Wallis test followed by Dunn's *post hoc* test.

of individuals that have AD are misdiagnosed as having other neurologic disorders (Monsell et al., 2015). To avoid use of samples with uncertain diagnose we employed samples from individuals whose clinical diagnosis was confirmed by CSF Aβ42 and tau. Using these criteria 63 subjects from the UCSD Shiley-Marcos Alzheimer's Disease Research Center were identified (31 cognitively intact biomarker-negative controls, 16 CSF biomarker-positive MCI, and 16 CSF biomarker-positive AD) and their plasma used to isolate neural exosomes. RNA was extracted from neural exosomes, reversed transcribed and analyzed by qRT-PCR for five of the 12 miRNAs found to be altered in AD brains plus two miRNAs used to assess neuronal origin (miR-9 and miR-451a). The five miRNAs (miR-132-3p, miR-182-5p, miR-32-5p, miR-219a-5p, and miR-591) analyzed were chosen because they were consistently elevated in AD vs. control brain by >1.5-fold (**Tables 3**, **4**). In accord with our initial experiments using L1CAM-isolated exosomes (**Figure 3**), neuron-specific miR-9 was readily detected in all EV preps ($Ct \leq 35$) and at higher levels than the peripherally derived miR-451a ($Ct \leq 40$). Similar to brain samples, fold-changes of miR-9 and miR-451a were comparable between disease groups when normalized to miR-16 (**Figures 4A,B**).

miRNA-219a-5p could not be reliably detected in neural exosomes, and miR-32-5p, miR-182-5p, and miR-591 were unchanged between disease groups (**Supplementary Figure S3**). In contrast, miR-132 was significantly decreased (**Figure 4C**). miR-132, a miRNA that was regulated between AD, HPC, and control brains in our study, as well as in prior studies (Wong et al., 2013; Salta et al., 2016; Pichler et al., 2017), was decreased by ∼9-fold (log2 fold decrease of 3.15) in plasma-derived neural exosomes in AD vs. controls, and ∼5.4 fold in AD vs. AD-MCI (**Figure 4C**). Based on this result and the fact that miRNAs within the same cluster are often co-regulated, we sought to test whether miR-212, a miRNA in tandem to miR-132, was also altered in AD. Strikingly, the levels of miR-212 were reduced 4-fold in AD samples compared to controls (**Figure 4D**). Interestingly, higher CSF Tau/Aβ1-42 levels showed modest, but statistically significant association with lower levels of both miR-132 and miR-212 in plasma neural exosomes. Collectively, these results suggest that concerted dysregulation of miR-132 and miR-212 occurs in AD and that measuring the levels of these miRNAs in neurally derived exosome may offer a window on changes occurring in AD brain.

Receiver operating characteristic (ROC) curves is a common tool used to assess the diagnostic utility of novel biomarkers. ROC analysis (**Figures 5A,B**) revealed that miR-132 levels separated controls from AD-MCI with an AUC of 0.58 (95% CI: 0.38–0.78), and controls from AD dementia with an AUC of 0.77 (95% CI: 0.61–0.93). miR-212 showed better discrimination than miR-132 between both AD-MCI and controls, and AD and controls (**Figure 5**). ROC analysis of miR-212 levels separated controls from AD-MCI with an AUC of 0.68 (95% CI: 0.5–0.86), and controls from AD dementia with an AUC of 0.84 (95% CI: 0.72–0.96) (**Figures 5C,D**). miR-212 achieves a sensitivity (the ability to predict AD cases) of 92.2% (95% CI: 68.5–99.6%), and a specificity (the ability to exclude controls) of 69.0% (95% CI: 50.8–82.7%) at the best cut-off point determined by Youden's J statistics. Overall, our ROC analyses indicate that measurement of miR-212 in neurally derived plasma exosomes showed sufficient diagnostic sensitivity and specificity to pursue its use as a potential screening assay for AD.

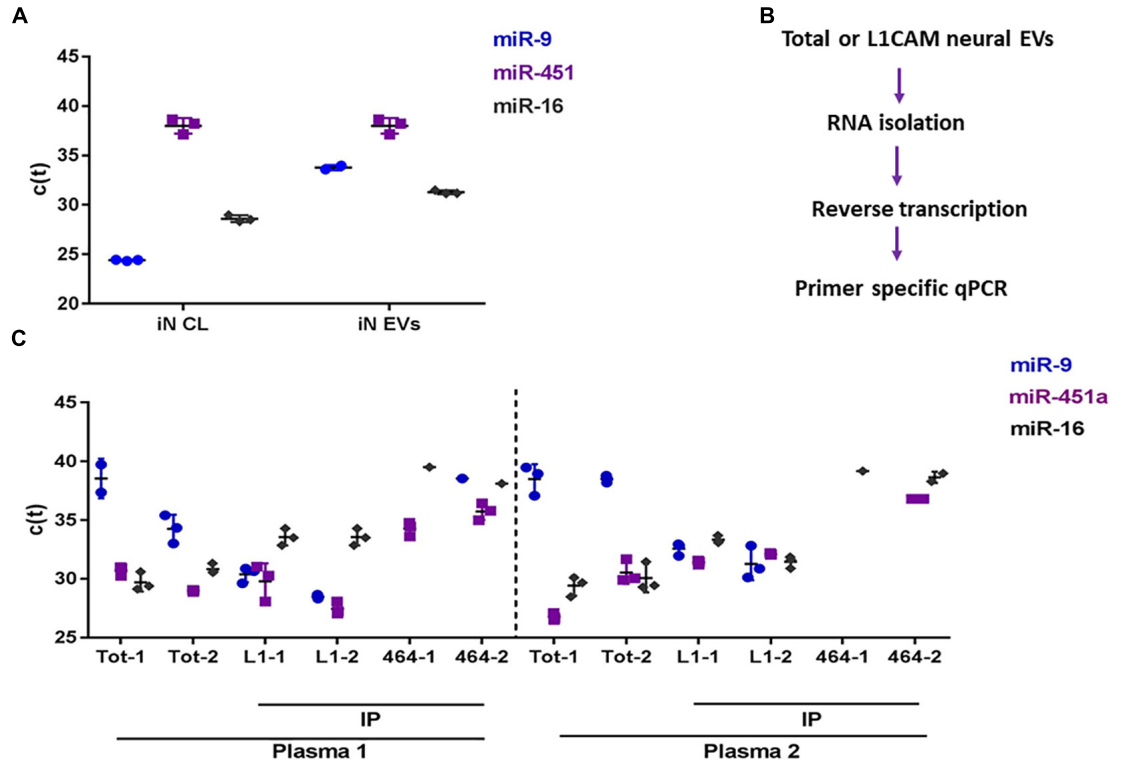

FIGURE 3 | miRNA analysis of brain-derived exosomes in blood. **(A)** C(t) values for neuron-specific miR-9, plasma abundant miR-451a, and ubiquitously expressed miR-16 from induced neuronal (iNs) cell lysates (CL), and iN exosomes isolated by ultracentrifugation of iN conditioned medium. **(B)** Flow chart for the detection of miRNAs from plasma exosomes. RNAs were isolated from total plasma exosomes (Exoquick pellets), or neural exosomes immunoprecipitated (IP) from total plasma exosomes with anti-L1CAM antibody. RNA was reverse transcribed with Qiagen's HiFlex buffer to generate cDNAs, and subsequently used as template for qPCR using miRNA-specific primers for miRNA detection. C(t) values for miR-9, miR-451a, and miR-16 from **(C)** plasma-derived total- and L1CAM (L1)-immunoprecipitated exosomes. As a negative control, an irrelevant antibody, 46-4 was used for immunoisolation. Total and IP'ed exosomes were isolated in duplicate (#1 and #2) from 2 healthy control donors (Plasma 1 and plasma 2). Low Ct values indicate high levels of miRNA, and high Ct values indicate low levels of miRNA. The reliable CT limit is ~40.

DISCUSSION

Despite considerable progress in our understanding of AD significant gaps remain and there is a desperate need for disease biomarkers that can offer insight about pathogenesis and which may serve as theragnostic indicators. To address this void, we exploited two exciting areas of AD research, namely miRNAs and neural exosomes. miRNAs are small regulatory molecules that post-transcriptionally repress gene expression and thereby regulate diverse biological processes, including neuronal differentiation, plasticity, survival, and regeneration (Kosik, 2006; Sambandan et al., 2017). Several neuronal miRNAs have been directly linked to AD, but there has been controversy as to which miRNAs are most important (Herrera-Espejo et al., 2019; Swarbrick et al., 2019).

In order to better define the most relevant miRNAs that are dysregulated in AD we conducted unbiased profiling of frontal cortex from three distinct groups of age-matched elderly individuals. Unlike some previous studies which compared only AD vs. controls (Salta et al., 2016; Pichler et al., 2017) we also compared AD vs. HPCs to distinguish between miRNAs that were altered by active neurodegeneration vs. those that may change in the absence of disease, but in response to amyloid and tangles. To ensure the robustness of our data we analyzed the same 5 AD, 5 HPC and 5 control samples in several different ways and then examined these 15 samples alongside additional AD, HPC and control samples. Initially, we used miRNA array analysis in an unbiased effort to profile differences between pools of RNA from AD, HPCs, and controls. Thereafter, we used miR-specific qRT-PCR to investigate the levels of 12 miRNAs that were most altered in the array experiments using both disease group pools of RNA, and RNA from individual brains. This approach yielded similar results regardless of the method used or whether RNA was from pools or individual brains, and these changes were maintained when additional brains were analyzed. Although all 12 miRNAs showed consistent fold differences (>1.5 fold) between AD, HPCs, and controls, only three miRNAs (miR-182-5p, miR-32-5p, and miR-132-3p) stood out in terms of group-based differences.

When we turned to analyze neural exosomes, we assessed miR-182-5p, miR-32-5p, and miR-132-3p, plus two other miRNAs (miR-219a-5p and miR-591) which in brain tissue showed consistent fold changes. Based on our iPSC-neuron experiments, we also used miR-9 and miR-451a to assess the neuronal origin

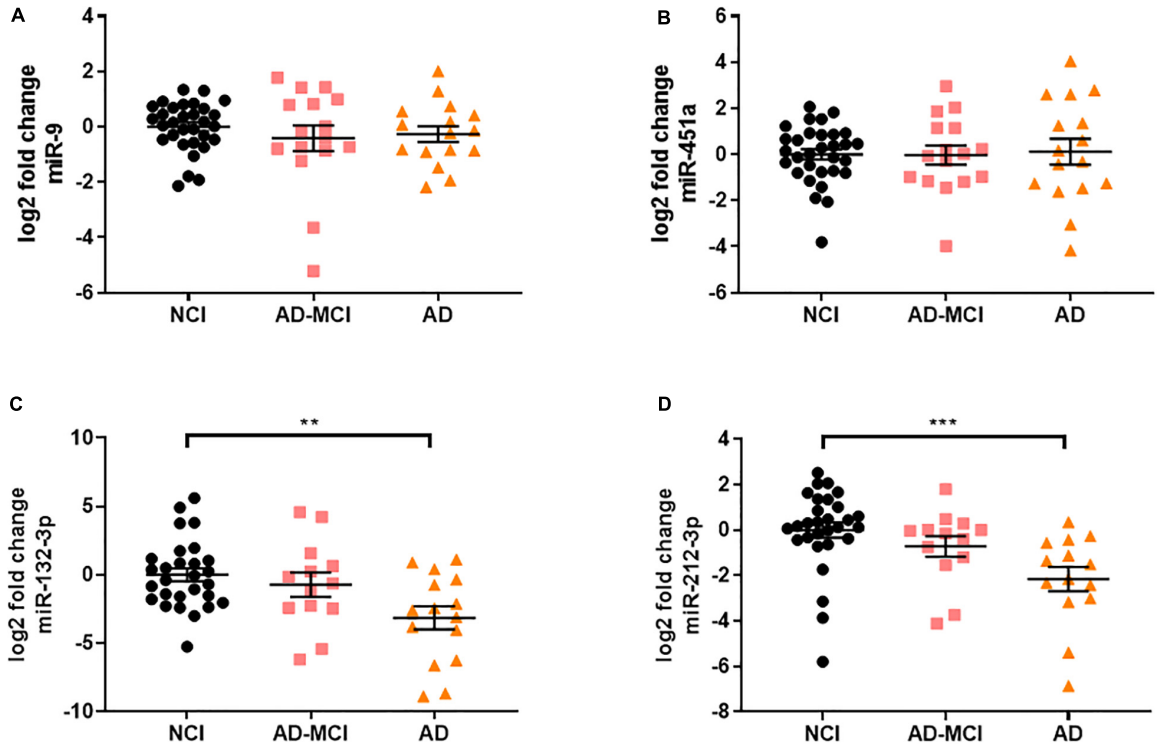

FIGURE 4 | miR-132/212 is significantly decreased in AD neural exosomes isolated from plasma. **(A)** neural-specific miR-9 was abundantly detected in all measured samples and was not significantly different between disease groups [$X^2(2) = 1.195$, $p = 0.550$]. **(B)** non-specific miR-451a were also detected in samples, but was unchanged between disease groups [$F(2) = 0.035$, $p = 0.965$]. Of the miRNAs significantly altered in AD brains, **(C)** miR-132 was significantly decreased in neural-derived plasma exosomes from AD subjects (** = 0.0333). **(D)** miR-212, a miRNA transcribed in tandem to miR-132, was also significantly decreased in AD (*** = 0.001). Significance was determined by one-way ANOVA followed by Tukey's *post hoc* test for normally distributed data. Otherwise, Kruskal–Wallis test followed by Dunn's *post hoc* test was used.

of our exosome preparations. miR-9 is one of the most highly expressed miRNAs in the vertebrate brain (Coolen et al., 2013) and here we show that miR-9 is enriched in human iPSC-derived neurons and neuronal exosomes. As we had anticipated, the peripherally expressed miR-451a (Okamoto et al., 2018) was barely detected in human neurons or neuronal exosomes. Applying these markers to our L1CAM-isolated plasma exosomes we found that miR-9 was readily detected, whereas miR-451a was present at only low levels. It is important to note that L1CAM is not uniquely expressed in brain, but is also found in kidney cells. Therefore, we cannot completely rule out, that a small contribution may come from L1CAM-positive kidney exosomes. However, the relative enrichment of neural-to-peripheral miRNAs in L1CAM-isolated exosomes indicates that the bulk of these exosomes are of neuronal origin. Consequently, the use of miR-9 should provide the field with a to tool to differentiate between neural and non-neuronal exosomes.

Of the four miRNAs most dysregulated in AD brain only miR-132 was significantly altered in AD neural exosomes. miR-219 could not be reliably detected, whereas, miR-32 and miR-182 were reliably detected, but their levels were similar across disease groups in neural exosomes. Why these miRNAs are dysregulated in brain, but unaltered in bona fide neural exosomes is not completely clear, but it is reasonable to assume that the miRNAs measured in brain tissue are derived from many different cell types, whereas our neural exosomes are predominantly neuronal in origin. In this regard, it is interesting to note that miR-132 is one of the most abundant brain-enriched miRNAs, whereas miR-182 is highly enriched in cells of myeloid linage (Pucella et al., 2015). Indeed, in future studies it will be important to determine if the four miRNAs we found to be most changed in AD brain are dysregulated in exosomes from microglia, astrocytes or oligodendrocytes.

Notwithstanding the importance of investigating miRNAs in exosomes from other brain cell types, it is intriguing that miR-132 is downregulated in both AD brain and neural exosomes. This finding is consistent with numerous other studies which have found miR-132 to be dysregulated in AD brain and with a host of studies which tie miR-132 down-regulation to AD pathogenesis (Lau et al., 2013; Wong et al., 2013; Hernandez-Rapp et al., 2016; Salta et al., 2016; Patrick et al., 2017; Pichler et al., 2017). For instance, reductions in miR-132 appears to occur before neuronal loss and *in vitro* miR-132 protects neurons against both Aβ and glutamate (Wong et al., 2013), and overexpression of miR-132 reduces tau pathology and caspase-3-dependent apoptosis in tau transgenic mice (El Fatimy et al., 2018). Since miRNAs within the same cluster are often co-regulated, we measured miR-212 in neural exosomes. The sequence of miR-212 is closely similar

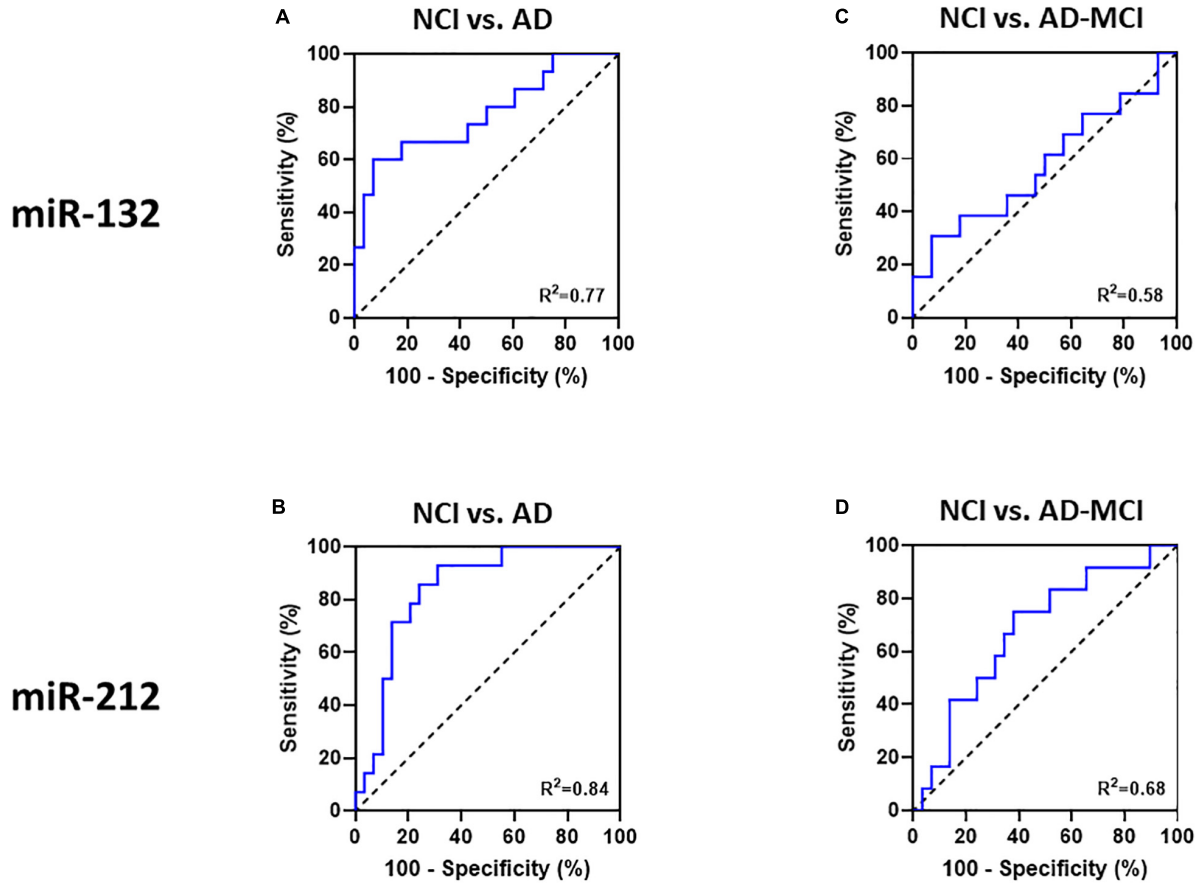

FIGURE 5 | Receiver-operator-characteristics (ROC) curves demonstrate that miR-132 and miR 212 in neural exosomes evidence good separation between NCI and AD. ROC curves of **(A)** miR-132, and **(B)** miR-212 allowed good separation of NCI from AD patients. Neither **(C)** miR-132, nor **(D)** miR-212 levels in NCI vs. AD-MCI patients allowed good separation. Area under the curves (AUC) for all ROC analyses were calculated using a non-parametric approach.

to that of miR-132 and both are enriched in neurons and exert regulatory functions on neuronal survival, maturation, plasticity and memory (Wanet et al., 2012). Moreover, downregulation of the miR-132/212 cluster in the frontal cortex had been reported for patients with amnestic MCI and mild AD (Weinberg et al., 2015). Here, we found that miR-212 was strongly dysregulated in AD neural exosomes, and tended to be decreased in AD brain. Why the decrease in miR-212 was significant in neural exosomes, but not brain is unclear, but (as with miR-182) this may relate to the relative distribution of miRNAs in neurons vs. glia.

Importantly, ROC analysis indicated that measurement of miR-132-3p and miR-212-3p in neurally derived plasma exosomes showed good sensitivity and specificity to diagnose AD, but did not effectively separate individuals with AD-MCI from controls. The criteria used to identify dysregulated miRNAs in AD brain required that they were specifically altered in AD vs. both HPCs and controls. Given that at least some HPCs maybe on path to AD it is perhaps not surprising that miRNAs that are preferentially dysregulated in AD brain compared with HPC brain do not discriminate AD from AD-MCI when measured in neural exosomes. Future studies should investigate whether miRNAs that are dysregulated in HPC brain compared to control brain might discriminate AD-MCI from controls when quantified in neural exosomes. Nonetheless, quantification of miR-132 and miR-212 in neural exosomes should aid diagnosis of symptomatic patients. While this is not the population most in need of blood-based biomarkers, measurement of neural exosome miR-132 and miR-212 may have theragnostic potential and it would be particularly interesting to measure these markers longitudinally. Future studies should determine whether the observed changes in miR-132 and miR-212 can also be seen in total plasma exosomes or are specific for neural exosomes.

DATA AVAILABILITY STATEMENT

The raw data from our array experiments can be accessed through https://www.ebi.ac.uk/arrayexpress/browse.html?query= under the accession number E-MTAB-8283. All other data supporting the conclusions of this manuscript will be made available by the authors, without undue reservation, to any qualified researcher. Religious Orders Study resources can be requested at the Rush Alzheimer's Disease Center Research Resource Sharing Hub at www.radc.rush.edu.

ETHICS STATEMENT

The studies involving human participants were reviewed and approved by the Partners Institutional Review Board. The patients/participants provided their written informed consent to participate in this study.

AUTHOR CONTRIBUTIONS

DW conceived the project, designed and supervised the research, and wrote the manuscript. DC performed the exosome isolations, analyzed the brain tissue and exosomes for miR content, analyzed data, prepared figures, and wrote the manuscript. DM coded and decoded the specimen designations to ensure all experiments were done blind to the disease status of donors/patient, conducted statistical analysis, prepared figures, and wrote the manuscript. WL dissected the brain tissue and assisted with preparation of iPSC-derived neurons. DS provided the critical guidance. MM and DK provided expert guidance on the preparation of neural exosomes. DG and RR supplied archived samples and relevant clinical data. DB provided brain samples, and detailed clinical and postmortem data. All authors critically appraised the manuscript.

FUNDING

This work was supported by grants to DW from the Alzheimer's Drug Discovery Foundation and by an Alzheimer's Association Zenith Award. DM is a research fellow funded by the German Research Foundation (DFG ME 4858/1-1). DW is an Alzheimer's Association Zenith Fellow. The Religious Orders Study was supported by NIA grants P30AG10161 and R01AG15819.

ACKNOWLEDGMENTS

We are grateful to brain donors and their families. We thank clinician colleagues for referring the patients, collecting blood, and performing lumbar punctures. We acknowledge the ARCND for providing access to the real-time PCR system. We also thank Dr. Tracy Young-Pearse for YZ1 human iPSC cells used to generate the iPSC neurons employed in this study.

SUPPLEMENTARY MATERIAL

The Supplementary Material for this article can be found online at: https://www.frontiersin.org/articles/10.3389/fnins.2019.01208/full#supplementary-material

FIGURE S1 | Identification of AD and AD-MCI subjects based on cognitive testing and best available CSF biomarkers used for subsequent exosome isolation. A total of 63 plasma samples were obtained from the UCSD biomarker collection. CSF from these subjects was analyzed and levels of Aβ42 and tau yielded clear segregation of the disease groups.

FIGURE S2 | Replicate plates within pooled disease groups show good correlation. Spearman correlation between replicates of different plates run on different days for the same sample/cDNA show high correlation with an $R^2 > 0.99$ for all.

FIGURE S3 | miR-32-5p, miR-182-5p, and miR-591 in plasma neural exosomes are unchanged between diagnostic groups. **(A)** miR-32-5p, **(B)** miR-182-5p, **(C)** miR-591, were measured in plasma neural Exosomes, but were not significantly changed ($p > 0.05$). Significance was determined by one-way ANOVA followed by Tukey's *post hoc* test for normally distributed data. Otherwise, Kruskal–Wallis test followed by Dunn's *post hoc* test was used.

TABLE S1 | miRNA list and primers.

REFERENCES

Abner, E. L., Jicha, G. A., Shaw, L. M., Trojanowski, J. Q., and Goetzl, E. J. (2016). Plasma neuronal exosomal levels of Alzheimer's disease biomarkers in normal aging. *Ann. Clin. Transl. Neurol.* 3, 399–403. doi: 10.1002/acn3.309

Banzhaf-Strathmann, J., Benito, E., May, S., Arzberger, T., Tahirovic, S., Kretzschmar, H., et al. (2014). MicroRNA-125b induces tau hyperphosphorylation and cognitive deficits in Alzheimer's disease. *EMBO J.* 33, 1667–1680. doi: 10.15252/embj.201387576

Bao, W., Jia, H., Finnema, S., Cai, Z., Carson, R. E., and Huang, Y. H. (2017). PET Imaging for Early Detection of Alzheimer's Disease: from pathologic to physiologic biomarkers. *PET Clin.* 12, 329–350. doi: 10.1016/j.cpet.2017.03.001

Bateman, R. J., Blennow, K., Doody, R., Hendrix, S., Lovestone, S., Salloway, S., et al. (2019). Plasma biomarkers of AD emerging as essential tools for drug development: an EU/US CTAD task force report. *J. Prev. Alzheimers Dis.* 6, 169–173. doi: 10.14283/jpad.2019.21

Bennett, D. A., Buchman, A. S., Boyle, P. A., Barnes, L. L., Wilson, R. S., and Schneider, J. A. (2018). Religious orders study and rush memory and aging project. *J. Alzheimers Dis.* 64, S161–S189. doi: 10.3233/JAD-179939

Bennett, D. A., Schneider, J. A., Arvanitakis, Z., Kelly, J. F., Aggarwal, N. T., Shah, R. C., et al. (2006). Neuropathology of older persons without cognitive impairment from two community-based studies. *Neurology* 66, 1837–1844. doi: 10.1212/01.wnl.0000219668.47116.e6

Bhatnagar, S., Chertkow, H., Schipper, H. M., Yuan, Z., Shetty, V., Jenkins, S., et al. (2014). Increased microRNA-34c abundance in Alzheimer's disease circulating blood plasma. *Front. Mol. Neurosci.* 7:2. doi: 10.3389/fnmol.2014.00002

Blennow, K., Zetterberg, H., and Fagan, A. M. (2012). Fluid biomarkers in Alzheimer disease. *Cold Spring Harb. Perspect. Med.* 2:a006221. doi: 10.1101/cshperspect.a006221

Chevillet, J. R., Kang, Q., Ruf, I. K., Briggs, H. A., Vojtech, L. N., Hughes, S. M., et al. (2014). Quantitative and stoichiometric analysis of the microRNA content of exosomes. *Proc. Natl. Acad. Sci. U.SA.* 111, 14888–14893. doi: 10.1073/pnas.1408301111

Coolen, M., Katz, S., and Bally-Cuif, L. (2013). miR-9: a versatile regulator of neurogenesis. *Front. Cell Neurosci.* 7:220. doi: 10.3389/fncel.2013.00220

Denk, J., Oberhauser, F., Kornhuber, J., Wiltfang, J., Fassbender, K., Schroeter, M. L., et al. (2018). Specific serum and CSF microRNA profiles distinguish sporadic behavioural variant of frontotemporal dementia compared with Alzheimer patients and cognitively healthy controls. *PLoS One* 13:e0197329. doi: 10.1371/journal.pone.0197329

El Fatimy, R., Li, S., Chen, Z., Mushannen, T., Gongala, S., Wei, Z., et al. (2018). MicroRNA-132 provides neuroprotection for tauopathies via multiple signaling pathways. *Acta Neuropathol.* 136, 537–555. doi: 10.1007/s00401-018-1880-5

Fiandaca, M. S., Kapogiannis, D., Mapstone, M., Boxer, A., Eitan, E., Schwartz, J. B., et al. (2015). Identification of preclinical Alzheimer's disease by a profile of

pathogenic proteins in neurally derived blood exosomes: a case-control study. *Alzheimers Dement.* 11, 600.e1–607.e1. doi: 10.1016/j.jalz.2014.06.008

Fruhbeis, C., Frohlich, D., and Kramer-Albers, E. M. (2012). Emerging roles of exosomes in neuron-glia communication. *Front. Physiol.* 3:119. doi: 10.3389/fphys.2012.00119

Galasko, D. (2015). Expanding the repertoire of biomarkers for alzheimer's disease: targeted and non-targeted approaches. *Front. Neurol.* 6:256. doi: 10.3389/fneur.2015.00256

Goetzl, E. J., Boxer, A., Schwartz, J. B., Abner, E. L., Petersen, R. C., Miller, B. L., et al. (2015a). Altered lysosomal proteins in neural-derived plasma exosomes in preclinical Alzheimer disease. *Neurology* 85, 40–47. doi: 10.1212/WNL.0000000000001702

Goetzl, E. J., Boxer, A., Schwartz, J. B., Abner, E. L., Petersen, R. C., Miller, B. L., et al. (2015b). Low neural exosomal levels of cellular survival factors in Alzheimer's disease. *Ann. Clin. Transl. Neurol.* 2, 769–773. doi: 10.1002/acn3.211

Goetzl, E. J., Ledreux, A., Granholm, A. C., Elahi, F. M., Goetzl, L., Hiramoto, J., et al. (2019). Neuron-derived exosome proteins may contribute to progression from repetitive mild traumatic brain injuries to chronic traumatic encephalopathy. *Front. Neurosci.* 13:452. doi: 10.3389/fnins.2019.00452

Guix, F. X., Corbett, G. T., Cha, D. J., Mustapic, M., Liu, W., Mengel, D., et al. (2018). Detection of aggregation-competent tau in neuron-derived extracellular vesicles. *Int. J. Mol. Sci.* 19:E663. doi: 10.3390/ijms19030663

Hebert, S. S., Horre, K., Nicolai, L., Papadopoulou, A. S., Mandemakers, W., Silahtaroglu, A. N., et al. (2008). Loss of microRNA cluster miR-29a/b-1 in sporadic Alzheimer's disease correlates with increased BACE1/beta-secretase expression. *Proc. Natl. Acad. Sci. U.S.A.* 105, 6415–6420. doi: 10.1073/pnas.0710263105

Heinzelman, P., Bilousova, T., Campagna, J., and John, V. (2016). Nanoscale extracellular vesicle analysis in Alzheimer's disease diagnosis and therapy. *Int. J. Alzheimers Dis.* 2016:8053139. doi: 10.1155/2016/8053139

Hernandez-Rapp, J., Rainone, S., Goupil, C., Dorval, V., Smith, P. Y., Saint-Pierre, M., et al. (2016). microRNA-132/212 deficiency enhances Abeta production and senile plaque deposition in Alzheimer's disease triple transgenic mice. *Sci. Rep.* 6:30953. doi: 10.1038/srep30953

Herrera-Espejo, S., Santos-Zorrozua, B., Alvarez-Gonzalez, P., Lopez-Lopez, E., and Garcia-Orad, A. (2019). A Systematic Review of MicroRNA Expression as Biomarker of Late-Onset Alzheimer's Disease. *Mol. Neurobiol*. doi: 10.1007/s12035-019-01676-9 [Epub ahead of print].

Jack, C. R. Jr., Bennett, D. A., Blennow, K., Carrillo, M. C., Dunn, B., Haeberlein, S. B., et al. (2018). NIA-AA research framework: toward a biological definition of Alzheimer's disease. *Alzheimers Dement.* 14, 535–562. doi: 10.1016/j.jalz.2018.02.018

Jack, C. R. Jr., Knopman, D. S., Jagust, W. J., Petersen, R. C., Weiner, M. W., Aisen, P. S., et al. (2013). Tracking pathophysiological processes in Alzheimer's disease: an updated hypothetical model of dynamic biomarkers. *Lancet Neurol.* 12, 207–216. doi: 10.1016/S1474-4422(12)70291-0

Janelidze, S., Stomrud, E., Palmqvist, S., Zetterberg, H., Van Westen, D., Jeromin, A., et al. (2016). Plasma beta-amyloid in Alzheimer's disease and vascular disease. *Sci. Rep.* 6:26801. doi: 10.1038/srep26801

Johnstone, R. M., Adam, M., Hammond, J. R., Orr, L., and Turbide, C. (1987). Vesicle formation during reticulocyte maturation. Association of plasma membrane activities with released vesicles (exosomes). *J. Biol. Chem.* 262, 9412–9420.

Kapogiannis, D., Boxer, A., Schwartz, J. B., Abner, E. L., Biragyn, A., Masharani, U., et al. (2015). Dysfunctionally phosphorylated type 1 insulin receptor substrate in neural-derived blood exosomes of preclinical Alzheimer's disease. *FASEB J.* 29, 589–596. doi: 10.1096/fj.14-262048

Kosik, K. S. (2006). The neuronal microRNA system. *Nat. Rev. Neurosci.* 7, 911–920. doi: 10.1038/nrn2037

Lau, P., Bossers, K., Janky, R., Salta, E., Frigerio, C. S., Barbash, S., et al. (2013). Alteration of the microRNA network during the progression of Alzheimer's disease. *EMBO Mol. Med.* 5, 1613–1634. doi: 10.1002/emmm.201201974

Monsell, S. E., Kukull, W. A., Roher, A. E., Maarouf, C. L., Serrano, G., Beach, T. G., et al. (2015). Characterizing apolipoprotein E epsilon4 carriers and noncarriers with the clinical diagnosis of mild to moderate alzheimer dementia and minimal beta-amyloid peptide plaques. *JAMA Neurol.* 72, 1124–1131. doi: 10.1001/jamaneurol.2015.1721

O'Brien, J., Hayder, H., Zayed, Y., and Peng, C. (2018). Overview of MicroRNA biogenesis, mechanisms of actions, and circulation. *Front. Endocrinol.* 9:402. doi: 10.3389/fendo.2018.00402

Okamoto, M., Fukushima, Y., Kouwaki, T., Daito, T., Kohara, M., Kida, H., et al. (2018). MicroRNA-451a in extracellular, blood-resident vesicles attenuates macrophage and dendritic cell responses to influenza whole-virus vaccine. *J. Biol. Chem.* 293, 18585–18600. doi: 10.1074/jbc.RA118.003862

Pan, B. T., Teng, K., Wu, C., Adam, M., and Johnstone, R. M. (1985). Electron microscopic evidence for externalization of the transferrin receptor in vesicular form in sheep reticulocytes. *J. Cell Biol.* 101, 942–948. doi: 10.1083/jcb.101.3.942

Paolicelli, R. C., Bergamini, G., and Rajendran, L. (2019). Cell-to-cell communication by extracellular vesicles: focus on microglia. *Neuroscience* 405, 148–157. doi: 10.1016/j.neuroscience.2018.04.003

Patrick, E., Rajagopal, S., Wong, H. A., Mccabe, C., Xu, J., Tang, A., et al. (2017). Dissecting the role of non-coding RNAs in the accumulation of amyloid and tau neuropathologies in Alzheimer's disease. *Mol. Neurodegener.* 12:51. doi: 10.1186/s13024-017-0191-y

Pichler, S., Gu, W., Hartl, D., Gasparoni, G., Leidinger, P., Keller, A., et al. (2017). The miRNome of Alzheimer's disease: consistent downregulation of the miR-132/212 cluster. *Neurobiol. Aging* 50:167.e1-167 e10. doi: 10.1016/j.neurobiolaging.2016.09.019

Pucella, J. N., Yen, W. F., Kim, M. V., Van Der Veeken, J., Luo, C. T., Socci, N. D., et al. (2015). miR-182 is largely dispensable for adaptive immunity: lack of correlation between expression and function. *J. Immunol.* 194, 2635–2642. doi: 10.4049/jimmunol.1402261

Raposo, G., and Stoorvogel, W. (2013). Extracellular vesicles: exosomes, microvesicles, and friends. *J. Cell Biol.* 200, 373–383. doi: 10.1083/jcb.201211138

Salloway, S., Sperling, R., and Brashear, H. R. (2014). Phase 3 trials of solanezumab and bapineuzumab for Alzheimer's disease. *N. Engl. J. Med.* 370:1460.

Salta, E., Sierksma, A., Vanden Eynden, E., and De Strooper, B. (2016). miR-132 loss de-represses ITPKB and aggravates amyloid and TAU pathology in Alzheimer's brain. *EMBO Mol. Med.* 8, 1005–1018. doi: 10.15252/emmm.201606520

Sambandan, S., Akbalik, G., Kochen, L., Rinne, J., Kahlstatt, J., Glock, C., et al. (2017). Activity-dependent spatially localized miRNA maturation in neuronal dendrites. *Science* 355, 634–637. doi: 10.1126/science.aaf8995

Swarbrick, S., Wragg, N., Ghosh, S., and Stolzing, A. (2019). Systematic review of miRNA as biomarkers in alzheimer's disease. *Mol. Neurobiol.* 56, 6156–6167. doi: 10.1007/s12035-019-1500-y

Vella, L. J., Hill, A. F., and Cheng, L. (2016). Focus on extracellular vesicles: exosomes and their role in protein trafficking and biomarker potential in Alzheimer's and Parkinson's disease. *Int. J. Mol. Sci.* 17:173. doi: 10.3390/ijms17020173

Wanet, A., Tacheny, A., Arnould, T., and Renard, P. (2012). miR-212/132 expression and functions: within and beyond the neuronal compartment. *Nucleic Acids Res.* 40, 4742–4753. doi: 10.1093/nar/gks151

Weinberg, R. B., Mufson, E. J., and Counts, S. E. (2015). Evidence for a neuroprotective microRNA pathway in amnestic mild cognitive impairment. *Front. Neurosci.* 9:430. doi: 10.3389/fnins.2015.00430

Winston, C. N., Goetzl, E. J., Akers, J. C., Carter, B. S., Rockenstein, E. M., Galasko, D., et al. (2016). Prediction of conversion from mild cognitive impairment to dementia with neuronally derived blood exosome protein profile. *Alzheimers Dement.* 3, 63–72. doi: 10.1016/j.dadm.2016.04.001

Wong, H. K., Veremeyko, T., Patel, N., Lemere, C. A., Walsh, D. M., Esau, C., et al. (2013). De-repression of FOXO3a death axis by microRNA-132 and -212 causes neuronal apoptosis in Alzheimer's disease. *Hum. Mol. Genet.* 22, 3077–3092. doi: 10.1093/hmg/ddt164

Conflict of Interest: DW is an employee of Biogen Inc.

The remaining authors declare that the research was conducted in the absence of any commercial or financial relationships that could be construed as a potential conflict of interest.

frontiers in Neuroscience

REVIEW
published: 12 December 2019
doi: 10.3389/fnins.2019.01347

Exosome Production Is Key to Neuronal Endosomal Pathway Integrity in Neurodegenerative Diseases

Paul M. Mathews[1,2,3]* *and Efrat Levy*[1,2,3,4]*

[1] Center for Dementia Research, The Nathan S. Kline Institute for Psychiatric Research, Orangeburg, NY, United States, [2] Department of Psychiatry, New York University Langone Health, New York, NY, United States, [3] NYU Neuroscience Institute, New York University Langone Health, New York, NY, United States, [4] Department of Biochemistry and Molecular Pharmacology, New York University Langone Health, New York, NY, United States

OPEN ACCESS

Edited by:
Francesc Xavier Guix,
Severo Ochoa Molecular Biology Center (CSIC-UAM), Spain

Reviewed by:
Archan Ganguly,
University of California, San Diego, United States
Melissa Calegaro Nassif,
Major University, Chile

***Correspondence:**
Paul M. Mathews
paul.mathews@nki.rfmh.org
Efrat Levy
efrat.levy@nki.rfmh.org

Specialty section:
This article was submitted to Neurodegeneration, a section of the journal Frontiers in Neuroscience

Received: 29 July 2019
Accepted: 29 November 2019
Published: 12 December 2019

Citation:
Mathews PM and Levy E (2019) Exosome Production Is Key to Neuronal Endosomal Pathway Integrity in Neurodegenerative Diseases. Front. Neurosci. 13:1347. doi: 10.3389/fnins.2019.01347

Dysfunction of the endosomal–lysosomal system is a prominent pathogenic factor in Alzheimer's disease (AD) and other neurodevelopmental and neurodegenerative disorders. We and others have extensively characterized the neuronal endosomal pathway pathology that results from either triplication of the amyloid-β precursor protein (APP) gene in Down syndrome (DS) or from expression of the apolipoprotein E ε4 allele (APOE4), the greatest genetic risk factor for late-onset AD. More recently brain exosomes, extracellular vesicles that are generated within and released from endosomal compartments, have been shown to be altered in DS and by APOE4 expression. In this review, we discuss the emerging data arguing for an interdependence between exosome production and endosomal pathway integrity in the brain. *In vitro* and *in vivo* studies indicate that altered trafficking through the endosomal pathway or compromised cargo turnover within lysosomes can affect the production, secretion, and content of exosomes. Conversely, exosome biogenesis can affect the endosomal–lysosomal system. Indeed, we propose that efficient exosome release helps to modulate flux through the neuronal endosomal pathway by decompressing potential "traffic jams." Exosome secretion may have the added benefit of unburdening the neuron's lysosomal system by delivering endosomal–lysosomal material into the extracellular space, where other cell types may contribute to the degradation of neuronal debris. Thus, maintaining robust neuronal exosome production may prevent or mitigate endosomal and lysosomal abnormalities linked to aging and neurodegenerative diseases. While the current evidence suggests that the exosomal system in the brain can be modulated both by membrane lipid composition and the expression of key proteins that contribute to the formation and secretion of exosomes, how exosomal pathway-regulatory elements sense and respond to perturbations in the endosomal pathway is not well understood. Based upon findings from the extensively studied DS and APOE4 models, we propose that enhanced neuronal exosome secretion can be a protective response, reducing

pathological disruption of the endosomal–lysosomal system in disease-vulnerable neurons. Developing therapeutic approaches that help to maintain or enhance neuronal exosome biogenesis and release may be beneficial in a range of disorders of the central nervous system.

Keywords: endosome, lysosome, extracellular vesicle, multi-vesicular body, neurodegeneration, apolipoprotein E, Alzheimer's disease, Down syndrome

INTRODUCTION

In Alzheimer's disease (AD), early alterations of the endosomal system in neurons is followed by extensive disruption of autophagic and lysosomal compartments (Colacurcio et al., 2018). Neuronal endosomal pathway disruption has been suggested to result from multiple pathological insults in AD, including, for example, intravesicular amyloid-β (Aβ) (Willen et al., 2017). Our laboratories and collaborators have focused on the apparently Aβ-independent endosomal pathway changes that are seen in Down syndrome (DS) (Cataldo et al., 2000, 2003, 2008) and as a result of the expression of the apolipoprotein E ε4 allele (ApoE4) (Nuriel et al., 2017). In DS, which leads to early onset AD, the elevated levels of the β-site cleaved carboxyl-terminal fragment (βCTF) of the amyloid-β precursor protein (APP) that result from the triplication and overexpression of the APP gene are sufficient to cause early endosomal changes (Cataldo et al., 2003; Salehi et al., 2006; Jiang et al., 2010, 2016; Nixon, 2017). Expression of APOE4, the most important genetic risk factor for late-onset AD (Corder et al., 1993; Farrer et al., 1997; Bu, 2009; Liu et al., 2013), leads to morphologically similar neuronal endosomal pathway changes in humans as well as in mouse models (Cataldo et al., 2000; Nuriel et al., 2017; Zhao et al., 2017). More recently, research focus in these models of AD-related endosomal disruption has extended to exosomes, membrane-bound vesicles that are generated within the endosomal pathway and secreted into the extracellular space (Kreimer et al., 2015; van der Pol et al., 2015). A widely held opinion is that extracellular vesicles (EVs), including exosomes, can be harmful within the brain. These stable vesicles may allow toxic material to be transported between cells and brain regions, and may promote the accumulation of this material in the extracellular space (Valdinocci et al., 2017; Perez et al., 2019).

Nevertheless they may also be beneficial, discarding potentially toxic material that a neuron has targeted for degradation, as well as through the transport of neuroprotective proteins. Indeed, exosome secretion was originally described as a process that can complement and supplement lysosomal and proteasomal degradation for the removal of obsolete membrane and cytosolic materials (Johnstone et al., 1987). While the *in vivo* functions of exosomes in the brain are likely to be a mixture of beneficial and potentially pathological effects, in this review, we have chosen to emphasize the beneficial role that exosome production may play in supporting neuronal endosomal–lysosomal function. Emerging evidence now links endosomal pathway function and the generation and secretion of exosomes into the brain extracellular space. Perturbations of the neuronal endosomal–lysosomal pathway, which can alter endosomal pathway flux and lead to inefficient degradation in lysosomes, appear to affect exosome secretion. Additionally, it appears that disease-driven deficiencies in exosomal production can negatively affect flux and catabolism through the endosomal–lysosomal pathway. Thus, our hypothesis is that exosome production plays a key role in maintaining neuronal endosomal pathway integrity and that disruption of these integrated systems can contribute to neurodegenerative diseases.

DISCUSSION

Extracellular Vesicles in the Brain

Extracellular vesicles are secreted into tissue extracellular space, biological fluids, and, in culture, conditioned media. Their membrane is rich in phospholipids and they contain lipids, proteins, and RNA (mRNA and miRNA). Multiple types of EVs have been described with different sites of cellular origin (reviewed in van der Pol et al., 2012; Kowal et al., 2014; Kalra et al., 2016) and with distinct molecular and biological properties (Lai et al., 2016; Willms et al., 2016). *Microvesicles* derive from the plasma membrane, have a diameter of 100–1000 nm, and are continuously released from the cell membrane of apparently all cells, although under pathological conditions their release from the cell can also be triggered (Borroto-Escuela et al., 2015). The *exosome* is the most extensively studied EV species, 20–150 nm vesicles formed by the intraluminal invagination of the limiting-membrane of the late endosome/multi-vesicular body (MVB; so named because of the presence of these nascent vesicles within the larger endosomal lumen) (reviewed in Kreimer et al., 2015; van der Pol et al., 2015; **Figure 1**). Exosomes are these intraluminal vesicles (ILVs) once they are released into the extracellular space upon fusion of MVBs with the plasma membrane (Colombo et al., 2014). During the budding of both microvesicles and ILVs cytosolic content is captured within the lumen of the inchoate vesicle, contributing to the vesicle's eventual content. Additionally, these vesicles contain membrane lipids and various membrane-associated molecules, some of which are unique to each vesicle subtype. In addition to microvesicles and exosomes, lysosomal exocytosis releases lysosomal luminal contents into the extracellular space. This is, in part, a calcium-regulated process that entails fusion of the lysosomal limiting membrane with the plasma membrane (Stinchcombe et al., 2004). Lysosomes can also transiently contain ILVs delivered from the MVB which are released into the extracellular space upon lysosomal exocytosis (Migliano and Teis, 2018). Dysfunction of the endosomal–lysosomal pathway in AD appears to cause lysosomal components to

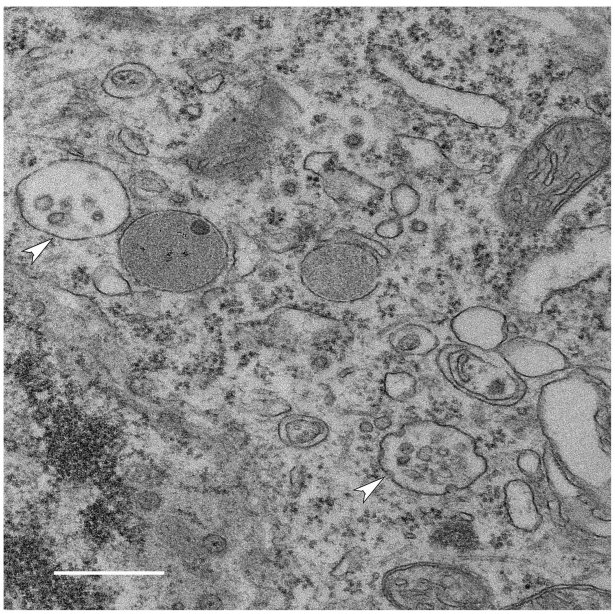

FIGURE 1 | Generation of intraluminal vesicles (ILVs) within MVBs in a neuron. Electron micrograph of MVBs (arrowheads) in a neuron in the brain of a wild-type mouse (bar 500 nm) shows multiple ILVs along with invaginations of the MVB limiting membrane that are likely to represent the formation of nascent ILVs. Once released into the extracellular space, these ILVs are exosomes.

leak into the extracellular fluid around amyloid plaques and into the cerebrospinal fluid (CSF) (Schwagerl et al., 1995; Nixon and Cataldo, 2006; Colacurcio et al., 2018). Lysosomal proteins, such as cathepsins B and D and lysosome-associated membrane protein 1 (LAMP-1) were identified in brain EVs, suggesting that autophagic-lysosomal dysfunction of neurons in AD may result in vesicular lysosomal exocytosis (Andrews, 2000; Ihara et al., 2012; Urbanelli et al., 2013). Additionally, higher levels of autophagic- and lysosomal-related proteins have been found in neuronal exosomes isolated from the blood in patients with AD compared to non-demented control individuals (Goetzl et al., 2015).

Microvesicles, exosomes, and vesicles resulting from lysosome secretion are typically co-isolated by experimenters from tissues, biological fluids such as plasma, CSF and urine, and from cell-culture conditioned media. These complex EVs preparations can be further purified to enrich for exosomes (Pérez-González et al., 2012, 2017). Exosomes themselves can be specifically identified by various markers such as the transmembrane tetraspanin proteins (e.g., CD63) and the endosomal sorting complex required for transport (ESCRT) machinery proteins (e.g., tumor susceptibility gene 101, TSG101 and ALG-2-interacting protein X, Alix, also called programmed cell death 6-interacting protein, PDCD6IP) involved in ILV formation (van Niel et al., 2018). Nevertheless, a full characterization and cataloging of the various types of EVs found in the brain has not been completed, and any experimental preparation at this point should be assumed to contain more than one type of EVs. An additional complexity is the multiple cell types within the brain that are potential sources of EVs. In this discussion, we have generally defaulted to the inclusive terminology of EVs except when the experimental evidence specifically supports changes in exosomes: we present such data as exosome findings.

Potential Contribution of EVs to the Spread of Pathogenic Molecules Within the Brain

Extracellular vesicles appear to have roles in cell signaling functions (Record et al., 2011), by shuttling cargo between cells and between tissues (Smalheiser, 2007). In the brain, this may contribute to the regulation of neurotransmitter receptor levels at the synapse (Faure et al., 2006), synapse number (Lee et al., 2018), the production and turnover of myelin membrane proteins (Bakhti et al., 2011; Kramer-Albers and Hill, 2016; Tassew et al., 2017), as well as, unfortunately, the progression and propagation of neurodegenerative diseases (Gould et al., 2003; Vella et al., 2008; Izquierdo-Useros et al., 2011; Budnik et al., 2016). The potential for deleterious functions of EV movement between cells was initially based upon the idea that EVs can efficiently transfer pathogens between cells. In the brain, one such pathogenic molecule that uses EV release is misfolded prion protein (PrP), causing transmissible neurodegenerative diseases such as Creutzfeldt–Jakob disease in humans and bovine spongiform encephalopathy in cattle (Vella et al., 2008; Vilette et al., 2018). α-synuclein, involved in the pathogenesis of Parkinson's disease, is also secreted in a calcium-dependent manner via EVs (Emmanouilidou et al., 2010; Alvarez-Erviti et al., 2011; Danzer et al., 2012; Stuendl et al., 2016; Ngolab et al., 2017), and the transfer of α-synuclein fibrils between cells appears to be an important component of α-synuclein pathology, spread of the misfolded protein to distant sites, and the activation of immune cells (reviewed in Tofaris, 2017; Grozdanov and Danzer, 2018; Stefanis et al., 2019). In Parkinson's disease, mutations in the leucine-rich repeat kinase 2 (LRRK2) gene are a frequent genetic cause of the disorder, and it has also been suggested that EV-associated LRRK2 carries pathogenic-potential for the disease (reviewed in Wang and West, 2019).

In AD, EVs have been proposed to contribute to the spread of Aβ and Aβ pathology in the brain (Rajendran et al., 2006) as well as the spread of hyper-phosphorylated pathogenic tau between neurons (Saman et al., 2012; Wang et al., 2017; Guix et al., 2018; Winston et al., 2019). We and others have shown that EVs contain full-length APP, the CTFs of APP generated through cleavage by β-secretase (βCTFs) or α-secretase (αCTFs), Aβ, and the enzymes that are responsible for these cleavage steps (Rajendran et al., 2006; Vingtdeux et al., 2007; Escrevente et al., 2008; Sharples et al., 2008; Pérez-González et al., 2012; Laulagnier et al., 2018; Miranda et al., 2018). The endosomal pathway is critical for the processing of APP (Nixon, 2017), with β-secretase cleavage mediated by BACE1 occurring in endosomes (Koo, 2002; Kinoshita et al., 2003; Small and Gandy, 2006). Thus, the finding that endosome pathway-derived exosomes contain abundant CTFs is not unexpected (Pérez-González et al., 2012; Gauthier et al., 2017). In addition to being the precursor of

the neurotoxic Aβ, the βCTF itself has the potential to be a neurotoxic protein that causes neuronal endosomal–lysosomal abnormalities (Jiang et al., 2010, 2016, 2019; Nixon, 2017) and functional sequelae including memory loss (Neve et al., 1996; Oster-Granite et al., 1996; Neve and Robakis, 1998; McPhie et al., 2001; Jiang et al., 2010; Deyts et al., 2012; Flammang et al., 2012; Lauritzen et al., 2012, 2016; Oules et al., 2012; Tamayev and D'Adamio, 2012; Tamayev et al., 2012). The propagation of βCTFs via exosomes from neuron to neuron may have deleterious effects separate from the propagation of Aβ by these vesicles.

EV Production Within the Brain May Also Be Protective

While it has been shown that EVs can propagate Aβ within the brain (Howitt and Hill, 2016; Xiao et al., 2017), a study has shown that exogenous EVs can paradoxically clear Aβ from the brain of APP overexpressing transgenic mice (Yuyama et al., 2014). *In vitro*, EVs released by neuroblastoma and primary cortical neurons can bind Aβ and can support Aβ fibril formation on their surface (Yuyama et al., 2012). While consistent with the proposed Aβ seeding properties of EVs, EV-bound Aβ can also be taken up by microglia for degradation. *In vivo*, continuous intracerebral infusion of exogenous neuroblastoma-produced EVs apparently trapped and targeted for microglial phagocytosis sufficient Aβ in the brain of APP overexpressing transgenic mice to reduce Aβ levels, amyloid deposition, and synaptotoxicity in the hippocampus (Yuyama et al., 2014). These findings support the idea that the balance that determines whether EVs drive pathology spread or serve as a pathway for the removal of toxic molecules within the brain is likely to be dependent on how efficiently EVs are removed from the brain parenchyma.

The release of the materials contained in an EV may be of benefit to the cell releasing this material. We advance the idea that the appropriate modulation of exosome production is essential to the normal functioning of the endosomal–lysosomal pathway in a neuron. We argue for three overlapping mechanisms by which exosome production can be supportive of the function of the neuronal endosomal–lysosomal system: (1) the transport of beneficial endosomal–lysosomal cargo within the brain; (2) the removal from the lysosomal system of a neuron of potentially deleterious material for degradation by other cells within the brain; and (3) the maintenance of membrane and vesicular-content flux through a neuron's endosomal–lysosomal pathway.

Transporting Protective Endosomal–Lysosomal Cargo Within the Brain

Exosomes are unique in that their limiting membrane renders them more stable in the extracellular environment than is the case for secreted, soluble proteins (reviewed in Simpson et al., 2008). Therefore, the association of neuroprotective/neurotrophic proteins with exosomes likely prolongs the extracellular survival of these proteins, extending their ability to exert protective effects both over time and spatially within the brain. An illustrative example is the cysteine-protease inhibitor cystatin C (CysC), which is contained within the endosomal–lysosomal pathway and implicated in neuroprotection and repair in the nervous system in response to diverse insults (reviewed in Tizon and Levy, 2006; Gauthier et al., 2011; Mathews and Levy, 2016). CysC is also secreted from cells, both in a soluble form and in association with EVs, including exosomes (Ghidoni et al., 2011). We have recently demonstrated that CysC-containing, exosome-enriched EVs protect cultured cells from nutrient deprivation-induced death (Pérez-González et al., 2019). While both CysC-containing and CysC-deficient EVs were taken up by the cultured cells, only EVs containing CysC protected the cells. Interestingly, both exogenous CysC and transgene-mediated overexpression of CysC can promote the secretion of EVs by cultured cells (Pérez-González et al., 2019). Transgene overexpression of CysC also leads to higher EV levels in the brain, showing that this effect of CysC expression occurs *in vivo* (Pérez-González et al., 2019). Thus, the release of EV-associated CysC may lead to a positive-feedback loop further amplifying the protective effects of CysC within the brain. The exosome association of CysC and other neurotrophic proteins such progranulin, which is also both secreted and localized to the endosomal pathway (Benussi et al., 2016), likely prolongs the extracellular survival of these proteins, extending their ability to exert beneficial effects. We have shown that EVs secreted by CysC-deficient cells, subsequently loaded with exogenous CysC, significantly protected primary neurons from nutrients-deprivation-induced death (Pérez-González et al., 2019), revealing the potential for the loading of EVs with CysC and other neuroprotective proteins for clinical purposes.

Removal of Endosomal–Lysosomal Material From Neurons for Uptake by Phagocytic Cells and Subsequent Degradation

The production of exosomes moves lipids and proteins from the endosomal–lysosomal pathway into the extracellular space. Exosomes released by a neuron that are degraded by non-neuronal cells such as microglia or otherwise removed from the brain would result in the net elimination of neuronal endosomal–lysosomal content (Yuyama et al., 2012; Joshi et al., 2015). This would also limit neuron-to-neuron propagation of pathological molecules via exosomes (Yuyama et al., 2012; Joshi et al., 2015). Some studies have shown that EV uptake by microglia is more efficient than that by neurons (Fitzner et al., 2011; Yuyama et al., 2012). However, the relative contribution of different cell types to brain exosome uptake is not clear, and neuron-to-neuron exosome trafficking has been shown (Chivet et al., 2014). Indeed, the balance of beneficial clearance versus pathogenic propagation mediated by exosomes and EVs more generally is likely to be complex and dynamic over time, dependent upon such factors as outward CSF and interstitial fluid flux, localized inflammation and gliosis, and the activation status of microglia. As better tools are developed for labeling and tracking EVs *in vivo*, more details will emerge regarding the metabolism of brain EVs and the impact of aging and neurodegenerative diseases upon these processes.

Maintaining Flux Through the Endosomal-Autophagy-Lysosomal System

As previously noted, a fundamental effect of exosome production is to remove lipids and proteins from a cell's

endosomal–lysosomal pathway. Our recent findings, particularly in DS and APOE4 carriers, support the idea that exosome release plays an important role in maintaining endosomal–lysosomal function by allowing for an "outlet" other than degradation within the lysosome. We expand upon these findings in support of this idea throughout the following discussion, first summarizing the endosomal-autophagic-lysosomal changes seen in AD and then the effect DS and APOE4 expression has on exosome biology and the impact this has on the endosomal–lysosomal pathway.

AD Risk, Abnormalities of the Neuronal Endosomal–Lysosomal and Exosome Generation and Release

The neuronal endosomal–lysosomal and autophagy systems are vulnerable to pathogenic changes in AD (Troncoso et al., 1998; Cataldo et al., 2000, 2004; Nixon et al., 2008). Alterations in early and late endosomes include morphologic changes such as enlargement and increased endosome numbers (Cataldo et al., 2000), and are likely to include alterations in endocytosis and flux through endosomal compartments (Cataldo et al., 2008; Small, 2008; Jiang et al., 2010). Autophagic vacuoles accumulate in neurons during AD, most prominently in neuronal processes such as axons, often in proximity to β-amyloid plaques (Yang et al., 2011). Lysosomal alterations were the first AD-driven changes in this system to be described, and include proliferation of lysosomes and increased levels of lysosomal proteins, including degradative lysosomal hydrolases (Cataldo et al., 1995). Findings in mouse models as well as the progression of these changes as seen in human AD are generally consistent with an underlying failure of efficient lysosomal hydrolysis and of autophagosome-lysosome fusion. This failure in turnover is thus an important contributor to both autophagosome accumulation and the proliferation of apparently degradation-deficient lysosomes loaded with undigested material (Colacurcio et al., 2018). AD appears to compromise the efficient movement of cargo through the lysosomal system and its subsequent degradation.

Neuronal endosome enlargement and proliferation appears to be an earlier event than either autophagy or lysosome dysfunction, and endosomal pathway alterations are uniformly seen in late-onset AD cases (Cataldo et al., 2000; Colacurcio et al., 2018). While multiple mechanisms are likely to contribute to the vulnerability of this pathway in neurons during aging and early in AD pathobiology, two extensively studied genetic causes of AD-like endosomal changes are chromosome 21 trisomy in DS (Cataldo et al., 2000, 2004, 2008; Takahashi et al., 2004; Jiang et al., 2010) and inheritance of the APOE4 allele (Cataldo et al., 2000; Nuriel et al., 2017; Zhao et al., 2017), the most important genetic risk factor for AD (Corder et al., 1993; Farrer et al., 1997; Bu, 2009; Liu et al., 2013).

Once early endosomal cargoes are delivered to the late endosome there are two possible fates for these proteins and lipids: either lysosome degradation or packaging into exosomes for release. Exosome secretion has the potential to allow for flux through the endosomal–lysosomal pathway that is independent of lysosomal delivery. Moreover, a neuron's secreted exosomes can be degraded by other cells or removed from the brain into the periphery. Since the late endosome/MVB regulates endosomal trafficking to the lysosome as well as exosome production, it is not unexpected that changes in brain exosomes have been seen in systems showing AD-like endosomal–lysosomal pathway alterations. Our studies have focused on the effects of DS and APOE4 genotype upon brain exosomes, where we have identified changes in brain exosome production and secretion as well as changes in their protein and lipid constituents (Gauthier et al., 2017; Peng et al., 2019).

A similar integrated relationship has been well established between autophagy and the exosome pathway. Exosome biogenesis and autophagy are linked by their function: exosomes remove cytoplasmic cargo into the extracellular space while autophagy removes cytoplasmic components via lysosome-dependent degradation. Recent studies have revealed shared molecular machinery between exosome biogenesis and autophagy, as well as substantial crosstalk between these two processes via fusion of autophagosomes with MVBs to form amphisomes (reviewed in Xu et al., 2018). For example, knockout of the ESCRT member Alix, which is important for ILV formation, reduces not only exosome generation but also basal autophagy flux, demonstrating a shared regulation between autophagy and exosome biogenesis (Murrow et al., 2015).

Additionally, exosome release is negatively regulated by the mechanistic target of rapamycin complex 1 (mTORC1), the protein complex containing mTOR that acts as the cell's master nutrient and energy sensor to regulate protein synthesis and autophagy. Sustained activation of mTORC1 reduces the release of exosomes by cells and in animal models, resulting in the intracellular accumulation of ILVs. Conversely, exosome release is stimulated by inhibition of mTORC1 by rapamycin or nutrient and growth factor deprivation (Zou et al., 2019). Inhibition of autophagy by wortmannin or CRISPR/Cas9-mediated knockout of the autophagy protein Atg5 (autophagy-related 5) in neuronal cell lines increased the release of exosomes, documenting this interrelationship in neurons as well as other cell types (Dias et al., 2016).

A pathology relevant interrelationship between exosomal release and autophagy has been seen in cell culture models of α-synuclein aggregation and in α-synuclein transgenic mice: inhibiting autophagy with bafilomycin A reduced the intracellular aggregation of α-synuclein but increased the secretion of smaller oligomers that were predominantly released through exosomes (Poehler et al., 2014). Poehler et al. (2014) suggested that impaired autophagy in the diseased brain not only limits intracellular degradation of misfolded proteins such as α-synuclein, but can also lead to detrimental effects in the local microenvironment due to enhanced α-synuclein secretion. Similarly, inhibition of autophagosome formation by silencing ATG5 in α-synuclein, overexpressing neurons increased the secretion of exosome-associated α-synuclein while blocking exosomal secretion using GW4869 exacerbated α-synuclein-induced cell death (Fussi et al., 2018). Thus, exosomal secretion of α-synuclein is apparently increased after impaired formation of autophagosomes, which can reduce intracellular α-synuclein

burden and limit α-synuclein-induced neuronal cell death (Fussi et al., 2018). These findings document the interdependence of autophagy and the exosomal pathway while also highlighting the sometimes contradictory outcome of exosome release. Under pathological conditions, dysfunction of the endosomal–lysosomal and/or autophagic pathways can lead to changes in exosome generation and secretion, which may help to preserve needed flux through the system as a whole. This enhanced exosome production may be protective for the cell secreting the exosomes, yet potentially damaging to neighboring cells and within the local microenvironment.

Exosome Secretion Is Enhanced in the DS Brain

Given that an increase in early endosomal drive was demonstrated in DS, one would predict a necessary compensatory increase in either lysosome degradation or exosome release. Indeed, enhanced exosome secretion in DS would help to shed excessive neuronal endosomal content into the brain extracellular space (**Figure 2**). Endosomal pathology has been shown in human DS neurons, in neurons of DS mouse models, and in human DS fibroblasts in culture (Cataldo et al., 2000, 2004, 2008; Takahashi et al., 2004; Jiang et al., 2010). We have shown that higher levels of exosomes occur in each of these systems. In samples of frontal cortices of DS patients who did not have β-amyloid pathology, higher exosome levels in the brain parenchyma were found compared to age-matched diploid controls (Gauthier et al., 2017). Higher exosome levels were also found in the brain extracellular space of two DS mouse models, Ts[Rb(12.17^{16})]2Cje (Ts2) and Ts65n, as compared to diploid littermate controls (Gauthier et al., 2017). Examination of exosome secretion into the media of cultured human fibroblasts showed that these DS fibroblasts, which have AD-like endosomal abnormalities (Cataldo et al., 2008), secrete more EVs compared to age-matched diploid control fibroblasts (Gauthier et al., 2017).

While higher levels of exosomes in the growth media of DS fibroblast is consistent with the idea that DS cells produce greater numbers of exosomes, levels of exosomes in the brain are dependent upon both production and turnover. Recent findings argue that it is brain exosome production, and more specifically neuronal exosome production, which is higher in DS compared to diploid controls. Using high-resolution electron microscopy and quantitative analyses of MVBs in neurons of the frontal cortex of Ts2 mice, we recently showed that Ts2 MVBs are larger, more abundant, and contain a higher number of ILVs per neuron compared to littermate diploid controls (D'Acunzo et al., 2019). While not neuron specific, higher levels in Ts2 mice compared to controls of ILV proteins within the brain subcellular fractions that also contained endosomal markers corroborated these electron microscopy findings (D'Acunzo et al., 2019).

Further evidence for higher exosome production in DS has been provided by examining the expression of key molecular regulators of exosome biogenesis. The formation of ILVs in the late endosome/MVB is regulated by the ESCRT machinery and by an ESCRT independent system that includes tetraspanins (van Niel et al., 2011). Unlike most tetraspanins that are present in the plasma membrane, CD63 is uniquely enriched in the membrane of MVBs and of secreted exosomes (Pols and Klumperman, 2009; van Niel et al., 2011). Several Rab GTPases and SNARE proteins regulate the intracellular trafficking of MVBs toward the plasma membrane for fusion (Eitan et al., 2016). Among them, rab35 likely plays a role in the docking of MVBs to the plasma membrane (Hsu et al., 2010; Klinkert and Echard, 2016). Given the important role that these proteins play in exosome generation and secretion, changes in their expression levels within a cell or tissue are likely to reflect changes in ILV biogenesis and/or exosome secretion. While the expression levels of the ESCRT machinery proteins Alix and TSG101 did not differ in the brains of human DS patients and in DS fibroblasts as compared with diploid controls, the expression of other regulators of exosome production did differ. We have shown higher levels of CD63 and rab35 proteins in brain-tissue homogenates from human DS patients and the Ts2 mouse model compared to diploid controls (Gauthier et al., 2017). CD63 mRNA is up-regulated in the hippocampus of Ts2 mice (Gauthier et al., 2017), arguing that higher levels of CD63 in the brain represents higher expression levels of tetraspanin machinery driving ILV formation, not simply higher amount of CD63 associated with brain exosomes. In contrast, rab35 mRNA is not higher in the Ts2 hippocampus as compared with controls. Unlike CD63, rab35 is not tethered to secreted exosomes, remaining within the cell's cytoplasm after the fusion of the late endosome/MVB with the plasma membrane and therefore is found in secreted exosomes only in modest amounts (Gauthier et al., 2017). Thus while the amount of rab35 protein is higher, the cell's need for an ongoing, robust increase in rab35 expression is likely to be less than the need for CD63, which is consumed during exosome production, a difference that is reflected in the greater change in CD63 mRNA levels.

Together these findings in the brain support our model that exosome production itself is higher in DS (**Figure 2**) and are consistent with the finding that DS fibroblasts secret more exosomes into the cultured media compared to diploid control cells. Like DS brain, CD63 is overexpressed in DS fibroblasts (Gauthier et al., 2017). Importantly, while knockdown of CD63 expression in fibroblasts using interference RNA (siRNA) did not affect exosome secretion by wild-type diploid cells, reducing CD63 expression in DS cells led to reduced exosomes secretion into the cell culture media (Gauthier et al., 2017).

In addition to confirming that higher CD63 expression is necessary for the higher levels of exosome production by DS cells, this manipulation showcased the interdependence between endosomal pathway function and exosome production and secretion. While CD63 knockdown had no effect on exosome production or endosome morphology in diploid cells, CD63 knockdown led to a worsening of the early endosomal phenotype in DS fibroblasts, including further enlargement and increased numbers (Gauthier et al., 2017). This argues that partially blocking exosome generation in DS cells increases the intracellular accumulation of endosomal compartments, worsening the DS endosomal pathology. In contrast, silencing CD63 in normal cells without endosomal pathology did not affect exosome release or accumulation of endosomes, suggesting that

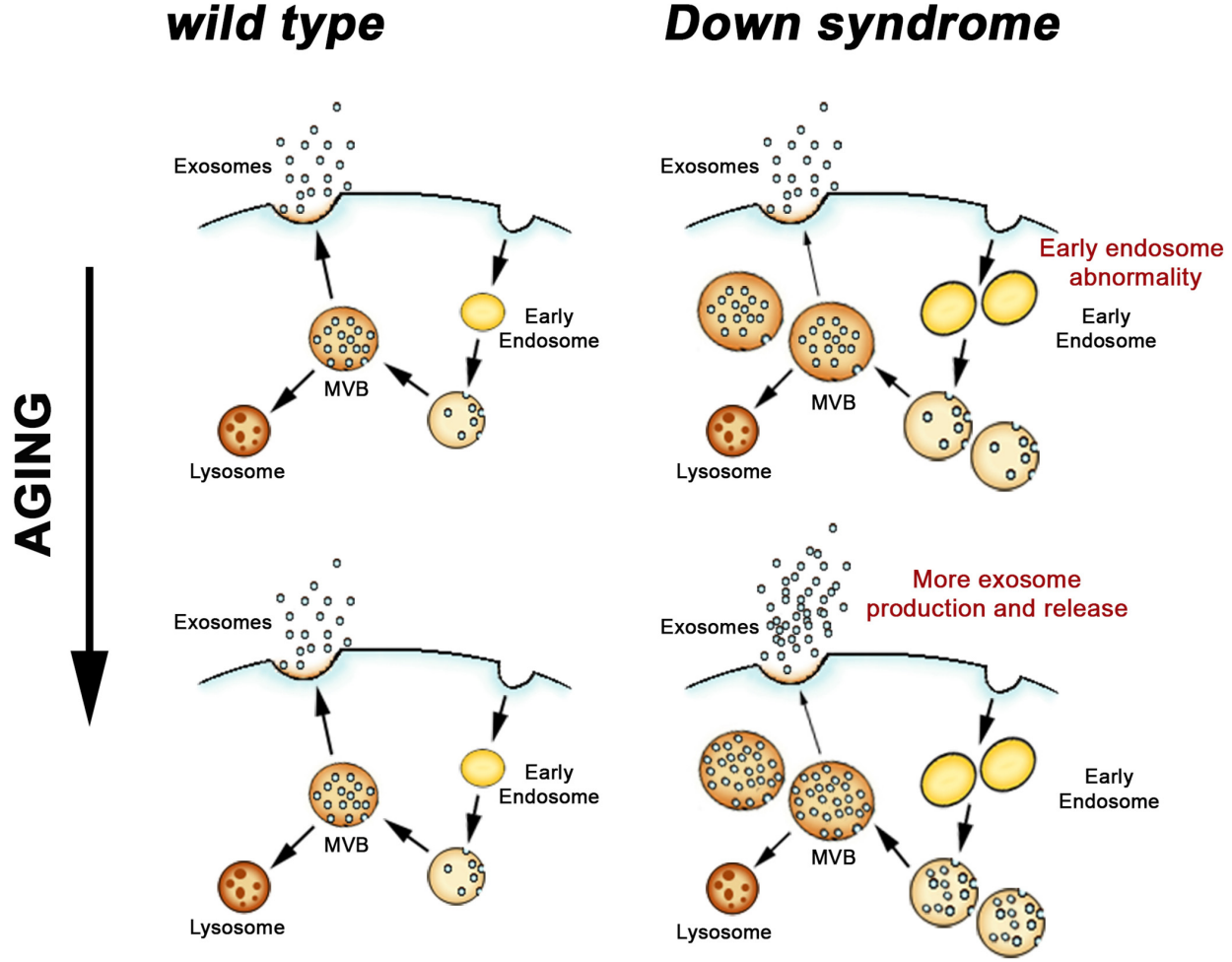

FIGURE 2 | Endosomal and exosomal changes in the DS brain. Endocytosed material is sorted through early endosomes and late endosomes/MVB for either degradation in lysosomes or exosomal secretion. In DS, where neuronal endosome dysfunction begins before birth, an age-dependent increase in exosome release appears to be a compensatory response to limit the extent of the endosomal pathway pathology that results from DS genetic effects.

homeostatic exosome release can be maintained in diploid cells even with a perturbation in the expression of a protein involved in exosome generation. CD63 levels may be particularly relevant to the formation of more ILVs when the endosomal-exosomal system is disrupted, as it is in DS.

These findings support our idea that the release of more exosomes by a DS cell allows the cell to regulate its endosomal pathway, albeit not to the point that normal endosomal function can be maintained (Gauthier et al., 2017). Suggesting that this may be a more generalized phenomenon, a recent study reported higher levels of another member of the tetraspanin family, tetraspanin-6, in the brains of AD patients (Guix et al., 2017). In the same study, tetraspanin-6 overexpression was linked *in vitro* to the generation of more exosomes (Guix et al., 2017). We propose that in DS, where endosome dysfunction begins before birth (Cataldo et al., 2000), greater ongoing exosome release moderates, but is not sufficient, to prevent endosomal pathology (**Figure 2**). These findings in DS emphasize the importance of endosomal-exosomal regulation as a risk factor for neurodegenerative disease and serve to reiterate the interdependence of the endosomal and exosomal pathways.

Exosome Production Is Compromised by APOE4 Expression

Of the three alleles of apolipoprotein E (APOE) (Mahley, 1988; Mahley and RallJr, 2000), APOE4 is the single most important genetic risk-factor for AD (Corder et al., 1993; Farrer et al., 1997; Bu, 2009; Liu et al., 2013). APOE3 is risk-neutral for AD (Corder et al., 1993; Mahley and RallJr, 2000; Liu et al., 2013) and APOE2 expression is associated with a lower risk of AD (Corder et al., 1994; Liu et al., 2013). Multiple mechanisms appear to drive the pathogenic effects of the APOE4 allele in the brain, including enhancing Aβ deposition while reducing Aβ clearance and degradation; modulating synaptic integrity; modulating cholesterol levels in the brain and the availability of cholesterol and other lipids to neurons; and inducing changes in reactive O_2 scavenging in the CNS (Strittmatter et al., 1993;

Ma et al., 1994; Bales et al., 1997; Higgins et al., 1997; Haan et al., 1999; Holtzman et al., 2000; Shibata et al., 2000; Bu, 2009; Kim et al., 2009; Kolovou et al., 2009; Andrews-Zwilling et al., 2010; Verghese et al., 2011; Villemagne et al., 2011; Leung et al., 2012; Mahley and Huang, 2012; Andrews et al., 2013; Liu et al., 2013; Reinvang et al., 2013; Zlokovic, 2013; Rodriguez et al., 2014). In the absence of a dementia diagnosis, human APOE4-carriers still display structural and functional differences within regions of the hippocampus and cortex, and cognitive decline compared to age-matched non-carriers (Bookheimer and Burggren, 2009; Filippini et al., 2009; Olofsson et al., 2010; Sheline et al., 2010; Wisdom et al., 2011; Liu et al., 2013; Di Battista et al., 2016), and mouse models show cognitive deficits linked to APOE4 expression without AD pathology (Leung et al., 2012; Peng et al., 2017; East et al., 2018).

Mice humanized for the expression of APOE4 do not develop β-amyloid or tau pathology (Wang et al., 2005). However, expression of APOE4 is sufficient to drive dysfunction of the neuronal endosomal–lysosomal pathway in these mouse models in comparison to APOE3 (Nuriel et al., 2017; Zhao et al., 2017). Cataldo et al. (2000) first suggested that APOE4 expression might impact neuronal endosomes when they reported more robust early endosome changes in cortical neurons when comparing APOE4 to APOE3 early stage AD patients. In a number of aspects the APOE4-driven endosomal disruption resembles that seen in DS, including an increase in size and a proliferation in the number of early endosomes (Nuriel et al., 2017; **Figure 3**). However, the DS endosomal pathway alterations appear to be independent of age and the overexpression of APP that is essential to this phenotype is sufficient to drive endosomal pathway changes in multiple cell types, both *in vivo* and *in vitro* (Cataldo et al., 2003; Salehi et al., 2006; Jiang et al., 2010). This appears not to be the case with APOE4 expression, where the *in vivo* neuronal early endosomal phenotype requires aging. Comparing layer II/III pyramidal neurons of the cingulate cortex of APOE4 to APOE3 mice, early endosomal changes were apparent at 18 months of age but not at 12 (Nuriel et al., 2017). The timing and aging-dependence of early endosome changes in APOE4 mice is particularly intriguing given our subsequent study examining APOE4 effects on brain exosome levels and production (Peng et al., 2019). In aged, non-AD human brain and brain tissue from humanized APOE mice, APOE4 expression decreased brain exosome levels (Peng et al., 2019). The mouse findings, however, showed that this decrease in brain exosome levels is aging-dependent, apparent at 12 but not evident at 6 months of age. 12 months of age is earlier than when endosomal changes were seen (Nuriel et al., 2017). Thus, a reduction in brain exosome levels precedes the neuronal endosomal changes in the brain of APOE4 expressing mice (**Figure 3**).

In contrast to the findings from DS mouse models, APOE4 expression results in a downregulation of exosome generation and secretion from the endosomal pathway. As we showed in Peng et al. (2019), APOE4 expression reduced both TSG101 and rab35 expression in the brains of aged mice. Decreasing the expression of ESCRT proteins such as TSG101 reduces exosome secretion *in vitro* (Colombo et al., 2013), and inhibition of rab35 *in vitro* leads to impaired exosome secretion by inhibiting fusion of the MVB with the cell membrane (Hsu et al., 2010). An interpretation of these findings from APOE4 mice that is consistent with these prior studies is that exosome biogenesis and secretion are reduced in the brain. Based upon the data from the mouse models, APOE4 expression appears to first disrupt exosome production, followed by broader neuronal endosomal–lysosomal system alterations.

The mechanism connecting expression of the lipid-carrier APOE4 with reduced expression of TSG101 and rab35, and therefore reduced exosome production, is not known. However, because APOE4 compared with APOE3 expression disrupts neuronal and peripheral cholesterol metabolism (Sing and Davignon, 1985; Michikawa et al., 2000), and membrane-lipid changes may compromise the endosomal-exosomal pathway, we examined EV lipids from the brains of humanized APOE mice. We found higher cholesterol levels in the EVs isolated from the brain of APOE4 compared with APOE3 mice, differences that likely reflect altered lipid metabolism within the endosomal pathway from which exosomes originate (Peng et al., 2019). The accumulation of lipids, including cholesterol, in endosomal and lysosomal vesicles occurs in AD and is pathogenic in a subset of genetic lysosomal storage disorders (Distl et al., 2001; Kuech et al., 2016). Increased membrane cholesterol levels, which can result in the secondary accumulation of sphingolipids, can disrupt the endosomal pathway affecting both the morphology and motility of endosomal compartments (Lebrand et al., 2002; Marquer et al., 2014). The functions of several rubs are known to be modulated by endosomal cholesterol levels (Choudhury et al., 2004; Glodowski et al., 2007). For example, endosomal cholesterol accumulation can disrupt MVB mobility and fusion by altering the function of rab7 (Lebrand et al., 2002; Chen and Lamb, 2008). Thus, APOE4-driven changes in cholesterol metabolism and therefore intracellular cholesterol levels may be directly associated with compromised exosome production (Peng et al., 2019). While it has not been determined whether rab35's function is also affected by cholesterol levels, the changes in rab35 levels in the brain of APOE4 mice (Peng et al., 2019) warrant further studies to determine whether it too is regulated by cholesterol levels in the MVB.

Showing that APOE4 leads to a failure in brain exosome production in an *in vivo* model lacking hallmark AD pathology (Peng et al., 2019) adds further to the evidence that the endosomal–lysosomal system within neurons is extensively disrupted by the expression of this allele (Nuriel et al., 2017). Functional changes within the endosomal–lysosomal system can result in the accumulation of debris in neuronal endosomes and lysosomes (Nixon, 2004), and it appears that dysfunction of this system is an important factor contributing to neuron vulnerability in multiple neurodegenerative disorders, including AD (Nixon, 2005; Schreij et al., 2016). We have proposed that releasing endosomal material into the extracellular space via exosomes can be an important mechanism by which neurons remove endosomal–lysosomal pathway debris (Peng et al., 2019). Indeed, in DS a failure in exosome production worsens the endosomal pathway disturbances (Gauthier et al., 2017). APOE4-driven failure of the neuronal endosomal–lysosomal and exosomal pathways during aging is likely to disturb essential

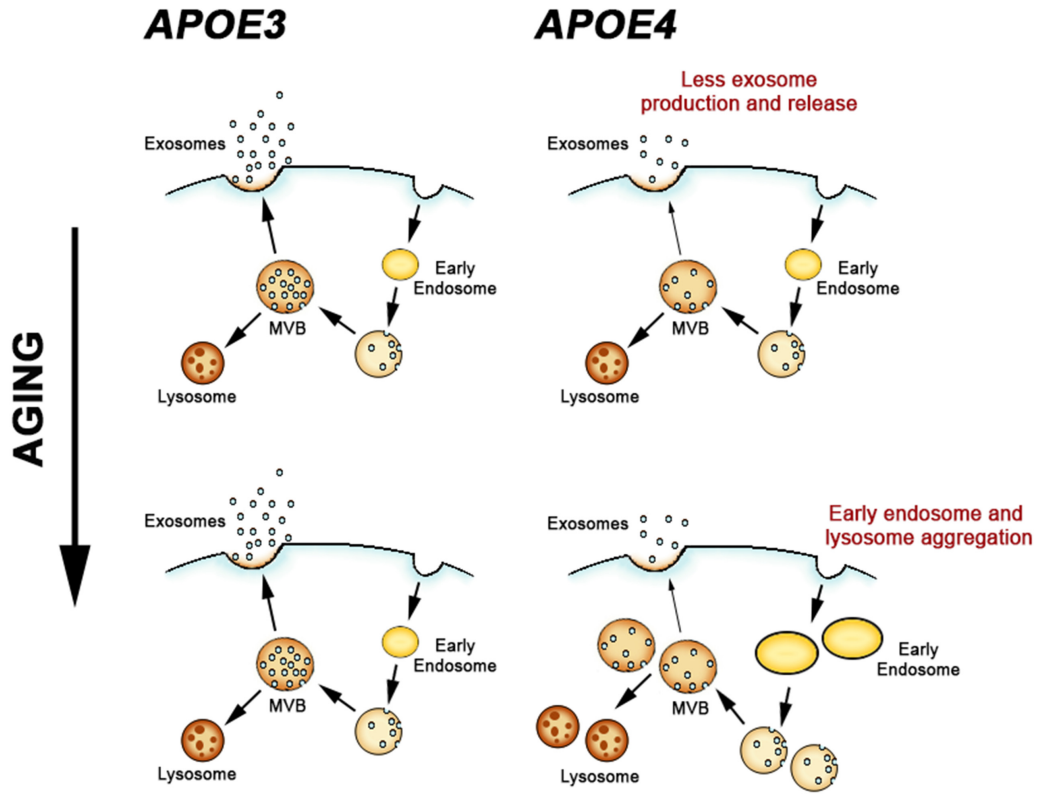

FIGURE 3 | Apolipoprotein E-genotype effects on the endosomal and exosomal pathways. APOE4 expression leads to a deficiency in exosome generation and release in the brain, which subsequently leads to pathogenic alterations in early endosomes and lysosomes during aging.

functions of this system, including the efficient degradation of unneeded cellular materials, thus contributing to the risk of neurodegenerative diseases such as AD (Nixon, 2017).

CONCLUSION

We have argued that in two AD relevant systems, DS and APOE4 expression, there is strong evidence linking alterations in the endosomal pathway with changes in exosome biology. This interrelationship has been demonstrated in neuronal systems, including the intact brain. These findings are consistent with a model in which flux through the exosomal pathway – i.e., ILV generation and fusion of the MVB with the cell surface to release exosomes – is an essential component of endosomal pathway integrity. In the case of DS, exosome biogenesis appears to be increased to partially compensate for increased endosomal pathway activity. APOE4 expression appears to reduce exosome production with a subsequent impact on the endosomal–lysosomal pathway. While it cannot be ruled out that in the diseased brain the protective effects of the exosome secretion on the endosomal pathway may be offset by the spread and seeding of toxic materials associated with exosomes, we would argue that it is misnomer to discuss exosomes exclusively in the context of promoting the spread and propagation of pathology in neurodegenerative disorders (Howitt and Hill, 2016; Xiao et al., 2017). Indeed, while reducing exosome secretion has been suggested as a potential therapeutic intervention for AD (Dinkins et al., 2014; Asai et al., 2015), our experimental findings in DS models (Gauthier et al., 2017) would argue that such an intervention would lead to greater endosomal pathway pathology, which is likely to be detrimental. Detrimental consequences of limiting exosome production have been shown in an *in vitro* model of α-synuclein pathology (Fussi et al., 2018) and *in vivo* in a transgenic mouse overexpressing a mutant form of the toxic protein TDP-43 (Iguchi et al., 2016). Finally, we have interpreted our findings with APOE4 expression to argue that enhanced exosome production would be protective, which emphasizes the risk of a therapeutic paradigm involving reduced exosome secretion. In summary, exosome production may be protective through the removal of endosomal–lysosomal material from a vulnerable neuron, where this material can be removed from the brain or degraded by support cells. Additionally, exosome secretion can help maintain the homeostatic function of the endosomal–lysosomal and autophagic pathways by offering an additional pathway for the flux of material when lysosomal degradation is insufficient. These beneficial effects of exosome production are most apparent to the neuron secreting the exosomes and are likely to be important in mitigating aging vulnerability to a neuron's endosomal-autophagy-lysosomal system and the vulnerability this systems sees due to AD.

In this review, we argue that the interrelationship between the endosomal-autophagic-lysosomal system and exosome release has important implications for the survival of neuronal cells. The potential for exosomes to relieve neurons of accumulated, toxic material argues for the importance of developing drugs that can enhance their release. While such compounds are not currently available, greater insight into the biology that drives exosome production as well as exosome clearance in the brain will hopefully guide the therapeutic strategies that can maintain or, in a neurodegenerative disease, restore the integrity of the endosomal-exosomal pathway. Solid evidence has emerged that maintaining the integrity of the overall lysosomal system is critical for the wellbeing of neurons. Tapping into the exosomal pathway appears to be one way to support the stability of this system during aging and with disease.

AUTHOR CONTRIBUTIONS

PM and EL conceived the review and wrote the manuscript.

FUNDING

This work was supported by the NIH (P01 AG017617, RF1 AG057517, R56 AG052524, and R01 AG056732).

ACKNOWLEDGMENTS

The authors thank Drs. Pasquale D'Acunzo and Chris N. Goulbourne for the electron micrograph (**Figure 1**) and Dr. Katherine Y. Peng for the graphic drawings in **Figures 1**, **2**.

REFERENCES

Alvarez-Erviti, L., Seow, Y., Schapira, A. H., Gardiner, C., Sargent, I. L., Wood, M. J., et al. (2011). Lysosomal dysfunction increases exosome-mediated α-synuclein release and transmission. *Neurobiol. Dis.* 42, 360–367. doi: 10.1016/j.nbd.2011.01.029

Andrews, K. A., Modat, M., Macdonald, K. E., Yeatman, T., Cardoso, M. J., Leung, K. K., et al. (2013). Atrophy rates in asymptomatic amyloidosis: implications for Alzheimer prevention trials. *PLoS One* 8:e58816. doi: 10.1371/journal.pone.0058816

Andrews, N. W. (2000). Regulated secretion of conventional lysosomes. *Trends Cell Biol.* 10, 316–321. doi: 10.1016/s0962-8924(00)01794-3

Andrews-Zwilling, Y., Bien-Ly, N., Xu, Q., Li, G., Bernardo, A., Yoon, S. Y., et al. (2010). Apolipoprotein E4 causes age- and Tau-dependent impairment of GABAergic interneurons, leading to learning and memory deficits in mice. *J. Neurosci.* 30, 13707–13717. doi: 10.1523/JNEUROSCI.4040-10.2010

Asai, H., Ikezu, S., Tsunoda, S., Medalla, M., Luebke, J., Haydar, T., et al. (2015). Depletion of microglia and inhibition of exosome synthesis halt tau propagation. *Nat. Neurosci.* 18, 1584–1593. doi: 10.1038/nn.4132

Bakhti, M., Winter, C., and Simons, M. (2011). Inhibition of myelin membrane sheath formation by oligodendrocyte-derived exosome-like vesicles. *J. Biol. Chem.* 286, 787–796. doi: 10.1074/jbc.M110.190009

Bales, K. R., Verina, T., Dodel, R. C., Du, Y., Altstiel, L., Bender, M., et al. (1997). Lack of apolipoprotein E dramatically reduces amyloid (-peptide deposition. *Nat. Genet.* 17, 263–264. doi: 10.1038/ng1197-263

Benussi, L., Ciani, M., Tonoli, E., Morbin, M., Palamara, L., Albani, D., et al. (2016). Loss of exosomes in progranulin-associated frontotemporal dementia. *Neurobiol. Aging* 40, 41–49. doi: 10.1016/j.neurobiolaging.2016.01.001

Bookheimer, S., and Burggren, A. (2009). APOE-4 genotype and neurophysiological vulnerability to Alzheimer's and cognitive aging. *Annu. Rev. Clin. Psychol.* 5, 343–362. doi: 10.1146/annurev.clinpsy.032408.153625

Borroto-Escuela, D. O., Agnati, L. F., Bechter, K., Jansson, A., Tarakanov, A. O., and Fuxe, K. (2015). The role of transmitter diffusion and flow versus extracellular vesicles in volume transmission in the brain neural-glial networks. *Philos. Trans. R. Soc. Lond. B Biol. Sci.* 370, 20140183. doi: 10.1098/rstb.2014.0183

Bu, G. (2009). Apolipoprotein E and its receptors in Alzheimer's disease: pathways, pathogenesis and therapy. *Nat. Rev. Neurosci.* 10, 333–344. doi: 10.1038/nrn2620

Budnik, V., Ruiz-Canada, C., and Wendler, F. (2016). Extracellular vesicles round off communication in the nervous system. *Nat. Rev. Neurosci.* 17, 160–172. doi: 10.1038/nrn.2015.29

Cataldo, A. M., Barnett, J. L., Berman, S. A., Li, J., Quarless, S., Bursztajn, S., et al. (1995). Gene expression and cellular content of cathepsin D in Alzheimer's disease brain: evidence for early up-regulation of the endosomal-lysosomal system. *Neuron* 14, 671–680. doi: 10.1016/0896-6273(95)90324-0

Cataldo, A. M., Mathews, P. M., Boiteau, A. B., Hassinger, L. C., Peterhoff, C. M., Jiang, Y., et al. (2008). Down syndrome fibroblast model of Alzheimer-related endosome pathology: accelerated endocytosis promotes late endocytic defects. *Am. J. Pathol.* 173, 370–384. doi: 10.2353/ajpath.2008.071053

Cataldo, A. M., Petanceska, S., Peterhoff, C. M., Terio, N. B., Epstein, C. J., Villar, A., et al. (2003). App gene dosage modulates endosomal abnormalities of Alzheimer's disease in a segmental trisomy 16 mouse model of down syndrome. *J. Neurosci.* 23, 6788–6792. doi: 10.1523/jneurosci.23-17-06788.2003

Cataldo, A. M., Petanceska, S., Terio, N. B., Peterhoff, C. M., Durham, R., Mercken, M., et al. (2004). Aβ localization in abnormal endosomes: association with earliest Aβ elevations in AD and Down syndrome. *Neurobiol. Aging* 25, 1263–1272. doi: 10.1016/j.neurobiolaging.2004.02.027

Cataldo, A. M., Peterhoff, C. M., Troncoso, J. C., Gomez-Isla, T., Hyman, B. T., and Nixon, R. A. (2000). Endocytic pathway abnormalities precede amyloid β deposition in sporadic Alzheimer's disease and Down syndrome: differential effects of APOE genotype and presenilin mutations. *Am. J. Pathol.* 157, 277–286. doi: 10.1016/s0002-9440(10)64538-5

Chen, B. J., and Lamb, R. A. (2008). Mechanisms for enveloped virus budding: can some viruses do without an ESCRT? *Virology* 372, 221–232. doi: 10.1016/j.virol.2007.11.008

Chivet, M., Javalet, C., Laulagnier, K., Blot, B., Hemming, F. J., and Sadoul, R. (2014). Exosomes secreted by cortical neurons upon glutamatergic synapse activation specifically interact with neurons. *J. Extracell. Vesicles* 3:24722. doi: 10.3402/jev.v3.24722

Choudhury, A., Sharma, D. K., Marks, D. L., and Pagano, R. E. (2004). Elevated endosomal cholesterol levels in Niemann-Pick cells inhibit rab4 and perturb membrane recycling. *Mol. Biol. Cell* 15, 4500–4511. doi: 10.1091/mbc.e04-05-0432

Colacurcio, D. J., Pensalfini, A., Jiang, Y., and Nixon, R. A. (2018). Dysfunction of autophagy and endosomal-lysosomal pathways: roles in pathogenesis of Down syndrome and Alzheimer's Disease. *Free Radic. Biol. Med.* 114, 40–51. doi: 10.1016/j.freeradbiomed.2017.10.001

Colombo, M., Moita, C., van Niel, G., Kowal, J., Vigneron, J., Benaroch, P., et al. (2013). Analysis of ESCRT functions in exosome biogenesis, composition and secretion highlights the heterogeneity of extracellular vesicles. *J. Cell Sci.* 126(Pt 24), 5553–5565. doi: 10.1242/jcs.128868

Colombo, M., Raposo, G., and Thery, C. (2014). Biogenesis, secretion, and intercellular interactions of exosomes and other extracellular vesicles. *Annu. Rev. Cell Dev. Biol.* 30, 255–289. doi: 10.1146/annurev-cellbio-101512-122326

Corder, E. H., Saunders, A. M., Risch, N. J., Strittmatter, W. J., Schmechel, D. E., Gaskell, P. C., et al. (1994). Protective effect of apolipoprotein E type 2 allele for late onset Alzheimer's Disease. *Nat. Genet.* 7, 180–184. doi: 10.1038/ng0694-180

Corder, E. H., Saunders, A. M., Strittmatter, W. J., Schmechel, D. E., Gaskell, P. C., Small, G. W., et al. (1993). Gene dose of apolipoprotein E type 4 allele and the risk of Alzheimer's disease in late onset families. *Science* 261, 921–923. doi: 10.1126/science.8346443

D'Acunzo, P., Hargash, T., Pawlik, M., Goulbourne, C. N., Pérez-González, R., and Levy, E. (2019). Enhanced generation of intraluminal vesicles in neuronal late

endosomes in the brain of a down syndrome mouse model with endosomal dysfunction. *Dev. Neurobiol* 79, 656–663. doi: 10.1002/dneu.22708

Danzer, K. M., Kranich, L. R., Ruf, W. P., Cagsal-Getkin, O., Winslow, A. R., Zhu, L., et al. (2012). Exosomal cell-to-cell transmission of α synuclein oligomers. *Mol. Neurodegener* 7:42. doi: 10.1186/1750-1326-7-42

Deyts, C., Vetrivel, K. S., Das, S., Shepherd, Y. M., Dupre, D. J., Thinakaran, G., et al. (2012). Novel GalphaS-protein signaling associated with membrane-tethered amyloid precursor protein intracellular domain. *J. Neurosci.* 32, 1714–1729. doi: 10.1523/JNEUROSCI.5433-11.2012

Di Battista, A. M., Heinsinger, N. M., and Rebeck, G. W. (2016). Alzheimer's disease genetic risk factor APOE-ε4 also affects normal brain function. *Curr. Alzheimer Res.* 13, 1200–1207. doi: 10.2174/1567205013666160401115127

Dias, M. V., Teixeira, B. L., Rodrigues, B. R., Sinigaglia-Coimbra, R., Porto-Carreiro, I., Roffe, M., et al. (2016). PRNP/prion protein regulates the secretion of exosomes modulating CAV1/caveolin-1-suppressed autophagy. *Autophagy* 12, 2113–2128. doi: 10.1080/15548627.2016.1226735

Dinkins, M. B., Dasgupta, S., Wang, G., Zhu, G., and Bieberich, E. (2014). Exosome reduction in vivo is associated with lower amyloid plaque load in the 5XFAD mouse model of Alzheimer's disease. *Neurobiol. Aging* 35, 1792–1800. doi: 10.1016/j.neurobiolaging.2014.02.012

Distl, R., Meske, V., and Ohm, T. G. (2001). Tangle-bearing neurons contain more free cholesterol than adjacent tangle-free neurons. *Acta Neuropathol.* 101, 547–554.

East, B. S., Fleming, G., Peng, K., Olofsson, J. K., Levy, E., Mathews, P. M., et al. (2018). Human apolipoprotein E genotype differentially affects olfactory behavior and sensory physiology in mice. *Neuroscience* 380, 103–110. doi: 10.1016/j.neuroscience.2018.04.009

Eitan, E., Suire, C., Zhang, S., and Mattson, M. P. (2016). Impact of lysosome status on extracellular vesicle content and release. *Ageing Res. Rev.* 32, 65–74. doi: 10.1016/j.arr.2016.05.001

Emmanouilidou, E., Melachroinou, K., Roumeliotis, T., Garbis, S. D., Ntzouni, M., Margaritis, L. H., et al. (2010). Cell-produced α-synuclein is secreted in a calcium-dependent manner by exosomes and impacts neuronal survival. *J. Neurosci.* 30, 6838–6851. doi: 10.1523/JNEUROSCI.5699-09.2010

Escrevente, C., Morais, V. A., Keller, S., Soares, C. M., Altevogt, P., and Costa, J. (2008). Functional role of N-glycosylation from ADAM10 in processing, localization and activity of the enzyme. *Biochim. Biophys. Acta* 1780, 905–913. doi: 10.1016/j.bbagen.2008.03.004

Farrer, L. A., Cupples, L. A., Haines, J. L., Hyman, B., Kukull, W. A., Mayeux, R., et al. (1997). Effects of age, sex, and ethnicity on the association between apolipoprotein E genotype and Alzheimer disease. A meta-analysis. APOE and Alzheimer disease meta analysis consortium. *JAMA* 278, 1349–1356. doi: 10.1001/jama.278.16.1349

Faure, J., Lachenal, G., Court, M., Hirrlinger, J., Chatellard-Causse, C., Blot, B., et al. (2006). Exosomes are released by cultured cortical neurones. *Mol. Cell Neurosci.* 31, 642–648. doi: 10.1016/j.mcn.2005.12.003

Filippini, N., Rao, A., Wetten, S., Gibson, R. A., Borrie, M., Guzman, D., et al. (2009). Anatomically-distinct genetic associations of APOE ε4 allele load with regional cortical atrophy in Alzheimer's disease. *Neuroimage* 44, 724–728. doi: 10.1016/j.neuroimage.2008.10.003

Fitzner, D., Schnaars, M., van Rossum, D., Krishnamoorthy, G., Dibaj, P., Bakhti, M., et al. (2011). Selective transfer of exosomes from oligodendrocytes to microglia by macropinocytosis. *J. Cell Sci.* 124(Pt 3), 447–458. doi: 10.1242/jcs.074088

Flammang, B., Pardossi-Piquard, R., Sevalle, J., Debayle, D., Dabert-Gay, A. S., Thevenet, A., et al. (2012). Evidence that the amyloid-β protein precursor intracellular domain, AICD, derives from β-secretase-generated C-terminal fragment. *J. Alzheimers Dis.* 30, 145–153. doi: 10.3233/jad-2012-112186

Fussi, N., Hollerhage, M., Chakroun, T., Nykanen, N. P., Rosler, T. W., Koeglsperger, T., et al. (2018). Exosomal secretion of α-synuclein as protective mechanism after upstream blockage of macroautophagy. *Cell Death Dis.* 9:757. doi: 10.1038/s41419-018-0816-2

Gauthier, S., Kaur, G., Mi, W., Tizon, B., and Levy, E. (2011). Protective mechanisms by cystatin C in neurodegenerative diseases. *Front. Biosci.* 3:541–554. doi: 10.2741/s170

Gauthier, S. A., Pérez-González, R., Sharma, A., Huang, F. K., Alldred, M. J., Pawlik, M., et al. (2017). Enhanced exosome secretion in Down syndrome brain - a protective mechanism to alleviate neuronal endosomal abnormalities. *Acta Neuropathol. Commun.* 5:65. doi: 10.1186/s40478-017-0466-0

Ghidoni, R., Paterlini, A., Albertini, V., Glionna, M., Monti, E., Schiaffonati, L., et al. (2011). Cystatin C is released in association with exosomes: a new tool of neuronal communication which is unbalanced in Alzheimer's disease. *Neurobiol. Aging* 32, 1435–1442. doi: 10.1016/j.neurobiolaging.2009.08.013

Glodowski, D. R., Chen, C. C., Schaefer, H., Grant, B. D., and Rongo, C. (2007). RAB-10 regulates glutamate receptor recycling in a cholesterol-dependent endocytosis pathway. *Mol. Biol. Cell* 18, 4387–4396. doi: 10.1091/mbc.e07-05-0486

Goetzl, E. J., Boxer, A., Schwartz, J. B., Abner, E. L., Petersen, R. C., Miller, B. L., et al. (2015). Altered lysosomal proteins in neural-derived plasma exosomes in preclinical Alzheimer disease. *Neurology* 85, 40–47. doi: 10.1212/WNL.0000000000001702

Gould, S. J., Booth, A. M., and Hildreth, J. E. (2003). The Trojan exosome hypothesis. *Proc. Natl. Acad. Sci. U.SA.* 100, 10592–10597. doi: 10.1073/pnas.1831413100

Grozdanov, V., and Danzer, K. M. (2018). Release and uptake of pathologic α-synuclein. *Cell Tissue Res.* 373, 175–182. doi: 10.1007/s00441-017-2775-9

Guix, F. X., Corbett, G. T., Cha, D. J., Mustapic, M., Liu, W., Mengel, D., et al. (2018). Detection of aggregation-competent Tau in neuron-derived extracellular vesicles. *Int. J. Mol. Sci.* 19:E663. doi: 10.3390/ijms19030663

Guix, F. X., Sannerud, R., Berditchevski, F., Arranz, A. M., Horre, K., Snellinx, A., et al. (2017). Tetraspanin 6: a pivotal protein of the multiple vesicular body determining exosome release and lysosomal degradation of amyloid precursor protein fragments. *Mol. Neurodegener.* 12:25. doi: 10.1186/s13024-017-0165-0

Haan, M. N., Shemanski, L., Jagust, W. J., Manolio, T. A., and Kuller, L. (1999). The role of APOE ε4 in modulating effects of other risk factors for cognitive decline in elderly persons. *JAMA* 282, 40–46.

Higgins, G. A., Large, C. H., Rupniak, H. T., and Barnes, J. C. (1997). Apolipoprotein E and Alzheimer's disease: a review of recent studies. *Pharmacol. Biochem. Behav.* 56, 675–685.

Holtzman, D. M., Bales, K. R., Tenkova, T., Fagan, A. M., Parsadanian, M., Sartorius, L. J., et al. (2000). Apolipoprotein E isoform-dependent amyloid deposition and neuritic degeneration in a mouse model of Alzheimer's disease. *Proc. Natl. Acad. Sci. U.S.A.* 97, 2892–2897. doi: 10.1073/pnas.050004797

Howitt, J., and Hill, A. F. (2016). Exosomes in the Pathology of Neurodegenerative diseases. *J. Biol. Chem.* 291, 26589–26597. doi: 10.1074/jbc.R116.757955

Hsu, C., Morohashi, Y., Yoshimura, S., Manrique-Hoyos, N., Jung, S., Lauterbach, M. A., et al. (2010). Regulation of exosome secretion by Rab35 and its GTPase-activating proteins TBC1D10A-C. *J. Cell Biol.* 189, 223–232. doi: 10.1083/jcb.200911018

Iguchi, Y., Eid, L., Parent, M., Soucy, G., Bareil, C., Riku, Y., et al. (2016). Exosome secretion is a key pathway for clearance of pathological TDP-43. *Brain* 139(Pt 12), 3187–3201. doi: 10.1093/brain/aww237

Ihara, Y., Morishima-Kawashima, M., and Nixon, R. (2012). The ubiquitin-proteasome system and the autophagic-lysosomal system in Alzheimer disease. *Cold Spring Harb. Perspect. Med.* 2, a006361. doi: 10.1101/cshperspect.a006361

Izquierdo-Useros, N., Naranjo-Gomez, M., Erkizia, I., Puertas, M. C., Borras, F. E., Blanco, J., et al. (2011). HIV and mature dendritic cells: trojan exosomes riding the Trojan horse? *PLoS Pathog.* 6:e1000740. doi: 10.1371/journal.ppat.1000740

Jiang, Y., Mullaney, K. A., Peterhoff, C. M., Che, S., Schmidt, S. D., Boyer-Boiteau, A., et al. (2010). Alzheimer's-related endosome dysfunction in Down syndrome is Aβ -independent but requires APP and is reversed by BACE-1 inhibition. *Proc. Natl. Acad. Sci. U.S.A.* 107, 1630–1635. doi: 10.1073/pnas.0908953107

Jiang, Y., Rigoglioso, A., Peterhoff, C. M., Pawlik, M., Sato, Y., Bleiwas, C., et al. (2016). Partial BACE1 reduction in a down syndrome mouse model blocks Alzheimer-related endosomal anomalies and cholinergic neurodegeneration: role of APP-CTF. *Neurobiol. Aging* 39, 90–98. doi: 10.1016/j.neurobiolaging.2015.11.013

Jiang, Y., Sato, Y., Im, E., Berg, M., Bordi, M., Darji, S., et al. (2019). Lysosomal dysfunction in Down syndrome is APP-dependent and mediated by APP-βCTF (C99). *J. Neurosci.* 39, 5255–5268. doi: 10.1523/JNEUROSCI.0578-19.2019

Johnstone, R. M., Adam, M., Hammond, J. R., Orr, L., and Turbide, C. (1987). Vesicle formation during reticulocyte maturation. Association of plasma membrane activities with released vesicles (exosomes). *J. Biol. Chem.* 262, 9412–9420.

Joshi, P., Benussi, L., Furlan, R., Ghidoni, R., and Verderio, C. (2015). Extracellular vesicles in Alzheimer's disease: friends or foes? Focus on Aβ-vesicle interaction. *Int. J. Mol. Sci.* 16, 4800–4813. doi: 10.3390/ijms16034800

Kalra, H., Drummen, G. P., and Mathivanan, S. (2016). Focus on extracellular vesicles: introducing the next small big thing. *Int. J. Mol. Sci.* 17:170. doi: 10.3390/ijms17020170

Kim, J., Basak, J. M., and Holtzman, D. M. (2009). The role of apolipoprotein E in Alzheimer's disease. *Neuron* 63, 287–303. doi: 10.1016/j.neuron.2009.06.026

Kinoshita, A., Fukumoto, H., Shah, T., Whelan, C. M., Irizarry, M. C., and Hyman, B. T. (2003). Demonstration by FRET of BACE interaction with the amyloid precursor protein at the cell surface and in early endosomes. *J. Cell Sci.* 116(Pt 16), 3339–3346. doi: 10.1242/jcs.00643

Klinkert, K., and Echard, A. (2016). Rab35 GTPase: a central regulator of phosphoinositides and F-actin in endocytic recycling and beyond. *Traffic* 17, 1063–1077. doi: 10.1111/tra.12422

Kolovou, G., Damaskos, D., Anagnostopoulou, K., and Cokkinos, D. V. (2009). Apolipoprotein E gene polymorphism and gender. *Ann. Clin. Lab. Sci.* 39, 120–133.

Koo, E. H. (2002). The β-amyloid precursor protein (APP) and Alzheimer's disease: does the tail wag the dog? *Traffic* 3, 763–770. doi: 10.1034/j.1600-0854.2002.31101.x

Kowal, J., Tkach, M., and Thery, C. (2014). Biogenesis and secretion of exosomes. *Curr. Opin. Cell Biol.* 29, 116–125. doi: 10.1016/j.ceb.2014.05.004

Kramer-Albers, E. M., and Hill, A. F. (2016). Extracellular vesicles: interneural shuttles of complex messages. *Curr. Opin. Neurobiol.* 39, 101–107. doi: 10.1016/j.conb.2016.04.016

Kreimer, S., Belov, A. M., Ghiran, I., Murthy, S. K., Frank, D. A., and Ivanov, A. R. (2015). Mass-spectrometry-based molecular characterization of extracellular vesicles: lipidomics and proteomics. *J. Proteome Res.* 14, 2367–2384. doi: 10.1021/pr501279t

Kuech, E. M., Brogden, G., and Naim, H. Y. (2016). Alterations in membrane trafficking and pathophysiological implications in lysosomal storage disorders. *Biochimie* 130, 152–162. doi: 10.1016/j.biochi.2016.09.011

Lai, R. C., Tan, S. S., Yeo, R. W., Choo, A. B., Reiner, A. T., Su, Y., et al. (2016). MSC secretes at least 3 EV types each with a unique permutation of membrane lipid, protein and RNA. *J. Extracell. Vesicles* 5:29828. doi: 10.3402/jev.v5.29828

Laulagnier, K., Javalet, C., Hemming, F. J., Chivet, M., Lachenal, G., Blot, B., et al. (2018). Amyloid precursor protein products concentrate in a subset of exosomes specifically endocytosed by neurons. *Cell Mol. Life Sci.* 75, 757–773. doi: 10.1007/s00018-017-2664-0

Lauritzen, I., Pardossi-Piquard, R., Bauer, C., Brigham, E., Abraham, J. D., Ranaldi, S., et al. (2012). The β-secretase-derived C-terminal fragment of βAPP, C99, but not Aβ, is a key contributor to early intraneuronal lesions in triple-transgenic mouse hippocampus. *J. Neurosci.* 32, 16243–16255. doi: 10.1523/jneurosci.2775-12.2012

Lauritzen, I., Pardossi-Piquard, R., Bourgeois, A., Pagnotta, S., Biferi, M. G., Barkats, M., et al. (2016). Intraneuronal aggregation of the β-CTF fragment of APP (C99) induces Aβ-independent lysosomal-autophagic pathology. *Acta Neuropathol.* 132, 257–276. doi: 10.1007/s00401-016-1577-6

Lebrand, C., Corti, M., Goodson, H., Cosson, P., Cavalli, V., Mayran, N., et al. (2002). Late endosome motility depends on lipids via the small GTPase Rab7. *Embo. J.* 21, 1289–1300. doi: 10.1093/emboj/21.6.1289

Lee, S. H., Shin, S. M., Zhong, P., Kim, H. T., Kim, D. I., Kim, J. M., et al. (2018). Reciprocal control of excitatory synapse numbers by Wnt and Wnt inhibitor PRR7 secreted on exosomes. *Nat. Commun.* 9:3434. doi: 10.1038/s41467-018-05858-2

Leung, L., Andrews-Zwilling, Y., Yoon, S. Y., Jain, S., Ring, K., Dai, J., et al. (2012). Apolipoprotein E4 causes age- and sex-dependent impairments of hilar GABAergic interneurons and learning and memory deficits in mice. *PLoS One* 7:e53569. doi: 10.1371/journal.pone.0053569

Liu, C. C., Kanekiyo, T., Xu, H., and Bu, G. (2013). Apolipoprotein E and Alzheimer disease: risk, mechanisms and therapy. *Nat. Rev. Neurol.* 9, 106–118. doi: 10.1038/nrneurol.2012.263

Ma, J., Yee, A., Brewer, H. B. Jr., Das, S., and Potter, H. (1994). Amyloid-associated proteins α 1-antichymotrypsin and apolipoprotein E promote assembly of Alzheimer (-protein into filaments. *Nature* 372, 92–94. doi: 10.1038/372092a0

Mahley, R. W. (1988). Apolipoprotein E: cholesterol transport protein with expanding role in cell biology. *Science* 240, 622–630. doi: 10.1126/science.3283935

Mahley, R. W., and Huang, Y. (2012). Apolipoprotein E sets the stage: response to injury triggers neuropathology. *Neuron* 76, 871–885. doi: 10.1016/j.neuron.2012.11.020

Mahley, R. W., and Rall, S. C. Jr. (2000). Apolipoprotein E: far more than a lipid transport protein. *Annu. Rev. Genomics. Hum. Genet.* 1, 507–537. doi: 10.1146/annurev.genom.1.1.507

Marquer, C., Laine, J., Dauphinot, L., Hanbouch, L., Lemercier-Neuillet, C., Pierrot, N., et al. (2014). Increasing membrane cholesterol of neurons in culture recapitulates Alzheimer's disease early phenotypes. *Mol. Neurodegener.* 9:60. doi: 10.1186/1750-1326-9-60

Mathews, P. M., and Levy, E. (2016). Cystatin C in aging and in Alzheimer's disease. *Ageing Res. Rev.* 32, 38–50. doi: 10.1016/j.arr.2016.06.003

McPhie, D. L., Golde, T., Eckman, C. B., Yager, D., Brant, J. B., and Neve, R. L. (2001). β-secretase cleavage of the amyloid precursor protein mediates neuronal apoptosis caused by familial Alzheimer's disease mutations. *Brain Res. Mol. Brain Res.* 97, 103–113. doi: 10.1016/s0169-328x(01)00294-7

Michikawa, M., Fan, Q. W., Isobe, I., and Yanagisawa, K. (2000). Apolipoprotein E exhibits isoform-specific promotion of lipid efflux from astrocytes and neurons in culture. *J. Neurochem.* 74, 1008–1016. doi: 10.1046/j.1471-4159.2000.0741008.x

Migliano, S. M., and Teis, D. (2018). ESCRT and Membrane Protein Ubiquitination. *Prog. Mol. Subcell. Biol.* 57, 107–135. doi: 10.1007/978-3-319-96704-2_4

Miranda, A. M., Lasiecka, Z. M., Xu, Y., Neufeld, J., Shahriar, S., Simoes, S., et al. (2018). Neuronal lysosomal dysfunction releases exosomes harboring APP C-terminal fragments and unique lipid signatures. *Nat. Commun.* 9:291. doi: 10.1038/s41467-017-02533-w

Murrow, L., Malhotra, R., and Debnath, J. (2015). ATG12-ATG3 interacts with Alix to promote basal autophagic flux and late endosome function. *Nat. Cell Biol.* 17, 300–310. doi: 10.1038/ncb3112

Neve, R. L., Boyce, F. M., McPhie, D. L., Greenan, J., and Oster-Granite, M. L. (1996). Transgenic mice expressing APP-C100 in the brain. *Neurobiol. Aging* 17, 191–203. doi: 10.1016/0197-4580(95)02074-8

Neve, R. L., and Robakis, N. K. (1998). Alzheimer's disease: a re-examination of the amyloid hypothesis. *Trends Neurosci.* 21, 15–19. doi: 10.1016/s0166-2236(97)01168-5

Ngolab, J., Trinh, I., Rockenstein, E., Mante, M., Florio, J., Trejo, M., et al. (2017). Brain-derived exosomes from dementia with Lewy bodies propagate α-synuclein pathology. *Acta Neuropathol. Commun.* 5:46. doi: 10.1186/s40478-017-0445-5

Nixon, R. A. (2004). Niemann-Pick Type C disease and Alzheimer's disease: the APP-endosome connection fattens up. *Am. J. Pathol.* 164, 757–761.

Nixon, R. A. (2005). Endosome function and dysfunction in Alzheimer's disease and other neurodegenerative diseases. *Neurobiol. Aging* 26, 373–382. doi: 10.1016/j.neurobiolaging.2004.09.018

Nixon, R. A. (2017). Amyloid precursor protein and endosomal-lysosomal dysfunction in Alzheimer's disease: inseparable partners in a multifactorial disease. *FASEB J.* 31, 2729–2743. doi: 10.1096/fj.201700359

Nixon, R. A., and Cataldo, A. M. (2006). Lysosomal system pathways: genes to neurodegeneration in Alzheimer's disease. *J. Alzheimers Dis.* 9 3(Suppl.), 277–289. doi: 10.3233/jad-2006-9s331

Nixon, R. A., Yang, D. S., and Lee, J. H. (2008). Neurodegenerative lysosomal disorders: a continuum from development to late age. *Autophagy* 4, 590–599. doi: 10.4161/auto.6259

Nuriel, T., Peng, K. Y., Ashok, A., Dillman, A. A., Figueroa, H. Y., Apuzzo, J., et al. (2017). The endosomal-lysosomal pathway Is dysregulated by APOE4 expression in vivo. *Front. Neurosci.* 11:702. doi: 10.3389/fnins.2017.00702

Olofsson, J. K., Nordin, S., Wiens, S., Hedner, M., Nilsson, L. G., and Larsson, M. (2010). Odor identification impairment in carriers of ApoE-ε4 is independent of clinical dementia. *Neurobiol. Aging* 31, 567–577. doi: 10.1016/j.neurobiolaging.2008.05.019

Oster-Granite, M. L., McPhie, D. L., Greenan, J., and Neve, R. L. (1996). Age-dependent neuronal and synaptic degeneration in mice transgenic for the C terminus of the amyloid precursor protein. *J. Neurosci.* 16, 6732–6741. doi: 10.1523/jneurosci.16-21-06732.1996

Oules, B., Del Prete, D., Greco, B., Zhang, X., Lauritzen, I., Sevalle, J., et al. (2012). Ryanodine receptor blockade reduces amyloid-β load and memory impairments in Tg2576 mouse model of Alzheimer disease. *J. Neurosci.* 32, 11820–11834. doi: 10.1523/jneurosci.0875-12.2012

Peng, K. Y., Mathews, P. M., Levy, E., and Wilson, D. A. (2017). Apolipoprotein E4 causes early olfactory network abnormalities and short-term olfactory memory impairments. *Neuroscience* 343, 364–371. doi: 10.1016/j.neuroscience.2016.12.004

Peng, K. Y., Pérez-González, R., Alldred, M. J., Goulbourne, C. N., Morales-Corraliza, J., Saito, M., et al. (2019). Apolipoprotein E4 genotype compromises brain exosome production. *Brain* 142, 163–175. doi: 10.1093/brain/awy289

Perez, M., Avila, J., and Hernandez, F. (2019). Propagation of tau via extracellular vesicles. *Front. Neurosci.* 13:698. doi: 10.3389/fnins.2019.00698

Pérez-González, R., Gauthier, S. A., Kumar, A., and Levy, E. (2012). The exosome-secretory pathway transports amyloid precursor protein carboxyl terminal fragments from the cell into the brain extracellular space. *J. Biol. Chem.* 287, 43108–43115. doi: 10.1074/jbc.M112.404467

Pérez-González, R., Gauthier, S. A., Kumar, A., Saito, M., Saito, M., and Levy, E. (2017). A method for isolation of extracellular vesicles and characterization of exosomes from brain extracellular space. *Methods Mol. Biol.* 1545, 139–151. doi: 10.1007/978-1-4939-6728-5_10

Pérez-González, R., Sahoo, S., Gauthier, S. A., Kim, Y., Li, M., Kumar, A., et al. (2019). Neuroprotection mediated by cystatin C-loaded extracellular vesicles. *Sci. Rep.* 9:11104. doi: 10.1038/s41598-019-47524-7

Poehler, A. M., Xiang, W., Spitzer, P., May, V. E., Meixner, H., Rockenstein, E., et al. (2014). Autophagy modulates SNCA/ α-synuclein release, thereby generating a hostile microenvironment. *Autophagy* 10, 2171–2192. doi: 10.4161/auto.36436

Pols, M. S., and Klumperman, J. (2009). Trafficking and function of the tetraspanin CD63. *Exp. Cell Res.* 315, 1584–1592. doi: 10.1016/j.yexcr.2008.09.020

Rajendran, L., Honsho, M., Zahn, T. R., Keller, P., Geiger, K. D., Verkade, P., et al. (2006). Alzheimer's disease β-amyloid peptides are released in association with exosomes. *Proc. Natl. Acad. Sci. U.S.A.* 103, 11172–11177. doi: 10.1073/pnas.0603838103

Record, M., Subra, C., Silvente-Poirot, S., and Poirot, M. (2011). Exosomes as intercellular signalosomes and pharmacological effectors. *Biochem. Pharmacol.* 81, 1171–1182. doi: 10.1016/j.bcp.2011.02.011

Reinvang, I., Espeseth, T., and Westlye, L. T. (2013). APOE-related biomarker profiles in non-pathological aging and early phases of Alzheimer's disease. *Neurosci. Biobehav. Rev.* 37, 1322–1335. doi: 10.1016/j.neubiorev.2013.05.006

Rodriguez, G. A., Burns, M. P., Weeber, E. J., and Rebeck, G. W. (2014). Young APOE4 targeted replacement mice exhibit poor spatial learning and memory, with reduced dendritic spine density in the medial entorhinal cortex. *Learn. Mem.* 20, 256–266. doi: 10.1101/lm.030031.112

Salehi, A., Delcroix, J. D., Belichenko, P. V., Zhan, K., Wu, C., Valletta, J. S., et al. (2006). Increased app expression in a mouse model of Down's syndrome disrupts NGF transport and causes cholinergic neuron degeneration. *Neuron* 51, 29–42. doi: 10.1016/j.neuron.2006.05.022

Saman, S., Kim, W., Raya, M., Visnick, Y., Miro, S., Jackson, B., et al. (2012). Exosome-associated Tau is secreted in tauopathy models and is selectively phosphorylated in cerebrospinal fluid in early Alzheimer disease. *J. Biol. Chem.* 287, 3842–3849. doi: 10.1074/jbc.M111.277061

Schreij, A. M., Fon, E. A., and McPherson, P. S. (2016). Endocytic membrane trafficking and neurodegenerative disease. *Cell Mol. Life Sci.* 73, 1529–1545. doi: 10.1007/s00018-015-2105-x

Schwagerl, A. L., Mohan, P. S., Cataldo, A. M., Vonsattel, J. P., Kowall, N. W., and Nixon, R. A. (1995). Elevated levels of the endosomal-lysosomal proteinase cathepsin D in cerebrospinal fluid in Alzheimer disease. *J. Neurochem.* 64, 443–446. doi: 10.1046/j.1471-4159.1995.64010443.x

Sharples, R. A., Vella, L. J., Nisbet, R. M., Naylor, R., Perez, K., Barnham, K. J., et al. (2008). Inhibition of (-secretase causes increased secretion of amyloid precursor protein C-terminal fragments in association with exosomes. *FASEB J.* 22, 1469–1478. doi: 10.1096/fj.07-9357com

Sheline, Y. I., Morris, J. C., Snyder, A. Z., Price, J. L., Yan, Z., D'Angelo, G., et al. (2010). APOE4 allele disrupts resting state fMRI connectivity in the absence of amyloid plaques or decreased CSF A(42. *J. Neurosci.* 30, 17035–17040. doi: 10.1523/JNEUROSCI.3987-10.2010

Shibata, M., Yamada, S., Kumar, S. R., Calero, M., Bading, J., Frangione, B., et al. (2000). Clearance of Alzheimer's amyloid-((1-40) peptide from brain by LDL receptor-related protein-1 at the blood-brain barrier. *J. Clin. Invest.* 106, 1489–1499. doi: 10.1172/jci10498

Simpson, R. J., Jensen, S. S., and Lim, J. W. (2008). Proteomic profiling of exosomes: current perspectives. *Proteomics* 8, 4083–4099. doi: 10.1002/pmic.200800109

Sing, C. F., and Davignon, J. (1985). Role of the apolipoprotein E polymorphism in determining normal plasma lipid and lipoprotein variation. *Am. J. Hum. Genet.* 37, 268–285.

Smalheiser, N. R. (2007). Exosomal transfer of proteins and RNAs at synapses in the nervous system. *Biol. Direct.* 2:35. doi: 10.1186/1745-6150-2-35

Small, S. A. (2008). Retromer sorting: a pathogenic pathway in late-onset Alzheimer disease. *Arch. Neurol.* 65, 323–328. doi: 10.1001/archneurol.2007.64

Small, S. A., and Gandy, S. (2006). Sorting through the cell biology of Alzheimer's disease: intracellular pathways to pathogenesis. *Neuron* 52, 15–31. doi: 10.1016/j.neuron.2006.09.001

Stefanis, L., Emmanouilidou, E., Pantazopoulou, M., Kirik, D., Vekrellis, K., and Tofaris, G. K. (2019). How is α-synuclein cleared from the cell? *J. Neurochem.* 150, 577–590. doi: 10.1111/jnc.14704

Stinchcombe, J., Bossi, G., and Griffiths, G. M. (2004). Linking albinism and immunity: the secrets of secretory lysosomes. *Science* 305, 55–59. doi: 10.1126/science.1095291

Strittmatter, W. J., Saunders, A. M., Schmechel, D., Pericak-Vance, M., Enghild, J., Salvesen, G. S., et al. (1993). Apolipoprotein E: high-avidity binding to (-amyloid and increased frequency of type 4 allele in late-onset familial Alzheimer's Disease. *Proc. Natl. Acad. Sci. U.S.A.* 90, 1977–1981. doi: 10.1073/pnas.90.5.1977

Stuendl, A., Kunadt, M., Kruse, N., Bartels, C., Moebius, W., Danzer, K. M., et al. (2016). Induction of α-synuclein aggregate formation by CSF exosomes from patients with Parkinson's disease and dementia with Lewy bodies. *Brain* 139(Pt 2), 481–494. doi: 10.1093/brain/awv346

Takahashi, R. H., Almeida, C. G., Kearney, P. F., Yu, F., Lin, M. T., Milner, T. A., et al. (2004). Oligomerization of Alzheimer's β-amyloid within processes and synapses of cultured neurons and brain. *J. Neurosci.* 24, 3592–3599. doi: 10.1523/jneurosci.5167-03.2004

Tamayev, R., and D'Adamio, L. (2012). Inhibition of (-secretase worsens memory deficits in a genetically congruous mouse model of Danish dementia. *Mol. Neurodegener.* 7:19. doi: 10.1186/1750-1326-7-19

Tamayev, R., Matsuda, S., Arancio, O., and D'Adamio, L. (2012). β- but not (-secretase proteolysis of APP causes synaptic and memory deficits in a mouse model of dementia. *EMBO Mol. Med.* 4, 171–179. doi: 10.1002/emmm.201100195

Tassew, N. G., Charish, J., Shabanzadeh, A. P., Luga, V., Harada, H., Farhani, N., et al. (2017). Exosomes mediate mobilization of autocrine Wnt10b to promote axonal regeneration in the injured CNS. *Cell Rep.* 20, 99–111. doi: 10.1016/j.celrep.2017.06.009

Tizon, B., and Levy, E. (2006). "Protease inhibitors and their involvement in neurological disorders," in *Handbook of Neurochemistry and Molecular Neurobiology*, ed. A. Lajtha, (New York, NY.: Springer Publishers).

Tofaris, G. K. (2017). A critical assessment of exosomes in the pathogenesis and stratification of parkinson's disease. *J. Parkinsons Dis.* 7, 569–576. doi: 10.3233/JPD-171176

Troncoso, J. C., Cataldo, A. M., Nixon, R. A., Barnett, J. L., Lee, M. K., Checler, F., et al. (1998). Neuropathology of preclinical and clinical late-onset Alzheimer's disease. *Ann. Neurol.* 43, 673–676.

Urbanelli, L., Magini, A., Buratta, S., Brozzi, A., Sagini, K., Polchi, A., et al. (2013). Signaling pathways in exosomes biogenesis, secretion and fate. *Genes* 4, 152–170. doi: 10.3390/genes4020152

Valdinocci, D., Radford, R. A., Siow, S. M., Chung, R. S., and Pountney, D. L. (2017). Potential modes of intercellular α-synuclein transmission. *Int. J. Mol. Sci.* 18:E469. doi: 10.3390/ijms18020469

van der Pol, E., Boing, A. N., Gool, E. L., and Nieuwland, R. (2015). Recent developments on the nomenclature, presence, isolation, detection and clinical impact of extracellular vesicles. *J. Thromb. Haemost.* 14, 48–56. doi: 10.1111/jth.13190

van der Pol, E., Boing, A. N., Harrison, P., Sturk, A., and Nieuwland, R. (2012). Classification, functions, and clinical relevance of extracellular vesicles. *Pharmacol. Rev.* 64, 676–705. doi: 10.1124/pr.112.005983

van Niel, G., Charrin, S., Simoes, S., Romao, M., Rochin, L., Saftig, P., et al. (2011). The tetraspanin CD63 regulates ESCRT-independent and -dependent

endosomal sorting during melanogenesis. *Dev. Cell* 21, 708–721. doi: 10.1016/j.devcel.2011.08.019

van Niel, G., D'Angelo, G., and Raposo, G. (2018). Shedding light on the cell biology of extracellular vesicles. *Nat. Rev. Mol. Cell Biol.* 19, 213–228. doi: 10.1038/nrm.2017.125

Vella, L. J., Sharples, R. A., Nisbet, R. M., Cappai, R., and Hill, A. F. (2008). The role of exosomes in the processing of proteins associated with neurodegenerative diseases. *Eur. Biophys. J.* 37, 323–332. doi: 10.1007/s00249-007-0246-z

Verghese, P. B., Castellano, J. M., and Holtzman, D. M. (2011). Apolipoprotein E in Alzheimer's disease and other neurological disorders. *Lancet Neurol.* 10, 241–252. doi: 10.1016/S1474-4422(10)70325-2

Vilette, D., Courte, J., Peyrin, J. M., Coudert, L., Schaeffer, L., Andreoletti, O., et al. (2018). Cellular mechanisms responsible for cell-to-cell spreading of prions. *Cell Mol. Life Sci.* 75, 2557–2574. doi: 10.1007/s00018-018-2823-y

Villemagne, V. L., Pike, K. E., Chetelat, G., Ellis, K. A., Mulligan, R. S., Bourgeat, P., et al. (2011). Longitudinal assessment of A(and cognition in aging and Alzheimer disease. *Ann. Neurol.* 69, 181–192.

Vingtdeux, V., Hamdane, M., Loyens, A., Gele, P., Drobeck, H., Begard, S., et al. (2007). Alkalizing drugs induce accumulation of amyloid precursor protein by-products in luminal vesicles of multivesicular bodies. *J. Biol. Chem.* 282, 18197–18205. doi: 10.1074/jbc.m609475200

Wang, C., Wilson, W. A., Moore, S. D., Mace, B. E., Maeda, N., Schmechel, D. E., et al. (2005). Human apoE4-targeted replacement mice display synaptic deficits in the absence of neuropathology. *Neurobiol. Dis.* 18, 390–398. doi: 10.1016/j.nbd.2004.10.013

Wang, S., and West, A. B. (2019). Caught in the act: LRRK2 in exosomes. *Biochem. Soc. Trans.* 47, 663–670. doi: 10.1042/BST20180467

Wang, Y., Balaji, V., Kaniyappan, S., Kruger, L., Irsen, S., Tepper, K., et al. (2017). The release and trans-synaptic transmission of Tau via exosomes. *Mol. Neurodegener.* 12:5. doi: 10.1186/s13024-016-0143-y

Willen, K., Edgar, J. R., Hasegawa, T., Tanaka, N., Futter, C. E., and Gouras, G. K. (2017). Aβ accumulation causes MVB enlargement and is modelled by dominant negative VPS4A. *Mol. Neurodegener.* 12:61. doi: 10.1186/s13024-017-0203-y

Willms, E., Johansson, H. J., Mager, I., Lee, Y., Blomberg, K. E., Sadik, M., et al. (2016). Cells release subpopulations of exosomes with distinct molecular and biological properties. *Sci. Rep.* 6:22519. doi: 10.1038/srep22519

Winston, C. N., Aulston, B., Rockenstein, E. M., Adame, A., Prikhodko, O., Dave, K. N., et al. (2019). Neuronal exosome-derived human Tau is toxic to recipient mouse neurons in vivo. *J. Alzheimers Dis.* 67, 541–553. doi: 10.3233/JAD-180776

Wisdom, N. M., Callahan, J. L., and Hawkins, K. A. (2011). The effects of apolipoprotein E on non-impaired cognitive functioning: a meta-analysis. *Neurobiol. Aging* 32, 63–74. doi: 10.1016/j.neurobiolaging.2009.02.003

Xiao, T., Zhang, W., Jiao, B., Pan, C. Z., Liu, X., and Shen, L. (2017). The role of exosomes in the pathogenesis of Alzheimer' disease. *Transl. Neurodegener.* 6:3. doi: 10.1186/s40035-017-0072-x

Xu, J., Camfield, R., and Gorski, S. M. (2018). The interplay between exosomes and autophagy - partners in crime. *J. Cell Sci.* 131:jcs215210. doi: 10.1242/jcs.215210

Yang, D.-S., Stavrides, P., Mohan, P., Kaushik, S., Kumar, A., Ohno, M., et al. (2011). Reversal of autophagy dysfunction in the TgCRND8 mouse model of Alzheimer's disease ameliorates amyloid pathologies and memory deficits. *Brain* 134, 258–277. doi: 10.1093/brain/awq341

Yuyama, K., Sun, H., Mitsutake, S., and Igarashi, Y. (2012). Sphingolipid-modulated exosome secretion promotes the clearance of amyloid-β by microglia. *J. Biol. Chem.* 287, 10977–10989. doi: 10.1074/jbc.M111.324616

Yuyama, K., Sun, H., Sakai, S., Mitsutake, S., Okada, M., Tahara, H., et al. (2014). Decreased amyloid-β pathologies by intracerebral loading of glycosphingolipid-enriched exosomes in Alzheimer model mice. *J. Biol. Chem.* 289, 24488–24498. doi: 10.1074/jbc.m114.577213

Zhao, N., Liu, C. C., Van Ingelgom, A. J., Martens, Y. A., Linares, C., Knight, J. A., et al. (2017). Apolipoprotein E4 impairs neuronal insulin signaling by trapping insulin receptor in the endosomes. *Neuron* 96, 115.e5–129.e5. doi: 10.1016/j.neuron.2017.09.003

Zlokovic, B. V. (2013). Cerebrovascular effects of apolipoprotein E: implications for Alzheimer disease. *JAMA Neurol* 70, 440–444. doi: 10.1001/jamaneurol.2013.2152

Zou, W., Lai, M., Zhang, Y., Zheng, L., Xing, Z., Li, T., et al. (2019). Exosome release is regulated by mTORC1. *Adv. Sci.* 6:1801313. doi: 10.1002/advs.201801313

Conflict of Interest: The authors declare that the research was conducted in the absence of any commercial or financial relationships that could be construed as a potential conflict of interest.

frontiers in Neuroscience

ORIGINAL RESEARCH
published: 21 April 2020
doi: 10.3389/fnins.2020.00246

Intrastriatal Administration of Exosome-Associated Pathological Alpha-Synuclein Is Not Sufficient by Itself to Cause Pathology Transmission

*Mantia Karampetsou[1†], Vasia Samantha Sykioti[1†], Emmanouela Leandrou[1], Katerina Melachroinou[1], Alexandros Lambiris[1], Antonis Giannelos[1], Evangelia Emmanouilidou[1,2] and Kostas Vekrellis[1]**

[1] Center for Basic Research, Biomedical Research Foundation Academy of Athens, Athens, Greece, [2] Laboratory of Biochemistry, Department of Chemistry, National and Kapodistrian University of Athens, Athens, Greece

OPEN ACCESS

Edited by:
Grant Thomas Corbett, Brigham and Women's Hospital and Harvard Medical School, United States

Reviewed by:
Kelvin C. Luk, University of Pennsylvania, United States
Xiaoli Yu, University of Colorado Anschutz Medical Campus, United States

***Correspondence:**
Kostas Vekrellis
vekrellis@bioacademy.gr

[†] These authors have contributed equally to this work

Specialty section:
This article was submitted to Neurodegeneration, a section of the journal Frontiers in Neuroscience

Received: 29 July 2019
Accepted: 04 March 2020
Published: 21 April 2020

Citation:
Karampetsou M, Sykioti VS, Leandrou E, Melachroinou K, Lambiris A, Giannelos A, Emmanouilidou E and Vekrellis K (2020) Intrastriatal Administration of Exosome-Associated Pathological Alpha-Synuclein Is Not Sufficient by Itself to Cause Pathology Transmission. Front. Neurosci. 14:246. doi: 10.3389/fnins.2020.00246

α-Synuclein (α-syn) has been genetically and biochemically linked to the pathogenesis of Parkinson's disease (PD). There is accumulating evidence that misfolded α-syn species spread between cells in a prion-like manner and seed the aggregation of endogenous protein in the recipient cells. Exosomes have been proposed to mediate the transfer of misfolded α-syn and thus facilitate disease transmission, although the pathological mechanism remains elusive. Here, we investigated the seeding capacity of exosome-associated α-syn, *in vivo*. Disease-associated α-syn was present in exosome fractions isolated from transgenic A53T mouse brain. However, following intrastriatal injection of such exosomes in wild-type (wt) mice, we were not able to detect any accumulation of endogenous α-syn. In addition, recombinant fibrillar α-syn, when loaded to isolated brain exosomes, induced minor pathological α-syn brain accumulation at 7 months post injection. These data suggest that exosomes neutralize the effect of toxic α-syn species and raise additional questions on their paracrine modulatory role in disease transmission.

Keywords: α-synuclein (a-synuclein), propagation, exosomes, Parkinson's, aggregation

INTRODUCTION

Extracellular α-synuclein (α-syn) has been involved in the transmission of pathology from diseased to healthy neurons, where misfolded α-syn might serve as a template to induce the oligomerization of the soluble protein. Exosomal release and transport of misfolded α-syn were reported by us and several other groups *in vitro* and *in vivo* (Emmanouilidou et al., 2010; Alvarez-Erviti et al., 2011). Exosomes are small extracellular cup-shaped vesicles that are released intact, following fusion of the plasma membrane with the multivesicular bodies (Vekrellis et al., 2011). Besides their physiological role in cell–cell communication, exosomes have been proposed to be involved in the pathogenesis of many neurodegenerative diseases. Exosome-associated pathological proteins, like Aβ 42, tau, and α-syn, have been found in biological fluids of patients with neurodegenerative diseases, yet their pathological potential is still not elucidated (Vella et al., 2016). The misfolded pathological α-syn loaded to exosomes has been proposed not only to seed the accumulation of endogenous

soluble protein of the recipient neuronal cells but also to trigger the inflammatory response of glial cells (Soria et al., 2017). In this regard, exosomes might be able to facilitate the spread of pathology of aggregation-prone proteins in a prion-like manner and thus contribute to Parkinson's disease (PD) progression. However, it remains unclear how much of the α-syn release occurs through exosomes. Danzer et al. (2012) were the first to show that oligomeric α-syn is present in both the lumen and the surface of exosomes. Importantly, the exosome-associated oligomers were transferred more efficiently to the cells than were the free oligomeric forms. Moreover, mutant A53T α-syn has been shown to associate more efficiently to extracellular vesicles (EVs) than the wild-type (wt) α-syn in cultured cells (Gustafsson et al., 2018). In addition, exosome release has been suggested to be a key mechanism of clearing oligomeric α-syn (Poehler et al., 2014). Dysfunction in the autophagy/lysosome pathway and mitochondrial impairment, which are both related to PD pathology, has been proposed to increase the transfer of α-syn via exosomes (Alvarez-Erviti et al., 2011; Pan-Montojo et al., 2012).

The levels of exosomal α-syn detected in PD patients have been shown to be variable, with some studies indicating an increase of exosomal α-syn in the plasma and cerebrospinal fluid (CSF) of PD patients (Shi et al., 2014). Still, the interaction between α-syn and exosomes is not understood, and whether exosomes play an important role in PD pathogenesis is still unclear. Recently, exosomes isolated from the CSF of PD patients were shown to seed α-syn pathological aggregation using a reporter cell line (Stuendl et al., 2016). *In vivo*, administration of PD patient plasma-derived exosomes barely colocalize with neuronal cells in contrast to their strong preference for microglia cells near the injection site. Nonetheless, human α-syn was detected in the Substantia Nigra pars compacta (SNpc) neurons, which implies a glia–neuron transmission process as well (Xia et al., 2019).

Recombinant α-syn preformed fibrils (PFFs) have been shown to be readily taken up by neighboring neurons *in vitro* and *in vivo* and induce endogenous α-syn accumulation and cell death in the recipient neurons (Volpicelli-Daley et al., 2011; Luk et al., 2012; Karampetsou et al., 2017). To study whether exosomes could interfere with the process of α-syn misfolding, Grey and colleagues examined the aggregation kinetics of α-syn in the presence of exosomes. Importantly, they showed that exosomes could aid the aggregation of α-syn as efficiently as low concentrations of PFFs (Grey et al., 2015). The present work demonstrates that exosome-associated pathological α-syn cannot seed robust Lewy body (LB)-like pathology in neuronal cells and thus initiate propagation in the wt mouse brain. Consequently, the exosomal load was not sufficient to impair neuronal viability even after prolonged incubation time.

MATERIALS AND METHODS

Whole-Brain Exosome Isolation and Purification

Exosomes were isolated from whole mouse brains as previously described (Papadopoulos et al., 2018) with slight modifications. A53T (A53T alpha-synuclein PRP/M83 mice, Jackson Laboratory) and KO (C57BL6/JOlaHsd mice, Harlan Laboratories) exosomes were isolated from 10- to 12-month old mice. Exosomes used for the binding assay with the PFFs were isolated from 2- to 4-month-old KO mouse brains. Excised brains were dissociated enzymatically upon incubation with papain (20 units/ml, Worthington) diluted in Hibernate A solution (6 ml/brain; BrainBits) at 37°C for 15 min. Tissue was homogenized by adding two volumes of cold Hibernate A solution, and the suspension was passed through a 40-μm cell strainer and a 0.2-μm syringe filter. The filtrate was centrifuged at 300*g* (10 min, 4°C), and then the supernatant was further centrifuged at 2,000*g* (10 min, 4°C), 10,000*g* (30 min, 4°C), and finally 100,000*g* (70 min, 4°C). Following aspiration of the supernatant, exosome pellet was washed in 22–24 ml of cold phosphate-buffered saline (PBS) and centrifuged again at 100,000 × *g* (70 min, 4°C). Exosome pellet was then diluted in 1.5 ml of sucrose solution (0.95 M), loaded on a sucrose gradient column, and centrifuged at 200,000 × *g* (16 h, 4°C). Sucrose gradient comprises six fractions (2–0.25 M, 1.5 ml each). Following centrifugation, seven fractions were separated according to the gradient (a–g from the top to the bottom), collected individually, and diluted to PBS up to 22 ml of final volume. All fractions were centrifuged at 100,000 × *g* (70 min, 4°C) and pellets were resuspended in PBS. To access the exosome enriched fractions, we measured the acetylcholinesterase activity as described by Savina et al. (2002). Briefly, 10 μl of the isolated exosomal fractions or known concentrations of recombinant AchE were added to individual wells on a 96-well flat-bottomed microplate; 1.25 mM of acetylthiocholine and 0.1 mM of 5,5′-dithiobis (2-nitrobenzoic acid) in PBS were added in a final volume of 250 μl. Following 30-min incubation [room temperature (RT), shaking, in the dark], the absorbance at 405 nm was measured. Total protein of the exosomal fraction was measured by Bradford protein assay. Fractions c and d were enriched in exosomes and used for the intrastriatal injections.

Electron Microscopy

Exosome-enriched fraction was fixed with 4% paraformaldehyde overnight at 4°C. Five microliters were loaded on 300-mesh copper grids with carbon-coated formvar film and incubated for 20 min. The grids were washed with PBS and incubated with 1% glutaraldehyde for 5 min. Finally, grids were stained with uranyl oxalate (pH 7, 5 min) and methyl cellulose–uranyl acetate (10 min on ice) and allowed to dry. Samples were examined with a Philips 420 Transmission Electron Microscope at 60 kV.

Preformed Fibrils Binding to Exosomes

Isolated exosomes from two KO mouse brains (Fraction c in PBS, pH 7.4) and mouse PFFs (in Tris 50 mM, NaCl 150 mM, pH 7.5) were incubated at a ratio of 1.5:1 (180 μg of exosomes: 120 μg of PFFs) with an equal volume of 0.2 M of sodium acetate pH 5.2 (Qazi et al., 2009). After 30-min incubation at RT, Tris 2 M (pH 11) was added to neutralize the pH; and the mixture was incubated for 45 min at RT. After the incubation, the mixture was resuspended in 0.95 M of sucrose at a final

volume of 1.5 ml. The exosome–PFF preparation was then applied on a sucrose step gradient column (six 1.5-ml steps starting from 2.0 M of sucrose up to 0.25 M of sucrose), as described previously in the "Materials and Methods" section. Each fraction was centrifuged for 70 min at 100,000 × *g* at 4°C in a T865 rotor; and the pellets were resuspended in PBS. Fraction d of the sucrose gradient column contains the exosome-bound PFFs.

Staining and Uptake Assay of Exosomes

Exosomes (20 μg) from mouse neuronal primary culture conditioned medium were diluted in PBS and labeled with 1.2 μM of BODIPY TR Ceramide (Thermo Fisher Scientific) for 1 h at 37°C. The final volume of the labeling reaction was 500 μl. Excess dye was removed by ultrafiltration using Vivaspin 50-kDa filters previously equilibrated in PBS. The resultant 50 μl of exosome solution was stored at 4°C for 16 h before further analysis or used immediately. For internalization assays, primary mouse cortical cultures were prepared from E16 C57BL/6 embryos as described previously (Karampetsou et al., 2017). Cells were seeded on poly-D-lysine precoated coverslips. Labeled exosomes (2 μg) were added to the culture media of the recipient cells and incubated for 3 h at 37°C. Following incubation with 2 μM of calcein-AM (LIVE/DEAD viability/cytotoxicity kit, Invitrogen) for 30 min, cells were washed with PBS to remove the excess of the dye.

Stereotaxic Injections

Male C57/BL6 mice, 2–3 months old, were injected under general isoflurane anesthesia. The Kopf stereotaxic frame was used to properly align the animals (Kopf Instruments, United States), and the right dorsal striatum was targeted using the following coordinates from bregma: anteroposterior of +0.5 mm, mediolateral of −2 mm, and dorsoventral in two depths of −3.2 and −3.4 mm according to the brain atlas of Paxinos and Franklin. A total of 5.5 μg (4 μl) of isolated mouse brain exosomes (KO/A53T) were injected at a constant flow rate of 0.27 μl/min (10 mice/group). For the PFF experiments, 2.5 μg of mouse PFFs or the respective amount of exosomes containing the same quantity of bound PFFs was used to inoculate mouse striatum. Between target depths, a 5-min interval was followed. Animals receiving KO or A53T-derived exosomes were sacrificed 5 months post injection, whereas mice injected with free or exosome-bound PFFs were sacrificed 2 or 7 months post injection.

Tissue Fractionation

Midbrain, cortex, hippocampus, and striatum from mice were dissected and weighed, and total protein was extracted following a two-step protocol. Initially, the tissue was homogenized (7 ml/g) in 1% Triton X extraction buffer (150 mM of NaCl, 50 mM of Tris pH 7.6, 1% Triton X-100), sonicated, and centrifuged at 100,000 × *g* for 30 min, at 4°C. The resulting supernatants comprise the Triton X-soluble fraction. The remaining pellets were washed twice with PBS buffer and dissolved in 1% sodium dodecyl sulfate (SDS) radioimmunoprecipitation assay (RIPA) buffer (50 mM of Tris, pH 8.0, 150 mM NaCl, 5 mM of EDTA, 1% NP-40, 0.5% sodium deoxycholate, and 1% SDS). The supernatant recovered represents the SDS-soluble fraction. Protease and phosphatase inhibitors (Roche) were added. Protein concentration was estimated by the Bradford assay (Bio-Rad).

Primary Neuronal Cultures

Primary cortical neurons were prepared from embryonic day E16 mouse brains as previously described (Karampetsou et al., 2017). A total of 1.7 × 10^6 cells/well plated in a six-well plate were cultured in Neurobasal medium containing 2% B27 supplement (Gibco, Invitrogen), 0.5 mM of L-glutamine, and 1% penicillin/streptomycin. By day 5, cultures were treated for 8 and 24 h with free and exosome-bound PFFs (0.3 μg/105 cells) or PBS and KO exosomes as controls. Following two brief washes with 0.05% trypsin–EDTA, cells were collected in trypsin, and the enzyme was deactivated in 10% fetal bovine serum (FBS)-containing medium. The cell pellet (400 g, 5 min) was washed twice in PBS, resuspended in 1% Triton X extraction buffer, and solubilized by sonication. Protease and phosphatase inhibitors were added. The Triton X-soluble fraction was recovered following centrifugation at 16,000 × *g* for 40 min at 4°C. For the immunocytochemical analysis, 5-day-old primary cortical cultures, plated on glass coverslips (10^5 cells/cm^2), were treated with free or exosome-bound PFFs for 48 h, and neurons were fixed in 4% (wt/vol) formaldehyde.

Sodium Dodecyl Sulfate–Polyacrylamide Gel Electrophoresis and Immunoblotting

Denaturing gel electrophoresis was performed on 13% SDS-PAGE Tris-glycine gels. Proteins were subsequently transferred onto nitrocellulose membranes (Whatman) and analyzed by immunoblotting. The following primary antibodies were used: α-syn Syn-1 (human, mouse, rat, monoclonal, BD Transduction), α-syn 4B12 (human, monoclonal, Genetex), α-syn C20 (human, mouse, rat, polyclonal, Santa Cruz), pS129 α-syn (monoclonal, Abcam), Flotillin-1 antibody (human, mouse, rat, polyclonal, Abcam), GAPDH (monoclonal, Millipore), and γ-tubulin (monoclonal, Sigma). Differences in protein expression levels were quantified using both Gel Analyser v1.0 and Fiji v 2.0.0 software after normalization of all values with the loading control.

Immunofluorescence Analysis

Mice were anesthetized and perfused intracardially first with ice-cold PBS (30 ml) and then 4% paraformaldehyde (30 ml) in PBS, under a constant flow rate using a pump. Brains were post-fixed overnight at 4°C and then incubated in 30% sucrose in PBS for 48 h at 4°C. For snap freezing, brains were immersed into frozen iso-pentane (−45°C) for 30 s and stored at −80°C. Free-floating sections of 35 μm were collected using a Leica cryostat at −25°C. For immunohistochemistry, the sections were rinsed in three changes of PBS for 15 min each and then blocked for 60 min in 5% normal goat serum (NGS) in PBS containing 0.1% Triton X (blocking buffer). Sections were then incubated with the primary antibodies in blocking buffer for 48 h at 4°C. Following 3 × 15 min of washes in PBS, sections were incubated with the secondary antibodies diluted in blocking buffer, for 2 h at RT,

and washed again as above. For the mounting, Superfrost plus slides (VWR) were used. For immunocytochemistry, fixed cells were incubated first in blocking buffer for 1 h at RT and then with the primary antibodies diluted in blocking buffer for 16 h at 4°C. Following five washes in PBS, secondary antibodies diluted in blocking buffer were added for 2 h at RT. After final PBS washes, the coverslips were mounted on a slide using Vectashield (Vector-labs) as a mounting medium. The following primary antibodies were also used: tyrosine hydroxylase (TH) (polyclonal, 1:2,000, Millipore), Tuj-1 (β-tubulin III, monoclonal, 1:1,000, Sigma), Syn-1 (monoclonal, 1:1,000, BD transduction), α-syn C20 (human, mouse, rat, polyclonal, Santa Cruz), and pS129 α-syn (monoclonal, Abcam).

Stereology

The total number of TH-positive neurons in the *SNpc* was counted using the Stereo Investigator v10.0 software (MBF Bioscience, United States). For each animal, nine sections of 35-μm thickness were collected every four throughout the rostro-caudal axis and stained for TH. Following incubation with the secondary antibody (Vectastain Elite ABC kit, Vector labs), 3,3′-diaminobenzidine (DAB; Dako) was used as a chromogen as previously described (Karampetsou et al., 2017). For the stereological analysis, a total number of four animals per group were used. Drawing of counting contours was performed with the 2.5 × objective, and counting was performed using a 63 × glycerol immersion objective. For the analysis, the following parameters were set: optical dissector height (12 μm), grid size (85 μm), and counting frame (50 μm). A coefficient of error (Gundersen, $m = 1$) of ≤ 0.1 was accepted.

Confocal Microscopy

Images were obtained with both Leica SP5-II upright and inverted confocal microscopes. Phosphorylated accumulations were counted manually from tiled SNpc confocal images. Five sections from each animal, starting from −2.66-mm anteroposterior distance relative to bregma (Paxinos and Franklin, 2004) and collected every four, were used for the counting. Fluorescent images were processed with LAS AF (Leica Microsystems) and Fiji v2.0.0 software. A 3D reconstruction of confocal images was performed by Imaris 9.5.1 software.

Behavioral Analysis

Motor behavior of mice inoculated with A53T and KO exosomes at 5 months post injection was assessed by the following tests. Animals were handled for 1 week before the starting date to minimize stress and anxiety. Prior to each behavioral experimentation, mice were allowed to acclimate to the testing room for a minimum of 30 min.

Open Field

To assess the general locomotor activity, mice were placed separately in the center of an open-field apparatus that consisted of a squared Plexiglass chamber. Free-moving animals within the arena were monitored individually by a digital camera. The Ethovision XT 8.5 (Noldus) software was used to track moving mice for 15 min and to analyze the following parameters: (a) total distance traveled, (b) mean velocity, and (c) time spent in the center zone region.

Challenging Beam Traversal

The challenging beam was used to access fine-motor coordination as previously described (Karampetsou et al., 2017). A Plexiglass beam (1 m long) consisted of four parts with different widths (3.5, 2.5, 1.5, and 0.5 cm) was used. Mice were placed in the wider part (starting point) and trained to traverse along the beam up to the end of the narrowest part (final point), where their home cage was placed. All animals were trained to perform the task for 2 days (5 trials/animal/day). On the following day (test day), a wire mesh was placed approximately 1 cm over the beam, and the traversal of each animal was recorded by a digital camera (5 trials/animal). Error steps (error: each time limbs slip through the mesh) and total steps (step: forward movement of the animal with each forelimb) were counted, and the results were expressed as mean average of total errors/steps.

Pole Test

Balance and motor coordination were assessed by pole test as previously described (Karampetsou et al., 2017). To perform this task, mice were placed on the top of a wooden pole (50 cm), which is fixed vertically to a stable base. Each animal is facing up, and all four limbs grasp the pole. The animals were trained for 2 days to orient downward and reach the wooden base (5 trials/animal). On the test day, each animal was recorded to perform the task, and two parameters were calculated: (a) time to orient downward and (b) total time to descend the pole. The mean of 4–5 trials/animal was analyzed.

Statistical Analysis

The data are shown as the mean ± SEM. The statistical analysis was performed with the GraphPad Prism 6 software using Student's *t*-test. Differences of $p < 0.05$ were considered significant.

Ethical Approval

All animals were caged in the Laboratory Animal Unit of Centre of the Biomedical Research Foundation of the Academy of Athens. Animal experimental protocol was approved by an authorized veterinarian committee in accordance to Greek legislation (Presidential Decree 56/2013, in compliance with the European Directive 2010/63).

RESULTS

Isolation and Characterization of Brain Exosomes

To investigate the role of exosome-associated α-syn on the pathogenesis and progression of pathology *in vivo*, we isolated exosomes from α-syn null (KO) and symptomatic 10- to 12-month-old A53T transgenic mice (Giasson et al., 2002). Initially, we characterized the nature and levels of α-syn in these mouse brains. Triton X-soluble and SDS-soluble fractions from null,

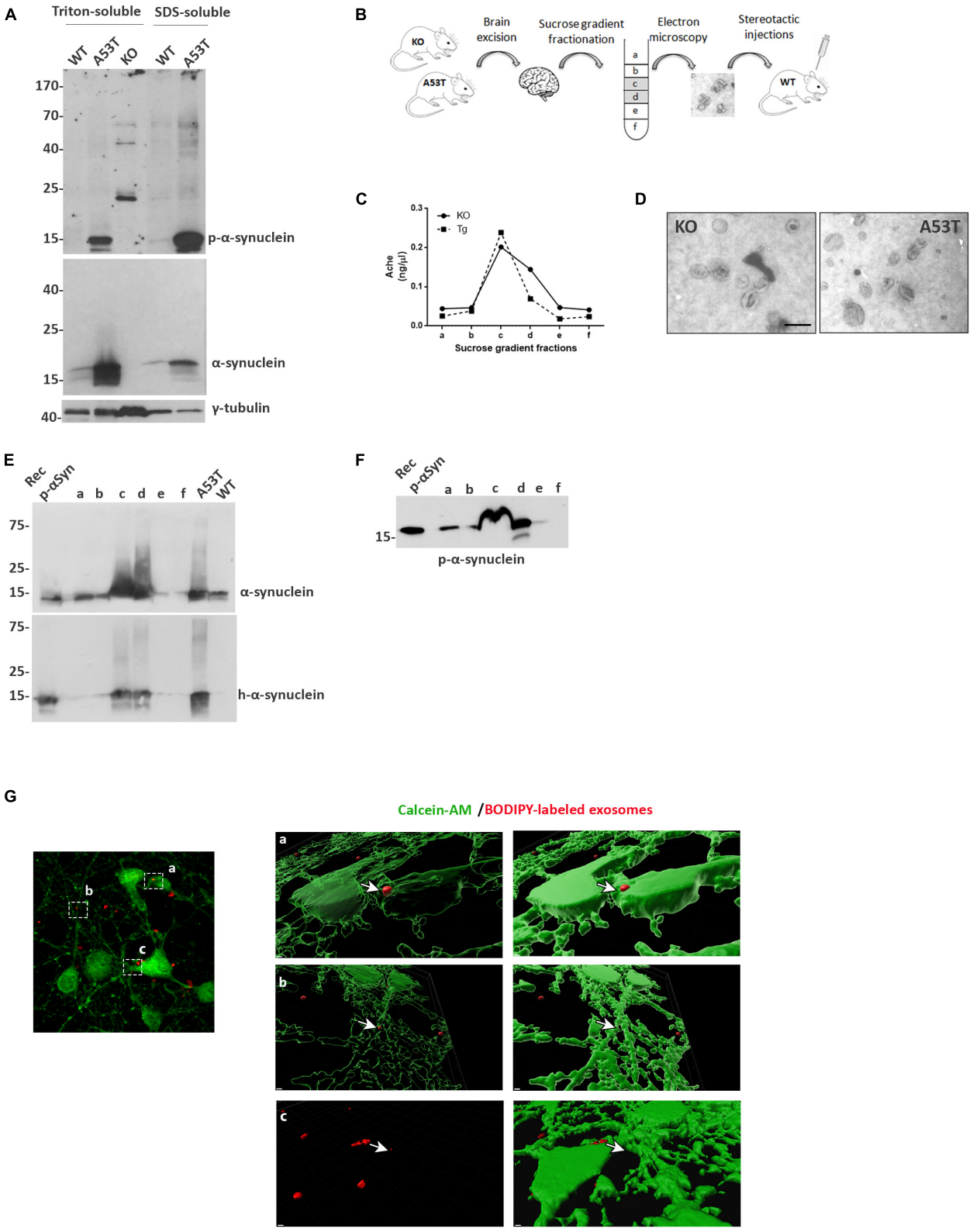

FIGURE 1 | Continued

FIGURE 1 | Continued
Isolation and characterization of mouse brain exosomes. **(A)** Brain tissue from wild-type (wt), A53T, and KO mice was separated into Triton X- and sodium dodecyl sulfate (SDS)-soluble fractions. α-Synuclein species were detected by western blot analysis with the Syn-1 and pS129 antibodies. Increased detergent-soluble and detergent-insoluble α-synuclein species were detected in the A53T mice. γ-Tubulin was used as loading control. **(B)** Schematic representation of the procedure followed for the isolation of whole brain exosomes. **(C)** Graph depicting the concentration of AchE enzyme contained in the isolated exosomal fractions. **(D)** Electron microscopy images of isolated exosomes from KO and A53T mouse brains. Scale bar, 200 nm. Human and total **(E)** as well as phospho-α-synuclein **(F)** species were detected in the isolated exosomal fractions from A53T mouse brains using the 4B12, Syn-1, and pS129 antibodies, respectively. Recombinant α-syn protein, A53T, and wt brain lysates were used as controls. **(G)** Primary mouse cortical cultures were incubated in the presence of BODIPY-labeled exosomes (red) for 3 h, and incorporation of the fluorescent lipophilic dye was monitored by confocal microscopy. Neurons were stained with calcein-AM. Internalization of dyed exosomes was assessed by using the Imaris software. Scale bar represents 2 μm.

wt, and A53T Tg brain homogenates were prepared. Western blotting with the Syn-1 antibody revealed elevated levels of α-syn in the brains of the A53T-expressing mice in the Triton X- and SDS-soluble fractions, compared with wt littermates (**Figure 1A**). As expected, α-syn was absent in the null mice. Phosphorylation of α-syn has been suggested to constitute a primary trigger for α-syn-induced pathology. Examination of the phosphorylated levels of α-syn in the same fractions showed that A53T-Tg mice exhibit increased levels of both detergent-soluble and detergent-insoluble phosphorylated α-syn species. These results confirm that A53T-Tg mice, compared with age-matched wt littermates, contain elevated phosphorylated α-syn species in their brains.

We then went on to isolate exosomal vesicles from null and A53T-Tg mouse brains. Following mild tissue homogenization with papain, brain membrane vesicles were isolated on a sucrose gradient as depicted in **Figure 1B**. To confirm the presence of membrane vesicles in our preparations and to quantify the amount of vesicles with exosomal characteristics present in the different fractions, we assessed the activity of acetylcholinesterase, an enzyme enriched to exosomes. As shown in **Figure 1C**, Fractions c and d of our preparations were enriched in exosome-like vesicles. Electron microscopy (EM) was also used to verify the morphology, size, and intact structure of the isolated exosomes in these fractions (**Figure 1D**).

Then we sought to examine the α-syn biochemical profile in the isolated exosomes. To this end, we characterized only fractions obtained from A53T-Tg brains because we confirmed the absence of α-syn in the brains of α-syn null mice. Western blotting of the exosome-containing fractions with the human specific anti-α-syn antibody 4B12 demonstrated the presence of human α-syn in the fractions obtained from the A53T Tg mouse brain (**Figure 1E**). The presence of α-syn in the same fractions was further confirmed with the Syn-1 antibody for the total α-syn (**Figure 1E**). We also examined whether the α-syn associated with exosomal vesicles was phosphorylated at sites that are usually linked with PD. Interestingly, we observed the abundance of phosphorylated S129 α-syn species in the exosomal fractions isolated from the A53T mouse brain (**Figure 1F**). To confirm that the isolated exosomes could be taken up by cells, we labeled exosomes with the fluorescent lipophilic dye BODIPY, and we assessed their uptake by primary mouse neuronal cultures following exosome application for 3 h. Confocal microscopy imaging followed by Imaris software analysis revealed the presence of labeled exosomes entering the cytoplasm of living calcein-AM-positive cells (**Figure 1G**). These results suggest that isolated brain exosomes are intact and can be incorporated into recipient cells.

Injections of Exosomes Carrying Mutant A53T α-Synuclein Do Not Induce α-Synuclein Pathology in the Brains of Recipient Wild-Type Mice

To better elucidate the seeding potential of brain exosomes and their ability to induce oligomerization and accumulation of α-syn pathology *in vivo*, we performed stereotaxic injections targeting the mouse right dorsal striatum with exosomes isolated from null and A53T mouse brains. C57BL/6 male 2- to 3-month-old mice were inoculated with 5.5 μg of A53T or KO exosomes. To examine the potential of exosomal preparations to seed pathology, we chose the time point of 150 days post injection (dpi) for our analyses. As a first readout for α-syn pathology, we measured by western blotting the amount of total α-syn in the Triton and SDS detergent-soluble brain fractions of the injected and control hemispheres; 150-dpi cortex, midbrain, striatum, and hippocampal regions were analyzed using the Syn-1 antibody. As shown in **Figures 2A–H**, the densitometric analysis revealed no significant differences in the levels of α-syn between the ipsilateral and contralateral sides of null and A53T exosome-injected mice in all the brain regions studied. To further investigate pathological α-syn species in the exosome-injected brains, we also determined by western blotting the levels of phosphorylated α-syn (a marker of pathological α-syn) in the striatum and midbrain. These areas have been shown to accumulate endogenous phosphorylated α-syn following intrastriatal injections of recombinant misfolded α-syn species. Injected mice displayed similar levels of phosphorylated α-syn in the SDS-soluble fractions in the regions examined (**Figures 3A,B**). Together, these results suggest the lack of induction of pathological α-syn from exosomes carrying the A53T α-syn form. These observations were further confirmed by the immunohistochemical analysis of the midbrain and the cortex of mice that received isolated exosomes. Coronal sections from each animal were immunostained for phosphorylated α-syn (phospho-Ser129) and TH for the *SNpc* (**Figure 3C**) or the α-syn-specific antibody Syn-1 and the neuronal Tuj-1 marker for the cortex (**Figure 3D**). As shown in **Figures 3C,D**, exosomal α-syn cargo does not influence the accumulation of endogenous α-syn in our *in vivo* setting. Additionally, immunofluorescent counts of the TH-positive neurons in the *SNpc* revealed no changes in the number of surviving neurons (**Figure 3E**).

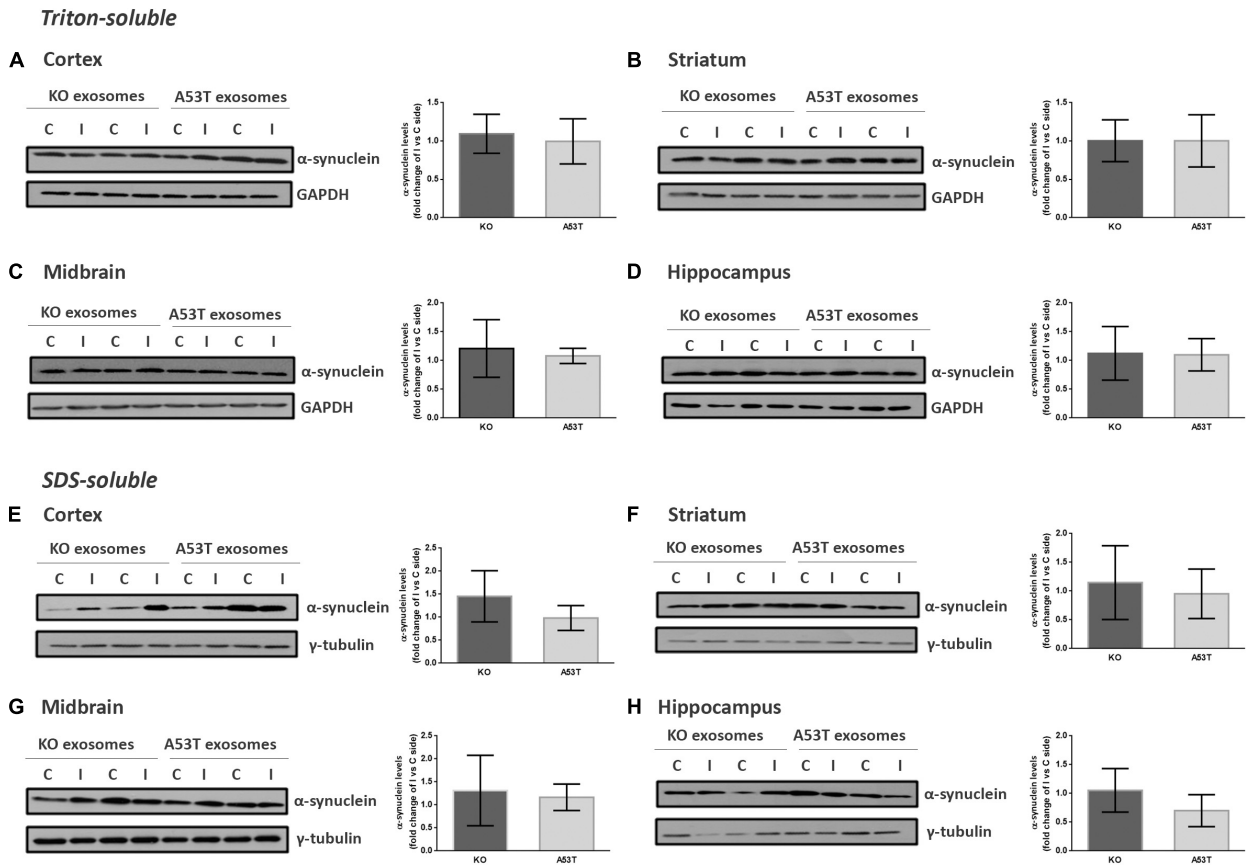

FIGURE 2 | Wild-type (wt) mice injected with KO or A53T brain exosomes display similar levels of detergent-soluble and detergent-insoluble α-syn in their brains. The cortex, striatum, midbrain, and hippocampus were isolated from exosome-injected wt mice at 150 dpi. Brain homogenates from the ipsilateral and contralateral sides were analyzed by immunoblotting using the Syn-1 antibody to α-syn. GAPDH and γ-tubulin were used as loading controls for Triton X- and sodium dodecyl sulfate (SDS)-soluble fractions, respectively. Representative (in duplicate) immunoblots from **(A/E)** cortex, **(B/F)** striatum **(C/G)**, midbrain, and **(D/H)** hippocampus are depicted. Differences in the levels of α-syn in the Triton X-soluble and SDS-soluble fractions were further evaluated by densitometry quantification. The fold changes between the ipsilateral and contralateral sides in α-syn levels are shown in the graphs. No significant differences in the levels of α-syn species were detected. Data are presented as mean ± SEM of $n = 4$ animals/group.

Behavioral Phenotyping of Exosome-Injected Mice

A battery of behavioral tests was conducted on male wt mice injected with either KO or A53T exosomes. To assess gross motor function, we used the open field test. KO and A53T exosome-injected mice displayed a similar locomotor activity, as measured by the total distance traveled and speed in the course of 15 min (**Supplementary Figures S1A,B**). Although A53T exosome-injected mice tended to spend slightly less time in the central area of the arena, which is indicative of an anxiety-like behavior, this trend was not statistically significant (**Supplementary Figure S1C**). To further characterize the fine-motor activity of the injected animals, such as their balance and coordination, we performed the pole task and the beam walking test. The analysis showed that KO and A53T exosome-injected mice performed in the same manner during the pole test, with no significant differences in the time to orient downward and descend from the pole (**Supplementary Figures S1D,E**). Likewise, measurements recorded during the beam walking test revealed no significant differences between the two cohorts, as expressed by the ratio of the total errors per steps (**Supplementary Figure S1F**).

Exosome-Bound Preformed Fibrils Induce Minor Pathology Following Injection in Wild-Type Mouse Brain

We further sought to investigate whether the association of PFFs with exosomes could modify their capacity in seeding pathological α-syn *in vivo*. To this end, we loaded sonicated mouse PFFs on exosomes isolated from null mouse brains, and we injected exosome-bound and exosome-free PFFs in wt mouse striata. Initially, α-syn PFFs were loaded on exosomes as described in the "Materials and Methods" section. The resulting exosome-bound PFFs were purified by ultracentrifugation on a sucrose gradient. Western immunoblotting of the isolated fractions for α-syn revealed the expected shift of exosome-bound PFFs in lower-density sucrose fractions when compared with PFFs alone (**Figure 4A**). In order to estimate the concentration of PFFs that were bound on exosomes, different dilutions of

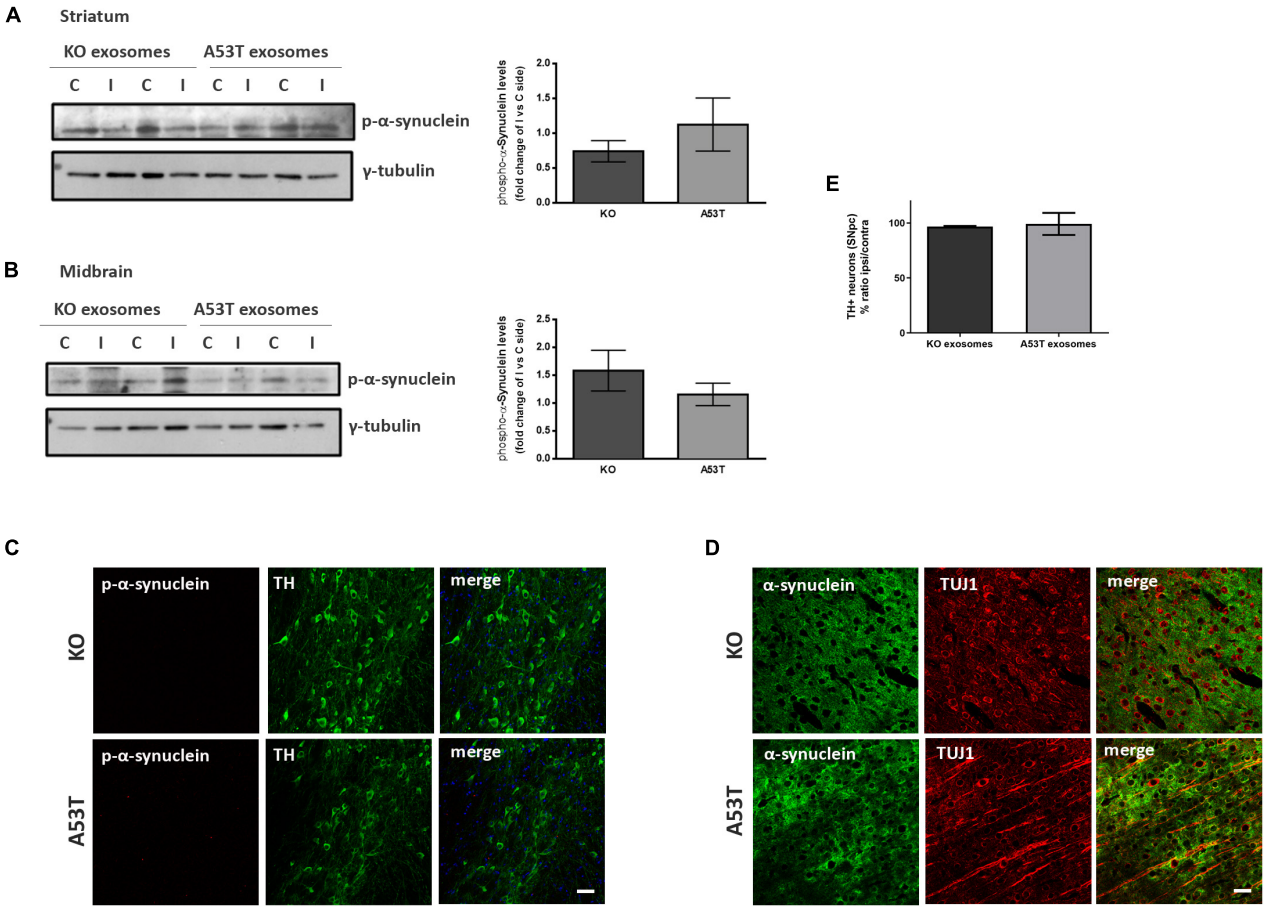

FIGURE 3 | Exosomal cargo does not induce the accumulation of phosphorylated α-syn in the brains of recipient mice. The sodium dodecyl sulfate (SDS)-soluble fractions of striatum **(A)** and midbrain **(B)** of wild-type (wt) mice injected with KO or A53T isolated brain exosomes were examined for the presence of phosphorylated α-syn species using the pS129 antibody. γ-Tubulin was used as a loading control. The fold change between the ipsilateral and contralateral sites in phosphorylated α-syn levels is shown in the graphs. No significant differences in the levels of phosphorylated α-syn species were detected. Data are presented as mean ± SEM of $n = 4$ animals. Nigral **(C)** and cortex **(D)** sections of mice injected with KO or A53T exosomes were stained for phosphorylated α-synuclein and total α-syn, respectively. pS129-positive inclusions were not evident in the ipsilateral tyrosine hydroxylase (TH)-positive neurons of KO- and A53T-injected animals. Labeling with the Syn-1 specific α-syn antibody and neuronal Tuj-1 is showing the absence of endogenous α-syn accumulations. Scale bar, 50 μm. **(E)** Coronal sections containing the SNpc from mice injected with exosomes from KO and A53T mouse brains were immunolabeled with anti-TH antibody. The numbers of TH-positive neurons were quantified in each section using the ImageJ software ($n = 3$). Graph shows the% ratio of ipsilateral to contralateral side of TH-positive neurons. Statistical analysis by Student's *t*-test did not reveal any statistical differences between the groups.

the exosome–PFF-enriched fraction (Fraction d) were compared with known concentrations of PFFs by the western blot analysis with the α-syn (C20) antibody (**Figure 4B**). Following the densitometric analysis, a total of 2.5 μg of PFFs, either exosome bound or free, was injected stereotactically in the right dorsal striatum of 2- to 3-month-old wt mice. Pathology transmission was examined by assessing phosphorylated α-syn pathological accumulations in the SNpc of injected mice. As shown in **Figure 4C**, at 60 dpi, only free PFFs induced the robust accumulation of phosphorylated α-syn in the SNpc of injected mice. Exosome-bound PFFs promoted a minor accumulation of phosphorylated α-syn as judged by immunofluorescence staining with the pS129 antibody. Western blotting further verified the increase in the levels of phosphorylated α-syn species in the SDS-soluble fraction of the ipsilateral midbrain of injected animals. In order to follow the progress of pathology induced by exosome-bound PFFs, we analyzed a second group of animals at 210 dpi. Even at this prolonged time point, free PFF-injected animals accumulated significantly more inclusions within TH-positive neurons than did the exosome-bound PFF-injected animals (% phospho α-syn accumulation/TH: 6.57 ± 0.27 vs. 1.23 ± 0.33, respectively) (**Figure 4D**). As expected, PFFs had significantly impaired the survival of the dopaminergic neurons given the development of extensive pathological accumulations already within the first 2 months post injection. The stereological analysis of TH-positive neurons at 210 dpi revealed a significant loss of dopaminergic neurons in the free PFF-injected animals compared with those injected with exosome-bound PFFs (% TH ratio ipsi/contra: 59.74 ± 6.014 vs. 95.86 ± 2.809, respectively) (**Figure 4E**). Again, over time, exosome-bound PFF-injected

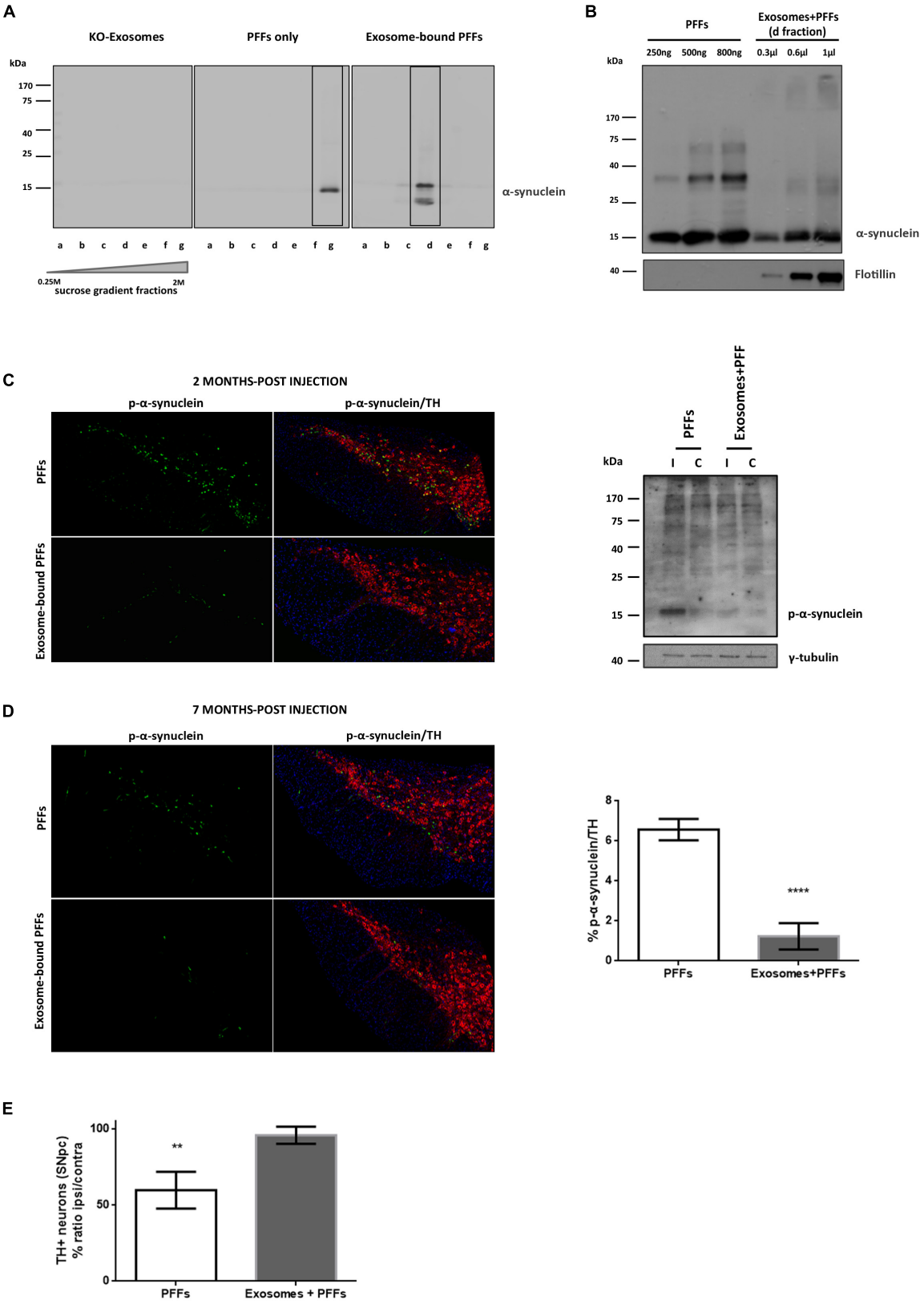

FIGURE 4 | Continued

FIGURE 4 | Continued
Exosome-bound preformed fibrils (PFFs) induce minor pathology following injection in wild-type (wt) mouse brain. **(A)** Exosomes from α-syn KO brains were loaded with recombinant α-syn PFFs. Successful binding of PFFs on exosomes was verified by the shift of the purified exosome–PFF complex to fractions of lower sucrose density following ultracentrifugation on sucrose gradient as assessed with the Syn-1 antibody. **(B)** The amount of PFFs loaded to exosomes was determined by western blot analysis using the C20 antibody and comparing different dilutions of the exosome–PFF fraction with known concentrations of PFFs. Flotillin was used as a vesicular marker. Coronal midbrain sections of free and exosome-bound PFF-injected animals at 2 **(C)** and 7 **(D)** months post injection were stained with antibodies to phosphorylated α-syn and TH. At 2 months post injection, robust pathology was detected following free PFF injection as seen by accumulation of phosphorylated α-syn. Western blot analysis verified the presence of sodium dodecyl sulfate (SDS)-soluble phosphorylated α-syn species in the midbrain of PFF-injected animals. **(D)** At 7 months post injection, phosphorylated α-syn accumulations were significantly more in PFFs compared with exosome-bound PFF-injected animals. Graph shows the% phosphorylated α-syn accumulations within tyrosine hydroxylase (TH) neurons. **(E)** Stereological assessment of SNpc neurons in PFFs and exosome-bound PFF-injected animals at 7 months post injection. Significant TH-neuronal loss occurs following free PFF injections. Graph depicts the TH neurons as a % ratio of ipsilateral to contralateral side. Statistical analysis by Student's *t*-test, $n = 4$ per group. $^{****}p < 0.0001$, $^{**}p < 0.01$.

mice developed few phosphorylated α-syn loci in the absence of dopaminergic neuronal loss in the SNpc.

Exosomes Impede Preformed Fibril Uptake in Primary Cortical Neurons

We next asked whether the association of PFFs with exosomes could affect the ability of PFFs to enter recipient neurons. To this end, we incubated 5-day-old primary mouse neuronal cultures with free or exosome-bound PFFs and investigated their uptake by the recipient cells at 8 and 24 h. Following trypsinization, cell lysates were extracted with Triton X-100. Internalized α-syn species were detected in the fractions by western blotting with the specific α-syn antibody C-20. As shown in **Figure 5A**, free PFFs were readily taken up by neuronal cells as early as 8 h. By 24 h, the presence of high-molecular-weight α-syn species intracellularly was evident. Interestingly, compared with free PFFs, exosome-associated PFFs demonstrated reduced uptake by primary neurons, whereas a substantial amount of insoluble material still remained trapped in the stacking gel (PFFs 15.68 ± 1.91 vs. exosome-bound PFFs 6.91 ± 1.66) (**Figure 5A**). Treatment of mouse primary neurons for 48 h with free or exosome-bound PFFs further confirmed the reduced uptake of PFFs by neurons upon exosomal binding. As depicted in **Figure 5B**, immunocytochemical staining with the neuronal marker Tuj-1 and the α-syn antibody C20 revealed that exosome-associated PFFs cannot efficiently enter recipient neurons. Interestingly, the 3D reconstruction analysis of the images using the Imaris (9.5.1) software revealed that exosome-bound PFFs are sequestered on the cell membranes. As shown in **Figure 5B** (transparent vs. opaque), the majority of C-20 immunostained exosome-bound PFFs were partly colocalized with Tuj-1. On the contrary, free PFFs seem to be fully internalized following 48-h incubation with primary neurons (**Figure 5B**). To gain some insight as to why the exosome-bound PFFs are not readily taken up by neurons and hence lose their capacity to induce pathological accumulation of α-syn and impair neuronal integrity, we incubated 1.25 μg of exosomes with 1 μM of PFFs *in vitro* (final volume 150 μl in PBS) at 37°C and assessed the effects of this association up to 24 h. The western blot analysis with the anti-α-syn-specific antibodies C20 and Syn-1 showed that over time PFFs appear to assemble into higher-order multimers upon *in vitro* binding to exosomes with gradual loss of the monomer (**Figure 5C**). Interestingly, probing with the Syn-1 antibody also revealed the generation of α-syn species with molecular weights lower than 15 kDa. It is possible that these are the results of cleavage by exosomal proteases due to the absence of cells in the *in vitro* preparation. No multimerization was observed when PFFs were incubated in the absence of exosomes for the same amount of time.

DISCUSSION

Exosomes could facilitate the spreading of α-syn disease pathology by the transfer of α-syn oligomers to unaffected neurons where they could initiate the oligomerization of endogenous α-syn. It was previously shown that exosomal α-syn oligomers are efficiently internalized into recipient cells (Danzer et al., 2012). Homozygous A53T α-syn mice have been shown to develop α-syn inclusions in the striatum, thalamus, sparsely in the motor cortex, brain stem, and spinal cord, which is accompanied with a severe motor phenotype between 8 and 16 months. We have previously shown that A53T Tg mice have increased levels of extracellular α-syn in their interstitial fluid (ISF) (Emmanouilidou et al., 2011). Considering that the exosome environment may provide a local concentration gradient of α-syn (as opposed to free α-syn), as well as offer protection from degradation (Lee et al., 2005), we assumed that exosomes from A53T mice would be a key template for the accumulation and the transmission of α-syn pathology. Here, we hypothesized that exosomal α-syn species from mice with excessive mutant α-syn may serve as transporters of disease pathology. We also inferred that α-syn had to be phosphorylated because in patients with synucleinopathies greater than 90% of the LBs contain phosphorylated α-syn at serine residue 129 (Oueslati, 2016). Following final purification on a sucrose gradient, we obtained fractions that were analyzed by EM for purity and the presence of EVs. As judged by the AchE/Bradford assays, similar amounts of exosomes were obtained from null and A53T mouse brains. We then examined the cargo of brain-derived exosomes for oligomerized proteins. In this regard, aged transgenic A53T mice exhibited increased levels of Triton X-soluble and Triton X-insoluble α-syn as well as phosphorylated α-syn species (**Figure 1**). Exosomal α-syn levels in the Tg mouse correlated with the expression levels of the protein in the brain. In addition, we found that exosomes isolated from Tg mice were rich in phosphorylated α-syn and carried, as expected, human α-syn. The EM analysis further demonstrated that the density gradient-isolated brain exosomes were intact. In our hands,

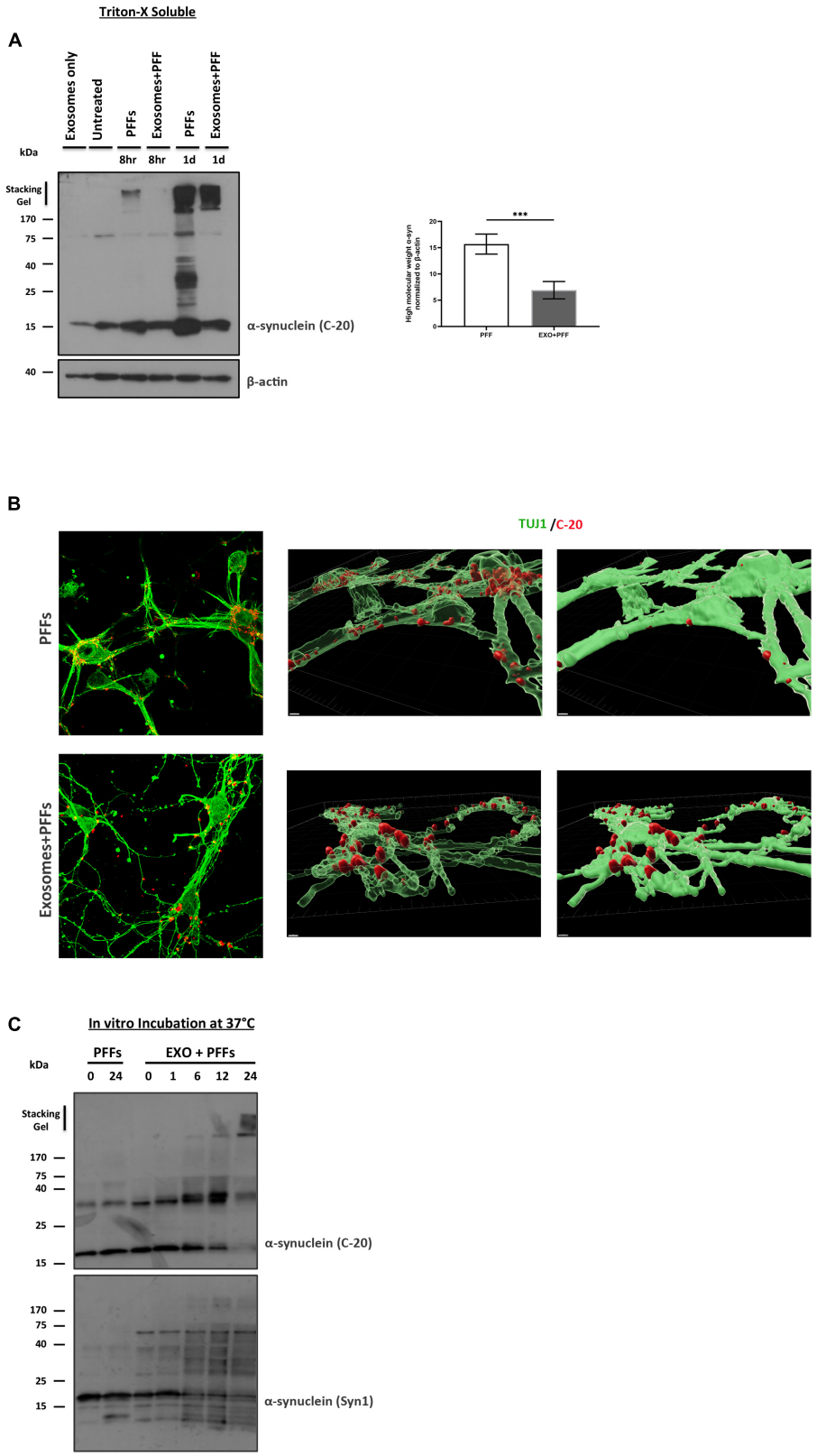

FIGURE 5 | Continued

FIGURE 5 | Continued
Exosomes impede the uptake of preformed fibrils (PFFs) by neuronal cultures. **(A)** Primary mouse neuronal cultures (5div) were treated with either free or exosome-bound PFFs for 8 and 24 h. Following trypsinization, cell lysates were extracted with Triton X-100 and analyzed for the presence of α-syn species by western blotting using the specific α-syn antibody C-20. Increased α-syn high-molecular-weight species were evident in PFF-treated primary cultures as early as 8 h and significantly increased at 24 h. Graph shows the densitometric quantification from three independent experiments. Statistical analysis was with Student's *t*-test. **(B)** Immunofluorescent confocal images of mouse primary cortical neurons treated for 48 h with free or exosome-bound PFFs following staining with Tuj-1 and C-20 antibodies. 3D reconstruction analysis revealed the differential localization of free PFFs versus exosome-bound PFFs in neuronal cultures. Imaris software was used for image processing. Scale bar represents 5 μm. **(C)** PFFs were incubated *in vitro* in the presence or absence of exosomes for up to 24 h and analyzed by western blotting with the C-20 and Syn-1 antibodies. Figure shows the gradual formation of higher-molecular-weight α-syn species (gel excluded) in the presence of exosomes. α-Syn (Syn-1) antibody further detected the presence of cleaved α-syn products below 15 kDa. $^{***}p < 0.001$.

secreted vesicle-associated α-syn appears to be internalized by primary neurons. This is in agreement with data of Xia et al., who also observed that exogenous exosomes are taken up by neuronal and microglia cells, both *in vitro* and *in vivo* (Xia et al., 2019). Moreover, human α-syn has been shown to accumulate in neuronal cells following hippocampal injection of exosomes derived from patients with dementia with LBs (DLB) (Ngolab et al., 2017). Isolated exosomes from the brains of aged A53T Tg mice and null α-syn mice, as an α-syn independent control, were further analyzed for their potential to induce oligomerization of α-syn and propagation, *in vivo*, in wt mice. Considering seeded α-syn pathology develops in a time-dependent manner, we chose to examine the late time-point of 5 months post injection to assess any exosome-induced pathology, because this would be sufficient for accumulation detection. We also opted to use the same donor and recipient species in our study in an attempt to eliminate any exosome uptake obstruction due to species differences. Despite the presence of phosphorylated α-syn species in the A53T brain exosomal preparations, we did not observe any accumulation of α-syn in mice that received these exosomes. Null and A53T-derived exosomes did not affect soluble or insoluble levels of total α-syn in all the brain regions tested. In addition, phosphorylated SDS-soluble α-syn levels were found unaffected in the midbrain and the striatum of exosome-recipient mice. PD patient-derived serum exosomes have been shown to induce features of LB-like pathology and dopaminergic loss when injected in mice (Han et al., 2019). In our experimental setup, we were not able to detect pathological accumulation or reduced neuronal viability. This discrepancy may be attributed to differences in the concentrations of exosomes injected. Unlike the study of Han et al., where the mice were injected with 200 μg of exosomes in total on a weekly basis for 2 months, we used a single dose of 5.5 μg of exosome fractions for intrastriatal injections, which might not be sufficient as pathogenic seed. Of note, the injected amount used in our setup is in accordance with other studies using exosomes as a potential pathogenic material (Ngolab et al., 2017; Zheng et al., 2017; Winston et al., 2019).

Moreover, Xia et al. (2019) demonstrated transmission of pathology in the mouse brain following injection of plasma exosomes derived from PD patients. Although not neuronal in origin, the plasma exosomes isolated from PD patients may contain the α-syn species necessary for the templating and seeding of the endogenous α-syn. In our study, the levels of α-syn species with true seeding capacity originating from exosomes isolated from the A53T mice may be absent or low, and this may have had functional consequences for the transmission of α-syn pathology. Variance in α-syn amount as exosomal cargo has been reported previously between DLB and PD exosomes. In the study by Stuendl et al. (2016), DLB CSF exosomes, although fewer in absolute numbers, contained substantially more α-syn per exosome than did PD CSF exosomes. The absence of α-syn-induced pathology in our *in vivo* setting was further confirmed by confocal imaging. The behavioral analysis showed that mice injected with α-syn null or A53T exosomes performed similarly in almost all assays of motor function, exhibiting intact gross and fine-motor features such as locomotor activity, balance, and motor coordination. Our findings with exosomes isolated from A53T mouse brains indicate that perhaps not all of the misfolded α-syn species are able to generate exosomes carrying α-syn seeds. To this end, Tsika and collaborators provided a biochemical characterization of *in vivo* formed oligomeric intermediates of α-syn in the A53T α-syn transgenic mice. This study showed that despite their similar biochemical properties, oligomeric α-syn isolated from different brain regions exhibited variances in aggregate formation and toxicity (Tsika et al., 2010). We should note here that the Tg A53T animals used in our study were symptomatic, and we hypothesized that this may have critically affected the generation of exosomes with efficient α-syn seeding cargoes. In this regard, it should be noted that the A53T mice do not exhibit dopaminergic cell loss, suggesting that the α-syn pathology observed does not directly correlate with toxicity (Giasson et al., 2002). A recent study showed that prion protein seeds, although widely distributed in the brain, cause degeneration in certain areas and that misfolded prion protein alone does not necessarily induce neurodegeneration (Alibhai et al., 2016).

To further address the role of exosomes on intercellular transmission of proteopathic α-syn seeds, we went on to load them with toxic α-syn fibrils, known to induce pathological accumulation in the brain (Luk et al., 2012). Following successful binding of mouse PFFs to exosomes, the complexes were purified on sucrose gradient and injected in the striatum of wt mice. Even at 210 dpi, exosome-bound PFFs failed to promote a sufficient accumulation of pathological α-syn in the injected mice, although minor α-syn phosphorylated puncta were observed. As expected, injection of free PFFs templated the seeding of pathological phosphorylated α-syn as early as 60 dpi and significantly impaired dopaminergic neuron integrity by 210 dpi. Further analysis using primary neuronal cultures revealed that this lack of pathology induction by the PFF/exosome complex might be

due to reduced internalization of the complex by the recipient neurons. Although it is not clear why exosome-bound PFFs only partially enter neurons, we found that *in vitro* incubation of PFFs with purified isolated mouse brain exosomes caused their multimerization into high-molecular-weight assemblies. The exact nature of these α-syn multimers that form upon binding to the exosomal membranes remains to be identified. Given the high affinity of fibrillar α-syn to the membranes, we can speculate that mouse PFFs may act as linkers by sequestering exosomes in high-molecular-weight aggregates with limited accessibility to the cells. As shown in **Figure 5B**, these clusters are located at the interface between the intracellular and extracellular space of primary cortical neurons. Although it remains to be proven, it is plausible that in our *in vivo* setup, the neuronal terminals might be unable to uptake these assemblies and thus be protected from the toxic PFFs, as judged by the absence of neuronal loss even following a 7-month incubation period. Our results are in agreement with those of An et al., who demonstrated that isolated exosomes were protective against Aβ-induced long-term potentiation (LTP) impairment by sequestering Aβ oligomers at their surface (An et al., 2013). Moreover, the absence of pathology in exosome–PFF-injected animals might be the result of limited access of the endogenous α-syn to the aggregated-prone structure of the PFFs, due to complete or partial masking by the exosomes. Together, our results, using exosomes as carrier vesicles of pathological α-syn, indicate that exosomes alone are insufficient to induce robust LB-like pathology in wt mouse brains. We should note here that irrespective of the pathogenic potential of their α-syn cargo, we and others have noticed that exosomes are taken up less efficiently from neurons than other cell types, like microglia (Xia et al., 2019). This limited access might also affect their potential to recruit the endogenous neuronal α-syn and transmit pathology *in vivo*.

Considering that neurodegeneration is influenced by not only the buildup of misfolded proteins but also the district cellular environment (Brettschneider et al., 2015; Goedert, 2015; Peng et al., 2018), it is possible that exosome uptake and contribution to pathology spreading are selectively governed by as-yet-unknown mechanisms between emitting and receiving cells. However, it is still not clear whether misfolded α-syn follows a prion-like transmission pattern for the progression of the disease or whether other signals trigger the pathological accumulation in vulnerable neurons (Walsh and Selkoe, 2016). In this sense, under pathological conditions, exosome-associated α-syn might be triggering immune responses when taken up by brain glia cells that in turn aid the seeding of endogenous neuronal α-syn. More studies are needed to elucidate whether exosomes are a complementary or essential mechanism of disease transmission.

DATA AVAILABILITY STATEMENT

All datasets generated for this study are included in the article/**Supplementary Material**.

ETHICS STATEMENT

The animal study was reviewed and approved by the Centre of the Biomedical Research Foundation of the Academy of Athens. The competent Regional Veterinary authority approved the experimental protocol in accordance to Greek legislation (Presidential Decree 56/2013, in compliance with the European Directive 2010/63).

AUTHOR CONTRIBUTIONS

VS and MK performed the exosome isolation, stereotactic injections, biochemical analysis, *in vitro* and *in vivo* experiments, and behavioral assessments. EL, KM, and AG performed the immunohistochemistry and biochemical analyses of mice. AL and MK performed the immunohistochemistry and TH counting. EE, MK, and KM performed the figure preparation and data analysis. VK supervised the experiments and performed the data interpretation. KV and MK wrote the manuscript. All authors contributed to the drafting of the manuscript.

FUNDING

Part of this work has been financially supported by a grant to KV from the European Regional Development Fund of the European Union and Greek national funds through the Operational Program Competitiveness, Entrepreneurship and Innovation, under the call RESEARCH–CREATE–INNOVATE (Project Code: T1EDK-03884).

ACKNOWLEDGMENTS

We thank Drs. Hilal Lashuel and Anne-Laure Mahul Mellier (EPFL, Switzerland) for providing the mouse PFF material. We would like to thank Dr. Georgia Minakaki for assisting with immunocytochemistry of stained exosomes. We also thank Dr. Tasos Delis and the Bioimaging Core Unit of BRFAA for technical assistance and Dr. Ismini Kloukina for assistance with acquisition of EM images.

SUPPLEMENTARY MATERIAL

The Supplementary Material for this article can be found online at: https://www.frontiersin.org/articles/10.3389/fnins.2020.00246/full#supplementary-material

FIGURE S1 | Behavioral profile of mice injected with KO and A53T exosomes. Exosome injected mice exhibit normal gross and fine motor function. In the open field test the parameters assessed for general locomotor activity during the course of 15 min were **(A)** total distance travelled in centimeters **(B)** velocity and **(C)** total time spent in the center of the field expressed in seconds. **(D,E)** represent the latency to orient and descend from the pole expressed in seconds. **(F)** Represents the challenging beam traversal performance in exosome-injected animals, expressed in total errors/steps. $n = 10$ animals/group. Data are plotted as mean ± SEM. Differences were estimated using Student's test.

REFERENCES

Alibhai, J., Blanco, R. A., Barria, M. A., Piccardo, P., Caughey, B., Perry, V. H., et al. (2016). Distribution of misfolded prion protein seeding activity alone does not predict regions of neurodegeneration. *PLoS Biol.* 14:e1002579. doi: 10.1371/journal.pbio.1002579

Alvarez-Erviti, L., Seow, Y., Schapira, A. H., Gardiner, C., Sargent, I. L., Wood, M. J. A., et al. (2011). Lysosomal dysfunction increases exosome-mediated alpha-synuclein release and transmission. *Neurobiol. Dis.* 42, 360–367. doi: 10.1016/j.nbd.2011.01.029

An, K., Klyubin, I., Kim, Y., Jung, J. H., Mably, A. J., O'Dowd, S. T., et al. (2013). Exosomes neutralize synaptic-plasticity-disrupting activity of Abeta assemblies in vivo. *Mol. Brain* 6:47. doi: 10.1186/1756-6606-6-47

Brettschneider, J., Del Tredici, K., Lee, V. M.-Y., and Trojanowski, J. Q. (2015). Spreading of pathology in neurodegenerative diseases: a focus on human studies. *Nat. Rev. Neurosci.* 16, 109–120. doi: 10.1038/nrn3887

Danzer, K. M., Kranich, L. R., Ruf, W. P., Cagsal-Getkin, O., Winslow, A. R., Zhu, L., et al. (2012). Exosomal cell-to-cell transmission of alpha synuclein oligomers. *Mol. Neurodegen.* 7:42. doi: 10.1186/1750-1326-7-42

Emmanouilidou, E., Elenis, D., Papasilekas, T., Stranjalis, G., Gerozissis, K., Ioannou, P. C., et al. (2011). Assessment of alpha-synuclein secretion in mouse and human brain parenchyma. *PloS One* 6:e22225. doi: 10.1371/journal.pone.0022225

Emmanouilidou, E., Melachroinou, K., Roumeliotis, T., Garbis, S. D., Ntzouni, M., Margaritis, L. H., et al. (2010). Cell-produced alpha-synuclein is secreted in a calcium-dependent manner by exosomes and impacts neuronal survival. *J. Neurosci.* 30, 6838–6851. doi: 10.1523/JNEUROSCI.5699-09.2010

Giasson, B. I., Duda, J. E., Quinn, S. M., Zhang, B., Trojanowski, J. Q., and Lee, V. M.-Y. (2002). Neuronal alpha-synucleinopathy with severe movement disorder in mice expressing A53T human alpha-synuclein. *Neuron* 34, 521–533. doi: 10.1016/s0896-6273(02)00682-7

Goedert, M. (2015). Neurodegeneration. Alzheimer's and Parkinson's diseases: The prion concept in relation to assembled Abeta tau and alpha-synuclein. *Science* 349:1255555. doi: 10.1126/science.1255555

Grey, M., Dunning, C. J., Gaspar, R., Grey, C., Brundin, P., Sparr, E., et al. (2015). Acceleration of alpha-synuclein aggregation by exosomes. *J. Biol. Chem.* 290, 2969–2982. doi: 10.1074/jbc.M114.585703

Gustafsson, G., Loov, C., Persson, E., Lazaro, D. F., Takeda, S., Bergstrom, J., et al. (2018). Secretion and uptake of alpha-synuclein via extracellular vesicles in cultured cells. *Cell. Mol. Neurobiol.* 38, 1539–1550. doi: 10.1007/s10571-018-0622-5

Han, C., Xiong, N., Guo, X., Huang, J., Ma, K., Liu, L., et al. (2019). Exosomes from patients with Parkinson's disease are pathological in mice. *J. Mol. Med.* 97, 1329–1344. doi: 10.1007/s00109-019-01810-z

Karampetsou, M., Ardah, M. T., Semitekolou, M., Polissidis, A., Samiotaki, M., Kalomoiri, M., et al. (2017). Phosphorylated exogenous alpha-synuclein fibrils exacerbate pathology and induce neuronal dysfunction in mice. *Sci. Rep.* 7:16533. doi: 10.1038/s41598-017-15813-8

Lee, H.-J., Patel, S., and Lee, S.-J. (2005). Intravesicular localization and exocytosis of alpha-synuclein and its aggregates. *J. Neurosci.* 25, 6016–6024. doi: 10.1523/JNEUROSCI.0692-05.2005

Luk, K. C., Kehm, V., Carroll, J., Zhang, B., O'Brien, P., Trojanowski, J. Q., et al. (2012). Pathological alpha-synuclein transmission initiates Parkinson-like neurodegeneration in nontransgenic mice. *Science* 338, 949–953. doi: 10.1126/science.1227157

Ngolab, J., Trinh, I., Rockenstein, E., Mante, M., Florio, J., Trejo, M., et al. (2017). Brain-derived exosomes from dementia with Lewy bodies propagate alpha-synuclein pathology. *Acta Neuropathol. Commun.* 5:46. doi: 10.1186/s40478-017-0445-5

Oueslati, A. (2016). Implication of Alpha-synuclein phosphorylation at S129 in synucleinopathies: what have we learned in the last decade? *J. Parkinson Dis.* 6, 39–51. doi: 10.3233/JPD-160779

Pan-Montojo, F., Schwarz, M., Winkler, C., Arnhold, M., O'Sullivan, G. A., Pal, A., et al. (2012). Environmental toxins trigger PD-like progression via increased alpha-synuclein release from enteric neurons in mice. *Sci. Rep.* 2:898. doi: 10.1038/srep00898

Papadopoulos, V. E., Nikolopoulou, G., Antoniadou, I., Karachaliou, A., Arianoglou, G., Emmanouilidou, E., et al. (2018). Modulation of beta-glucocerebrosidase increases alpha-synuclein secretion and exosome release in mouse models of Parkinson's disease. *Hum. Mol. Genet.* 27, 1696–1710. doi: 10.1093/hmg/ddy075

Paxinos, G., and Franklin, K. B. (2004). *The Mouse Brain in Stereotaxic Coordinates*, 2nd Edn, San Diego: Elsevier.

Peng, C., Gathagan, R. J., Covell, D. J., Medellin, C., Stieber, A., Robinson, J. L., et al. (2018). Cellular milieu imparts distinct pathological alpha-synuclein strains in alpha-synucleinopathies. *Nature* 557, 558–563. doi: 10.1038/s41586-018-0104-4

Poehler, A.-M., Xiang, W., Spitzer, P., May, V. E. L., Meixner, H., Rockenstein, E., et al. (2014). Autophagy modulates SNCA/alpha-synuclein release, thereby generating a hostile microenvironment. *Autophagy* 10, 2171–2192. doi: 10.4161/auto.36436

Qazi, K. R., Gehrmann, U., Domange Jordo, E., Karlsson, M. C. I., and Gabrielsson, S. (2009). Antigen-loaded exosomes alone induce Th1-type memory through a B-cell-dependent mechanism. *Blood* 113, 2673–2683. doi: 10.1182/blood-2008-04-153536

Savina, A., Vidal, M., and Colombo, M. I. (2002). The exosome pathway in K562 cells is regulated by Rab11. *J. Cell Sci.* 115(Pt 12), 2505–2515.

Shi, M., Liu, C., Cook, T. J., Bullock, K. M., Zhao, Y., Ginghina, C., et al. (2014). Plasma exosomal alpha-synuclein is likely CNS-derived and increased in Parkinson's disease. *Acta Neuropathol.* 128, 639–650. doi: 10.1007/s00401-014-1314-y

Soria, F. N., Pampliega, O., Bourdenx, M., Meissner, W. G., Bezard, E., and Dehay, B. (2017). Exosomes, an unmasked culprit in neurodegenerative diseases. *Front. Neurosci.* 11:26. doi: 10.3389/fnins.2017.00026

Stuendl, A., Kunadt, M., Kruse, N., Bartels, C., Moebius, W., Danzer, K. M., et al. (2016). Induction of alpha-synuclein aggregate formation by CSF exosomes from patients with Parkinson's disease and dementia with Lewy bodies. *Brain J. Neurol.* 139(Pt 2), 481–494. doi: 10.1093/brain/awv346

Tsika, E., Moysidou, M., Guo, J., Cushman, M., Gannon, P., Sandaltzopoulos, R., et al. (2010). Distinct region-specific alpha-synuclein oligomers in A53T transgenic mice: implications for neurodegeneration. *J. Neurosci.* 30, 3409–3418. doi: 10.1523/JNEUROSCI.4977-09.2010

Vekrellis, K., Xilouri, M., Emmanouilidou, E., Rideout, H. J., and Stefanis, L. (2011). Pathological roles of alpha-synuclein in neurological disorders. *Lancet. Neurol.* 10, 1015–1025. doi: 10.1016/S1474-4422(11)70213-7

Vella, L. J., Hill, A. F., and Cheng, L. (2016). Focus on extracellular vesicles: exosomes and their role in protein trafficking and biomarker potential in Alzheimer's and Parkinson's Disease. *Intern. J. Mol. Sci.* 17:173. doi: 10.3390/ijms17020173

Volpicelli-Daley, L. A., Luk, K. C., Patel, T. P., Tanik, S. A., Riddle, D. M., Stieber, A., et al. (2011). Exogenous alpha-synuclein fibrils induce Lewy body pathology leading to synaptic dysfunction and neuron death. *Neuron* 72, 57–71. doi: 10.1016/j.neuron.2011.08.033

Walsh, D. M., and Selkoe, D. J. (2016). A critical appraisal of the pathogenic protein spread hypothesis of neurodegeneration. *Nat. Rev. Neurosci.* 17, 251–260. doi: 10.1038/nrn.2016.13

Winston, C. N., Aulston, B., Rockenstein, E. M., Adame, A., Prikhodko, O., Dave, K. N., et al. (2019). Neuronal exosome-derived human tau is toxic to recipient mouse neurons in vivo. *J. Alzheimer Dis. JAD* 67, 541–553. doi: 10.3233/JAD-180776

Xia, Y., Zhang, G., Han, C., Ma, K., Guo, X., Wan, F., et al. (2019). Microglia as modulators of exosomal alpha-synuclein transmission. *Cell Death Dis.* 10:174. doi: 10.1038/s41419-019-1404-9

Zheng, T., Pu, J., Chen, Y., Mao, Y., Guo, Z., Pan, H., et al. (2017). Plasma exosomes spread and cluster around beta-amyloid plaques in an animal model of Alzheimer's Disease. *Front. Aging Neurosci.* 9:12. doi: 10.3389/fnagi.2017.00012

Conflict of Interest: The authors declare that the research was conducted in the absence of any commercial or financial relationships that could be construed as a potential conflict of interest.

Advantages of publishing in Frontiers

OPEN ACCESS
Articles are free to read for greatest visibility and readership

FAST PUBLICATION
Around 90 days from submission to decision

HIGH QUALITY PEER-REVIEW
Rigorous, collaborative, and constructive peer-review

TRANSPARENT PEER-REVIEW
Editors and reviewers acknowledged by name on published articles

Frontiers
Avenue du Tribunal-Fédéral 34
1005 Lausanne | Switzerland

Visit us: www.frontiersin.org
Contact us: info@frontiersin.org | +41 21 510 17 00

REPRODUCIBILITY OF RESEARCH
Support open data and methods to enhance research reproducibility

DIGITAL PUBLISHING
Articles designed for optimal readership across devices

FOLLOW US
@frontiersin

IMPACT METRICS
Advanced article metrics track visibility across digital media

EXTENSIVE PROMOTION
Marketing and promotion of impactful research

LOOP RESEARCH NETWORK
Our network increases your article's readership